

Queens' College



UNIVERSITY OF
CAMBRIDGE



Identification and functional characterisation of different inner mitochondrial membrane supercomplexes

Margherita Protasoni

Dissertation submitted for the degree of Doctor of Philosophy
September 2020

Declaration

This dissertation describes the results of my own work, except for the experiments performed by collaborators, which are specified in the figure legends. This work was carried out between October 2016 and September 2019 under the supervision of Prof Massimo Zeviani assisted by Dr Erika Fernandez-Vizarra (Senior Investigator Scientist) and between October 2019 and September 2020 under the supervision of Dr Julien Prudent at the MRC Mitochondrial Biology Unit. Information derived from other sources has been referenced accordingly. This thesis has not been submitted, in whole or in part, for a degree at this or any other institution and the length of it does not exceed the prescribed word limit.

The results described in Section 5 led to a publication: Respiratory supercomplexes act as a platform for complex III-mediated maturation of human mitochondrial complexes I and IV. Protasoni M, Pérez-Pérez R, Lobo-Jarne T, Harbour ME, Ding S, Peñas A, Diaz F, Moraes CT, Fearnley IM, Zeviani M, Ugalde C, Fernández-Vizarra E. EMBO J. 2020 Feb 3;39(3).

Margherita Protasoni
September 2020

Acknowledgments

I would like to express my sincere gratitude to my PhD supervisor, Dr Julien Prudent, and Dr Erika Fernandez-Vizarra for the invaluable guidance and support during my PhD, and for having shared their enthusiasm and knowledge with me. I would also like to thank my first supervisor, Prof Massimo Zeviani, for giving me the opportunity to carry out my work in the MBU and the MRC, who funded my research. A special thank you to Dr Caterina Garone, her passion for science and life is contagious.

I would like to thank all the past Mitochondrial Medicine lab members, for all the discussions, the advices, and the encouragement you gave me since the very first day, especially Pedro, Aggelos, Cris, Dario, and Anil. Thanks also to my fellow PhD friends Juliette, Anja, and Dan for facing and sharing this challenge with me.

A special thank you to the Mitochondrial Physiology group, that adopted me and made me feel part of the family. A weird, crazy family, but I could not imagine anything better. Thank you to Vincent, for being my source of hugs and deep conversations, to Gonçalo, for always helping me and being such a role model, to LuisCa, for being so caring and supportive, and to Jordan, Filipa, Hanish, Roy, and Mark, for making the lab such an amusing place. Thank you also to Anezka, who greatly contributed to the MCU project with her hard work and resilience.

In particular, a huge thank you to Lisa, the one I literally shared every good and bad moment of this PhD with and who taught me so much about life, love, and friendship.

I would also like to express my gratitude to the mass spectrometry facility, the microscopy facility, and all the wonderful people working in administration and IT.

Thanks to my other Cambridge family, the numerous housemates I have shared laughs, ideas, and affection with during the last four years, and the incredibly vibrant Queens' College community. To Luz, my teammate and companion during the apocalypse, who knew since freshers week we were going to stick together and have quite an adventure, Aaron and Arian, for their support and the fun moments spent together (and especially for the mitochondria-related jokes), Ara and Ivan, for all the laughs we shared and for making our little house feel

like home, Martin, for giving me the confidence and the encouragement I needed, and to Le, Toby, Ankita, Andrej, Chels, Matt, Cindy, Henry and all the Cambridge friends for the amazing time I had. I had an incredible and irreplaceable experience and all thanks to you.

Lastly, I would like to thank my parents, without you none of this would have been possible.

Summary

The inner mitochondria membrane (IMM) is densely packed with proteins necessary for mitochondrial activity, including oxidative phosphorylation (OXPHOS) complexes and transporters. Mitochondrial respiratory chain (MRC) complexes, which generate ATP by OXPHOS, associate in higher-order assemblies, known as supercomplexes (SC), that are structurally interdependent. Numerous patients carrying mutations in a single complex, indeed, present with combined enzyme deficiencies and, in particular, the destabilisation of complex I (CI) has been often described in the absence of complex III (CIII). To clarify the structural and functional relationships between complexes, we have analysed a MTCYB-deficient human cell line, unable to assemble CIII. Our results showed that in this line, CI biogenesis was blocked by preventing the incorporation of the NADH module, the last step of CI assembly, rather than decreasing its stability. Moreover, complex IV (CIV) biogenesis was impaired as well, and CIV subunits appeared sequestered within CIII subassemblies. Therefore, we propose that CIII is central not only for the formation of SC but also for the maturation of the other electron transport chain complexes. These results challenge the previous SC model that described the formation of fully assembled individual complexes before the association in SC. In contrast, they support a cooperative-assembly model in which the main role of CIII in SC is to provide a structural and functional platform for the completion of overall MRC biogenesis.

Next, we identified and characterised the interaction between CIV and the mitochondrial calcium uniporter complex (MCUC), responsible for mitochondrial calcium uptake and homeostasis. Our data, indeed, showed a specific physical interaction between this ETC enzyme and various subunits of MCUC in first and second dimension blue native PAGE, SILAC labelling/pulldown, and BioID proteomic-based methods. We then investigated the effects of this association with CIV, measuring enzyme activity and mitochondrial respiration, but also on MCUC and CIV distribution in the IMM, by N-structured illuminated super-resolution microscopy (N-SIM). Our results showed a specific reduction in CIV activity in the absence of MICU1, the main regulator of the uniporter, but surprisingly no effects were observed after MCU downregulation or pharmacological inhibition of mitochondrial Ca^{2+} entry. Instead, the lack of CIV seems to have an impact on MCU-containing complexes

formation and induces a re-localisation of MCU from the cristae membrane to the inner boundary membrane. Further experiments will be performed to shed light on the physiological relevance of this interaction.

Abbreviations

$\Delta\Psi$	membrane potential
1D/2D	first/second dimension
ADHD	attention deficit hyperactivity disorder
ADP	adenosine diphosphate
AOX	alternative oxidase
Apaf-1	apoptotic protease activating factor-1
ATP	adenosine triphosphate
BioID	proximity-dependent biotin identification
BLAST	basic local alignment search tool
BN-PAGE	blue native gel electrophoresis
bp	base pairs
BSA	bovine serum albumin
Ca ²⁺	calcium
CCCP	carbonyl cyanide <i>m</i> -chlorophenyl hydrazone
CCD	the coiled-coil domain
CHCHD2	coiled-coil-helix-coiled-coil helix domain containing 2
CHCHD3	coiled-coil-helix-coiled-coil helix domain containing 3
CI	complex I
CII	complex II
CIII	complex III
CIV	complex IV
CJ	cristae junction
CL2	containment level 2
CM	cristae membrane
CO ₂	carbon dioxide
COX	cytochrome c oxidase
CS	citrate synthase
Cu	copper
CV	complex V

CYC1	cytochrome <i>c1</i>
D-loop	displacement loop
DCPIP	2,6-dichlorophenolindophenol
DDM	n-dodecyl- β -D-maltoside
DID	DIME interacting domain
DISC	death-inducing signalling complex
DMEM	Dulbecco's modified eagle's medium
DMSO	dimethyl sulfoxide
DNA	deoxyribonucleic acid
DNAJC11	dnaJ homolog subfamily C member 11
Drp1	dynamamin-related/-like protein 1
DTNB	5', 5'-Dithiobis 2-nitrobenzoic acid
DTT	dithiothreitol
EM	electron microscopy
EMRE	essential MCU regulator
ER	endoplasmic reticulum
ETC	electron transport chain
EV	empty vector
FAD	flavin adenine dinucleotide
FBS	foetal bovine serum
Fe	iron
FMN	flavin mononucleotide
FPLC	fast protein liquid chromatography
G	gram
GHITM	growth hormone inducible transmembrane protein
GTP	guanosine triphosphate
GTPases	Guanosine Triphosphatase
H ⁺	proton
H ₂ O	water
HA	hemagglutinin
HEK	human embryonic kidney
hr	hours
IBM	inner boundary membrane
IGA	in-gel activity

IMM	inner mitochondrial membrane
IMS	inter-membrane space
Ins(1,4,5)P ₃ Rs	inositol 1,4,5-triphosphate receptors
IP	immunopurification
ISCU	iron-sulphur cluster assembly enzyme
KD	knockdown
K _d	dissociation constant
kDa	kilodalton
KO	knockout
LB	lysogeny broth
LC-MS	liquid chromatography mass spectrometry
LHD	linker helix domain
LHON	Leber's hereditary optic neuropathy
M	molar
MCIA	mitochondrial complex I assembly
MCU	mitochondrial calcium uniporter
MCUC	mitochondrial calcium uniporter complex
MCUR1	mitochondrial calcium uniporter regulator 1
MELAS	mitochondrial myopathy, encephalopathy, lactic acidosis and stroke-like episodes
Mfn1/Mfn2	mitofusin 1/2
mHCX	mitochondrial H ⁺ /Ca ²⁺ exchangers
MIA	mitochondrial intermembrane space assembly machinery
MICOS	mitochondrial contact site and cristae organizing system
MICU1	mitochondrial Calcium Uptake 1
MICU2	mitochondrial Calcium Uptake 2
min	minutes
MIOREX	mitochondrial ribosomes and the mitochondrial organization of gene expression complex
MIP	mitochondrial intermediate protease
MITRAC	mitochondrial translation regulation assembly intermediate of cytochrome c oxidase
ml	millilitre
mM	millimolar

Mn ²⁺	manganese
mNCX	mitochondrial Na ⁺ / Ca ²⁺ exchangers
MOMP	mitochondrial outer membrane permeabilisation
MPP	mitochondrial matrix protease
MPTP	mitochondrial permeability transition pore
MS	mass spectrometry
Mt	mitochondria
MTCYB	cytochrome b
mtDNA	mitochondrial DNA
MTS	mitochondrial targeting signal
Mtx1/Mtx2	metaxin-1 and 2
MUT	mutant cybrids
N-SIM	Nikon structured illumination microscope
NAD	nicotinamide adenine dinucleotide
NARP	neurogenic muscle weakness, ataxia and retinitis pigmentosa syndrome
nDNA	nuclear DNA
ng	nanograms
NTD	N-terminal domain
O ₂	oxygen
O ₂ ^{•-}	super oxide radicals
OH•	hydroxyl radicals
OMM	outer mitochondrial membrane
OPA1	optic atrophy type 1
OSCP	oligomycin sensitivity-conferring protein
OXPPOS	oxidative phosphorylation
PBS	phosphate buffered saline
PCR	polymerase chain reaction
Pi	inorganic phosphate
PKA	protein kinase A
PMF	proton-motive force
PVDF	polyvinylidene difluoride
Q•	semiquinone
Q, coQ	ubiquinone or coenzyme Q

RET	reverse electron transfer
RNA	ribonucleic acid
RNAi	RNA interference
ROS	reactive oxygen species
rpm	revolutions per minute
rRNA	ribosomal RNA
RT	room temperature
RT-PCR	reverse transcription polymerase chain reaction
RyRs	ryanodine receptors
S	sulphur
SAD	single-wavelength anomalous dispersion
SAM50	sorting assembly machinery 50 kDa subunit
SC	supercomplex
SCaMC1	ATP-Mg ²⁺ /P _i transporter
SDH	succinate dehydrogenase
SDS-PAGE	sodium dodecyl sulphate-polyacrylamide polyacrylamide gel electrophoresis
shRNA	small hairpin RNA
SILAC	stable isotope-labelled amino acids in cell culture
siRNA	short interfering RNA
SR	sarcoplasmic reticulum
TBE	tris/borate/EDTA
TCA	tricarboxylic acid cycle
TG	triton/glycerol
TIM	transporter of the inner membrane
T _m	melting temperature
TMD	transmembrane domain
TMPD	N,N,N',N'-Tetramethyl-p-phenylenediamine dihydrochloride
TOM	translocase of the outer membrane
tRNAs	transfer RNAs
UQCRFS1	Rieske protein
UTR	untranslated region
UV	ultraviolet
V	volts

VDAC	voltage-dependent anion channel
V_{\max}	maximal velocity
WB	western blot
WT	wild type
μg	microgram
μl	microlitre
μM	micromolar

DECLARATION	I
ACKNOWLEDGMENTS	II
SUMMARY	IV
INTRODUCTION	1
SECTION 1: MITOCHONDRIA.....	2
1.1 ORIGIN OF MITOCHONDRIA AND MITOCHONDRIAL GENOME	2
1.2 MITOCHONDRIAL DNA MUTATIONS.....	2
1.3 MITOCHONDRIAL MEMBRANES	3
1.4 MITOCHONDRIAL CRISTAE	5
1.5 PROTEIN TRANSPORT THROUGH MITOCHONDRIAL MEMBRANES	7
1.6 MITOCHONDRIAL DYNAMICS	8
1.7 FUNCTIONS OF MITOCHONDRIA	9
1.7.1 <i>Energy production</i>	10
1.7.2 <i>Apoptosis</i>	11
1.7.3 <i>Heme synthesis</i>	12
1.7.4 <i>Fe/S clusters synthesis</i>	13
SECTION 2: ELECTRON TRANSPORT CHAIN.....	15
2.1 PROTON GRADIENT AND PROTON MOTIVE FORCE.....	15
2.2 ELECTRON TRANSPORT AND OXIDATIVE PHOSPHORYLATION	16
2.3 COMPLEX I.....	20
2.3.1 <i>Structure and assembly</i>	20
2.3.2 <i>Pathologies associated with complex I deficiency</i>	24
2.4 COMPLEX II.....	27
2.4.1 <i>Structure and assembly</i>	27
2.4.2 <i>Pathologies associated with complex II deficiency</i>	29
2.5 COMPLEX III	30
2.5.1 <i>Structure and subunits</i>	30
2.5.2 <i>Assembly</i>	32
2.5.3 <i>Pathologies associated with complex III deficiency</i>	39
2.6 COMPLEX IV	40
2.6.1 <i>Structure and subunits</i>	40
2.6.2 <i>Assembly</i>	41
2.6.3 <i>Pathologies associated with complex IV deficiency</i>	45
2.7 COMPLEX V	47
2.7.1 <i>Structure and assembly</i>	47
2.7.2 <i>Pathologies associated with complex V deficiency</i>	49
2.8 LOCALISATION OF THE OXPHOS MACHINERY IN THE IMM	49
2.9 SUPERCOMPLEXES	51
2.9.1 <i>Existing models</i>	51
2.9.2 <i>Species of supercomplexes and complex-complex interactions</i>	53
2.9.3 <i>Possible functional roles of supercomplexes</i>	55
2.9.4 <i>Assembly of supercomplexes</i>	57
SECTION 3: CALCIUM AND MITOCHONDRIA.....	59
3.1 THE MICRODOMAIN MODEL - MITOCHONDRIA AND ER CONTACT SITES	61
3.2 THE MCU COMPLEX	64
3.3 MCU.....	65
3.3.1 <i>MCUb</i>	67
3.4 MICU1	67
3.4.1 <i>MICU1 localisation and cristae remodelling</i>	70
3.4.2 <i>MICU1.1</i>	71
3.5 MICU2.....	71
3.5.1 <i>MICU1-MICU2 dimer</i>	72
3.5.2 <i>MICU1-MICU2 dimer assembly and interaction with MCU</i>	74
3.6 MICU3.....	76
3.7 EMRE.....	76
3.8 MCUR1	77

3.9 ANIMAL MODELS.....	78
3.9.1 Evolutionary conservation of MCUC proteins.....	78
3.9.2 MCUC animal models.....	78
3.9.3 <i>Drosophila melanogaster</i>	79
3.9.4 Mouse.....	79
3.10 PATHOLOGIES ASSOCIATED WITH MCU COMPLEX DEFECTS.....	81
3.11 OXPHOS AND CALCIUM.....	83
SECTION 4: MATERIALS AND METHODS.....	87
4.1 CELL CULTURE METHODS.....	87
4.1.1 CELL LINES.....	87
4.1.2 CULTURE CONDITIONS.....	88
4.1.3 CELL GROWTH ANALYSIS.....	88
4.2 DNA-BASED METHODS.....	89
4.2.1 CLONING OF THE GENE OF INTEREST BY PCR.....	89
4.2.1.1 Templates of genes of interest.....	89
4.2.2 Purification of PCR product by extraction from agarose gel.....	90
4.2.3 TOPO-TA cloning.....	91
4.2.4 Plasmid cloning by restriction enzymes digestion.....	91
4.2.5 Transformation of <i>E. coli</i> chemically competent cells.....	92
4.2.6 DNA extraction from competent cells.....	93
4.2.7 Screening of colonies and DNA sequencing.....	93
4.2.8 Site-directed mutagenesis.....	93
4.2.9 STABLE CELL LINES PRODUCTION: 2ND GENERATION LENTIVIRUS EXPRESSION SYSTEM.....	96
4.2.10 shRNA.....	99
4.2.11 siRNA.....	101
4.2.12 NDUFAF2 TRANSFECTION.....	102
4.2.13 GENE EXPRESSION LEVELS QUANTIFICATION.....	102
4.3 PROTEIN-BASED METHODS.....	104
4.3.1 PROTEIN QUANTIFICATION.....	104
4.3.2 MITOCHONDRIA ISOLATION.....	104
4.3.3 FRACTIONATION.....	105
4.3.4 SDS-PAGE GEL ELECTROPHORESIS (SDS-PAGE).....	105
4.3.5 BLUE NATIVE GEL ELECTROPHORESIS (BN-PAGE).....	106
4.3.6 WESTERN BLOT ANALYSIS.....	106
4.3.7 QUANTITATIVE SILAC MASS SPECTROMETRY.....	108
4.3.8 COMPLEXOME PROFILING.....	109
4.3.9 ASSEMBLY KINETICS ASSAYS.....	110
4.4 BIOCHEMICAL METHODS.....	111
4.4.1 BIOCHEMICAL ANALYSIS OF COMPLEXES ACTIVITY.....	111
4.4.2 IN GEL ACTIVITY – COMPLEX I ASSAY.....	114
4.4.3 OXYGRAPHIC MEASUREMENTS: OROBOROS OXYGRAPH-2K (O2k).....	114
4.4.3.1 Oxygraph measurements: respiration in intact cells.....	115
4.4.3.2 Oxygraph measurements: respiration in permeabilised cells.....	115
4.5 MICROSCOPY-BASED METHODS.....	117
4.5.1 IMMUNOFLUORESCENCE (IF) - MTCYB PROJECT.....	117
4.5.2 CLONING AND TRANSFECTION OF FUSION PROTEINS FOR IMAGING (FIXED CELLS) - MCU PROJECT.....	118
4.5.3 N-SIM IMAGING AND ANALYSIS.....	120
4.5.4 DRAGONFLY IMAGING AND ANALYSIS.....	121
4.6 STATISTICAL ANALYSIS.....	121
SECTION 5: ANALYSING COMPLEX III ASSEMBLY AND ITS ROLE IN SUPERCOMPLEXES FORMATION AND ETC MATURATION.....	123
5.1 INTRODUCTION.....	123
5.2 CIII ASSEMBLY: LACK OF MTCYB CAUSES ACCUMULATION OF CIII ASSEMBLY INTERMEDIATES.....	124
5.2.1 EFFECTS OF $\Delta 4$ -CYB MUTATION ON CIII.....	124
5.2.2 CHARACTERISATION OF THE UQCR10 AND CYC1-CONTAINING INTERMEDIATES.....	129
5.2.2.1 Cloning of <i>UQCR10-HA</i> and <i>CYC1-HA</i>	129
5.2.3 CYC1-HA ACCUMULATES AT THE MITOCHONDRIAL SURFACE IN $\Delta 4$ -CYB CELLS.....	132
5.3 SEARCHING FOR CANDIDATE CIII ASSEMBLY FACTORS.....	136

5.3.1 CHARACTERISATION OF THE ROLE OF GHITM/MICS1 AND CHCHD3/MIC19 IN CIII ASSEMBLY AND/OR FUNCTION.....	139
5.3.2 SILENCING OF GHITM IN WT AND Δ 4-CYB CYBRIDS.....	142
5.3.3 SILENCING OF CHCHD3/MIC19 IN WT AND Δ 4-CYB CYBRIDS.....	144
5.3.4 CHCHD3/MIC19 OVEREXPRESSION IN WT AND Δ 4-CYB CYBRIDS.....	149
5.4 CHARACTERISATION OF Δ 4-CYB CYBRIDS: COMBINED MITOCHONDRIAL RESPIRATORY CHAIN DEFICIENCY.....	152
5.5 CI ASSEMBLY: INCOMPLETE MATURATION IN THE ABSENCE OF MTCYB.....	156
5.6 ROLE OF CIII ACTIVITY ON CI ASSEMBLY: AOX OVEREXPRESSION.....	167
5.7 THE ASSEMBLY OF CII AND CIV, BUT NOT OF CV, IS ALTERED IN Δ 4-CYB CYBRIDS.....	171
5.8 CONCLUSIONS.....	175
SECTION 6: DISCUSSION AND FUTURE DIRECTIONS.....	177
SECTION 7: ANALYSIS OF COMPLEX IV AND MCU COMPLEX INTERACTION.....	187
7.1 INTRODUCTION AND PRELIMINARY DATA.....	187
7.2 CHARACTERISATION OF MCUC-CIV INTERACTION.....	189
7.2.1 ANALYSIS OF MCUC SUBUNITS INTERACTION NETWORK.....	189
7.2.2 EFFECTS OF LACK OF CIV ON MCUC.....	191
7.2.3 SPECIFICITY OF THE MCUC-CIV INTERPLAY.....	195
7.2.4 CHALLENGES IN THE ANALYSIS OF COX15 ROLE IN MCUC-CIV INTERACTION.....	196
7.3 EFFECTS OF LACK OF MCUC SUBUNITS ON CIV.....	198
7.4 STUDY OF THE EFFECTS OF MCU ACTIVITY ON OXPHOS.....	204
7.5 ANALYSIS OF THE EFFECTS OF MCUC-CIV INTERACTION ON THE ORGANISATION OF THE IMM.....	206
7.6 CONCLUSIONS.....	214
SECTION 8: DISCUSSION AND FUTURE DIRECTIONS.....	217
BIBLIOGRAPHY.....	225
9.1 APPENDIX A.....	279
9.2 APPENDIX B.....	299

Introduction

Mitochondria are ubiquitous intracellular organelles found in almost all eukaryotes and involved in various aspects of cellular life, with a primary role in energy production. The interest in this organelle has grown stronger with the discovery of their link to various pathologies, including cancer, ageing and neurodegenerative diseases. Indeed, dysfunctional mitochondria cannot provide the required energy to tissues with a high-energy demand, such as heart, brain and muscles, leading to a large spectrum of clinical phenotypes. Mitochondrial defects are at the origin of a group of clinically heterogeneous pathologies, called mitochondrial diseases, with an incidence of 1 in 5000 live birth (Schaefer et al., 2004; Smeitink et al., 2006). Primary mitochondrial diseases are associated with genetic mutations both in nuclear and mitochondrial DNA (mtDNA), affecting genes involved in every aspect of the organelle function. As a consequence, it is difficult to find a common cause for mitochondrial diseases, and subsequently to offer a precise clinical definition of the pathology. Moreover, the complexity of this condition makes it challenging to identify possible therapies or drug targets.

During my Ph.D. program, I have worked on cellular models derived from patients carrying mutations in different complexes of the oxidative phosphorylation (OXPHOS) machinery, the metabolic pathway used for energy production in the cells, and I have studied multiple aspects of mitochondrial biology. In this thesis, I will present the data originated from two separate projects. In the first project, we analysed the effects of a severe mutation in cytochrome b (MTCYB), that leads to complete absence of the respiratory chain complex III (CIII), on the formation and the functionality of the rest of the respiratory chain. In the second project, we studied the interaction between the mitochondrial calcium uniporter complex (MCUC), that regulates mitochondrial calcium homeostasis, and the OXPHOS machinery, using cells derived from patients carrying complex IV (CIV) mutations as a model.

Section 1: Mitochondria

1.1 Origin of mitochondria and mitochondrial genome

According to current theories, mitochondria evolved from free-living bacteria and participated in the origin of eukaryotic cells through a process known as endosymbiosis (Margulis, 1970). The endosymbiotic hypothesis proposes that original anaerobic eukaryotic cells engulfed the primitive mitochondria and established a favourable interaction for both the organisms. Indeed, mitochondria were able to drastically improve the cell energy production generating adenosine triphosphate (ATP) through the respiratory chain, while the host cell offered a safe environment for bacterial proliferation (Cavalier-Smith, 2006).

This theory was supported by the discovery in the 1960s of mitochondrial DNA (mtDNA) and of an independent mitochondrial translation system. Indeed, mitochondria contain their own genetic material, mtDNA, which have maintained the typical features of bacterial DNA: in humans, it is a circular 16,569-base pairs (bp) double-stranded molecule, does not contain introns and is polycistronic (Chinnery and Hudson, 2013). In fact, apart from one non-coding region, called the displacement loop or D-loop, each gene is contiguous to the next one. Moreover, contrary to nuclear DNA, mtDNA is present in many copies in the cell, between 100 and 10 000 copies, proportionally to the energy demand of the specific tissue (Chinnery and Hudson, 2013). Finally, mtDNA genetic code differs slightly from nuclear DNA, presenting different codons encoding for tryptophan and methionine and only two stop codons. During evolution, most of the mitochondrial genes were lost or transferred to the nuclear DNA, and today mtDNA only contains 37 genes: 11 messenger ribonucleic acids (mRNAs), translated to 13 proteins, 2 ribosomal RNAs (rRNAs, 12S and 16S), and 22 tRNAs (Gustafsson et al., 2016). The structure of mtDNA is represented in Figure 1.1.

1.2 Mitochondrial DNA mutations

As for nuclear DNA mutations, alterations in mtDNA can have important pathological consequences. However, because of the differences between mitochondrial and nuclear DNA,

mtDNA inheritance does not follow the canonical mendelian genetics. Firstly, in sexuate organisms, mtDNA is maternally inherited (Giles et al., 1980), therefore only the mother can transmit mutant mtDNA to children. Secondly, while nuclear genes are present in only two copies per cell, every cell contains multiple copies of mtDNA. These copies can be all identical in sequence, giving a condition known as homoplasmy. However, inheritance of mutated copies, replication errors, oxidative stress or inefficient DNA repair, might lead to mtDNA mutations in a percentage of copies, causing heteroplasmy (Chinnery and Hudson, 2013). The proportion of mutant DNA versus the wild type variety has a strong impact on the development and the severity of the pathological phenotypes.

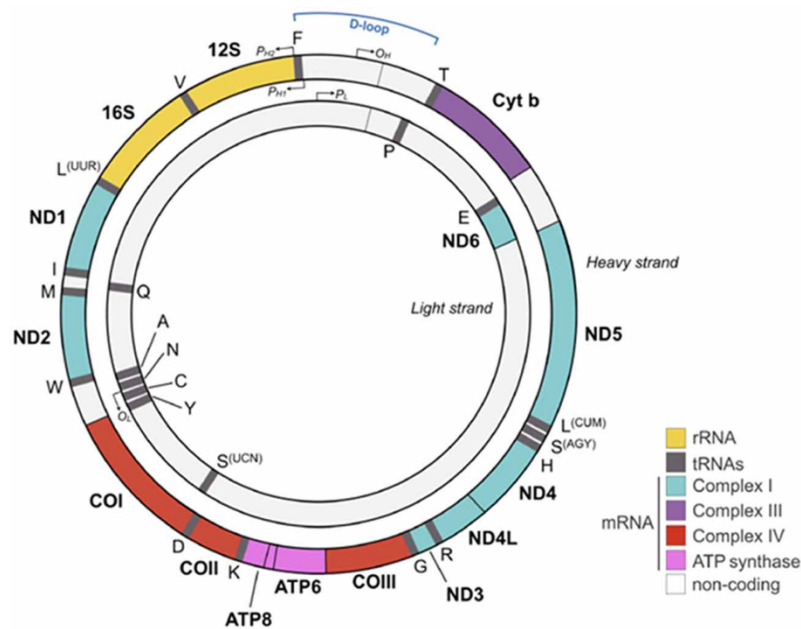


Figure 1.1: schematic representation of mitochondrial DNA (mtDNA). Each protein-encoding gene is indicated with a coloured bar and all the genes encoding for subunits of the same complex are represented with the same colour. rRNAs are indicated in yellow and tRNAs in grey. Source: Hoffmann and Spengler, 2018.

1.3 Mitochondrial membranes

Mitochondria are surrounded by two phospholipidic membranes, the outer mitochondrial membrane (OMM) and the inner mitochondrial membrane (IMM), which divide the organelle into two spaces, the matrix and the intermembrane space (IMS) (Kuhlbrandt, 2015). The two

membranes present significant differences in lipid composition, characteristics and roles of the transmembrane proteins, permeability, and shape, and are the result of the endosymbiotic origin of the organelle. Indeed, the OMM is more similar in lipid composition to eukaryotic cell membranes, while the IMM resembles the cardiolipin-containing bacterial membranes (Cavalier-Smith, 2006). The IMM is characterised by a higher protein:lipid ratio and forms highly packed invaginations in the matrix, called cristae (Ernster, 1981). Embedded in the cristae resides, together with many other proteins, the OXPHOS machinery and one proposed reason for the IMM folding is to increase the available surface for energy production. The part of the IMM that does not protrude in the matrix but, instead, runs parallel to the OMM is called inner boundary membrane (IBM). Cristae and IBM are connected via narrow tubular or slit-like structures, the cristae junctions (CJs) (Palade, 1953) (Figure 1.2).

Moreover, OMM and IMM differ largely for what concerns their permeability. While the OMM allows the passage of ions and small molecules through voltage-dependent anion channel (VDAC) (Colombini, 1989), only water, oxygen (O_2), and carbon dioxide (CO_2) can pass freely through the IMM. This selectivity allows the formation of an electrochemical gradient across the membrane, which is necessary for ATP production, and the tight regulation of other ions concentrations, such as calcium, largely used in cell signalling (De Stefani et al., 2011; Nicholls, 1974).

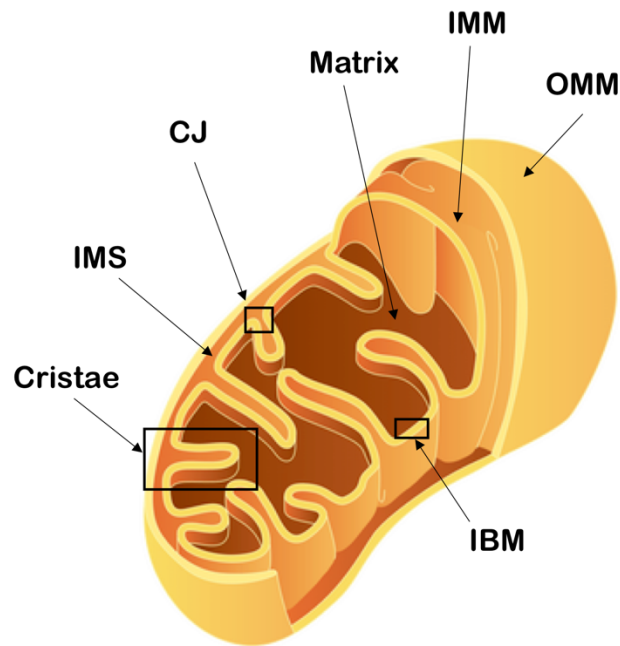


Figure 1.2: schematic representation of mitochondrial architecture.

1.4 Mitochondrial cristae

Mitochondria are internally organised with cristae, invaginations of the IMM, which can be dynamically reorganised according to various stimuli, such as changes in energy requirements or apoptotic signals, becoming more or less compact (Cogliati et al., 2016a). The formation and maintenance of these structures is a complex process that requires the participation of many proteins, including the mitochondrial contact site and cristae organizing system (MICOS) and the fusion protein Optic atrophy type 1 (OPA1). MICOS and OPA1 have been widely associated with the regulation of the cristae architecture, specifically at the cristae junction (Cogliati et al., 2016b).

The MICOS complex was originally characterised and largely studied in yeast, where it is composed of six subunits: Mic10/MINOS1, Mic12/Aim5, Mic19/CHCHD3, Mic26/ApoO, Mic27/ApoOL, and Mic60/Mitofilin (Pfanner et al., 2014). In mammals, this system is more complicated and two additional subunits have been described: Mic25/CHCHD6, paralog of

Mic19 in metazoans (An et al., 2012), and Mic13/QIL1 (Guarani et al., 2015). All of these subunits are transmembrane proteins, except for Mic19 and Mic25.

Mic60 and Mic10 are the core subunits of the two sub-complexes forming the MICOS architecture (Figure 1.3). From one side, Mic60 contacts directly Mic19 and Mic25, while the remaining subunits assemble with Mic10 (Rampelt, 2017). Both subcomplexes are necessary for the formation and stabilisation of the cristae at CJ. Mic10 interacts with Mic26 and Mic27 and is stabilised by QIL1 (Guarani et al., 2015). Mic10 has been shown to be able to induce membrane curvature even in the absence of the other MICOS subunits (Barbot, 2015). The Mic60/Mic19 module is also associated with the OMM. Indeed, Mic19 has been shown to form a bridge between Mic60 and Sorting Assembly Machinery 50 kDa subunit (SAM50), the outer membrane protein that regulates the import and assembly of β -barrel proteins (Darshi et al., 2011), creating tight OMM and IMM contact sites. Other proteins have been specifically associated with this OMM-IMM junction such as Metaxin-1 and 2 (Mtx1/Mtx2) and DnaJ homolog subfamily C member 11 (DNAJC11) (Huynen et al., 2016), which for the MIB complex (mitochondrial intermembrane space bridging complex). These OMM-IMM interactions create a specific environment of closed apposition of the two membranes favourable for protein import, and lipid and phospholipid transport (Scharwey et al., 2013).

In addition to this, immunoprecipitation experiments indicated that both Mic19 and Mic60 interact with OPA1. OPA1 is an IMM protein with a double role in mitochondrial dynamics and architecture: it is involved in the fusion of the IMM and it participates in cristae remodelling (Cipolat et al., 2004; Frezza et al., 2006). Indeed, OPA1 has been shown to be upstream and epistatic to MIC60 and to be the sole regulator of cristae width and junction diameter and number (Glytsou et al., 2016).

Finally, the formation of the cristae rims has been proposed to be linked also to the dimerization of the ATP synthase. Indeed, Complex V (CV) dimers reside at the very bottom of the cristae and, when the dimerization is abolished, the IMM loses the typical tubular organisation of the cristae and forms onion-like structures instead, a typical feature associated with MICOS deregulation (Paumard et al., 2002)

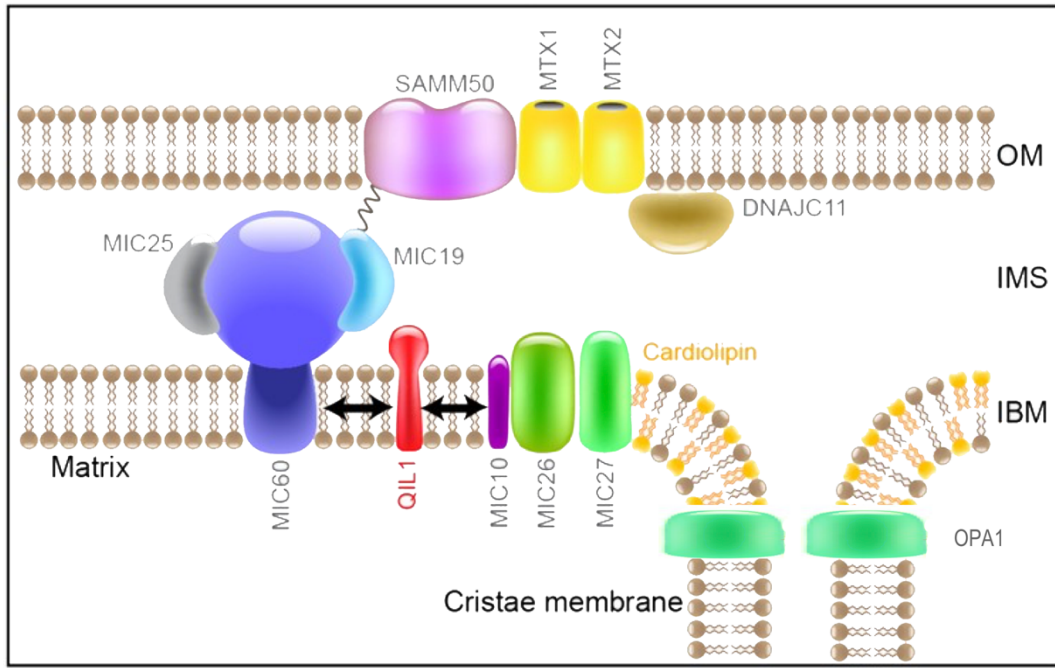


Figure 1.3: cartoon of the MICOS complex at the cristae junction. Source: Guarani et al., 2015.

1.5 Protein transport through mitochondrial membranes

The mechanisms of protein and ion transport through the OMM and the IMM differ in many aspects (Palmieri et al., 2010; Calvo et al., 2015). As described previously, the IMM is much less permeable than the OMM and is characterised by α -helical transport proteins such as protein translocases and other carriers for metabolites and ions. The OMM, instead, contains channel-forming proteins, such as β -barrel transmembrane hydrophilic pores, that allow the passage of precursor proteins, small hydrophilic metabolites and ions.

mtDNA only contains 37 genes, while it has been estimated that mitochondrial proteome is composed of approximately 1200 proteins (Sickmann et al., 2003). Consequently, most of the proteins required are encoded by nuclear genes, translated in the cytosol and transported to or into the organelle. Indeed, newly synthesized proteins carrying a mitochondrial targeting signal are transported to the OMM by chaperones and, according to the nature of their signal, they can be inserted in the OMM, imported in the IMS or transported to the IMM translocases (Neupert, 1997). At the OMM, proteins transport is ensured by the two main complexes: the Translocase of the Outer Membrane (TOM) complex and Sorting and Assembly Machinery

(SAM) complex (Mori et al., 1998; Wiedemann et al., 2003). For insertion of proteins in the OMM, integral proteins containing one or more spanning helices are not imported, but inserted in the OMM via initial interaction with TOM70 (receptor subunit of TOM) and then, in yeast, with Mim1, while β -barrel proteins pass through TOM40 (pore subunit of TOM) and are then transported by chaperones to SAM. The main component of SAM is SAM50, a β -barrel protein, which interacts with the new protein, accommodates the folding, and inserts it laterally into the membrane (Stroud et al., 2011).

Proteins localised in the IMS can have different fates: they can undergo modifications to stabilise the protein and prevent retrograde transport, such as insertion of a heme group or oxidation of cysteine residues in order to form a disulphide bridge via the Mia40 pathway (Mordas and Tokatlidis, 2015). In addition, modified proteins with a specific target peptide can be directed to the IMM or the matrix via TIM23 (Fox et al., 2012).

Proteins that have to be inserted in the IMM are delivered by the IMS chaperones TIM9-10 to the IMM insertase/translocase complex TIM22, main pathway for import of polytopic inner membrane proteins (Sirrenberg et al., 1996). The import through TIM22 requires mitochondrial membrane potential but is not ATP driven (Rehling et al., 2003). Finally, Oxa1, a conserved membrane protein, mediates the insertion of both nuclear and mitochondria-encoded precursors into the inner mitochondrial membrane (Krüger et al., 2012).

For matrix targeted protein, the translocase involved in this process is TIM23 and three different forces drive the transport: the membrane potential, the increasing affinities of the precursor proteins to the components on the trans side of the translocase, and the motor force generated upon ATP hydrolysis by the chaperone mtHsp70 and its associated subunits (Demishtein-Zohary et al., 2017).

1.6 Mitochondrial dynamics

Mitochondria are dynamic organelles that form a complex network of tube-like structures (Tilokani et al., 2018). They undergo opposing fusion and fission events to generate a specific mitochondrial morphology network according to the cellular energy needs, the metabolic state of the cell or to adapt to cellular cues. Mitochondrial fusion allows the organelles to share

metabolites, proteins, and mtDNA, and a hyperfused mitochondrial morphology is associated with a mechanism of defence to enhance cell survival. In contrast, while mitochondrial fragmentation is often associated with mitochondrial dysfunction and cell death, this process is also required for mitochondrial motility or segregation of damaged portions of the reticulum for degradation through a process known as mitophagy (Pickles et al., 2018).

Mitochondrial dynamics are controlled by Guanosine Triphosphatase (GTPases) proteins belonging to the Dynamin family of proteins, where GTP hydrolysis leads to structural change subsequently driving membrane remodelling (Kraus and Ryan, 2017). During mitochondrial division, the constriction of the tubule and membrane scission of one mitochondrion in two separate organelles is carried-out by recruitment of the cytosolic GTPase Dynamin-related/-like protein 1 (Drp1) to mitochondria-endoplasmic reticulum (ER) contact sites (Tilokani et al., 2018). At these sites, Drp1 oligomerizes in a ring-like structure and upon GTP hydrolysis drives mitochondrial division. Mitochondrial fusion, instead, is a two-step mechanism with the OMM localised GTPases mitofusin 1 and 2 (Mfn1 and Mfn2) ensuring OMM fusion, and the IMM GTPase OPA1 responsible for IMM fusion.

Mitochondria need to move within the cell and their localisation is crucial for different functions, such as cell division (Frederick and Shaw, 2007). Directed mitochondrial transport happens on microtubule filaments, typically through force-generating motor proteins, classified into three families: myosins, kinesins and dyneins (Hollenbeck and Saxton, 2005). Milton, syntabulin, and the GTPase Miro have been identified as mitochondria-specific molecules involved in microtubule-based transport (Frederick and Shaw, 2007).

Mitochondrial trafficking is fundamental for a constant supply of healthy mitochondria generating ATP at the right time and place, especially in neuronal cells, where organelles have to move over long distances along the axon, from the cell body to the presynaptic terminal (Zheng et al., 2019).

1.7 Functions of mitochondria

Mitochondria are commonly known as the ‘powerhouse of the cell’, due to their role in energy production. However, in the last 30 years, mitochondria have been characterised also as a signalling organelle involved in numerous physiological functions, including calcium

homeostasis (which will be treated in Section 3), apoptosis, heme and iron-sulphur clusters synthesis.

1.7.1 Energy production

The main source of energy in cells derives from the de-phosphorylation of an ATP molecule to an Adenosine diphosphate (ADP) molecule. To make this process sustainable, the cell needs to use nutrients to re-generate the ATP molecules used. This process is known as cellular respiration, where a glucose molecule is gradually broken down into carbon dioxide, and its hydrogens are stripped and used to combine with oxygen to form water. The first stage of this mechanism takes place in the cytosol, is anaerobic and is mitochondria-independent (Alberts, 2002). This pathway is known as glycolysis, and it produces only two molecules of ATP from one of glucose metabolised, generating two molecules of pyruvate. To optimise ATP production, glycolysis is coupled to a second pathway, known as the citric acid cycle (or tricarboxylic acid cycle or Krebs cycle, Figure 1.4), which takes place in mitochondria and is aerobic. This cycle is composed of nine different enzymatic reactions and each round generates 3 nicotinamide adenine dinucleotide (NADH) molecules, 1 flavine adenine dinucleotide (FADH₂), and 1 guanosine triphosphate (GTP). One molecule of glucose leads to two cycles, producing in total 6 NADH, 2 FADH₂ and 2 GTP. NADH and FADH₂ molecules can then be used in the last part of cellular respiration, known as oxidative phosphorylation, where the majority of the energy is finally converted to ATP. This process consists of the passage of electrons from NADH and FADH₂ to the final acceptor, oxygen, through the electron transport chain (ETC), which will be discussed more in detail in Section 2.2. In total, the complete oxidation of a single molecule of glucose is used by the cell to produce 30 ATP molecules. This process, which involves molecular oxygen as a sink for binding electrons is known as respiration.

Alternately, NADH and FADH₂ can be produced by a process known as fatty acid β -oxidation. A fatty acid is converted to fatty acyl-CoA and then to acyl carnitine, in order for it to enter the mitochondria and eventually be reconverted in intramitochondrial acyl-CoA. In the organelle, a long-chain acyl-CoA is broken down to acetyl-CoA molecules, producing 1 NADH and 1 FADH₂ for each couple of carbons forming the initial molecule (Adeva-Andany et al., 2019).

The proton gradient produced during respiration, similar to a capacitor, supplies energy to operate the ATP synthase (complex V) which, through dissipating it, provides the energy to condensate ADP and P_i into ATP. Thus, respiration is distinct but coupled to phosphorylation, in the oxidative phosphorylation pathway.

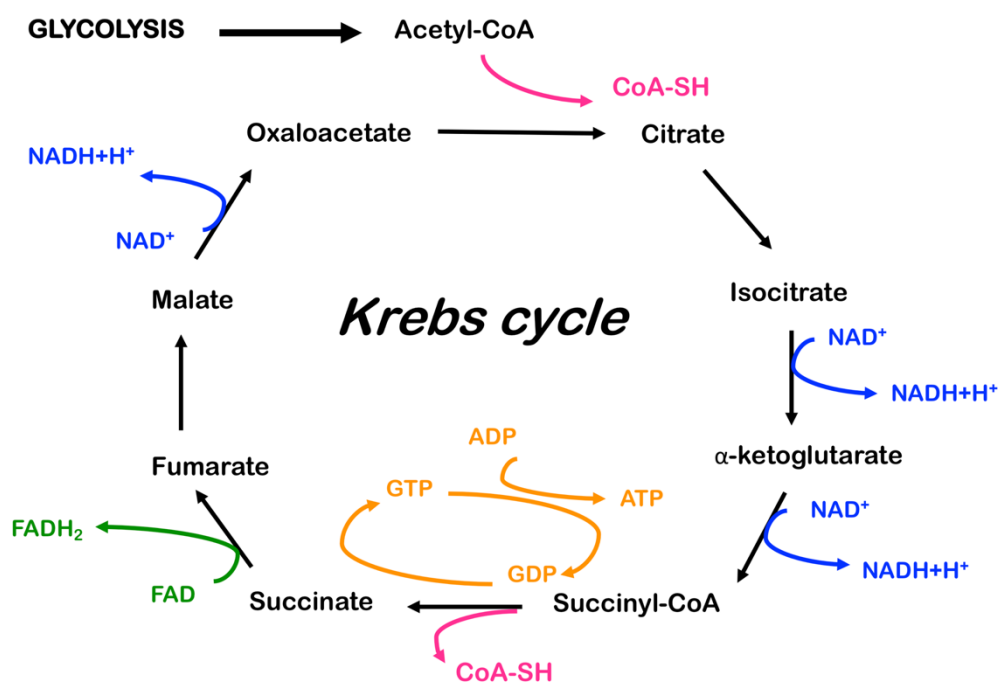


Figure 1.4: schematic representation of the tricarboxylic acid cycle or Krebs cycle.

1.7.2 Apoptosis

Mitochondria have also a role in the regulation of programmed cell death, called apoptosis, which is required for embryonic development and numerous physiological functions. Apoptosis leads to a controlled and programmed cell death, which can occur as a response to various damages or stressors, such as DNA-damage, oxidative stress, immune reactions and absence of certain growth factors, hormones and cytokines, or as a natural part of development and ageing (Elmore, 2007). Different apoptotic pathways exist, characterised by different triggers but with a common final execution pathway. Indeed, these different pathways lead to activation of initiator caspase (as caspase 8 and 9), which then activate executioner caspases

(as caspase 3 or 7), to finally induce cellular components degradation. The extrinsic or death receptor pathway, which does not directly involve mitochondria, is activated by extracellular ligands binding to death receptors on the plasma membrane and leads to the formation of the death-inducing signalling complex (DISC), which subsequently activates the initiator caspase 8 and then the executioner caspase 3 (Igney and Krammer, 2002). The best characterised is the mitochondrial or intrinsic pathway of apoptosis. Mitochondrial apoptosis is initiated by internal signals of stress or damage and it consists of the mitochondrial outer membrane permeabilisation (MOMP), regulated by the Bcl-2 family of proteins. Upon stressors, the pro-apoptotic members BAX and BAK oligomerise at the OMM (Große et al., 2016; Salvador-Gallego et al., 2016), where they induce the release of pro-apoptotic proteins from the IMS into the cytosol, including cytochrome *c* (Tait and Green, 2013). Once in the cytosol, cytochrome *c* binds and activates apoptotic protease activating factor-1 (Apaf-1), as well as procaspase-9, forming a complex known as “apoptosome”. Active caspase 9 is then able to cleave and activate caspase 3, starting the communal execution pathway (Chinnaiyan et al., 1999; Hill et al., 2004). The execution pathway leads to DNA fragmentation, degradation of cytoskeletal and nuclear proteins, cross-linking of proteins and formation of apoptotic bodies.

1.7.3 Heme synthesis

Heme is an iron-containing porphyrin, essential in numerous biological processes, such as oxygen transport and storage, drug and steroid metabolism, signal transduction, and microRNA processing (Chiabrando et al., 2014). Moreover, heme is incorporated in some subunits of the electron transport chain and it is necessary for cellular respiration (Lodish, 2000).

The synthesis of this compound occurs both partially in the mitochondria and in the cytosol (Ogun, 2019). Heme is generated by the insertion of ferrous iron into the tetrapyrrole macrocycle of protoporphyrin IX (Ajioka et al., 2006) catalysed by a mitochondrial matrix enzyme, called ferrochelatase. Protoporphyrin IX is produced through a series of reactions both in the mitochondria and in the cytosol, starting from glycine and succinyl-CoA.

The majority of heme production takes place in erythroid progenitors, while the remaining 15% is generated in the liver for the formation of heme-containing enzymes (Ajioka et al., 2006). The synthesis pathway is conserved in these two cellular types, while its regulation differs. The heme synthesis machinery in the liver has a rapid turnover in order to respond quickly to

changes in metabolic requirements, while the synthesis in developing red cells is tied to the availability of iron.

1.7.4 Fe/S clusters synthesis

Iron-sulphur (Fe/S) clusters are prosthetic groups with a variety of biological functions. Indeed, several enzymes, such as glycosylases, helicases, primases, and respiratory chain enzymes, require the incorporation of Fe/S centres for their activity (Maio, 2015). Both the proteins containing these centres and the proteins that are part of the biosynthesis machinery are highly conserved in prokaryotes and eukaryotes, suggesting an important role in the origin of life (Imlay, 2006). These cofactors originated probably in an environment characterised by low oxygen and co-evolved when the oxygen levels started increasing in the atmosphere, leading to the adaptation of anaerobic electron-transport chains for an aerobic habitat. Most of Fe/S proteins contain the rhomboid $[\text{Fe}_2/\text{S}_2]$, the cuboidal $[\text{Fe}_3/\text{S}_4]$ or the cubane $[\text{Fe}_4/\text{S}_4]$ cluster (Beinert et al., 1997). The most common protein ligand is cysteine, but also histidine, serine and arginine can form a bond (Maio, 2015).

In yeast, Fe/S cluster synthesis takes place exclusively in mitochondria, while in mammals they are produced in both mitochondria and the cytosol (Ye, 2010). However, in impaired mitochondria, cytosolic synthesis is compromised as well. The central actor of the synthesis pathway found in eukaryotic mitochondria is known as iron-sulphur cluster assembly enzyme (ISCU), which acts as a scaffold for the initial synthesis of a $[2\text{Fe}-2\text{S}]$ cluster. This cluster will be the basis for the formation of both mitochondrial and cytosolic Fe/S groups. The sulphide ions used in this process are obtained from cysteine side chains, thanks to the activity of enzymes called cysteine desulphurases (Roche et al., 2013), while it is not clear how iron is delivered to the ISCU, frataxin may be involved (Dean and Dos Santos, 2015).

Section 2: Electron transport chain

The enzymatic machinery performing cellular respiration, the electron transport chain (ETC), is composed of four protein complexes embedded in the IMM and two mobile electron carriers (ubiquinone, or coenzyme Q, and cytochrome *c*). Electrons are transported from electrons carriers reduced during glycolysis and the Krebs cycle (NADH and FADH₂) to coenzyme Q and cytochrome *c*, eventually transferred to O₂, forming H₂O. The final aim of this chain of redox reactions is the generation of an electrochemical proton gradient across the IMM, which is used by complex V or F₁F₀ ATP synthase to generate ATP (Capaldi and Aggeler, 2002; Reid et al., 1966).

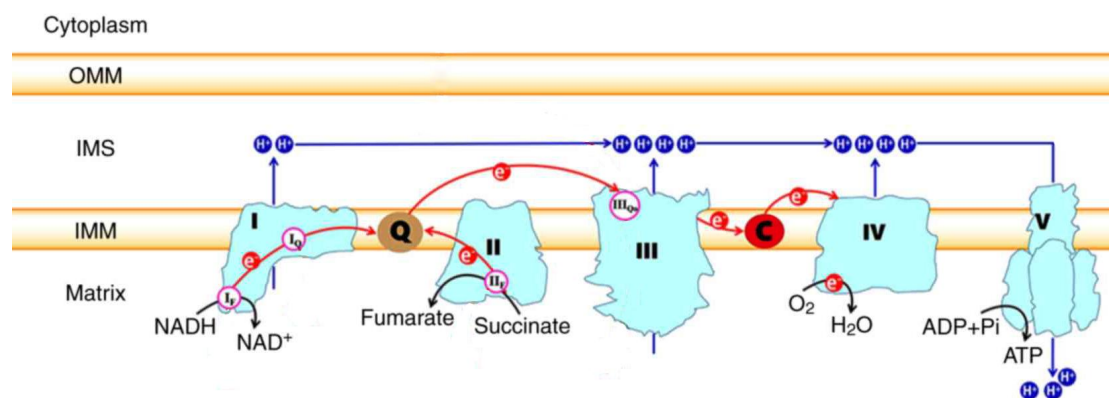


Figure 2.1: cartoon representation of the OXPHOS machinery. NADH and FADH₂ molecules generated during glycolysis and Krebs cycle are oxidised by CI and CII, respectively. Electrons are then passed to ubiquinone (Q), that transfers them to CIII. Here, they are transferred to cytochrome *c* and to CIV, where they are used to reduce O₂ to H₂O. Coupled to electron transfer, protons are pumped from the matrix to the IMS and the proton motive force generated is used by CV to produce ATP. Source: adapted from Zhao et al., 2019.

2.1 Proton gradient and proton motive force

The formation of the electrochemical gradient is made possible by the nature of the phospholipidic bi-layer that forms the IMM. Indeed, the membrane is impermeable to the passage of protons, which require protein transporters to cross it. These transporters are

complexes I, III and IV and the energy necessary for the proton pumping derives from the transport of electrons. This electrochemical gradient will be used by ATP synthase or complex V to produce ATP.

This gradient produces the proton-motive force (PMF or Δp), which can be described as a measure of the potential energy stored across the IMM. Since protons are electrically charged particles, the PMF has both chemical and electric components. The electric component corresponds to the voltage difference across the membrane and the free energy is calculated as $\Delta G = -F\Delta\Psi$ (F =Faraday constant; $\Delta\Psi$ =membrane potential). The chemical component, instead, has a free energy calculated as $\Delta G = RT \ln([H^+]_i/[H^+]_o)$ where $[H^+]_i$ and $[H^+]_o$ refer to the proton concentrations inside and outside the IMM, respectively, R is the gas constant of 1.987 cal/(degree·mol), and T is the temperature (in degrees Kelvin). Combining these two components, the PMF is calculated as $\Delta p = \Delta\Psi - (RT/F) * \ln([H^+]_i/[H^+]_o)$. Under physiological conditions, the magnitude of the PMF is about -220 mV (Lodish, 2000). As a consequence of the difference in protons concentration, the matrix side of the inner mitochondrial membrane is negatively charged and slightly alkaline (pH=8).

2.2 Electron transport and oxidative phosphorylation

The first actors in the electron transport chain are NADH and FADH₂ (Figure 2.2). NAD⁺ and FAD⁺ are reduced to NADH and FADH₂, respectively, during glycolysis and the citric acid cycle. A 1:1 mixture of NADH and NAD⁺ has a redox potential of -320 mV, while the midpoint redox potential of FADH₂ is around -220 mV. This means that both these molecules have a strong tendency to donate electrons (Alberts, 2002). The $\Delta G^{\circ'}$ values for these strongly exergonic reactions are -52.6 kcal/mol (NADH) and -43.4 kcal/mol (FADH₂) (Lodish, 2000).

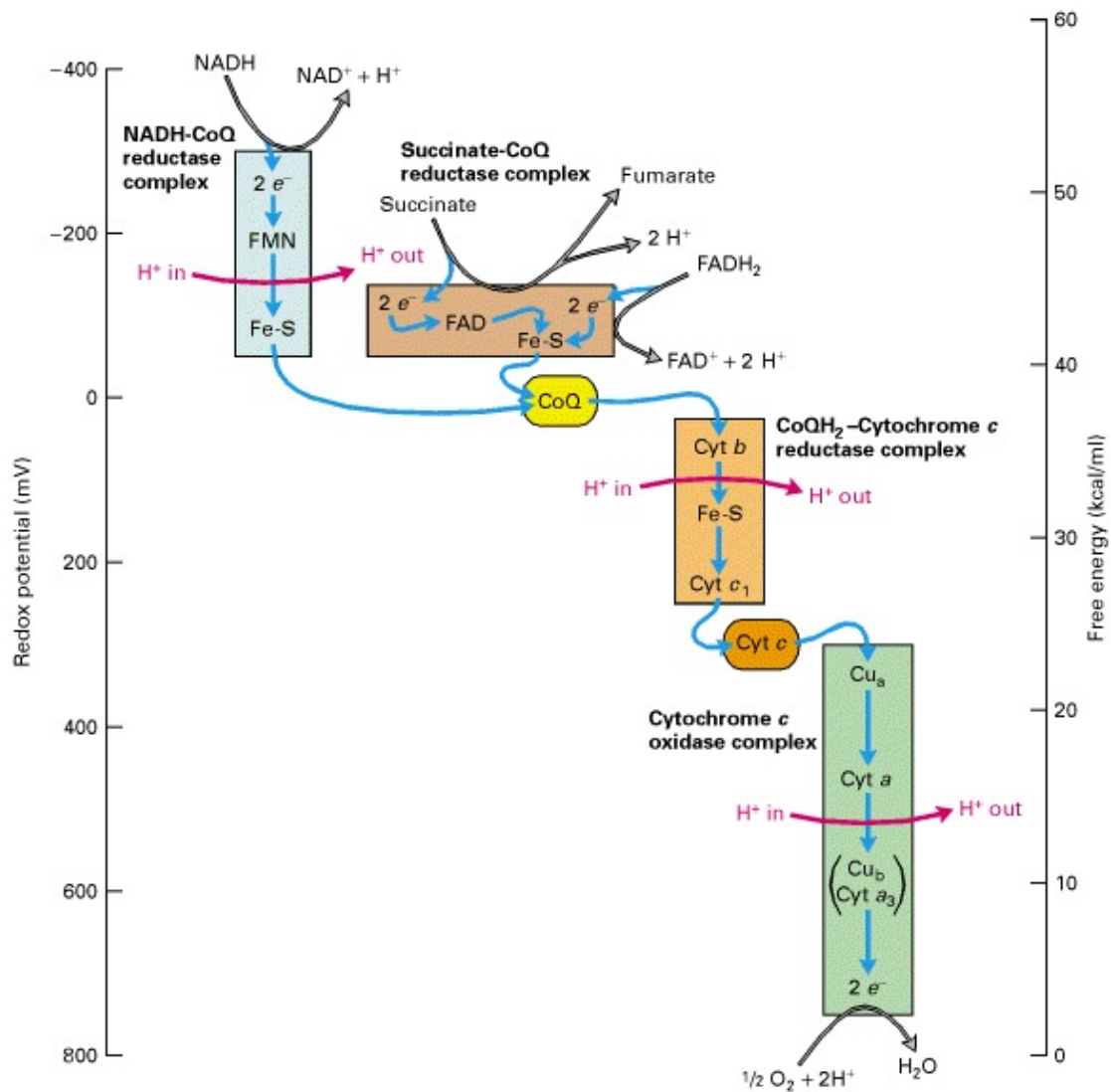


Figure 2.2: graphic representation of electrons flow through the ETC from NADH, succinate, and FADH₂ to O₂. The catalytic centres of the four electron transport chain complexes are represented. Electrons pass in sequence from carriers with a lower reduction potential to those with a higher potential. The energy released from the passage of electrons through the chain is coupled with the pumping of protons across the inner membrane, establishing the proton motive force (PMF). Source: Lodish, 2000.

NADH binds to complex I (CI, NADH dehydrogenase) and is oxidised to NAD⁺, donating two electrons to a flavin mononucleotide (FMN) (Figure 2.2), inserted in CI subunit NDUFV1. Electrons are then passed to a chain of 8 iron-sulphur (Fe/S) clusters, in order to be eventually transferred to the oxidised form of coenzyme Q or ubiquinone (Q), which uptakes two protons to form ubiquinol (QH₂). As the electrons are transferred to one redox centre to the other, four protons are pumped through CI out of the matrix. Despite the numerous biochemical and

structural studies on CI, a definitive model of redox-coupled proton pumping does not exist yet. Many models have been proposed: first hypotheses suggested conformational changes in antiporter-like subunits in the P-module, allowed by the energy produced during electron transport (Efremov and Sazanov, 2011; Hunte et al., 2010), or transient hydration changes able to generate water-gated pathways for proton transfer between conserved ionizable residues along the membrane domain (Kaila et al., 2014). The energy necessary for the proton translocation could be provided by two processes: a two-stroke mechanism where the pumping is coupled with N2 (the terminal cluster in the Fe/S chain) reduction/re-oxidation, which occurs twice for every NADH oxidized assuming the transfer of one electron at the time, or a single-stroke mechanism, where all four protons are translocated together after the reduction of coenzyme Q (Brandt et al., 2011; Hirst and Roessler, 2016; Verkhovsky et al., 2012). More recent analyses of the X-ray structure of the *Y. lipolytica* enzyme, instead, led to the hypothesis that proton pumping is linked to the coordinated conformational rearrangement of three loops in subunits ND1, NDUFS2, and ND3, triggered by the binding with negatively charged ubiquinone (Cabrera-Orefice et al., 2018).

FADH₂ derives from the reduction of succinate to fumarate by complex II (CII, succinate reductase) during the Krebs cycle, reaction that reduces FAD⁺ to FADH₂, a cofactor bound to the flavoprotein subunit (SDHA). Then, two electrons are transferred to the Fe/S clusters contained in SDHB, which will eventually pass them to Q (Figure 2.2). This process results in an increased ubiquinol pool, but does not influence directly the proton gradient, because CII is not a proton pump.

Coenzyme Q is a mobile co-factor that can interact with CI and CII and transports the electrons received to complex III (CIII, Q-cytochrome c oxidoreductase). CIII oxidises QH₂ to Q and passes the electrons to another soluble carrier, cytochrome *c*, during a process known as Q-cycle (Figure 2.3). The Q-cycle consists of two parallel reactions, which involve the three prosthetic groups of the enzyme: the heme groups contained in cytochrome *c1* and cytochrome *b* and the 2Fe/2S cluster contained in UQCRFS1 (Mitchell, 1976). The first reaction requires the passage of one electron from QH₂ bound to the Q_o binding site, to the iron/sulphur group and then to cytochrome *c1* leading to the reduction of cytochrome *c*. Each cytochrome *c* is able to bind only one electron and, when reduced, moves from CIII to complex IV (CIV, cytochrome *c* oxidase). The second electron from QH₂, is passed to the two heme *b* groups (b_L and b_H) contained in cytochrome *b* and terminates on a second ubiquinone molecule bound to

a different binding site of the enzyme (Q_i site). This ubiquinone is partially reduced to a semiquinone ($Q\cdot$) during the first Q-cycle and completely reduced to QH_2 following a second catalytic cycle (Iwata et al., 1998; Trumpower et al., 1990; Xia et al., 1997; Zhang et al., 1998). One QH_2 molecule is then recycled and two electrons are eventually passed to two cytochrome *c* molecules. For each QH_2 molecule that is oxidised, there is the release of two protons to the intermembrane space. QH_2 has a redox potential around 0 mV, while CIII centres have a positive potential, allowing the passage of electrons. In order to permit the two branches of the Q-cycle, different centres of CIII must have different redox potential, ranging between 72.5 mV of cytochrome *b*, low enough to allow the recycling of electrons through semiquinone, and 242 mV of cytochrome *c1*, which passes the electron to cytochrome *c* (251 mV) (Peters et al., 2018; Urban and Klingenberg, 1969).

During the Q-cycle, CoQ is present in three different forms, according to its redox state: ubiquinone (Q), semiquinone ($Q\cdot$) and ubiquinol (QH_2). According to the phase of the cycle and the consequent state of reaction, CoQ molecules can bind CIII in different binding sites: Q_o , which faces the IMS, and catalyses the oxidation of ubiquinol to ubiquinone, and Q_i , which faces the matrix and catalyses the reduction of ubiquinone to semiquinone and ubiquinol (Saraste, 1999).

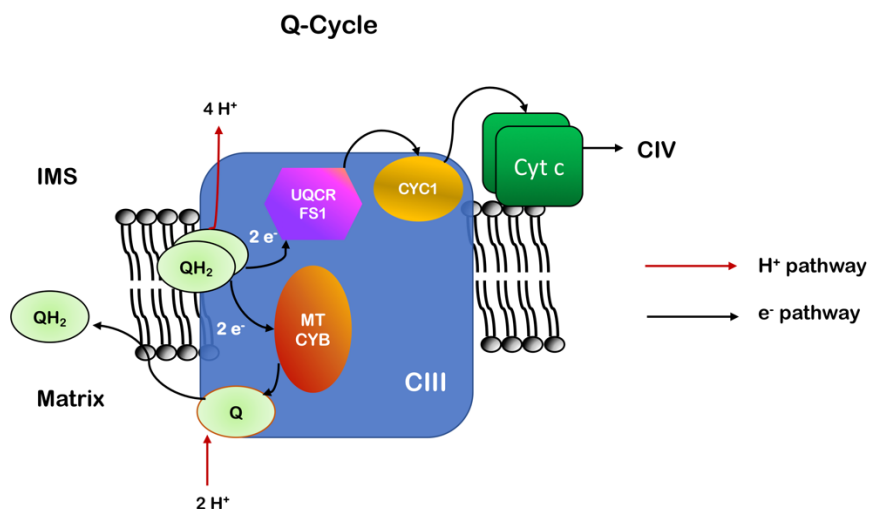


Figure 2.3: schematic representation of the Q-cycle.

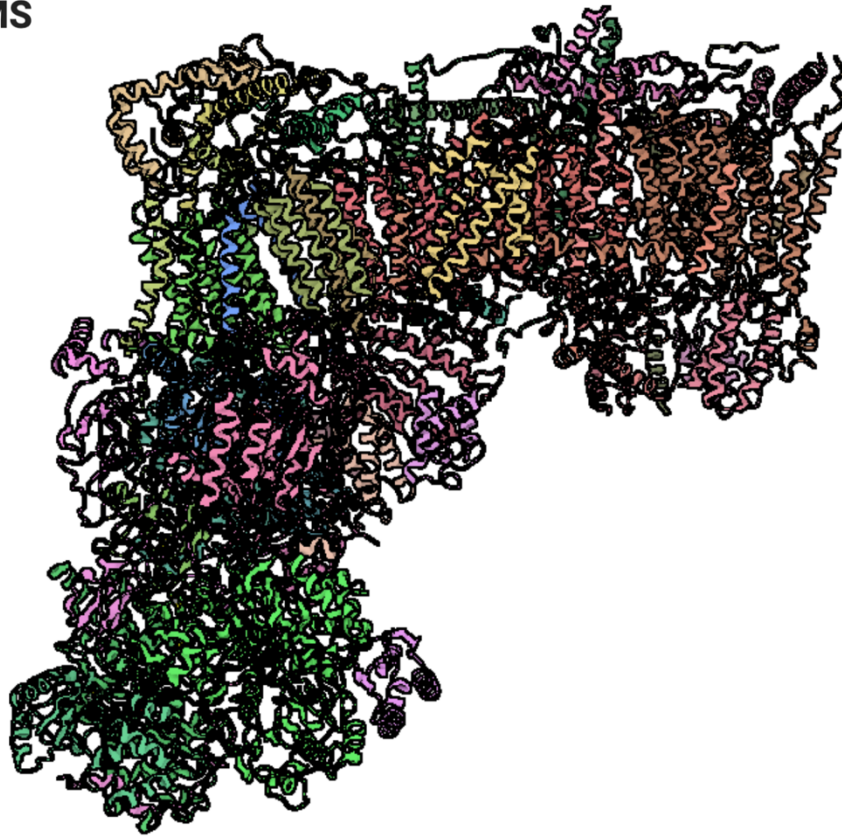
The last steps of oxidative phosphorylation take place in CIV (the terminal oxidase), which allows the passage of electrons from cytochrome *c* to oxygen (redox potential=820 mV), generating water. Since cytochrome *c* carries only one electron, four molecules are oxidised in order to generate two H₂O molecules from one molecule of O₂. In the meantime, four substrate protons are taken from the matrix to form two H₂O and other four protons are pumped into the IMS (Michel, 1999; Wikstrom, 2004). CIV contains two heme groups (cytochromes *a* and *a*₃) and two copper atoms (Cu_A and Cu_B) (Pilet et al., 2004). Electrons are transferred through the Cu_A centre and heme *a* to the heme *a*₃/Cu_B group. When both heme *a*₃ and Cu_B are reduced, one O₂ molecule is recruited to form a peroxide bridge between these two prosthetic groups. This bound is broken by the reaction with protons picked up by the mitochondrial matrix and two H₂O molecules are formed (Yoshikawa and Shimada, 2015).

2.3 Complex I

2.3.1 Structure and assembly

NADH dehydrogenase (Complex I, CI) is the first step of the electron transport chain and is composed of 44 different subunits in mammals (Vinothkumar et al., 2014), organized in three structural domains: a membrane arm, or P-module, and two peripheral domains, the N- and the Q-modules, protruding in the mitochondrial matrix. The N-module contains the FMN co-factor and is responsible of the binding and the oxidation of NADH, while the Q-module contains the ubiquinone binding site. The passage of electrons between these two extremities occurs in Fe/S clusters in both the N- and the Q-modules. The peripheral arm is composed of nuclear-encoded proteins, 7 'core' subunits (NDUFV1, NDUFV2, NDUFS1, NDUFS2, NDUFS3, NDUFS7 and NDUFS8) and 30 accessory subunits necessary to stabilise the enzyme and to protect it from reactive oxygen species (ROS) damage (Vartak et al., 2014). The P-module, instead, is assigned to the proton pumping activity and contains 7 mitochondrial-encoded proteins: ND1, ND2, ND3, ND4, ND4L, ND5 and ND6. ND1 forms the reduction site for ubiquinone, while ND2, ND4 and ND5 have been found to share a similar structure to sodium and potassium antiporters and may be involved in proton pumping (Carroll et al., 2013). Mammalian CI structure is represented in Figure 2.4.

IMS



Matrix

Figure 2.4: representation of C1 structure. Image has been created with BioRender.com using the structural data retrieved from PDB (5LC5).

Due to the large number of subunits forming CI, the assembly pathway of this enzyme is particularly complex and requires the involvement of many assembly factors. The first stage is the synthesis of the various subunits, both inside mitochondria and in the cytoplasm, and is coupled with the import in the organelle of the nuclear-encoded components. Most CI subunits have N-terminal mitochondrial targeting sequences (MTS), while 11 are imported into the organelle thanks to uncharacterised internal signals within the mature protein (Claros and Vincens, 1996). Several core subunits need further maturation and the insertion of the prosthetic groups. However, it is difficult to identify assembly factors with this role using the traditional proteomic analysis, probably because of the transient and labile interaction between them and the forming enzyme (Sanchez-Caballero et al., 2016). The only assembly factor known to be involved in the incorporation of 4Fe/4S clusters in the peripheral arm is NUBPL, a member of the Mrp/NBP35 ATP-binding proteins family (Bych et al., 2008; Sheftel et al.,

2009). Moreover, it is not clear if the insertion of the iron/sulphur clusters happens before or after the incorporation of the single subunit in an assembly intermediate.

The second step of CI assembly is the formation of 6 independent modules, N, Q, ND1/P_{P-a}, ND2/P_{P-b}, ND4/P_D and ND5/P_{D-b}, and the incorporation of each of them in a specific order (Signes and Fernandez-Vizarra, 2018). All the known CI assembly factors are summarised in Table 2.1.

The ND2 module is the first detectable after inhibition of mitochondrial protein biosynthesis (Guerrero-Castillo et al., 2017). This subassembly binds to numerous assembly factors: ACAD9, ECSIT, TMEM126B, NDUFAF1, COA1 and the putative assembly factor TMEM186, which form the mitochondrial complex I intermediate assembly (MCIA) (Formosa et al., 2020). Moreover, TMEM186 was found strongly interacting with the newly synthesized MT-ND3, which is added to the intermediate together with MT-ND6 and MT-ND4L, forming a 385 kDa structure.

In parallel to this, an intermediate of the Q-module starts forming, binding to NDUFAF3 and NDUFAF4 and generating a ~170 kDa structure. This submodule will then bind to the assembly factor TIMMDC1 and the subunits ND1, NDUFA3, NDUFA8 and NDUFA13, to yield a 283 kDa complex (Guerrero-Castillo et al., 2017).

The ND4 module, instead, involves the subunits NDUFB1, NDUFB4, NDUFB5, NDUFB6, NDUFB10, and NDUFB11 together with the assembly factors FOXRED1, ATP5SL and TMEM70. This 230 kDa module binds initially to the N2 module and then to the ND1/Q modules intermediate (Guerrero-Castillo et al., 2017).

The ND5 module, which forms the distal extremity of the membrane arm, is the second to last intermediate inserted in the forming enzyme. It is composed by the subunits NDUFB2, NDUFB3, NDUFB7, NDUFB8, NDUFB9 and NDUFAB1 and it is known to bind one assembly factor: DMAC1/TMEM261 (Stroud et al., 2016). This late intermediate lacking the N-module is stabilised by NDUFAF2/NDUFA12L/B17.2L.

Finally, the N-module, composed by NDUFV1, NDUFV2, NDUFS1 and NDUFA2, forming a 160 kDa assembly, is incorporated (Guerrero-Castillo et al., 2017). This last passage

Table 2.1: CI assembly factors. Adapted from Giachin, 2016 and Sanchez-Caballero et al., 2016.

Assembly factor	Function	CI interacting module	References
ACAD9	Binding of ND2 module	ND2/P _P -b module	(Haack et al., 2010; Nouws et al., 2010)
ECSIT	Insertion of ND2	ND2/P _P -b module	(Vogel et al., 2007)
FOXRED1	Binding of ND4 module	ND4/P _D module	(Formosa et al., 2015; Rendón, 2016)
ATP5SL	Binding of ND4 module	ND4/P _D module	(Andrews et al., 2013)
TMEM70	Binding of ND4 module	ND4/P _D module	(Cizkova et al., 2008; Sánchez-Caballero et al., 2020)
NDUFAF1	Insertion of ND2 module	N module, ND1	(Vogel et al., 2005)
NDUFAF2	Binding of N module	N module	(Ogilvie et al., 2005)
NDUFAF3	Binding of Q with P _P -a	Q module	(Saada et al., 2009)
NDUFAF4	Binding of Q with P _P -a	Q module	(Saada et al., 2008)
NDUFAF5	Methyltransferase activity	Not known	(Sugiana et al., 2008; Rhein et al., 2016)
NDUFAF6	Squalene/phytoene synthase activity	Not known	(McKenzie et al., 2011)
NDUFAF7	Methyltransferase activity	Not known	(Carilla-Latorre et al., 2010; Rhein et al., 2013)
NUBPL	4Fe/4S clusters insertion. Necessary for the entire enzyme stability	Supposed to interact with the developing N module and possibly Q module	(Sheftel et al., 2009; Bych et al., 2008; Protasoni et al., 2020)
TIMMDC1	Translocase of inner mitochondrial membrane domain-containing protein 1	ND1/P _P -a	(Andrews et al., 2013; Guarani et al., 2014)
TMEM126B	Required for formation of the ND2 module	ND2/P _P -b module	(Heide et al., 2012)
TMEM186	Not known	ND2/P _P -b module	(Guerrero-Castillo et al., 2017)
DMAC1/TMEM261	Stabilisation and/or assembly of ND5	ND5/P _D -b	(Stroud et al., 2016)
COA1	CIV assembly factor, found bound to CI assembly intermediates	ND2/P _P -b module	(Guerrero-Castillo et al., 2017)

2.3.2 Pathologies associated with complex I deficiency

Mutations affecting CI stability or activity are responsible for a wide range of pathological phenotypes (Janssen et al., 2006). Missense mutations affecting the mtDNA-encoded subunits (ND subunits) have been associated with Leber's hereditary optic neuropathy (LHON), mitochondrial encephalomyopathy, lactic acidosis and stroke-like syndrome (MELAS), and

Leigh syndrome. Many mutations in nuclear-encoded subunits have been identified in patients with CI deficiency, causing Leigh syndrome, leukoencephalopathy, leukodystrophy, encephalopathy, cardiomyopathy and other neurological defects. In addition, assembly factors and chaperones involved in CI assembly can also be at the origin of the pathogenesis of these diseases (Scheffler, 2015). The main pathological mutations found in CI subunits or assembly factors are summarised in Table 2.2.

Table 2.2: CI subunits and assembly factors associated with mitochondrial diseases.

Gene/protein	OMIM	Associated phenotype	Reference
<i>Complex I subunits</i>			
MTND1	516000	Leber Optic Atrophy, MELAS syndrome, dystonia, spasticity, myopathy.	(Howell et al., 1991; Kirby et al., 2004; Simon et al., 2003)
MTND2	516001	Leber Optic Atrophy.	(Johns and Berman, 1991)
MTND3	516002	Infantile encephalopathy, Leigh syndrome.	(McFarland et al., 2004)
MTND4	516003	Leber Optic Atrophy, MELAS syndrome.	(Lertrit et al., 1992; Torroni et al., 1997)
MTND4L	516004	Leber Optic Atrophy.	(Brown et al., 2002)
MTND5	516005	Leber Optic Atrophy, MELAS syndrome.	(Brown et al., 1992; Liolitsa et al., 2003)
MTND6	516006	Leber Optic Atrophy, MELAS syndrome.	(Brown et al., 1992; Ravn et al., 2001)
NDUFV1	161015	Severe encephalopathy, neurologic abnormalities.	(Bénit et al., 2001; Schuelke et al., 1999)
NDUFV2	600532	Hypertrophic cardiomyopathy, truncal hypotonia, and encephalopathy.	(Bénit et al., 2003)
NDUFS1	157655	Growth retardation, axial hypotonia, hepatomegaly, dystonia, and persistent hyperlactatemia.	(Bénit et al., 2001)
NDUFS2	602985	Neonatal lactic acidosis and hypertrophic cardiomyopathy.	(Loeffen et al., 2001)
NDUFS3	603846	Leigh syndrome, severe axial dystonia with oral and pharyngeal motor dysfunction, dysphagia, and a tetraparetic syndrome.	(Bénit et al., 2004)
NDUFS4	602694	Muscular hypotonia, absence of visual and auditive attention, cardiac defects.	(Budde et al., 2000)
NDUFS6	603848	Fatal infantile lactic acidosis.	(Spiegel et al., 2009)
NDUFS7	601825	Leigh syndrome, feeding problems, dysarthria, and ataxia.	(Smeitink and van den Heuvel, 1999)
NDUFS8	602141	Leigh syndrome, poor feeding and episodes of apnoea and cyanosis.	(Loeffen et al., 1998)

NDUFA11	612638	Fatal infantile metabolic acidosis, brain atrophy, no motor development, and hypertrophic cardiomyopathy.	(Berger et al., 2008)
NDUFA1	300078	Leigh syndrome, hypotonia, nystagmus, generalized choreoathetosis, and decreased reflexes.	(Fernandez-Moreira et al., 2007)
NDUFA2	602137	Leigh syndrome, hypertrophic cardiomyopathy and developmental delay.	(Hoefs et al., 2008)
NDUFA6	602138	Intrauterine growth retardation, respiratory insufficiency, lactic acidosis, and hypoglycemia.	(Alston et al., 2008)
NDUFA8	603359	Severe neonatal hypotonia, dysmorphic features, epilepsy, and signs of brainstem involvement.	(Bugiani et al., 2004)
NDUFA9	603834	Respiratory and metabolic acidosis, hearing loss, apneas, retinitis pigmentosa.	(Van der Bosch et al., 2012)
NDUFA10	603835	Leigh syndrome, delayed psychomotor development.	(Hoefs et al., 2011)
NDUFA12	614530	Leigh syndrome, progressive loss of motor abilities, scoliosis, dystonia.	(Ostergaard et al., 2011)
NDUFA13	609435	Delayed development, hypotonia, poor eye contact, abnormal eye movements, and poor feeding, encephalopathy, hearing loss.	(Angebault et al., 2015)
NDUFB3	603839	Encephalopathy, myopathy, hypotonia, developmental delay, and lactic acidosis.	(Haack et al., 2012)
NDUFB9	601445	Progressive hypotonia associated with increased serum lactate.	(Haack et al., 2012)
NDUFB10	603843	Lethal complex I deficiency.	(Friederich et al. 2017)
NDUFB11	300403	Linear skin defects, cardiomyopathy, and other congenital anomalies.	(van Rahden et al., 2011)
<i>Complex I assembly factors</i>			
ACAD9	611103	Cardiorespiratory depression, hypertrophic cardiomyopathy, encephalopathy, and severe lactic acidosis.	(Haack et al., 2010)
FOXRED1	613622	Leigh syndrome, congenital lactic acidosis, athetoid movements of the limbs in early childhood, hypotonia, and cerebellar atrophy.	(Calvo et al., 2010)
NDUFAF1	606934	Hypertrophic cardiomyopathy, developmental delay, lactic acidosis, hypotonia, and Wolff-Parkinson-White syndrome.	(Dunning et al., 2007)
NDUFAF2	609653	Ataxia, lethargy, nystagmus, hypotonia, optic atrophy, and episodic respiratory insufficiency.	(Ogilvie et al., 2005)
NDUFAF3	612911	Macrocephaly, weak cry, no eye contact, wide anterior fontanel, and axial hypotonia.	(Saada et al., 2009)
NDUFAF4	611776	Severe encephalopathy and antenatal cardiomyopathy.	(Saada et al., 2008)

NDUFAF5	612360	Facial dysmorphism, progressive lactic acidosis, neurological defects.	(Sugiana et al., 2008)
NDUFAF6	612392	Focal seizures, decreased movement and strength, ataxia, lactic acidosis, and Leigh syndrome.	(Pagliarini et al., 2008)
NDUFAF8	618461	Leigh syndrome.	(Alston et al., 2020)
NUBPL	613621	Infantile-onset hepatopathy, renal tubular acidosis, developmental delay, short stature, leukoencephalopathy, myopathy, nystagmus, ataxia.	(Sheftel et al., 2009); Bych et al., 2008; Protasoni et al., 2020)
TIMMDC1	615534	Infantile-onset hypotonia, failure to thrive, delayed or minimal psychomotor development, sensorineural deafness, dysmetria, dyskinetic movements, peripheral neuropathy, nystagmus, and Leigh syndrome.	(Kremer et al., 2017)
TMEM126B	615533	Exercise intolerance, muscle weakness, myalgia, early onset renal tubular acidosis, and hypertrophic cardiomyopathy.	(Alston et al., 2016; Sánchez-Caballero et al., 2016)
COA7	615623	Autosomal recessive spinocerebellar ataxia with axonal neuropathy-3 .	(Martinez Lyons et al., 2016)

2.4 Complex II

2.4.1 Structure and assembly

Succinate dehydrogenase (SDH, complex II, CII) is a ~ 120 kDa integral membrane complex, involved in both the TCA cycle and the ETC. Indeed, this enzyme catalyses the oxidation of succinate to fumarate, central step of the citric acid cycle, producing FADH₂, and reduces ubiquinone to ubiquinol (Rutter et al., 2010). CII is the only complex of the chain that does not pump protons across the membrane and that is entirely encoded by the nuclear DNA.

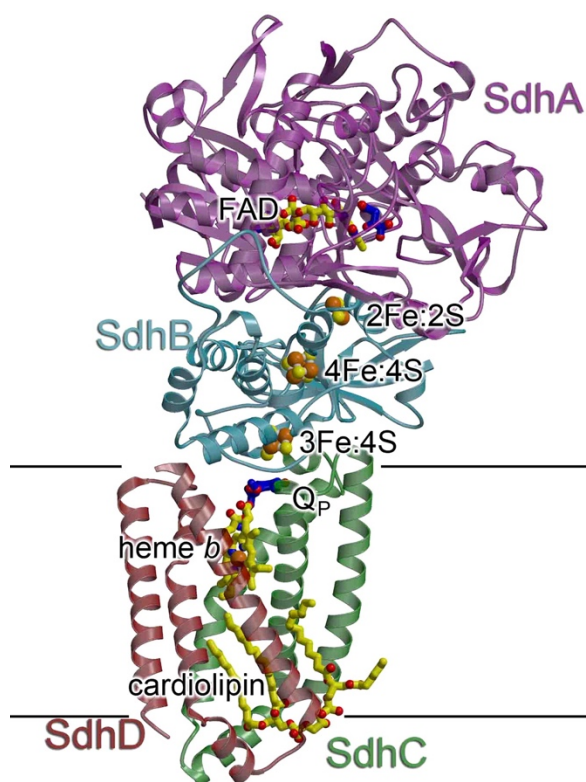


Figure 2.6: representation of *E. Coli* CII structure. The four subunits forming the complex (SDHA-D) are showed in different colours and labelled with the letters A to D. FAD, Fe/S centres, heme b and ubiquinone binding site are indicated. Source: Iverson, 2013.

CII is composed of 4 subunits, named SDHA-D, forming two domains. The hydrophilic head of CII comprises SDHA and SDHB and is required for the oxidation of succinate. FAD⁺ binds to SDHA and the electrons are transferred to SDHB, containing three Fe/S clusters ([2Fe-2S], [4Fe-4S], and [3Fe-4S]) (Cecchini et al., 2003). The hydrophobic membrane domain of the enzyme is composed of SDHC and SDHD and contains a heme b group and two ubiquinone binding sites (Sun et al., 2005).

The mature forms of SDHA and SDHB are generated independently before the complex assembly, while SDHC and SDHD are able to form an intermediate subcomplex (Van Vranken et al., 2015). SDHA is initially imported in the matrix as an apo-protein and the FAD cofactor is inserted thanks to the interaction with the assembly factor SDHAF2/Sdh5 (Hao et al., 2009). Then, mature SDHA binds to SDHAF4/Sdh8, a chaperone that protects the subunit from auto-oxidation and facilitates the assembly with SDHB. Mature SDHB contains Fe/S clusters, which are inserted by SDHAF1 (Ghezzi et al., 2009; Maio et al., 2016). SDHB stability is then maintained by the association with a LYR motif protein recently identified in yeast, Sdh7 (SDHAF3/ACN9/LYRM10, human ortholog), which shields one or more of the prosthetic centres from oxidants (Dwight et al., 2017). Mature SDHA and SDHB are then able to

assemble together and join SDHC and SDHD, synthesised and inserted in the membrane via a still uncharacterised mechanism.

2.4.2 Pathologies associated with complex II deficiency

Patients presenting with a specific CII defect are quite rare, less than 10% of OXPHOS deficiency cases (Munnich et al., 2001). Two main phenotypes can originate from mutations in CII subunits or assembly factors. Mutations in SDHAF1 and SDHA lead to encephalomyopathy and leukoencephalopathy (Alston et al., 2012; Ghezzi et al., 2009), while variants in SDHA, SDHB, SDHC, SDHD and SDHAF2 are responsible for hereditary paraganglioma (Baysal et al., 2000, 2004; Hao et al., 2009; Skoldberg et al., 1998). Moreover, other genes involved in FAD and Fe/S clusters synthesis can impair CII activity and stability (Ghezzi, 2018). The main pathological mutations found in CII subunits or assembly factors are summarised in Table 2.3.

Table 2.3: CII subunits and assembly factors associated with mitochondrial diseases.

Gene/protein	OMIM	Associated phenotype	Reference
SDHA	600857	Leigh syndrome, neonatal dilated cardiomyopathy, catecholamine-secreting extraadrenal paraganglioma.	(Parfait et al, 2000; Levitas et al., 2010; Burnichon et al., 2010)
SDHB	185470	Paraganglioma, pheochromocytoma, gastrointestinal stromal tumors.	(Astuti et al., 2001; Janeway et al., 2011)
SDHC	602413	Paraganglioma and gastric stromal sarcoma.	(Baysal et al., 2004; McWhinney et al., 2007)
SDHD	602690	Paraganglioma, pheochromocytoma, gastric stromal sarcoma.	(Baysal et al., 2000; McWhinney et al., 2007)
SDHAF1	612848	Leukoencephalopathy, spastic quadriplegia, psychomotor regression.	(Ghezzi et al., 2009)
SDHAF2	613019	Paraganglioma.	(Hao et al., 2009)

2.5 Complex III

2.5.1 Structure and subunits

The ubiquinol:cytochrome *c* oxidoreductase (cytochrome *bc*₁, complex III, CIII) is the central element of the respiratory chain. In yeast, it is formed of 10 different subunits, while in mammals an additional subunit was identified, corresponding to the mitochondrial targeting sequence of the Rieske protein (UQCRFS1), which remains anchored to the complex after the proteolytic cleavage (Brandt et al., 1993). However, recent studies proposed that the latter is not a stoichiometric subunit and that the N-terminal UQCRFS1 peptide needs to be eliminated in order to maintain the functionality of CIII (Bottani et al., 2017; Fernandez-Vizarra and Zeviani, 2018). All CIII subunits are encoded by nuclear DNA except cytochrome *b* (MTCYB), which is encoded by mtDNA (Iwata et al., 1998; Schagger et al., 1986). CIII is always dimeric and high-resolution crystal structures of the bovine, chicken and yeast *bc*₁ complexes have been resolved (Berry et al., 1999; Lange, 2002; Xia et al., 1997; Yu et al., 1996) (Figure 2.7).

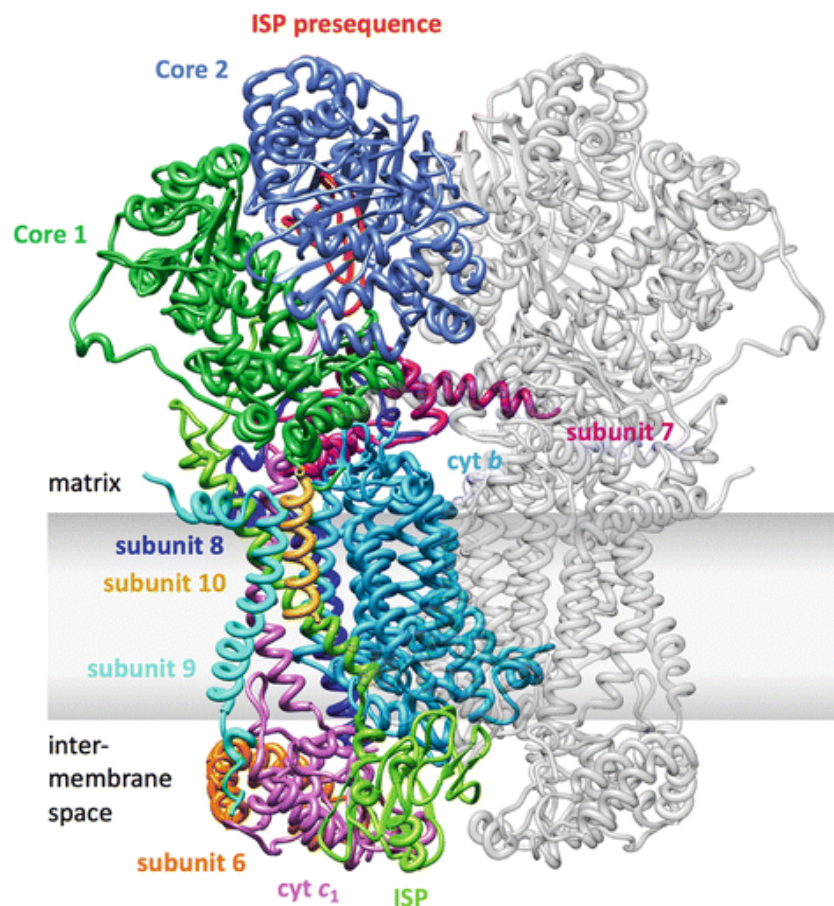


Figure 2.7: representation of bovine CIII structure. CIII is shown as a dimer, the only form in which it is found in cells. All the 10 subunits are represented with a different colour in one monomer. Source: Sousa et al., 2018.

Both in yeast and mammals, CIII contains three protein subunits with redox prosthetic groups: cytochrome *b*, which contains both the high-potential b_H (*b562*) and the lower-potential b_L (*b565*) heme centres, cytochrome *c1* (CYC1), containing the *c*-type heme c_1 , and the Rieske iron-sulphur protein (Rip1 in yeast, UQCRFS1 protein in mammals) with a 2Fe–2S cluster (Kim, 2012). The di-heme cytochrome *b* polypeptide forms eight transmembrane helices and contains two histidine residues in each of the second (helix B) and fourth (helix D), forming the binding site for quinone (Yun et al., 1991). The low-potential heme b_L is located on the intermembrane space side of the IMM, while the high-potential heme b_H is positioned in a cavity accessible from the matrix, where it can receive electrons from b_L and pass them to the Q_i site, where it reduces one bound ubiquinone to semiquinone (Kim, 2012). CYC1 has a wedge-like structure containing the heme group and is anchored in the membrane through a C-terminal transmembrane anchor next to helix E of cytochrome *b* (Zhang et al., 1998). The heme group binds a CXXCH domain, highly conserved in *c*-type cytochromes. UQCRFS1 contacts MTCYB on one of the two CIII heterodecamer with its N-terminal transmembrane domain, where it receives one electron and undergoes a conformational change that makes it reach CYC1 on the other one (Iwata et al., 1999). The maturation of UQCRFS1 has been studied in details in simpler organisms, such as *Neurospora Crassa* and *Saccharomyces Cerevisiae* (Graham et al., 1994). The newly synthesised protein undergoes two post-translational modifications: the cleavage of a targeting pre-sequence and the insertion of the iron-sulphur cluster in the mitochondrial matrix. Initially, the MTS is cleaved by a mitochondrial matrix protease (MPP), and finally, an extra 8-amino acids-long sequence is removed by a mitochondrial intermediate protease (MIP). Contrary to yeast and birds, mammalian UQCRFS1 iron-sulphur protein maturation generates a 78-amino acid-long fragment, which remains temporally bound to CIII as an eleventh subunit, Subunit 9 (Su9) (Brandt et al., 1993). This additional subunit localises between the two core subunits UQCRC1 and UQCRC2 and it has been proposed that these two are responsible for the cleavage of UQCRFS1, due to the conservation of their MPP function (Deng et al., 1998; 2001; Berry et al., 2013).

The remaining subunits are accessory and their function is mainly to support and stabilise the complex (Barel et al., 2008; Haut et al., 2003).

2.5.2 Assembly

CIII assembly pathway has been studied in depth in *S. cerevisiae* (Ndi et al., 2018; Smith et al., 2012; Zara et al., 2007, 2009a, b) and a human CIII assembly model has been constructed by homology, as some of the steps have been shown to be analogous to yeast (Fernandez-Vizarra and Zeviani, 2015).

The first step of CIII assembly, both in yeast and in mammals, is the synthesis and the insertion in the IMM of cytochrome *b*. Yeast cytochrome *b* gene contains introns and requires processing (Christianson, 1983), while mammalian *MTCYB* is transcribed as a polycistronic segment. MtDNA is organised so that mRNAs coding for proteins are divided by tRNAs, which assume a specific secondary structure, and function as punctuation marks between the genes. tRNAs are then cleaved by mitochondrial RNase P at the 5' ends and by RNase Z at the 3' ends, and mRNAs are then translated (Hallberg, 2014). Moreover, studies in mice suggested the involvement of PTC2 (pentatricopeptide repeat domain protein 2) in processing the pre-processed *ND5-CYTB* RNA transcript (Xu et al., 2008).

The transcription and translation of cytochrome *b* must be coordinated with the synthesis of nuclear proteins. This mitochondrial-nuclear communication is possible thanks to a group of proteins called translational activators. These nuclear-encoded factors regulate the expression of mitochondrial genes and their own expression in relation to the OXPHOS activity, in order to limit the accumulation of unused subunits, which can have toxic effects on the organelle. In yeast, four translational activators of COB have been identified: Cbp1, Cbs1, Cbs2 and the complex Cbp3/Cbp6 (Ndi et al., 2018). These factors interact with mitochondrial ribosomes and the mitochondrial organization of gene expression (MIOREX) complex (Kehrein, 2015). The primary role of Cbp1 is to protect *COB* mRNAs and to transfer it to the translational apparatus (Islas-Osuna et al., 2003). Cbs1 and Cbs2 have been found associated in the same high-molecular-weight complex with mitochondrial ribosomes, but they might also form other sub-complexes including different activator proteins, such as COX-specific activators (Krause-Buchholz et al., 2005; Naithani et al., 2003). Recent studies on Cbs1 determined that this protein binds to a segment of the 5' UTR of *COB* mRNA, sequestering it and repressing the translation. Cbs1 is then replaced by the complex Cbp3/Cbp6 liberated during assembly, which activates the translation (Salvatori et al., 2020). These proteins, necessary for the stability of COB mRNA and its translation, do not have orthologs in mammals (Ndi et al., 2018).

Cbp3-Cbp6 complex, instead, plays a role in the second phase of translation, binding the nascent polypeptide exiting the ribosome, and it does not leave the protein until the incorporation of the b_L heme group (Gruschke et al., 2011; Hildenbeutel et al., 2014). This complex has orthologs in mammals named ubiquinol-cytochrome *c* reductase complex assembly factors 1 and 2 (UQCC1 and UQCC2), with the same function (Tucker et al., 2013). Cbp3 interacts directly with Cbp4 (human ortholog: UQCC3), an assembly factor anchored in the IMM and protruding into the intermembrane space. Cbp4 is not necessary for complete translation and release from ribosomes of cytochrome *b*, but it has a role in the stabilization of the semihemylated intermediate that contains the b_L (Gruschke et al., 2011; Hildenbeutel et al., 2014). Together, Cbp3–Cbp6, Cbp4 and cytochrome *b* compose the intermediate I. In yeast, the now mature cytochrome *b* forms a subcomplex with the subunits Qcr7 and Qcr8, called intermediate II. Deletion of any one of the genes encoding cytochrome *b*, Qcr7, and Qcr8, leads to the almost complete loss of the other two subunits and Qcr6, while the other subunits are only partially reduced (Zara et al., 2004). Similarly, the mammalian orthologs UQCRB and UQCRQ are incorporated in the early stages of CIII assembly in mammals, provoking the release of the UQCC1-UQCC2 complex.

The following steps of CIII assembly have been described in yeast, but are still unclear in mammals, because of the difficulties in identifying both possible vertebrate-specific assembly factors involved in the process and intermediate subassemblies. The order of incorporation in *S. cerevisiae* was determined by generating yeast mutants for single CIII subunits and studying the stability of the remaining components of the complex (Zara et al., 2007, 2009a, b). The third intermediate step involves the insertion of four subunits: Qcr6 (UQCRH in humans), the two large structural core subunits Cor1 and Cor2 (UQCRC1 and UQCRC2), and cytochrome *c1* (Cyt1). At this stage, dimerization occurs by joining assembly intermediate II and the Cor1/2 modules (Stephan and Ott, 2020).

Interestingly, Cor1, Cor2 and cytochrome *c1* have been found associated in a subassembly module, even if the contacts between the core proteins and the catalytic subunits in the fully assembled enzyme are minimal (Zara et al., 2007). Surprisingly, the complex Cor1/Cor2 has been detected in various subcomplexes in two-dimensional electrophoresis. This behaviour might be due to the association of these subunits with other proteins or ETC complexes in the IMM or to the formation of Cor1/Cor2 aggregates. However, these subassemblies are detectable only in mutant strains and disappear when the complex is assembled correctly, therefore they might not represent a physiological intermediate. The last assembly factor that

might have a role in the early or intermediate phases of CIII assembly is Bca1, an inner membrane protein found only in fungi (Mathieu et al., 2011). However, its function is not clear yet and there are no known mammalian ortholog.

An essential step for the generation of intermediate III is the synthesis, the import and the maturation of Cyt1. Cyt1 contains a single heme centre and is anchored to the IMM via a single transmembrane segment near its C-terminus (Xia et al., 1997). The precursor of this subunit is translated in the cytosol and transported through TOM and TIM complexes into the mitochondria. The cytochrome c_1 precursor protein contains an N-terminal cleavable bipartite pre-sequence (Sadler et al., 1984). The first of the two independent sequences, a strongly basic region of 35 amino acids, is a mitochondrial targeting signal and it is proteolytically removed by MPP in the matrix. The second sequence is a hydrophobic sorting sequence, which targets Cyt1 to the IMM. However, two models have been proposed to explain this process. The first one proposes that the whole protein and therefore both the targeting sequences, reach the mitochondrial matrix and that only in a second step the second sequence is re-located into the membrane, allowing the proteolytic cleavages (Arnold et al., 1998). Instead, in the second model, only the first segment reaches the mitochondrial matrix while the second internal hydrophobic sequence remains anchored in the membrane, stopping the import. In the matrix, the positive-charged mitochondrial targeting sequence is cleaved by MPP. At the same time, the C-terminal alpha-helix gets inserted in the membrane and the heme centre is attached to the protein. The hemylation is mediated by holocytochrome c_1 synthetase (Cyt2 or HCCS1 in mammals) (Zollner et al., 1992). This modification provokes a conformational change that allows the exposure and the cleavage of the second targeting sequence by Imp2 (inner membrane peptidase 2), leaving the N-terminal of the mature Cyt1 soluble in the intermembrane space (van Loon et al., 1987).

In the late assembly stages, three subunits are incorporated: Qcr9 (UQCR10 in mammals), Qcr10 (UQCR11) and Rip1 (UQCRFS1). Firstly, Qcr9 is inserted (Phillips et al., 1990). This small (7.3 kDa) accessory subunit is necessary for the functionality of the complex and its deletion results in the formation of a nearly inactive enzyme. Indeed, it has been observed that, lacking Qcr9, the conformation of Rip1 is altered and the Fe/S cluster is not incorporated correctly (Phillips et al., 1993). The last two proteins to be inserted are Qcr10 and Rip1. Qcr10 is an 8.5 kDa supernumerary subunit inserted before the Rieske protein and required for its stabilisation. However, it is not clear yet how and when it is recruited (Brandt et al., 1994).

Many studies, instead, have been published about the maturation and insertion of the Rieske protein both in yeast and mammals.

Prior to the insertion, Rip1 is imported in mitochondria and receives its 2Fe/2S centre, likely by the resident iron-sulphur cluster (ISC) system. In yeast, the import is followed by two proteolytic steps that eliminate the N-terminal MTS. The precursor form is first processed by a matrix MPP protease into an intermediate form (Fu et al., 1990). The second cleavage generates the mature form of the protein and is catalysed by the mitochondrial intermediate peptidase (MIP). At this point, Rip1 is transported back across the IMM in the intermembrane space, where it is assembled in the complex. In mammals, however, UQCRFS1 N-terminal import signal is cleaved in a single step when the protein is already incorporated in the complex and the cleaved segment remains attached to the enzyme (Brandt et al., 1993).

Two assembly factors are necessary for the Rieske protein assembly in both mammals and yeast: Bcs1 (BCS1L in mammals) and Mzm1 (LYRM7). Bcs1 is a 456 amino acids protein formed by three different domains: a positively charged 126 amino acids N-terminal target signal (Fölsch et al., 1996), a central Bcs1p-specific domain and a highly conserved C-terminal AAA-ATPase domain (Nouet et al., 2009). It has been initially proposed that Bcs1p might have a role in the Fe/S cluster insertion, act as a chaperone (Nobrega et al., 1992) or bind to the partially formed CIII in an ATP-dependent manner, keeping it in a state that allows the incorporation of the Rieske protein (Cruciat et al., 1999). The most recent theory is that Bcs1 is responsible for the export of the Rieske Fe/S domain from the matrix into the IMS (Wagener et al., 2011). Bcs1, indeed, is able to recognize the correctly folded Rieske protein and act as a protein translocase. This model has been confirmed by the determination of the cryogenic electron microscopy (cryo-EM) structure of Bcs1 in yeast (Kater et al., 2020) and mouse (Tang et al., 2020), which suggested an airlock-like mechanism for Rip1/UQCRFS1 translocation. Bcs1, indeed, seems to form two large aqueous vestibules, a bigger one on the matrix side and a smaller one in the inner membrane, through which UQCRFS1 is transported.

Mzm1 is a 14 kDa protein located in the mitochondrial matrix. It was initially thought to be involved in the modulation of the zinc pool and to this function it dues its name (mitochondrial zinc maintenance 1) (Atkinson et al., 2010). However, in addition to the reduced zinc pool, cells lacking Mzm1 have a defect in CIII due to faulty insertion of Rip1 (Atkinson et al., 2011).

Its role is to stabilize Rip1 in the matrix before the translocation to the IMM. The same function is shared by the human ortholog, LYRM7 or MZM1L (Sanchez et al., 2013).

Finally, third factor necessary for UQCRFS1 metabolism, that does not have a yeast ortholog, is TTC19 (Ghezzi et al., 2011). TTC19 binds to CIII after the incorporation of UQCRFS1 and is involved in the clearance of UQCRFS1 fragments, process that is necessary to keep the complex in a functionally competent state (Bottani et al., 2017).

A complete list of CIII subunits is indicated in Table 2.4 and the latest model of CIII biogenesis pathway is represented in Figure 2.8.

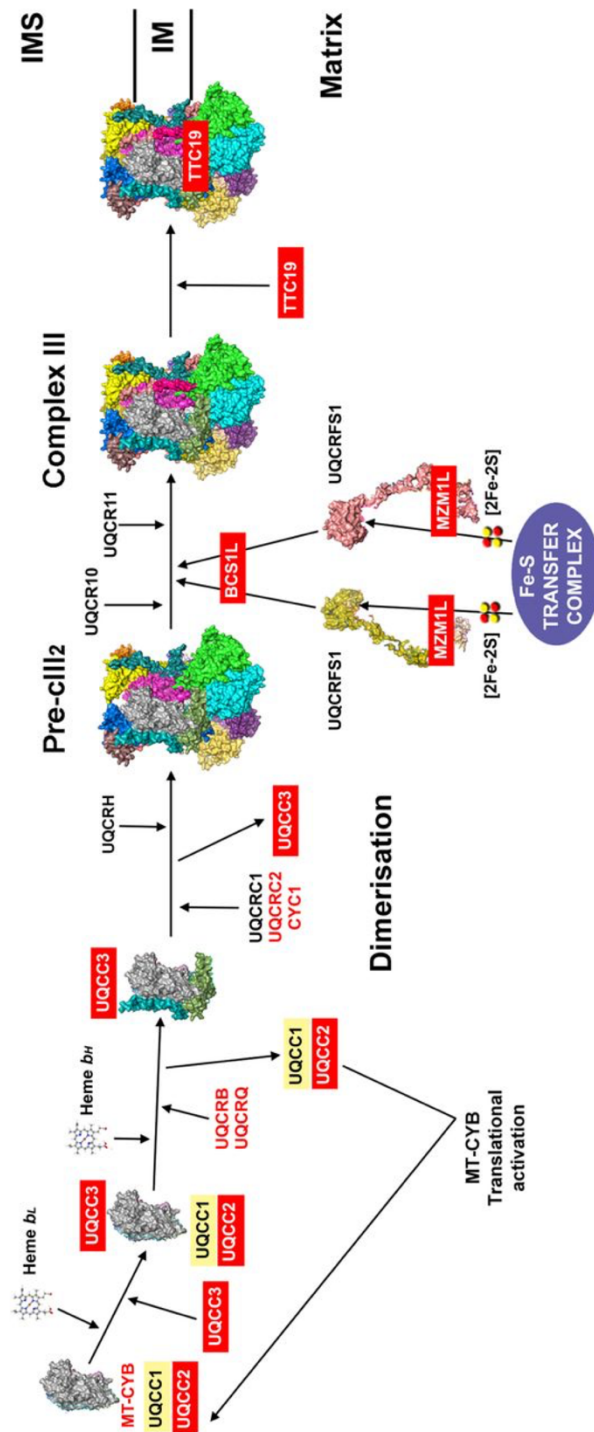


Figure 2.8: complex III assembly model based on the bovine CIII₂ crystal structure with PDB ID: 1BGY (Iwata et al., 1998) and the models proposed in references Fernandez-Vizarra and Zeviani, 2015, 2018. Proteins indicated in red are associated with pathological mutations. Source: Signes and Fernandez-Vizarra, 2018.

Table 2.4: list of CIII subunits and factors involved in CIII assembly, both in *S. cerevisiae* and humans.

<i>S. cerevisiae</i>		<i>Homo sapiens</i>			
Gene	Protein	Gene	Protein	Reference (id yeast)	
<i>Complex III subunits</i>					
COR1	Cor1	<i>UQCRC1</i>	UQCRC1	(Tzagoloff et al., 1986)	
COR2	Cor2	<i>UQCRC2</i>	UQCRC2	(Oudshoorn et al., 1987)	
COB	Cytb	<i>MT-CYB</i>	Cytochrome <i>b</i>	(Nobrega and Tzagoloff, 1980)	
CYT1	Cyte1	<i>CYC1</i>	CYC1	(Sadler et al., 1984)	
RIP1	Rip1	<i>UQCRFS1</i>	UQCRFS1	(Beckmann et al., 1987)	
QCR6	Qcr6	<i>UQCRH</i>	UQCRH	(Van Loon et al., 1984)	
QCR7	Qcr7	<i>UQCRB</i>	UQCRB	(De Haan et al., 1984)	
QCR8	Qcr8	<i>UQCRQ</i>	UQCRQ	(Maarse and Grivell, 1987)	
QCR9	Qcr9	<i>UQCR10</i>	UQCR10	(Phillips et al., 1990)	
QCR10	Qcr10	<i>UQCR11</i>	UQCR11	(Brandt et al., 1994)	
-	-	<i>UQCRFS1</i>	UQCRFS1	-	
<i>Translation factors</i>				Function	Reference
CBP1	Cbp1	-	-	Translational activator of COB mRNA	(Dieckmann et al., 1982)
CBS1	Cbs1	-	-	Translational activator of COB mRNA	(Rödel et al., 1986)
CBS2	Cbs2	-	-	Translational activator of COB mRNA	(Rödel et al., 1986)
CBP3	Cbp3	<i>UQCC1</i>	UQCC1	Translational activator of COB	(Wu et al., 1989)
CBP6	Cbp6	<i>UQCC2</i>	UQCC2	Translational activator of COB	(Dieckmann et al., 1985)
<i>Assembly factors</i>					
CBP3	Cbp3	<i>UQCC1</i>	UQCC1	Cytochrome <i>b</i> assembly factor	(Wu et al., 1989)
CBP6	Cbp6	<i>UQCC2</i>	UQCC2	Cytochrome <i>b</i> assembly factor	(Dieckmann et al., 1985)
CBP4	Cbp4	<i>UQCC3</i>	UQCC3	Cytochrome <i>b</i> assembly factor	(Crivellone et al., 1994; Wanschers et al., 2014)
FMP25	Bca1	-	-	Early/intermediate stages assembly factor in fungi	(Mathieu et al., 2011)
CYT2	Cyt2	<i>VPS53</i>	HCCS1	Heme lyase (Cytochrome <i>c1</i>)	(Zollner et al., 1992)
CYC2	Cyc2	-	-	Cytochrome <i>c1</i> and cytochrome <i>c</i> assembly factor	(Dumont et al., 1993)
BCS1	Bcs1	<i>BCS1L</i>	BCS1L	AAA-ATPase involved in Rieske protein incorporation	(Cruciat et al., 1999; Fernandez-Vizarra et al., 2007; Nobrega et al., 1992; Wagener et al., 2011)

MZM1	Mzm1	<i>LYRM7</i>	LYRM7	Matrix protein involved in Rieske protein incorporation	(Atkinson et al., 2010; Cui et al., 2012; Sanchez et al., 2013)
-	-	<i>TTC19</i>	TTC19	Rieske protein metabolism	(Ghezzi et al., 2011)

2.5.3 Pathologies associated with complex III deficiency

Pathologies due to deficiencies in CIII activity are relatively infrequent and most of them derive from mutations in *MTCYB*, the only mitochondrial-encoded subunit. Mutations in this protein are generally associated with myopathy and exercise intolerance (Ghezzi, 2018). Defects in nuclear-encoded subunits are rarer, but a handful of mutations have been found in several patients. The majority of the pathological variants associated with mitochondrial CIII deficiency of nuclear origin are found in *BCS1L* (Baker et al., 2019). The genes found mutated in patients with CIII deficiency and the relative clinical phenotype are summarised in Table 2.5.

Table 2.5: CIII subunits and assembly factors associated with mitochondrial diseases.

Gene/protein	OMIM	Associated phenotype	Reference
<i>Complex III subunits</i>			
UQCRC2	191329	Hypoglycemia, lactic acidosis, ketosis, and hyperammonaemia.	(Miyake et al., 2013)
MTCYB	516020	Leber optic atrophy, exercise intolerance, encephalomyopathy, cardiomyopathy, multisystemic disorder.	(Andreu et al., 2000; Bouzidi et al., 1993; Brown et al., 1992; Keightley et al., 2000; Wibrand et al., 2001)
CYC1	123980	Neurologic deterioration, insulin-responsive hyperglycemia, ketoacidosis with increased serum lactate, liver failure, and hyperammonaemia.	(Gaignard et al., 2013)
UQCRB	191330	Gastroenteritis, liver enlargement, hypoglycemia, metabolic acidosis, but normal psychomotor development at age 4.	(Haut et al., 2003.)
UQCRQ	612080	Severe neurologic phenotype.	(Barel et al., 2008)
UQCRFS1	191327	Cardiomyopathy and alopecia totalis.	(Gusic et al., 2020)
<i>Complex III assembly factors</i>			
BCS1L	603647	GRACILE Syndrome, Bjornstad Syndrome, myopathy, encephalopathy, proximal tubulopathy and liver failure.	(Baker et al., 2019; Blázquez et al., 2009; de Lonlay et al., 2001; Fernandez-Vizarra et al., 2007; Gil-Borlado et al., 2009; Hinson

			et al., 2007; Oláhová et al., 2019; Siddiqi, 2013; Visapaa, 1998)
TTC19	613814	Progressive encephalopathy, ataxia, spastic paraparesis, psychiatric phenotype.	(Ghezzi et al., 2011; Habibzadeh et al., 2019; Mordaunt et al., 2015; Morino et al., 2014; Nogueira et al., 2013)
LYRM7	615831	Neurological decompensation and regression, leukoencephalopathy, liver failure.	(Dallabona et al., 2016; Invernizzi et al., 2013)
UQCC2	614461	Intrauterine growth retardation, neonatal lactic acidosis and renal tubular dysfunction.	(Feichtinger et al., 2017; Tucker et al., 2013)
UQCC3	616097	Lactic acidosis, hypoglycemia, hypotonia and delayed development.	(Wanschers, 2014)

2.6 Complex IV

2.6.1 Structure and subunits

Cytochrome *c* oxidase (COX, complex IV, CIV) is the terminal step of the ETC. The enzyme has a molecular mass of about 200 kDa and in mammals it is composed of 13 subunits, 10 nuclear-encoded and 3 encoded by the mtDNA (MTCO1, MTCO2 and MTCO3), which form the functional core of the complex (Capaldi, 1990) (Figure 2.9). However, recently a 14th subunit, NDUFA4, previously attributed to CI, has been described (Balsa et al., 2012; Pitceathly et al., 2013) and was found to be incorporated in the structure of monomeric human CIV (Zong et al., 2018).

MTCO1 contains three prosthetic groups: cytochrome a_3 and Cu_B , which form the bi-nuclear centre that binds oxygen, and cytochrome *a*. MTCO2 incorporates the Cu_A centre (Hill, 1993) and MTCO3 does not have catalytic activity. The remaining subunits (COX4, 5A, 5B, 6A, 6B, 6C, 7A, 7B, 7C, 8A) are thought to have a structural role in the stabilisation of the complex. Interestingly, CIV is the only ETC complex that evolved tissue-, developmental-, and species-specific isoforms for COX subunits 4, 6A, 6B, 7A, 7B, and 8A (Sinkler et al., 2017), probably in order to regulate ATP and energy production in different conditions (Kadenbach et al., 2015).

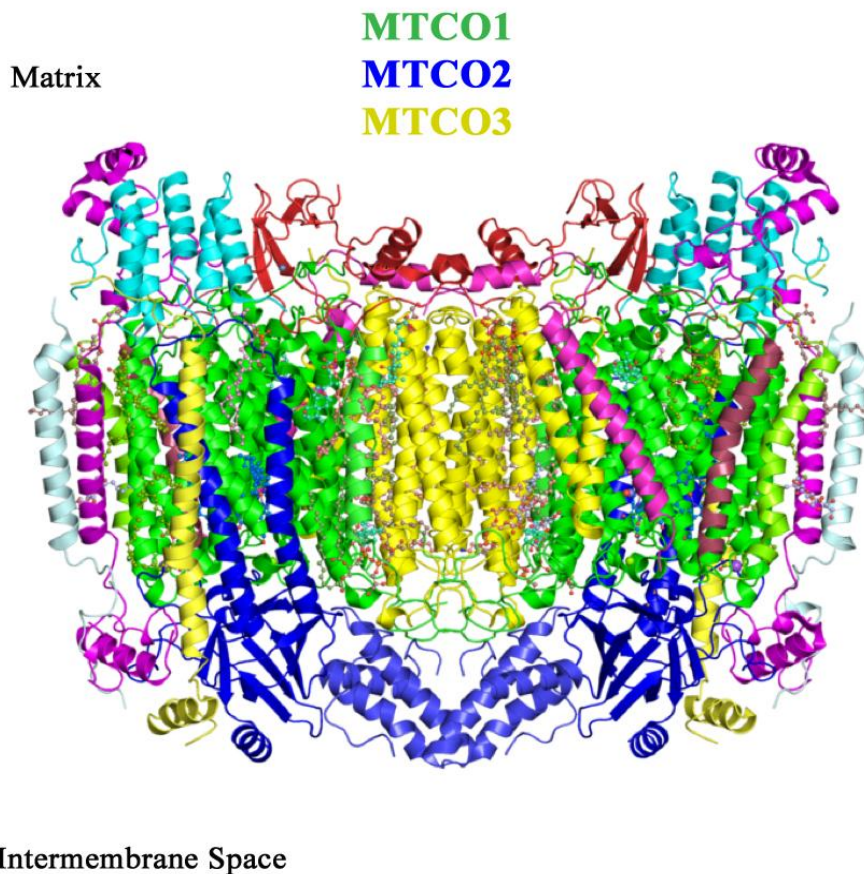


Figure 2.9: representation of bovine CIV dimeric structure, obtained from X-ray crystallography (SFX). The functional core of the complex is composed of the mitochondrial encoded subunits MTCO1 (green), MTCO2 (dark blue) and MTCO3 (yellow). Source: adapted from Ishigami et al., 2017.

2.6.2 Assembly

CIV assembly is now understood as a modular process. MTCO1 was classically considered the ‘seed’ around which the rest of the complex assembles (Nijtmans et al., 1998; Timón-Gómez et al., 2018). However, recent evidences indicated that the first CIV subassembly is formed by the association between two nuclear-encoded subunits, COX4I1 and COX5A (Vidoni et al., 2017). This module contains also HIGD1A, a protein initially proposed to be involved in the regulation of CIV activity during hypoxia (Hayashi et al., 2015).

In parallel, the MTCO1 module, also known as ‘MITRAC’ (MItochondrial TRanslation Regulation Assembly intermediate of Cytochrome *c* oxidase) (Dennerlein et al., 2015; Mick et

al., 2012) is formed, composed of the CIV subunit and a series of assembly factors necessary for its maturation and stabilisation. The first level of regulation of this module is translational, with the activity of the mitochondrial RNA-binding protein LRPPRC (Xu et al., 2004) and the translational activator TACO1 (Weraarpachai et al., 2009). After translation, the newly synthesised protein has to be inserted in the IMM. The first factors binding MTCO1 are COX14/C12ORF62 and COA3/CCDC56/MITRAC12 (Clemente et al., 2013; Mick et al., 2012, 2010; Szklarczyk et al., 2012). These two chaperones assist MTCO1 during and after its insertion in the membrane and avoid the aggregation of MTCO1 subunits. The transient complex MTCO1/COX14/COA3 is stabilised by another assembly factor, CMC1 (Bourens et al., 2017).

At this point of the pathway, MTCO1 needs the incorporation of the three prosthetic groups. Heme *a* biosynthesis is carried-out by COX10 and COX15 catalysing the conversion of heme *b* to heme *o*, and then heme *o* to heme *a* (Antonicka et al., 2003a; Diaz et al., 2015). On the other hand, the assembly factor SURF1 has been proposed to participate in its delivery (Timón-Gómez et al., 2018). In addition, PET117 might also have a role in this process because it was found interacting with COX15 in yeast, but its involvement still has to be proven in mammals (Taylor et al., 2017). Cu_B incorporation is mediated by the metallochaperone COX11 (Hiser et al., 2000), which is maintained in the correct redox state by COX19 (Bode et al., 2015). The coppers are donated by COX17 (Glerum et al., 1996).

MTCO2 requires binding with COX18 in order to be inserted in the IMM (Mansilla et al., 2018), and with COX20/FAM36A and TMEM177 for stabilisation (Bourens et al., 2014; Lorenzi et al., 2018). Secondly, the Cu_A centre must be inserted in MTCO2. This process is regulated by the copper-binding proteins COX17, SCO1 and SCO2 (Leary et al., 2007, 2004, 2009) together with COA6 (Pacheu-Grau et al., 2015; Stroud et al., 2015) and COX16 (Aich et al., 2018; Cerqua et al., 2018). The MTCO2 module (MTCO2 + COX5B + COX6C + COX7C + COX8A and, most probably COX7B) is incorporated in intermediate steps of the assembly process joining the COX4I1-COX5A and the MTCO1 modules forming the ‘S3’ intermediary. This intermediary binds three assembly factors, PET100 (Church et al., 2005), PET117 (Taylor et al., 2017) and MR-1S (Vidoni et al., 2017). MR-1S is a vertebrate-specific chaperone that interacts with the highly conserved factors PET100 and PET117. An additional assembly factor, APOPT1 or COA8, was proposed to have a role in the intermediate steps of CIV assembly in mouse and human mitochondria (Signes et al., 2019). Finally, the MTCO3

module (MTCO3 + COX6A1 + COX6B1 + COX7A2) is incorporated (Vidoni et al., 2017), followed by NDUFA4 initially described as a CI subunit and later assigned to CIV (Timon-Gomez et al., 2018). All known CIV assembly factors are summarised in Table 2.6 and a comprehensive representation of CIV assembly pathway is shown in Figure 2.10.

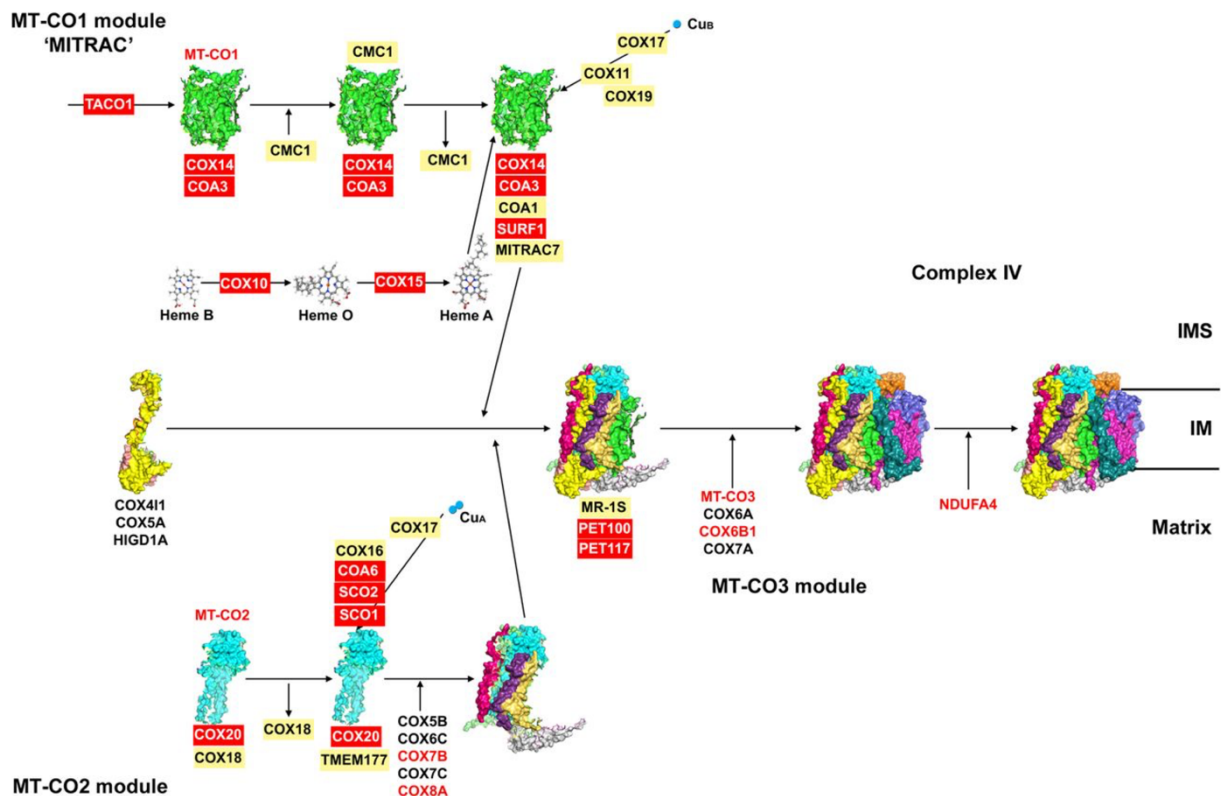


Figure 2.10: Schematic representation of complex IV assembly model based on the bovine crystal structure with PDB ID: 2OCC (Yoshikawa et al., 1998) and the model proposed in Vidoni et al., 2017. Red colour indicates proteins with described pathological mutations. Source: Signes and Fernandez-Vizarra, 2018.

Table 2.6: Factors involved in mammals CIV assembly. When present, the yeast orthologue is indicated.

Assembly factor (Yeast)	Assembly factor (Mammals)	Function	CIV interacting module	References
<i>RNA stability and translation</i>				
-	TACO1	Translational activator of mitochondria-encoded MTCO1.	MTCO1 - translation	(Weraarpachai et al., 2009)

-	LRPPRC	Mitochondrial mRNA stability.	-	(Xu et al., 2004)
<i>Heme a biosynthesis and insertion</i>				
Cox10	COX10	Heme <i>a</i> synthesis (conversion of heme <i>b</i> into heme <i>o</i>).	MTCO1 module	(Antonicka et al., 2003a; Nobrega et al., 1990)
Cox15	COX15	Heme <i>a</i> synthesis (conversion of heme <i>o</i> into heme <i>a</i>).	MTCO1 module	(Antonicka et al., 2003b; Glerum et al., 1997)
Shyl	SURF1	Involved in the insertion or stabilization of heme <i>a</i> ₃ .	Early MTCO1 subcomplexes	(Smith et al., 2005)
<i>Copper metabolism and insertion</i>				
Coa6	COA6	Copper homeostasis and transport to CIV.	MTCO2 module	(Stroud et al., 2015; Vögtle et al., 2012)
Sco1	SCO1	Incorporation of copper atoms.	MTCO2 module	(Leary et al., 2004; Schulze et al., 1988)
-	SCO2	Incorporation of copper atoms.	MTCO2 module	(Papadopoulou et al., 1999)
Cox11	COX11	Copper chaperone.	MTCO1 module	(Hiser et al., 2000; Tzagoloff et al., 1990)
Cox16	COX16	MTCO2 maturation.	MTCO2 module	(Carlson et al., 2003; Cerqua et al., 2018)
Cox17	COX17	Copper transfer.	MTCO1 module	(Glerum et al., 1996)
Cox19	COX19	Stabilisation of COX11.	MTCO1 module	(Bode et al., 2015; Nobrega et al., 2002)
<i>Assembly</i>				
Coa3	COA3/MITRA C12	Required for MTCO1 stability and assembly. Involved in translational regulation of MTCO1 and prevention of MTCO1 aggregation before assembly.	MTCO1 module	(Clemente et al., 2013; Mick et al., 2010)
-	COA7	Unknown.	Unknown	(Martinez Lyons et al., 2016)
Cox14	COX14/c12orf6 2	MTCO1 stability and assembly; avoids MTCO1 aggregation.	MTCO1 module	(Szklaarczyk et al., 2012; Weraarpachai et al., 2012)
Cmc1	CMC1	Stabilizes the interaction between MTCO1, COX14 and COA3.	MTCO1 module	(Bourens et al., 2017)
-	COX20/FAM36 A	MTCO2 chaperone for copper metalation.	MTCO2 module	(Hell et al., 2000)

Pet100	PET100	Assembly factor.	S3 intermediary	(Church et al., 1996; Lim et al., 2014; Oláhová et al., 2015)
Pet117	PET117	Assembly factor; possible role in Cox15 oligomerization and function.	S3 intermediary	(McEwen et al., 1993; Renkema et al., 2017; Taylor et al., 2017)
-	MR-1S	Interacts with PET117 and PET100.	S3 intermediary	(Vidoni et al., 2017)
-	APOPT1/COA8	Intermediate assembly steps. Putative role in CIV protection from ROS damage.	Unknown	(Signes et al., 2019)
Cox18	COX18	Promotes the translocation of MTCO2 globular domain through the IMM.	MTCO2	(Bourens and Barrientos, 2017; Souza et al., 2000)

2.6.3 Pathologies associated with complex IV deficiency

After CI-related pathologies, defects in CIV are the most common OXPHOS defects associated with mitochondrial diseases (Ghezzi, 2018). The most frequent clinical phenotypes associated with CIV deficiencies are myopathy, affecting the skeletal muscles, and systemic pathologies, such as Leigh's disease and multiorgan failure (<https://rarediseases.org/rare-diseases/cytochrome-c-oxidase-deficiency/>). As in most of the mitochondrial diseases, symptoms can be very heterogeneous and the severity of the pathology can vary greatly. While most of the pathological mutations found in patients are associated with assembly factors of the enzyme or mitochondrial tRNAs, only few cases of mutations in CIV structural subunits have been reported. This observation suggests that mutations in CIV subunits might be incompatible with life. The genes found mutated in patients with CIV deficiency and the relative clinical phenotype are summarised in Table 2.7.

Table 2.7: CIV subunits and assembly factors associated with mitochondrial diseases.

Gene/protein	OMIM	Associated phenotype	Reference
<i>Complex IV subunits</i>			
MTCO1	516030	MELAS syndrome, myopathy, myoglobinuria, motor neurone	(Comi et al., 1998; D'Aurelio et al., 2001; Lamperti et al., 2012;

		disease, exercise intolerance, epilepsy, multisystem disorders, deafness, LHON or mitochondrial sensorineural hearing loss.	Nishigaki et al., 2010; Valente et al., 2009).
MTCO2	516040	Encephalomyopathy, LHON, myopathy, hypertrophic cardiomyopathy.	(Abu-Amero et al., 2006; Clark et al., 1999; Rahman et al., 1999; Wei et al., 2006)
MTCO3	516050	MIDD, LHON, myopathy, Leigh disease, myoglobinuria, sporadic bilateral optic neuropathy, rhabdomyolysis, encephalopathy.	(Bosley et al., 2008; Hanna et al., 1998; Horvath et al., 2002; Marotta et al., 2011; Mkaouar-Rebai et al., 2011; Tabebi et al., 2015)
COX4I1	123864	Short stature, poor weight gain, mild dysmorphic features, and Fanconi anemia.	(Abu-Libdeh et al., 2017)
COX5A	603773	Early-onset pulmonary arterial hypertension, lactic acidemia, failure to thrive.	(Baertling et al., 2017)
COX6A2	602009	Muscle weakness and hypotonia, cardiomyopathy.	(Inoue et al., 2019)
COX8A	123870	Leigh-like syndrome presenting with leukodystrophy and severe epilepsy.	(Hallmann et al., 2016)
COX6B1	124089	Severe infantile encephalomyopathy.	(Massa et al., 2008)
COX6A1	602072	Charcot-Marie-Tooth disease.	(Tamiya et al., 2014)
COX7B	300885	Microphthalmia with linear skin lesions.	(Indrieri et al., 2012)
NDUFA4	603833	Leigh syndrome.	(Pitceathly et al., 2013)
<i>Complex IV assembly factors</i>			
SURF1	185620	Leigh Syndrome.	(Tiranti et al., 1998)
COA3/MITRAC12	614775	Mild phenotype, exercise intolerance, peripheral neuropathy, obesity and short stature.	(Mick et al., 2012)
COA7	615623	Ataxia and peripheral neuropathy, cognitive impairments, leukodystrophy.	(Martinez Lyons et al., 2016)
COX14/c12orf62	614478	Severe lactic acidosis and dysmorphic features.	(Weraarpachai et al., 2012)
COX20/FAM36A	614698	Growth delay, hypotonia, and cerebellar ataxia.	(Szklarczyk et al., 2013)
PET100	614770	Early-onset psycho-motor delay, seizures, hypotonia, and Leigh Syndrome.	(Lim et al., 2014; Oláhová et al., 2015)
PET117	614771	Neurodevelopmental regression.	(Renkema et al., 2017)
APOPT1/COA8	616003	Leukodystrophy, neurological signs.	(Melchionda et al., 2014)
SCO1/SCO2	603644/604272	Cardioencephalomyopathy, Leigh Syndrome-like symptoms, spinal muscular atrophy-like presentations, Charcot-Marie-Tooth disease type 4.	(Pronicki et al., 2010; Rebelo et al., 2018)

COX10/COX15	602125/603646	Leigh syndrome, encephalopathy, cardiomyopathy, sensorineural deafness and metabolic acidosis.	(Antonicka et al., 2003a, b)
COA6/C1orf31	614772	Fatal infantile cardioencephalopathy.	(Baertling et al., 2015)
TACO1	612958	Leigh syndrome.	(Weraarpachai et al., 2009)

2.7 Complex V

2.7.1 Structure and assembly

ATP synthase (Complex V, CV) is the enzyme that catalyses the synthesis of ATP from ADP and phosphate. It is composed of two distinct domains: the F_1 domain, which faces the mitochondrial matrix, and the F_0 domain, located in the IMM (Abrahams et al., 1994; Jonckheere et al., 2012). The human CV is composed of 29 proteins of 18 kinds, only two of which are encoded by the mtDNA (ATP6 and ATP8) (He et al., 2018). A schematic representation of the main domains of CV is shown in Figure 2.11. F_1 domain is composed of three copies of subunits α and β , and one copy of subunits γ , δ and ϵ . γ , δ and ϵ subunits form the central stalk of the complex, while α and β are the subunits that physically interact with the ADP and ATP molecules (Jonckheere et al., 2012). F_0 , instead, is composed of a ring of c subunits and one copy each of subunits a, b, d, F_6 and the oligomycin sensitivity-conferring protein (OSCP). The c-ring stoichiometry is not constant, but can vary, ranging from 8 copies in vertebrates to 15 in photosynthetic organisms (Watt et al., 2010).

Each c-subunit is able to bind one proton in the IMS, which interacts with a conserved carboxylate group from a glutamate or aspartate side chain. The protonation of these subunits provokes the rotation of the c-ring, until the final dissociation of the proton at the matrix side favoured by the positive charge on a conserved arginine residue (A210) of subunit a (Berg et al., 2002). The c-ring is structurally linked to the γ and ϵ subunits and its rotation provokes the turn of these subunits inside the $\alpha_3\beta_3$ hexamer unit of F_1 . On the external side, the $\alpha_3\beta_3$ hexamer is prevented from rotating by the peripheral stalk formed by the two b chains and the d subunit. The result of the proton transport, therefore, is first the rotation of the c-ring, followed by the rotation of the γ subunit, and the consequent synthesis of ATP through the binding-change mechanism of $\alpha_3\beta_3$. The binding-change mechanism is based on the fact that the interactions between the γ subunit and the three β subunits are not identical. The result is three different

conformations for the three β subunits: T (tight), L (loose), and O (open). The subunit in T conformation binds ATP very strongly and its affinity for the molecule is so high that it will induce the conversion $\text{ADP} + \text{P}_i$ into ATP. The subunit in the L conformation, instead, is able to bind ADP and P_i but it cannot release the nucleotides. Finally, the O conformation allows the release of the formed ATP. The result of the γ subunit rotation is the change in these subunits conformations allowing the passage through all the stages and the generation of ATP (Berg et al., 2002).

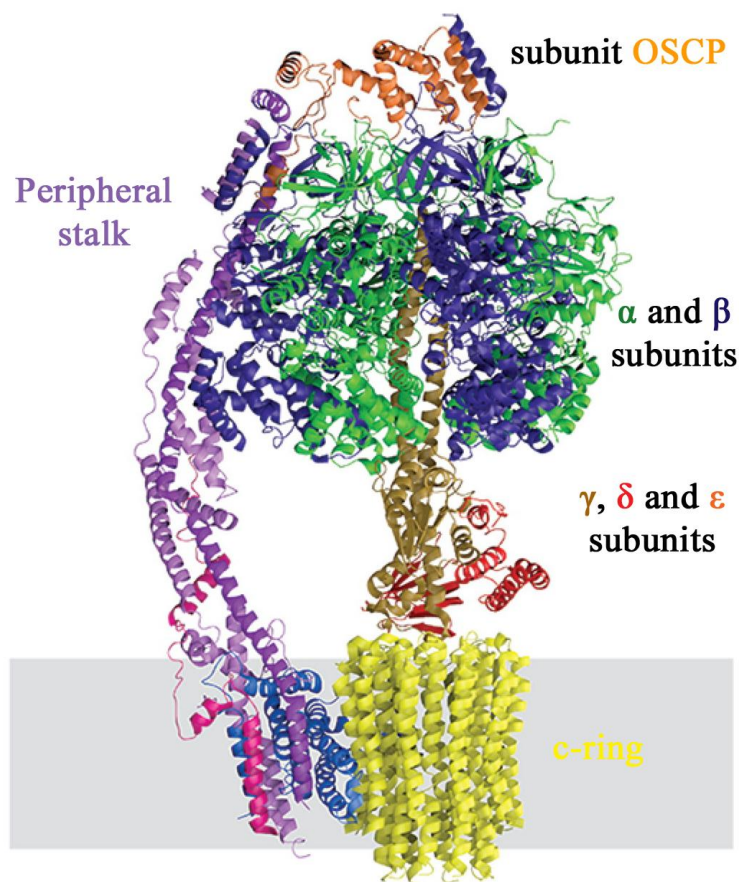


Figure 2.11: representation of Saccharomyces cerevisiae CV structure. The main subunits of the enzyme are indicated and showed in different colours. Source: adapted from Kuhlbrandt, 2019.

As for other complexes described, CV assembly is also modular. Three sub-assemblies are formed individually and then put together: the F_1 module, the c-ring and the peripheral stalk (Wittig and Schagger, 2008). The F_1 subcomplex formation requires the activity of the chaperones ATPAF1/ATP11 and ATPAF2/ATP12, which bind ATP5B and ATP5A1,

respectively (Ackerman and Tzagoloff, 1990). Initially, the F₁ and the c-ring module assemble. The peripheral stalk, instead, is incorporated in two additional steps: the incorporation of b/ATP5F1, d/ATPH, F₆/ATP5J and OSCP/ATP5O first and the addition of e/ATP5I, g/ATP5L and f/ATP5J2 in a second moment (He et al., 2017; Walker, 2013). Different assembly factors involved in this process have been identified in yeasts. Atp25 stimulates the synthesis and assembly of the subunit c of the c-ring (Zeng et al., 2008), while the protease Atp23 processes and stabilises the membrane-inserted yeast Atp6, unprocessed in mammals (Rak et al., 2011). Finally, the inner membrane assembly complex (INAC), composed of Ina17 and Ina22 (Lytovchenko et al., 2014), binds and stabilises two distinct assembly intermediates of the yeast ATP synthase: the newly assembled c-ring and an assembly intermediate composed of the F₁ domain and the peripheral stalk.

2.7.2 Pathologies associated with complex V deficiency

Patients presenting with CV defects are rare and generally associated with neonatal-onset hypotonia and hypertrophic cardiomyopathy, lactic acidosis and 3-methylglutaconic aciduria (Ghezzi, 2018). Only few pathological mutations in CV subunits or assembly factors have been found in patients so far. The majority of these mutations were identified in MT-ATP6, responsible for neurogenic muscle weakness, ataxia and retinitis pigmentosa (NARP) syndrome (López-Gallardo et al., 2009), MT-ATP8 (Jonckheere et al., 2008), while rarer cases were found in ATP5E, ATP5A1, ATPAF2 and TMEM70 (Hejzlarová et al., 2014; Jonckheere et al., 2008; Jonckheere et al., 2013; Mayr et al., 2010; Tatuch and Robinson, 1993).

2.8 Localisation of the OXPHOS machinery in the IMM

The OXPHOS machinery is embedded in the IMM, together with a variety of other mitochondrial proteins. Indeed, the IMM is one of the most protein-rich lipid bilayers in biological systems, with a protein/lipid mass ratio of ~75:25 (Scheffler, 1999). Many protein complexes which localise in this compartment are not distributed randomly, but tend to cluster in specific regions, according to their individual function. As discussed previously, the IMM can be divided into two subdomains: the inner boundary membrane (IBM), opposite to the

OMM, and the cristae membrane (CM), alias for invaginations of the membrane in the matrix, connected by the cristae junctions.

Results obtained with quantitative immunogold-EM on mammalian mitochondria and yeast cells demonstrated that the preferential location of OXPHOS complexes is the CM, but that both sub-compartments are dynamic and the distribution of mitochondrial proteins can change according to the physiological state of the cell (Gilkerson et al., 2003; Vogel et al., 2006). In particular, it has been observed that OXPHOS enzymes - or intermediates of them - might localise in different regions of the membrane in different stages of maturation. With the only exception of CII, the respiratory chain enzymes are composed by both nuclear- and mitochondrial-encoded subunits, and their biogenesis is the result of the coordination between two temporally and spatially separated protein synthesis machineries. Consequently, it was proposed that, while proteins synthesised in the matrix are translated and inserted directly in the cristae, subunits that must be imported from the cytosol are preferentially inserted in the IBM (Vogel et al., 2006). More recent analyses by super-resolution microscopy and quantitative cryo-immunogold-EM have helped to determine where specifically CIII, CIV and CV subunits are translated and inserted in the yeast inner membrane (Stoldt et al., 2018). This study confirmed that, under steady-state conditions, the mature form of CIII, CIV and CV localise mainly in the CM, while early stages of assembly are more enriched in the IBM. Indeed, mitoribosomes translating *COB* mRNA (the very first step of CIII assembly) and Cbp3 and Cbp6 (markers for the early assembly of the enzyme) were found more present in the IBM, while Cbp4 (a marker of the early-to-mid-assembly phase) was already less enriched in this sub-compartment. Conversely, the integration of the Rieske protein, last step of maturation, which takes place after CIII dimerization, happened predominantly in the CM. Similarly, Stoldt and colleagues investigated the localisation of markers of the early (Pnt1, Cox18, Coa1, and Cox20) and the late (Pet100) phases of CIV assembly, finding the earliest stages of maturation enriched in the IBM and the late phases in the CM. By contrast, the entire assembly pathway of CV seems to occur mainly in the CM (Stoldt et al., 2018).

2.9 Supercomplexes

The picture of the OXPHOS machinery as individual enzymes sitting in the IMM is a simplified vision of what happens in the mitochondria of living cells. A second level of complexity is added by the formation of supercomplexes (SC), stable structures composed of the association of the respiratory chain enzymes.

The development of blue native PAGE techniques (Schägger, 1991) allowed the separation and detection of both the individual complexes and the supercomplexes, composed of different combinations of CI, CIII₂ and CIV. However, many questions remained open in the field. Firstly, it was necessary to characterise the type and strength of these inter-complex interactions, in order to hypothesise a realistic model of IMM organisation. Secondly, it was essential to attempt to explain the biological and physiological function of these structures. This second aspect will be one of the central questions of this thesis.

2.9.1 Existing models

The models to explain the organisation of the respiratory chain enzymes have changed in time. The first proposal, known as the ‘fluid state’ model, describes the mitochondrial complexes as individual and independent units that float in the inner membrane and collide randomly with each other, allowing the passage of electrons. According to this theory, cytochrome *c* would be diffusing in three dimensions, in order to transport electrons between complexes, and this transient and casual formation of each SC specie by collision would allow the cell to adapt to different energy demands. This model was the most accepted one during the 1980s, following the presentation of the Random Collision Model of Hackenbrock (Hackenbrock et al., 1986). The fluid model is supported by the very high protein-to-lipid ratio in the membrane, which allows the frequent interaction of the enzymes. Scanning calorimetry (Höchli et al., 1979) and freeze-fracture electron microscopy (Sowers et al., 1981) studies, besides, showed that the intramembrane particles are randomly distributed in the IMM. Moreover, independent studies showed that CoQ is a mobile carrier (Fato et al., 1986; Lenaz et al., 1999), confirming an essential part of this theory. On the other hand, however, both blue native and electron microscopy experiments in different systems, such as mammals, bacteria, yeasts and plants, suggested a more stable interactions between these particles (Dudkina et al., 2005; Schäfer et

al., 2006; Schägger et al., 2000, 2001; Stroh et al., 2004). In the original experiments it was necessary to solubilise the membranes with strong detergent in order to isolate the single enzyme, while milder detergents such as digitonin used in blue native studies preserve the various species of SC intact.

The second and opposite model proposed was the ‘solid state’ model, which supported the vision that the different activities and redox centres were contained in an undissociated protein matrix. These structures were also thought to contain Q and cyt *c* (Chance and Williams, 1955; Keilin and Hartree, 1947). This view, however, was challenged by the observation that the isolated complexes were functional and that they could diffuse within the lipid bilayer as well as activity rate values were compatible with a mechanism of random collision (Hatefi et al., 1962). The ‘solid state’ model remained the most accepted view until the development of the native electrophoretic techniques described above, which showed the co-existence of supercomplexes of different sizes and the individual respiratory chain complexes. From a functional point of view, the proximity of the enzymes and the molecular carriers involved would increase the interactions and prevent the intermediates from escaping or being sequestered by other enzymes for use in secondary metabolic pathways (Trouillard et al., 2011). Indeed, in the model in which the different supramolecular species coexist and trap the mobile electron carriers, the association of CI, III and IV and, on the other side, CIII and IV, would define two different functional CoQ populations: CoQ dedicated to transferring electrons originating from NADH (CoQ_{NADH}), which is trapped in SC containing CI, and free CoQ in the inner mitochondrial membrane for use by CII and other enzymes that use FAD (CoQ_{FAD}) (Lapiente-Brun et al., 2013). However, this system is not compatible with the kinetics of the CoQ pool, and recent additional studies indicated that cytochrome *c* diffuses freely in the membrane in yeast (Trouillard et al., 2011) and that only one CoQ and cytochrome *c* pools are present, accessible to all the enzymes (Blaza et al., 2014). An additional interesting analysis has been proposed after inserting AOX (an alternative oxidase) *in vitro*, a cyanide-insensitive quinol oxidase originally from *Trypanosoma brucei*, in bovine heart mitochondria (Fedor and Hirst, 2018). AOX receives electrons from ubiquinone, bypassing CIII and CIV. In the case of two separate pools of ubiquinone, the ‘respirasome pool’ should continue to provide a substantial flux of electrons through the supercomplex. Instead, a competition between respirasomes and AOX was observed increasing AOX supplementation, confirming the theory that ubiquinone is not channelled but can move freely in the IMM.

In conclusion, putting together the information available today, the most realistic proposal is a middle-ground and more dynamic model in which various species of supercomplexes and free respiratory complexes coexist. For now, the model that explains this phenomenon is the so-called ‘dynamic aggregate’ or ‘plasticity’ model, which proposes a dynamic interchange of the complexes in their ‘free’ and associated states into SC in response to varying energetic demands. A premise for the model is that the complexes are pre-assembled individually before associating among each other (Acin-Perez and Enriquez, 2014; Acin-Perez et al., 2008).

2.9.2 Species of supercomplexes and complex-complex interactions

Structures of the I_1III_2IV and I_1III_2 SC from mammals and plants have been resolved by single-particle electron cryo-EM (Gu et al., 2016; Guo et al., 2017; Letts et al., 2019; Letts et al., 2016) and by electron cryo-tomography (cryo-ET) (Davies et al., 2018; Dudkina et al., 2011). The yeast *Saccharomyces cerevisiae* lacks CI and complexes III and IV form two SC species III_2IV_1 and III_2IV_2 , the structures of which have been recently solved (Hartley et al., 2019; Rathore et al., 2019).

In mammals, the main supercomplexes species are III_2IV_1 , I_1III_2 and the respirasomes $I_1III_2IV_1$. The existence of a “Megacomplex” with a $I_2III_2IV_2$ stoichiometry, which might also bind CII, was reported in cultured human cells (Guo et al., 2017). Additionally, CIV and CV can form homodimers and CIV is involved in the formation of other high-molecular-weight structures not yet identified, but visible in blue native experiments (Schagger, 2002; Vukotic et al., 2012; Wittig and Schagger, 2008). ‘Megacomplexes’ containing also CII have been proposed as well, but their existence is debated.

Since *Saccharomyces cerevisiae* lacks CI (Marcet-Houben et al., 2009), yeast-based studies of the respirasomes have been conducted in *Yarrowia lipolytica* (Davies et al., 2018). In this model, CI and CIII interactions are comparable to what has been observed in mammals, while CIV was found in various positions around $CIII_2$, but not in the position most commonly observed in the porcine heart respirasomes, contacting the ND5 module of CI (Figure 2.12).

In plants, on the other side, CIV was never observed in the respirasomes and the only apparent supercomplex was I_1III_2 . Interestingly, supercomplexes are not universal and simpler organisms such as *Escherichia coli*, which express CI, CII and CV homologues, but not CIII,

do not present such structures (Friedrich et al., 2016). In these bacteria, the different complexes have been shown to not to co-localise together and to not sub-localise in specific domains over the membrane surface (Llorente-Garcia et al., 2014).

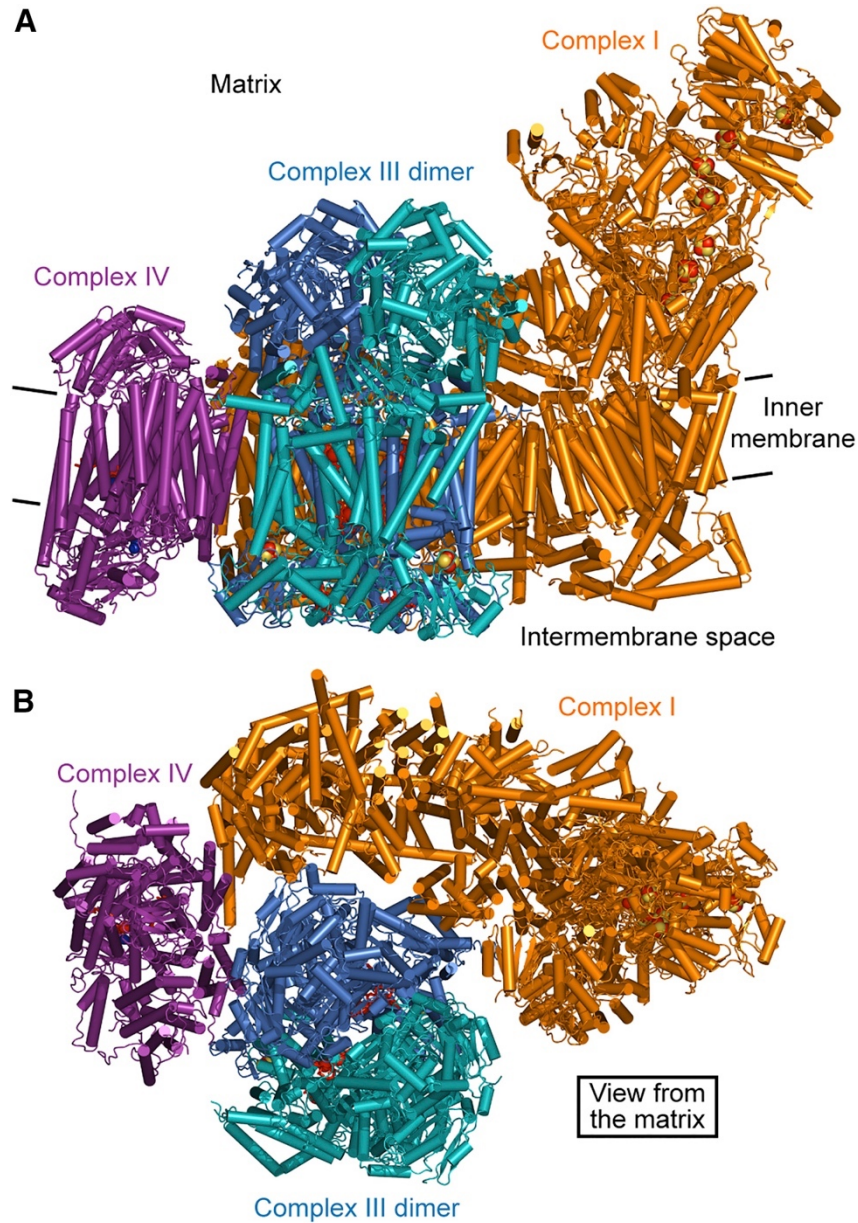


Figure 2.12: overall structure of porcine respirasome (I₁III₂IV₁). Source: adapted from Milenkovic et al., 2017.

Interestingly, the percentage of free complexes vs. SC varies largely between different species. In bovine heart mitochondria, electron cryo-tomography indicated that only 56% of CI was associated with other complexes (Davies et al., 2018). However, BN-PAGE-based

quantifications of the same cell type estimated that only 14-16% of free CI was present (Schägger, 2001). On the other hand, blue native-PAGE experiments using human mitochondria show a minimal population of CI (~10% at the most, in the presence of digitonin) migrating as an individual complex (Lobo-Jarne et al., 2018). In any case, there seems to be more of 'free' CI in mitochondria from different tissues in mammalian organisms such as sheep, pigs or mouse than in humans (Acin-Perez et al., 2008; Letts and Sazanov, 2017). These differences might be due to various reasons, including artefacts introduced during the sample preparation or actual differences in the regulation of energy demands between different organisms.

In addition, in the same organism, not all the complexes engage in the formation of SC in the same proportion. Indeed, in humans, it has been estimated that while 85%–100% of CI is inserted in a supercomplex structure, only 55%–65% of CIII, and 15%–25% of CIV, are found in SC (Greggio et al., 2017; Lobo-Jarne et al., 2018; Lobo-Jarne and Ugalde, 2018; Schägger, 2001).

Structural analyses have been important also to define which subunits are involved in the complex-complex interaction. The association between CI and CIV seem to involve subunit COX7A of CIV, ND5 and NDUFA9 of CI (Letts et al., 2016). COX7A, together with COX8B, could be involved also in the interaction with CIII, through binding of UQCRC1, UQCRQ, UQCR10 or UQCR11 (Letts et al., 2016; Davies et al., 2018; Gu et al., 2016). Concerning the connection between CI and CIII, subunit NDUFA11 of CI seems to face and contact the transmembrane region of CIII, close to UQCRB and UQCRQ (Gu et al., 2016; Letts et al., 2016). Other CI subunits that might be involved in the interaction are NDUFAB1 and NDUFB9, contacting UQCRC1 of CIII.

2.9.3 Possible functional roles of supercomplexes

The biological function of SC is still highly debated and various hypotheses have been proposed. The first theory proposes that their role is substrate channelling, increasing OXPHOS efficiency due to the physical proximity of all the machinery components (Mileykovskaya et al., 2012). The second possible function of SC might be to minimise ROS production. ROS are

generated by the reduction of oxygen by electrons leaked from the ETC and are physiologically used as a signalling molecule (Turrens, 2003). However, if there is an imbalance between the excessive formation of ROS and limited antioxidant defences, ROS can become deleterious and damage mtDNA, lipids and proteins. In this case, the formation of supra-structures might decrease electron or proton leakages during respiration. This theory is supported by two studies. In the first one, ROS production by CI has been shown to increase in two experimental conditions that inhibit the formation of CI and CIII interactions: treating bovine heart mitochondria or liposome-reconstituted supercomplex I-III with dodecyl maltoside, and reconstructing CI and CIII at high phospholipids:protein ratio (Maranzana et al., 2013). In the second study, the difference in SC formation in astrocytes and neurons has been analysed, showing how astrocytes, which present a higher percentage of free CI, are characterised by poorer mitochondrial respiration but higher ROS production (Lopez-Fabuel et al., 2016).

The last hypothesis, which will be the basis of the first project presented in this thesis, is that the formation of SC is necessary for the assembly and/or stability of the single enzymes. This theory is supported by the observation that defects in one enzyme can lead to multi-complex deficiencies. Indeed, mutations in MTCYB, fundamental for CIII assembly, induce also CI deficiencies (Andreu et al., 1999; Blakely et al., 2005; Lamantea et al., 2002). Similarly, patients presenting with mutations in CIII assembly factors, such as BCS1L, can display defects in both CI and CIV (Moran et al., 2010), while the suppression of CIV in mouse fibroblasts affects CI assembly or stability (Diaz et al., 2006). An explanation for this phenomenon was that CI was destabilized after its complete assembly by an active oxidative stress-triggered degradation (Acin-Perez et al., 2004; Diaz et al., 2012; Guaras et al., 2016). However, a multistep model for SC assembly that sees CI intermediates binding CIII and CIV subunits before the completion of the mature enzyme was proposed (Moreno-Lastres et al., 2012). In the same study, UQCRFS1 was shown to insert preferentially within the III₂+IV supercomplex, instead of dimeric CIII₂.

Finally, an additional role of SC is reserved to the ATP synthase. CV does not seem to interact with the rest of the respiratory chain, but it is able to form dimers and more complex supra-structures such as tetramer and hexamers (Habersetzer et al., 2013). These supercomplexes localise specifically at the tips of the cristae, where they appear to enforce a strong local curvature on the inner membrane, necessary for the formation of the invagination (Strauss et al., 2008).

2.9.4 Assembly of supercomplexes

Being that the assembly of the monomeric forms of the OXPHOS enzymes requires the participation of a number of assembly factors, it has been proposed that additional proteins should be involved in the formation of supercomplexes.

The first proposed assembly factor was COX7A2L or SCAF1 (supercomplex assembly factor 1), an isoform of the CIV subunit COX7A, described originally to have a role in the inclusion of CIV in III₂+IV and I+III₂+IV₁₋₄ (Lapiente-Brun et al., 2013). However, following studies showed that the lack of COX7A2L affects the formation of the SC III₂+IV, but not of respirasomes (Lobo-Jarne et al., 2018; Mourier et al., 2014; Pérez-Pérez, 2016; Williams et al., 2016). Pérez-Pérez data also showed how COX7A2L binds to CIII₂ early during its assembly, indicating a preferential interaction with this complex (Pérez-Pérez et al., 2016). Thus, it might have a role in the establishment of a checkpoint for the regulation of CIII₂ levels and its incorporation into SC (Lobo-Jarne et al., 2018).

Another study showed how the incorporation of different COX7A isoforms might determine which CIV-containing species (monomer, dimer or respirasome) is formed (Cogliati et al., 2016a). Thus, the CIV subunit COX7A2 is replaced by COX7A2L in supercomplexes with both CIV and CIII, and by COX7A1 in CIV dimers. Moreover, other CIV tissue-specific subunit isoforms might play a role in this as well, as dimers appeared to be stabilised by the COX6A2 isoform rather than COX6A1. COX6A subunits are localised at the interface between the two monomers, position that would favour the regulation of the dimerization. COX7A2 and COX6A1, instead, would favour the free CIV form.

Analyses conducted in *Saccharomyces cerevisiae* suggested the participation of Rcf1 and Rcf2 in the formation of respirasomes (Vukotic et al., 2012). In yeast, the loss of Rcf1 affects CIV function and the correct insertion of Cox13 (equivalent to human COX6A). These data showed also deficiency in SC formation, but recent reports point to this being an indirect effect due to CIV defects (Dawitz et al., 2019; Hartley et al., 2020; Strogolova et al., 2019). While Rcf2 is specific to yeast, two orthologs of Rcf1 have been identified in humans: RCF1a/HIGD1A and RCF1b/HIGD2A. HIGD1A has been confirmed to bind CIV and it has been suggested to affect the interaction between CIV and cytochrome *c*, or to act in a still unclear way on the heme centres (Hayashi et al., 2015; Vidoni, 2017). Another study found HIGD1A directly involved in CIII biogenesis, promoting the final incorporation of UQCRFS1, and suggested its

participation in the formation of CIII-containing SC (Timón-Gómez et al., 2020). Concerning HIGD2A, instead, two independent groups demonstrated that the knockdown of this protein leads to impaired SC formation by the release of CIV from respirasomes (Chen et al., 2012; Rieger et al., 2017). However, HIGD2A was identified as a MTCO3 module assembly factor and it is possible that its impact on SC is a pleotropic effect due to impaired CIV biogenesis (Hock et al., 2020; Timón-Gómez et al., 2020).

Concerning oligomerisation of CV, the role of post-translational modifications in Atp20 have been investigated (Reinders et al., 2007). Specifically, the molecular mechanism seems to revolve around the phosphorylation of serine 62, which inhibits the dimerization of the ATP synthase.

Finally, also the lipid composition of the IMM, and in particular the level of cardiolipin, is important for the stabilisation of SC. In yeast lacking Taz1, the acyltransferase involved in the remodelling of cardiolipin, CIII and CIV associations are destabilised (Brandner et al., 2005). In Barth syndrome patients, harbouring mutations in Tafazzin (the human ortholog of Taz1), the assembly and stability of CIV and its SC forms are affected, with a secondary effect also on CI+III associations (McKenzie et al., 2006).

Section 3: Calcium and mitochondria

Calcium ion (Ca^{2+}) is a secondary messenger involved in numerous cellular signalling and transducing pathways. Two characteristics make Ca^{2+} the perfect regulator for many cellular processes: ubiquity and versatility (Berridge et al., 2000). Indeed, the oscillation in Ca^{2+} concentration can be finely regulated in terms of space and time, from extremely localised Ca^{2+} bursts, which lead to rapid peaks of high ions concentrations, to gradual diffusion, that generates Ca^{2+} waves in larger areas. The first case is optimal for rapid responses, such as muscle contraction and synaptic transmission, while the second case allows less localised and more persistent signals, such as in non-excitable cells, where Ca^{2+} regulates transcription, cell cycle or apoptosis (Carafoli, 2002).

Each of these patterns creates a different response in the cell, as many proteins can be activated or regulated by Ca^{2+} . For this reason, Ca^{2+} must also be compartmentalised within the cell, to control its mobility and concentration, in different organelles. The main sources for Ca^{2+} are the external environment and internal organelles such as the endoplasmic reticulum (ER) or the sarcoplasmic reticulum (SR) in muscle cells (with an average concentration of Ca^{2+} of 100–500 μM), but also to lesser extend the Golgi apparatus (100–300 μM), lysosomes (200–500 μM) and mitochondria (Lam and Galione, 2013; Suzuki et al., 2016).

The first evidence of Ca^{2+} in mitochondria was reported in 1953, but its uptake was described as a passive process (Slater and Cleland, 1953). In 1955, instead, Britton Chance demonstrated that Ca^{2+} , which was so far believed to be a generic mitochondrial uncoupler, showed an unexpected behaviour, uncoupling cellular respiration reversibly (Chance, 1955). Following this observation, two groups reported that these organelles were able to use ATP-derived energy to actively uptake Ca^{2+} (Deluca and Engstrom, 1961; Vasington and Murphy, 1962), and in 1963 it was confirmed that Ca^{2+} was actually transported inside mitochondria in exchange for protons (Saris, 1963). Indeed, mitochondria require a constant presence of a large electric gradient across the IMM (~180 mV), which generates the driving force that pushes positively charged Ca^{2+} ions into the matrix (Rizzuto et al., 2012). In the following 60 years, numerous studies have been conducted to characterise the nature of this relationship: how Ca^{2+}

regulates or affects mitochondria and, vice versa, how mitochondria regulate Ca^{2+} signalling and what machineries are involved in these processes.

Ca^{2+} is involved in the regulation of numerous cellular processes, such as muscle contraction, exocytosis and gene transcription (Raffaello et al., 2016). In mitochondria, one of the major roles of Ca^{2+} is to activate pyruvate, isocitrate, and 2-oxoglutarate dehydrogenases, involved in the TCA cycle, stimulating mitochondrial respiration and ATP production (Rizzuto et al., 2000). The effects of Ca^{2+} signalling on TCA cycle and OXPHOS will be discussed more in detail in Section 3.10.

Another event regulated by mitochondrial Ca^{2+} is cell death. Indeed, it is well established that the excessive and prolonged accumulation of Ca^{2+} in the organelle can induce the opening of the mitochondrial permeability transition pore (mPTP) (Hunter and Haworth, 1979). Many mechanisms have been proposed to explain this physiological phenomenon, including the involvement of dimeric ATP synthase complex (Giorgio et al., 2013) and VDAC (Crompton, 1999), but the molecular basis of mPTP opening is still unclear. This phenomenon provokes an increase in the permeability of the IMM to low molecular weight solutes (<1.5 kDa), osmotic swelling, drop of membrane potential and consequent inhibition of mitochondrial respiration and ATP production (Bonora et al., 2015). mPTP opening is mainly known to be linked to necrosis, a non-programmed form of cell death, but it has been recently reported to be interconnected with apoptosis (Danese et al., 2017).

The deregulation of Ca^{2+} , therefore, is associated with mPTP opening, loss of $\Delta\Psi_m$, and drop in ATP production, which leads to several pathologies, such as cerebrovascular or cardiovascular disease, neurodegeneration and motor disorders, and cancer development (Granatiero et al., 2019; Sterea and El Hiani, 2020; Tamargo and Lopez-Sendon, 2011). Therefore, a deep understanding of Ca^{2+} regulation has a vital role in the study of the pathophysiology of numerous diseases.

In addition to energy production and cell death, mitochondria are important in the regulation of intracellular calcium homeostasis, acting as Ca^{2+} buffer. Indeed, mitochondria can uptake Ca^{2+} rapidly during cell stimulation, and successively release it slowly back into the cytosol, shaping the cytosolic Ca^{2+} signal (Pozzan et al., 1994; Rutter and Rizzuto, 2000). Under resting conditions, Ca^{2+} concentration inside the organelle is around 100–200 nM, while under

stimulation these organelles can accumulate between 1 and 500 μM (Giorgi et al., 2018; Montero et al., 2000).

3.1 The microdomain model - Mitochondria and ER contact sites

The main route for Ca^{2+} import into mitochondria is the mitochondrial calcium uniporter (MCU). MCU is characterised by low affinity for Ca^{2+} under physiological conditions (K_d around 10–20 μM), making it necessary to have high cytoplasmic Ca^{2+} concentrations to initiate the uptake. However, this condition does not occur in healthy cells and how MCU was able to uptake Ca^{2+} in the matrix was subject to intense debate. This discrepancy was solved in the late '90s by the microdomain model: the fast uptake of mitochondrial Ca^{2+} depends on the close proximity between mitochondria and the site of Ca^{2+} release, the ER (Rizzuto et al., 1998). The formation of a spatially and temporally controlled microdomain of high Ca^{2+} concentration ($[\text{Ca}^{2+}] > 10 \mu\text{M}$) meets the low affinity of the channel, allowing rapid and controlled mitochondrial Ca^{2+} uptake, while preventing Ca^{2+} overload and unspecific signalling.

ER-mitochondria contact sites are areas of close apposition, but not fusion, between the membranes of the two organelles (~20-50 nm) (Scorrano et al., 2019). It has been estimated that ~5–20% of the ER surface is in close proximity to the mitochondria (Csordás et al., 2006), where it facilitates the exchange of different molecules, including Ca^{2+} , lipids, amino acids, and metals (Burgoyne et al., 2015; Lahiri et al., 2015) (Figure 3.1). The establishment of these restricted areas of juxtaposition is thought to be promoted by the presence of tethering forces resulting from protein–protein or protein–lipid interactions, which involve both ER and mitochondrial proteins (Paillusson et al., 2016).

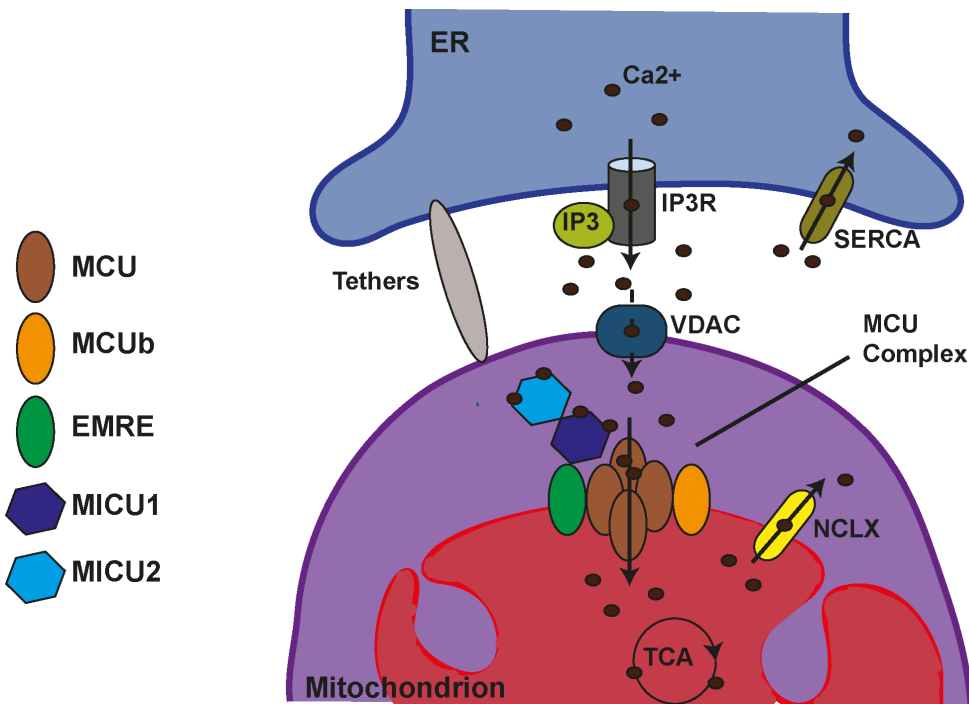


Figure 3.1: cartoon representation of calcium exchange at the ER-mitochondria contact sites. *Ins(1,4,5)P₃R*s (or IP₃R) in the ER membrane are activated by IP₃ binding and release Ca²⁺ in the cytosol or into neighbouring organelles. At ER-mitochondria contact sites, VDAC1 in the OMM and MCU in the IMM uptake Ca²⁺. The close proximity of the two organelles ensures highly localised and concentrated Ca²⁺ microdomains, necessary for the passage of Ca²⁺ through MCU. Source: Paupe and Prudent, 2018.

The release of Ca²⁺ into the cytosol or other organelles, is mediated by two receptors: ryanodine receptors (RyRs) and inositol 1,4,5-triphosphate receptors (Ins(1,4,5)P₃R). Ins(1,4,5)P₃R are enriched at the membrane contact sites with mitochondria and are activated by the binding with the signalling molecule IP₃ (inositol 1,4,5-triphosphate), generated by phospholipase C (PLC)-mediated cleavage of phosphatidylinositol 4,5-bisphosphate (PIP₂), triggering Ca²⁺ release (Giorgi et al., 2018). The existence of regions of high local Ca²⁺, close to IP₃-gated channels was demonstrated for the first time in 1993 by Rizzuto and colleagues, using mitochondrially targeted recombinant aequorin, a Ca²⁺-sensitive photo-protein (Rizzuto et al., 1993). These data confirmed the formation of close contact points between ER and mitochondria, deputed to the formation of Ca²⁺ microdomain and ER-Ca²⁺ transfer. Upon prolonged ER-Ca²⁺ release, the reduction of Ca²⁺ in the ER store is then counterbalanced by an influx from the extracellular space through the Ca²⁺ release-activated Ca²⁺ (CRAC) channels (Figure 3.2), in a process called Store-operated calcium entry (SOCE). This process leads to an influx of Ca²⁺ into the cytosol,

which will be refilled in the ER lumen by the sarco/endoplasmic reticulum Ca^{2+} -ATPase (SERCA) pump (Berridge et al., 2000; Raffaello et al., 2016).

Once released from ER at the membrane contact sites, Ca^{2+} ions pass the OMM through voltage-dependent anion-selective channel proteins (VDACs), in particular VDAC1, (De Stefani et al., 2012), and the IMM through MCU. Contrary to the uncontrolled release of Ca^{2+} through mPTP, the controlled export of mitochondrial matrix Ca^{2+} relies on the mitochondrial $\text{Na}^+/\text{Ca}^{2+}$ exchangers (mNCX) (Palty et al., 2010) and mitochondrial $\text{H}^+/\text{Ca}^{2+}$ exchangers (mHCX) (Gunter and Pfeiffer, 1990). The downregulation of mNCX, indeed, has been shown to inhibit mitochondrial Ca^{2+} efflux, whereas its overexpression enhances Ca^{2+} clearance.

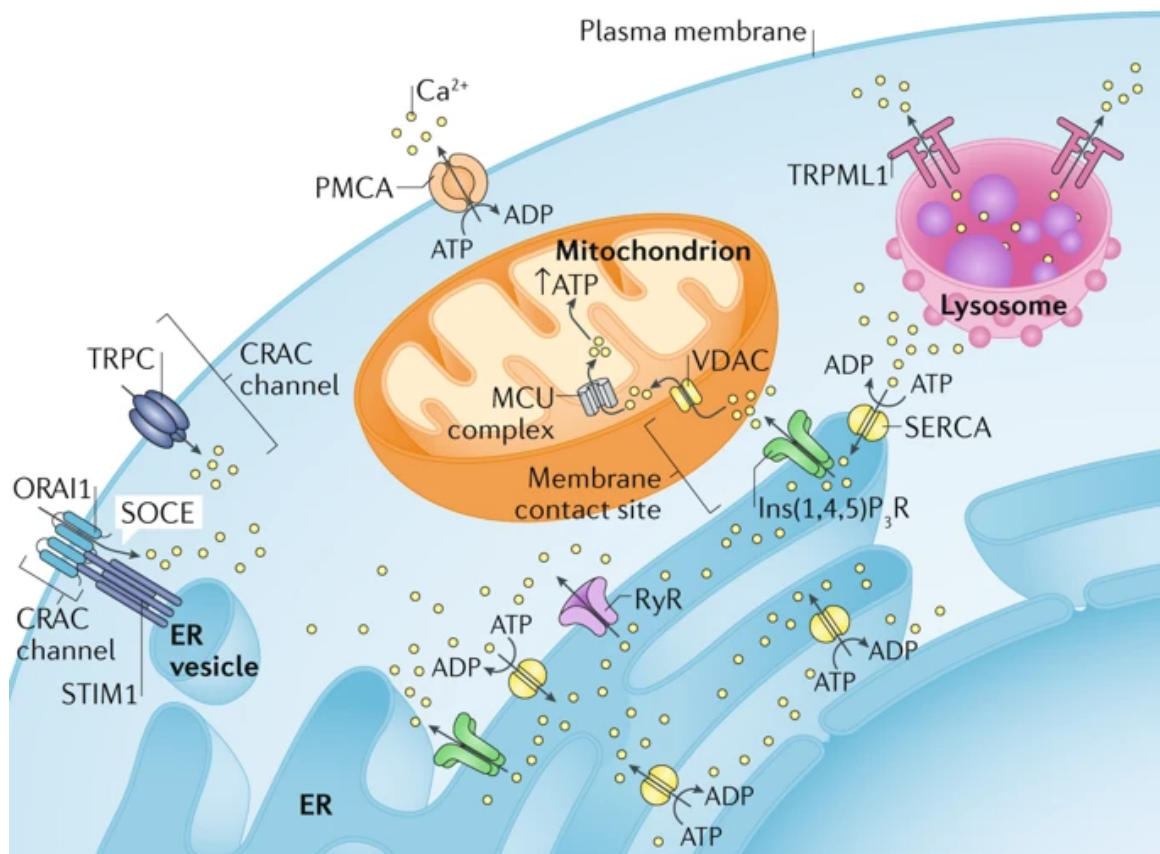


Figure 3.2: schematic representation of components involved in intracellular Ca^{2+} signalling. Ca^{2+} is imported into the cell via the CRAC channel and is transported in the ER lumen by the SERCA pumps. The release of Ca^{2+} from the ER occurs through two channels, the RyR and the IP3Rs. This last one is responsible for the transport of Ca^{2+} from the ER to the mitochondria at the ER-mitochondria contact sites, where Ca^{2+} is imported through VDAC1 in the OMM and MCUC in the IMM. Source: Giorgi et al., 2018.

3.2 The MCU complex

Table 3.1: Subunits forming the MCU complex.

Subunit	Function	Reference
MCU (Mitochondrial Calcium Uniporter)	Channel-forming subunit of the uniporter.	(Baughman et al., 2011; De Stefani et al., 2011)
MICU1 (Mitochondrial Calcium Uptake 1) <ul style="list-style-type: none"> MICU1.1 - splicing variant 	Contains EF-hands domains able to sense Ca^{2+} , regulates MCU opening.	(Perocchi et al., 2010; Vecellio Reane D, 2016)
MICU2 (Mitochondrial Calcium Uptake 2) <ul style="list-style-type: none"> MICU3 - paralog 	Contains EF-hands domains able to sense Ca^{2+} , regulates MCU opening.	(Plovanich, 2013; Patron et al., 2019)
EMRE (Essential MCU REgulator)	Required for the interaction of MCU with MICU1/MICU2 and for MCU stability.	(Sancak et al., 2013)
MCUb (Mitochondrial Calcium Uniporter b)	Paralog of MCU, negative regulator of the channel.	(Raffaello et al., 2013)
MCUR1 (Mitochondrial Calcium Uniporter Regulator 1)	Regulator of Ca^{2+} uptake? CIV assembly factor?	(Mallilankaraman et al., 2012)

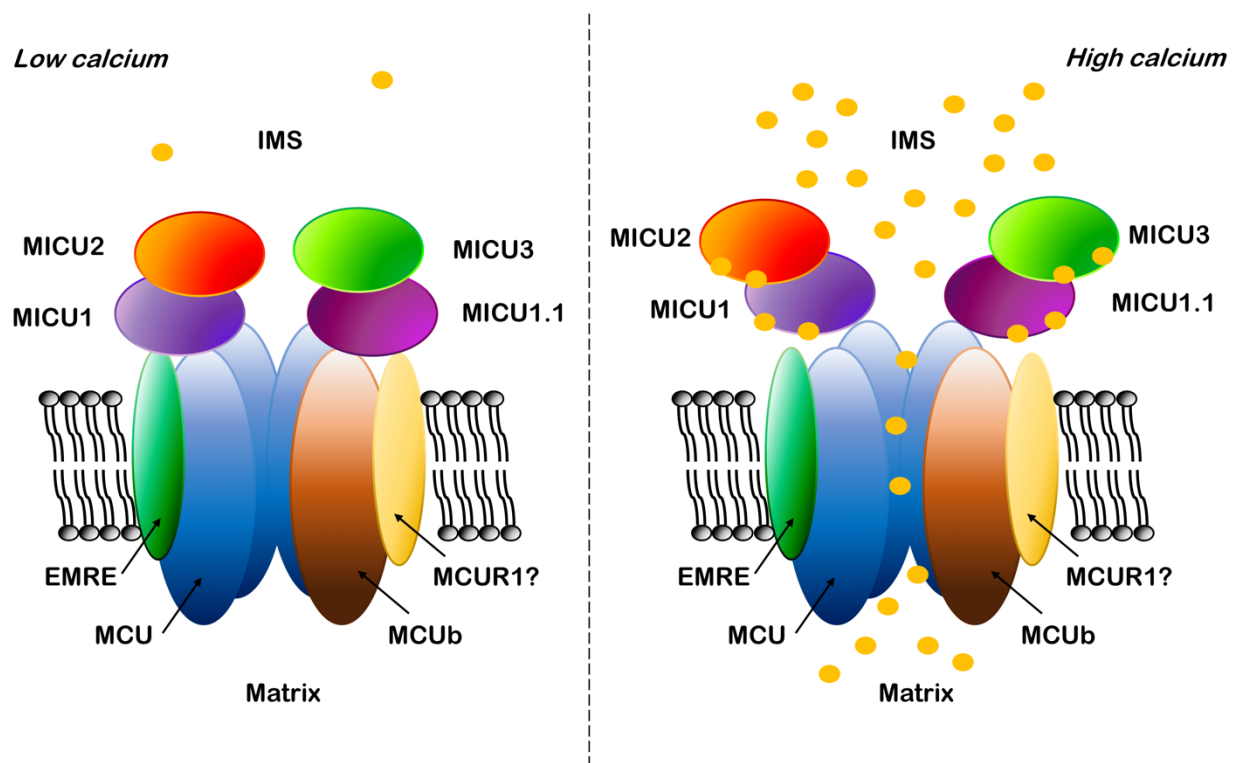


Figure 3.3: Cartoon representation of the mitochondrial calcium uniporter (MCU) complex subunits, in low and high Ca^{2+} conditions. MCU and MCB are the pore-forming subunits, together with the

essential mitochondrial Ca²⁺ uniporter regulator (EMRE). MICU1, MICU1.1, MICU2, and MICU3 face the intermembrane space and sense Ca²⁺ concentrations thanks to their EF-hand domains. MCU regulator 1 (MCUR1) is a potential member of the complex.

3.3 MCU

The first subunit of the mitochondrial calcium uniporter complex identified in 2010 was MICU1 (Perocchi et al., 2010), while only the following year two independent laboratories identified MCU as a 40 kDa IMM protein (previously known as CCDC109A (Pagliarini et al., 2008)) essential for Ca²⁺ uptake into mitochondria (Baughman et al., 2011; De Stefani et al., 2011). Indeed, the purified MCU protein showed channel activity in planar lipid bilayers in patch-clamp electrophysiology experiments (De Stefani et al., 2011). In addition, MCU overexpression or MCU silencing in both intact or permeabilised cells led to increased or decreased mitochondrial Ca²⁺ content, respectively (Baughman et al., 2011; Liu et al., 2020b).

MCU presents with a broad expression profile in all mammalian tissues and it has homologs in invertebrates and kinetoplastids, but not in the yeast *Saccharomyces cerevisiae* (Docampo and Lukes, 2012; Yamamoto et al., 2016). Each MCU subunit is composed of two transmembrane α -helices, which are highly conserved among different species, and both the N- and C- termini are localised within the matrix (Kamer and Mootha, 2015). The two α -helices are connected by a 9-aa linker with a four-residue “DIME” motif (or DXXE, based on its amino acid sequence) (Lee et al., 2015). The DIME motif facing the IMS is fundamental for MCU activity, since it is responsible for MCU ion selectivity filter (Cao et al., 2017) and for the interaction with MICU1 (Paillard et al., 2018; Patron, 2014).

Since every MCU subunit contains only two transmembrane domains, it has been suggested that the functional uniporter was composed by MCU oligomers. The first proposed model was a tetramer, in which eight helices form the putative pore, generating also a cluster of charged residues in the proximity of the pore that provides the negative electrostatic potential that favours the flux of positively charged ions (Raffaello et al., 2013). This architecture has been confirmed in X-ray and cryo-EM studies of the fungal and zebrafish uniporter (Baradaran et al., 2018; Fan et al., 2018; Yoo et al., 2018) and of the human MCU-EMRE complex (Wang, 2019) (Figure 3.4).

The structure of the single MCU subunit differs in different species (Wang et al., 2019). In particular, while the fungal protein is composed of only three structural domains, each human MCU subunit can be divided into four: the N-terminal domain (NTD), the linker helix domain (LHD) -absent in fungi-, the coiled-coil domain (CCD), and the transmembrane domain (TMD) (Figure 3.4). The NTD domain is important for the formation of MCU dimers, while the beginning of the second transmembrane domain, contains the DIME motif, which faces the intermembrane space (Baughman et al., 2011; Oxenoid et al., 2016).

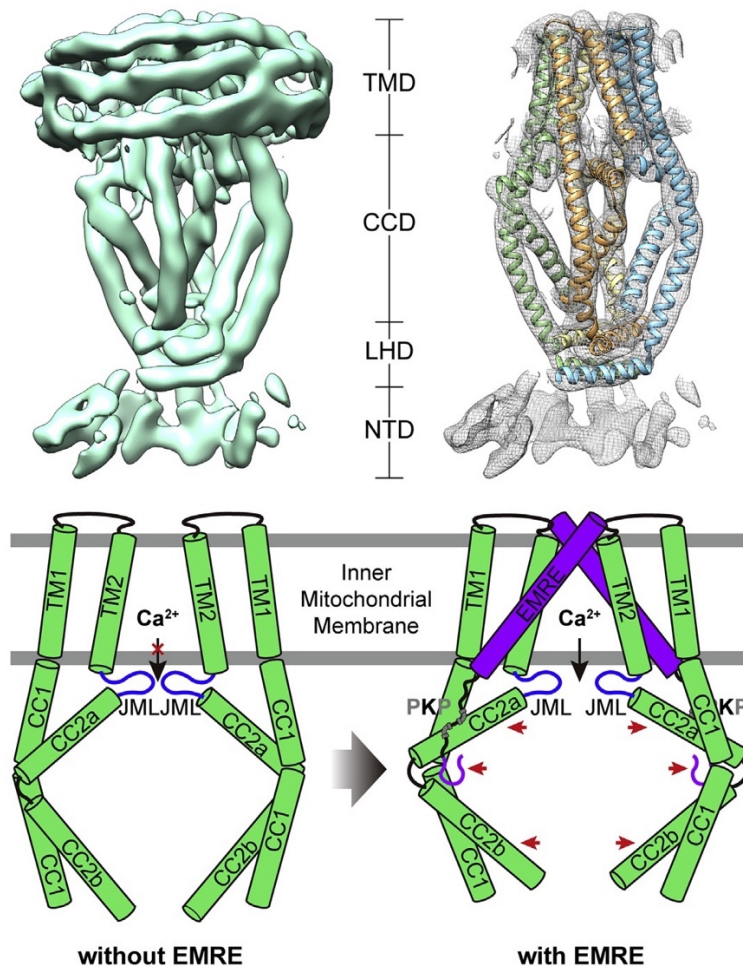


Figure 3.4: cryo-EM structure and model of the human MCU (7.7 Å) with helices from the TMD, CCD, LHD, and NTD modelled into the electron density. Source: Wang et al., 2019.

3.3.1 MCUB

MCU is not the only pore-forming unit of the MCU complex: MCU paralog gene (*CCDC109b*) encodes for a protein called MCUB, which acts as a negative regulator of the uniporter activity both in lipid bilayer experiments and in mammalian cells (Raffaello et al., 2013). It has been suggested that the role of MCUB is to interrupt the interaction between the MCU pore and the dimer MICU1/MICU2, altering the macromolecular assembly and stoichiometry of the complex subunits. Indeed, fast protein liquid (FPLC) size-exclusion chromatography in MCUB knockout cells showed an increase in high-molecular-weight complexes containing MCU, MICU1, and MICU2 (Lambert et al., 2019), while overexpression decreases the levels of MCU/MICUs complexes. These results are supported also by the discovery that MCUB does not interact directly with the MICUs proteins (Lambert et al., 2020).

However, this regulation mechanism does not seem to be conserved in every organism expressing MCUB. For example, in protozoa such as *Trypanosoma cruzi*, MCUB acts as a conducting subunit of the pore and its overexpression increases Ca^{2+} uptake (Chiurillo et al., 2017). Instead, in another trypanosomatid, *Trypanosoma brucei*, two more MCU isoforms are expressed, MCUC and MCUD, both positive regulators of the uniporter (Huang and Docampo, 2018).

In addition to differences between species, MCUB expression might change in different tissues. The amount of MCU-mediated Ca^{2+} uptake, indeed, varies between tissues and regulatory mechanisms such as the modulation of MCU but also MCUB levels might play a key role (Fieni et al., 2012). For example, MCUB is expressed at higher levels than MCU in lungs and heart, known to have lesser maximal Ca^{2+} uptake capacity, while it is strongly downregulated compared to MCU in skeletal muscles and liver, tissues which experience elevated calcium oscillations (Raffaello et al., 2013).

3.4 MICU1

MICU1 was the first identified subunit of the MCU complex (Perocchi et al., 2010). Since the identification of MCU itself was not known at the time, MICU1 was discovered through a

focused RNA interference (RNAi) strategy designed to identify mitochondrial proteins required for Ca^{2+} entry. The RNAi library was prepared following the observation that vertebrates and kinetoplastids show similar mitochondrial Ca^{2+} uniporter activity, while there is no evidence in the yeast *Saccharomyces cerevisiae* (Balcavage et al., 1973; Carafoli et al., 1971).

Further investigations showed that MICU1's main role is to work as a gatekeeper and keep the channel closed at low Ca^{2+} concentration, preventing a massive and toxic uncontrolled entrance of Ca^{2+} into the mitochondrial matrix. Indeed, in experiments conducted on cultured cells, and in knockout animals, loss of MICU1 leads to constitutive Ca^{2+} accumulation in the matrix through MCU, which results in increased sensitivity to mPTP opening and apoptosis, and to reduced ATP production (Csordás et al., 2013; Mallilankaraman et al., 2012). In high Ca^{2+} concentrations, instead, MICU1 functions as a positive regulator of the transporter activity, promoting the Ca^{2+} uptake.

MICU1 is a soluble IMS localised protein containing two canonical EF domains (EF1 and EF4), which bind Ca^{2+} and allow MICU1 to sense cytosolic Ca^{2+} concentration. EF domains are typical of a protein family known as EF-hand proteins, which includes nearly 600 members. These domains can both bind Ca^{2+} and regulate the protein through conformational change (Carafoli, 2002). The role of the MICU1 canonical EF domains has been examined by rescuing MICU1 knockdown (KD) cells by either reintroducing wild-type MICU1 or MICU1 with both the EF-hands mutated, which is stably expressed but unable to bind Ca^{2+} (Csordás et al., 2013). While the wild-type MICU1 was perfectly able to restore the normal Ca^{2+} dose-response curve, the mutated MICU1 was only able to re-establish the inhibition effect in low Ca^{2+} concentration. This result suggests that the physical presence of the protein itself is enough to restore the inhibition of MCU, which is lost in the KD, but the lack of Ca^{2+} binding ability affects the cooperative activation of the pore. MICU1 is, therefore, the modulator of the apparent Ca^{2+} affinity of the uniporter ($\sim K_D=10-20 \mu\text{M}$ under physiological conditions) (Mallilankaraman et al., 2012).

Another proposed function of MICU1 is to confer MCU selectivity for Ca^{2+} over Mn^{2+} . Indeed, MCU has been shown to be able to transport Mn^{2+} , since the DIME motif of the pore is not specific for calcium (Kamer et al., 2018). Moreover, mitochondrial uptake of Mn^{2+} shares many properties with Ca^{2+} uptake through MCU: it is sensitive to Ru360, a strong MCU inhibitor, it

is enhanced in the presence of phosphate, and it is dependent on mitochondrial membrane potential (Konji et al., 1985). Without selectivity, Mn^{2+} would compete with Ca^{2+} for the transport into the matrix, affecting the calcium signalling. The presence of MICU1 ensures the Ca^{2+} selectivity of MCU and prevents Mn^{2+} derived toxicity inside the organelle (Chance, 1966).

MICU1 crystal structures, both free and binding Ca^{2+} , were revealed using single-wavelength anomalous dispersion (SAD) at the resolution of 3.2 Å and 2.7 Å, respectively (Wang et al., 2014). Four domains were identified: the N-domain, the N-lobe, the C-lobe, and the C-helix (Figure 3.5). The N-domain of the protein is characterised by a poly-lysine domain, which potentially interacts with negatively-charged phospholipids and with EMRE. Indeed, EMRE possesses a highly conserved C-terminal polyaspartate tail, typically composed of one glutamate followed by 5–7 aspartates, which is negatively charged and complementary to the MICU1 positively charged polybasic sequence (KKKKR) (Tsai et al., 2016).

The two calcium-binding EF-hands localise in the N-lobe and in the C-lobe, together with two other helix-loop-helix structural units (referred to as pseudo-EF2 and pseudo-EF3) (Wang et al., 2014). The C-helix, instead, is necessary for the formation of MICU1 oligomers. Indeed, in the absence of Ca^{2+} , MICU1 exists predominantly as a hexamer, while it is able to generate various oligomeric forms in the presence of Ca^{2+} . Moreover, between the C-lobe and the C-helix a putative DIME interacting domain (DID) has been identified, required for both gatekeeping and cooperative activation of MCU. In this domain, two arginines (R440 and R443) have been proposed to form salt bridges with the D-ring of MCU, connecting the two subunits (Paillard et al., 2018).

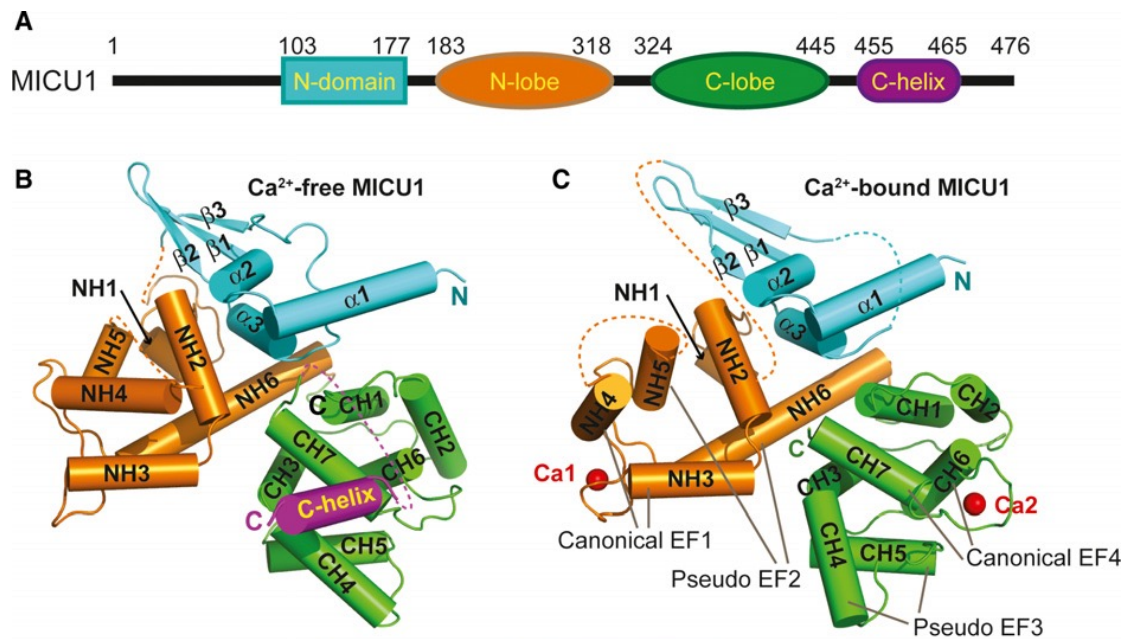


Figure 3.5: representation of the crystal structures of human MICU1. A) schematic drawing of the four domains of human MICU1: N-domain, N-lobe, C-lobe, C-helix. B, C) Cartoon representation of the overall structure of MICU1 in the Ca²⁺-free and the Ca²⁺-bound state. Source: Wang et al., 2014.

3.4.1 MICU1 localisation and cristae remodelling

Since its characterisation, MICU1 has been considered part of the MCU complex and involved exclusively in the regulation of Ca²⁺ uptake. However, in the last year, it was proposed an alternative -or possibly parallel- function of MICU1 at the IBM (Gottschalk et al., 2019). This study used super-resolution structured illumination microscopy (SIM) to sub-localise MICU1, MCU and EMRE in the mitochondrial cristae, under normal conditions and in the presence of Ca²⁺ stimuli. The authors showed that MICU1 is exclusively localised in the non-cristae structure of the IMM, the IBM, both in the presence and in the absence of Ca²⁺. MCU and EMRE, instead, are normally localised in the cristae and are recruited to the IBM only under Ca²⁺ stimulation, in a MICU1-dependent manner. In addition, this study also revealed that MICU1 can regulate cristae junctions (CJ) stability. Indeed, MICU1 knockdown leads to widening of the CJ by ~58%, mitochondrial depolarization, and sensitivity to stress-induced cytochrome *c* release, a phenotype similar to OPA1 depletion (Frezza et al., 2006). A second study, currently in preprint, confirmed these finding and showed that MICU1, but not MCU, interacts with the MICOS subunit MIC60 and with coiled-coil-helix-coiled-coil helix domain

containing 2 (CHCHD2) (Meng et al., 2017), both present at the IBM and involved in cristae remodelling (Tomar et al., 2019).

Moreover, Gottschalk and colleagues suggested that the C-helix domain and the formation of MICU1 oligomers are responsible for the IBM localisation (Gottschalk et al., 2019). Indeed, the truncated Δ C-MICU1 construct they generated, which does not form multimers, is able to localise at the IBM only in the presence of endogenous MICU1, while it distributes through the entire IMM in cells depleted of endogenous MICU1.

3.4.2 MICU1.1

As introduced previously, signalling pathways in different cell types have different needs in terms of Ca^{2+} concentrations. For example, in skeletal muscle the consumption of oxygen needs to increase dramatically to allow maximal aerobic exercise, while the cytosolic ATP free energy must be maintained constant in order to preserve the normal cellular functions (Glancy et al., 2013). It has been proposed that Ca^{2+} can play a critical role in this process, leading to the highest mitochondrial Ca^{2+} transients in skeletal muscle compared to other tissues (Fieni et al., 2012). This led to the discovery in this tissue of a MICU1 splicing variant, called MICU1.1 (Vecellio Reane et al., 2016). This isoform is characterised by the addition of a micro-exon coding for four amino acids. The variant is able to dimerise with MICU2 and has similar behaviour to the canonical MICU1 concerning the ability to inhibit Ca^{2+} uptake at low Ca^{2+} concentrations. However, its sensitivity to Ca^{2+} is one order of magnitude higher, allowing the activation of the uniporter at lower Ca^{2+} concentrations in the IMS. As a consequence, in skeletal muscle the activation of MCU by the dimer MICU1.1-MICU2 leads to an increased Ca^{2+} entry into mitochondria compared to MICU1-MICU2 after stimulation, allowing mitochondria to respond to high energy demands.

3.5 MICU2

MICU2 is a paralog of MICU1, sharing with it 25% of the AA sequence, and also contains two canonical EF-hands separated by a long stretch of residues predicted to form α -helices

(Plovanich, 2013). As for MICU1, EF-motifs in MICU2 are strongly conserved across evolution and play a crucial role in Ca²⁺ sensing.

The X-ray structure of the unbound form of *Mus musculus* MICU2 has been recently produced at 2.5-Å resolution (Kamer et al., 2019). The central part of the protein shares the same structure observed in MICU1: two lobes, each containing one canonical Ca²⁺-binding EF-hand (EF1, EF4) and one structural or pseudo-EF-hand (EF2, EF3). The extremities of the two subunits, instead, differ partially: the N-domain of MICU2 is less extensive and more integrated with the N-lobe, compared to MICU1, missing the highly charged poly-lysine domain that allows the interaction with EMRE (Hoffman et al., 2013). The C-helix, instead, is longer and extends away from the core of the protein. This domain does not seem to be necessary *in vitro* to form the MICU1/MICU2 complex, however, it is required for MICU2's function in cells (Kamer et al., 2019).

Through its interaction with MICU1, MICU2 acts as Ca²⁺ sensor and MCU gatekeeper, preventing Ca²⁺ uptake under resting conditions and allowing it at high cytosolic Ca²⁺ concentrations. However, the mechanism through which MICU2 regulates MICU1 gatekeeper activity has been intensely debated. A possible explanation was found studying the MICU1-MICU2 dimer and the effects of silencing these two subunits on mitochondrial Ca²⁺ modulation, as discussed in the next section.

3.5.1 MICU1-MICU2 dimer

MICU1 and MICU2 have been shown to form a ~96 kDa dimer, binding covalently through disulphide bridges (Patron et al., 2014). However, the specific function of each of the two subunits is still debated. The functional studies of the MICU proteins are made more difficult since modulation of the expression levels of one of the two components has different effects on the other half. MICU1 has been shown to regulate MICU2 steady-state levels, causing a reduction of the protein expression in MICU1 knockout and an increase after overexpression. On the other side, the downregulation of MICU2 does not consistently affect MICU1 expression (Plovanich et al., 2013). Indeed, MICU1 can bind MCU in the absence of MICU2, while the opposite is not possible (Kamer et al., 2014; Patron et al., 2014). As a consequence, the silencing of MICU1 affects indirectly MICU2, making the data interpretation challenging.

Mootha's group proposed a similar negative activity of MICU1 and MICU2 on MCU opening (Kamer et al., 2014). In this scenario, the absence of MICU1 (and therefore of MICU2) should lead to an increased Ca^{2+} influx in the matrix, while the downregulation of MICU2 alone still allows MICU1 to operate a certain inhibition on the transporter. On the other side, Rizzuto's group claimed that the two proteins have an opposite effect on MCU (Patron et al., 2014). According to their model, MICU2 is the real inhibitor of the pore, while MICU1 would act as an MCU activator. In this case, both downregulating MICU2 directly or indirectly through MICU1 silencing, mitochondrial Ca^{2+} gatekeeping is abolished leading to increased Ca^{2+} import.

Another observation reported in support of this model is that MICU1 overexpression clearly shows a stimulation of mitochondrial calcium uptake (Patron et al., 2014). However, contrary to MICU2, MICU1 has a strong preference for forming homodimers when in excess, which leads to a shift in the equilibrium from the canonical heterodimer to MICU1-MICU1 complexes in models overexpressing MICU1 or downregulating MICU2. The recent resolution of the crystal structures of the MICU1-MICU2 heterodimer and of the MICU1 homodimer (Park et al., 2020) suggests that the MICU1-MICU2 heterodimer has a lower Ca^{2+} binding affinity ($K_d = 620 \text{ nM}$) compared with that of the MICU1 homodimer ($K_d \approx 300 \text{ nM}$). MICU1 homodimer prevalence, therefore, would increase the Ca^{2+} uptake, explaining why in Patron et al. study, silencing MICU1 or MICU2, or overexpressing MICU1, all lead to higher mitochondrial Ca^{2+} measurements in intact HeLa cells (Figure 3.6).

Finally, another recent study addressed the question of MICU1 and MICU2 individual functions in the MCUC and suggested that the activation of mitochondrial Ca^{2+} uptake can have two different components, one transient and one permanent, which are differently affected by the knockdown of MICU1 or MICU2 (Matesanz-Isabel et al., 2016). Indeed, it showed that in the absence of MICU2, MCU uptakes Ca^{2+} in a persistent way, while the knockdown of MICU1 triggers both a transient and a persistent response. The transient uptake would be MICU1-dependent, while the persistent component would be an indirect effect of the simultaneous loss of MICU2. This study concludes that the two proteins have similar roles and cooperate in keeping MCU closed at low Ca^{2+} concentrations and setting the threshold of MCU activation.

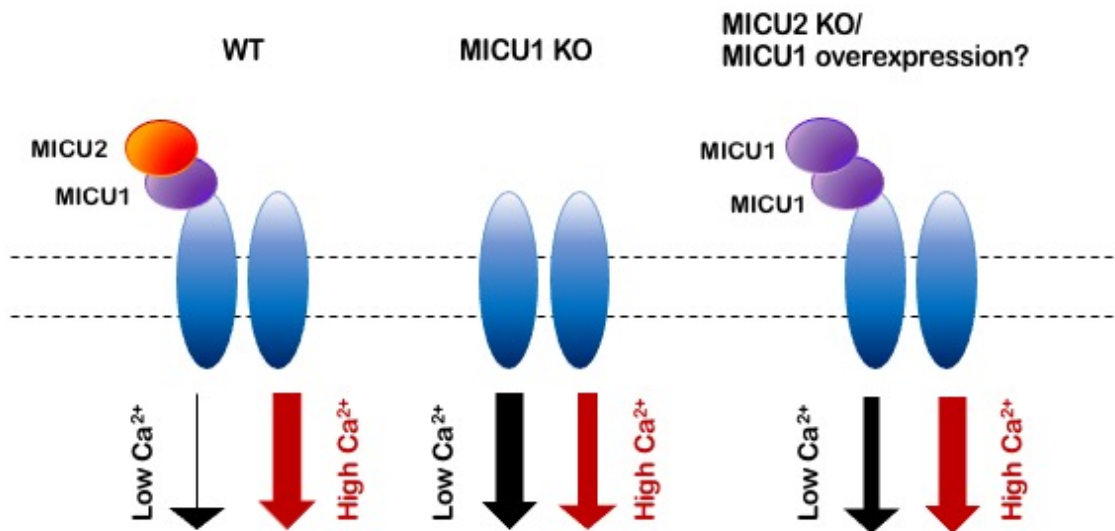


Figure 3.6: proposed kinetics of the mitochondrial Ca^{2+} uptake in normal conditions versus models downregulating MICU1 or MICU2 or overexpressing MICU1. In physiological conditions, the heterodimer MICU1-MICU2 is formed and prevents the entry of Ca^{2+} into mitochondrial matrix at low cytosolic concentrations, while it allows the opening of the uniporter at high levels. In the absence of MICU1 -and consequently MICU2- Ca^{2+} is constantly transported and leads to overload. Contrarily, MICU2 removal and the consequent formation of MICU1 homodimers, is responsible for persistent increase in mitochondrial Ca^{2+} uptake at high cytosolic Ca^{2+} concentrations and to lowering of the threshold necessary for MCU pore opening.

3.5.2 MICU1-MICU2 dimer assembly and interaction with MCU

The process of dimerization of MICU1 and MICU2 and their interaction with the rest of the MCU complex has been only recently explored. It has been observed that MICU1 interacts with Mia40 in the IMS, a chaperone involved in the import and folding of mitochondrial proteins containing a CxxC motif (Chacinska et al., 2004) and that Mia40 mediates the dimerization between MICU1 and MICU2 (Petrungaro et al., 2015). The only cysteine conserved in MICU1 and thought to be responsible for both the disulphide bonds with MICU2 and Mia40 is Cys463 (Patron et al., 2014). This cysteine is localised in an alpha-helix and is surrounded by hydrophobic residues, a typical motif found in other Mia40 substrates (Koch and Schmid, 2014; Milenkovic et al., 2009; Sideris et al., 2009). Interestingly, although MICU1 and MICU2 have a high sequence similarity, MICU2 does not contain this recognition motif and is not able to bind Mia40 (Petrungaro et al., 2015).

Riemer's group, however, observed that in the absence of Cys463, MICU1 can still bind MCU, suggesting that the first interaction MICU1 forms after the import is with MCU, followed by the link to Mia40, which allows the dimerization with MICU2, while MICU1 is still linked to the pore subunit (Petrungaro et al., 2015). Once the complex is mature, the interaction between MCU and the dimer is regulated by the Ca^{2+} levels. Indeed, different levels of Ca^{2+} might affect the conformation of the dimer, so that at low Ca^{2+} , it interacts with MCU, while this bond is lost at high Ca^{2+} concentrations, allowing Ca^{2+} uptake through the uniporter. This property has been demonstrated by showing that with the increase of Ca^{2+} concentrations, the amount of MICU1-MICU2 dimer co-immunoprecipitated with MCU decreases proportionally (Petrungaro et al., 2015). It is not clear yet how the re-recruitment of the dimer works when the concentration of Ca^{2+} drops and the transporter must be closed again. It has been suggested a role of EMRE in this context, but no experimental data is currently available. This model is supported also by the observation that MCU has a longer half-life than MICU1, suggesting that MICU1 and MICU2 can be exchanged more frequently than the intramembrane components of the pore, without affecting the transporter stability.

Moreover, a study on the crystal structure of human MICU2 investigated more in details the MICU1-MICU2 interaction in low and high Ca^{2+} concentrations (Wu et al., 2019). The Ca^{2+} binding to the MICU1 and MICU2 EF-hands provokes a conformational change, where MICU2 pulls MICU1 in a tighter complex, causing the loss of direct interactions with the D-ring of MCU. In this scenario, EMRE would maintain its interaction with the MICU1-MICU2 dimer, keeping it at the opening of the pore and preventing its free diffusion in the intermembrane space.

However, this model contrasts with the proposed localisation of MICU1 at the IBM and the recruitment of MCU only during Ca^{2+} spikes (Gottschalk et al., 2019). Assuming that both models are correct, the only explanation could be two separate sub-populations of MICU1, with different functions in the mitochondria, one interacting with the CJ proteins and one dimerising with MICU2.

3.6 MICU3

MICU3, paralog of MICU2, was found expressed predominantly in skeletal muscle and the central nervous system (Plovanich et al., 2013). In particular, the silencing of MICU3 in primary cortical neurons leads to impairment in the synaptic activity, suggesting a specific role in the modulation of neuronal excitability (Patron et al., 2019). MICU3 interactions with the rest of the MCU complex have been recently studied in HeLa cells, which do not express it in physiological conditions (Patron et al., 2019). This study showed that MICU3 can bind MICU1, but not MICU2, and that it is able to mediate a more rapid response to Ca^{2+} fluctuations, essential in excitable cells.

3.7 EMRE

EMRE (essential MCU regulator) is a 10 kDa single-pass transmembrane protein, identified by Mootha's group through a SILAC/mass spectrometry-based proteomic approach using MCU-FLAG as a bait (Sancak et al., 2013). EMRE and MCU are the minimal pore unit allowing Ca^{2+} entry, as shown by reconstructing the different components of the complex in yeast (Kovacs-Bogdan et al., 2014). In addition, silencing of EMRE in cell cultures leads to a similar effect observed with the loss of MCU, causing a reduced Ca^{2+} uptake (Sancak et al., 2013).

EMRE interacts with MICU1 in the IMS and with MCU oligomers in the inner membrane, therefore one of the first hypotheses was that it might bridge the interaction between the pore and the MICU proteins. However, EMRE is present only in metazoans, while it is not found in plants, fungi, or protozoa, where MCU and MICU1 are still expressed and are able to assemble in a functional complex (Bick et al., 2012; Sancak et al., 2013). Another suggested function was the regulation of MCU sensitivity to matrix Ca^{2+} (Vais et al., 2016). According to this model, MCU would need Ca^{2+} sensors on both sides of the IMM, MICUs proteins facing the IMS and EMRE facing the matrix. This hypothesis, however, has been challenged by other studies that focused on the structure and the topology of EMRE (Tsai et al., 2016; Yamamoto et al., 2016). Indeed, while Vais and colleagues proposed that the C-terminal tail of the protein should be involved in sensing of matrix Ca^{2+} , additional observations demonstrated that the

short N-terminus is actually exposed to the matrix, while its acidic C-terminus faces the IMS, where it interacts with MICU1 (Yamamoto et al., 2016).

Another interesting aspect of the EMRE-MCU interaction is the importance of the correct stoichiometry between the two proteins. Overexpression of EMRE by inhibition of its degradation pathway (Konig et al., 2016) or by expression of proteolytic-resistant EMRE constructs (Vais et al., 2016), leads to uncontrolled MCU channel opening and Ca^{2+} overload. For this reason, EMRE steady-state levels are strictly regulated and dependent on MCU levels, while the opposite is not true.

3.8 MCUR1

The last subunit that has been proposed being part of the MCU complex is the mitochondrial Ca^{2+} uniporter regulator 1 (MCUR1). MCUR1 is a coiled-coil-containing integral inner membrane protein encoded by the *CCDC90A* gene, identified by an RNAi screen for proteins involved in MCU activity (Mallilankaraman et al., 2012). Indeed, the silencing of MCUR1 reduces Ca^{2+} uptake and affects oxidative phosphorylation and ATP production, leading to AMP kinase-dependent autophagy.

However, these results have been challenged and MCUR1 has been suggested to act as a CIV assembly factor instead, and to cause defects in Ca^{2+} uptake only indirectly (Paupe et al., 2015). Indeed, the silencing of MCUR1 provokes a CIV assembly defect and consequent reduction in mitochondrial respiration and mitochondrial membrane potential. MCU activity depends on membrane potential, explaining the reduced Ca^{2+} import. This idea is supported by two other observations: firstly, MCUR1 was not found associated with the MCU complex in proteomic analysis, suggesting it might play a role outside of the uniport complex (Sancak et al., 2013), and secondly an MCUR1 orthologue is present in budding yeast, which lacks MCU (Sickmann et al., 2003).

Nevertheless, more recent studies in conditional knockout mouse models reported that MCUR1 is required for efficient MCU activity and proposed a third possible role, showing that MCUR1 binds to MCU and EMRE and functions as an ‘MCU assembly factor’ (Tomar et al., 2016). In particular, the formation of higher-order oligomeric MCU, or MCU-containing

supercomplexes, seems to depend on the presence of MCUR1, while it is not affected by the silencing of other MCUC subunits, such as MICU1.

3.9 Animal models

3.9.1 Evolutionary conservation of MCUC proteins

Homologues of MCU have been identified in a variety of organisms, including plants and metazoans, while it is absent in certain protozoan and fungal lineages (Bick et al., 2012; Liu et al., 2017). The existence of organisms lacking any uniporter shows that MCU structure or activity is not fundamental for mitochondrial integrity or function and that other systems involved in Ca^{2+} trafficking might be present.

Similarly, MICU1 is present in most organisms, with the exception of *Neurospora crassa* (Bick et al., 2012), while MICU2 is less evolutionarily conserved. In particular, it does not exist in two models used in research: *Drosophila melanogaster* and *Arabidopsis Thaliana*. In this last case, MICU1 has three EF-hands instead of two, perhaps incorporating MICU1 and MICU2 function within a single protein. Finally, EMRE is specific for metazoans (Sancak et al., 2013). In order to better understand the functions and the characteristics of each subunit of the MCUC, many animal models have been generated.

3.9.2 MCUC animal models

The effects of MCU silencing or knockout on living organisms have been studied in a variety of models. In *Trypanosoma brucei*, belonging to a group of parasites, for example, the KD of *TbMCU* by RNA interference or by conditional knockout led to a strong decrease in mitochondrial Ca^{2+} import without affecting membrane potential, and marked growth defects *in vitro* and reduced infectivity *in vivo* (Huang et al., 2013). The KO of *mcu1*, the *C. elegans* ortholog of MCU, led to impairment in mitochondrial Ca^{2+} uptake after wounding and alterations in tissue repair (Xu and Chisholm, 2014). In addition, an MCU knockdown zebrafish model showed that MCU is involved in the control of embryonic cell movements, since embryos lacking this protein displayed blastomer migration defects leading to alterations in the anteroposterior axis formation (Prudent et al., 2013).

However, the two main organisms used to study MCUC are the *Drosophila melanogaster* and murine models.

3.9.3 *Drosophila melanogaster*

The first time that MCU and MICU1 were genetically manipulated in *Drosophila melanogaster* was during a screen, which identified them as possible candidate genes that could affect the animal memory when silenced (Walkinshaw et al., 2015). Following this study, an MCU knockdown *Drosophila* line was generated, demonstrating its viability and confirming the impaired memory formation, without impacting the learning capacity of the flies (Drago and Davis, 2016). Another group started working on the biochemical consequences of MCU loss-of-function in *Drosophila*, discovering that this model did not show significant changes in body weight, metabolism, and autophagic flux compared with control flies (Choi et al., 2017).

A more recent study reported a genetic characterisation of all the MCUC subunits conserved in *Drosophila* (Tufi et al., 2019). The first model generated is an *MCU* null mutant incapable of rapid Ca^{2+} uptake buffering. These flies showed a modest reduction in ATP levels and in CI and CII-linked respiration. However, mitochondrial morphology and axonal transport were not affected, resulting in a mild phenotype at the organismal level. The second knockout produced was *EMRE*. This model was also viable, and presented an even milder phenotype than *MCU*, a part of being characterised by a shortened lifespan. In contrast, *MICU1* KO was found to be larval lethal. Not being able to analyse the adult, only data concerning the larvae are available, showing a substantial mitochondrial impairment and significantly reduced axonal transport. Finally, since *MICU2* ortholog is absent in flies, *MICU3*, which is conserved and expressed in neuronal tissue, was assessed. This knockout model slightly affects the animal lifespan and leads to neuro-motorial defects.

3.9.4 Mouse

The first full-body *MCU* mouse model was generated in 2013 by the Finkel's group (Pan et al., 2013). As observed in the fly model, this mouse showed a particularly mild phenotype, even with a clear defect in Ca^{2+} uptake into the mitochondria, presenting only with slightly

smaller size and modest defects in skeletal muscle strength. A similar observation was described two years before, when no significant difference in weight or organ pathology was detected following continuous MCU silencing via short interfering RNA (shRNA) in mouse liver (Baughman et al., 2011).

Two other important evidences came from Pan et al. study. Firstly, even if mitochondrial matrix Ca^{2+} in MCU KO mice was strongly reduced, it was not completely inhibited. Indeed, mutant animals showed about 25% of control levels, suggesting an alternative mechanism for Ca^{2+} entry. One possible explanation of this phenomenon is that, in the absence of MCU, the other mitochondrial calcium exchangers, in particular the $\text{Na}^+/\text{Ca}^{2+}$ exchanger, might work in the opposite direction, allowing the entrance of Ca^{2+} in the matrix in high cytosolic Ca^{2+} conditions (Murphy et al., 2014; Samanta et al., 2018). These compensatory systems are probably slower and less efficient than MCU, but might be sufficient in non-stress conditions. During exercise, instead, these mutant mice showed a significant decrease in the muscle capacity. Besides, other routes of Ca^{2+} entry into mitochondria have been hypothesised, after the identification through patch-clamp experiments in mitoplasts isolated from HeLa cells of Ca^{2+} currents independent from the presence of MCU protein (Bondarenko et al., 2014).

Secondly, MCU KO does not seem to affect cell death. The KO of MCU, indeed, did not give protection from cell death through the inhibition of Ca^{2+} -induced mPTP opening as expected. On one side, it is possible that mPTP-independent modes of death are upregulated in the KO mutants. On the other, mPTP might be triggered by MCU-independent pathways. Indeed, it has been reported that mPTP opening might take place in yeast as well, which do not express an MCU equivalent (Jung et al., 1997).

Afterward, conditional KO mouse models of MCU were generated, allowing the acute KO of the gene in specific tissues by Cre-mediated methods (Kwong et al., 2015; Luongo et al., 2015). Two groups focused on cardiac tissues in order to study how acute mitochondrial Ca^{2+} uptake impacts cardiac physiology. In these models, cells showed greater resistance to Ca^{2+} overload and decrease susceptibility to mPTP activation. The evident contradictions between models have not been clearly explained yet. They might be due to the methodologies used or to different cellular responses due to the different timing and duration of MCU deletion, since in the first case MCU is absent during the whole development phase, which could lead to

unknown adaptation mechanisms, while in the second model is mainly an acute effect (Liu et al., 2017).

On the contrary, manipulation of MICU1 is more challenging. The first attempts of MICU1 KO mice generation resulted in complete perinatal lethality shortly after birth (Antony et al., 2016). A second attempt in a different genetic background resulted in high but not total postnatal lethality (Liu et al., 2016). These mice presented with severe pathological phenotypes, including mitochondrial morphology alterations, decreased muscle ATP levels, elevated serum lactate, and neurological features such as ataxia. These defects are the consequence of increased Ca^{2+} uptake at low concentrations leading to Ca^{2+} overload in the matrix. Interestingly, this phenotype was rescued by the KO of EMRE on one allele, which affects MCU structure and ability to uptake Ca^{2+} . It suggests that the relative expression of the MCUC subunits could have important *in vivo* consequences on Ca^{2+} transport.

Following this analysis, an EMRE KO mouse was generated, confirming that, lacking EMRE, mitochondria are unable to rapidly uptake Ca^{2+} (Liu et al., 2020a). Although these mice are born less frequently, they seem to have normal basal metabolism and not significantly impaired exercise capacity, providing a similar picture to what is observed in the MCU model.

Taken these data together, it is possible to summarise that the lack of subunits forming the main structure of the pore, MCU and EMRE, do not induce strong pathological phenotypes in flies and mice. On one side, reduced Ca^{2+} uptake is less toxic than Ca^{2+} overload and shows effects mainly in stress conditions; on the other, compensatory mechanisms are probably available in order to maintain a basal level of Ca^{2+} import. On the contrary, MICU1 deficiency causes Ca^{2+} overload, impacting severely the organism.

3.10 Pathologies associated with MCU complex defects

Loss-of-function homozygous mutations in MICU1 have been observed in different cohorts of patients (Lewis-Smith et al., 2016; Logan et al., 2014; Musa et al., 2019). As expected, the loss of MICU1 results in increased mitochondrial Ca^{2+} load in patients' fibroblasts, both at basal cytosolic Ca^{2+} levels and after low-frequency and transient increases in concentrations. The

resulting pathological phenotype is characterised by early-onset proximal muscle weakness, fatigue, lethargy, elevated serum creatine kinase levels, learning difficulties, and a variety of motor signs, such as chorea, tremor, dystonic posturing and orofacial dyskinesia. Additional neurological features, typical of mitochondrial diseases, have been reported, including ataxia, microcephaly, ophthalmoplegia, ptosis, optic atrophy and axonal peripheral neuropathy. Interestingly, studies conducted on patient fibroblasts did not reveal significant OXPHOS defects or alterations in membrane potential, but highlighted a fragmented mitochondrial network (Bhosale et al., 2017).

Only two human patients with MICU2 deficiency have been described so far (Shamseldin et al., 2017). These siblings are characterised by delayed cognitive development, severe intellectual disability and severe attention deficit hyperactivity disorder (ADHD). Interestingly, compared to MICU1 patients, MICU2 mutations do not result in evident muscular and movement disorders. The analysis performed on these patients' fibroblasts showed that, similarly to MICU1 patients, MICU2 loss-of-function leads to Ca^{2+} overload during resting states, but they show significant slowing of Ca^{2+} influx in response to stimuli. Moreover, MICU2 patient fibroblasts present increased sensitivity to oxidative stress and altered membrane potential. For both MICU1 and MICU2 patients, a compensatory activity of sodium-calcium exchanger (NLCXm) has been proposed (Bhosale et al., 2017). The continuous mitochondrial Ca^{2+} influx might be balanced by Ca^{2+} efflux through the NLCXm. However, the increased -and futile- activity of the $\text{Na}^+/\text{Ca}^{2+}$ exchanger could trigger an abnormal activity of the Na^+/H^+ transporter as well, resulting in matrix proton overload, which would undermine the PMF and ATP synthesis, resulting in energy loss and affecting high-energy-demand tissues. The molecular mechanisms behind the consequences of MICU1 and MICU2 mutations on patients, however, remain unclear.

Patients carrying pathological mutations in MICU3, EMRE and MCUR1 have not been described yet. Similarly, no cases of patients with typical mitochondrial disease phenotype have been associated with mutation in MCU. This is not surprising, considering that the mouse and fly models lacking MCU does not show evident phenotypes. However, the MCU complex might have relevance in other pathologies, due to its potential role in mediating cell death. For example, alteration in MCU and MICU1 levels has been observed in a majority of cancer tissues, such as colorectal, ovarian, pancreatic, stomach, and prostate cancer, while MICU2 seems to be upregulated in thyroid, prostate and breast cancer, and MCUb was found in most

colorectal cancers and in breast, cervical, and ovarian cancers (Ren et al., 2017; Vultur et al., 2018; Wiel et al., 2014; Yu et al., 2017). Another group of pathologies where Ca^{2+} regulation and MCU might have an important impact is neurodegenerative disorders such as ALS, multiple sclerosis, Alzheimer's disease, and Parkinson's disease. Indeed, Ca^{2+} overload and consequent mPTP opening has been considered key in neuronal cells death (Kalani et al., 2018).

3.11 OXPHOS and calcium

Calcium release from the ER stores and uptake in the mitochondrial matrix are involved in the regulation of oxidative phosphorylation and energy production. Different mechanisms have been proposed to explain the modulation of mitochondrial respiration by Ca^{2+} . Matrix Ca^{2+} has long been known for being responsible for the activation of pyruvate, isocitrate, and 2-oxoglutarate dehydrogenases, three Krebs cycle dehydrogenases (Denton, 2009). However, many aspects of the molecular mechanisms involved in the dehydrogenases activations still have to be explained. Firstly, it has been speculated that these enzymes should contain an EF-hand domain in order to bind the Ca^{2+} ions, but the analysis of the sequences of NAD-isocitrate dehydrogenase and oxoglutarate dehydrogenase did not show a putative Ca^{2+} binding site (Nichols and Denton, 1995). Secondly, the three dehydrogenases do not seem to share the same molecular basis of Ca^{2+} binding. For example, isocitrate dehydrogenase requires the presence of isocitrate, adenine and magnesium ions, while oxoglutarate dehydrogenase does not need additional ligands (Rutter and Denton, 1989). Moreover, there are differences in the level of Ca^{2+} necessary to activate the enzymes: in conditions of low ATP/ADP ratios oxoglutarate dehydrogenase is more sensitive to Ca^{2+} fluctuations, followed closely by pyruvate dehydrogenase and finally NAD-isocitrate dehydrogenase. This suggests a hierarchy in the activation of different steps of the cycle.

In addition, Ca^{2+} might have a role regulating other mitochondrial proteins, such as transporters. For example, the malate-aspartate shuttle contains a cytosolic EF domain and is regulated by extramitochondrial Ca^{2+} (Palmieri et al., 2001). Moreover, the ATP- $\text{Mg}^{2+}/\text{P}_i$ transporter (SCaMC1) is also stimulated by extramitochondrial Ca^{2+} (Traba et al., 2012). The

increased availability of substrates might have an additional role in the activation of mitochondrial respiration.

More recent analysis highlighted other effects of Ca^{2+} on complexes of the OXPHOS machinery. The F_1F_0 ATP synthase, for example, could be directly stimulated by Ca^{2+} ions (Territo et al., 2000). This study, however, was conducted on isolated porcine heart mitochondria and does not take into account the possible additional action of Ca^{2+} on the transport of OXPHOS substrates, such as glutamate (Gellerich et al., 2010).

Another electron transport chain complex that has been proposed to be modulated by Ca^{2+} is CIII (Murphy et al., 1990). Indeed, it has been shown in rat isolated mitochondria that Ca^{2+} stimulation leads to increase respiration when using succinate or durohydroquinone as substrate, but not in the presence of ascorbate and TMPD, which donate electrons to cytochrome *c* and subsequently to CIV, bypassing CIII. They concluded that a Ca^{2+} -sensitive site must be present in the electron transport chain within the span of ubiquinone through the cytochrome *b-c1* complex to cytochrome *c*. However, these data have never been confirmed by follow-up studies and deeper analysis of the complex structure never identified Ca^{2+} binding sites, while other metal such as zinc are known to bind and inhibit CIII (Berry et al., 2000).

Finally, numerous studies suggested a direct or indirect action of Ca^{2+} on CIV activity. A first hypothesis is that CIV activity can be modulated through phosphorylation and that the pathway controlling this post-translational modification might be the cAMP-dependent protein kinases. Many phosphorylation sites have been identified by mass spectrometry and crystal structure analysis in several CIV proteins: Tyr-218 in MTCO2, Ser-1 in COX5a, Ser-2 in COX5b, Ser-1 in COX7c (Helling et al., 2012), Tyr-304, Ser115 and Ser116 in MTCO1 (Fang et al., 2007; Lee et al., 2005) and Ser34, Ser67, Ser136 and Thr52 in COX4-1 (Fang et al., 2007; Olsen et al., 2010; Steenaart and Shore, 1997). According to this model, CIV is inhibited by cAMP-dependent phosphorylation by protein kinase A (PKA), which can decrease both the maximal velocity (V_{max}) of the enzyme and its affinity for cytochrome *c*, while bursts of calcium would activate Ca^{2+} -dependent phosphatase that can reverse this effect (Bender and Kadenbach, 2000). However, very large concentrations of Ca^{2+} ($> 100 \mu\text{M}$) seem to be required for the dephosphorylation of the complex and no effect was measured on the activity of the isolated enzyme (Lee et al., 2002). These data suggest that this process might take place only in extreme situations and might not be relevant in physiological conditions.

The second hypothesis is that Ca^{2+} might bind CIV directly and modulate its activity. It has been proposed that CIV contains a cation binding site, which is able to bind Ca^{2+} and Na^+ . The site is located in MTCO1, facing the IMS (Vygodina et al., 2013). Unfortunately, the crystal structure of CIV is available only for the Na^+ -bound form, and there is no direct evidence of Ca^{2+} binding. However, this might be due to the competitive binding between Na^+ and Ca^{2+} and the high levels of Na^+ contained in buffers used for crystallography (Kirichenko et al., 2005; Marechal et al., 2013). Konstantinov's group investigated the idea that CIV can be inhibited by the binding of Ca^{2+} ions in the IMS to the cation binding site, by analysing the enzyme activity and oxygen consumption rates in *in vitro* models with purified CIV and in isolated mitochondria (Vygodina et al., 2013; Vygodina et al., 2017).

It has been calculated that the equilibrium dissociation constant of Ca^{2+} binding with CIV cation binding site (K_d) is $\sim 1 \mu\text{M}$, but taking into account also the competition with Na^+ present in the cytosol, the effective K_d for Ca^{2+} should rise to $\sim 10 \mu\text{M}$. This amount of Ca^{2+} is not available in resting conditions, but can be in the range of extramitochondrial Ca^{2+} concentrations during the Ca^{2+} spikes induced by Ca^{2+} release from the ER, at membrane contact sites (Clapham, 2007; Vygodina et al., 2013). This process could appear in contradiction with the activation of the mitochondrial Krebs cycle dehydrogenases and the mitochondrial transporters in the presence of Ca^{2+} . However, this stimulation is observed at relatively low concentrations of extramitochondrial free Ca^{2+} ($0.3\text{--}5 \mu\text{M}$), condition in which CIV would still be fully protected from the Ca^{2+} inhibition by sodium ions (Denton, 2009). This inhibition process, instead, would have a transient nature and take place only for short periods, during the Ca^{2+} spikes. Konstantinov's group suggested that CIV transient inhibition could have a role in the modulation of calcium uptake by mitochondria, in order to avoid overload and reduce energy expenses for superfluous Ca^{2+} transportation to the matrix via MCU, and outside the matrix via the $\text{Na}^+/\text{Ca}^{2+}$ transporter (Vygodina et al., 2013).

Section 4: Materials and Methods

4.1 Cell culture methods

4.1.1 Cell lines

MTCYB project: Cybrids containing a mitochondrial DNA cytochrome b 4-base pair deletion (#17.3 Δ 4-CYB) have been used for this project (Rana et al., 2000). The cybrids have been generated by the fusion between ρ 0 143B osteosarcoma cells and enucleated fibroblasts from a previously described patient with Parkinsonism carrying the mutation (De Coo et al., 1999). Clones containing different levels of heteroplasmy have been generated and selected in order to obtain both homoplasmic wild type (WT) and mutant (MUT) cybrids.

MCU project: Five cell models have been used in this project. Most of the experiments were performed on a cybrid model containing homoplasmic frameshift mutation in MTCO3 (Tiranti et al., 2000), a CIV subunit involved in the late stages of complex assembly. For this cell line, two clones have been generated, as described for Δ 4-CYB lines, with a wild type mtDNA homoplasmic (WT 73) and a mutant mtDNA homoplasmic for the mutation (MTCO3). This MTCO3 mutant cells have been characterised and the accumulation of assembly intermediates have been shown (Vidoni, 2017). Another mtDNA mutant cybrid model carrying a mutation in MTCO1 (Bruno et al., 1999; D'Aurelio et al., 2001; Lobo-Jarne et al., 2020) has been used to validate the results obtained with the first model. MTCO1 is one of the first CIV subunits inserted during assembly, therefore this model is characterised by a more severe defect in the enzyme biogenesis and present no subassembly formation. The third model used is HeLa cells (European Collection of Authenticated Cell Cultures; Cat# 93021013). This model has been chosen to analyse the effect of the loss of the mitochondrial calcium uptake machinery (MCUM) on RC complex assembly, and to confirm the data obtained on the cybrid models with super resolution microscopy. Indeed, cybrids cells tend to be spherical cells with fairly fragmented mitochondria, while HeLa cells are a well acknowledged cell model for microscopy, harbouring a tubular mitochondrial network and a more spread shape. Finally, cells lacking CI and CIII were used as control: CI-deficient immortalised fibroblasts from a

patient carrying two compound heterozygous mutations in NUBPL, a CI assembly factor, characterised by complete loss of CI (Protasoni et al., 2020), compared to a control line of immortalised fibroblasts, and the CIII-deficient $\Delta 4$ -CYB cybrids and respective WT control described previously.

4.1.2 Culture conditions

Cybrids were grown at 37°C and 5% CO₂ in Dulbecco's Modified Eagle Medium (DMEM, Gibco), supplemented with 10% foetal bovine serum (FBS, Gibco), and 50 µg/ml uridine (Sigma-Aldrich). Supplementation with uridine is necessary for cells displaying severe OXPHOS defects, in order to compensate for the reduced synthesis of pyrimidine. Indeed, the *de novo* pyrimidine biosynthesis pathway depends on the activity of an ETC-dependent enzyme, the dihydroorotate dehydrogenase. Cybrids used in the MTCYB project were grown in the presence of 1% penicillin and streptomycin (both from Invitrogen). HeLa cells were cultured in DMEM with high glucose and GlutaMAX™, supplemented with 10% FBS. Cells were trypsinised (Gibco) and collected after washing with sterile phosphate-buffered saline (PBS) (Life technologies).

Cell stocks were stored in liquid nitrogen after being re-suspended in DMEM with 10% DMSO (Dimethyl sulfoxide).

4.1.3 Cell growth analysis

Growth curves were assessed using an IncuCyte HD instrument (Essen Bioscience), with an algorithm to calculate cell confluency based on inverted microscope imaging. Cells were seeded in a 24-well plate and images of each well were taken every 6 hour (h) for a total period of 78 h.

4.2 DNA-based methods

4.2.1 Cloning of the gene of interest by PCR

4.2.1.1 Templates of genes of interest:

- CYC1: synthetic constructs of *Homo sapiens* *CYC1* gene was obtained from Source BioScience (CCSBo5058F1281061D).
- CHCHD3, COX15 and COX8A: clones were obtained from cDNA synthesized from RNA extracted from immortalised control human fibroblasts.
- MCU and MICU1: clones were donated by Dr. Julien Prudent.
- AOX-HA: The HA-tagged *Emericella nidulans* AOX cDNA insert cloned into the pTNT vector was donated by M^a Pilar Bayona-Bafaluy (University of Zaragoza, Spain).
- NDUFAF2: obtained from cDNA clone (Cat# RC207387), OriGene Technologies.

Inserts were amplified using specific primers and C-terminal HA or FLAG tags were added by Polymerase chain reaction (PCR), following the protocol indicated in table 4.1. Primers used are indicated in table 4.3. Primers were designed with the following characteristics:

- Length ideally between 19 and 21 base pair (bp), which provides sequence specificity and allows efficient DNA binding;
- content of G's and C's around 50% of the total bases;
- presence of G or C bases in the 5' and 3' end of the primer, to help specific binding due to the stronger binding of G and C bases;
- not forming secondary structures, hairpins and cross dimers;
- melting temperature (T_m), the temperature at which the 50% of DNA dissociates to single strand, ideally between 55 and 80°C. Forward and reverse primers should have a similar T_m .

Table 4.1: PCR amplification protocol. Thermocycling conditions were optimised for every gene amplified.

(a) PCR amplification reaction set-up

Reagent	Volume/reaction	Final concentration
10× Cloned Pfu DNA polymerase reaction buffer	5 µL	1X
PCR nucleotide Mix, 2.5 mM each (Sigma-Aldrich)	4 µL	0.2 mM each dNTP
Forward primer (10 µM)	2 µL	0.4 µM
Reverse primer (10 µM)	2 µL	0.4 µM
Template DNA		50 ng
PfuTurbo DNA polymerase (2.5 U/ µl)	1 µL	2.5 U
Nuclease-Free Water to	50 µL	

(b) Thermocycling conditions

Step	Temperature	Time	Cycle
Initial denaturation	95 °C	3 min	1
Denaturation	95 °C	30-45 sec	25 to 35
Annealing	54-58 °C	30-45 sec	
Elongation	68-72 °C	1 min/kb	
Final elongation	72 °C	5 min	1
Hold	4 °C	∞	1

4.2.2 Purification of PCR product by extraction from agarose gel

PCR products were separated in a 1% [w/v] agarose gel (Thermo Scientific). Agarose was dissolved in 100 ml of Tris/Borate/EDTA (TBE) buffer (89 mM Tris-borate, 100 mM boric acid, 2 mM ethylenediaminetetraacetic acid (EDTA)) and boiled in a microwave. To visualise DNA, 10 µL of SYBR safe dye (10,000X, Invitrogen) were added to the agarose solution. Loading dye was added to the DNA samples with a final volume ratio of 1:6. The size of the DNA fragment was verified by running for each gel 5 µL of 1 Kb Plus DNA ladder (Invitrogen). The gel was run at 100 Volts (V) and the separate fragments were visualised with an ultraviolet (UV) light transilluminator. The band at the expected size was cut out of the gel and extracted using a QIAquick gel extraction kit (Qiagen). Gel slices were first dissolved in a high-salt binding buffer at 50°C. The mixture was then passed through a QIAquick spin column, in order to purify DNA. DNA was washed with 70% ethanol (EtOH) and finally eluted in 30-50 µL of water. Eluted DNA was then quantified using a nanodrop system.

4.2.3 TOPO-TA cloning

The purified PCR products were cloned in the pCR2.1 TOPO TA cloning kit (Invitrogen). Before the ligation, a poly-A tail was added to the PCR fragments. 18.5 μL of PCR product were incubated with 0.5 μL of TAQ polymerase (Thermo Scientific), 2.5 μL of 10X TAQ buffer, 2.5 μL of 25 mM MgCl_2 (Thermo Scientific) and 1 μL of 2.5 mM dATPs at 72 $^\circ\text{C}$ for 10 minutes (min). The TOPO vectors provided in the kit are linearized and have 3'-T overhangs that ligate with the poly-A tail of the PCR products. The enzyme DNA topoisomerase I, which functions both as a restriction enzyme and as a ligase, is covalently bound to the 3' phosphate on each end of the vector. The topoisomerase activity enables the vectors to readily ligate DNA sequences with compatible ends in only 10 min at room temperature (RT).

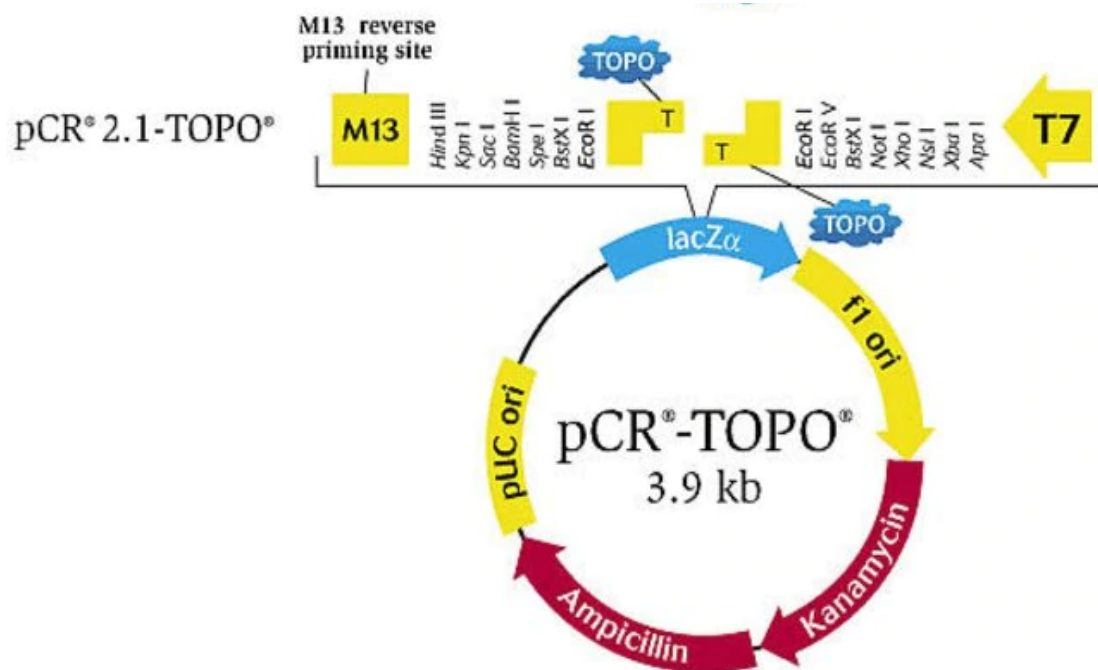


Figure 4.1: map of pCR[™]2.1 TOPO[®] TA vector.

4.2.4 Plasmid cloning by restriction enzymes digestion

In order to cleave DNA and create compatible sequences for cloning, adequate restriction enzymes have been used. The total volume of the gel extracted PCR product or 3-5 μg of donor plasmid containing insert and 3-5 μg of recipient plasmid were incubated for 2 hr at 37 $^\circ\text{C}$ with

1 μL of each appropriate and compatible restriction enzyme in 1X smart cut digestion buffer (as indicated on the NEB website for double digestions: <https://nebcloner.neb.com/#!/redigest>). The digested DNA fragments were resolved in a 0.7% agarose gel at 70 V for 2 h, the specific bands were cut out and DNA was extracted using QIAquick gel extraction kit (Qiagen), according to manufacturer's instructions.

Extracted DNA was quantified using a nanodrop system. 50 ng of recipient plasmid were used for each ligation. The amount of insert used in each reaction was calculated as follows: $\text{ng insert} = 3 * (\text{ng vector} * \text{Kb insert}) / \text{Kb vector}$. The correct amount of insert and vector were incubated overnight at 16°C with 1 μL of T4 DNA ligase (New England Biolabs), 1 μL of 10X ligase buffer and water to a final volume of 10 μL .

4.2.5 Transformation of E. coli chemically competent cells

2 μl of ligation product were added to a 50 μL aliquot of One Shot® TOP10 Chemically Competent E. coli (ThermoFisher) and kept on ice for 30 min. Then, cells were transformed by heat shock (45 seconds at 42 °C) in a thermoblock (AccuBlock Digital Dry Baths, Labnet, UK) and recovered adding 250 μl of SOC medium (2% tryptone, 0.5% yeast extract, 10 mM NaCl, 2.5 mM KCl, 10 mM MgCl₂, 10 mM MgSO₄, and 20 mM glucose). Cells were then incubated at 37 °C for 1 hr under agitation. Transformed cells were plated on LB (lysogeny broth, i.e. 10 g/L tryptone, 5 g/L yeast Extract, 5 g/L NaCl) agar plate with 100 $\mu\text{g/ml}$ of the selection antibiotics (ampicillin or kanamycin) and incubated at 37 °C overnight. In the case of TOPO-TA, the insertion of the PCR product interrupts the LacZ gene present in the vector, which encodes for the β -galactosidase enzyme. β -galactosidase hydrolyses the compound X-gal to 5-bromo-4-chloro-indoxyl, which spontaneously dimerizes and produces a blue pigment, 5,5'-dibromo-4,4'-dichloro-indigo. Therefore, in the case of TOPO-TA cloning, the plate was previously coated with 60 μL of 50 mg/ml X-Gal, in order to allow the screening of the colonies containing the insert versus the empty vector.

The following day, single colonies were picked and grown overnight in 5 ml of LB medium with 100 $\mu\text{g/ml}$ of the selection antibiotics (ampicillin or kanamycin) at 37 °C and 225 revolutions per minute (rpm). When a higher yield was required a midiprep was performed and cells were grown in 100 ml of LB under the same conditions.

4.2.6 DNA extraction from competent cells

Plasmids were extracted using a miniprep or a midiprep kit (QIAprep Spin Miniprep kit, and QIAGEN Plasmid Midi Kit), following the manufacturer's instruction. In both protocols, cells were lysed and the cellular debris were separated by centrifugation or filtering. Cleared lysates were then applied to a QIAprep column, where DNA binds to the membrane. In minipreps, DNA was washed with a washing buffer and eluted in 30-50 μ L of elution buffer. In midipreps, after the elution, DNA was precipitated in isopropanol, washed in 70% ethanol and solubilised in 0.5-1 ml of QLE elution buffer.

4.2.7 Screening of colonies and DNA sequencing

Each colony amplified was screened by digestion in order to differentiate between clones expressing the empty vector and clones that have incorporated the vector containing the insert of interest. 5 μ L of miniprep were digested with the same restriction enzymes used for the cloning, run in a 1% agarose gel and imaged with a ChemiDoc system (Biorad). Clones that resulted positive were verified by DNA Sanger sequencing (Source Bioscience UK Ltd., Cambridge, UK) and analysed by sequence alignment using Basic Local Alignment Search Tool (BLAST) online (accessible at <https://blast.ncbi.nlm.nih.gov/Blast.cgi>) and ExPASy translate tool (accessible at <https://web.expasy.org/translate/>).

4.2.8 Site-directed mutagenesis

Mutagenesis was performed with QuikChange II Site-Directed Mutagenesis Kit (Agilent), using as a template MICU1 and COX15 inserted in TOPO-TA vector and following the manufacturer's instructions. Each mutation has been inserted in a separate PCR (Table 4.2), using the primers indicated in Table 4.3.

Mutations in MICU1 have been inserted in order to inactivate its EF-hand domains, which bind and sense cytosolic calcium. Mutations in these domains abolish the sensitivity to large calcium pulses, without affecting the protein expression (Perocchi et al., 2010). As indicated in Perocchi et al., four point-mutations have been introduced into EF1 (D231A, E242K) and EF4 (D421A, E432K). One mutation was inserted in COX15 because the gene harbours a restriction site for BamHI within its coding sequence and BamHI digestion is necessary for cloning in a pWPXLd

vector. All the mutations inserted have been designed in order to not alter the corresponding amino-acids.

4.2.8.1 Primer design

The mutagenic primers used in this protocol were designed individually according to the desired mutation and with the following characteristics:

- Both of the primers must contain the desired mutation and anneal to the same sequence on opposite strands of the plasmid;
- Primers must have a length of 25-45 bases, with the desired mutation in the middle of the primer with ~10–15 bases of correct sequence on both sides;
- Primers should have a melting temperature (T_m) of $\geq 78^\circ\text{C}$.

Table 4.2: site-directed mutagenesis PCR amplification protocol.

(a) PCR amplification reaction set-up

Reagent	Volume/reaction	Final concentration
10× reaction buffer	5 μL	1x
dsDNA template	-	50 ng
Primer 1	1.25 μL	125 ng
Primer 2	1.25 μL	125 ng
dNTP mix	1 μL	0.25 mM each dNTP
PfuUltra HF DNA polymerase	1 μL	2.5 U
Nuclease-Free Water to	50 μL	-

(b) Thermocycling conditions

Step	Temperature	Time	Cycle
Initial denaturation	95°C	30 sec	1
Denaturation	95°C	30 sec	12
Annealing	55°C	1 min	
Elongation	68°C	1 min/kb of plasmid length	
Cooling	4°C	2 min	-

4.2.8.2 DpnI digestion of the PCR products

1 μ L of the DpnI restriction enzyme (10 U/ μ L) was added directly to each PCR reaction. The reactions were mixed and immediately incubate at 37°C for 1 hr to digest the parental (i.e., the nonmutated) supercoiled dsDNA. 1 μ L of the DpnI-treated DNA was used to transform competent cells, as indicated previously.

Table 4.3: Primers list

MTCYB project

Gene	Tag insertion (5' -> 3')
CYC1	Fw: GTTTTGACTCTCGTGGCG Rv -HA tag: TCAAGCGTAATCTGGAACATCGTATGGGTACTTGGGCGG
CHCHD3	Fw: GAAAAGAATCCAGGCCCTTC Rv -HA tag: TCAAGCGTAATCTGGAACATCGTATGGGTATCCTCCCTTCTCAAGCATG
AOX	Fw: GCCCATGAACAGCATGAGC Rv -HA tag: CCAGATTACGCCTGAATAAAC

MCU project

MICU1	HA tag insertion (5' -> 3')	EF domains mutagenesis (5' -> 3')
FW	TCATGTTTCGTCTGAACT C	D231A: CTTCAAGATGTTTGCTTTGAATGGAGATGG E242K: GAAGTAGATATGGAAAAATTGGAACAGGTTC D421A: GTTTGCACCTTTGCCTGTGATGGCAATGG E432K: CGAACTGAGCAATAAGAAATTTGTTTCCAT
RV	CGAGTTAAGCATAATCAG G	D231A: CCATCTCCATTCAAAGCAAACATCTTGAAG E242K: GAACCTGTTCAAATTTTCCATATCTACTTCT D421A: CCATTGCCATCACAGGCAAAGAGTGCAAAC E432K: ATGGAAACAAATTTCTTATTGCTCAGTTTCG

COX15	HA tag insertion (5' -> 3')	BamHI site – mutagenesis (5' -> 3')
FW	TGGCTGTTCCCTGTCATCAG	GGGAGAATCCTGGATACCGGAGGAC CTCTTT
RV	TCAAGCGTAATCTGGAACATC GTA TGG GTA TTTTGGGA CTCTTCGGAG	AAAGAGGTCCTCCGGTATCCAGGAT TCTCCC

4.2.9 Stable cell lines production: 2nd generation lentivirus expression system

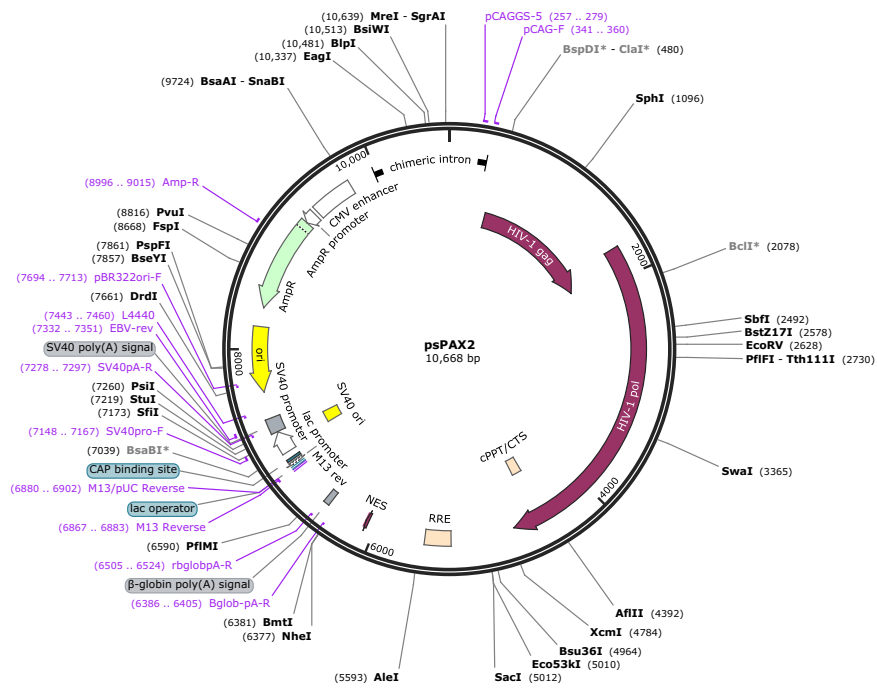
Lentiviral particles were used for cell transduction and stable expression of CYC1-HA, CHCHD3-HA, AOX-HA, COX15-HA, MICU1-HA, and MICU1^{EFmut}-HA.

4.2.9.1 Materials:

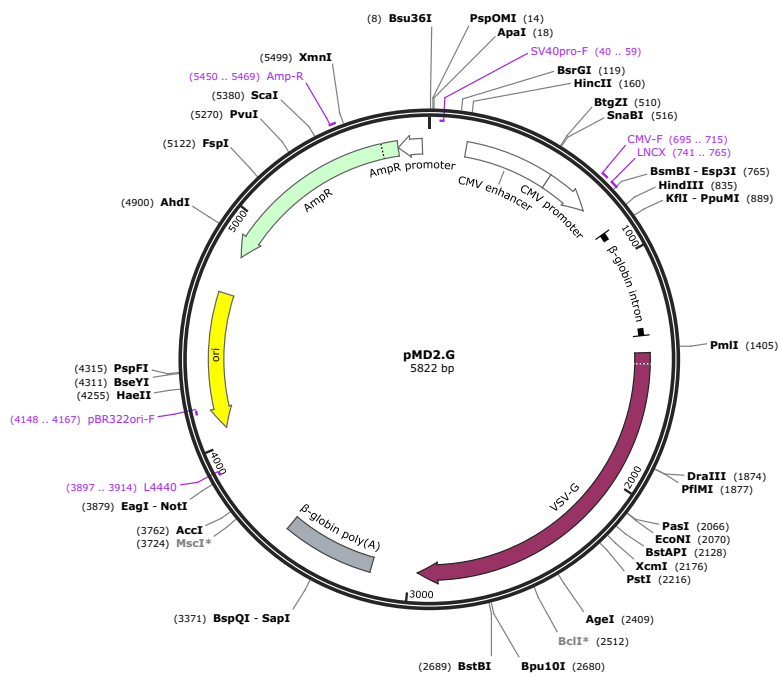
The components required for lentiviral particle generation are:

- 1) Packaging plasmid: psPAX2 (Addgene plasmid #12260, 2nd generation). This plasmid contains four genes essential for the transcription and the packaging of an RNA copy of the insert into the newly generated pseudoviral particles: Gag (group-specific antigen), Pol (the reverse transcriptase), Rev (regulator of expression of virion proteins) and Tat (HIV trans-activator).
- 2) Envelope plasmid: pMD2.G (Addgene plasmid # 12259). This plasmid contains the genes for the envelope surface glycoproteins, vesicular stomatitis virus GP (VSV-G). These glycoproteins give to the lentivirus a broad host-cell range selectivity (Cronin, Zhang and Reiser, 2005).
- 3) Transfer/expression plasmid: pWPXLd-based vectors, containing resistance genes for Hygromycin or Puromycin. It encodes the gene of interest and the resistance gene, which will be integrated in the host genome under the same promoter.

A



B



24 and 48 hr after transfection. The media containing the viral particles was centrifuged at 3,000 x g for 5 min at RT and filtered through a 0.45 µm filter. The filtered medium was stored at -80°C or used immediately to transduce the target cells. Target cells were incubated with 2 ml of medium containing the viral particles for 24 hr with the addition of 8 µg/ml of polybrene, a cationic polymer used to increase transduction efficiency. Infected cells were selected for puromycin (InvivoGen, 1 µg/ml) or hygromycin (InvivoGen, 100 µg/ml) resistance. Selection was considered completed when all the cells plated in a control plate in the absence of viruses died. After selection, transduced cells were cultured in medium without selection antibiotics. All the virus-related work was performed in a containment level 2 (CL2) cell culture room.

4.2.10 shRNA

Gene silencing of *CHCHD3* and *GHITM* was performed by lentiviral transduction of shRNA sequences. Lentiviral particles were produced as indicated previously. Transfer vectors were purchased from Sigma Aldrich (MISSION® shRNA Bacterial Glycerol Stock). Five shRNA constructs have been tested for each transcript of interest and the two clones with the most severe effects were selected for the study. All the constructs used are indicated in Table 4.4. As a control, stable cell lines expressing the pLKO.1 empty vector have been produced.

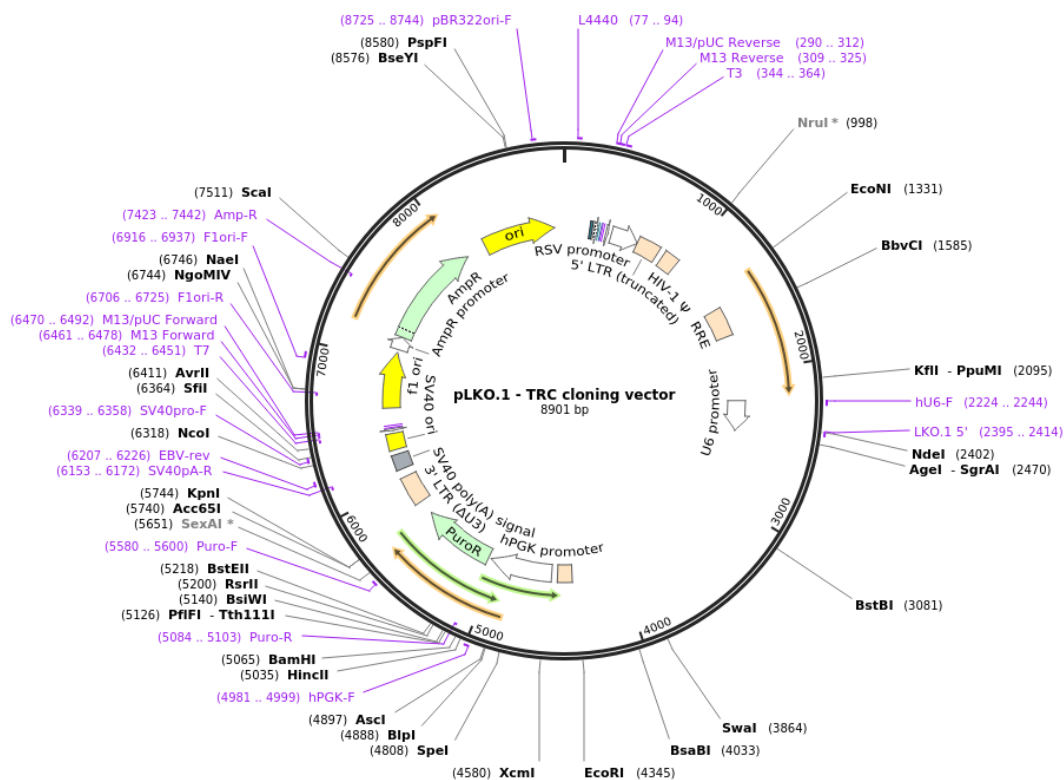


Figure 4.3: map of pLKO.1 vector, used for shRNA expression.

Table 4.4: shRNA list

Target mRNA	Sequence (5' -> 3')	Code
CHCHD3	CCGGCGGACGAGAATGAGAACATCACT CGAGTGATGTTCTCATTCTCGTCCGTTT TTTG	TRCN0000166698
	CCGGCGAAGATCAGAAACGACTAAACT CGAGTTTAGTCGTTTCTGATCTTCGTTT TTTG	TRCN0000160043
	CCGGCAGCAGAATCATTTCACGTTTCTC GAGAAACGTGAAATGATTCTGCTGTTTT TTG	TRCN0000160348
	CCGGCCTCAGTTTCTGATGAAGAATCTC GAGATTCTTCATCAGAAACTGAGGTTTT TTG	TRCN0000160532
	CCGGCGAGTGCTAAAGAAGCAGGATCT CGAGATCCTGCTTCTTTAGCACTCGTTT TTTG	TRCN0000164713
GHITM	CCGGGCAAACCTGTGTTTGCATATTCTC GAGAATATGCAAACACAGGTTTGCTTT	TRCN0000151131

TTTG	
CCGGGCAGAAGTATCACCAATGTATCT CGAGATACATTGGTGATACTTCTGCTTT TTTG	TRCN0000151432
CCGGGCAGTAATCCTCTCCCAAATACTC GAGTATTTGGGAGAGGATTACTGCTTTT TTG	TRCN0000155299
CCGGGAAAGTATCAAGCGTGCAGAACT CGAGTTCTGCACGCTTGATACTTTCTTT TTTG	TRCN0000154530
CCGGGTGGCAATGTACGGTGGATTACT CGAGTAATCCACCGTACATTGCCACTTT TTTG	TRCN0000157150

4.2.11 siRNA

25 μ L of Lipofectamine RNAiMAX transfection reagent (Thermo Fisher Scientific) were pipetted in a 10 cm dish containing 1 ml of Optimem medium (Gibco). 10 μ L of 20 μ M siRNA (final concentration of 20 nM) were added to the Optimem/RNAiMAX reaction and mixed by swirling. Plates were incubated at RT for 15 min. 10 ml of appropriate number of cells (~20% of confluency) were then plated directly on the mixture and incubated at 37°C overnight. The following day, the siRNA containing-medium was replaced with fresh medium. Transfected cells were splitted, if confluent, on the second day and collected after three days of treatment. The siRNAs used are indicated in Table 4.5.

Table 4.5: siRNAs list

Target gene	ID number/sequence	Producer
MCU	hs.Ri.MCU.13.7	Integrated DNA Technologies
MICU1	hs.Ri.MICU1.13.2	Integrated DNA Technologies
MICU2	DsiRNA, MICU2-si1	Integrated DNA Technologies
EMRE	L-016704-01-0005	Dharmacon
MIC60	AATTGCTGGAGCTGGCCTT	Sigma
NDUFAF2	HA13185513-039	Sigma
Negative control	Negative Control DsiRNA	Integrated DNA Technologies

4.2.12 NDUFAF2 transfection

The Myc-DDK (FLAG)-tagged NDUFAF2 cDNA clone (Cat# RC207387) and the control plasmid (empty vector, EV) pCMV6-entry mammalian expression vector (Cat# PS100001) were purchased from OriGene Technologies. Both the WT and the Δ 4-CYB cybrids were transfected with these vectors using FuGENE HD in a ratio 3:1 with DNA. Cells were transfected for 48 hr and were selected for neomycin resistance (Gibco-Thermo Fisher Scientific, 500 μ g/ml).

4.2.13 Gene expression levels quantification

4.2.13.1 RNA extraction

10⁶ cells were harvested by trypsinisation, washed twice in PBS and collected by centrifugation at 250 x g at RT for 5 min. Cells were then lysed with 200 μ l of TRIZOL reagent by repetitive pipetting. The homogenised sample was incubated for 5 min at RT to allow the complete dissociation of nuclear proteins and centrifuged at 300 x g for 5 min. 40 μ l of chloroform were added to the supernatant and incubated for three min at RT. Samples were then centrifuged at 12,000 x g for 15 min at 4°C in order to separate them in three phases: lower red, phenol-chloroform phase, interphase and a transparent upper phase, where the RNA localises. The upper phase was collected and RNA was precipitated adding 100 μ l of isopropanol. Samples were incubated at RT for 10 min and centrifuged at 12,000 x g for 10 min at 4°C. The pellet was washed with 200 μ l 70% ethanol and air-dried. RNA was finally resuspended in 50 μ l of water.

4.2.13.2 cDNA synthesis

cDNA was synthesised using the Omniscript Reverse Transcriptase (Qiagen). The master mix was prepared as indicated in Table 4.5. 15 μ l of master mix were mixed with 5 μ l of RNA and incubated at 37°C for 1 hr followed by 5 min at 95°C. Samples were diluted with 30 μ l of RNase free water.

Table 4.6: master mix protocol for reverse transcription.

Reagent	Amount (μ l)	Final concentration
10x RTase Buffer	2	1x
dNTPs (5mM each)	2	0.5 mM each
Random Hexamer (50 μM)	0.2	0.5 μ M
Oligo dT primer (50 μM)	0.2	0.5 μ M
RNase inhibitor (40 U/μl)	0.25	10 U
Omniscript RTase (4 U/μl)	1	4 U
RNase free water	9.35	-

4.2.13.3 Real-time reverse transcription-PCR (RT-PCR)

RT-PCR was used to quantify gene expression levels, using pre-tested and validated specific Gene Expression TaqMan assays (Thermo Fisher Scientific) for each of the transcripts of interest (Table 4.7). TaqMan probes consist in an oligonucleotide, which recognises the transcript of interest covalently bound to a 6-carboxyfluorescein (FAM) fluorophore at the 5'-end and a tetramethylrhodamine (TAMRA) quencher at the 3'-end. When the probe binds the specific DNA region, the Taq polymerase synthesises the new strand and degrades the probe, liberating the fluorophore and generating a fluorescent signal. The amplification cycle at which the fluorescence crosses the background threshold is called the threshold cycle (TC) and is used for the calculation of the expression levels, using the $\Delta\Delta$ Ct analysis.

Table 4.7: list of TaqMan probes used in the RT-PCR analysis.

Gene	TaqMan Assay ID
NDUFB8	Hs00428204_m1
NDUFB11	Hs00372638_g1
ND1	Hs02596873_s1
COX15	Hs00189238_m1
GAPDH	Hs02758991_g1

Each sample was measured in technical triplicates and in each well 5 μ l of cDNA were mixed with 10 μ l of master mix (Thermo Fisher Scientific), 1 μ l of TaqMan probe and 4 μ l of water. The RT-PCR was run as indicated in Table 4.8.

Table 4.8: Real time PCR thermocycling conditions.

Step	Temperature	Time	Cycles
Initial denaturation	95 °C	10 min	1
Denaturation	95 °C	15 sec	40
Annealing/Elongation	60 °C	1 min	

The fluorescence signals after cyclic annealing were collected, and the *GAPDH* transcript level was used to normalise the results. The quantitative analysis relative to control was performed.

4.3 Protein-based methods

4.3.1 Protein quantification

Proteins samples were quantified using a colorimetric DC Protein Assay (detergent compatible, Bio-Rad), following manufacturer's instructions. The change of solution's colour was measured with a SpectraMax Plus384 plate reader (Molecular Devices, Sunnyvale, CA, USA) at 750 nm at RT. The absorbance of the unknown samples was compared to a bovine serum albumin (BSA) standard curve with known concentrations from 0 to 2 mg/ml.

4.3.2 Mitochondria isolation

Mitochondria isolation was performed by differential centrifugation as described previously (Fernandez-Vizarra et al., 2010). Cells were harvested by trypsinisation, washed twice in PBS and collected by centrifugation at 250 x g for 5 min at RT. To ensure an optimal plasma membrane permeabilization, cells were resuspended in one pellet volume of cold hypotonic homogenisation buffer (IB 0.1x) (3.5 mM Tris-HCl, pH 7.8, 2.5 mM NaCl, 0.5 mM MgCl₂). Cells were then homogenised with a motor-driven Teflon pestle for 10-12 strokes at 4°C. Immediately after the homogenisation, 1/10 of the volume of hypertonic buffer (IB 10x) was added to make the medium isotonic again and avoid excessive mitochondrial damage. The homogenate was centrifuged at 1,200 x g for 5 min at 4°C and the supernatant, containing the mitochondria was transferred to a clean tube. The pellet, containing unbroken cells, debris and nuclei, was homogenised a second time, to increase the yield. Mitochondria were pelleted by

centrifugation at 15,000 x g for 2 min at 4°C and washed three times with a homogenisation medium (0.32 M sucrose, 1 mM EDTA, 10 mM Tris-HCl, pH 7.4).

4.3.3 Fractionation

Mitochondria were isolated from 10 T175 flasks, by differential centrifugation, as indicated above. In order to study mitochondrial localisation of the proteins of interest, isolated mitochondria were exposed to protease treatment before and after the removal of the outer membrane by hypotonic shock. Hypotonic shock was performed by incubating mitochondria in 10 mM Tris-HCl pH=7.4, 1 mM EDTA on ice for 10 min. Protease treatment was achieved with 100 and 150 µg/ml trypsin at RT for 30 min with rotation. Finally, one sample was treated with both trypsin and 1% triton as protein extracted control sample. 0.5 mg of mitochondrial protein was used for each treatment. Samples were separated using an SDS-PAGE Nu-PAGE 4-12% Bis-Tris gel (Invitrogen), including cytosolic fraction (supernatant after the 15,000 x g centrifugation), crude mitochondria (supernatant after the 1,200 x g centrifugation), and total cells, collected during the mitochondria extraction.

4.3.4 SDS-page gel electrophoresis (SDS-PAGE)

Cells were pelleted at 300 x g at RT and the pellet was washed twice with PBS. Cells were lysed in cold triton/glycerol (TG) lysis buffer (20 mM Tris-HCl pH 7.5, 500 mM NaCl, 1mM EDTA, 1% Triton-X-100, 10% Glycerol, 1.5 mM MgCl₂) (MTCYB project) or in RIPA buffer (25mM Tris pH 8.0, 150 mM NaCl, 1% Triton-X100, 0.5% Sodium deoxycolate, 0.1% SDS) (MCU project) with both buffers containing 1X protease inhibitor cocktail (Roche). The protein amount was detected with DC protein assay kit (BioRad) and 20 µg of proteins were loaded for each condition. Samples were prepared by mixing the extracted proteins with 4X Laemli buffer (200 mM tris-HCl pH 6.8, 40% glycerol, 8% w/v Sodium dodecyl sulphate (SDS), 0.04% v/v bromophenol blue, 400mM DTT or 20% β-mercaptoethanol). Samples were resolved by SDS polyacrylamide gel electrophoresis, using SDS-PAGE Nu-PAGE 4-12% Bis-Tris gel (Invitrogen). Gels were run in MES running buffer (50 mM MES, 50 mM Tris Base, 0.1% SDS, 1 mM EDTA, pH 7.3; Thermofisher Scientific). Proteins were transferred to a

Polyvinylidene difluoride (PVDF) membrane (Immobilon-P) at 100 V for 1 hr at 4°C in Tris-Glycine transfer buffer (25 mM Tris-HCl, 192 mM Glycine), 20% methanol, and 0.25% SDS.

4.3.5 Blue native gel electrophoresis (BN-PAGE)

5×10^6 cells were trypsinised, washed twice with PBS and pelleted at 300 x g at RT. A mitochondria-enriched fraction was extracted treating the cells with 8 mg/ml digitonin for 10 min on ice, to break plasma membrane and eliminate the cytosolic fraction, followed by centrifugation at 10,000 x g for 5 min. Samples were re-suspended in 1.5 M aminocaproic acid, 50 mM Bis-Tris/HCl pH=7 protein solubilising solution and lysed with 1% n-dodecyl- β -D-maltopyranoside (DDM), to analyse monomeric complexes, or digitonin, which is a milder detergent and preserves supercomplexes, for 5 min on ice. Samples were centrifuged for 30 min at 18,000 x g and 10 μ l of loading buffer (750 mM aminocaproic acid, 50 mM Bis-Tris/HCl pH=7, 0.5 mM EDTA and 5% Serva Blue G) were added to the supernatant. 50 μ g of proteins were loaded in a BN-PAGE. BN-PAGE was performed using 3–12% Bis-Tris separating gels (Invitrogen) and proteins were blotted to a PVDF membrane (Immobilon-P) at 300 mA for 1.5 hr in bicarbonate transfer buffer (0.318 mg/ml Na₂CO₃, 0.84 mg/ml NaHCO₃).

For second dimension (2D) PAGE, lanes from 1D BN were cut into strips and soaked in 1% SDS and 1% β -mercaptoethanol solution for 1.5 h, in order to denature proteins. Strips were loaded and turned by 90° into a 2D SDS-PAGE Nu-PAGE 4-12 % Bis-tris gel (Invitrogen). 2D BN were run and transferred following the procedure described for SDS-PAGE.

4.3.6 Western blot analysis

Membranes were blocked with 10% milk in PBS with 0.1% Tween 20 (PBS-T) for one hr at RT while shaking and then incubated overnight with specific primary antibodies in 2% milk in PBS-T at 4°C. Following three washes with PBS-T for 10 min at RT while shaking, membranes were incubated with horseradish peroxidase (HRP)-conjugated anti-mouse, anti-rabbit (Promega) or anti-rat (Santa Cruz Biotechnologies) IgG secondary antibodies at a dilution of 1:3000. Three additional washes in PBS-T were performed. Blots were developed by incubating membranes with Amersham™ ECL™ Western Blotting Detection Reagents (GE

Healthcare, Chalfont St Giles, UK) and visualising the signal on X-ray films (Fujifilm, Tokio, Japan) at different exposure times. Films were developed using an X-ray film processor (ECOMAX, Protec, Germany). Bands were quantified using Fiji (*Fiji Is Just ImageJ*). Primary and secondary antibodies used are indicated in Table 4.9.

Table 4.9: Antibody list

Antibody	Source	Catalogue Number	Dilution
Rabbit monoclonal anti-NDUFS1	Abcam	ab169540	1:5000
Mouse monoclonal anti-NDUFS3	Abcam	ab110246	1:500
Mouse monoclonal anti-NDUFA9	LifeTechnologies	LS459100	1:1000
Mouse monoclonal anti-NDUFB11	Proteintech	16720-1-AP	1:500
Mouse monoclonal anti-NDUFB8	Abcam	ab110242	1:1000
Mouse monoclonal anti-SDHA	Abcam	ab14715	1:1000
Mouse monoclonal anti-SDHB	Abcam	ab14714	1:1000
Mouse monoclonal anti-UQCRC1	Abcam	ab110252	1:1000
Mouse monoclonal anti-UQCRC2	Abcam	ab14745	1:1000
Mouse monoclonal anti-UQCRFS1	Abcam	ab14746	1:1000
Rabbit polyclonal anti-CYC1	Proteintech	10242-1-AP	1:500
Mouse monoclonal anti-UQCRQ	Abcam	ab110255	1:500
Rabbit polyclonal anti-UQCRQ	Abcam	ab136679	1:1000
Rabbit monoclonal anti-UQCRB	Abcam	ab190360	1:1000
Mouse monoclonal anti-COX4	Abcam	ab110272	1:1000
Mouse monoclonal anti-COX5A	Abcam	ab110262	1:1000
Mouse monoclonal anti-COX6B1	Abcam	ab110266	1:500
Mouse monoclonal anti-COX7B	Abcam	ab197379	1:1000
Mouse monoclonal anti-MTCO1	Abcam	ab14705	1:1000
Mouse monoclonal anti-MTCO2	Abcam	ab110258	1:1000
Mouse monoclonal anti-ATPalpha	Abcam	ab14748	1:1000
Rabbit polyclonal anti-ATPbeta	Santa Cruz Biotechnology	SC-33618	1:5000
Mouse monoclonal anti-ATPb	Santa Cruz Biotechnology	SC-514419	1:3000
Mouse monoclonal anti-β-actin	Sigma-Aldrich	AI978	1:5000
Mouse monoclonal anti-β-tubulin	Sigma-Aldrich	T5201	1:2000
Rabbit polyclonal anti-NDUFAF2	Proteintech	13891-1-AP	1:1000
Rabbit polyclonal anti-MCUR1/CCDC90A	LB Bioscience	LS-B9716	1:1000
Rabbit monoclonal anti-MCU	Cell Signalling	D2Z3B	1:500
Rabbit polyclonal anti-MICU1	AtLAS ANTIBODIES	HPA037480	1:500
Rabbit polyclonal anti-MICU2	Abcam	ab101465	1:1000

Rabbit polyclonal anti-EMRE	Santa Cruz	sc-86337	1:500
Rabbit polyclonal anti-TOMM20	Abcam	ab78547	1:1000
Mouse monoclonal anti-MIC60/Mitofilin	Abcam	ab110329	1:1000
Rabbit polyclonal anti-MIC19/CHCHD3	Proteintech	25625-1-AP	1:1000
Rabbit polyclonal anti-GHITM/MICS1	Proteintech	16296-1-AP	1:1000
Mouse monoclonal anti-flag	Sigma-Aldrich	F3165	1:1000
Rat monoclonal anti-HA	Roche	11867423001	1:1000
Goat anti-Mouse IgG	PROMEGA	W402B	1:3000
Goat anti-Rabbit IgG	PROMEGA	W401B	1:3000
Goat anti-Rat IgG	Cell Signaling Technology	70775	1:3000
Rabbit monoclonal anti-HA (Sepharose® Bead Conjugate)	Cell Signaling Technology	3956S	

4.3.7 Quantitative SILAC Mass Spectrometry

Cell lines were grown for at least 8 passages in “heavy” DMEM (Gibco-Thermo Fisher Scientific) containing ¹⁵N- and ¹³C-labeled Arg and Lys, respectively, and in “light” DMEM containing ¹⁴N- and ¹²C-labeled Arg and Lys, respectively (Sigma-Aldrich), complemented with 10% dialyzed serum (Gibco-Thermo Fisher Scientific) and 50 µg/ml Uridine. On the day of the experiment, cells were harvested and proteins were measured as described previously. Equal amounts of the differentially labelled cells were mixed and solubilised with 4 mg/ml digitonin. Solubilisation was followed by two washes in PBS and centrifugation at 13,000 x g for 5 min at 4°C. Pellets were then solubilized in a solubilisation buffer (10% glycerol in 1 X PBS with 1 x protease inhibitor, 1.5% (w/v) DDM and 1 X lipid stock (10X stock: 0.9 mg/ml 1-palmitoyl- 2-oleoyl-glycero-3-phosphocholine (POPC), 0.3 mg/ml 1-hexadecanoyl-2-(9Z-octadecenoyl)-sn-glycero-3-phosphoethanolamine (POPE), 0.3 mg/ml 1- palmitoyl-2-oleoyl-sn-glycero-3-phospho-(1'-rac-glycerol) (POPG), Avanti Polar Lipids)) and incubated on ice for 30 min. Insoluble material was removed by centrifugation at 21,000 x g for 10 min. Soluble material was then clarified by filtering it with a spin-X columns (Costar) by centrifugation at 1,000-4,000 x g. Affinity pulldown was performed by incubating the samples with anti-HA-agarose (Cell Signaling) beads overnight at 4°C in rotation. The following day, the unbound material was collected and the beads were washed with a washing buffer (10% glycerol, 1X protease inhibitors, 0.05% DDM in PBS). Samples were eluted with a denaturing elution buffer (200 mM glycine at pH 2.5 with 0.05% (w/v) DDM) for 5 min at RT. Samples were then prepared for mass spectrometry analysis. Firstly, cysteines were reduced and alkylated by 5

mM tris(2-carboxyethyl)phosphone (TCEP) (Sigma-Aldrich) at 37°C for 30 min. Samples were incubated 10 min at RT and alkylation was performed by addition of 15 mM iodoacetamide and incubation in dark at RT for 30 min. Finally, 25 mM Dithiothreitol (DTT, Melford Stores) was added to the samples to quench the excess of iodoacetamide. Proteins were separated through SDS-PAGE electrophoresis in a 10-well 10-20% tris glycine gel (Invitrogen). Each lane of the gel was cut in 11 0.6 mm slices and digested with trypsin. Extracted peptides were analysed by liquid chromatography mass spectrometry (LC-MS), using an LTQ XL-Orbitrap system (Thermo Fisher Scientific), as described previously (Rhein et al., 2013). Peptides were identified using Andromeda, a peptide search engine and the ratio between light and heavy signal was calculated with set of algorithms, MaxQuant (Cox and Mann, 2008).

Final results were based on two parallel experiments: experiment 1 - condition A in light medium mixed with condition B in heavy medium; experiment 2 - condition A in heavy medium mixed with condition B in light medium. Each experiment provides two results: first, proteins pulled-down which interact with the protein of interest, and second, a quantitative analysis of protein abundance in a condition compared to the other. Each protein identified in both the experiments was plotted as a point in a 'scatter plot', with ratios from one experiment on the X-axis and ratios from the second experiment on the Y-axis. Proteins which have been pulled-down but do not show a significant change in abundance in the two conditions cluster around the origin of the cartesian plan, while hits with consistent increase or decrease in abundance localise in the top right or bottom left quadrants, respectively. Proteins in the top left or bottom right quadrants are contaminants and do not give reproducible results in the two experiments. Statistical analysis was performed with Perseus (Cox and Mann, 2011; Tyanova et al., 2016).

4.3.8 Complexome profiling

Cell lines were conditioned in heavy and light SILAC mediums, as indicated in the previous section. Cells were collected by trypsinisation and pelleted at 250 x g for 5 min at RT. Cells were resuspended in 1 ml of PBS and proteins were quantified using a DC Protein Assay (BIORAD). Cells differentially labelled were mixed in a 1:1 protein ratio (experiment 1: condition A in light medium vs condition B in heavy medium; experiment 2: condition A in

heavy medium vs condition B in light medium). Mitochondria were extracted as indicated previously and solubilised in 1.6 mg DDM/mg of protein or 4 mg digitonin/mg of protein. The solubilised proteins were mixed with blue native loading buffer and loaded in a 10-well 3-12% native page gel. The gel was run overnight at 70 V at 4 °C. Each lane was then incubated in the fixing solution (50% methanol, 10% acetic acid, 10 mM ammonium acetate [pH 3]) for 60 min and cut in 64 slices, which were digested with trypsin and analysed by tandem mass spectrometry, as indicated in Heide et al., 2012 and Guerrero-Castillo et al., 2017.

The relative protein abundance across slices was estimated quantifying the peptide appearing in the greatest proportion of the total number of gel slices in both unlabelled (light) and labelled (heavy) samples. Data was processed in Microsoft Excel and represented as profiles of one protein or of the average of a cluster of proteins, or as heatmaps. Profiles show the relative peptide peak intensities along the lane, normalised to the slice with the highest intensity, setting the maximum to 1.0, versus the molecular weight of the complexes. The mass calibration used in complexome profiles was performed using respiratory chain complexes and supercomplexes as standards, as previously described (Guerrero--Castillo et al., 2016; Heide et al., 2012). Heat maps represent the normalised abundance in each gel slice by a three-colour code gradient (black/yellow/red) and were produced with the NOVA software v0.5 (Giese et al., 2015).

4.3.9 Assembly kinetics assays

[³⁵S]-L-Methionine (L-Methionine, [³⁵S]-Cell Labelling Grade, PerkinElmer) pulse and pulse-chase labelling of the mitochondrial peptides were performed as described previously (Chomyn, 1996; Fernandez-Silva et al, 2007). Cells were incubated with ³⁵S-Met and cycloheximide, which inhibits cytosolic translation. Samples were collected at 2, 5, and 24 hr after substituting medium containing ³⁵S-Met and cycloheximide with fresh medium. Samples were then extracted for SDS-PAGE and BN-PAGE, as indicated previously. SDS, 1D and 2D-BN were run as indicated previously and dried for 2 hr at 80°C and phosphor screens (GE Healthcare's Life Sciences) were exposed to the radioactive gels for several days at RT. The signal was detected using a laser scanner (Amersham Typhoon, GE Healthcare's Life Sciences, UK).

To block mitochondrial translation, 15 µg/ml doxycycline was added to the culture medium for 6 days. Cells were collected at different time points after removal of the drug, prepared and run for BN-PAGE, as described previously.

4.4 Biochemical methods

4.4.1 Biochemical analysis of complexes activity

The activities of respiratory chain complexes and citrate synthase (CS) were measured spectrophotometrically in cell samples. Cells were collected by trypsinisation and centrifugation at 250 x g for 5 min at RT. Pellets were resuspended in buffer A (20 mM MOPS, 250 mM sucrose, pH=7.4) and solubilised in 0.2 mg/ml digitonin for 5 min on ice. Digitonin-treated cells were centrifuged at 5,000 x g for 5 min at 4°C in order to separate the cytosolic fraction (in the supernatant) and the mitochondria-enriched pellet. Pellets were washed in buffer B (20 mM MOPS, 250 mM sucrose, 1 mM EDTA, pH=7.4) and centrifuged at 10,000 x g for 5 min at 4°C. Samples were stored at -80°C until use. On the day of the experiment, pellets were homogenized in 10 mM potassium phosphate (KP) buffer pH=7.4 and disrupted by three cycles of freezing/thawing in liquid nitrogen (N₂(l)) at 37°C.

The spectrophotometric activity of CI, CII, CIII, CIV, and CS, was measured as described in Bugiani et al., 2004. The Beer–Lambert law was applied in order to calculate absorbance: $A = \epsilon lc$ (A =absorbance, ϵ =molar absorption coefficient, l =optical pathlength, c =molar concentration).

$$\text{Specific activity} = \frac{\Delta Abs * Total Volume (ml)}{\epsilon * Sample volume (ml) * [prot] \left(\frac{mg}{ml} \right) * l (cm)}$$

CI activity was measured by following the decrease of NADH absorbance at 340 nm. Proteins were incubated during 2 min at 30°C in the reaction mix indicated in Table 4.10. The reaction was initiated adding 50 µM CoQ, followed for 2 min, and then inhibited with 5 µM rotenone. The reaction was followed for two additional min after rotenone inhibition, in order to subtract the CI-independent signal of NADH oxidation. $\epsilon_{\text{NADH340nm}} = 6.81 \text{ ml/nmol} \cdot \text{cm}$.

Table 4.10: Complex I enzymatic activity assay mixture and substrates.

Compound	Final concentration
KP buffer pH 8	20 mM
NADH	0.2 mM
Sodium azide (NaN₃)	1 mM
BSA (in EDTA 10 mM pH 7.4)	1 mg/ml
CoQ	50 μM
Rotenone	5 μM

Enzyme activity of respiratory chain CII was evaluated as described by Ragan, 1987. Proteins were preincubated for two min with the master mixture indicated in Table 4.11 at 30°C. The assay is based on 2,6-dichlorophenolindophenol (DCPIP), an artificial electron acceptor, which absorbs in the 600 nm range and change colour on reduction. DCPIP is reduced directly by CII and also by the quinol product of CII catalysis (Munujos et al., 1993). This reaction is followed after the injection of 16 μM succinate (SDH activity) and 50 μM CoQ (CII activity). $\epsilon_{\text{DCPIP600nm}} = 19 \text{ ml/nmol*cm}$.

Table 4.11: Complex II enzymatic activity assay mixture and substrates.

Compound	Final concentration
KP buffer pH 7	50 mM
Potassium cyanide (KCN)	1.5 mM
2,6-Dichlorophenolindophenol (DCPIP)	0.1 mM
Succinate	16 μM
CoQ	50 μM

CIII was assessed as described by Zheng et al., 1990. The reduction of cytochrome *c* was followed at 550 nm for 2 min at 30°C. Proteins were incubated with the master mixture indicated in Table 4.12. $\epsilon_{\text{Cyt}c550\text{nm}} = 21 \text{ ml/nmol*cm}$.

Table 4.12: Complex III enzymatic activity assay mixture and substrates.

Compound	Final concentration
KP buffer pH 7.4	50 mM
NaN₃	2 mM
BSA (in EDTA 10 mM pH 7.4)	1 mg/ml
Cytochrome c	50 μM
Decylubiquinone (DBH₂)	50 μM

CIV activity was measured at 550 nm following cytochrome *c* oxidation for 2 min at 37°C as described by Warthon, 1967. Proteins were incubated in the master mixture indicated in Table 4.13 for two min before starting the measurement. $\epsilon_{\text{Cyt}c550\text{nm}} = 18.5 \text{ ml/nmol}^* \text{ cm}$.

Table 4.13: Complex IV enzymatic activity assay mixture and substrates.

Compound	Final concentration
90-95 % reduced cytochrome c in 50 mM KP buffer pH 7	50 mM

All enzymatic activities were normalized for protein quantification (DC assay kit, Bio-Rad) and for CS activity. CS catalyses the reaction between acetyl-CoA and oxaloacetate. In this assay, this reaction is combined with the generation of 5-thio-2-nitrobenzoic acid (TNB) from 5', 5'-Dithiobis 2-nitrobenzoic acid (DTNB). This yellow product is followed by measuring the absorbance at 412 nm for 2 min at 30°C. The master mixture used in this assay is indicated in Table 4.14. $\epsilon_{\text{TNB}412\text{nm}} = 13.8 \text{ ml/nmol}^* \text{ cm}$.

Table 4.14: Citrate synthase enzymatic activity assay mixture and substrates.

Compound	Final concentration
Tris-HCl buffer pH 8	75 mM
5,5-dithio-bis-(2-nitrobenzoic acid (DTNB))	0.1 mM
Triton X-100	0.1 %
Acetyl-CoA	0.4 mM
Oxalacetate	0.5 mM

4.4.2 In gel activity – Complex I assay

In gel activity was performed on blue native samples, prepared as described above. Samples were run overnight at 4 °C in a 3-12% Bis-Tris native gels (Invitrogen) at 70 V. Gels were then incubated 1-2 hr at RT while gently shaking with 0.1 M Tris-HCl pH 7.4, 0.14 mM NADH, 1 mg/ml Nitro blue tetrazolium (NBT, Sigma-Aldrich). Finally, gels were washed with water and scanned with a professional scanner (EPSON Expression 1680 Pro, EPSON, UK).

4.4.3 Oxygraphic measurements: OROBOROS Oxygraph-2k (O2k)

Intact and permeabilised cells respiration measurements were conducted in Oroboros Oxygraph-2k. The Oroboros is composed of two chambers, allowing the analysis of two samples in parallel. Each chamber has a capacity of 2 ml and is equipped with oxygen sensors that can measure in real time both the oxygen concentration (nmol/ml) and the oxygen consumption (pmoles/sec/ml). Through the lid of each chamber, substrates and inhibitors are injected in medium or buffer containing resuspended cells or mitochondria. The suspension is kept agitated by a stirrer at the bottom of the chamber, therefore each substrate or inhibitor is evenly mixed in few seconds. The Oroboros is also equipped with a temperature controlling system, which maintains the samples at 37 °C during the measurement.

The reasons why this technique was preferred to other methods to measure oxygen consumption, such as the Seahorse, are two. Firstly, in the Oroboros, samples are kept in solution, while in the Seahorse approach, cells are grown on a monolayer in a special 8 to 96 well-plates. This characteristic allowed us to work with both intact cells and freshly digitonin permeabilised cells. Secondly, since all the injections are performed manually, each complex of the OXPHOS can be assessed independently in digitonised cells. In this protocol, combinations of substrates and complexes inhibitors allow the independent measurement of oxygen consumption due to electrons passage through CI+CIII+CIV, CII+CIII+CIV or CIV alone.

4.4.3.1 Oxygraph measurements: respiration in intact cells

Oxygen consumption rate per cell was measured with an Oroboros Oxygraph-2k (O2k) in intact cells resuspended in culture DMEM medium. An example of a standard experiment is summarised in Figure 4.4. Routine respiration (R) is followed by inhibition of ATP synthase (injection of 5 μ l of 20 μ M Oligomycin), leading to the non-phosphorylating LEAK state (L). Subsequently maximal capacity of the electron transfer system (ETS) is assessed injecting 250 μ M Carbonyl cyanide *m*-chlorophenyl hydrazone (CCCP) ([3-chlorophenyl]hydrazono]malononitrile). For each sample, a titration is performed, keeping adding the uncoupler until the maximal signal is reached. Finally, 1 μ l of 2 mM Rotenone and 2 μ l of 2.5 mM Antimycin A were added to completely inhibit respiration.

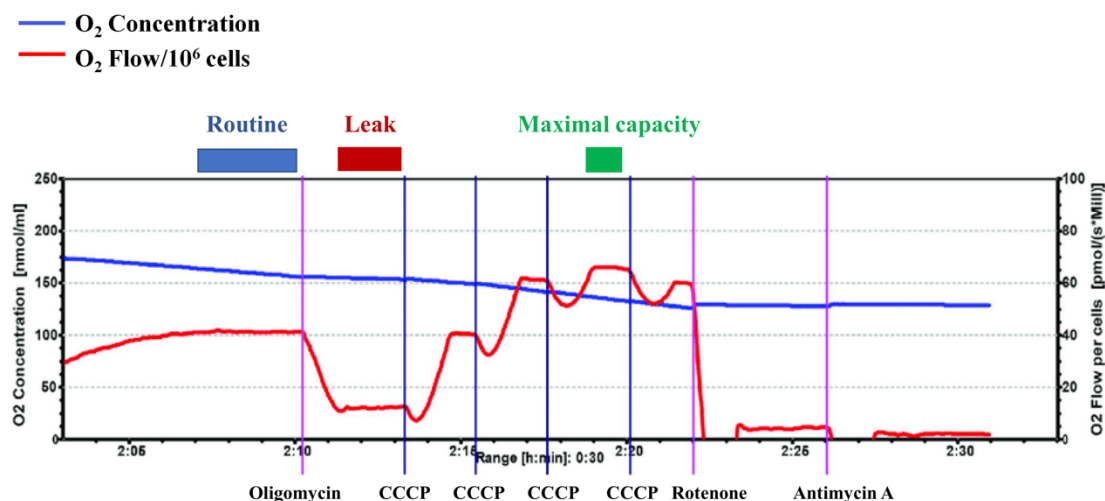


Figure 4.4: example of mitochondrial respiration analysis in OROBOROS Oxygraph-2k in intact cells: oxygen flow (red line) calculated as the negative time derivative of oxygen concentration in the closed respirometer chamber (blue line).

4.4.3.2 Oxygraph measurements: respiration in permeabilised cells

5*10⁶ cells for each sample were collected by trypsinisation followed by centrifugation before every measurement. The cell pellet was resuspended in 1 ml of medium A (20 mM Hepes, 250 mM sucrose, 10 mM MgCl₂, pH=7.1) and permeabilised for 1 min in 50 μ g/ml digitonin in medium A. The reaction was stopped with 4 ml of medium A and digitonised cells were collected by centrifugation at 350 x g for 3 min at RT. A second wash in medium A was

performed, in the same conditions. Cells were then resuspended in 2 ml of 'respiration buffer' (medium A supplemented with 1 mM ADP and 2 mM potassium phosphate) and loaded in the Oroboros chambers. Since cells can be lost after these passages, they were counted a second time after permeabilisation and final results were normalised for the final count.

The design of a standard experiment is summarised in Figure 4.5. Initially, the permeabilised cells are fed with glutamate and malate, which provide electrons to CI. Indeed, the addition of glutamate and malate to permeabilised cells or isolated mitochondria generates NADH, the electron donor of CI. Glutamate enters mitochondria through the glutamate-aspartate antiporter, which exchanges glutamate with aspartate and H^+ , and is transformed in 2-oxoglutarate, producing a NADH molecule. Malate is transported through the antiporter with 2-oxoglutarate and generates NADH when metabolised to oxaloacetate. After the inhibition of this pathway through the addition of rotenone, electrons are provided to CII by succinate and glycerol-3-phosphate. The first half of the respiratory chain is then inhibited by the CIII inhibitor antimycin A and the respiration through CIV is calculated as the difference between oxygen consumption after the injection of ascorbate and TMPD (tetramethyl-p-phenylenediamine) and after the inhibition of the enzyme by potassium cyanide (KCN). TMPD is a CIV specific electron donor, and ascorbate is added to the solution in order to maintain TMPD reduced and able to donate electrons to build a linear rate of CIV activity.

CI+CIII+CIV-linked respiration was calculated as the difference in oxygen consumption after the injection of 15 μ L of 1 M glutamate and 15 μ L of 1 M malate and the injection of 3 μ L of 2 mM rotenone. CII+CIII+CIV-linked respiration was measured as the difference between the oxygen consumption rate after the injection of 15 μ L of 1 M succinate and 15 μ L of 1 M glycerol-3-phosphate and the inhibition of CIII by 6 μ L of 4 mM antimycin A. For CIV-linked respiration, 15 μ L of 40 mM TMPD and 10 mM ascorbate and 15 μ L of 200 mM KCN were used.

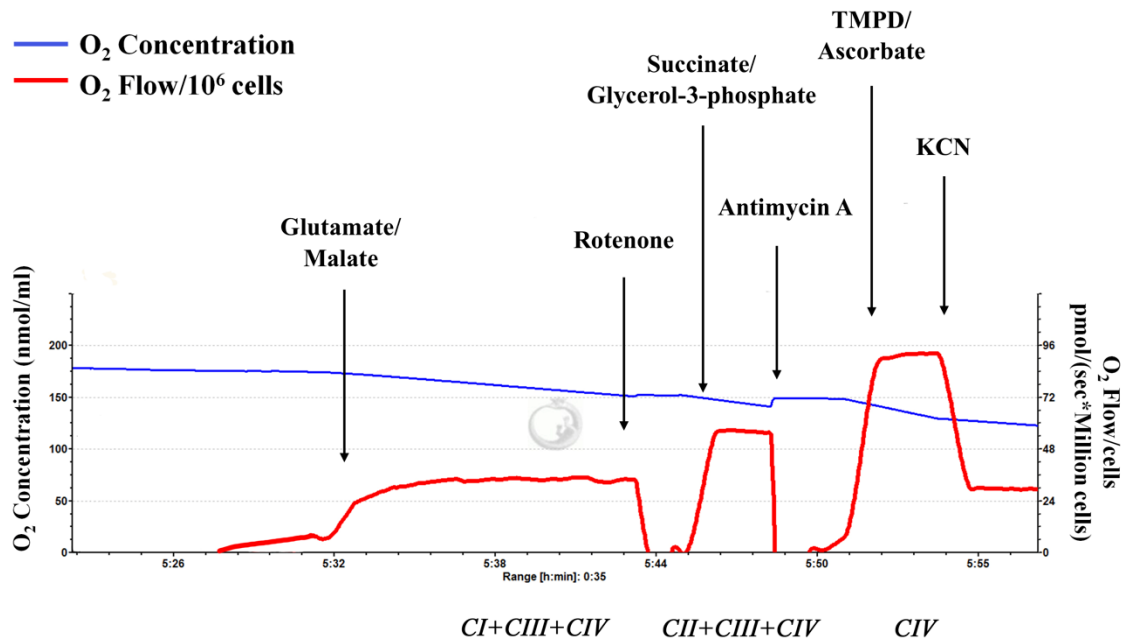


Figure 4.5: example of mitochondrial respiration analysis in OROBOROS Oxygraph-2k in permeabilised cells: oxygen flow (red line) calculated as the negative time derivative of oxygen concentration in the closed respirometer chamber (blue line).

4.5 Microscopy-based methods

4.5.1 Immunofluorescence (IF) - MTCYB project

Cells were cultured in 12-well plates containing coverslips and fixed with 3.7% formaldehyde in culture medium for 15 min at 37°C. Cells were then washed three times in PBS. In order to visualize inner membrane proteins, antigen retrieval was performed by incubation of the coverslips for 10 min in hot antigen retrieval buffer (100 mM Tris, 5% (w/v) urea, pH 9.5). Cells were permeabilised for 10 min at RT with 0.1% Triton-X-100, 0.05% sodium deoxycholate in PBS and blocked in 5% goat serum in PBS for 1 hr at RT. Cells were then incubated for 1 hr at RT or overnight at 4 °C with appropriate primary antibody (as indicated in Table 4.15) in blocking buffer. After four washes in PBS, cells were incubated with the corresponding secondary antibodies Alexa fluor 488 and 568 (Invitrogen) for 1 hr at RT. Coverslips were mounted with Prolong Gold mounting media (Thermo Fisher Scientific) and kept at RT for 48 h. Coverslips were then stored at -20°C.

Table 4.15: list of primary and secondary antibodies used for the IF experiments in the MTCYB project.

Antibody	Type	Producer	Dilution factor
SDHA	mouse	Abcam	1:200
TOMM20	rabbit	Santa Cruz Biotechnology	1:1000
-HA488	mouse	Cell Signaling	1:500
Anti-Mouse 488	Goat IgG(H+L)	Invitrogen	1:500
Anti-Mouse 568	Goat IgG(H+L)	Invitrogen	1:500
Anti-Rabbit 568	Goat IgG(H+L)	Invitrogen	1:500

4.5.2 Cloning and transfection of fusion proteins for imaging (fixed cells) - MCU project

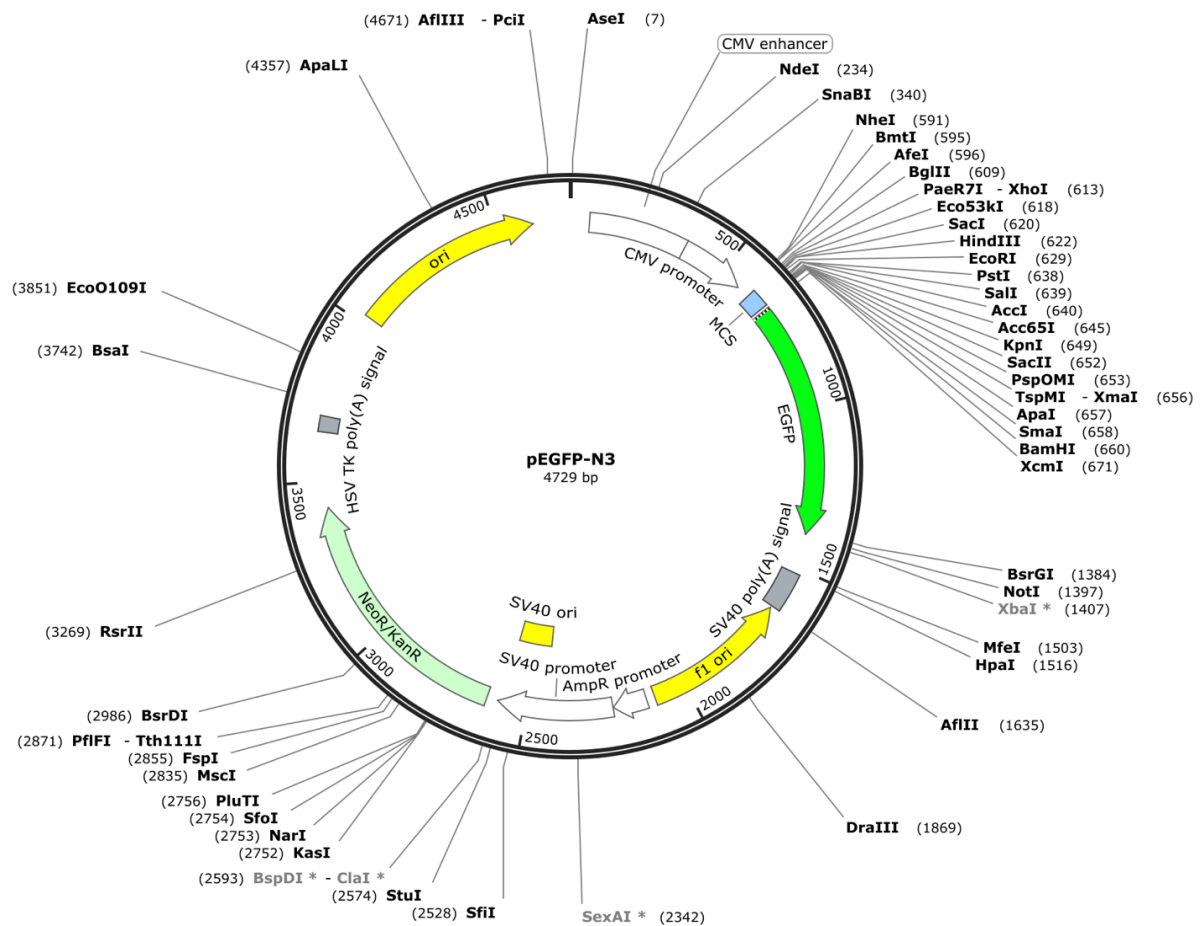
Table 4.16: list of primers used to clone fusion proteins for microscopy.

	Fusion with pEGFP-N3 (Figure 4.6 A)	Fusion with pmCherry-N1 (Figure 4.6 B)
Gene	Primers (5' -> 3')	Primers (5' -> 3')
MCU	Fw: GCTAGCATGGCGGCCCGCCGCAGG Rv: GGATCCCATAGATCCACCAGATC C	Fw: GCTAGCATGGCGGCCCGCCGCAGG Rv: GGATCCAACATAGATCCACCAGATC C
MICU1	Fw: GCTAGCGCCGCCACCATGTTTCG TCTGAACTC Rv: GGATCCCTGTTTGGGTAAAGC	Fw: GCTAGCGCCGCCACCATGTTTCG TCTGAACTC Rv: GGATCCTTCTGTTTGGGTAAAGC
COX8A	Fw: CGCGGGCCCGGGATCCATGTCCG TCCTGACGCC Rv: TGGTGGCGATGGATCCCTCTGGC CTCCTGTAGGTCTC	-

50.000 cells were plated in 24-well plates containing coverslips and transfected overnight with 0.1 μ g of each plasmid using FuGENE in a FuGENE:DNA ratio of 3:1. The constructs used were COX8A-EGFP-N3, MCU-EGFP-N3, MCU-pmCherry-N1, MICU1-EGFP-N3, IMM-mCherry-MITO7, and pMTS-mScarlet-N1 (cloned as indicated previously. Primers used are listed in Table 4.16). Cells were fixed with 5% para-formaldehyde in PBS for 15 min at 37°C and then washed three times in PBS. Coverslips were mounted with Prolong Gold mounting media (Invitrogen) and left 48 hr at RT. Coverslips were then stored at 4°C.

A

Created with SnapGene®



B

Created with SnapGene®

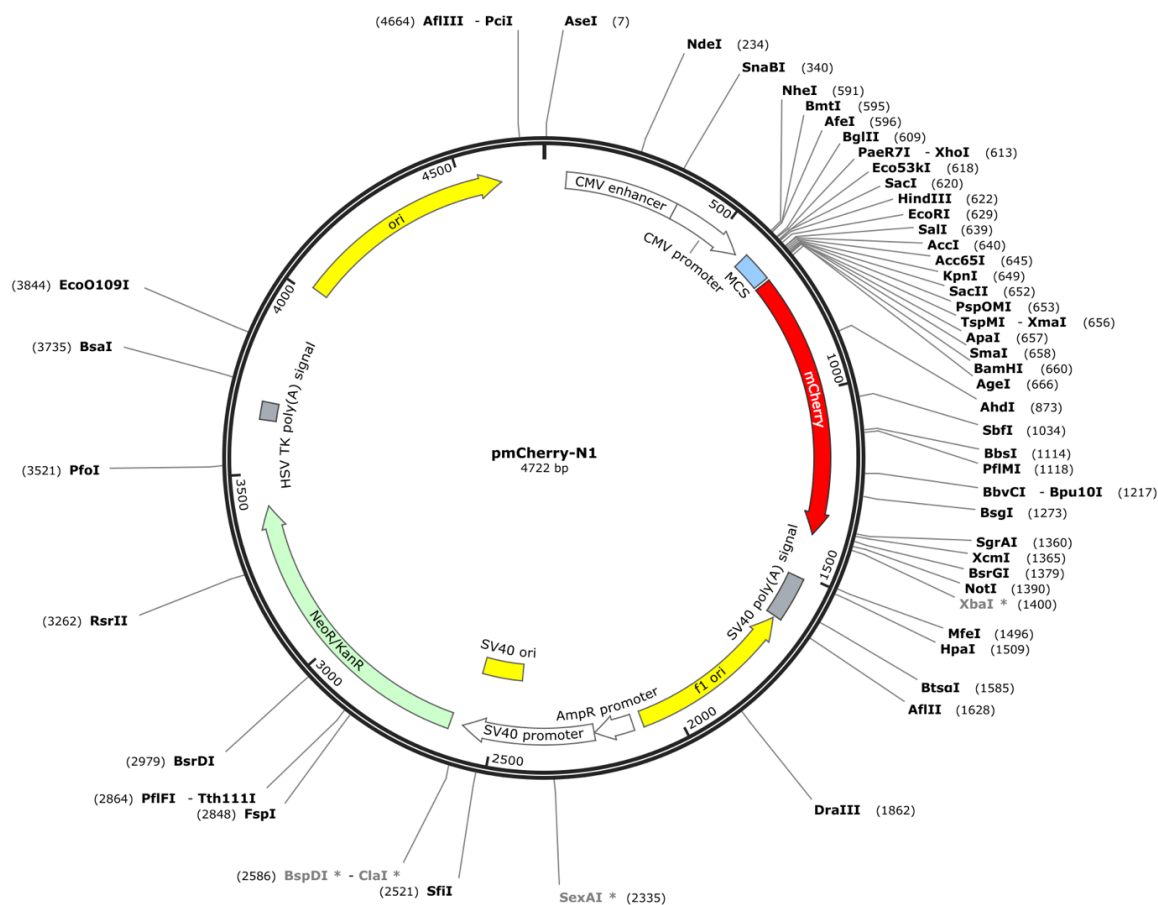


Figure 4.6: EGFP-N3 and pmCherry-N1 maps.

4.5.3 N-SIM imaging and analysis

Images were acquired with an N-SIM Nikon microscope (Structured Illumination super-resolution Microscope) using the 488 nm and 561 nm lasers. 7 Z-stack of 0.2 μm each were acquired using a SR Apo TIRF 100 \times 1.49 N.A. oil objective and a DU897 Ixon camera (Andor Technologies). Raw images were computationally reconstructed using the reconstruction slice system from NIS-Elements software (Nikon). Signals co-localisation were analysed by generating the cross-section intensity profiles of the two fluorophores with the FIJI (Fiji Is Just ImageJ) software. Additional co-localisation analysis was performed using Imaris 9.0 XT software (Bitplane Scientific Software). For each image, threshold was applied in the same way using automated ROI threshold for the sub-compartments channel and adjusted in the

same range for GFP staining. Pearson's coefficient in the co-localised volume was calculated for each image.

4.5.4 Dragonfly imaging and analysis

Images were acquired using an Andor Dragonfly 500 spinning disk confocal system (Andor technologies) equipped with a Nikon eclipse inverted microscope, using the 488 nm and 561 nm laser lines of a Carl Zeiss LSM880 confocal laser-scanning system. For mitochondrial morphology analysis, 7 stacks of 0.2 μm each were acquired using the 60X 1.49 N.A objective and Zylo sCMOS plus camera (Andor technologies). Images were processed using the FIJI software. Images were compiled by “max projection” and mitochondrial morphology was analysed and presented as tubular, elongated or fragmented. At least 50 cells per condition were analysed from each independent experiments.

4.6 Statistical Analysis

Data are presented in graphs as mean \pm SD or mean \pm SEM. Student's t-test was used for pair-wise comparison while 2-way ANOVA with Sidak's post-hoc test was used for multiple comparisons. All statistical analyses were performed with GraphPad Prism v.7.0e for Mac OS. AUC was defined by the peptide intensity in each gel slice in the MS complexome profiling analyses.

Section 5: analysing complex III assembly and its role in supercomplexes formation and ETC maturation.

5.1 Introduction

Transmitochondrial cybrids containing an out-of-frame 4-base pair deletion in the mitochondrial DNA gene encoding cytochrome *b* ($\Delta 4$ -CYB, clone #17.3), previously identified in a patient with parkinsonism, were found associated with a severe CIII defect (de Coo et al., 1999; Rana et al., 2000). In this project, $\Delta 4$ -CYB cybrids, and cybrids derived from the same patient but carrying unmutated mtDNA copies (WT, clone #4.1), were used to study two aspects of OXPHOS machinery biogenesis.

The first aim of the project was to study CIII assembly, as only the very first stages, the maturation and the insertion of MTCYB, followed by UQCRQ and UQCRB, and the final addition of the Rieske protein, have been described in humans. Indeed, while in *S. cerevisiae* all the steps of enzyme maturation are known, less data is available in mammals, and the human CIII assembly model is still based on the yeast model (Zara et al., 2007, 2009a, b). In contrast to CI and CIV, only few assembly factors specific for CIII are known, both in yeast and mammals. Therefore, comparing a WT cell model with one presenting severe impairment in CIII maturation, we aimed to analyse the possible formation of intermediate subassemblies and identify new possible assembly factors interacting with these subassemblies.

The second aim of the project was to investigate how the lack of CIII, both structurally and functionally, affects the formation of SC and the maturation of the other complexes of the respiratory chain. Indeed, as discussed in the introduction, CIII is part of every known respiratory SC species and many patient cases have been reported with multi-enzyme failure in the presence of severe CIII deficiency. The investigation of the role of CIII in the stabilisation or biogenesis of one or more other ETC enzymes would provide new evidence about the effective role of SC in humans, including if they are formed for functional reasons such as substrate channelling or protection from oxidative stress, or for structural reasons.

To answer these questions, we have used proteomics, biochemical, and biogenetic approaches to characterise the biogenesis of all the ETC components in the $\Delta 4$ -CYB cell model.

5.2 CIII assembly: lack of MTCYB causes accumulation of CIII assembly intermediates

5.2.1 Effects of $\Delta 4$ -CYB mutation on CIII

Firstly, the expression of the structural components of the mitochondrial respiratory chain (MRC) complexes and the ATP synthase in the $\Delta 4$ -CYB cells were analysed. Metabolic labelling with ^{35}S -methionine of the thirteen mtDNA-encoded subunits confirmed that MTCYB was not synthesised in the mutant cells, while the remaining proteins were still detectable (Figure 5.1A). We then decided to characterise the effects of this mutation on other CIII components. Since insertion of MTCYB is the initial step of CIII assembly, we wondered if all the other subunits were degraded because of not being able to be inserted in a complex, or if some of them were stabilised and were potentially able to form detectable subassemblies. To study this, we performed SDS-PAGE, Western blot (WB) and immunodetection analysis of the steady-state levels of seven nuclear-encoded structural subunits in WT versus $\Delta 4$ -CYB cybrids, using specific antibodies against these proteins. The only two subunits we did not include in the study were UQCRH and UQCR11, because no valid antibodies were commercially available. We could observe significantly lower levels of UQCRC1, UQCRC2, UQCRB, UQCRFS1 and UQCRQ in the $\Delta 4$ -CYB cybrids (Figure 5.1B, C), while cytochrome *c1* (CYC1) showed comparable steady-state levels in both cybrid lines. Similarly, the signal obtained by immunodetection with an anti-UQCRQ monoclonal mouse antibody revealed a band with unchanged levels between WT and mutant. Interestingly, the recognised protein showed a molecular size smaller than 10 kDa and the signal appeared dramatically different from the one detected with an anti-UQCRQ rabbit antibody (molecular weight >10 kDa and no signal in the $\Delta 4$ -CYB cybrids). These results suggest that the mouse antibody failed to reliably detect UQCRQ whereas, as it will be shown next (Figures 5.4, 5.5), it cross-reacts with UQCR10 (predicted to have a molecular weight of ~7 kDa). Therefore, we considered this signal as belonging to UQCR10.

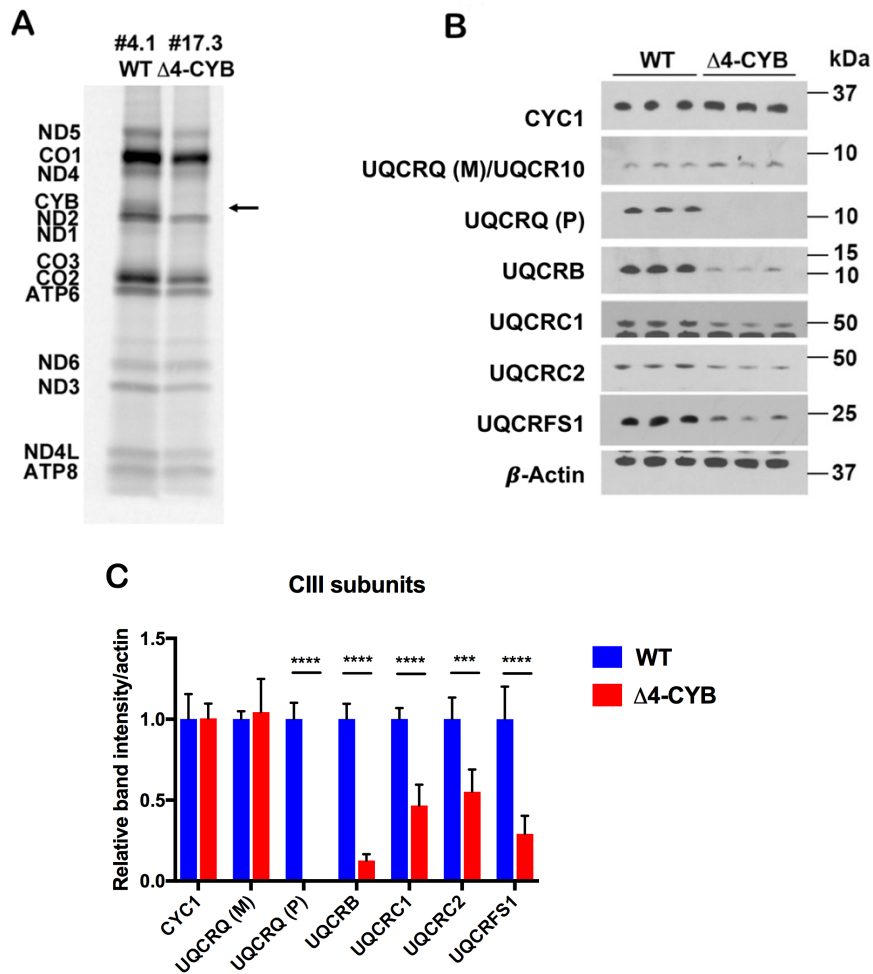


Figure 5.1: in the absence of MTCYB, CIII subunits steady-state levels are strongly decreased, with the exception of UQCR10 and CYC1. A) Labelling of the thirteen mtDNA-encoded MRC structural subunits. Cells were incubated with [³⁵S]-L-Met for 1 hr while inhibiting cytoplasmic translation with 100 μg/ml emetine. The arrow shows MTCYB signal. Experiment performed by Dr. Erika Fernández-Vizarra. B) Western blot and immunodetection of CIII structural subunits of total cell lysates separated by SDS-PAGE. Three independent biological replicates of WT and Δ4-CYB cells were run in the same gel and quantified. β-Actin was used as a loading control. UQCRQ (M) indicates the monoclonal antibody, UQCRQ (P) the polyclonal. C) The graph shows the densitometric quantification of the signals corresponding to each subunit normalised to that of β-Actin. Δ4-CYB samples signal has been calculated as relative to the mean of WT samples, set to 1.0. Values are plotted as the mean ± SD (n = 3). For statistical analysis two-way ANOVA with Sidak's multiple comparisons test was used. ****P < 0.0001; ***P = 0.0007.

To confirm these results and to better understand the reasons why some CIII subunits are stable in the Δ4-CYB cybrids, we performed reciprocal complexome profiling analyses with SILAC-labelled samples, comparing mitochondria extracts from WT and mutant cells. Differentially labelled mitochondria solubilised with 4 mg digitonin/mg of protein were resolved by BN-

PAGE, each lane was then excised into 64, 1-mm-thick slices, and protein distribution through the gel was determined by liquid chromatography–mass spectrometry (LC/MS) analysis. This experiment is highly informative because it compares the migration in a native gel, i.e. incorporation into different supramolecular entities, and abundance of all the proteins detectable by mass spectrometry in the two conditions analysed.

Firstly, we focused on CIII subunits and assembly factors. As expected, no fully assembled CIII or CIII-containing SC species were found in the mutant cells (Fig 5.2 and 5.3). Peptides corresponding only to four subunits, UQCRC2, UQCRFS1, CYC1, and UQCR10, and two assembly factors, BCS1L and MZM1L (LYRM7), both involved in the incorporation of the Rieske protein, were detected in mitochondria from both control and $\Delta 4$ -CYB cells (Figure 5.2). While UQCRC2 and UQCRFS1 mainly accumulate at the bottom of the gel, CYC1 and UQCR10 were found distributed along the entire lane, suggesting their association within (sub)complexes of different apparent molecular sizes. The amounts and distribution of UQCRFS1 assembly factors BCS1L and MZM1L, instead, did not change in the two cell lines.

In contrast, six additional structural CIII subunits and one additional assembly factor, were detected only in WT cells: UQCRC1, MTCYB, UQCRH, UQCRB, UQCRQ, and UQCR11, and UQCC2 (Figure 5.3). These results presented in “Heatmap” (Fig 5.3) confirmed the low steady-state levels of these proteins observed in mutant cells analysed by WB analyses (Fig 5.1).

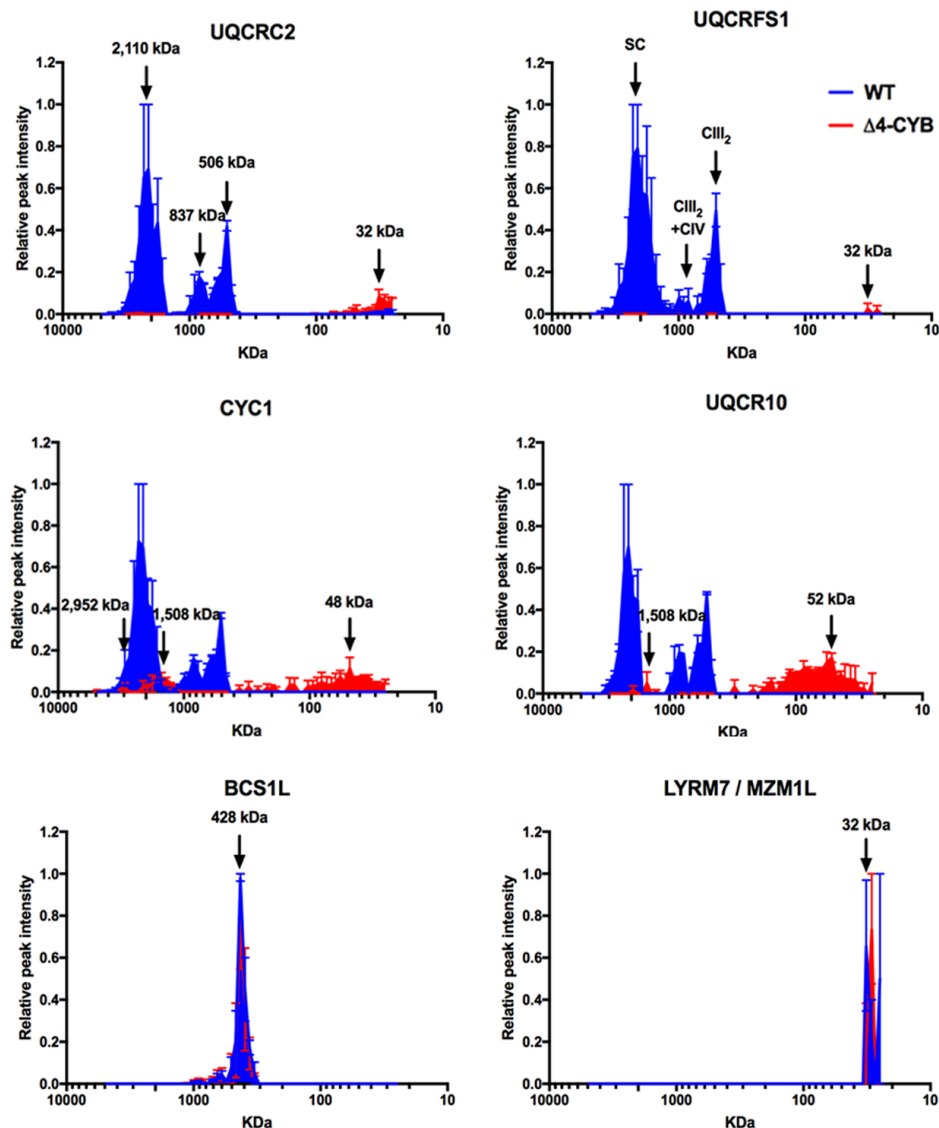


Figure 5.2: *UQCR10* and *CYC1* were detected in various high- and low-molecular-weight intermediates in $\Delta 4$ -*CYB* cells. Complexome profiles of *CIII* structural subunits generated by analysing the peptide content in each of the 64 slices in which the gel lanes were excised. The graphs plot the relative peptide peak intensities along the lane, setting the maximum to 1.0, versus the molecular mass calculated using the individual complexes and supercomplexes as the standards to generate a calibration curve. The relative amounts of the proteins between the two cell lines were determined by calculating the Heavy/Light ratios of peptides that were present in both WT (blue) and $\Delta 4$ -*CYB* samples (red). The represented values are the mean \pm SEM of the two reciprocal labelling experiments. The in-gel digestion and MS analysis, as well as the writing of Python and R scripts for data extraction and manipulation, were performed by Dr Michael E. Harbour.

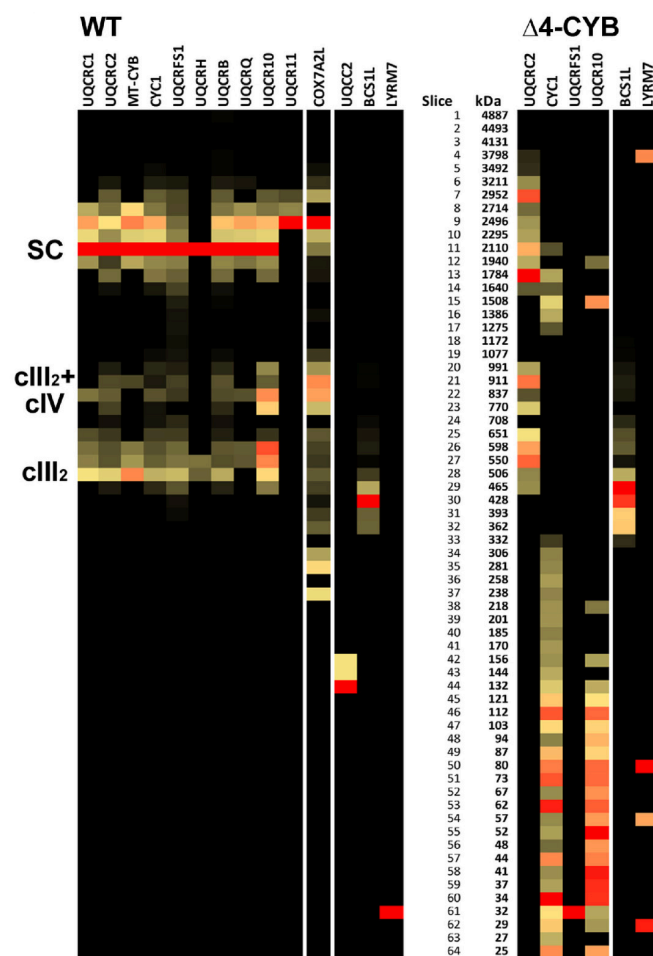


Figure 5.3: *only few CIII subunits are detectable in $\Delta 4$ -CYB cells, and they can be found in a variety of intermediates.* Heatmaps of CIII structural subunits and assembly factors derived from the complexome profiling experiment described in Figure 5.2, but analysing the most frequently found peptides in each labelling state independently, in WT or $\Delta 4$ -CYB cells. Black = 0; yellow = 0.5; red = 1 relative peptide intensities of the most frequent peptide found in each of the samples individually. Heatmaps were generated by Dr Erika Fernández-Vizarra.

Consequently, our attention moved to CYC1 and UQCR10, the only subunits still expressed and distributed in several intermediates in mutant cells with molecular sizes ranging from 25 to 2,952 kDa. Interestingly, while UQCR10 was not predicted to be part of a subassembly module, CYC1 was thought to be interacting with the core proteins before the incorporation in the nascent enzyme. Indeed, while subassemblies composed of Qcr1 (homolog of UQCRC1), Qcr2 (UQCRC2) and Cyt *c*₁ were identified in yeast mitochondria lacking cytochrome *b*, Qcr7 (UQCRB) or Qcr8 (UQCRQ) (Zara et al., 2007), our data from human samples showed that CYC1 not only does not stably interact with the core components during complex biogenesis but form other unknown associations.

5.2.2 Characterisation of the UQCR10 and CYC1-containing intermediates

5.2.2.1 Cloning of UQCR10-HA and CYC1-HA

Since UQCR10 and CYC1 are the only subunits of CIII that remain stable in the absence of the mature enzyme, we cloned the two proteins with an -HA tag in their C-terminus and performed stable lentiviral transduction of them in both WT and $\Delta 4$ -CYB cybrids. These cell lines were used to investigate the formation of uncharacterised assembly modules and the possible interaction with still unknown assembly factors. Moreover, UQCRQ, known to be inserted in the early stages of CIII biogenesis in humans, was also cloned with an -HA tag and overexpressed, in order to determine the behaviour of the HA-tagged subunit and relate it to its stability in the absence of MTCYB.

The expression of these constructs was verified by SDS-PAGE and WB analysis (Figure 5.4). UQCR10-HA expression was detectable both in WT and in $\Delta 4$ -CYB cells, while UQCRQ-HA was absent in the mutant cells. Interestingly, in samples from cells overexpressing CYC1-HA, immunodetection with an anti-HA tag antibody identified multiple bands between 25-35 kDa. As described in the introduction, CYC1 is subjected to a series of post-translational proteolytic cleavages which take place in the mitochondria. The smaller band most probably corresponds to the mature form of the protein, while the higher-molecular-weight bands represent the precursor forms of the protein, before the two cleavages that allow the transport and the insertion of CYC1 into the IMM. Interestingly, we observed that in mutant cells the proportional amount of these forms was shifted to the immature form, suggesting an accumulation of the precursor form and a decrease of mitochondrial import of the mature form. The investigation of this aspect is shown below in Figures 5.7 and 5.8.

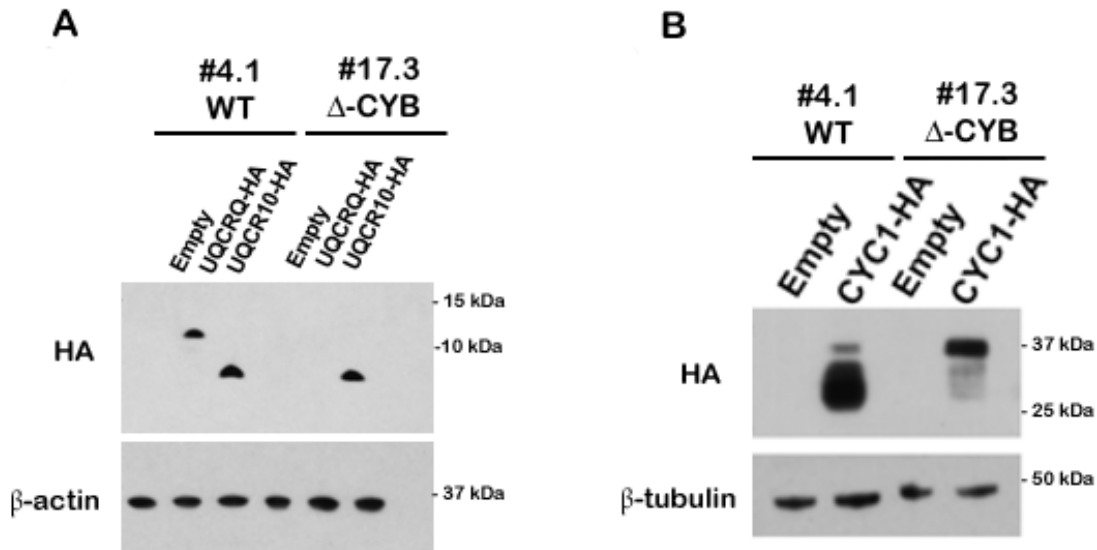


Figure 5.4: HA-tagged UQCRQ, UQCR10 (A) and CYC1 (B) constructs overexpressed in WT and Δ 4-CYB cells. SDS-PAGE, Western blot, and immunodetection analysis of total lysates from WT and mutant cybrids transduced with either the pWPXLd-ires-Puro^R empty vector (Empty), or the same expression vector containing the coding sequences for UQCRQ-HA, UQCR10-HA, or CYC1-HA. β -Actin and β -Tubulin were used as loading controls.

We then performed immunodetection analyses with anti-HA and endogenous antibody of samples from the CYC1-HA, UQCR10-HA and UQCRQ-HA overexpressing lines separated on first dimension (1D) BN-PAGE, using the cells transduced with the empty vector as controls. Two different detergents were used: digitonin, a mild detergent that preserves intact SC, and DDM, a stronger detergent that disrupts SC. As expected, the three overexpressed tagged-proteins were correctly incorporated into CIII and SC in WT cybrids (Figure 5.5 A, C). However, both CYC1-HA and UQCR10-HA were found associated with different high- and low-molecular-weight species in mutant cells when MTCYB is absent. These results corroborate the complexome profiles performed previously (Fig 5.2). Indeed, these results confirm that CYC1 and UQCR10 are likely to form intermediate complexes with other subunits, chaperones or scaffold proteins involved in the assembly.

The pattern of immunodetection obtained in BN-PAGE with the monoclonal anti-UQCRQ antibody (Figure 5.5B) was compatible with that of the native UQCR10 found in the MS analyses (Figure 5.2) and that of the immunodetected HA-tagged protein (Figure 5.5A). These results strongly suggested that this antibody actually recognised UQCR10 instead of UQCRQ, the latter being absent in the Δ 4-CYB cells.

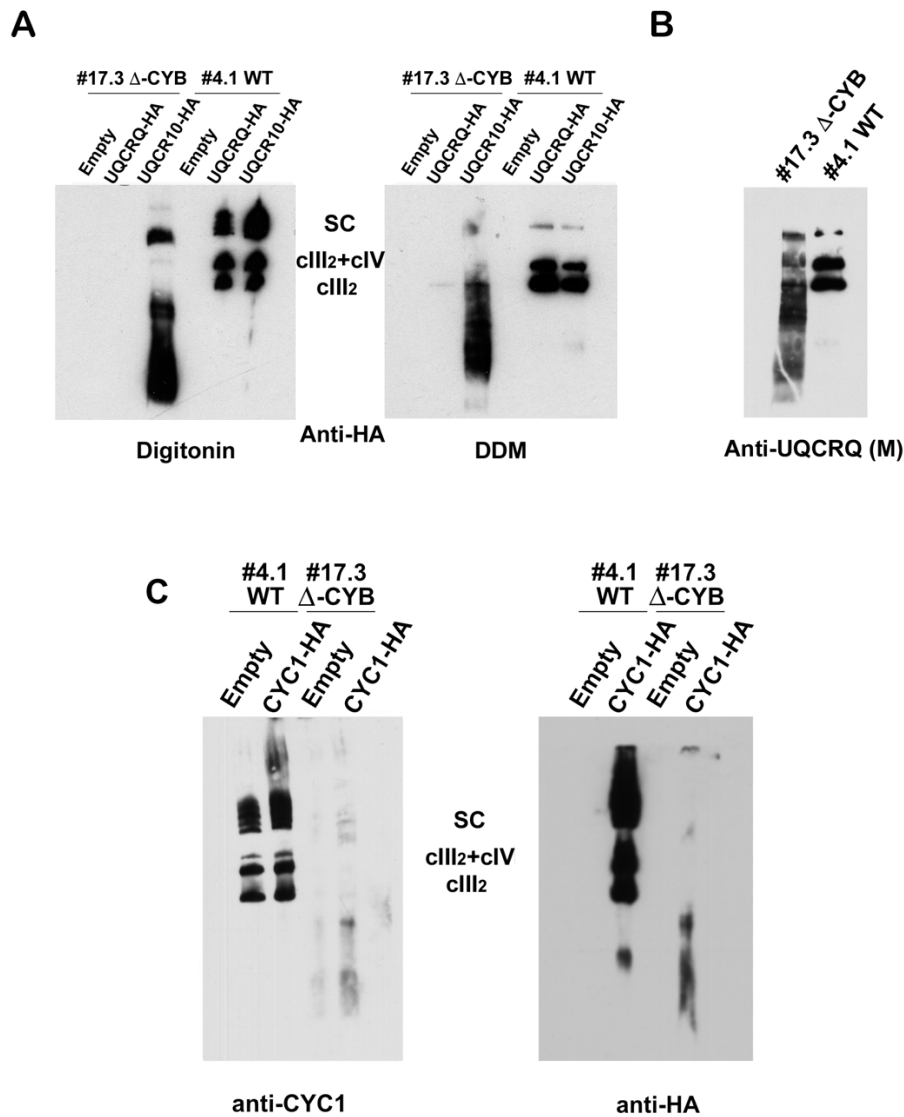


Figure 5.5: both tagged and endogenous UQCR10 and CYC1 were found in various high- and low-molecular-weight species in 1D BN-PAGE when MTCYB is absent. A) BN-PAGE, Western blot, and immunodetection, with an anti-HA tag antibody, of WT and Δ 4-CYB cells stably overexpressing UQCRQ-HA and UQCR10-HA and cells transduced with the pWPXLd-ires- Puro^R empty vector (lentiviral expression vector without any cDNA insert). Samples were solubilised in either 1% digitonin or 1% DDM. B) BN-PAGE, Western blot, and immunodetection of DDM-treated mitoplast samples of non-transduced Δ 4-CYB and WT cells. Membranes were blotted with the monoclonal (M) mouse anti-UQCRQ antibody (likely recognising UQCR10). 5.5A and B were performed by Dr Erika Fernández-Vizarra. C) BN-PAGE, Western blot, and immunodetection, with an anti-HA tag and an anti-CYC1 antibody, of WT and Δ 4-CYB cells stably overexpressing CYC1-HA and cells transduced with the empty vector.

5.2.3 CYC1-HA accumulates at the mitochondrial surface in $\Delta 4$ -CYB cells

As described above, the tag in CYC1-HA did not affect its incorporation and the assembly of CIII and SC in WT cells (Figure 5.5C). However, the overexpression in $\Delta 4$ -CYB cells led to the accumulation of the unprocessed precursor form of the protein (Figure 5.4B). It is plausible that CYC1 import and/or processing could be impaired when CIII assembly is largely compromised, representing an additional and unknown regulatory mechanism. The presence of a strong signal at ~ 35 kDa in the mutant line suggests that the immature CYC1-HA form is predominant, and might remain in the cytosol or anchored to the OMM. However, additional bands with an apparent molecular weight between 25 (mature form) and 35 (unprocessed form) kDa were also detected, both in the $\Delta 4$ -CYB and in the WT cells. CYC1 maturation is a two-step cleavage process (Arnold et al., 1998), and these bands might represent intermediate processed protein. To verify this, the subcellular and submitochondrial localisation of CYC1-HA was studied in both WT and mutant cells with fractionation (Figure 5.6) and super-resolution microscopy (N-SIM) experiments (Figure 5.7).

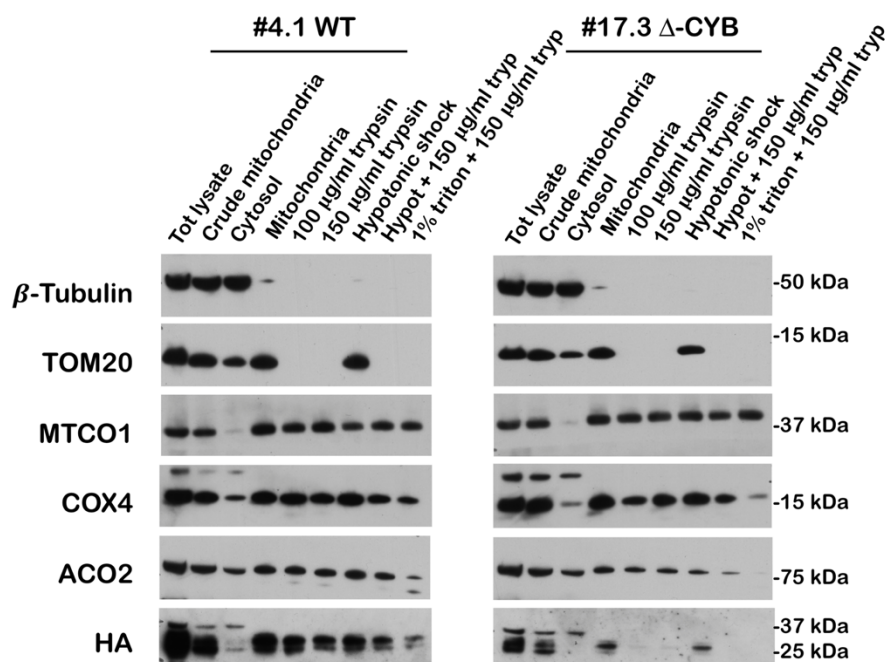


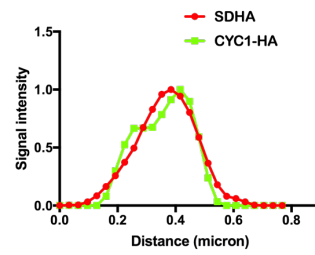
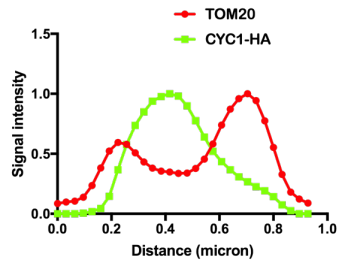
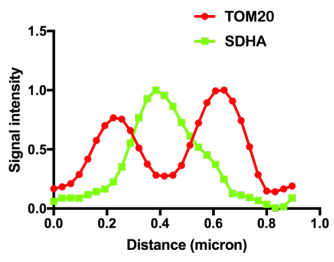
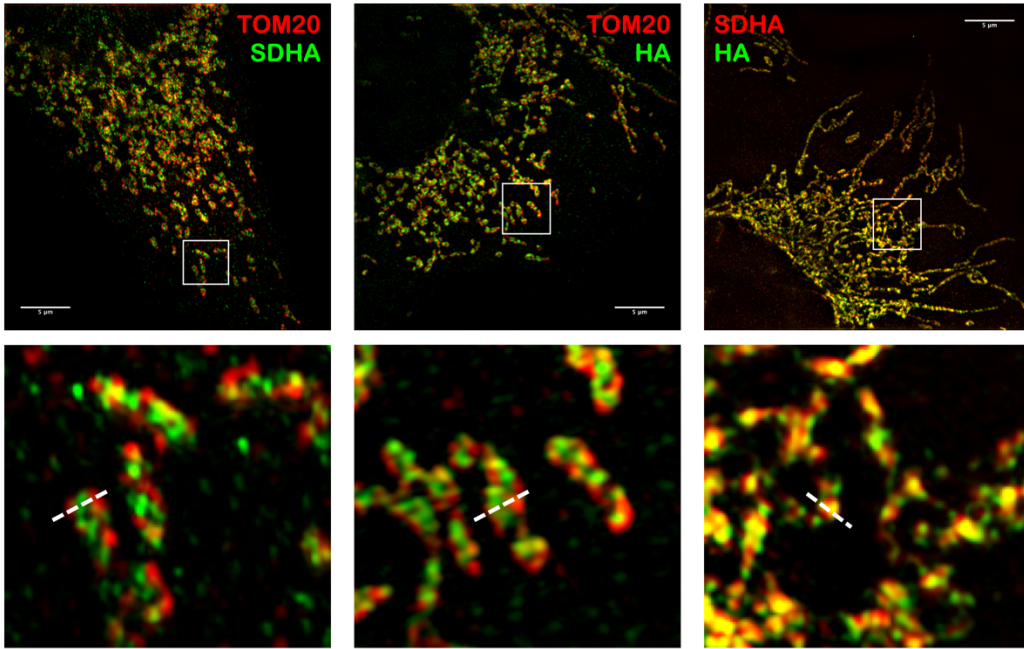
Figure 5.6: *CYC1-HA* mostly accumulates in the OMM when overexpressed in the $\Delta 4$ -CYB cells. SDS-PAGE and Western blot analysis of WT and $\Delta 4$ -CYB cybrids overexpressing *CYC1-HA* subcellular

fractions: total lysate, crude mitochondria (unwashed mitochondrial pellet), cytosol (post-mitochondrial extraction supernatant), mitochondria, and mitochondria undergone the following treatments: trypsin (100 µg/ml and 150 µg/ml), hypotonic shock, hypotonic shock + trypsin (150 µg/ml), and 1% triton + trypsin (150 µg/ml). TOM20 was used as an OMM marker, COX4 and MTCO1 as IMM markers and aconitase 2 (ACO2) as a matrix marker. β-tubulin was used as a cytosolic marker.

In both WT and Δ4-CYB cells, the CYC1-HA precursor band of approximately 35 kDa, is mainly found in the cytosolic fraction, while the mature form, with a size of 27 kDa, is in the mitochondrial fractions. As shown above (Figure 5.4), the precursor band tends to accumulate in the Δ4-CYB cells. Following treatment with trypsin, with or without hypo-osmotic shock, mature CYC1-HA form is still present in the mitochondrial fraction of WT cells, similarly to the IMM markers MTCO1 and COX4, indicating that the protein is imported in the IMM, where it is protected from the protease activity. In the mutant cells, instead, most of CYC1-HA is sensitive to the trypsin treatment even in intact mitochondria, similar to the OMM marker TOM20. These results indicate that in the Δ4-CYB cybrids, CYC1-HA remains partially at the mitochondrial surface as immature form and only a minor mature form reaches the IMM.

This behaviour was confirmed with submitochondrial analysis by N-SIM (Nikon structured illumination microscope) imaging (Figure 5.7). CYC1-HA was visualised with an anti-HA antibody, while outer or inner membrane were marked with anti-TOM20 or anti-SDHA primary antibodies, respectively. Fluorescence was detected using appropriate secondary antibodies conjugated to 488 nm and 568 nm fluorophores. As expected, in WT cells, CYC1-HA co-localised with the IMM marker SDHA (CII). Moreover, the HA fluorescent signal appears clearly separated and surrounded by the TOM20-labelled OMM, similar to SDHA labelling, indicating that CYC1-HA is localised to the IMM. In contrast to WT cells, the co-localisation of the HA and SDHA signals decreased and CYC1-HA was found co-localising more with TOM20 in mutant cells. Together, these results strongly indicate that CYC1-HA import is reduced in cells unable to assemble CIII.

#4.1 WT



#17.3 $\Delta 4$ -CYB

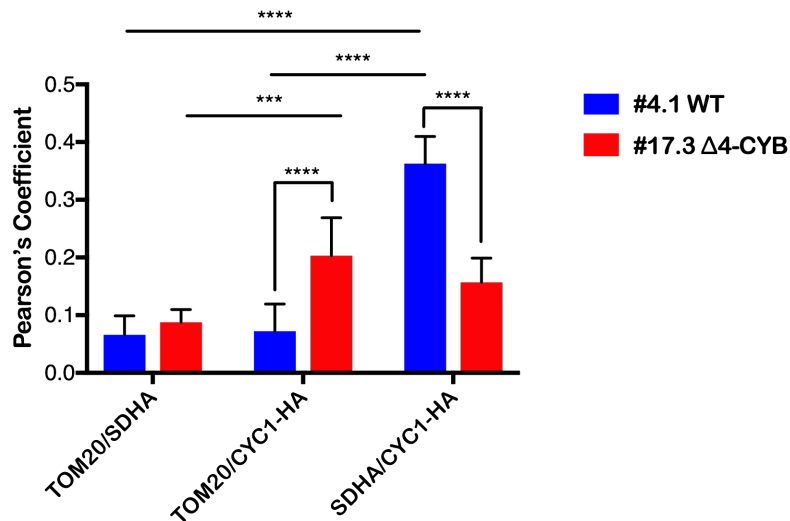
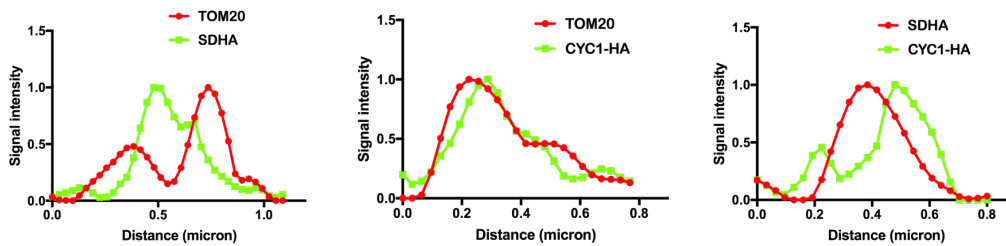
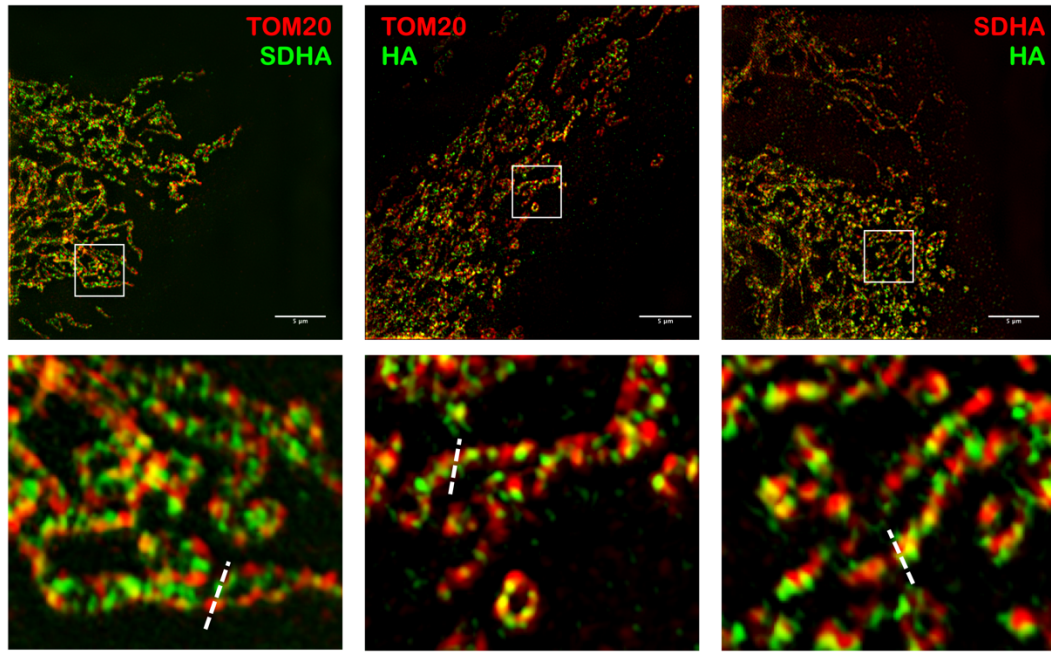


Figure 5.7: *CYC1-HA* submitochondrial localisation by N-SIM super resolution microscopy. Representative N-SIM images of WT and $\Delta 4$ -CYB cells overexpressing *CYC1-HA*. *CYC1-HA* was labelled with an anti-HA antibody Alexa Fluor® 488 Conjugate. Primary antibodies against TOM20 and SDHA and Alexa Fluor® conjugated secondary antibodies were used to label the OMM and the IMM, respectively. Bottom panels show line plots of the two channels through mitochondria at locations indicated by the white dashed lines. At least 5 images were taken for each condition. Scale bars: 5 μ m. The bar graph shows the Pearson's coefficient in co-localised volume of TOM20, SDHA, and *CYC1-HA*.

HA. Data show mean \pm SD ($n=5$). One-way ANOVA ($***P = 0.0004$ and $****P < 0.0001$) was employed for the statistical analysis.

5.3 Searching for candidate CIII assembly factors

In order to identify possible partner proteins interacting with the accumulated UQCR10 and CYC1-containing CIII assembly intermediates, quantitative SILAC and immunopurifications (IP) with an anti-HA antibody conjugated to Sepharose beads were performed. WT and mutant cells were grown in heavy “H” and light “L” SILAC medium and two experiments with reciprocal labelling were conducted for each condition. In the first experiment (Figure 5.8A), WT and mutant cybrids transduced with UQCR10-HA were compared. Consistent with the previous experiments, the immunopurified UQCR10 and CYC1 were found similarly abundant in the WT and in the mutant, while most of the other CIII subunits were strongly enriched in the WT cells ($< -5 \log_2$ ratios, 32-fold lower). Interestingly, UQCRH showed a similar behaviour to CYC1 and UQCR10, suggesting a possible participation of this subunit in the formation of pre-assembly intermediates. Unfortunately, lacking an antibody able to detect UQCRH in WB analyses, further analyses to confirm this hypothesis were not possible. The same experiment was performed with the cell lines overexpressing CYC1-HA (Figure 5.8B), which confirmed the enrichment in WT cells of UQCRC1, UQCRC2, and UQCRFS1 subunits in $\Delta 4$ -CYB cells. However, fewer proteins were identified by CYC1-HA IP compared to UQCR10-HA IP. This could be due to the lower amounts of mature CYC1-HA that reach the IMM in the mutant cells.

In addition, these experiments revealed several CIV structural subunits interacting with UQCR10-HA and CYC1-HA both in WT and in mutant cells. Interestingly these CIV subunits are mainly part of the MTCO2 module (MTCO2, COX5B, COX6C), intermediate stage of CIV assembly, with the only exception of COX6B1, belonging to the MTCO3 module, late assembly stage (Signes and Fernández-Vizarra 2018). These data suggest an involvement of CIV or of its assembly intermediates during CIII maturation. COX7A2L was also co-immunopurified with UQCR10-HA, showing strongly reduced levels in the $\Delta 4$ -CYB cybrids. This observation supports previous findings which saw COX7A2L as preferentially bound to CIII (Pérez-Pérez et al., 2016).

Finally, few other mitochondrial proteins were found to interact with UQCR10 or CYC1 and with positive \log_2 ratios. These proteins, which appear in the upper-right quadrant of the scatter plots (Figure 5.8), show greater enrichment in the mutant cybrids than in the WT, suggesting that they are probable chaperones or assembly factors that interact with the assembly intermediates or the free proteins. Proteins found interacting preferentially with UQCR10-HA in the mutant cells, were GHITM/MICS1, CHCHD3/MIC19, and HADHB, subunit beta of the fatty acid beta-oxidation trifunctional enzyme (Eaton et al., 2000). CYC1-HA was immunopurified with STOML2, involved in cardiolipin organisation and compartmentalisation (Ikon and Ryan, 2017), and HCCS, Cytochrome c-type heme lyase involved in the delivery and binding of the heme group to CYC1 (Dumont et al., 1987). We decided to focus on GHITM and CHCHD3 as CIII assembly factor candidates. These two proteins have been described as IMM proteins involved in the shaping of mitochondria, but their exact molecular role is still unknown. Therefore, we decided to investigate if they could have a role in the biogenesis of CIII, as suggested by our co-IP and proteomics experiments. GHITM (Growth hormone-inducible transmembrane protein) is a poorly characterised IMM protein required for the organisation of the mitochondrial network and cristae, which have been found to interact with CIII and CIV in *Drosophila* (Meng et al., 2017). CHCHD3, instead, is part of the MICOS complex and localises at the CJ, where the assembly of CIII starts (Stoldt et al., 2018).

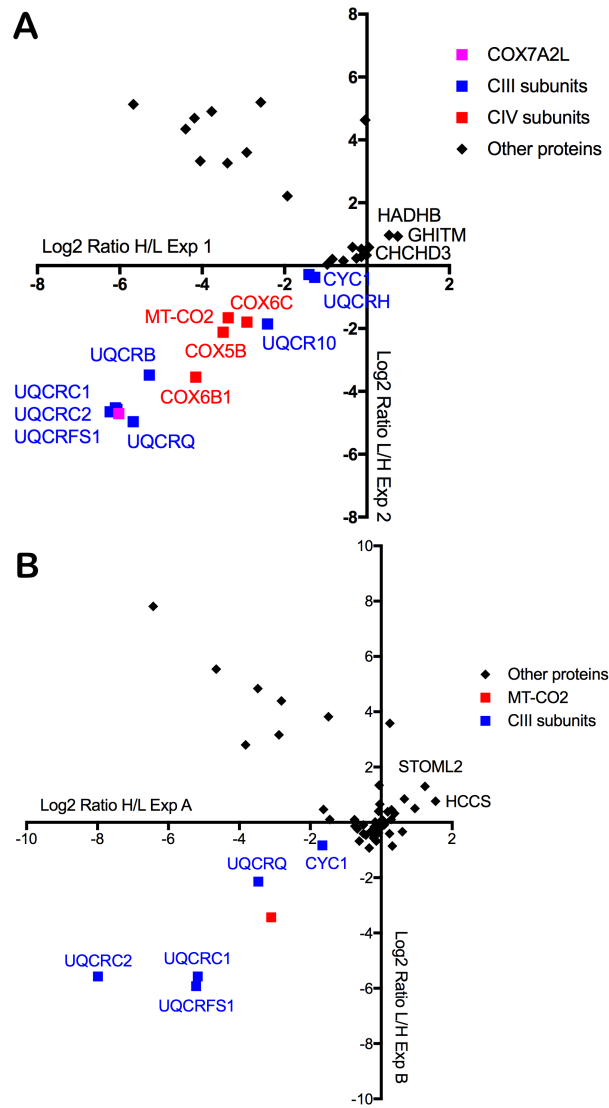


Figure 5.8: SILAC/co-immunopurification analysis of UQCR10-HA and CYC1-HA. Scatterplots showing the logarithmic heavy to light (H/L) ratios obtained after mass spectrometry analysis of –HA immunopurification (HA antibody conjugated to Sepharose beads) of WT and $\Delta 4$ -CYB cells transduced with UQCR10-HA (A) and CYC1-HA (B), after SILAC labelling. Two reciprocal labelling SILAC experiments were performed and plotted one in x-axis and the reverse in the y-axis. Proteins detected in the upper right quadrant were found interacting with UQCR10-HA or CYC1-HA in both WT and mutant cells, but were more abundant in the mutant line. Vice versa, proteins indicated in the bottom left quadrant were more abundant in the WT cells. Proteins localising in the upper left and in the bottom right quadrant are contaminant. 5.8A was performed by Dr Erika Fernández-Vizarra. The mass spectrometry samples and data were processed by Dr Shujing Ding.

5.3.1 Characterisation of the role of GHITM/MICS1 and CHCHD3/MIC19 in CIII assembly and/or function

In order to verify if GHITM/MICS1 and CHCHD3/MIC19 were affected by defects in the respiratory chain and specifically by CIII deficiency, we ran two experiments. Firstly, CHCHD3 and GHITM steady-state levels were analysed by WB and immunodetection after SDS-PAGE (Figure 5.9). In parallel, two MICOS complex subunits (MIC60 and MIC10) and TOM20 were analysed at the same time as controls. To verify if changes in protein levels were due to specific CIII deficiency or to more general OXPHOS defects, protein levels of GHITM and CHCHD3 were also analysed in two additional cell lines, one cybrid cell line homoplasmic for a mutation in MTCO3, presenting CIV assembly defects (Tiranti et al., 2000), and the 143B ρ^0 cells lacking mtDNA and therefore unable to form CI, CIII and CIV. Interestingly, while CHCHD3 did not show specific differences in the different cell lines tested, GHITM appeared significantly increased in $\Delta 4$ -CYB and ρ^0 cells, but not in the CIV deficient cells (Figure 5.9).

Secondly, CHCHD3 and GHITM distributions associated with the absence of MTCYB were then examined by SILAC-based complexome profiling on total mitochondrial extracts, solubilised with either 1.6 mg DDM/mg of protein or 4 mg digitonin/mg of protein (Figure 5.10). While CHCHD3 profile was not affected by CIII deficiency, GHITM profile showed a change in distribution characterised by a number of high- and low-molecular-weight complexes in mutant cells that do not exist in WT cells. This observation suggests a possible interaction with CIII intermediates in the mutant and a consequent role in the enzyme biogenesis.

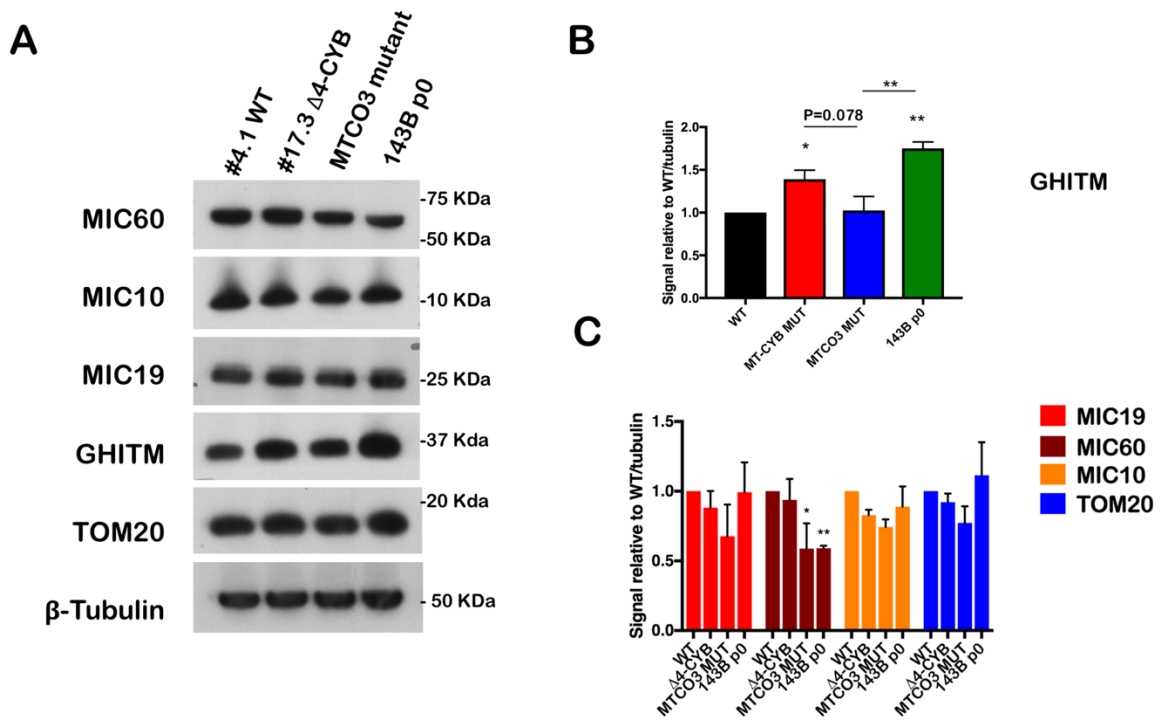


Figure 5.9: *GHITM* steady-state levels are increased in $\Delta 4$ -CYB cybrids and ρ^0 cells, but not in *MTCO3* mutant cells. A) SDS-PAGE, Western blot and immunodetection of samples extracted from total lysate of WT, $\Delta 4$ -CYB, *MTCO3* mutant cybrids and 143B ρ^0 cells. The graphs (B, C) show the densitometric quantification of the signals corresponding to each protein normalised to that of β -tubulin and referred to WT (1.0). Values are plotted as the mean \pm SD ($n = 3$). For statistical analysis two-way ANOVA test was used. * $P < 0.05$; ** $P = 0.01$. β -tubulin was used as loading control.

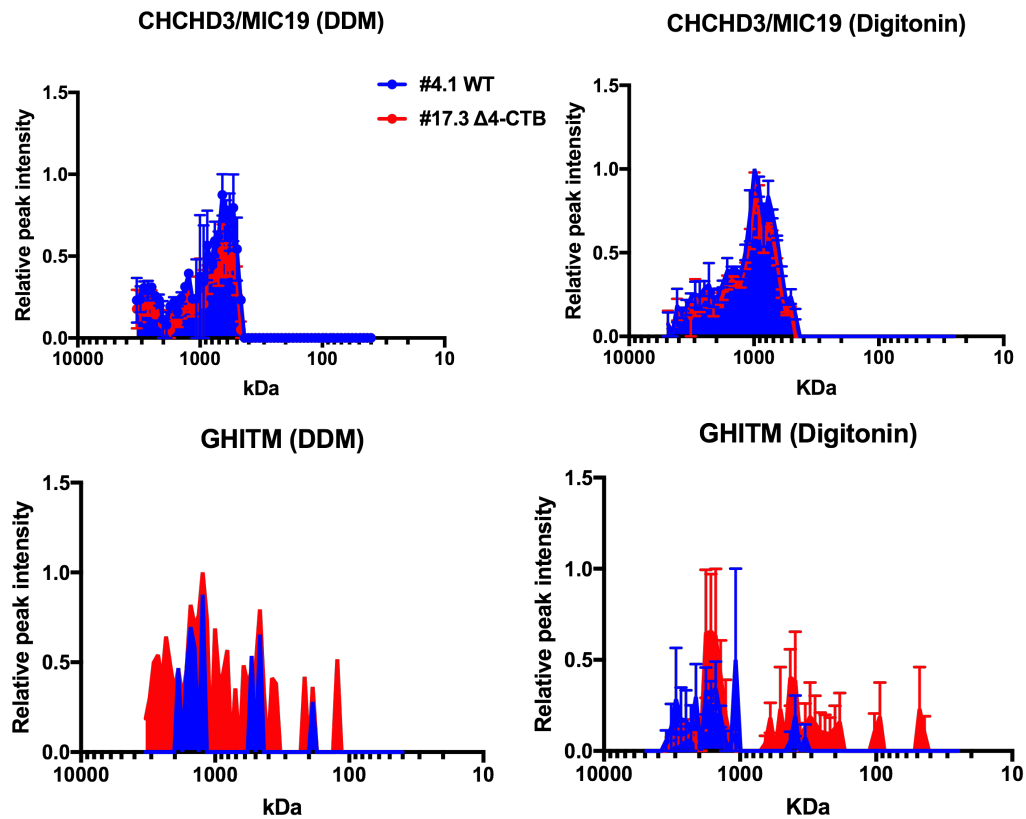


Figure 5.10: *GHITM* accumulates in many different high- and low-molecular-weight species in $\Delta 4$ -CYB cells, while *CHCHD3* complexome profile is not affected. Complexome profiles of *CHCHD3* and *GHITM* after either DDM or digitonin extractions. Profiles were generated by analysing the peptide content in each of the 64 slices in which the gel lanes were excised. The graphs plot the relative peptide peak intensities, setting the maximum to 1.0, versus the molecular mass calculated using the individual complexes and supercomplexes as the standards to generate a calibration curve. WT profiles are represented in blue and $\Delta 4$ -CYB profiles in red. Values are plotted as the mean \pm SEM of the two reciprocal labelling experiments, with the exception of *GHITM* (DDM) which was detected in only one experiment.

To verify this hypothesis, we analysed if downregulation of *CHCHD3* and *GHITM* impacted CIII assembly, analysing complex stability and activity. To assess this, RNA interference (RNAi) was performed through lentiviral transduction of small hairpin RNAs (shRNAs). WT and $\Delta 4$ -CYB cell lines stably expressing shRNAs specific for *CHCHD3* and *GHITM* were generated. For each gene, 5 different shRNAs were tested and the 2 leading to the strongest reduction in the protein of interest steady-state levels in SDS-PAGE and WB analysis were used for further experiments.

5.3.2 Silencing of GHITM in WT and $\Delta 4$ -CYB cybrids

The effects of GHITM knockdown on CIII structure, maturation and ability to form supercomplexes were tested in both SDS- and BN-PAGE combined with WB analyses. These experiments showed that reduced levels of GHITM do not lead to any alteration in the steady-state levels of UQCRQ or UQCRC1 (Figure 5.11A), both in WT and in $\Delta 4$ -CYB cybrids, nor evident defects in CIII and SC formation (Figure 5.11B). Surprisingly, CII, CIII and CIV, even if maintaining the same pattern, appear more abundant in cells transduced for GHITM-shRNAs.

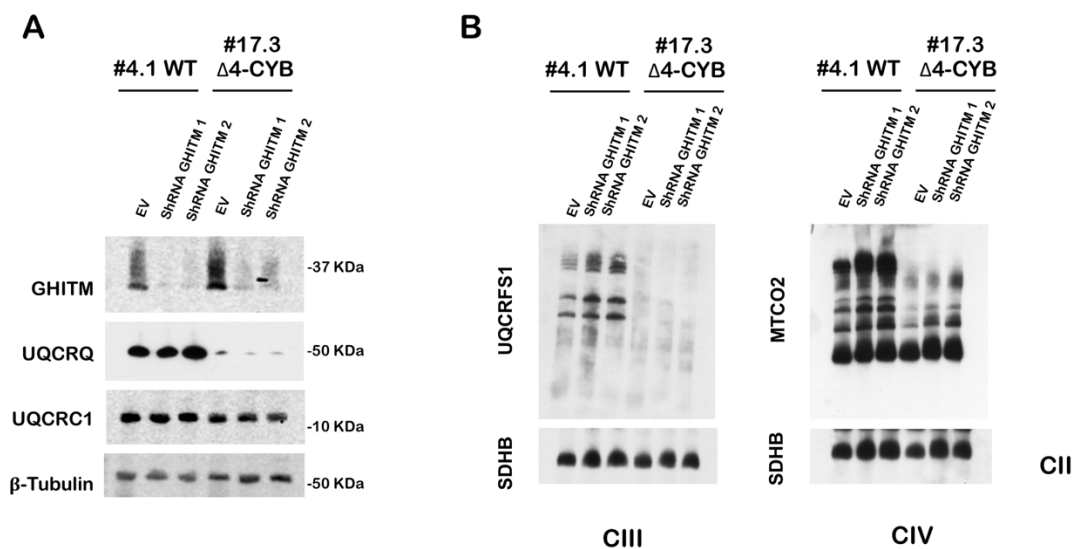


Figure 5.11: CIII subunits steady-state levels, CIII structure and SC formation are not affected by GHITM knockdown. A) SDS-PAGE, Western blot, and immunodetection of samples extracted from total lysate of WT and $\Delta 4$ -CYB stable lines transduced with pLKO.1 empty vector (EV) and two shRNA specific for GHITM. B) 1D BN-PAGE, Western blot, and immunodetection analysis of digitonin-solubilised samples from the same cell lines shown in (A). β -tubulin (A) and SDHB (B) were used as loading controls.

Once ruled out an effect of GHITM on CIII assembly, we then evaluated the effect of GHITM knockdown on the respiratory chain activity, measuring cellular respiration and ETC enzymes activity (Figure 5.12). No significant alteration in respiration and CIII activity was observed. However, an increase in CIV activity was found in one of the two GHITM knockdown clones, an observation that could request further investigations. Altogether these results indicate that while it co-migrates with UQCR10 in complexome profiling and is associated with different

molecular weight complexes in mutant cell lines, GHITM is not specifically involved in neither CIII biogenesis, nor activity.

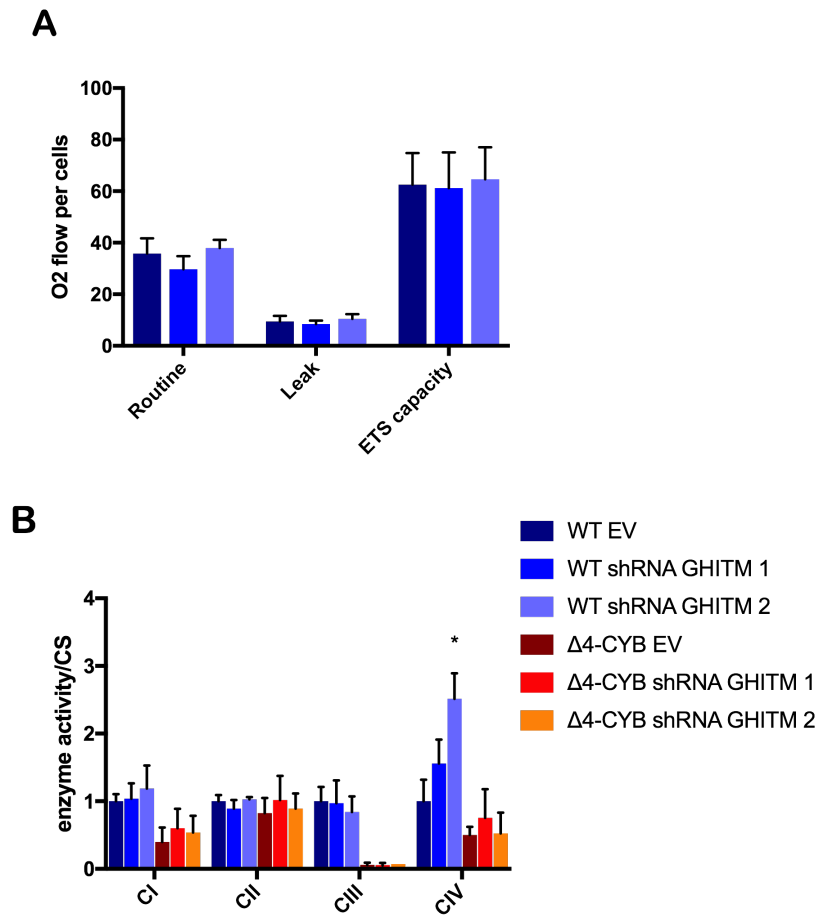


Figure 5.12: knockdown of GHITM expression does not decrease cellular respiration capacity and does not induce CIII enzymatic defects. *A*) Oxygen consumption rates measured in WT cybrids transduced with pLKO.1 empty vector (EV), or lentiviral vectors encoding two different shRNAs specific for GHITM mRNA (shRNA GHITM 1 and shRNA GHITM 2). Respiration was measured in whole cells in the basal state (Routine), in the presence of oligomycin (Leak) and uncoupled with CCCP (ETS capacity), in a O2K high-resolution respirometer (Oroboros instruments). The plotted values are the mean \pm SD ($n = 4$ for WT EV and WT shRNA GHITM 1 and $n = 3$ for WT shRNA GHITM 2). *B*) MRC enzyme activities in WT and $\Delta 4$ -CYB cells transduced with pLKO.1 empty vector (EV) or two shRNA specific for GHITM. Measurements were normalized to the activity of citrate synthase (CS) and referred to WT EV (1.0). The plotted values are the mean \pm SD ($n = 2$ biological replicates). Two-way ANOVA Tukey's multiple comparisons test was used. * $P = 0.0462$ (CIV).

5.3.3 Silencing of CHCHD3/MIC19 in WT and Δ 4-CYB cybrids

Next, WT and Δ 4-CYB cybrids stably downregulating CHCHD3 were characterised. Compared to GHITM, CHCHD3 has been studied more extensively, and it has been shown that its downregulation leads to an alteration in CJ architecture and cristae morphology, and mitochondrial fragmentation in HeLa cells (Darshi et al., 2011). However, its effect on the mitochondrial respiratory chain and more precisely on CIII maturation have not been investigated.

WT and Δ 4-CYB cells were transduced with five different shRNAs targeting CHCHD3, and the two clones exhibiting the strongest reduction were further analysed. Silencing of CHCHD3 was very efficient in the two clones, but neither displayed an evident reduction in either CIII subunits steady-state levels or CIII assembly and in SC formation (Figure 5.13). As for GHITM, these results indicate that CHCHD3 does not have a direct effect on CIII assembly or SC formation.

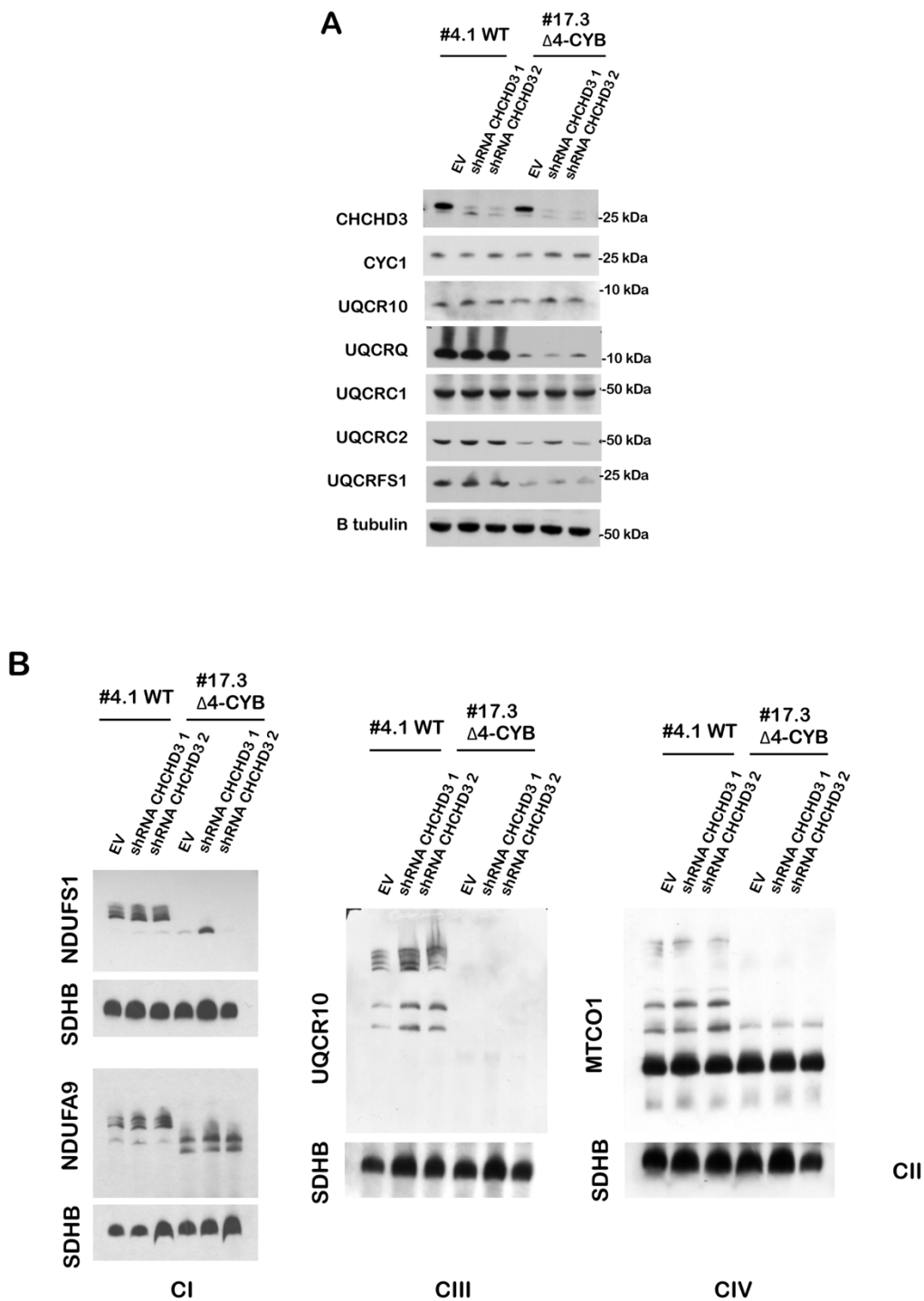


Figure 5.13: *CIII* subunits steady-state levels and *CIII* and *SC* formation are not affected by *CHCHD3* knock-down. *A*) SDS-PAGE, Western blot, and immunodetection of samples extracted from total lysate of WT and Δ 4-CYB stable lines transduced with pLKO.1 empty vector (EV) and two shRNA specific for *CHCHD3*/*MIC19*. β -tubulin was used as a loading control. *B*) 1D BN-PAGE, Western blot, and immunodetection analysis of digitonin-solubilised samples from the same cell lines shown in (*A*). *SDHB* (*CII*) was used as a loading control.

Mitochondrial bioenergetics analysis showed that, CHCHD3 depletion resulted in decreased basal and uncoupled cellular respiration (Figure 5.14A), confirming published results (Darshi et al., 2011). Surprisingly, this decrease in mitochondrial respiration did not correlate with a compromised activity of any of the ETC enzymes (Figure 5.14B). In view of these analyses, while CHCHD3 influences OXPHOS activity in an unknown mechanism, we can conclude that CHCHD3 is not a CIII assembly factor.

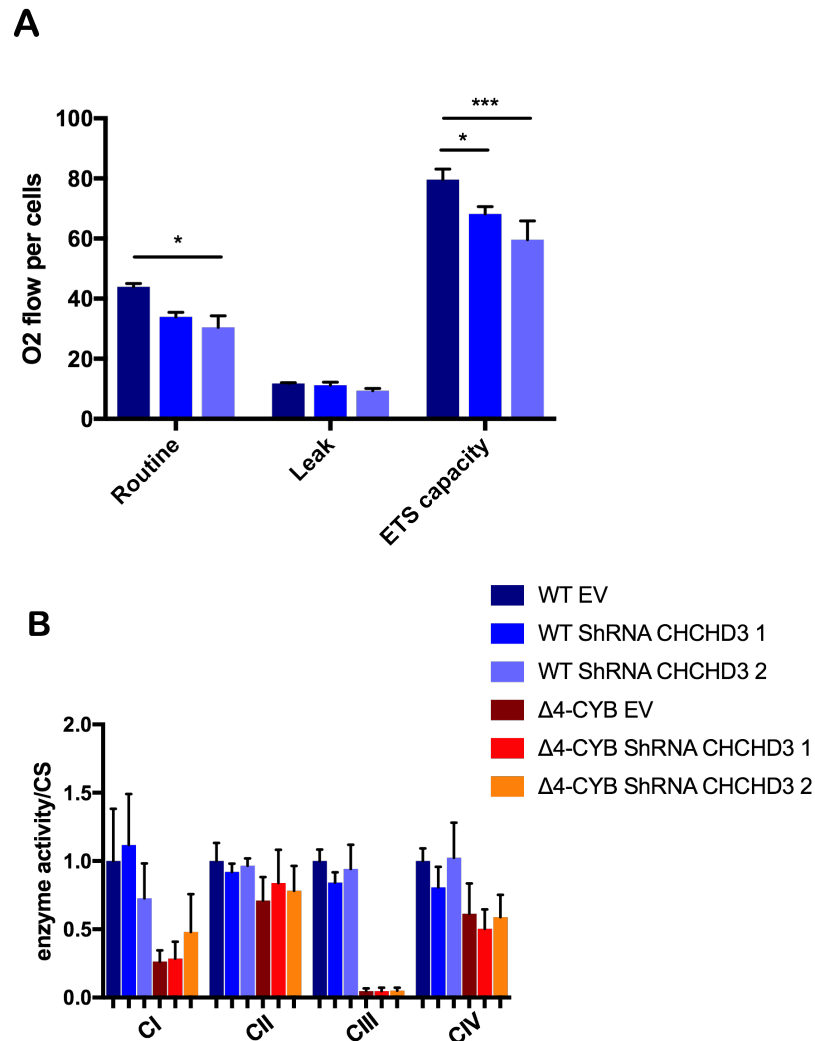


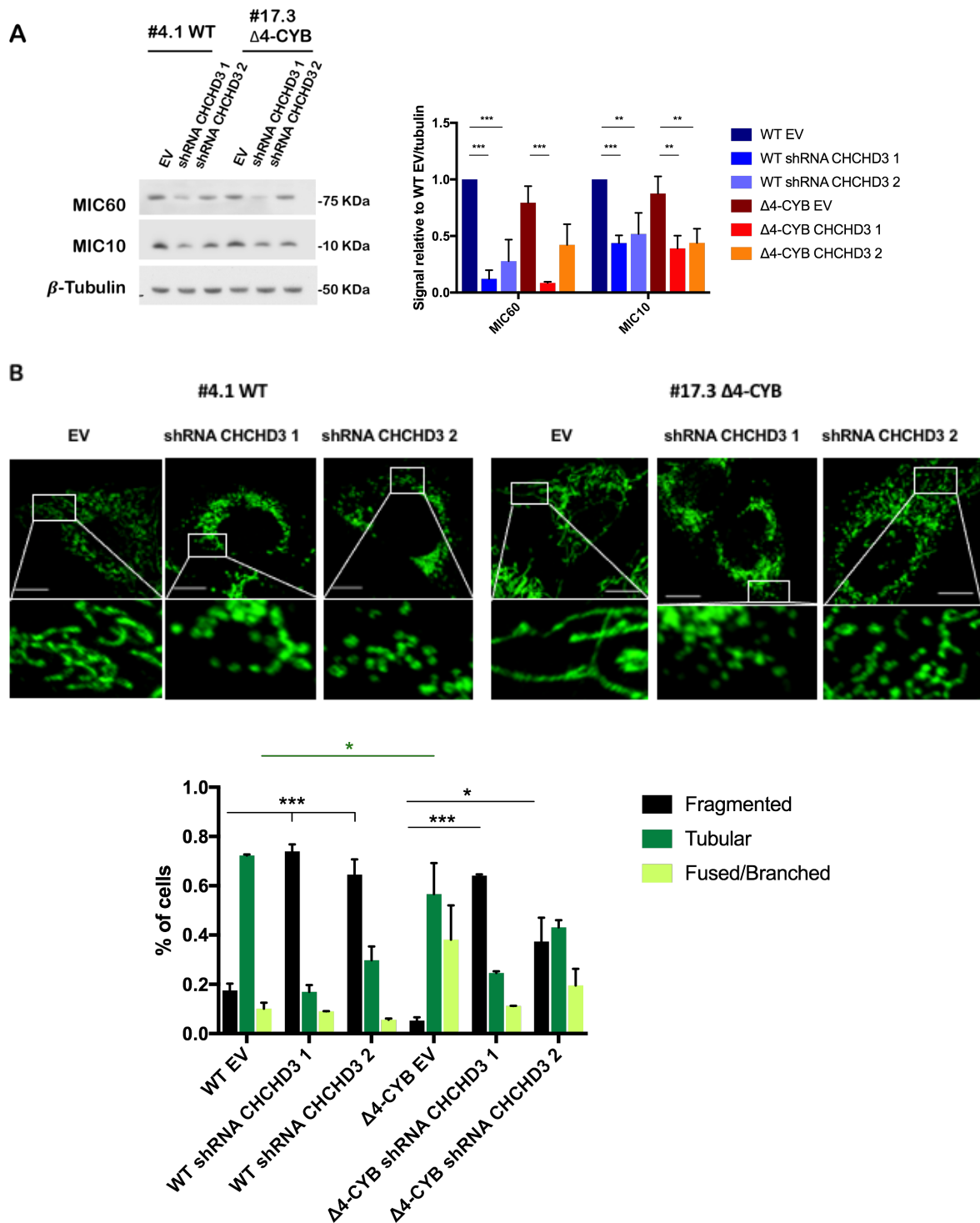
Figure 5.14: knockdown of CHCHD3 expression leads to decreased cellular respiration but does not induce specific CIII enzymatic defect. A) Oxygen consumption rates measured in WT cybrids transduced with pLKO.1 empty vector (EV), or lentiviral vectors encoding two different shRNAs specific for CHCHD3/MIC19 mRNA (shRNA CHCHD3 1 and shRNA CHCHD3 2). Respiration was measured in whole cells in the basal state (Routine), in the presence of oligomycin (Leak), and uncoupled with CCCP (ETS capacity), in a O₂K high-resolution respirometer (Oroboros instruments). The plotted

values are the mean \pm SD ($n = 4$). Two-way ANOVA Tukey's multiple comparisons test was used. * $P = 0.0126$ (Routine shRNA 2); * $P = 0.0386$ (ETS capacity shRNA 1); *** $P = 0.0002$ (ETS capacity shRNA 2). B) MRC enzyme activities in WT and $\Delta 4$ -CYB cells transduced with pLKO.1 empty vector (EV) or two shRNA specific for CHCHD3/MIC19. Measurements were normalised to the activity of citrate synthase (CS) and referred to WT EV (1.0). The plotted values are the mean \pm SD ($n = 4$ biological replicates).

Even if CHCHD3 stable downregulation by shRNA lentiviral transduction had been very efficient (Figure 5.13A), the effects at the level of ETC assembly and functionality were very modest (Figure 5.13B and 5.14), compared to data published before (Darshi et al., 2011). As mentioned above, CHCHD3 is an integral component of MICOS, therefore we decided to test the effects of CHCHD3 silencing on mitochondrial morphology in our cell lines. First, we analysed the steady-state levels of mitochondrial cristae remodelling proteins by SDS-PAGE, WB and immunodetection (Figure 5.15A). Second, we observed the mitochondrial morphology directly by spinning disc confocal microscopy (Figure 5.15B). As previously described in HeLa cells (Ott et al., 2015), stable knockdown of CHCHD3 both in WT and in $\Delta 4$ -CYB cells was associated with reduced levels of the core components of the MICOS complex, MIC60 and MIC10, (Figure 5.15A) and an increased mitochondrial fragmentation phenotype (Figure 5.15B). This confirmed the efficiency of CHCHD3 knockdown and the significant effects on mitochondrial morphology. However, our data does not show any evidence of supercomplex disorganisation when CHCHD3 is silenced in WT cells (Figure 5.13B). Similar results were observed also in yeast, where respiratory complexes and supercomplexes were found intact in Δ MICOS cells (Friedman et al., 2015). This is different to what was described in a model of OPA1-mediated cristae remodelling, where the loss of OPA1 was responsible not only for mitochondrial fragmentation and cristae structure defects, but also SC disassembly (Cogliati et al., 2013). However, in our case, while we can clearly observe mitochondrial fragmentation in CHCHD3 KD cells, more precise analysis of cristae organisation by transmission electron microscopy (TEM) should be performed to confirm cristae structure defects. Indeed, loss of cristae components protein levels is not always associated with structural cristae impairments (John et al., 2005).

Moreover, this experiment highlighted a significant difference in mitochondrial morphology between WT cells, prevalently characterised by tubular organelles, and the $\Delta 4$ -CYB mutant cybrids, with more elongated mitochondria. This is probably the consequence of a process

known as stress-induced mitochondrial hyperfusion (SiMH), which is a protective mechanism against autophagy and cell death required to enhance cell survival (Tondera et al., 2009).



of samples extracted from total lysate of WT and $\Delta 4$ -CYB stable lines transduced with pLKO.1 empty vector (EV) and two shRNA specific for CHCHD3/MIC19. In the graph, the quantification of three independent experiments immunodetecting MIC10 and MIC60 are shown. The plotted values are the mean \pm SD. Two-way ANOVA Tukey's multiple comparisons test was used. ** $P < 0.01$; *** $P < 0.001$. β -tubulin was used as a loading control. B) Representative images of mitochondrial morphology in the same cell lines used in (A). Scale bars represent 10 μ m. Mitochondria were labelled using an anti-SDHA antibody. The graph shows the quantification of mitochondrial morphology in $n = 2$ independent experiments, counting at least 60 cells/experiment. The plotted values are the mean \pm SD. Two-way ANOVA Tukey's multiple comparisons test was used. * $P < 0.05$; ** $P < 0.01$; *** $P < 0.001$. Stars in black indicate differences between EV and shRNA transduced cells, in green differences between WT and $\Delta 4$ -CYB cybrids.

5.3.4 CHCHD3/MIC19 overexpression in WT and $\Delta 4$ -CYB cybrids

Parallel to the characterisation of the cell lines with downregulated CHCHD3 expression, we generated stable lines overexpressing HA-tagged CHCHD3. Differently to CHCHD3 knockdown, its overexpression did not appear to alter the steady-state levels of MIC10 and MIC60 (Figure 5.16 A). CIII subunit steady-state levels were also unchanged in CHCHD3-HA overexpressing cells and no alterations in complex maturation and supercomplex patterns were observed (Figure 5.16 B, C). Moreover, CHCHD3-HA overexpression did not affect ETC complexes activity or cellular respiration (Figure 5.17), rejecting the hypothesis of CHCHD3 second role as a CIII assembly factor.

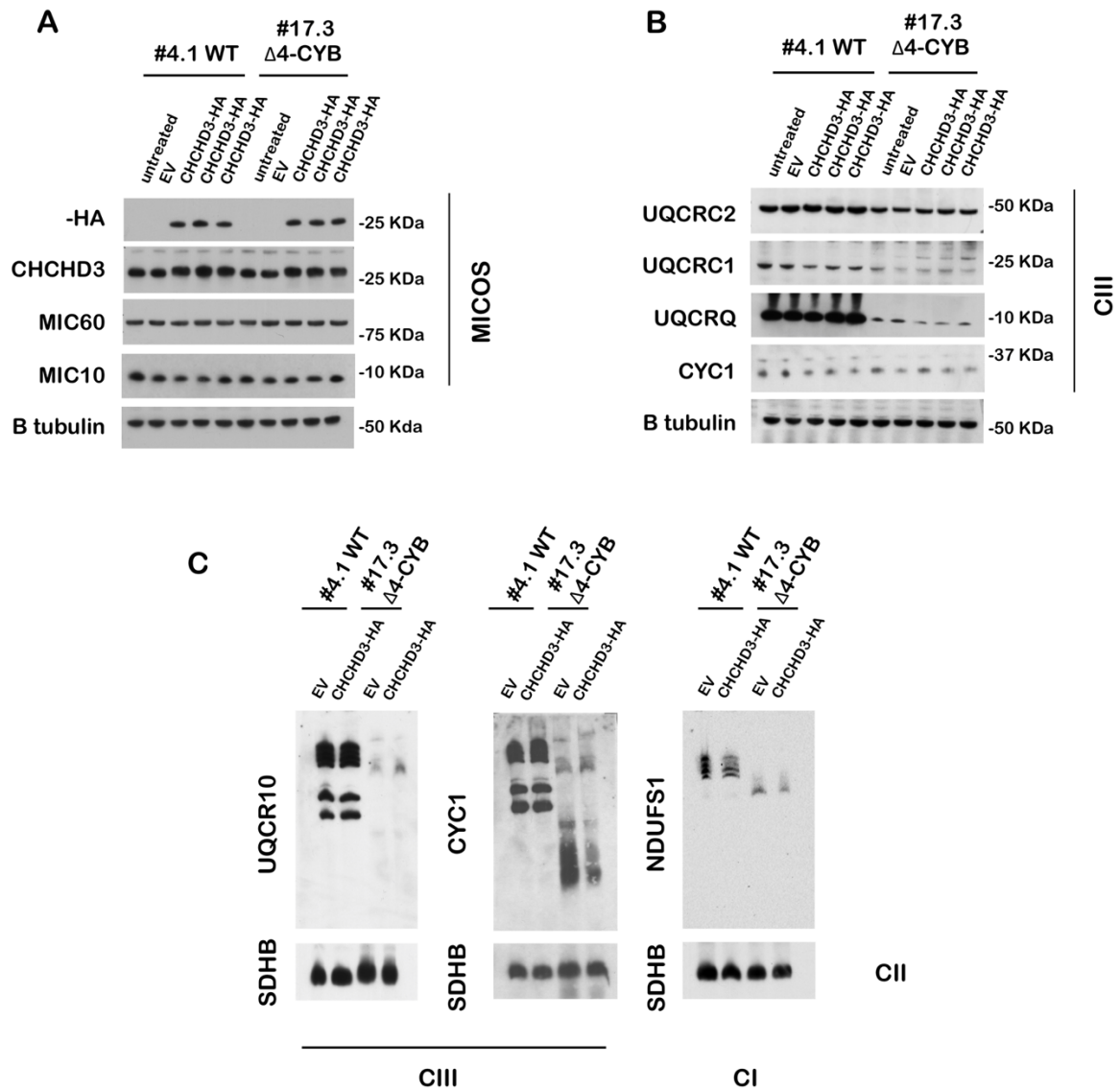


Figure 5.16: *CHCHD3-HA* overexpression does not impact MICOS complex and CIII subunits steady-state levels, or CIII maturation and supercomplexes formation. A, B) SDS-PAGE, Western blot, and immunodetection of samples extracted from total lysate of WT and $\Delta 4$ -CYB cybrids untreated, transduced with *pWPXLd-ires-Hygro^R* empty vector (EV), or *CHCHD3-HA* (three biological replicates). β -tubulin was used as a loading control. C) 1D BN-PAGE, Western blot, and immunodetection of the same cell lines in (A, B) solubilised in 1% digitonin. SDHB (CII) was used as a loading control.

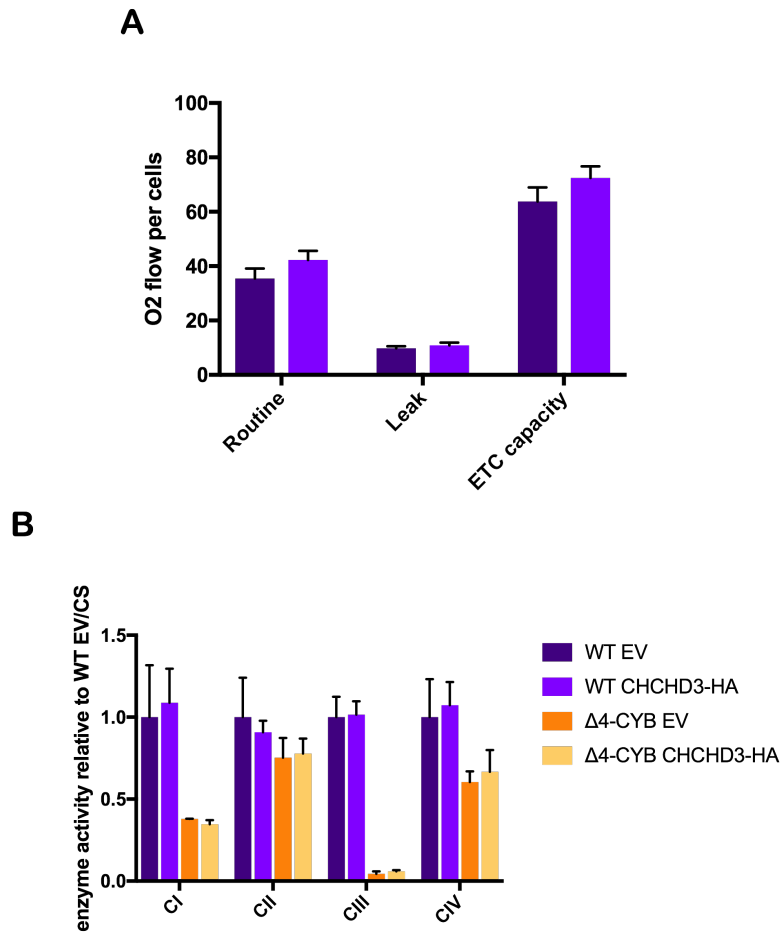


Figure 5.17: *CHCHD3-HA* overexpression did not affect cellular respiration or MRC enzymes activity. A) Oxygen consumption rates measured in WT cybrids transduced with *pWPXLd-ires-Hygro^R* empty vector (EV), or lentiviral vector encoding *CHCHD3-HA*. Respiration was measured in whole cells in the basal state (Routine), in the presence of oligomycin (Leak) and uncoupled with CCCP (ETS capacity), in a O₂K high-resolution respirometer (Oroboros instruments). The plotted values are the mean \pm SD ($n = 4$). B) MRC enzyme activities in WT and $\Delta 4$ -CYB cells transduced with *pWPXLd-ires-Hygro^R* empty vector (EV), or lentiviral vector encoding *CHCHD3-HA*. Measurements were normalised to the activity of citrate synthase (CS) and referred to WT EV (1.0). The plotted values are the mean \pm SD ($n = 3$ biological replicates).

5.4 Characterisation of $\Delta 4$ -CYB cybrids: combined mitochondrial respiratory chain deficiency

We then moved our attention to the effects of the lack of CIII on the other complexes of the respiratory chain, as it is well established that severe CIII defects have pleiotropic effects on the other components of the ETC, especially on CI (Andreu et al., 1999; Blakely et al., 2005; Lamantea et al., 2002). We tested the enzyme activity of each complex in WT and in our model of CIII-lacking cells. As expected, CIII activity was barely detectable in $\Delta 4$ -CYB cells, while CI and CIV activities were significantly lower than the WT ($25 \pm 13\%$ and $64 \pm 11\%$, respectively) (Figure 5.18). A slight non-significant decrease in CII activity was observed in the mutant.

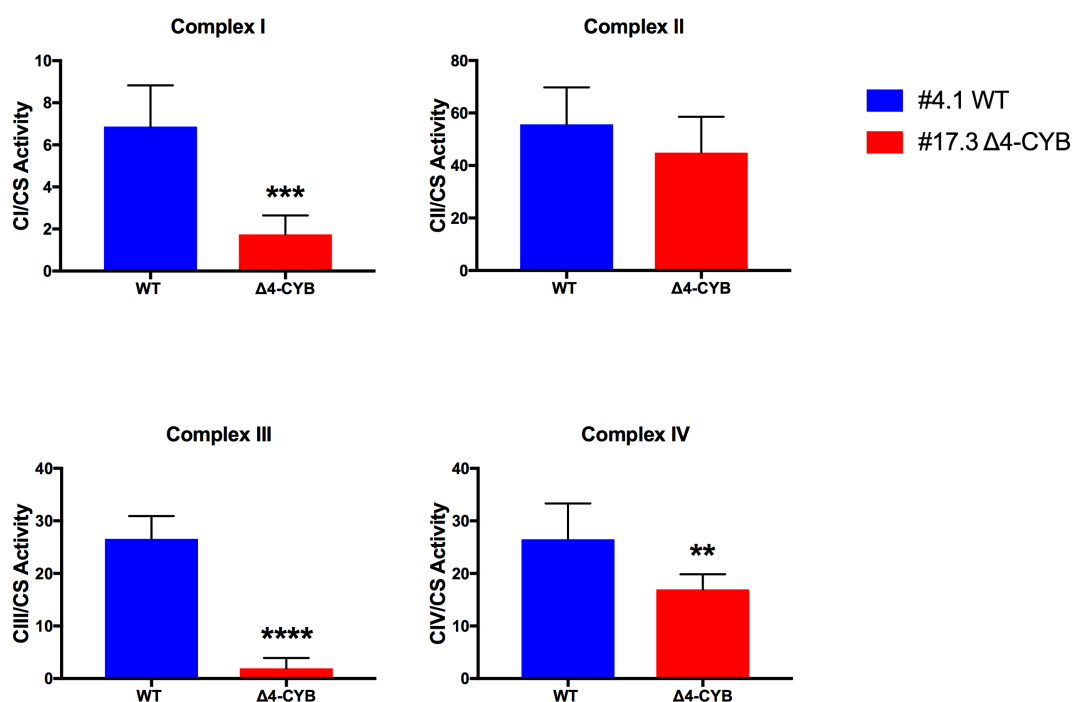
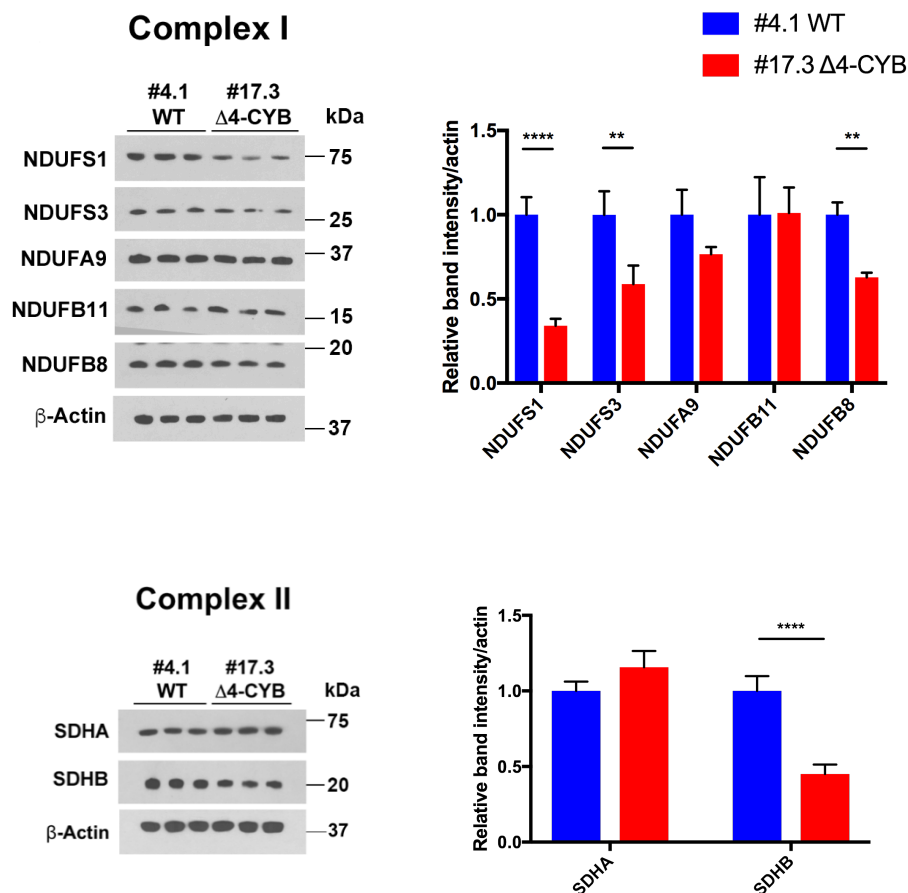


Figure 5.18: *combined respiratory chain complexes deficiency in $\Delta 4$ -CYB cells. The activities (mUnits/g of protein) of the respiratory chain enzymes were determined by spectrophotometric kinetic measurements in WT and $\Delta 4$ -CYB cells and normalised to citrate synthase (CS) activity. Results are expressed as mean \pm SD ($n = 4-6$ biological replicates). Unpaired Student's t -test was used. ** $P = 0.0100$; *** $P = 0.0002$; **** $P < 0.0001$.*

We then decided to study the reason for these biochemical deficiencies, evaluating the effect of the absence of CIII on the other complexes structure. We analysed the steady-state levels of various CI, CII, CIV and CV subunits by SDS-PAGE and WB analysis (Figure 5.19). CI appeared to be the most affected in $\Delta 4$ -CYB cells, with several subunits showing variable reduction. Interestingly, subunits that are part of modules inserted in the late stages of CI assembly were more impacted. Indeed, NDUFS1 of the N-module, showed the strongest reduction, followed by NDUFB8 (ND5-module) and NDUFS3 (Q-module). Contrarily, NDUFA9 and NDUFB11 of the early assembly ND2- and ND4-module, respectively, were not significantly reduced in the mutant samples. The steady-state levels of individual CIV subunits were not strongly changed in $\Delta 4$ -CYB cells, with the exception of COX6B1, being significantly reduced. Surprisingly, CII levels highlighted a reduction in SDHB amounts in mutant cybrids compared with WT, but not of SDHA. The residual SDHB, however, seems to be sufficient to ensure the assembly of the complex and a normal CII activity. CV subunits levels, instead, were not affected by the CIII defect.



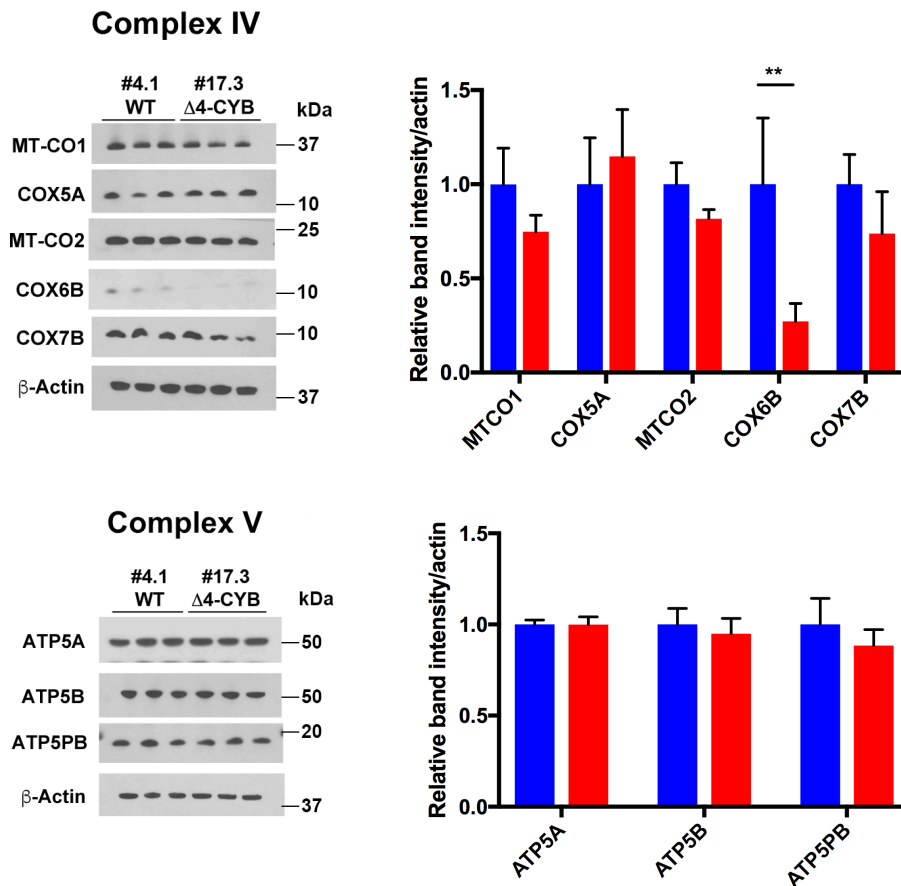


Figure 5.19: *certain, but not all, CI, CII and CIV subunits show lower steady-state levels in mutant cells. CV subunits are not affected. SDS-PAGE, Western blot, and immunodetection of CI, CII, CIV and CV structural subunits of total cell lysates from three independent replicates of WT (blue) and Δ4-CYB cells (red). The graphs show the densitometric quantification of the signals corresponding to each subunit normalised to that of the β-actin. All the measurements are relative to the mean of the three WT samples, set to 1.0. Data are plotted as mean ± SD (n = 3). Two-way ANOVA with Sidak's multiple comparisons test was used. ****P < 0.0001; **P < 0.01. β-Actin was used as loading control.*

Accordingly, the SILAC-based quantitative proteomics analysis of the Δ4-CYB and the WT cybrids solubilised with 1.6 mg DDM/mg protein showed a profound downregulation of CI and CIII subunits, followed by CIV and marginally CII, while CV levels were found unchanged (Figure 5.20). On the contrary, we found the CI assembly factor NDUFAF2 (Ogilvie et al., 2005), and the CII assembly factor SDHAF2 (Hao et al., 2009) significantly upregulated in the Δ4-CYB mutant cells, together with GHITM and its interactor CHCHD2 (Baughman et al., 2009; Oka et al., 2008), confirming the data presented earlier. This analysis included the relative quantification of 1,263 proteins.

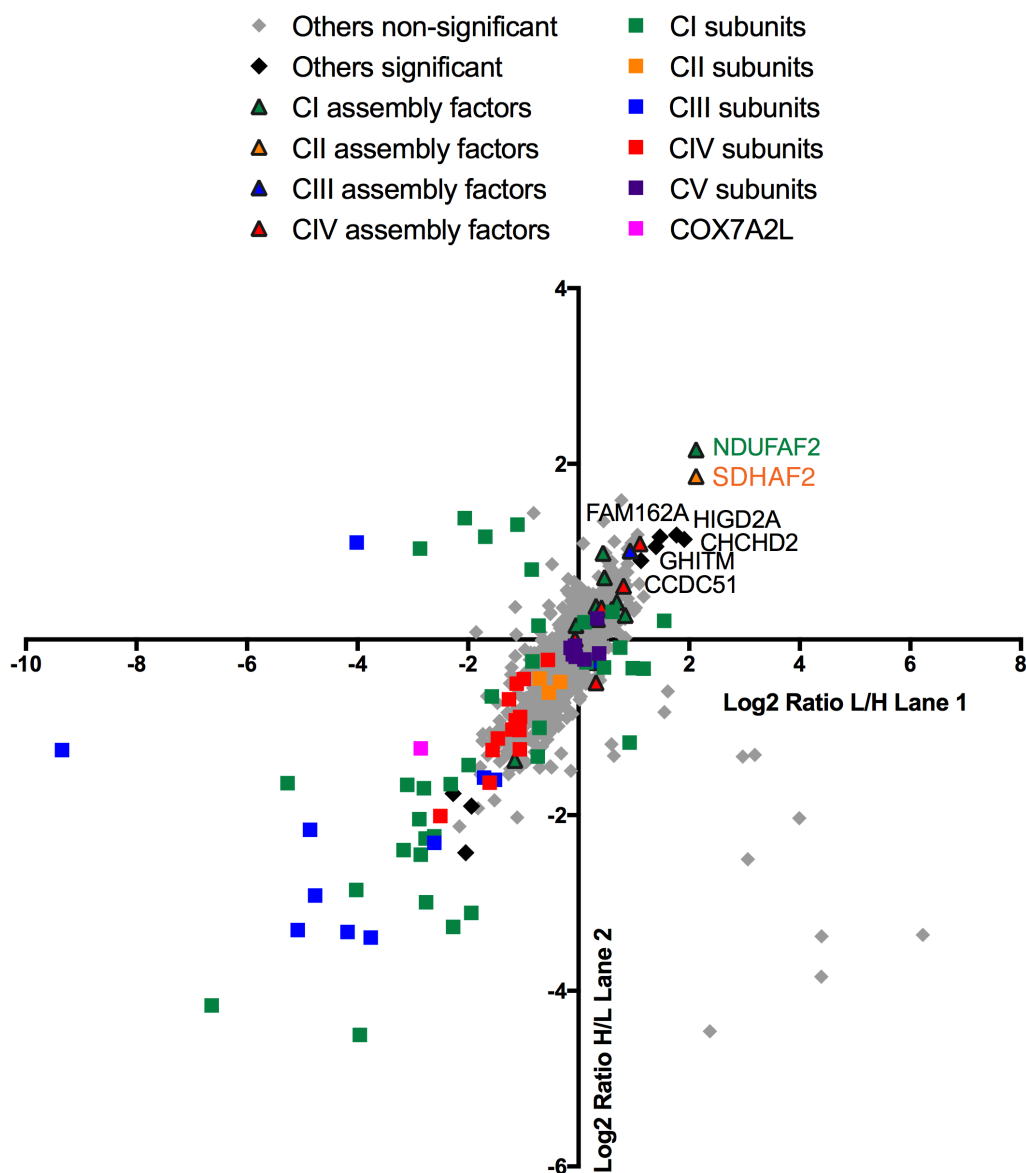


Figure 5.20: **quantitative proteomics analyses confirmed the reduced steady-state levels of ETC complexes subunits in $\Delta 4$ -CYB cells.** Scatter plot generated from the peptide content analysed by mass spectrometry in the complexome duplicate experiments performed with mitochondria isolated from WT and $\Delta 4$ -CYB cells and solubilised with 1.6 mg DDM/mg protein. Peptide content was analysed in each of the 64 slices excised from BN-PAGE and after quantifying the heavy-to-light (H/L) and light-to-heavy (L/H) ratios in both reciprocal labelling experiments. The logarithmic ratios were calculated using MaxQuant (Cox & Mann, 2008), and the statistical significance of the differences for the enrichment or depletion of the proteins was determined using Perseus (Cox & Mann, 2011; Tyanova et al., 2016).

To test whether the observed reduction of CI steady-state levels is the result of protein destabilisation due to impaired CI assembly and not due to a repression of subunit expression at the transcriptional level, we measured mRNA levels of several CI subunits by qPCR. In this assay, we included both mtDNA (MT-ND1) and nuclear-encoded subunits (NDUFB8 and NDUFB11), which belong to different assembly modules and showed different steady-state levels in the mutant cells. The transcriptional levels of these subunits were not reduced in $\Delta 4$ -CYB cybrids (Figure 5.21), indicating that the decreased levels of the proteins observed were not due to down-regulation of CI subunits transcription.

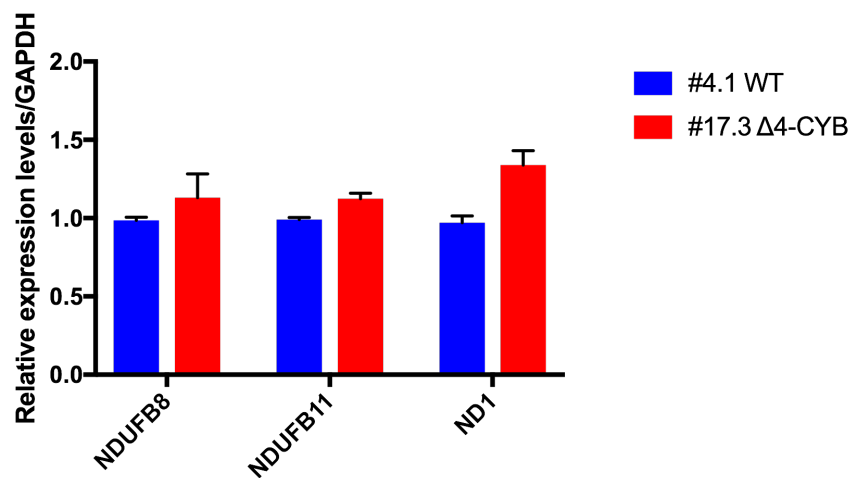


Figure 5.21: CI subunits mRNA levels are not reduced in $\Delta 4$ -CYB cells. Quantitative RT-PCR analysis of the expression at the mRNA level of three structural CI subunits. Total RNA was extracted from WT and $\Delta 4$ -CYB cells and was retrotranscribed. TaqMan Gene Expression Assay (Applied Biosystems, Thermo Fisher Scientific) was used to measure the levels of each transcript. NDUFB8, NDUFB11 and ND1 levels were normalised to that of the housekeeping gene GAPDH. Data are plotted as mean \pm SD ($n = 3$).

5.5 CI assembly: incomplete maturation in the absence of MTCYB

As discussed in the introduction, it has been often observed that strong CIII deficiencies can lead to multi-enzymes defects, affecting especially CI (Acin-Perez et al., 2004; Carossa et al., 2014; Lamantea et al., 2002). Accordingly, we observed a dramatic reduction of fully assembled CI in $\Delta 4$ -CYB cells in 1D BN-PAGE experiments (Figure 5.22). Previous studies

in a mouse fibroblast cell line carrying a missense mutation in MTCYB explained this phenomenon as destabilisation and consequent degradation of CI after its complete assembly, therefore, assuming the assembly of the enzyme as SC-independent and its subsequent stabilisation when included in the SC (Acin-Perez et al., 2004). However, as shown below, our complexome profiles analyses indicated stalling of nascent CI, suggesting a direct involvement of CIII during CI assembly (Figure 5.23).

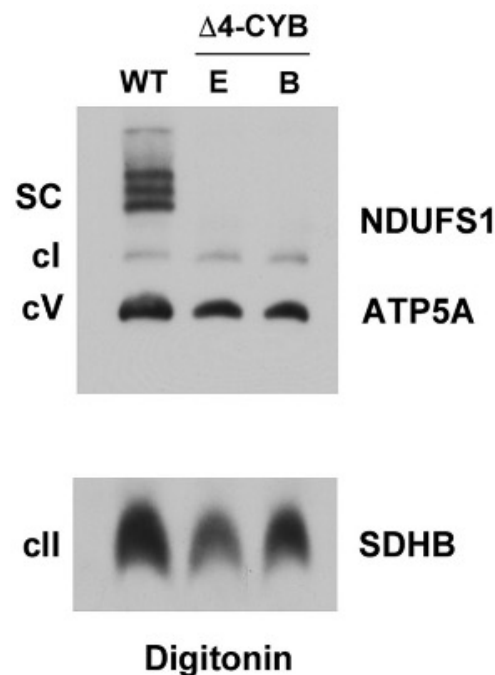


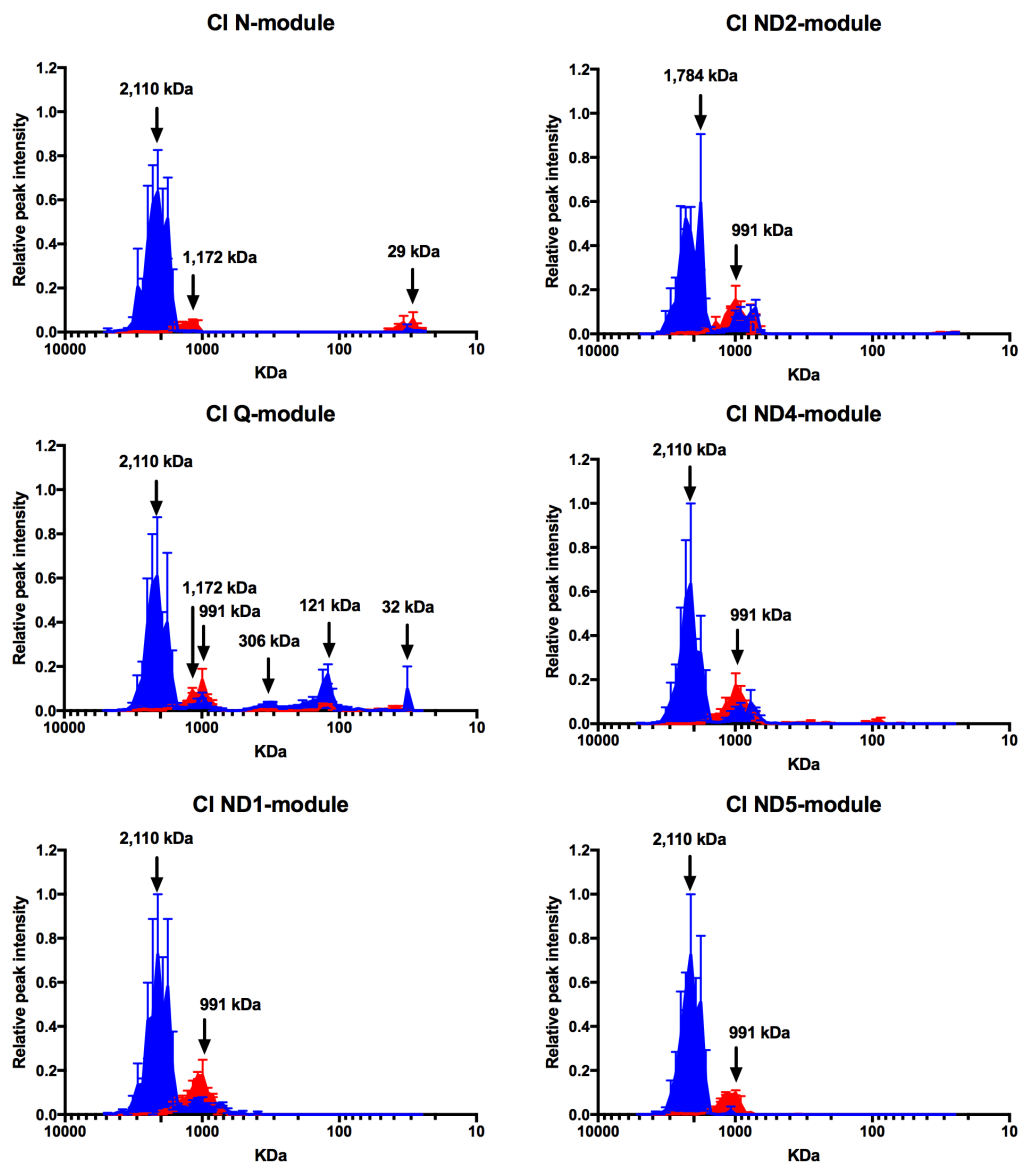
Figure 5.22: $\Delta 4$ -CYB mutation provokes profound reduction in fully assembled CI amounts. BN-PAGE, Western blot, and immunodetection of NDUFS1 (CI), ATP5A (CV), and SDHB (CII) on WT and two $\Delta 4$ -CYB samples (clones E and B). Clone E was the cell line used in all the other figures; clone B was a fresh batch of cells at the first passage. Samples were solubilised in 1% digitonin.

To determine the assembly state of CI, we also searched the CI subunits present in our reciprocal complexome profiling experiments performed with SILAC-labelled WT and $\Delta 4$ -CYB cybrids. Peptides from 31 of the 44 CI subunits were identified and quantified in both control and mutant samples. To simplify the analysis and data interpretation, CI subunits were grouped according to the structural and assembly modules to which they belong: N-, Q-, ND1-, ND2-, ND4-, and ND5- (Stroud et al., 2016; Guerrero-Castillo et al., 2017) (Figure 5.23A). In

agreement with the previous immunodetection experiments, mass spectrometry revealed profoundly decreased amounts of all CI structural subunits. To determine whether the quantifications in these experiments were reliable or not, we used three respiratory chain-unrelated mitochondrial proteins (TOM20, TOM22 and citrate synthase, CS) as internal controls, and showed that they were not significantly different between the two cell lines (Figure 5.23B) and that the quantities of the two differentially labelled cell lines were comparable during the mixing at the start of the experiment.

Examining the profiles of each CI module in the mutated cells, it is possible to see that, except for the N-module, CI subunits accumulate in a peak at an apparent molecular mass of 991 kDa in the mutant cybrids (Figure 5.23A). This peak corresponds to the “pre-complex I” (pre-CI) intermediate, that accumulates immediately before the incorporation of the N-module (Ogilvie et al., 2005).

The N-module, instead, was barely detected, forming a peak at an estimated size of 1,172 kDa, which corresponds to the fully assembled “free” CI, and with accumulation of some N-module subunits at the bottom of the gel (25 to 49 kDa), indicating impaired incorporation (Figure 5.23A).

A

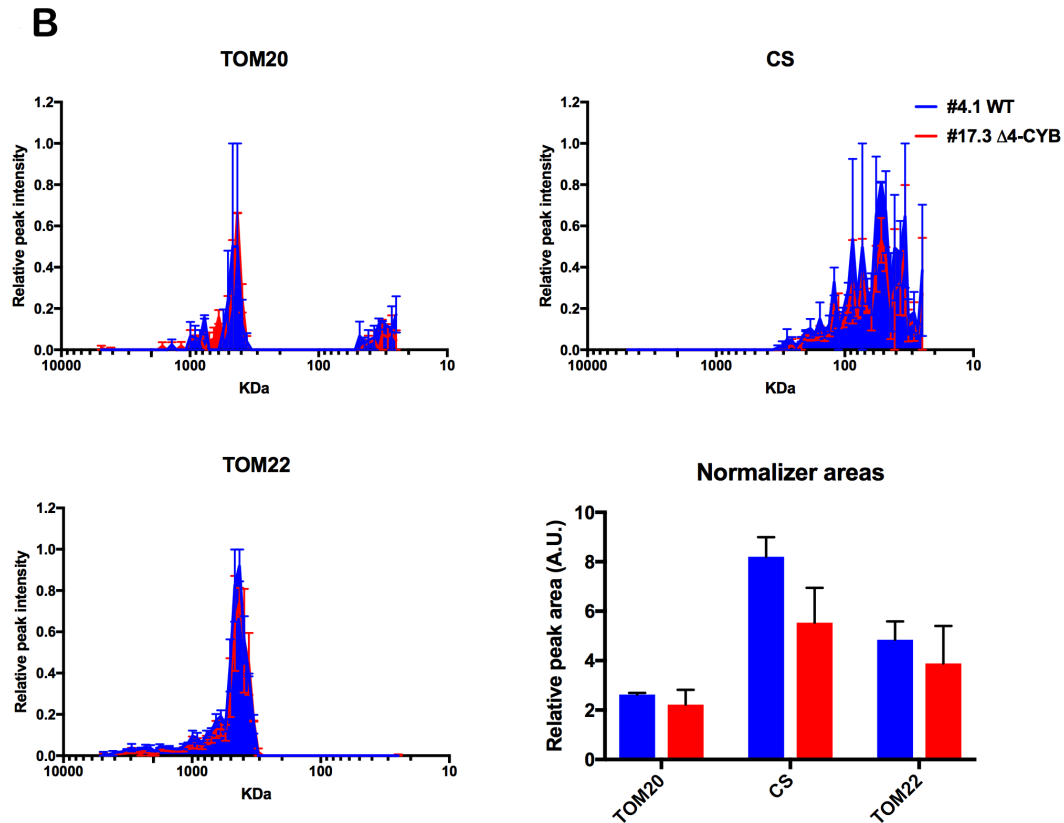


Figure 5.23: accumulation of CI assembly intermediates in $\Delta 4$ -CYB cells. A) Complexome profiles of CI structural modules. The detected subunits were organised in subgroups according to the assembly module they belong to and the peptide intensity values for the individual subunits were averaged to simplify the analysis. Values are plotted as mean \pm SEM of the two duplicate reciprocal labelling experiments. B) Complexome profiles of three ‘internal control’ proteins, citrate synthase (CS), and two members of the translocase of the outer membrane family (TOM20 and TOM22) were generated as in Figure 5.3. The bar graph represents the quantification of the total peak area under the curves (AUC) defined by the peptide intensity peaks for each protein. The plotted values are mean \pm SD ($n = 2$).

In addition, this analysis showed a large accumulation of NDUFAF2 in the 991 kDa peak in $\Delta 4$ -CYB cells, while it was only found at low-molecular mass positions in WT cybrids (Figure 5.24). This finding confirms that this peak identified the pre-CI assembly species, only lacking the N-module, since NDUFAF2 is a CI assembly factor that binds and stabilises this last intermediate (Ogilvie et al., 2005).

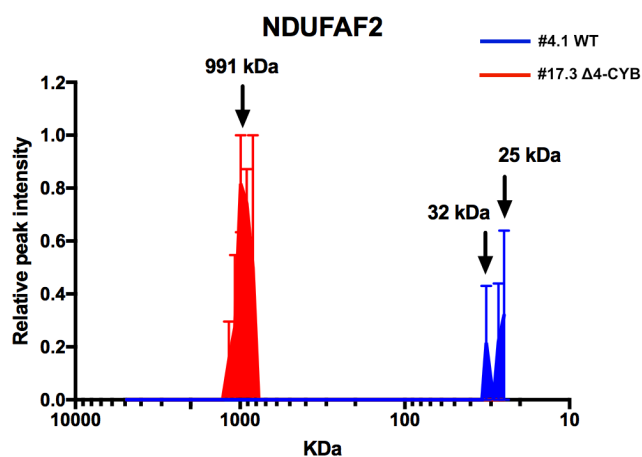


Figure 5.24: NDUF2F2 accumulates in the 991 kDa peak in Δ4-CYB cells. Complexome profiles of the CI assembly factor NDUF2F2 in WT (blue) and Δ4-CYB (red) mitochondria solubilised in digitonin. The graph was generated by analysing the peptide content in each of the 64 slices in which the gel lanes were excised and plotting the relative peptide peak intensities along the lane, setting the maximum to 1.0. The represented values are the mean \pm SEM of the two reciprocal labelling experiments.

NDUF2F2 binds and stabilises the Q-module of nascent CI, occupying a position similar to the N-module, probably temporarily engaging the binding site of its paralog, N-module subunit NDUF12 (Adjobo-Hermans et al., 2020; Ogilvie et al., 2005). In order to rule out the possibility that the impaired progression of CI assembly in our model was due to the increased levels of NDUF2F2, physically blocking the N-module binding site, we analysed CI maturation in cells silencing or overexpressing the assembly factor (Figures 5.25 and 5.26). Stable WT and Δ4-CYB cybrids overexpressing NDUF2F2 were generated by expression of a Myc-DDK (FLAG)-tagged version of the assembly factor and selected for neomycin resistance after 48 hours. The overexpression did not block CI maturation in WT cells, where a similar amount of assembled active CI was detected in mock transfected control cells by both WB of 1D BN-PAGE and in-gel activity assay (Figure 5.25B and C). In addition, spectrophotometric analysis of CI activity did not show any difference after NDUF2F2 overexpression in WT or Δ4-CYB cells compared to control (Figure 5.25D).

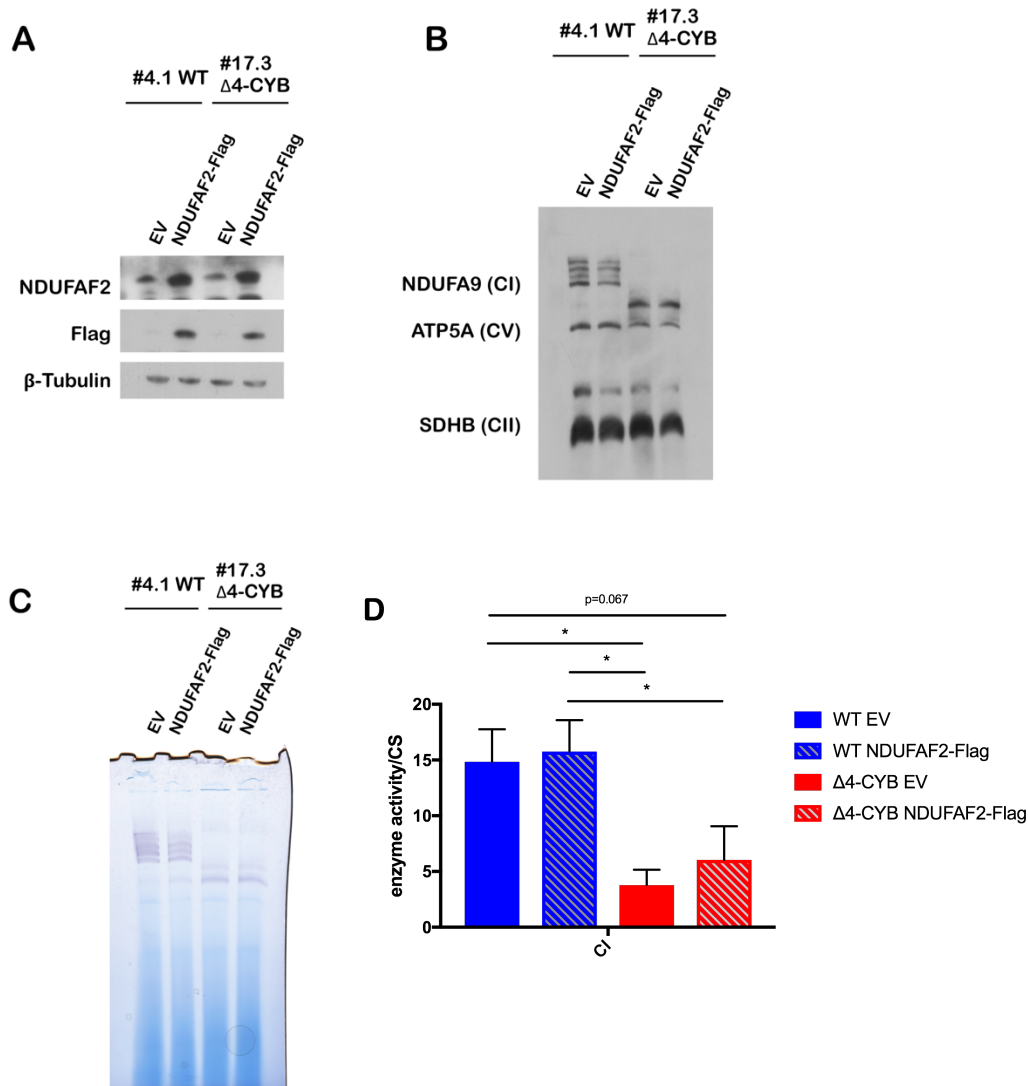
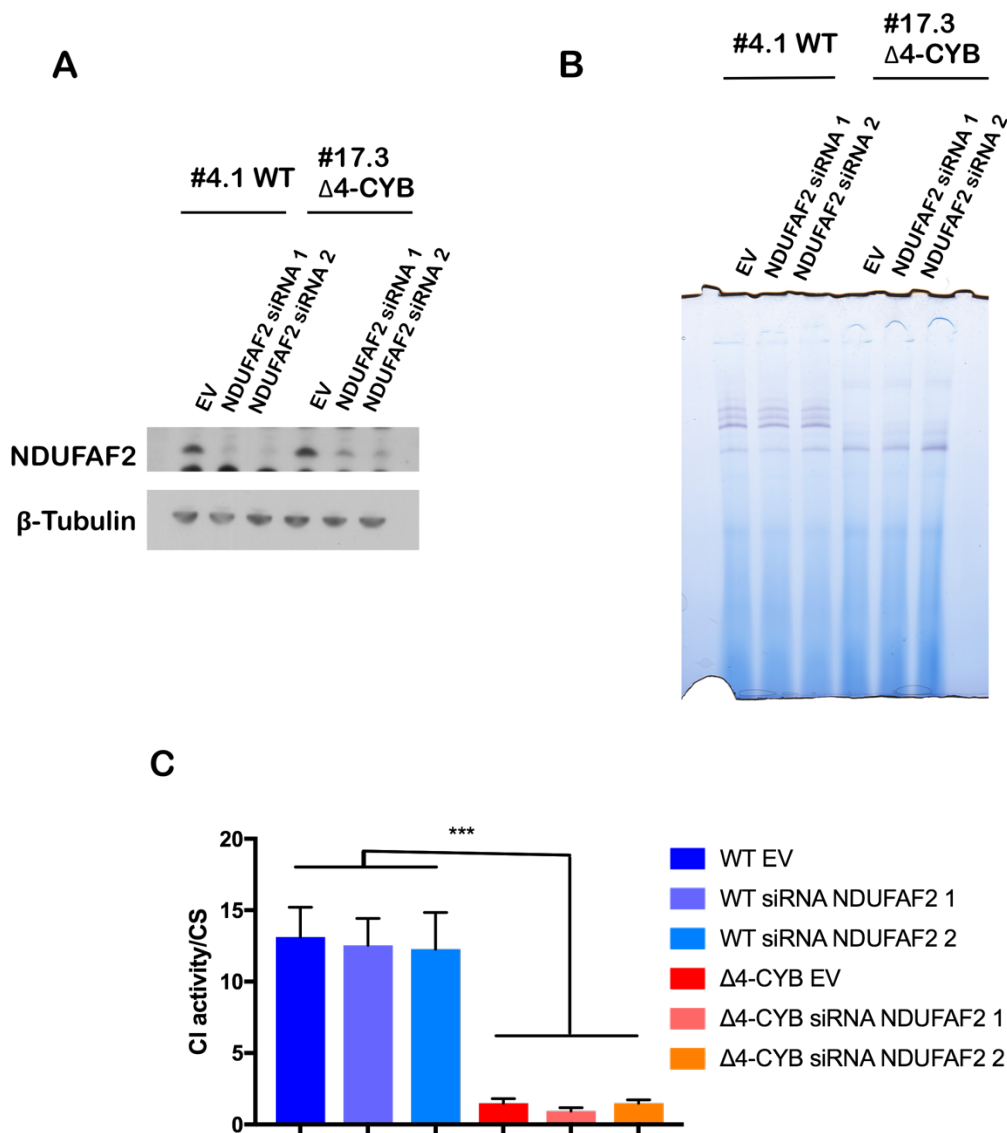


Figure 5.25: no significant differences in CI assembly and activity were found in cells overexpressing NDUF2F2. A) SDS-PAGE, Western blot, and immunodetection of total lysates of WT and Δ4-CYB cybrids stably expressing a Myc-DDK (FLAG)-tagged version of NDUF2F2 or the empty pCMV6-Entry vector (EV). Cells were transfected for 48h and selected against neomycin. β-Tubulin was used as loading control. B) BN-PAGE, Western blot, and immunodetection of samples extracted in 1% digitonin of the same cells used in (A). SDHB was used as loading control. C) CI in-gel activity assay performed in the NDUF2F2-overexpressing and negative control (EV) cell lines after solubilizing the samples with 1% digitonin and separating them on BN-PAGE. D) CI enzymatic activity assay performed in the same cell lines as in (A), normalised for CS activity. Results are expressed as mean ± SD (n = 3 biological replicates). One-way ANOVA with Tukey's multiple comparisons test was used. *P < 0.05.

Downregulation of NDUF2F2 was achieved with siRNA treatment. Two different siRNAs targeting the NDUF2F2 transcript were used and their efficiency was tested by immunodetection of WB after SDS-PAGE at three days after siRNA transfection (Figure

5.26A). Silencing of NDUFAF2 did not rescue CI maturation in the $\Delta 4$ -CYB cells (Figure 5.26B and C), confirming that the block in the enzyme assembly was not due to the physical interference of NDUFAF2 accumulation. Moreover, as previously observed by Schlehe et al. (Schlehe et al., 2013), silencing of NDUFAF2 did not impair CI assembly or activity in the WT cells. Whereas the lack of a CI defect in WT cells is surprising, it could be explained by the minimal but still detectable amount of residual protein after siRNA treatment, which could be enough to prevent a strong effect on CI assembly, as previously observed in full KO cells (Stroud et al., 2016).



*Figure 5.26: NDUF2 depletion does not promote CI maturation in the $\Delta 4$ -CYB cells. A) SDS-PAGE, Western blot, and immunodetection of total lysate samples of WT and $\Delta 4$ -CYB cybrids transfected with two different siRNAs targeting the NDUF2 transcript or the Sigma's siRNA Universal Negative Control #1 (EV). β -Tubulin was used as loading control. B) CI in-gel activity assay performed in the same cells described in (A), after solubilizing the samples with 1% digitonin and separating them on BN-PAGE. C) CI enzymatic activity assay performed in the same cells described in (A) normalised for CS activity. Results are expressed as mean \pm SD ($n = 3$ biological replicates). One-way ANOVA with Tukey's multiple comparisons test was performed. *** $P < 0.001$.*

We then questioned if the residual CI intermediate was the result of degradation of the destabilised fully assembled enzyme, or of assembly stalling of the nascent complex, a possibility that was highly suggested by our previously collected data. In order to answer this question, we studied CI assembly dynamics by analysing the incorporation of both the mtDNA- and nuclear-encoded subunits, through a collaboration with Dr Cristina Ugalde's group (Figure 5.27). Firstly, a pulse-chase [35 S]-L-Met metabolic labelling was performed to follow the stability and incorporation of the mtDNA-encoded subunits. Cells were collected after a 2-hour radioactive pulse and at chase times of 2, 5 and 24 hours. Samples were extracted and analysed by SDS, 1D BN and 2D BN-PAGE.

SDS-PAGE experiments showed that the turnover rates of the CI mitochondrial-encoded subunits (NDs) were comparable in WT and $\Delta 4$ -CYB cells (Figure 5.27A). The analysis of subunit incorporation was performed by BN-PAGE. 1D experiments detected neither fully assembled CI at any stage of enzyme maturation including SC, nor degradation products over time in $\Delta 4$ -CYB cells (Figure 5.27B). 2D analysis allowed us to follow the incorporation of each ND-subunit in the absence of CIII and to compare it with WT cells (Figure 5.27C). Initially, mtDNA-encoded subunits showed a similar pattern, except for the absence of MTCYB in $\Delta 4$ -CYB. In contrast, after only two hours of chase, ND-subunits were detected in SC of WT cells but they still remained inside the pre-CI in mutant cells. After 5- and 24-hours chase, CI assembly progressed directly from pre-CI to SC in WT cells, while it remained mainly stuck in pre-CI in $\Delta 4$ -CYB with the appearance of very low amounts of fully assembled CI simultaneously to the formation of SC in the WT cells.

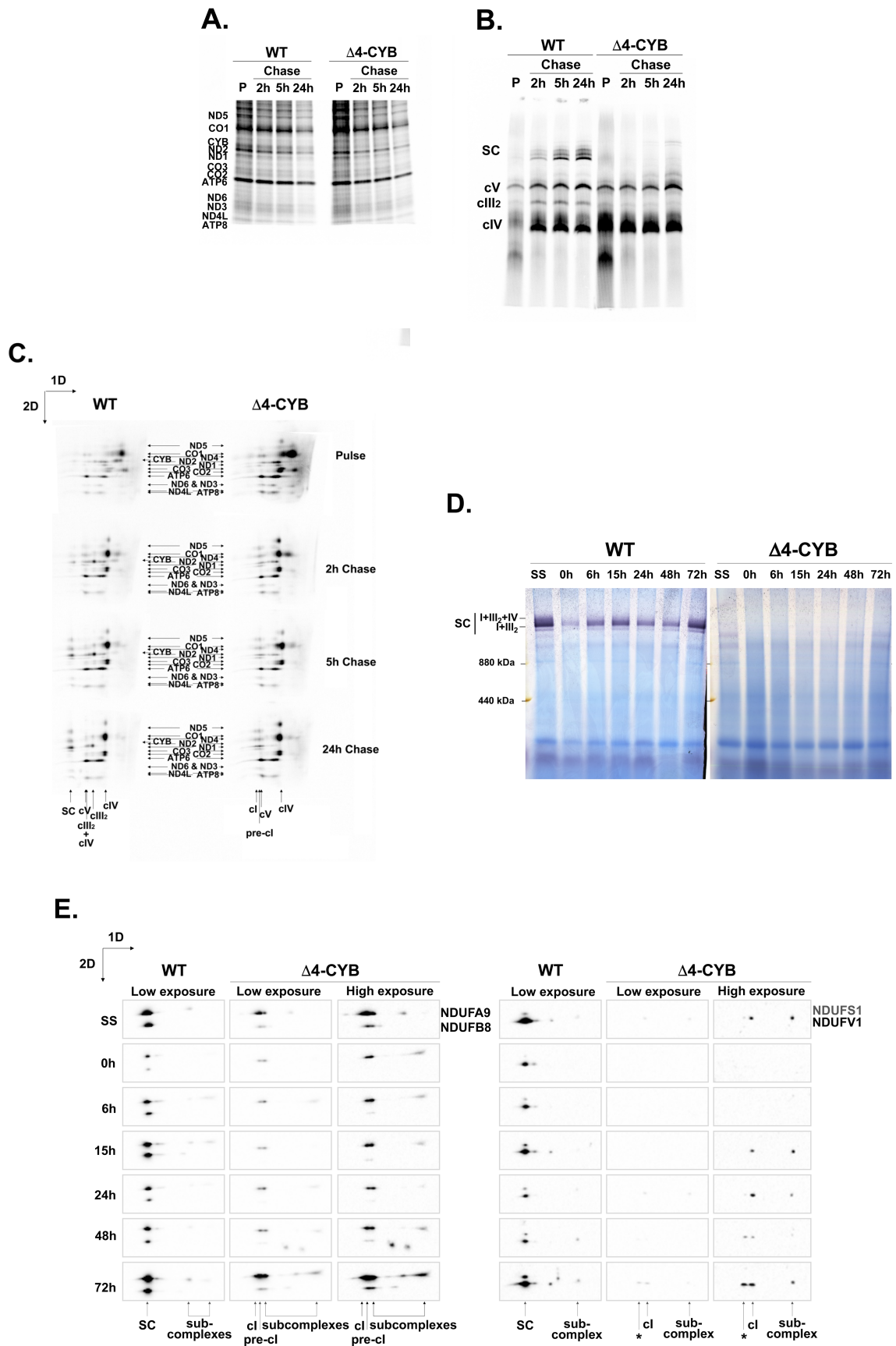


Figure 5.27: CI defects in $\Delta 4$ -CYB cells are due to incomplete maturation of the enzyme rather than destabilisation. A) SDS-PAGE resolving the pulse-chase [35 S]-L-Met metabolic labelled mitochondrial translation products. The 35 S-Met and the cycloheximide used to inhibit cytosolic translation were removed from the medium after a two-hour pulse (P), and cells were collected at the indicated chase times (0 (P), 2, 5, and 24 h). B) 1D BN-PAGE analysis of the same cells as in (A), solubilised in digitonin. C) 2D BN-PAGE analysis of the same samples as in (B). D) CI in-gel activity assay of digitonin-solubilised samples after inhibiting mitochondrial translation with doxycycline for 6 days (0 h) and at 6, 15, 24, 48 and 72 hours after removing the drug and restoring mtDNA-encoded proteins synthesis. The gels were incubated in the reaction mixture for 24 h. SS = steady state. The asterisk indicates the presence of a high-molecular weight CI-containing band of unknown nature. E) 2D BN-PAGE, Western blot, and immunodetection analysis of WT and $\Delta 4$ -CYB mitochondria from the same cells as in (D), to follow the incorporation kinetics of the indicated CI nuclear-encoded subunits, belonging to different structural modules. The blots shown were either exposed for 16 s. (low exposures) or 160 s. (high exposures) in order to visualise the qualitative signals in the $\Delta 4$ -CYB samples. Experiments indicated in A, B and C were performed by Dr Erika Fernandez-Vizarra, experiments in D and E were performed by Dr Rafael Pérez Pérez in Dr Cristina Ugalde's laboratory (Madrid, Spain).

Next, the incorporation over time of nuclear-encoded CI subunits was assessed. Cells were treated with doxycycline for 6 days in order to inhibit mtDNA-encoded protein synthesis and deplete cells of their mature OXPHOS complexes. Once the inhibitor was removed, cells were collected at different time points (0, 6, 15, 24, 48 and 72 hours). The first analysis was CI in-gel activity (Figure 5.27D), which showed how active CI progressively accumulates directly only in the SC in WT cells, while in the mutant cells, only a faint NADH-dehydrogenase reactive signal appeared at a molecular mass around 1,100 kDa, corresponding to free CI holocomplex.

Secondly, 2D BN-PAGE analysis on the same samples was performed, detecting four different subunits from distinct CI structural modules: NDUFA9 (ND2-module), NDUFB8 (ND5-module), NDUFS1 and NDUFV1 (N-module) (Figure 5.27E). In WT cells, CI nuclear subunits were principally detected in SC, with no noticeable accumulation of assembly intermediates. In $\Delta 4$ -CYB cells, instead, low amounts of NDUFA9 and NDUFB8 were mostly detected in pre-CI and subassemblies. In mutant cells, NDUFS1 and NDUFV1 were either undetected or detected in two very faint spots corresponding to the CI holocomplex and a higher uncharacterised molecular weight structure (asterisk) (Figure 5.27E). Both the faint bands in mutant cells with NADH oxidising activity (Figure 5.27D) and the signal marked with an asterisk (Figure 5.26E), likely correspond to a small second peak of CI N-module found in the complexome profiling analysis with an apparent molecular size of 1,386 kDa (Figure 5.23A). Confirming the very low abundance of CI subunits incorporated in a CI intermediate in mutant

cybrids, $\Delta 4$ -CYB blots needed to be exposed 10 times longer than those of the controls, in order to obtain detectable signals.

Together, these results confirm that the incorporation of the N-module is an extremely inefficient process in the absence of CIII, since this event takes place directly in the SC in normal conditions. These kinetic analyses also rule out the idea of CI destabilisation and consequent degradation in the mutant line.

5.6 Role of CIII activity on CI assembly: AOX overexpression

Another important aspect to investigate was if the CI assembly defect was due to the physical absence of CIII and CIII-containing SC or to the lack of ubiquinol oxidase activity, leading to a CoQ pool redox imbalance. Interestingly, it was demonstrated that in fungi, CIII and CIV are dispensable for the assembly and stability of CI, thanks to the upregulation of the alternative oxidase (AOX) (Maas et al., 2009). AOX is naturally expressed in plants, and in some fungi and parasites, and it can directly oxidise reduced CoQ, bypassing CIII and CIV, and consequently reducing the ROS production and stress in the absence of one or both of these complexes (Young et al., 2013). In order to verify this hypothesis, we stably expressed a HA-tagged version of *Emericella nidulans* AOX (AOX-HA), shown previously to be functional in mouse cultured cells (Guaras et al., 2016; Perales-Clemente et al., 2008), in both WT and $\Delta 4$ -CYB cybrids (Figure 5.28A). To prove the functionality of the expressed AOX in our cell models, we tested cell growth with and without uridine supplement in the culture medium (Figure 5.28B). In the absence of uridine, mutant cells proliferation is strongly impacted, since pyrimidine biosynthesis is dependent on the respiration-linked dihydroorotate de-hydrogenase (DHODH) which is required to overcome cell-cycle arrest (Bajzikova et al., 2019). $\Delta 4$ -CYB cybrids overexpressing AOX-HA, instead, were able to grow in culture medium without uridine, indicating the restoration of the CoQ pool redox balance.

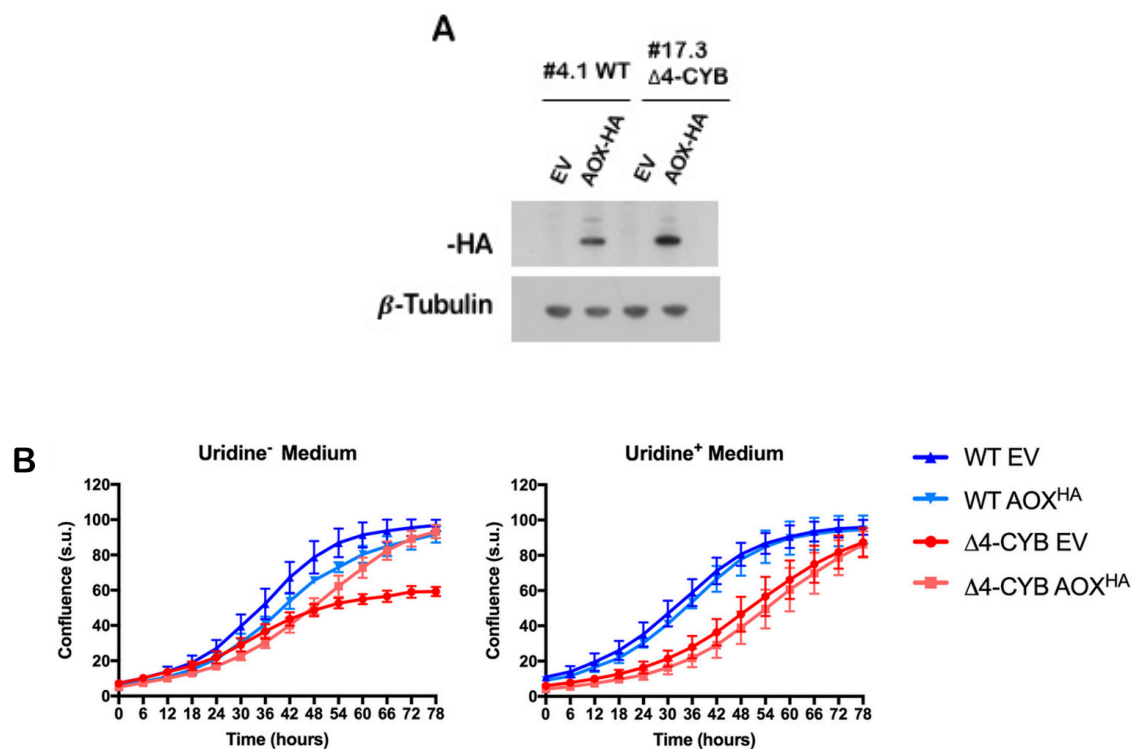


Figure 5.28: **functional AOX-HA was stably overexpressed in WT and $\Delta 4$ -CYB cybrids.** A) SDS-PAGE, Western blot, and immunodetection of AOX-HA in total lysate samples of WT and $\Delta 4$ -CYB cells transduced with AOX-HA/pWPXLd-ires-Hygro^R or empty pWPXLd-ires-Hygro^R (EV) lentiviral vector. β -Tubulin was used as loading control. B) Growth curves of the AOX-HA expressing cell lines and their corresponding EV controls. Cell growth was monitored every 6 hr after substituting the medium in two replicate 24-well plates, one plate with medium without uridine (Uridine⁻), and the second plate with medium supplemented with 50 μ g/ml uridine (Uridine⁺). The graphs show the average confluence \pm SD at each time point ($n = 6$ wells per cell line). Experiment performed by Dr Erika Fernandez-Vizarra.

As shown in Figure 5.29, the overexpression of AOX-HA did not have evident effects on WT cells, while it led to a partial recovery of the CI phenotype in $\Delta 4$ -CYB cybrids characterised by: increase of CI enzyme activity, from 25 to 55% of controls (A), CI-linked maximal respiratory capacity, up to 50% of the WT (B), CI subunits steady state levels (C), and CI assembly (D). However, in addition to an only partial structural and functional rescue, there were readily detectable amounts of NDUFAF2 still bound to pre-CI in the $\Delta 4$ -CYB AOX-HA cells (Figure 5.29D). These results suggest a role for CIII function in CI maturation, additionally to the structural one we described previously.

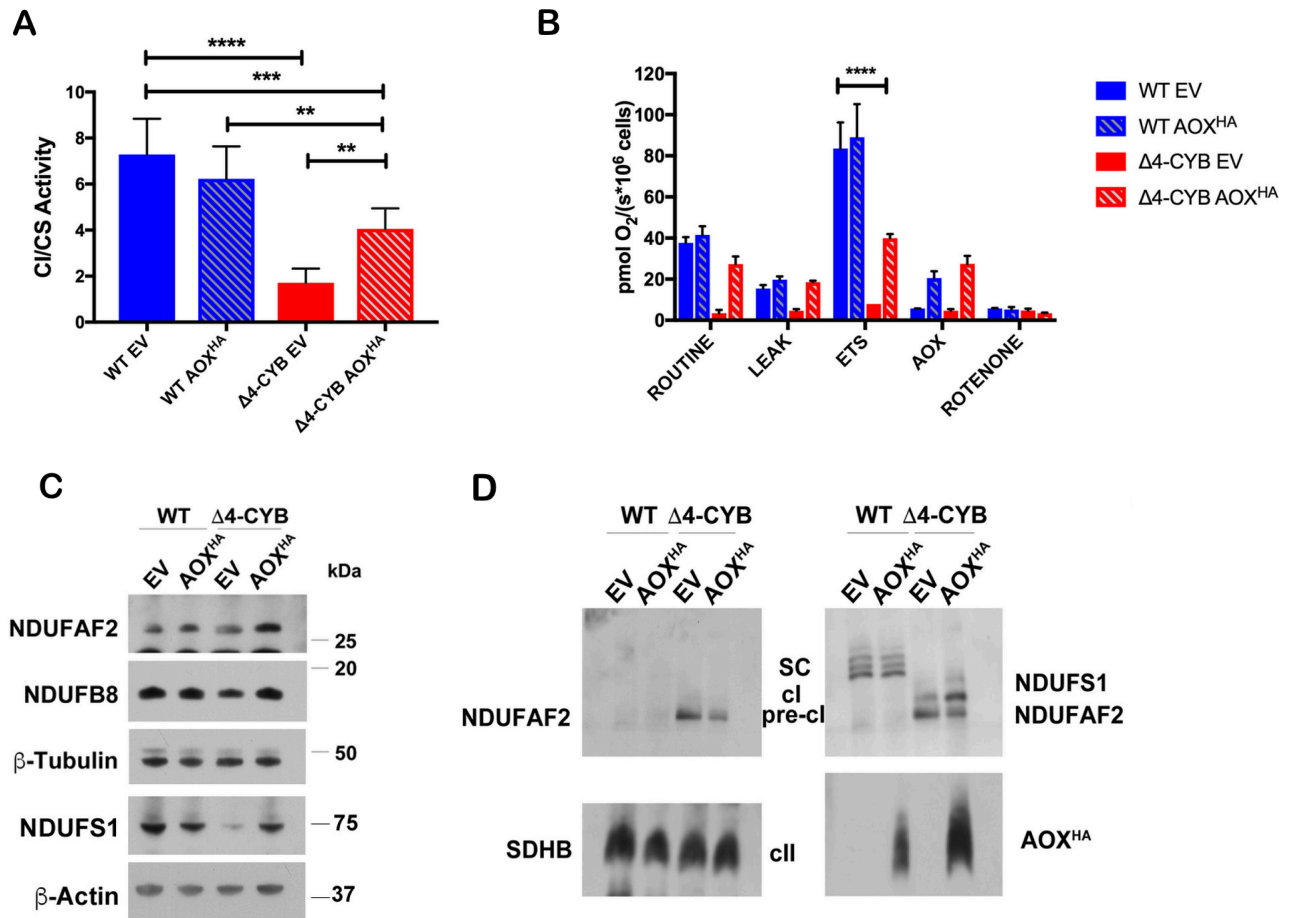


Figure 5.29: overexpression of functional AOX-HA leads to a partial rescue of activity defect and CI assembly in the absence of CIII. A) Spectrophotometric kinetic measurements of CI activity in WT and Δ 4-CYB cells transduced with AOX-HA/pWPXLd-ires-Hygro^R or empty pWPXLd-ires-Hygro^R (EV) lentiviral vector. CI activity was normalised for citrate synthase (CS) activity and results are expressed as mean \pm SD ($n = 5$ biological replicates). Two-way ANOVA with Tukey's multiple comparisons test was used. ** $P = 0.0077$ (WT AOX-HA versus Δ 4-CYB AOX-HA); ** $P = 0.0044$ (Δ 4-CYB EV versus Δ 4-CYB AOX-HA); *** $P = 0.0003$ (WT EV versus Δ 4-CYB AOX-HA); **** $P < 0.0001$. B) High-resolution respirometry analyses performed in the same cells in (A) in a O₂K high-resolution respirometer (Oroboros instruments). Respiration was measured in intact cells in DMEM medium in the basal state (Routine), in the presence of oligomycin (Leak) and uncoupled with CCCP (ETS capacity). AOX indicates oxygen consumption in the presence of antimycin A, which inhibits CIII activity but not AOX. ROTENONE indicates oxygen consumption in the presence of the CI inhibitor rotenone. In all cases, this was equal to the background. Results are expressed as mean \pm SD ($n = 2$ biological replicates). Two-way ANOVA with Tukey's multiple comparisons test was performed. **** $P < 0.0001$. This experiment was performed by Dr Erika Fernandez-Vizarra. C) SDS-PAGE, Western blot, and immunodetection of total lysates of the cells described in (A) β -Actin and β -Tubulin were used as loading controls. D) 1D BN-PAGE, Western blot, and immunodetection analyses of digitonin-solubilised mitochondria from the same samples as in (A). SDHB was used as loading control.

To better understand the role of the functional component of CIII on CI maturation and SC formation, WT cells expressing the AOX-HA construct or empty vector (EV) were treated with 2.5 μ M antimycin A, a CIII inhibitor, for seven days. This chronic treatment induced inhibition of mitochondrial respiration (Figure 5.30A), and consequently an imbalance in the ratio between oxidised and reduced CoQ (Guaras et al., 2016), without affecting CIII structure (Figure 5.30B). If the abolishment of CIII activity was enough to destabilise or to arrest the maturation of the rest of the OXPHOS machinery, an assembly defect should have been observed after seven days of antimycin A treatment. However, no significant destabilisation of CIII, CI, or SC was detected (Figure 5.30B). As expected, WT cells expressing functional AOX-HA treated with antimycin A showed normal respiration (Figure 5.30A), since this enzyme is able to bypass CIII, but no alteration in CI distribution or activity (Figure 5.30B). These results confirm that inhibition of CIII activity alone is not sufficient to impair CI assembly or its incorporation in the SC.

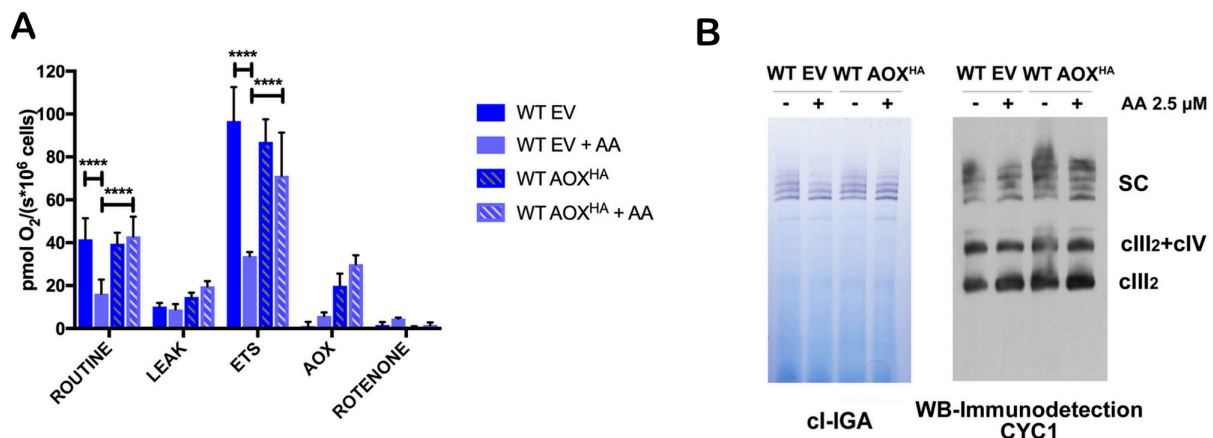


Figure 5.30: long-term inhibition of CIII activity does not induce CI assembly or stability impairments. A) High-resolution respirometry analyses performed on WT cells transduced with AOX-HA and empty vector (EV), untreated and treated with 2.5 μ M antimycin A for seven days, in a O2K high-resolution respirometer (Oroboros instruments). Respiration was measured in intact cells in DMEM medium in the basal state (Routine), in the presence of oligomycin (Leak), uncoupled with CCCP (ETS capacity), in the presence of antimycin A (AOX), and in the presence of rotenone (ROTENONE). Results are expressed as mean \pm SD ($n = 4$ biological replicates). Two-way ANOVA with Tukey's multiple comparisons test was used. **** $P < 0.0001$. B) 1D BN-PAGE analysis in digitonin-solubilised samples from the same cells used in (A) followed by CI in-gel activity (IGA) (left) or Western blot and immunodetection of CIII subunit CYC1 (right).

5.7 The assembly of CII and CIV, but not of CV, is altered in $\Delta 4$ -CYB cybrids

Even if CI deficiency was the most dramatic secondary effect of CIII deficiency in $\Delta 4$ -CYB cells, CIV and CII were also partially affected. Indeed, CII subunit SDHB was significantly reduced in $\Delta 4$ -CYB cells (Figure 5.19), while CIV enzyme activity was half of the WT (Figure 5.18). Therefore, we decided to investigate the effect of lack of CIII on these two enzymes and compared it to CV, which is not involved in the electron transport chain and in the formation of SC. To analyse the assembly state of the remaining OXPHOS complexes, we used SILAC/complexome profiling analyses.

Three out of four CII subunits were detected in both WT and mutant cells by mass spectrometry: SDHA, SDHB and SDHC (Figure 5.31). The amounts of SDHB and SDHC incorporated into CII were about half of the control, and SDHC was found in a ~91 kDa subassembly. In addition, even if SDHA steady-state levels were not affected (Figure 5.19), the amount of protein correctly incorporated in the mature enzyme decreased in the $\Delta 4$ -CYB cell line, while the rest accumulated in intermediate species at the bottom of the gel. It is possible to conclude that CIII absence impacts CII assembly, but the defect is not sufficient to cause significant reductions in the enzyme activity (Figure 5.18).

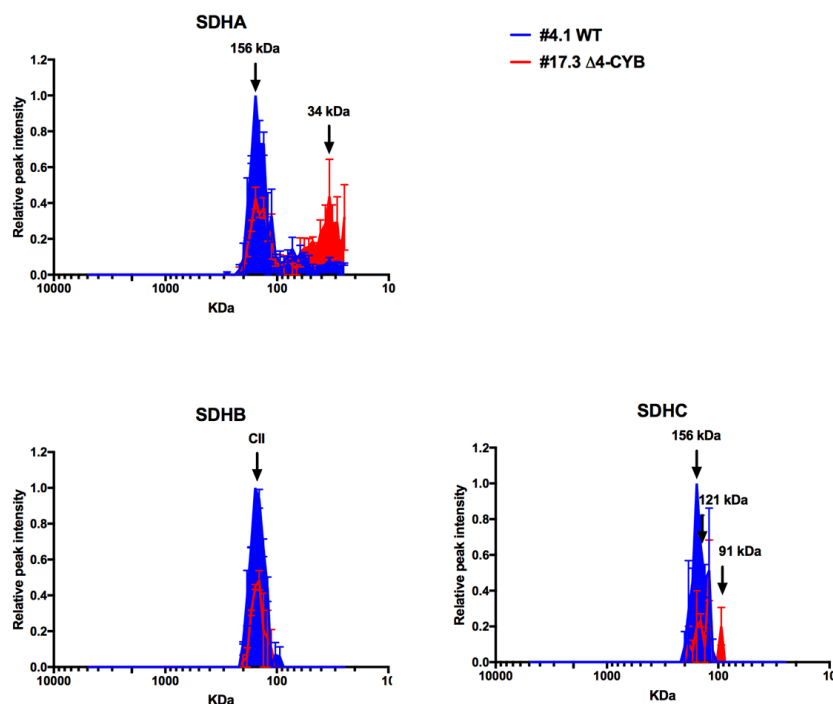


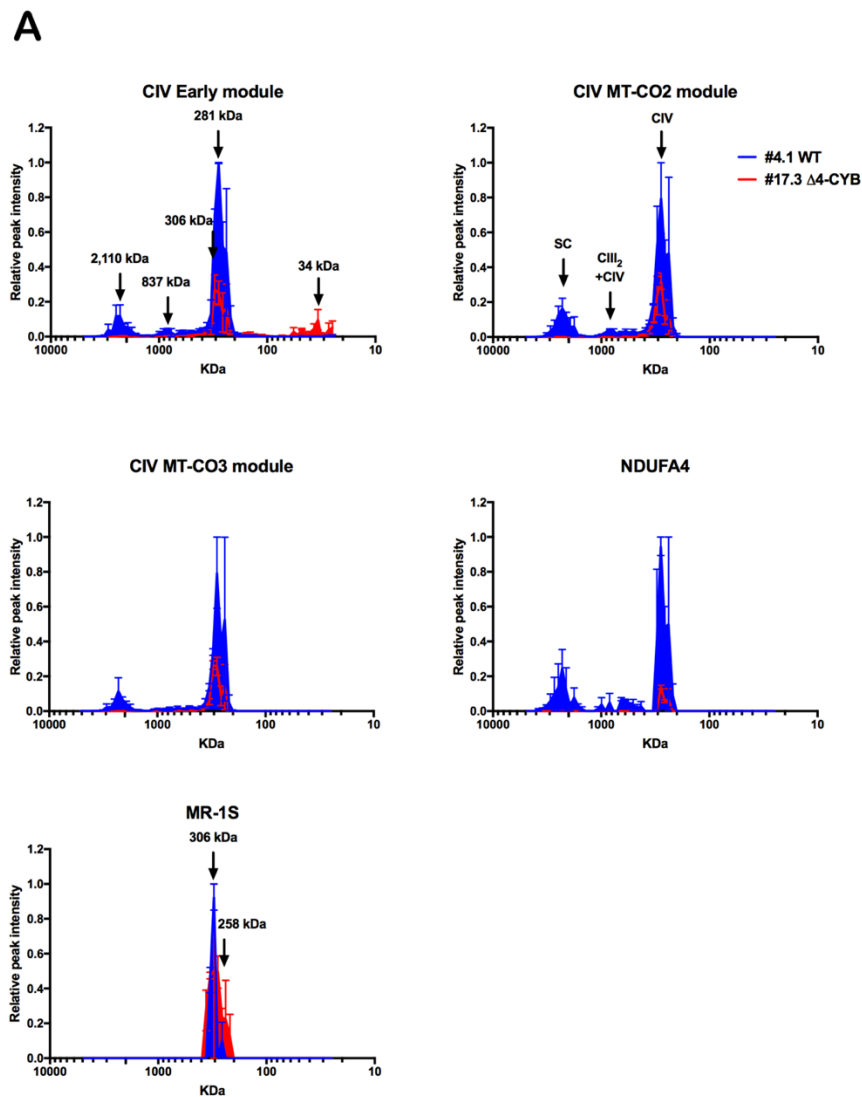
Figure 5.31: *in the absence of CIII, CII amount is reduced and subassemblies containing SDHA and SDHC, but not SDHB were detected.* Complexome profiles of the three detected CII subunits. The graphs were generated as in Figure 5.3. The represented values are the mean \pm SEM of the two reciprocal labelling experiments.

Analysis of the CIV subunits by mass spectrometry and immunodetection of samples separated by 1D BN-PAGE confirmed the alteration in CIV assembly in $\Delta 4$ -CYB cells, which can explain the observed reduced enzymatic activity (Figure 5.18). Also, for CIV, the detected subunits were clustered in three groups, according to the assembly stage they belong to: ‘early module’ (COX4 and COX5A), MTCO2 module, and MTCO3 module (Signes and Fernandez-Vizarra, 2018) (Figure 5.32). Peptides from MTCO1 and COX7B were not detected by mass spectrometry, therefore immunodetection data were used to complete this analysis. Proteins involved in the early stages of complex maturation (COX4, COX5A, HIGD1A, and MTCO1) and COX7B formed accumulation of low-molecular-weight subcomplexes, while the same does not happen to components of the later assembly stages MTCO2 and MTCO3 modules. All the modules, however, were significantly reduced in free CIV and absent in SC (Figure 5.32).

NDUFA4/COXFA4 was initially considered a CI subunit, but it was later proven to be a CIV subunit showing a more labile interaction and late incorporation in the assembly pathway

(Balsa et al., 2012; Pitceathly et al., 2013). This was the most reduced CIV protein in CIII mutant cells (Figure 5.32A), indicating an impairment in CIV maturation.

Moreover, the assembly factor MR-1S (Vidoni et al., 2017) was found accumulated in the CIV intermediates of $\Delta 4$ -CYB cells, forming peaks at 306 kDa and 258 kDa, despite the overall reduction in CIV amounts in this mutant. This was an additional indication that in the absence of CIII, not only CI, but also CIV assembly is stalled, leading to the accumulation of intermediates still bound to their specific assembly factors.



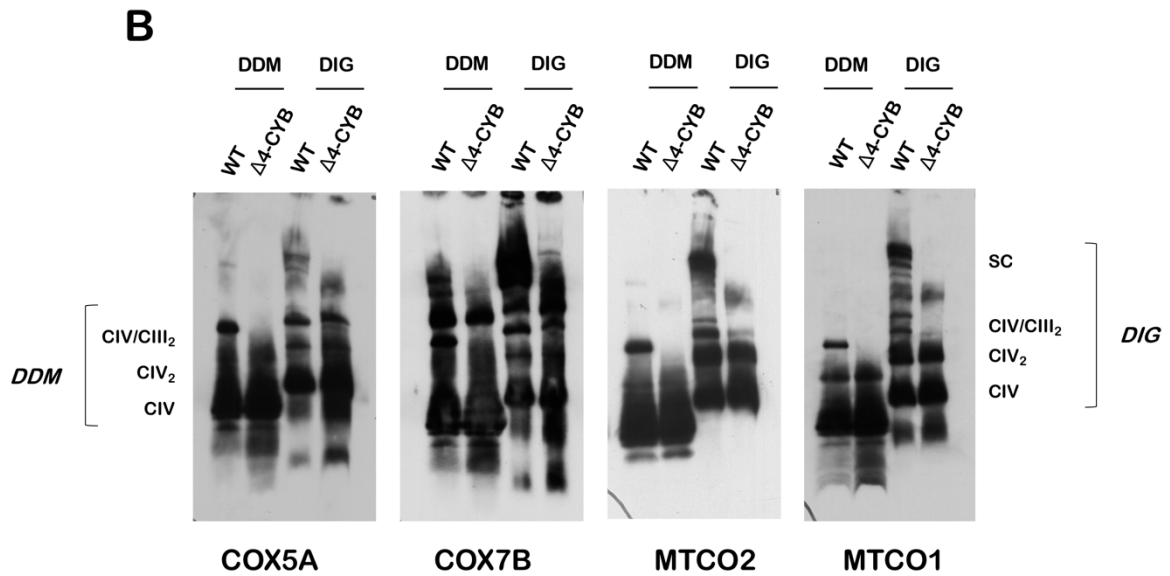


Figure 5.32: lack of CIII induces stalling of CIV assembly and intermediates accumulation. A) Complexome profiles of the different CIV subunits and assembly factors. Profiles were generated as in Figure 5.21 and the peptide intensity values of CIV subunits were grouped in the three main assembly modules and averaged, to simplify the analysis. The MR-1S assembly factor and the last subunit to be incorporated and only recently assigned to CIV, NDUFA4, are represented separately. The represented values are the mean \pm SEM of the two reciprocal labelling experiments. B) 1D BN-PAGE, Western blot, and immunodetection of samples from WT and $\Delta 4$ -CYB cells solubilised with 1% DDM and 1% digitonin (DIG). Two subunits not detected by mass spectrometry were included: MTCO1 and COX7B.

Various CV subunits were detected by mass spectrometry and in order to make the analysis and the visualisation of the data simpler, the subunits were clustered in the two main assembly modules. The F1 particle included α (ATP5A1), β (ATP5B), γ (ATP5C1), and ϵ (ATP5E) subunits, while the peripheral stalk included subunits b (ATP5F1), d (ATP5H), F6 (ATP5J), OSCP (ATP5O), e (ATP5I), f (ATP5J2), g (ATP5L), MT-ATP6, MT-ATP8, 6.8PL (MP68), and DAPIT. Both these modules did not show significant differences between WT and $\Delta 4$ -CYB cells (Figure 5.33).

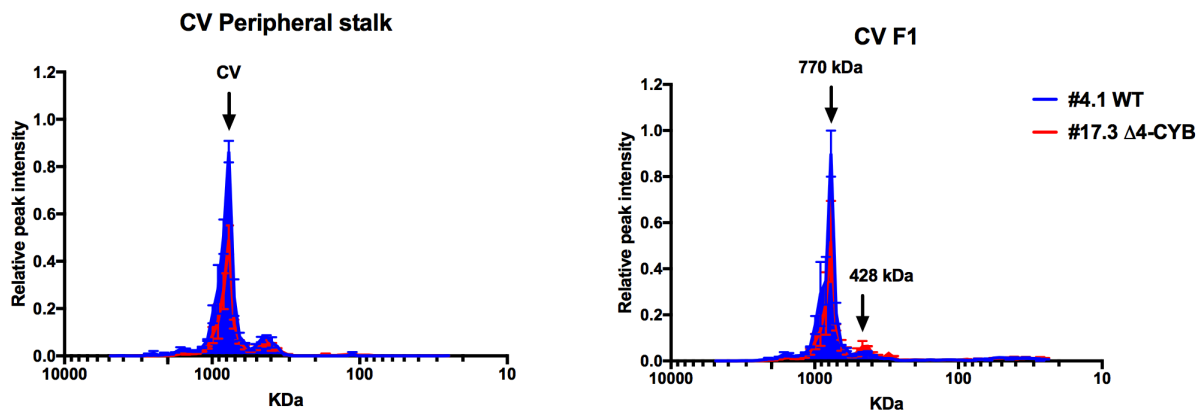


Figure 5.33: *CV assembly is not impacted by the absence of CIII*. Complexome profiles of CV subunits, generated as indicated in Figure 5.21. As for CI, subunits were grouped according to the assembly module they belong to and the peptide intensity values for the individual subunits' values were averaged. The represented values are the mean \pm SEM of the two reciprocal labelling experiments.

5.8 Conclusions

- In the presence of a truncating 4-base pair deletion in *MTCYB*, the catalytic subunit MTCYB was not synthesised. This resulted in the total absence of CIII activity and a dramatic reduction in CIII subunits steady-state levels, except for UQCR10 and CYC1.
- UQCR10 and CYC1 accumulated in a variety of high- and low-molecular-weight complexes or aggregates in the mutant cells, possibly involving also UQCRH. These results suggest that these subunits are involved in the formation of an assembly intermediate/s never described before.
- Several CIV structural subunits were found interacting with CYC1-HA and UQCR10-HA in the immunopurified fractions in both cell lines.
- The overexpression of CYC1-HA led to a reduced import and processing of CYC1 and to an accumulation of the protein in the OMM in cells lacking CIII, possibly as the result of an unknown control mechanism.
- SILAC/Co-immunopurification experiments identified new putative CIII assembly factor candidates, including CHCHD3/MIC19 and GHITM/MICS1. However, detailed studies of the role of these two proteins in CIII biogenesis and activity ruled out this hypothesis.

- The absence of CIII resulted in combined respiratory chain defects. In particular, mature CI was extremely reduced in mutant cells, in which the lack of CIII and SC blocked the incorporation of the N-module.
- Steady-state and kinetic analyses showed that the reduction in mature CI amount is due to stalled assembly of the enzyme, and not to destabilisation and degradation of a fully assembled CI, as suggested previously.
- CI assembly impairment is due to both structural and functional loss of CIII.
- Lack of CIII also impacts CIV and, to a lesser extent CII biogenesis. Indeed, both these complexes showed accumulation of assembly intermediates and CIV activity was significantly reduced in mutant cells.

Section 6: Discussion and future directions

The first aim of this project was to study CIII assembly in human cells. Before these analyses, the intermediate steps of CIII biogenesis in mammals were assumed to proceed as described in the yeast model. Yeast is a largely used model for OXPHOS studies, because it is possible to manipulate its mitochondrial and nuclear genome, and it tolerates well mutations that inactivate mitochondrial respiration and the complete loss of mitochondrial DNA, since it is able to satisfy its energy requirements by fermentation (Lasserre et al., 2015). The structural similarity and equal number of subunits, between the yeast and mammalian enzymes (Schagger et al., 1986; Iwata et al., 1998; Hartley et al., 2019) justified the assumption that the two organisms could share a similar assembly pathway. The only difference is the presence in mammalian CIII of the UQCRFS1 N-terminal import signal that remains bound between UQCRC1 and UQCRC2 and was considered to be an additional subunit (Subunit 9) (Brandt et al., 1993). However, our data suggest that the assembly mechanism could be partially different.

The early stage of CIII maturation in yeast involves the insertion of *Cytb*, the only mtDNA-encoded subunit of CIII, in the IMM, followed by the incorporation of Qcr8 (UQCRQ in humans) and Qcr7 (UQCRB). Two observations suggest that this phase is conserved in mammals. Firstly, as described in the introduction, homologous assembly factors involved in this process have been found: Cbp3/UQCC1, Cpb6/UQCC2 and Cpb4/UQCC3 (Tucker et al., 2013; Wanschers et al., 2014). Secondly, the lack of MTCYB in our cybrids led to a complete block of enzyme assembly and a very strong reduction of both UQCRQ and UQCRB steady-state levels compared to the other subunits. These observations indicate that in both yeasts and mammals MTCYB behaves as the seed around which the rest of the enzyme is built, while the similar instability of UQCRQ and UQCRB in mutant cells suggests they are probably inserted together and at the beginning of the assembly.

The second step of CIII maturation, however, seems to differ between the two models. In *S. cerevisiae*, the formation of a module including the catalytic subunit *Cyt c1*, and the two structural core subunits Qcr1 and Qcr2 was described, even if these proteins are spatially distant in the mature enzyme (Signes and Fernandez-Vizarra, 2018; Zara et al., 2009b). In contrast, a very recent study proposed that also in yeast Cor1/Cor2 module is formed independently of cytochrome *c1*, while Cyt1 was found interacting with Qcr6 (Stephan and

Ott, 2020). These new observations are in line with our data, which showed that the UQCRC1 and UQCRC2 steady-state levels are decreased in the absence of MTCYB, whereas CYC1 levels are comparable to WT. The fact that the latter subunit was found accumulated in different low- and high-molecular-weight structures is most probably the cause of its stability in the $\Delta 4$ -CYB cybrids. Moreover, another subunit, UQCR10, was found behaving similarly to CYC1. In the yeast assembly model, this subunit (Qcr9) is inserted only in the late stages of CIII assembly and was not found specifically interacting with other subunits before the incorporation in the enzyme (Zara et al., 2009). Further SILAC/co-immunopurification analysis of UQCR10-HA confirmed that UQCR10 and CYC1 are likely involved in the formation of stable intermediates and highlighted the possible participation of UQCRH, also not attributed to any specific assembly module in yeast, and of CIV subunits MTCO2, COX5B, COX6B1 and COX6C (Figure 5.34).

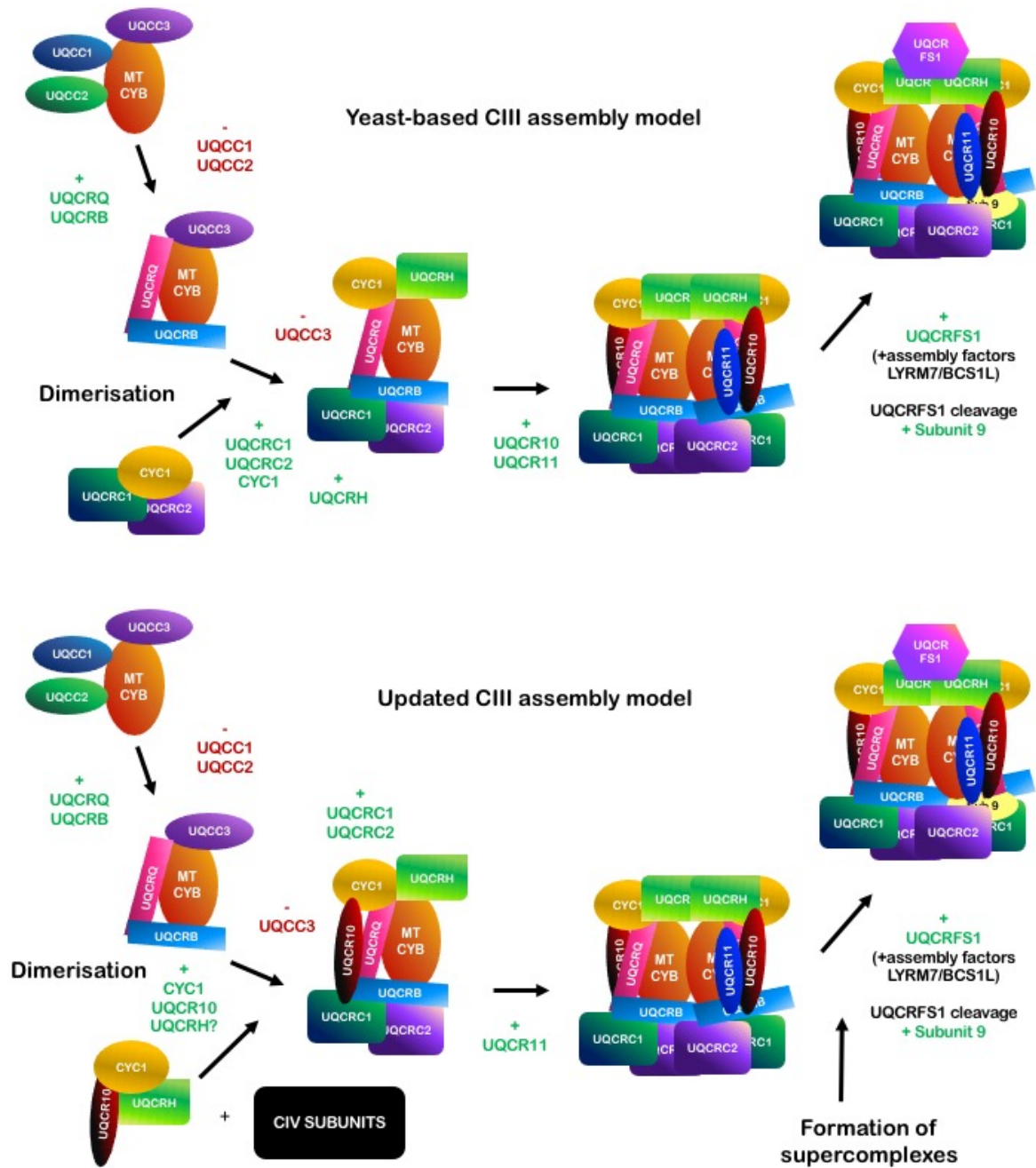


Figure 5.34: schematic representation of human CIII assembly model based on the homology with the available data for *S. cerevisiae* (Zara et al., 2007, 2009a,b; Atkinson et al., 2011; Gruschke et al., 2011, 2012; Wagener et al., 2011; Cui et al., 2012; Smith et al., 2012; Hildenbeutel et al., 2014; Stephan and Ott, 2020), and of our updated model.

On this basis, we performed mass spectrometry analysis on immunopurified fractions from cells overexpressing UQCR10-HA and CYC1-HA, in the hope of finding uncharacterised assembly factors or chaperones interacting with these assembly intermediates. While a variety of factors have been identified for every stage of CI and CIV maturation, only 6 are known for

CIII and all of them are involved in the maturation and assembly of either MTCYB or UQCRCFS1, which are the first and last step of CIII maturation, respectively. It is therefore difficult to imagine that the residual 8 subunits, incorporated in the intermediate assembly steps, can mature and be inserted completely independently.

Our analysis identified a few candidates: GHITM/MICS1, CHCHD3/MIC19, HADHB, and STOML2. We decided to focus on the first two, for which the function is currently unclear and appeared potentially to have an active role on CIII stabilisation and maturation or to interact directly with the enzyme during its biogenesis.

GHITM (Growth Hormone Inducible Transmembrane Protein), was initially described as a multipass IMM protein with a role in mitochondrial morphology and cytochrome *c* release (Oka et al., 2008). It was later found forming an interaction with CHCHD2 and stabilising Cyt *c* in the respiratory chain, allowing the proper electron flow from CIII to CIV in *Drosophila* (Meng et al., 2017). Moreover, it was found decreased in a *Par1^{-/-}* (the mitochondrial intramembrane-cleaving protease) mouse model, which displayed a specific CIII defect, together with TTC19, a well-characterised CIII biogenetical factor (Spinazzi et al., 2019). In our model, GHITM steady-state levels were increased specifically in the absence of CIII and complexome profiling analyses detected the protein in various complexes in the mutant cells that were absent in the WT cells. However, downregulation of GHITM did not affect CIII structure or activity, suggesting that its interaction with the enzyme is unrelated to the assembly pathway.

However, two observations were made working with GHITM knockdown cells. Firstly, BN-PAGE analyses showed that CII, CIII and CIV, appeared more abundant in cells transduced for the shRNAs, even if the formation of each SC specie was not altered. On one side, this could be due to an uncharacterised action of the protein on the whole OXPHOS machinery, but not specific for CIII. On the other, it is possible that the downregulation of GHITM modifies mitochondrial membranes properties and allows the extraction of a higher amount of proteins during BN samples solubilisation. Secondly, a potential effect on CIV activity was observed. Even if these data are very preliminary, it could be interesting to confirm it and explore this relationship more in depth in further studies, expanding the analysis also to CHCHD2 and its possible role in CIV assembly or stability. Indeed, silencing of CHCHD2 led to a significant decrease of CIV activity and a mild reduction of the assembled enzyme and CIV subunits steady-state levels in HEK293 cells (Baughman et al., 2009; Huang et al., 2018).

CHCHD3 (MIC19) is a known member of the MICOS complex involved in the connection between MIC60 in the IMM and the transporter SAM50 in the OMM. This protein localises specifically at the cristae junction, where the early stages of CIII and CIV assembly take place, and was the only MICOS member found associated with OXPHOS components (Sastri et al., 2017), in particular CIV subunits, suggesting a possible second role of this protein in OXPHOS regulation. However, the manipulation of CHCHD3 levels in WT and mutant cells did not confirm any specific involvement of this protein in CIII or CIV biogenesis. Moreover, as reported previously (Darshi et al., 2011), CHCHD3 depletion impaired mitochondrial respiration in our model. This defect is not specific for CHCHD3, since genetic removal of other MICOS subunits or proteins involved in cristae remodelling has been linked to reduced respiration, such as QIL1 (Guarani et al., 2015), OPA1 (Cogliati et al., 2016), and APOOL (Weber et al., 2013). These observations indicate that alteration in the cristae structure can lead to decreased respiration.

In conclusion, we found UQCR10- and CYC1-containing subassemblies within a wide range of molecular sizes that accumulate in the absence of MTCYB. Consequently, we aimed to take advantage of this fact to search for yet unknown CIII chaperones, but we were unable to prove a direct role on CIII biogenesis or activity for any of the identified interactors. However, an interesting observation emerged from these experiments: subunits belonging to the CIV assembly MTCO2-module were found consistently interacting with this intermediate in the $\Delta 4$ -CYB cybrids. These findings could suggest on one side that the nascent CIII might use CIV or CIV modules as a structural scaffold in a physiological context, on the other that it might sequester CIV specific subunits or intermediates when SC formation is impaired, as a control mechanism to inhibit CIV complete biogenesis. Both these hypotheses should be addressed in future work, in order to better define the association between the two enzymes. The generation of new models with different mutations in CIII subunits and different degrees of impairment in complex assembly could be useful to better characterise assembly intermediates and protein interactions.

In the second part of this project, we studied the structural and functional role of CIII in the assembly and maturation of the whole respiratory chain. CIII is central in the formation of all the main SC species (III_2IV_1 , I_1III_2 and the respirasomes $I_1III_2IV_1$ and $I_1III_2IV_2$) and its complete absence can lead to a deficiency in different ETC enzymes (Andreu et al., 1999;

Blakely et al., 2005, Schägger et al., 2004, Carossa et al., 2014; Feichtinger et al., 2017). Therefore, we took advantage of various proteomics and biochemical analyses to determine the origin of this CIII dependency for the biogenesis of the rest of the ETC, particularly that of CI. In addition to the virtually complete loss of CIII activity, $\Delta 4$ -CYB cybrids showed a dramatic reduction in CI activity and a significant decrease in CIV activity. In particular, analysing the structure of these enzymes, we found a severe decrease of fully-assembled CI in mutant cells, while mass spectrometry experiments highlighted the presence of a peak at 991 kDa (in digitonin solubilised samples) and 812 kDa (in DDM), which contained all the CI structural modules except the N-module and was bound to NDUFAF2. This indicated that the accumulated species corresponded to the previously described ~830 kDa pre-CI assembly intermediate (Ogilvie et al., 2005). Therefore, our analyses suggest that cells lacking CIII, and therefore unable to assemble SC, are not able to efficiently complete CI maturation.

The idea that respiratory complexes do not need to be fully assembled before associating with each other and that CIII and CIV might act as scaffolds to facilitate CI maturation was proposed in 2007 by Lazarou and colleagues (Lazarou et al., 2007), who also detected the assembly factor NDUFAF2 in CIII-containing high-molecular-weight complexes. Two years later, another paper was published reporting that newly imported nuclear-encoded CIV subunits were preferentially integrated into SC in the absence of monomeric CIV (Lazarou et al., 2009), while Moreno-Lastres (Moreno-Lastres et al., 2012) showed that the incorporation of the NADH dehydrogenase catalytic core in CI, and subsequent functional activation of the respirasome, takes place in the SC, instead of the monomeric CI. These data implied that the association between complexes is important for the formation and stability of CI. In addition, the incorporation kinetics of key CIII and CIV subunits indicated that there might be alternative biogenetical pathways for CIII and CIV depending on whether they are bound to the SC or not, even if the molecular mechanisms were still to be defined. This possibility has been recently corroborated with additional experimental evidence (Timón-Gómez et al., 2020).

Our observations of stalled CI assembly in the absence of SC, however, was in contrast with other studies previously published. Firstly, the most recent studies that analysed this pathway in detail and built the CI biogenesis model, considered that CI was assembled independently and before interacting with the other complexes (Guerrero-Castillo et al., 2017). Secondly, previous work on a murine cell line carrying mutations in the cytochrome *b* gene suggested

that the observed lack of fully assembled CI was due to instability and consequent degradation of the enzyme, once fully formed (Acin-Perez et al., 2004). The proposed explanations were that CIII might participate in CI maturation in an unknown way, such as through the possible peptidase activity of the two core subunits UQCRC1 and UQCRC2 (Acin-Perez et al., 2004), or that CI instability could be caused by the increased ROS production and consequent oxidative damage (Guaras et al., 2016). Indeed, in the case of CIII absence or damage, the CoQH₂/CoQ ratio is high and electrons from ubiquinol are transferred back to CI in a process known as Reverse Electron Transport (RET), which is responsible for the high production of O₂⁻ (Guaras et al., 2016).

The first experimental proof that contradicts the CI instability effect comes from our detailed kinetics analyses, which showed a comparable turnover of the MT-ND subunits between the Δ 4-CYB mutated cells and the control and did not highlight any sign of preferential degradation of the CI subunits. In addition, these experiments indicated clearly that in mutant cells CI assembly is stuck in the pre-CI stage, a ~830 kDa inactive intermediate lacking the N-module, while in WT cells CI subunits are detected in supercomplexes in early stages of maturation. Moreover, our complexome profiling analysis revealed that NDUFAF2, a CI assembly factor paralog of the NDUFA12 structural subunit able to bind to pre-CI and facilitate the insertion of the N-module, is upregulated and remains bound to the intermediate in the Δ 4-CYB cybrids (Ogilvie et al., 2005; Sanchez-Caballero et al., 2016). In normal assembly conditions, this assembly factor interacts with the nascent enzyme only transiently, while its accumulation indicates the stalling of complex formation in the mutant. Moreover, NDUFAF2 overexpression did not prevent CI assembly in WT cells, and its silencing did not rescue the biogenesis impairments in the mutant, confirming that NDUFAF2 accumulation is the consequence of pre-CI stalling, and not its cause.

Our data also showed that the absence of CIII has a double component in the assembly of CI: structural and functional. When CIII impaired function was replaced in Δ 4-CYB cells by the expression of AOX, we observed a partial recovery of the CI phenotype, similarly to what was reported in Guaras et al., 2016. On the other side, the presence of AOX did not lead to a full recovery of CI activity, nor prevent the pre-CI accumulation, and the pharmacological inhibition of CIII with antimycin A did not result in CI destabilisation or assembly defect in

WT cells, or in impairments in the SC formation. These observations imply that the lack of CIII activity alone is not sufficient to inhibit CI full maturation.

Moreover, the absence of CIII might influence the binding of the assembly factor NDUFAF2 to pre-CI, since the highly reduced CoQ pool generated might change the redox state of CI. Studies on *Y. lipolytica* suggested that N7BML's function (NDUFAF2 in humans) is to keep pre-CI in an 'open' state and to retain apo-proteins competent for interaction with the Fe/S cluster transfer machinery, before the binding of N7BM (NDUFA12) and the release of the assembly factor (Kmita et al., 2015), minimising the risk of ROS formation by RET. Highly reduced CoQ pool in CIII deficient cells, however, might reduce the Fe/S clusters and possibly block the incorporation of the N-module through electrostatic forces. The physical presence of CIII, instead, might induce a conformational change that helps the exchange between NDUFAF2 and NDUFA12, even if CIII does not contact directly the N-module of CI.

The contrasting data with what was previously published by Acin-Perez et al., (Acin-Perez et al., 2004) might be explained by different reasons. Firstly, the models used in the two studies are different, since our work was performed in human cell lines, while Acin-Perez et al., studied murine lines. As already discussed in the introduction, different species can present differences in supercomplex organisation and stoichiometry. In particular, humans may have a higher percentage of CI forming SC species, compared to other mammals and, if this observation is true, this might have an impact on the maturation pathway or the stability of the enzyme (Schägger, 2000; Davies et al., 2018). Moreover, the interpretation of data might have been influenced by technical reasons. Firstly, different species might present different turnover rates of the MRC complexes and the times used in the pulse-chase experiments of Acin-Perez et al. (2004) missed intermediate points (e.g., 2 and 5 h), taking only short and long chase times. Secondly, native samples of the *Mt-Cyb* mutants were solubilised in DDM, a stronger detergent than digitonin used in our study, which disrupts SC and might prevent the visualisation of relevant structures in BN-PAGE analyses.

Going from a focused to a wider perspective, the aim of this part of the project was also to collect new relevant data for the interpretation of the role of supercomplexes in humans. Many possible functions of these structures have been proposed, both structural and functional, together with different models describing the association between enzymes. Firstly, our data propose the role of CIII as a scaffold or 'platform' for CI and CIV assembly within the context of the SC, showing that there is no temporal gap between the complete assembly of CI and its

incorporation into SC. The ‘plasticity model’, therefore, which describes the simultaneous presence of SC and free enzymes, assuming that each complex is formed independently and forms higher grade associations subsequently, should be revised in the light of these findings. Secondly, we showed that in the context of CI assembly, the presence of CIII is necessary not only to offer structural support but also because of its functional component as a sensor of the redox state of the CoQ pool.

CI relies heavily on CIII presence to complete its maturation, but also CIV and, to a lesser extent CII are affected by MTCYB mutations. Indeed, CIV activity was reduced to approximately 60% of controls, as it has also been reported in a subset of patients with severe CIII deficiency of different genetic origins (Carossa et al., 2014; Feichtinger et al., 2017), the amount of fully assembled CIV was significantly decreased, and subassembly intermediates containing ‘early assembly stage’ subunits were accumulated in the mutant cells. These results indicate a general assembly defect in the absence of CIII and a probable stalling of CIV biogenesis, further supported by the increased amounts of MR-1S, a mammalian COX assembly factor which binds to a CIV intermediate, which lacks only the MTCO3 module (Vidoni et al., 2017).

For what concerns CII, reduced steady-state levels of SDHB and accumulation of SDHA and SDHC-containing intermediates were observed, even if these impairments did not result in significant loss of CII activity. Moreover, SDHAF2, a CII assembly factor binding SDHA and mediating its flavinylation (Hao et al., 2009; Kim et al., 2012), was found upregulated in the mutant cells. This result was surprising because CII is not generally considered as a component of SC, even if the existence of ‘megacomplexes’ containing all the ETC enzymes has been proposed (Acin-Perez et al., 2008; Guo et al., 2017). Moreover, both in our BN-PAGE and complexome profiling experiments, we never detected CII associating with other complexes or forming uncharacterised high-molecular-weight structures. The reduced expression of SDHB, the Fe/S cluster containing subunit, could be the result of a regulation mechanism in case of impaired OXPHOS, which results in accumulation of subassemblies containing the remaining subunits, which are now in excess. Another possibility is that, while in the case of CI and CIV, the physical absence of CIII has the strongest impact, together with a secondary functional component, the alteration of the CoQH₂/CoQ balance and the resulting oxidative stress might have the dominant role in CII assembly alterations. In order to further characterise this aspect, it could be interesting to measure SDHB expression and CII subassemblies

formation in WT cells chronically treated with antimycin A and in the AOX-HA overexpressing model we generated, to evaluate the effective weight of the redox state of the CoQ pool on the enzyme.

In conclusion, our work confirms the combined MRC enzyme deficiency associated with mutations in the CIII subunit MTCYB, that leads to complete loss of SC containing CIII and fully assembled CI, to the accumulation of an inactive pre-CI lacking the catalytic N-module, and to a reduction of fully assembled CIV levels. Many possible functions have been proposed for SC, including substrate channelling, structural support, and prevention of ROS formation, especially from CI (Maranzana et al., 2013; Lopez-Fabuel et al., 2016). These results provide new data in support of the hypothesis that a main function of SC is structural, acting as 'assembly stations' for the ETC complexes. Moreover, CIII is a central component of these stations, and might confer them also functional purposes. Firstly, SC could regulate the formation or the turnover of the ETC enzymes in different metabolic or stress conditions. Secondly, the stalling of CI in the pre-CI stage, which lacks the active NADH dehydrogenase module, and the control of the replacement of the N-module, would minimise superoxide formation in the absence of CIII and consequent high CoQH₂/CoQ ratio and reverse electron transport (Szczepanowska et al., 2020). These aspects should be better investigated in future research, analysing the formation and the stoichiometry of SC in different cell types, energy demand conditions and metabolic stresses.

Section 7: analysis of complex IV and MCU complex interaction

7.1 Introduction and preliminary data

The inner mitochondrial membrane is characterised by a high density of proteins, which spatially organise themselves in different subdomains and interact with each other. As described in the previous chapters, the components of the respiratory chain have been studied in depth and are today known to form supercomplexes (SC). However, the formation of still uncharacterised ETC-containing SC species to fulfil or regulate specific mitochondrial functions is still possible. In this project, we analysed the interaction between the mitochondrial calcium uniporter complex (MCUC) and cytochrome *c* oxidase (CIV), the terminal oxidase of the electron transport chain.

The starting point of the investigations described here was the finding of a physical interaction between CIV and MCU, in a SILAC/Pulldown experiment comparing a cybrid line with a homoplasmic frameshift mutation in *MTCO3* and a WT control (Tiranti et al., 2000) (Figure 7.1). The experiment was originally conducted to analyse CIV assembly pathway and identify new assembly factors, and data were published by Vidoni et al., 2017. Interestingly, in addition to OXPHOS subunits and assembly factors, peptides corresponding to MCU were also detected by mass spectrometry, showing that the protein could interact with CIV both in the WT and in the mutant cell line. The amounts of MCU in the immunopurified fractions were significantly enriched in eluates from control cells but not in the mutant line with impaired CIV assembly.

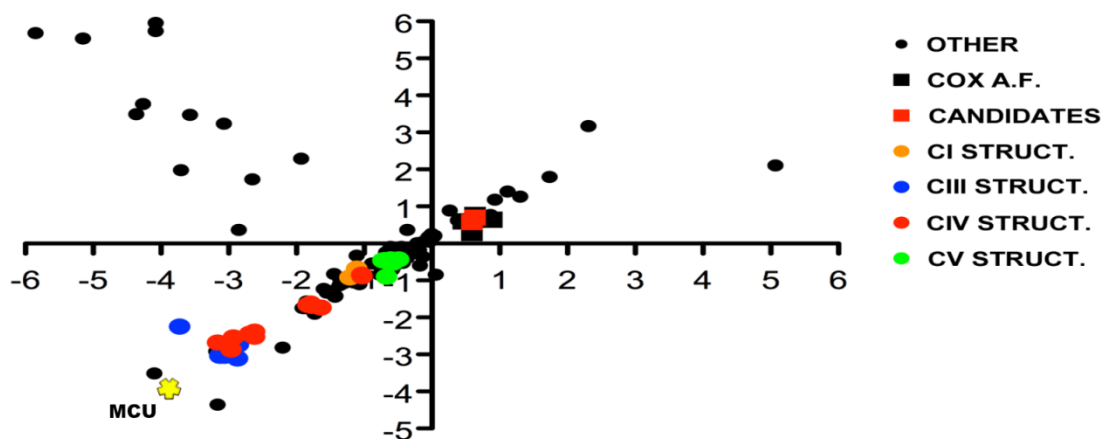


Figure 7.1: MCU interacts with CIV both in WT and MTCO3 mutant cells, and is less abundant in the mutant line. Scatterplots showing the logarithmic heavy to light (H/L) ratios obtained after mass spectrometry analysis of WT and MTCO3 mutant cybrid cell lines after bi-directional SILAC-labelling and COX immunocapture. Two reciprocal labelling SILAC experiments were performed and plotted one in x-axis and the reverse in the y-axis. Data obtained from Vidoni et al., 2017.

Based on these results, the project was divided in two aims: firstly, to confirm and characterise the MCUC-CIV interaction and whether the physical presence of one of the two complexes could stabilise the other or be relevant in its assembly; and secondly, to determine whether the activity of MCU, or one of the uniporter complex components and/or the regulation of mitochondrial calcium could have a functional role, important for the modulation of CIV and cellular respiration.

To address these questions, various experiments were performed on different cellular models. The effects of lack of CIV were studied in two cybrid lines, compared to the respective homoplasmic WT controls: one carrying a homoplasmic mutation in MTCO3, late-stage assembly subunit, which results in the accumulation of assembly intermediates, and used for the SILAC experiment shown in Figure 7.1, and one with a homoplasmic mutation in MTCO1, assembled in the early phases of enzyme biogenesis, which leads to the virtual absence of CIV (Bruno et al., 1999; D'Aurelio et al., 2001; Lobo-Jarne et al., 2020). To confirm the specificity of the results for CIV defects and not due to a general OXPHOS impairment, cells lacking CI and CIII were used as controls: CI-deficient immortalised fibroblasts from a patient carrying two compound heterozygous mutations in NUBPL, a CI assembly factor, which result in complete loss of CI (Protasoni et al., 2020), and the CIII-deficient $\Delta 4$ -CYB cybrids described in Section 5, characterised by complete loss of CIII and consequent impairment of CI assembly.

On the other side, to analyse CIV structure and activity in the absence of MCUC components, the same WT cybrids were treated with specific siRNA oligonucleotides, downregulating the expression of each MCUC subunit (Figure 7.8A).

7.2 Characterisation of MCUC-CIV interaction

7.2.1 Analysis of MCUC subunits interaction network

The first assay we performed to further investigate MCUC-CIV interaction was the recently developed proximity-dependent biotin identification (BioID) analysis (Roux et al., 2012), conducted on HEK293 cells in collaboration with Prof Eric Shoubridge (McGill University, Canada) and Prof Anne Claude Gringas (University of Toronto, Canada). Prof Shoubridge generated all the different cell lines expressing the ‘bait’ proteins and Prof Gringas performed the pulldown and mass spectrometry analysis. BioID is a method that allows the detection of proteins in close vicinity of a protein of interest in living cells, extending the sensitivity of canonical pulldown experiments from proteins stably binding the target, to proteins that are only transiently interacting with it or functioning in very close proximity (up to 10 nm). The principle is based on the capacity of a biotin ligase (BirA from E.coli) fused to a protein of interest to catalyse the proximity-dependent biotinylation of all the direct and close partners. For each constituent of the MCUC (MCU, MCUb, MICU1, MICU2, EMRE), we have generated a tetracycline inducible MCUC-BirA-FLAG stably integrated in HEK293 Flp-In T-Rex. Correct expression and mitochondrial localisation of the different constructs was confirmed by immunofluorescence. After 24 hours of expression, biotin was added to the cell media for another 24 hours and purification of biotinylated proteins by Streptavidin pulldown was performed, followed by their identification by mass spectrometry (Antonicka et al., 2020). Of note, the BioID of MCUR1 was performed by Dr Vincent Paupe and Prof Eric Shoubridge in an independent project.

In accordance with the co-immunopurification results, the BioID showed that CIV subunits and assembly factors are between the top hits identified for MICU1, MICU2, EMRE, and MCUR1, suggesting a frequent interaction or proximity between the two complexes (Figure 7.2). Interestingly, CIV subunits belonging to the early assembly modules and the assembly

factor COX15, which is involved, together with COX10, in the heme *a* synthesis and the maturation of MTCO1, scored the highest values. Of note, MCU and MCUB were found interacting only with each other and no specific interactions with other MCUC or CIV components were found. Indeed, the BirA was cloned in C-terminus of MCUC components, and, because of MCU and MCUB orientation in the IMM, biotinylated proteins were identified in the mitochondrial matrix and not in the IMS. As expected, instead, MICU1 and MICU2 were shown to interact with each other, and all the MICU proteins were identified in EMRE hits, validating the BioID results. In addition, these two conditions (MCU and MCUB) have been recently published by our collaborators (Antonicka et al., 2020), to demonstrate the specificity of the method.

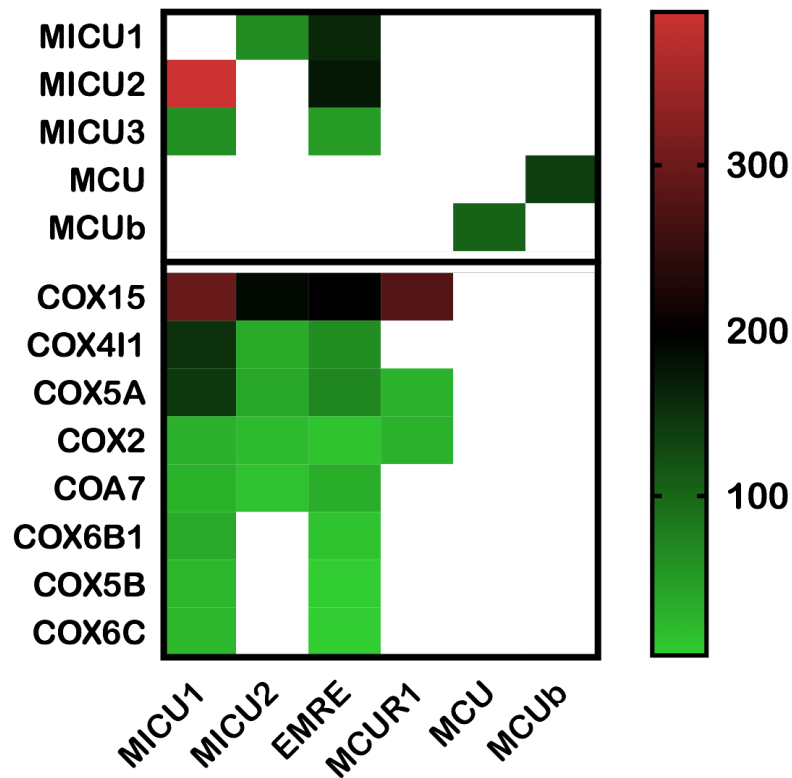
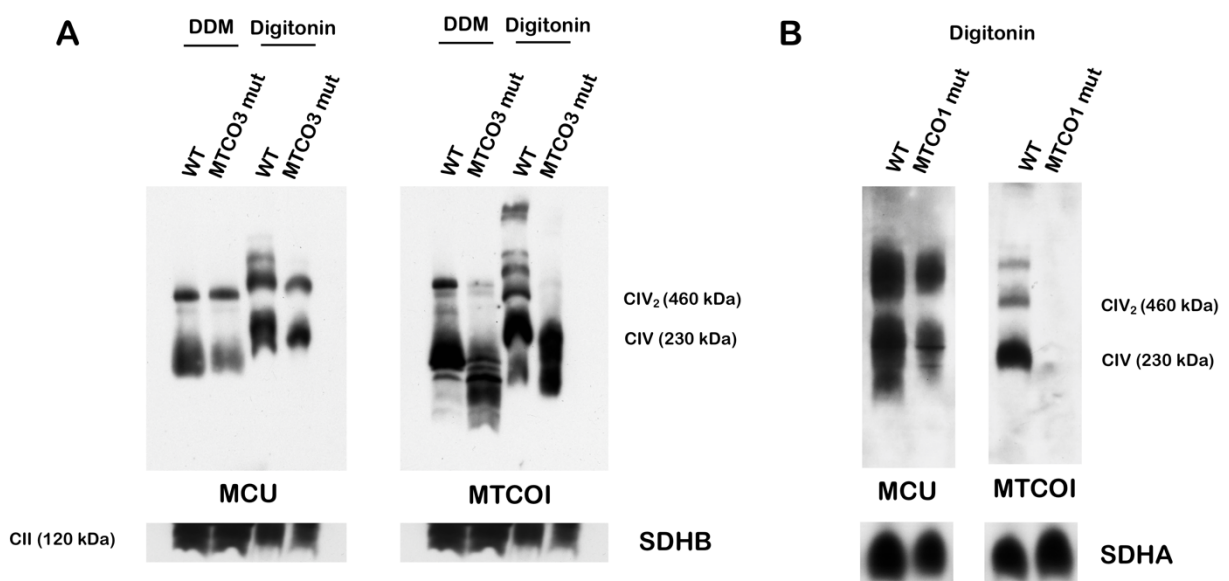


Figure 7.2: *MCUC components were found interacting with CIV subunits and assembly factors by BioID.* Heatmap of the abundance of protein interactions discovered by proximity-dependent biotin identification (BioID) for the baits of the different components of the MCUC, indicated at the bottom of the columns (MICU1, MICU2, EMRE, MCUR1, MCU, and MCUB). The colour gradient represents the normalised fold change of the proteins identified as interactors, while white boxes were used for proteins not found using the respective bait. Fold change was calculated as indicated in Antonicka et al., 2020. Experiment performed by Vincent Paupe and Eric Shoubridge.

7.2.2 Effects of lack of CIV on MCUC

To better characterise the potential interaction and functional relevance of the close association between CIV and the MCUC, we investigated how each complex is affected in the absence of the other one.

To evaluate if CIV deficiency has an impact on MCU organisation and formation of potential SC, we performed 1D BN-PAGE analyses on two cybrid lines with CIV assembly defects of different origin: MTCO3 and MTCO1 mutants (Figure 7.3A, B). Indeed, a recent study has shown using BN-PAGE experiments that MCU is present in different molecular-weight complexes, containing different combinations of the auxiliary subunits of the complex (Konig et al., 2016). Samples solubilised in both DDM and digitonin and analysed by 1D BN-PAGE revealed an alteration in the MCU complex pattern in the mutant lines. Indeed, in both CIV-deficient cell lines, the main MCU complex detected at ~230 kDa, which migrates at the same molecular weight as ‘monomeric’ CIV and is supposed to contain only MCU and EMRE (Koning et al., 2016), was considerably downregulated in both DDM and digitonin extraction conditions (Figure 7.3A, B). Moreover, we observed that the formation of SC containing MCU was also reduced in both MTCO1 and MTCO3 mutant cell lines. Finally, complexome profiling analyses with SILAC-labelled samples from mitochondria extracted from WT and MTCO3 mutant cells, also revealed an alteration of the MCU SC, confirming our results obtained in BN-PAGE and WB (Figure 7.3C).



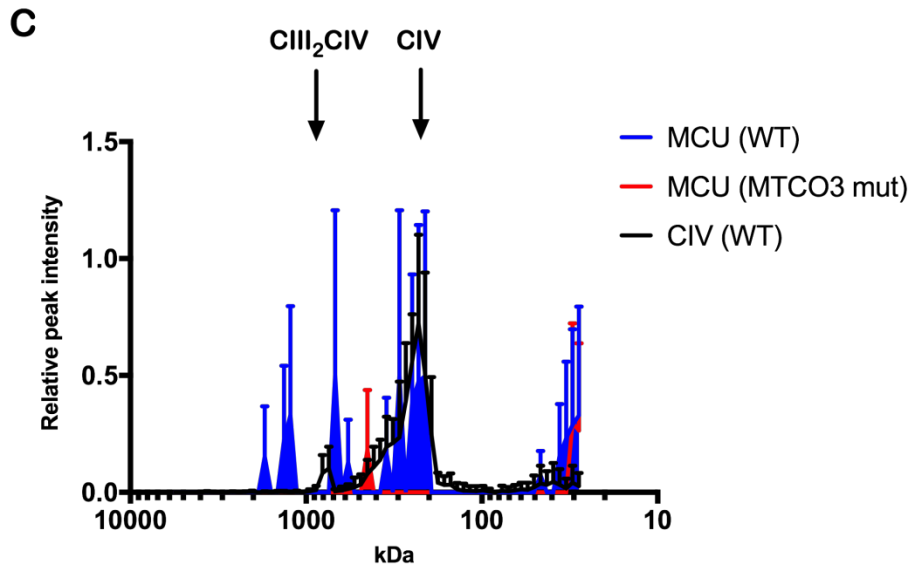


Figure 7.3: MCU pattern is altered in cells with CIV assembly defects. 1D BN-PAGE, Western blot, and immunodetection of MCU and MTCO1 (CIV) in two cybrid lines: one with a mutation in MTCO3 (A), and one with a mutation in MTCO1 (B), and respective WT lines. Samples were solubilised in 1% DDM or 1% digitonin, as indicated. CII (SDHB and SDHA) was used as a loading control. C) Complexome profiles of MCU and CIV in samples solubilised in 1.6 mg DDM/mg protein of WT and MTCO3 mutant cybrids. MCU profiles (WT in blue and mutant in red) were generated by analysing the peptide content in each of the 64 slices in which the gel lanes were excised. CIV profile (black) was generated plotting the average of all the CIV subunits identified in WT cells. The graphs plot the relative peptide peak intensities along the lane, setting the maximum to 1.0, versus the molecular mass calculated using the individual complexes and supercomplexes as the standards to generate a calibration curve. The relative amounts of the proteins between the two cell lines were determined by calculating the Heavy/Light ratios of peptides that were present in both WT and MTCO3 mutant samples. The represented values are the mean \pm SEM of the two reciprocal labelling experiments. The in-gel digestion and MS analysis, as well as the writing of Python and R scripts for data extraction and manipulation, were performed by Dr Michael E. Harbour. The experiment in B was performed by Anezka Kafkova. The experiment in C was performed by Dr Sara Vidoni.

To further validate these results, 2D BN-PAGE was performed to analyse digitonin-solubilised samples from WT and CIV mutant cybrids. In this method, each complex and SC is denatured in second-dimension electrophoresis, and the protein alignment allows the identification of co-migrating proteins or the shift towards high- or low-molecular-weight in comparison with other complexes. In the first experiment (Figure 7.4B), samples were immunoblotted against MICU2, MCU, CIV, CII, and CV. CII (~120 kDa) and CV (~770 kDa) patterns were not affected by the lack of CIV (Figure 7.4A), therefore they were used as reference points. In the second experiment (Figure 7.4C), samples were immunoblotted against MICU1, MCU, and MCUR1.

Firstly, our results confirmed what shown in Figure 7.3: MCU ~230 kDa complex co-migrates with monomeric CIV in WT cells and it is shifted towards high-molecular-weight in CIV mutant cells. Indeed, in Figure 7.4B, the red line indicating MCU is clearly closer to CV (black line) in MTCO1 mutant cells than in WT, while the distance between CII and CV is not affected. Similarly, in Figure 7.4C, the low-molecular-weight MCU signal is reduced in the absence of CIV. Secondly, MICU1 and MICU2 were detected mainly in low-molecular-weight complexes (Figure 7.4B, C), which do not co-localise with MCU and are not strongly impacted by the absence of CIV. MICU1 was detected also in high-molecular-weight complexes, possibly interacting with MCU and MCUR1 in WT, while this association was lost in MTCO3 mutant cells (Figure 7.4C). This last result, however, should be confirmed with additional experiments.

Taken together, these BN-PAGE-based experiments show results in the same direction as the proteomics analysis revealing the co-migration of MCUC, and in particular of MCU, with CIV and that CIV defects lead to a re-arrangement of MCUC SC.

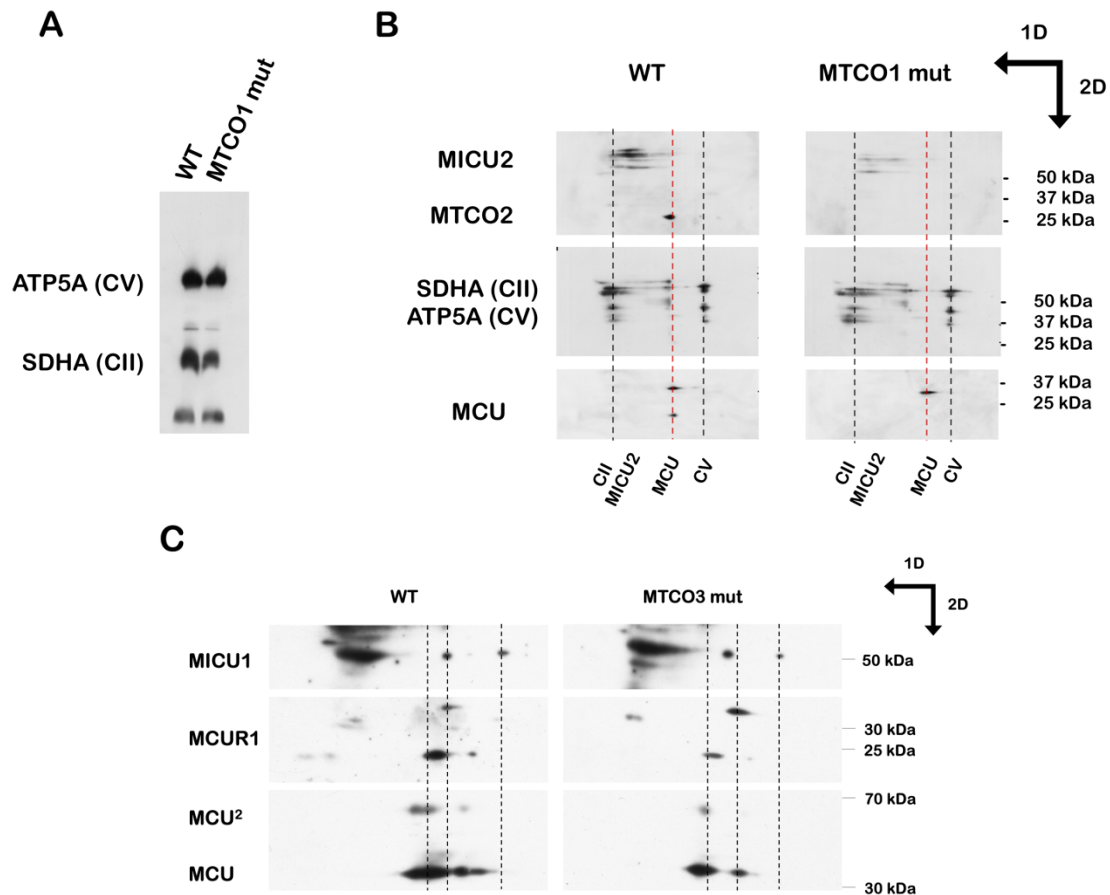


Figure 7.4: MCU, MICU1, MICU2, and MCUR1 patterns in 2D BN-PAGE in WT and CIV deficient cells. 1D (A) and 2D BN-PAGE (B), Western Blot, and immunodetection of samples from WT and MTCO1 mutant cybrids solubilised in 1% digitonin. SDHA (CII) and ATP5A (CV) were used as references points to evaluate the MCU and MICU2 subunits shifts. C) 2D BN-PAGE, Western Blot, and immunodetection of samples from WT and MTCO3 mutant cybrids solubilised in 1% digitonin.

Finally, the steady-state levels of MCUC subunits were also analysed in the two CIV-deficient cell lines compared to the respective WT controls by immunoblot analysis. No drastic changes were observed in MCUC protein levels in both mutant cell lines, except for a slight reduction in MICU1 and MCU signals in the absence of CIV (Figure 7.5). These results indicate that the differences observed in MCU complex and MCU-containing SC formation in cells lacking CIV are not due to significant differences in subunits steady-state levels.

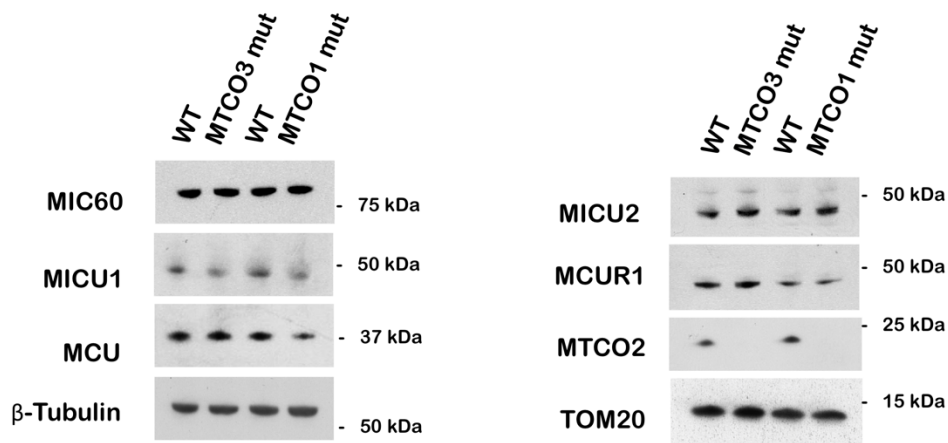


Figure 7.5: MICU1 and MCU steady-state levels are slightly reduced in the absence of CIV. SDS-PAGE, Western blot, and immunodetection of total cell lysate from cybrids with mutations in MTCO3, MTCO1 and respective controls. β-Tubulin, TOM20 and MIC60 were used as loading controls.

7.2.3 Specificity of the MCUC-CIV interplay

To establish if the changes in MCU-containing complexes were due specifically to CIV defects or to a general OXPHOS impairment, we analysed the MCU pattern in 1D BN-PAGE and immunoblotting in two additional cell models of RC deficiency: CIII-deficient cybrids (#17.3 Δ4-CYB), and CI-deficient immortalised fibroblasts (NUBPL mutant) (Figure 7.6). In both CI and CIII mutant cells, CIV-containing SC are missing or redistributed, but fully assembled CIV is still present (Figure 7.6). In these cells, MCU behaves differently than in CIV mutants, showing no major differences in the MCU complex and MCU-containing SC formation. However, we observed a slight increase of the MCU high-molecular-weight SC in the CIII-lacking samples (Figure 7.6). Moreover, the simultaneous immunodetection of MCU and CIII (Figure 7.6A) or CI (Figure 7.6B), showed that the two OXPHOS complexes do not co-migrate with MCU complex and therefore do not form supercomplexes with the uniporter.

Taking all our results together, we could, therefore, conclude that MCU interacts and forms complexes specifically with CIV, but not with the rest of the respiratory chain and that MCU SC pattern is affected only in cells lacking CIV.

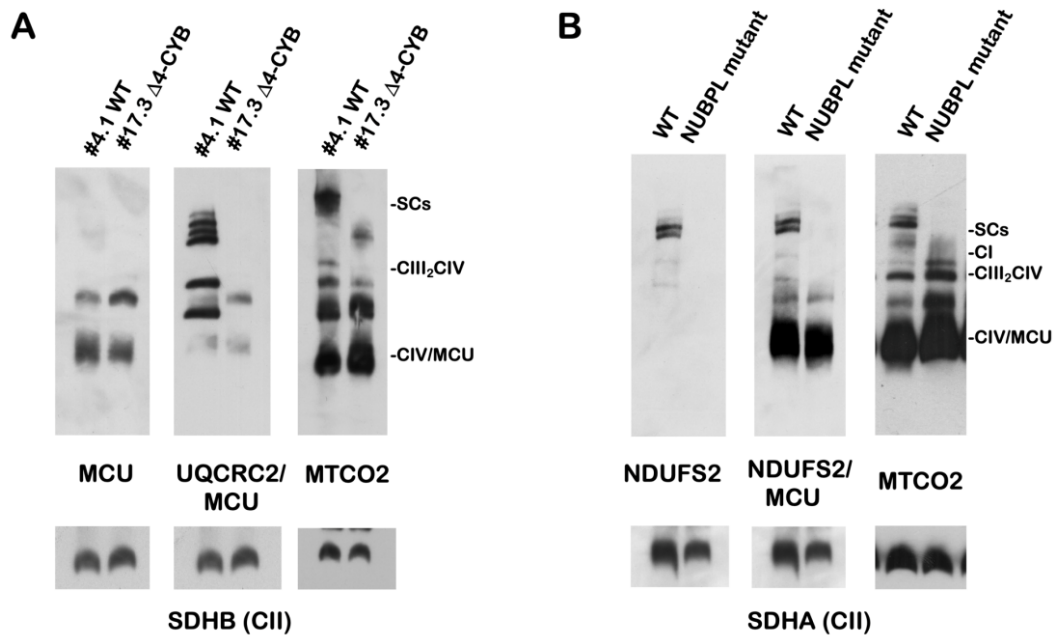


Figure 7.6: *MCU pattern is unaffected in cells lacking CI or CIII. 1D BN-PAGE, Western blot, and immunodetection of digitonin-solubilised samples from homoplasmic WT and $\Delta 4$ -CYB cybrids (A), and immortalised fibroblast with compound heterozygous mutations in NUBPL and control (B). SDHA and SDHB were used as loading controls.*

7.2.4 Challenges in the analysis of COX15 role in MCUC-CIV interaction

To conclude the analysis of the role of CIV in MCUC organisation, we decided to study the potential effects of silencing and overexpressing COX15, a CIV early-stage assembly factor, on the MCUC formation. Indeed, analysing our BioID results, we noticed that the first CIV component hit for MICU1, MICU2, EMRE, and MCUR1, was COX15. However, the lack of commercially available tools, such as valid antibodies and siRNAs constructs specific for COX15, did not allow us to perform a rigorous analysis of their potential interplay. Firstly, of the antibodies that we have tested, the only one recognising a band approximately at the COX15 predicted size (~46 kDa), was not specific for COX15, since the same band appeared in a sample derived from a COX15 knockout mouse model (Viscomi et al., 2011) (Figure 7.7A). Secondly, we tried to stably overexpress a C-terminal HA-tagged version of the protein. However, while the construct is inserted in the cells genome and the mRNA is expressed (Figure 7.7B), the protein was not detectable by SDS-PAGE and immunoblotting with an anti-HA antibody (data not shown). Finally, three different siRNAs targeting specifically COX15 were tested, and the residual amount of mRNA present in WT cells after six days of treatment

was measured by RT-PCR (Figure 7.7C). Only one siRNA led to a substantial decrease in *COX15* mRNA level, reducing it to 44% compared to control. However, we considered that the reduced *COX15* expression was not decreased enough to use it confidently as a model of *COX15* silencing. While *COX15* appeared to be a strongly conserved interactor of all the different MCUC members tested by BioID, the lack of tools made the investigation of the potential interplay of *COX15* with MCUC challenging. Further experiments will be needed to develop tools able to specifically manipulate *COX15* levels, in order to study its function in our model.

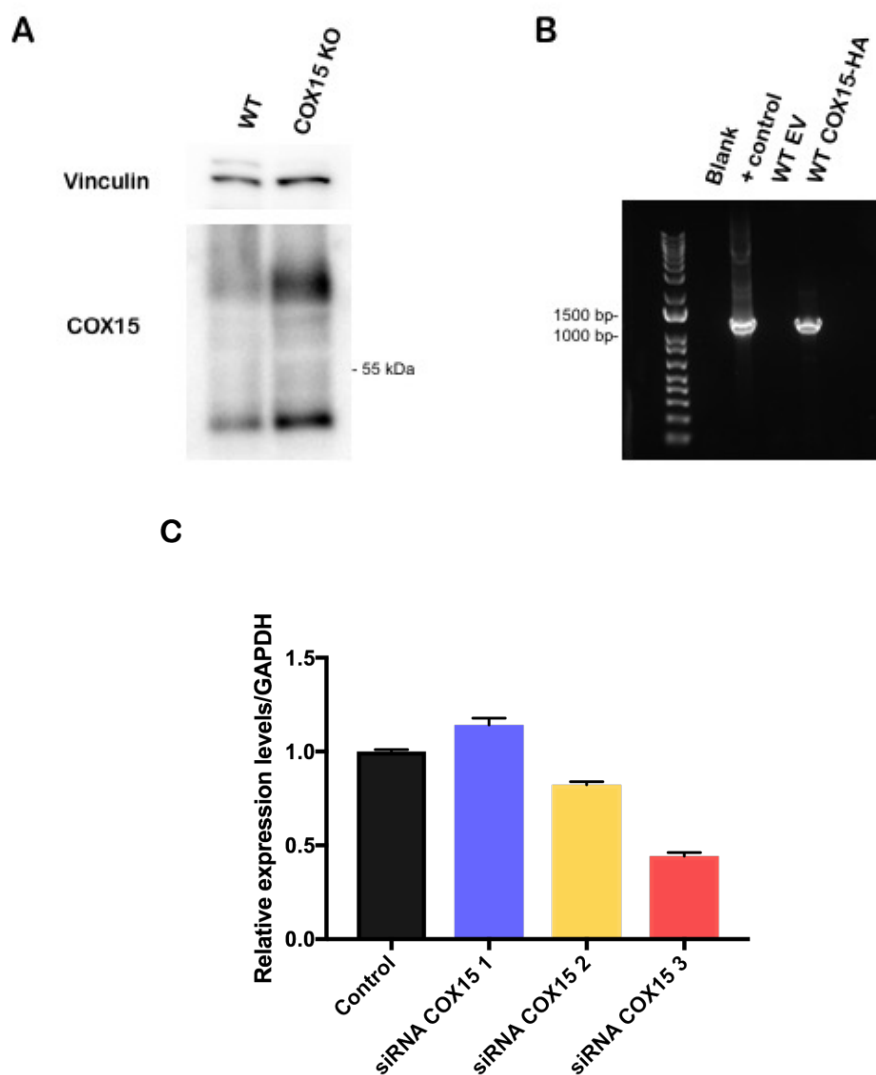


Figure 7.7: test of different approaches to visualise or modulate *COX15* expression. A) SDS-PAGE, Western blot, and immunodetection of samples from a WT and a knockout mouse model for *COX15*. Vinculin was used as a loading control. B) RNA was extracted from WT cells transduced with either the pWPXLd-ires-Hygro^R empty vector (EV), or containing *COX15*-HA, and retrotranscribed to cDNA. PCR was performed on the cDNA using *COX15* forward primer and a reverse primer specific for the HA sequence. As a positive control, the pWPXLd-ires-Hygro^R-*COX15*-HA construct used for

transduction and checked by Sanger sequencing was used. C) Quantitative RT-PCR analysis of the expression at the mRNA level of COX15 in WT cells treated with three different siRNAs targeting COX15. Total RNA was extracted and retrotranscribed. TaqMan Gene Expression Assay was used and COX15 levels were normalised to that of the housekeeping gene GAPDH and expressed as relative to control (1.0).

7.3 Effects of lack of MCUC subunits on CIV

After characterising the effects of CIV on MCUC, we moved on to investigating the role of each MCUC subunit on CIV activity and cellular respiration. To achieve this, we performed siRNA-mediated downregulation of MCU, MICU1, MICU2, and EMRE. The efficiency of each siRNA constructs was tested in every experiment, but a representative example is shown in Figure 7.8A, showing a significant knockdown of each subunit by specific siRNAs.

First, we evaluated CIV stability and ability to form supercomplexes when MCU, MICU1, MICU2, or EMRE expression was reduced (Figure 7.8B). In none of these conditions CIV assembly appeared significantly affected, ruling out the hypothesis that an interaction with the MCU complex is required for the biogenesis or stabilisation of the enzyme. However, while the canonical SC species described for CIV were found intact, by running the gel for a longer time and with a better separation of each single band, it was possible to observe two uncharacterised high-molecular-weight bands. Interestingly, while silencing of MCU or EMRE did not affect these high-molecular-weight SC species, loss of the MICU subunits led to a downregulation of the lower SC or both SC in MICU1 or MICU2 silenced cells, respectively (Figure 7.8B).

We then used the same methodology to evaluate the potential effects of MCUC subunits silencing on the rest of the OXPHOS machinery (Figure 7.8C). The immunodetection of CI and CIII subunits (using NDUFS2 and UQCRC2 as markers, respectively) from digitonin-solubilised samples of WT cells treated with MCUC siRNAs did not reveal any specific differences in the assembly of these enzymes or the formation of SC compared to control silenced cells, suggesting a specific interplay between MCUC and CIV.

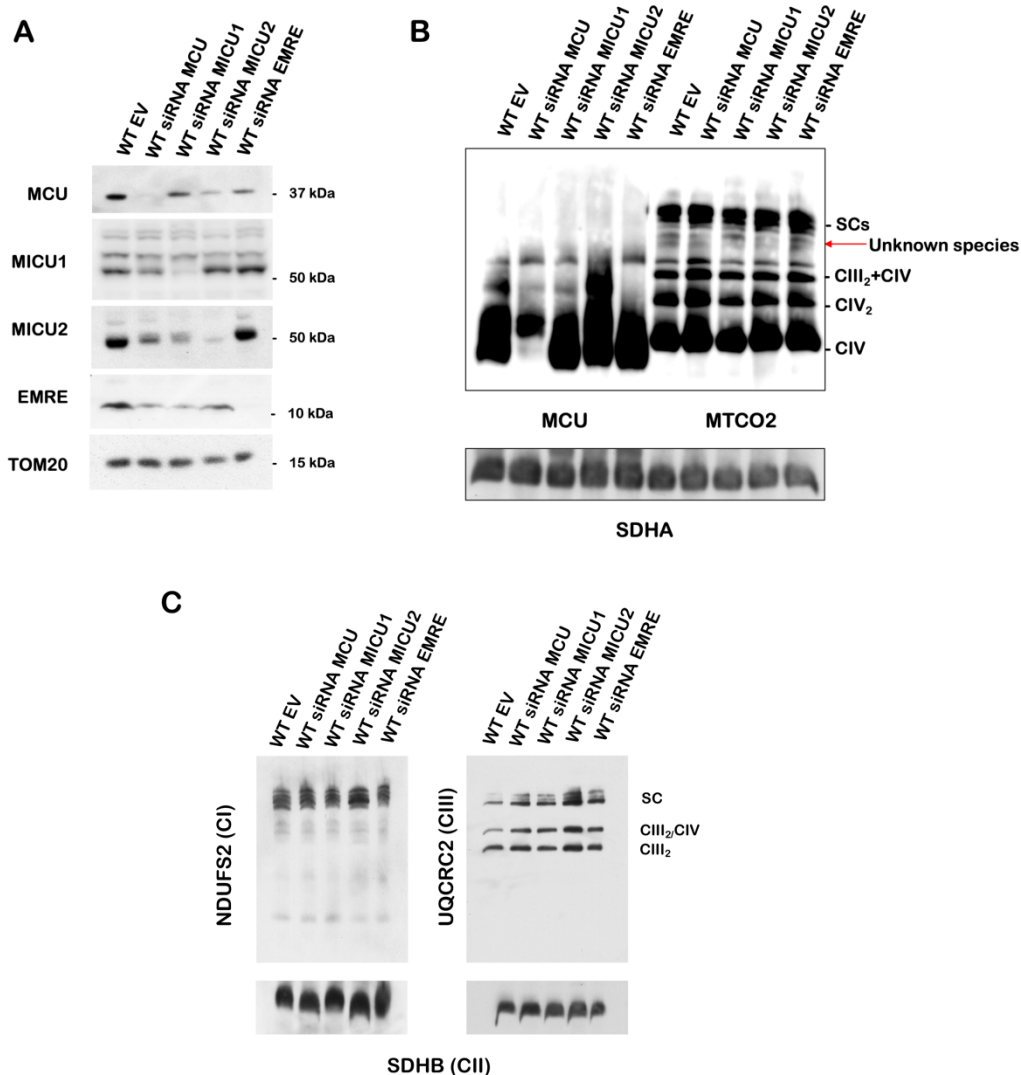


Figure 7.8: uncharacterised CIV supercomplexes are affected by knockdown of MICU1 and MICU2. A) SDS-PAGE, Western blot, and immunodetection of samples from WT cells treated for 3 days with siRNA specific for MCU, MICU1, MICU2, and EMRE, or with the siRNA negative control. TOM20 was used as loading control. B) 1D BN-PAGE, Western blot, and immunodetection of MCU and MTCO2 in 1% digitonin-solubilised samples from the cells described in (A). SDHA was used as a loading control. Experiment B was performed by Anezka Kafkova. C) 1D BN-PAGE, Western blot, and immunodetection of NDUFS2 and UQCRC2 in 1% digitonin-solubilised samples from the cells described in (A). SDHB was used as a loading control. The images are representative of experiments performed at least three times.

To try to better visualise and characterise the CIV-containing high-molecular-weight species observed in Figure 7.8B, we performed a complexome profiling analysis as a possible readout. We decided to compare control WT cells with cells downregulating MICU2, since in BN-PAGE analyses this condition showed the strongest effect on the formation of these unknown SC (Figure 7.8B). Values for the individual CIV subunits were averaged to simplify the graphic

representation (Figure 7.9). However, this technique appeared not to have enough sensitivity and resolution to detect and separate all the different SC bands. Indeed, complexome analysis showed that most of CIV was present as a monomer and only a small percentage was engaged in the formation of SC, resulting in a very strong signal at ~230 kDa and lower detection of high-molecular species. However, this quantitative proteomics analysis independently confirmed that downregulation of MICU2 does not affect the total amounts and assembly of the main CIV-containing species.

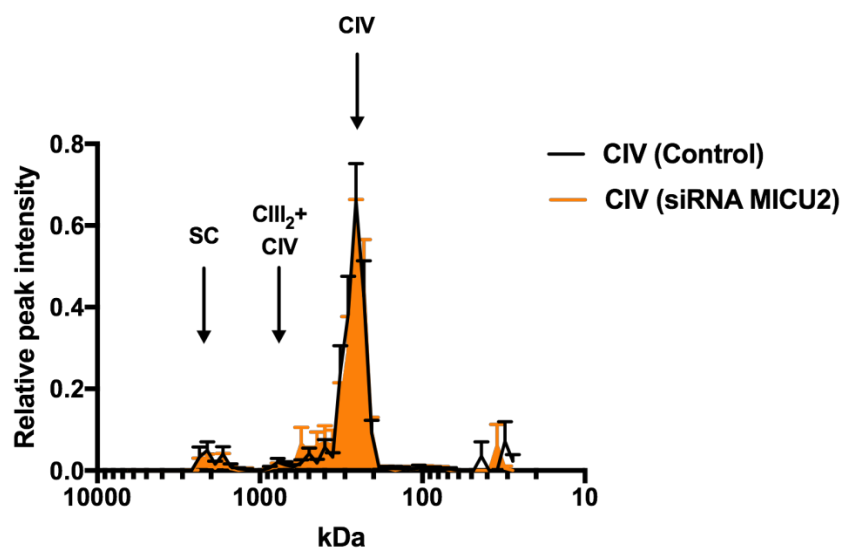


Figure 7.9: complexome profiles analysis did not provide a better visualisation of CIV SC species. Complexome profiles of CIV subunits in WT cells treated for three days with a siRNA specific for MICU2, or with the siRNA negative control. Samples were solubilised in 4 mg digitonin/mg of protein, 1D BN-PAGE was run overnight, and gel lanes were excised in 64 slices. The peptide content in each slice was analysed by mass spectrometry and the relative peptide peak intensities along the lane was plotted, setting the maximum to 1.0, versus the molecular mass calculated using the individual complexes and supercomplexes as the standards to generate a calibration curve. The relative amounts of the proteins between the two cell lines were determined by calculating the Heavy/Light ratios of peptides that were present in both control (black) and MICU2 knockdown (orange) samples. All detected CIV subunits were averaged and values are represented as mean \pm SEM of the two reciprocal labelling experiments.

Next, to have better insight of the functional relevance of the MCUC-CIV interaction, we measured the effects of MCUC subunits downregulation on CIV activity. To address this question, we performed two experiments: firstly, we measured oxygen consumption in permeabilised cells in an Oxygraph-2k respirometer, isolating CI-driven, CII-driven, and CIV

specific respiration (Figure 7.10A). Secondly, we analysed the enzyme activity of each complex of the ETC, by spectrophotometric kinetic measurements in different silenced cells (Figure 7.10B). Interestingly, the silencing of MCU and EMRE did not affect CIV activity, whereas the downregulation of MICU1 or MICU2 had an opposite impact on OXPHOS functionality. Indeed, MICU2 KD has a general effect that leads to increased respiration (Figure 7.10A) and enzyme activity (Figure 7.10B) of most of the ETC complexes, while reduced levels of MICU1 provoke a specific reduction of ~30% of CIV activity, while not affecting the rest of the ETC complexes, and of oxygen consumption.

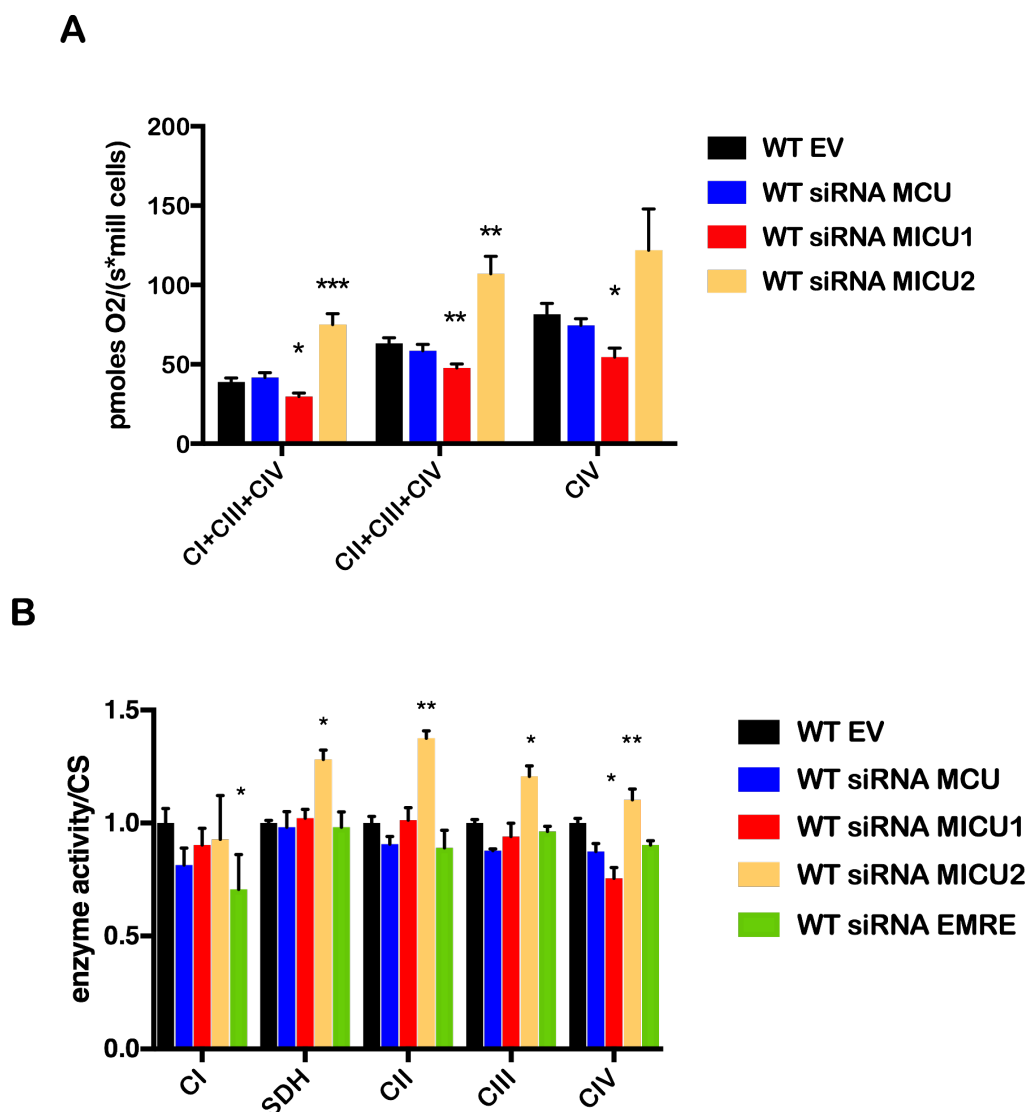


Figure 7.10: knockdown of MICU1 leads to a reduction in CIV activity and respiration, while knockdown of MICU2 provokes increased respiration and activity of CII, CIII and CIV. A) Oxygen consumption rates measured in permeabilised WT cybrids treated for 3 days with siRNA specific for MCU, MICU1, and MICU2, or with the siRNA negative control in an O2K high-resolution

respirometer. CI+III+IV: difference between rate of oxygen consumption in the presence of glutamate and malate, and after rotenone inhibition of CI. CII+III+IV: difference between rate of oxygen consumption in the presence of succinate and glycerol-3-phosphate, and after antimycin A inhibition of CIII. CIV: difference between rate of oxygen consumption in the presence of TMPD and ascorbate, and after CIV inhibition by KCN. Values are indicated as mean \pm SEM ($n = 4-7$ biological replicates). Unpaired Student's *t*-test was used (* $P < 0.05$; ** $P < 0.01$; *** $P < 0.001$). Experiment performed by Dr Erika Fernandez-Vizarra. B) The activities (mUnits/g of protein) of the respiratory chain enzymes were determined by spectrophotometric kinetic measurements in WT cybrids treated for 3 days with siRNA specific for MCU, MICU1, MICU2, and EMRE, or with the siRNA negative control and normalised to citrate synthase (CS) activity. Results are expressed as mean \pm SEM ($n = 6$ biological replicates). Two-way Anova test was used (* $P < 0.05$; ** $P < 0.01$; *** $P < 0.001$).

Since MICU1 was the only MCUC subunit showing an effect exclusively on CIV activity, we decided to study this protein in more details. Therefore, we cloned MICU1 wild type and MICU1^{EFmut}, with four point mutations in its EF-hand domains that abolish calcium-binding (Kamer and Mootha, 2014), with an -HA tag at their C-terminus and performed stable lentiviral transduction in WT cells. We then analysed the effects of MICU1 and MICU1^{EFmut} overexpression on the respiratory chain complexes, by SDS-PAGE (Figure 7.11A), BN-PAGE (Figure 7.11B), and spectrophotometric kinetic measurements of ETC enzymes activity (Figure 7.11C). Both MICU1 WT or EF^{mut} overexpression did not have any impact on the steady-state levels of the ETC subunits investigated, nor on CIV biogenesis and the formation of CIV SC (Fig 7.11A and B). However, a small reduction in CIII and CIV activity was observed in cells transduced for MICU1-HA, but not in cells overexpressing the Ca²⁺-binding-mutant protein (Fig 7.11C). This observation could be explained in two ways: on one side, it could reinforce the idea that MICU1 has a direct impact on the ETC activity and especially on CIV and that this impact is due to MICU1 Ca²⁺-sensing function and not to its physical presence, since MICU1^{EFmut} has no effect compared to MICU1-WT. On the other, the much higher expression levels of MICU1-HA compared to MICU1^{EFmut}-HA (Figure 7.11A), could play a role. Indeed, the non-physiological overexpression of MICU1 impacts MICU2 steady-state levels, and potentially the formation and assembly of MICU1/MICU2 dimers.

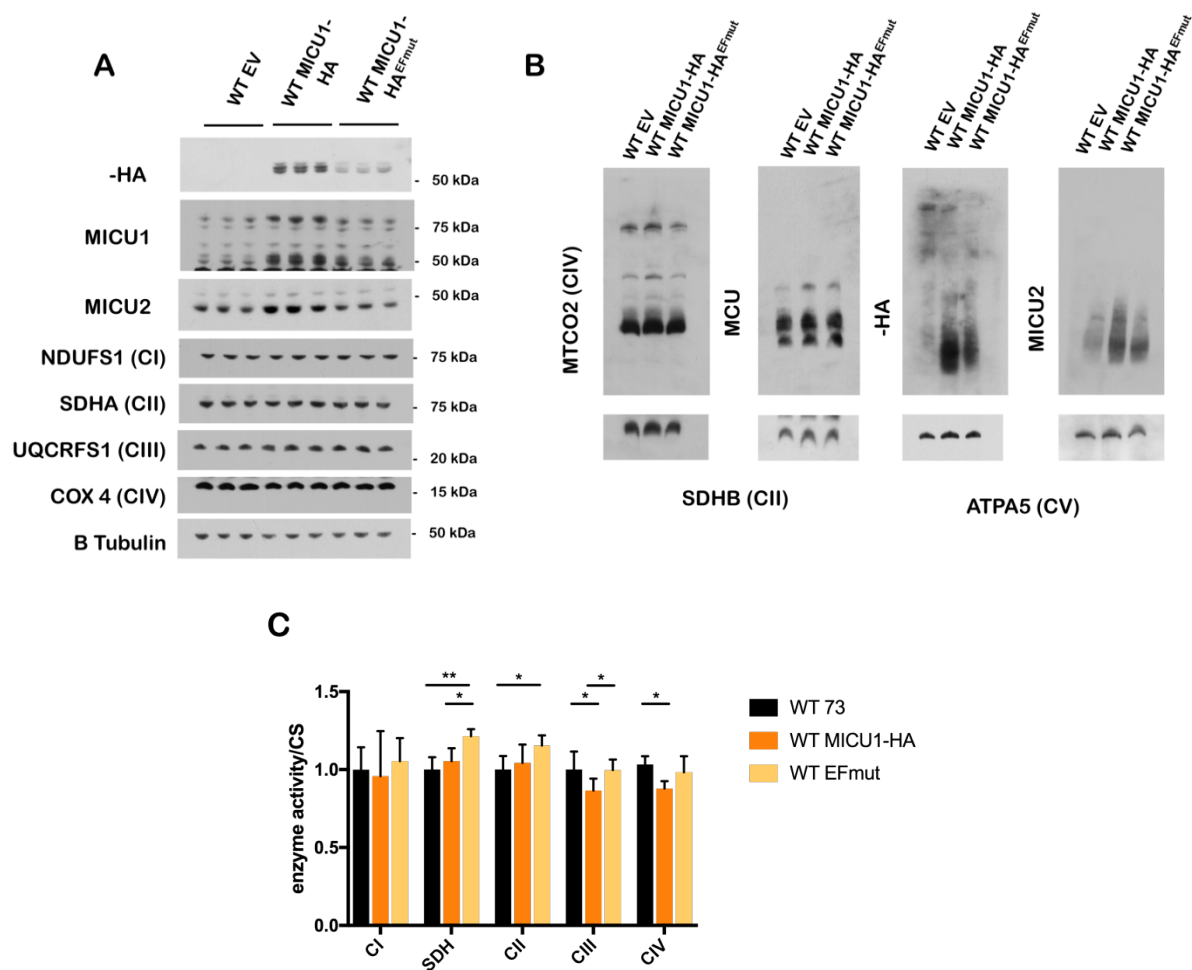


Figure 7.11: functionally active MICU1 overexpression did not affect CIV structure, but slightly reduced CIII and CIV activity. A) SDS-PAGE, Western blot, and immunodetection of total cell lysate from WT cybrids transduced with either the pWPXLd-ires-Puro^R empty vector (EV), or the same expression vector containing the coding sequences for MICU1-HA or MICU1^{EFmut}-HA. β -Tubulin was used as loading control. B) BN-PAGE, Western blot, and immunodetection of the same cells used in (A). C) MRC enzymes activities (mUnits/g of protein) determined by spectrophotometric kinetic measurements in the same cells in (A). Results were normalised to citrate synthase (CS) activity and expressed as mean \pm SD ($n = 6$ biological replicates). Two-way Anova test was used (* $P < 0.05$; ** $P < 0.01$; *** $P < 0.001$).

In conclusion, we observed a specific effect on CIV activity when MICU1 expression is altered, while MICU2 downregulation showed an opposite and not CIV-specific impact on the ETC. This effect appears to be linked to the functional role of these subunits and their ability to bind calcium, but further experiments should be conducted to better understand this behaviour.

7.4 Study of the effects of MCU activity on OXPHOS

Our experiments in cells in which MCU is downregulated, and therefore preventing both MCU activity and any possible physical interaction with CIV, showed no specific respiratory functional phenotype. However, when silencing or overexpressing MICU1, but not the inactive form MICU1^{EFmut}, we found a moderate but consistent defect in CIV activity. We then decided to study if in the presence of the fully assembled MCUC, the modulation of Ca²⁺ concentration in the mitochondrial matrix would have an impact on CIV activity and/or mitochondrial respiration. We did this by inhibiting MCU activity by treating the cells with 10 μ M Ru360, leading to decreased mitochondrial Ca²⁺ entrance (Kirichok et al., 2004). On the other hand, we induced an accumulation of mitochondrial calcium by treating the cells with 20 μ M CGP37157, a Na⁺/Ca²⁺ exchanger inhibitor (Baron and Thayer, 1997).

We first analysed the effects of Ru360 and CGP37157 chronic treatments (24 hours) on OXPHOS subunits steady-state levels, CIV stability and SC formation (Figure 7.12). No differences in protein levels of different MRC complexes analysed by WB, neither in CIV stability and SC formation by 1D BN-PAGE, were observed, suggesting that modulation of mitochondrial calcium does not alter CIV or the ETC from a structural point of view.

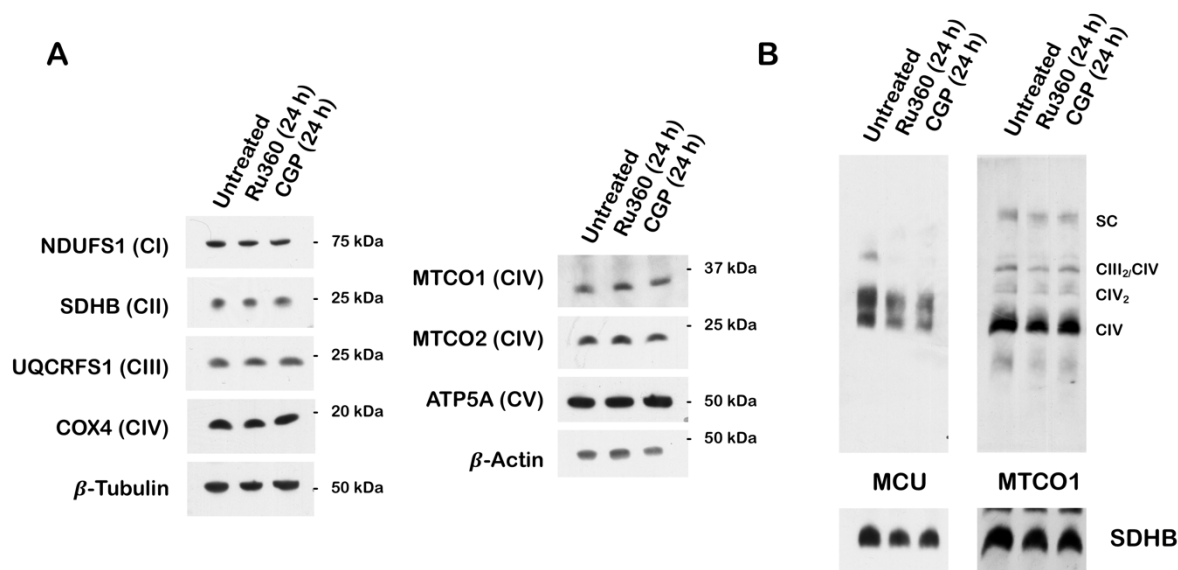


Figure 7.12: 24 hr treatment of WT cells with Ru360 or CGP does not affect CIV subunits steady-state levels or complex assembly. A) SDS-PAGE, Western Blot, and immunodetection of total lysates

from WT cells treated for 24 hours with 10 μM Ru360 (MCU inhibitor) or 20 μM CGP37157 (NCLX inhibitor). Antibodies against subunits of all the MRC complexes have been included. β -Tubulin and β -Actin were used as loading controls. B) BN-PAGE, Western blot, and immunodetection of samples from the same cells as in (A) solubilised in 1% digitonin. SDHB was used as loading control.

Next, we examined a possible effect of these treatments on CIV activity and OXPHOS regulation. To address this question, we analysed the effects of both a 24-hours treatment or an acute injection of Ru360 and CGP37157 on respiratory capacity, measuring oxygen consumption rate in permeabilised cells in a O2K high-resolution respirometer (Figure 7.13). In both acute and prolonged treatments, we did not observe any significant difference in oxygen consumption, apart from a slight decrease in CI-driven respiration after acute treatment with CGP. These data suggest that the uniporter activity and calcium depletion or accumulation in the matrix are not directly involved in the modulation of cellular respiration through CIV. Indeed, our results suggest that the MCUC-CIV interaction is probably linked to a structural role and that its function is not related to Ca^{2+} regulation.

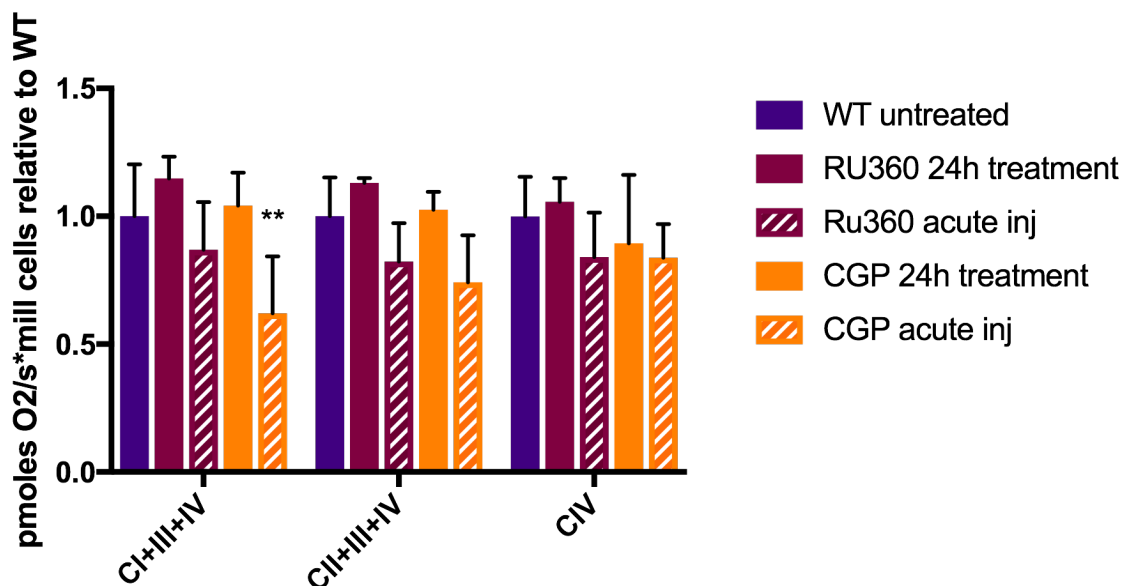


Figure 7.13: mitochondrial respiratory rates are not affected by Ru360 and CGP treatments. Oxygen consumption rates measured in permeabilised WT cybrids untreated, treated for 24 hours with 10 μM Ru360 (MCU inhibitor) or 20 μM CGP37157 (NCLX inhibitor), or after the acute injection of 10 μM Ru360 or 20 μM CGP37157 in the O2K high-resolution respirometer's chamber at the beginning of the measurement. CI+III+IV: difference between rate of oxygen consumption in the presence of glutamate and malate, and after rotenone inhibition of CI. CII+III+IV: difference between rate of oxygen consumption in the presence of succinate and glycerol-3-phosphate, and after antimycin A

inhibition of CIV. CIV: difference between rate of oxygen consumption in the presence of TMPD and ascorbate, and after CIV inhibition by KCN. Untreated: n=9; Ru360 acute injection: n=10; CGP acute injection: n=5; 24h treatments: n=3).

7.5 Analysis of the effects of MCUC-CIV interaction on the organisation of the IMM

In 2019, two interesting studies suggested an additional new role for MICU1 (Gottschalk et al., 2019; Tomar et al., 2019). According to Gottschalk's model, this MCUC subunit specifically localises at the cristae junctions (CJ) and is involved in the formation and maintenance of the cristae, leading to cristae widening when silenced. At the CJ, it has been proposed that MICU1 could recruit MCU and EMRE, normally found in the cristae, during calcium spikes. Supporting this model, Tomar's study showed that MICU1 interacts with components of the MICOS complex and proposed its involvement in the regulation of mitochondrial membrane dynamics and cristae organisation, independent of mitochondrial calcium uptake. The discovery of this additional function of MICU1 opened two further questions in the context of our study.

On one side, we questioned if the reduced CIV activity we observed after silencing of MICU1 was due only to a secondary effect of cristae disruption, and not to a direct role of MICU1 on the enzyme. To test this possibility, we analysed CIV assembly and activity in WT cells where MIC60, core subunit of the MICOS complex, was downregulated by siRNA treatment. MIC60 is responsible for cristae structure maintenance (Ott et al., 2015) and the loss of this subunit leads to strong defects in the IMM ultrastructure (John et al., 2005). Similarly to what is observed in cells downregulating MIC19 described in Section 5, while the silencing of MIC60 was efficient (Fig 7.14A), no defects in CIV and SC formation analysed by 2D BN-PAGE experiments (Fig 7.14B), nor in ETC complexes activity and cellular respiration (Figure 7.14C, D), were observed. These results support the hypothesis that MICU1 has a direct effect on CIV activity by specific interaction, rather than general disruption of IMM architecture.

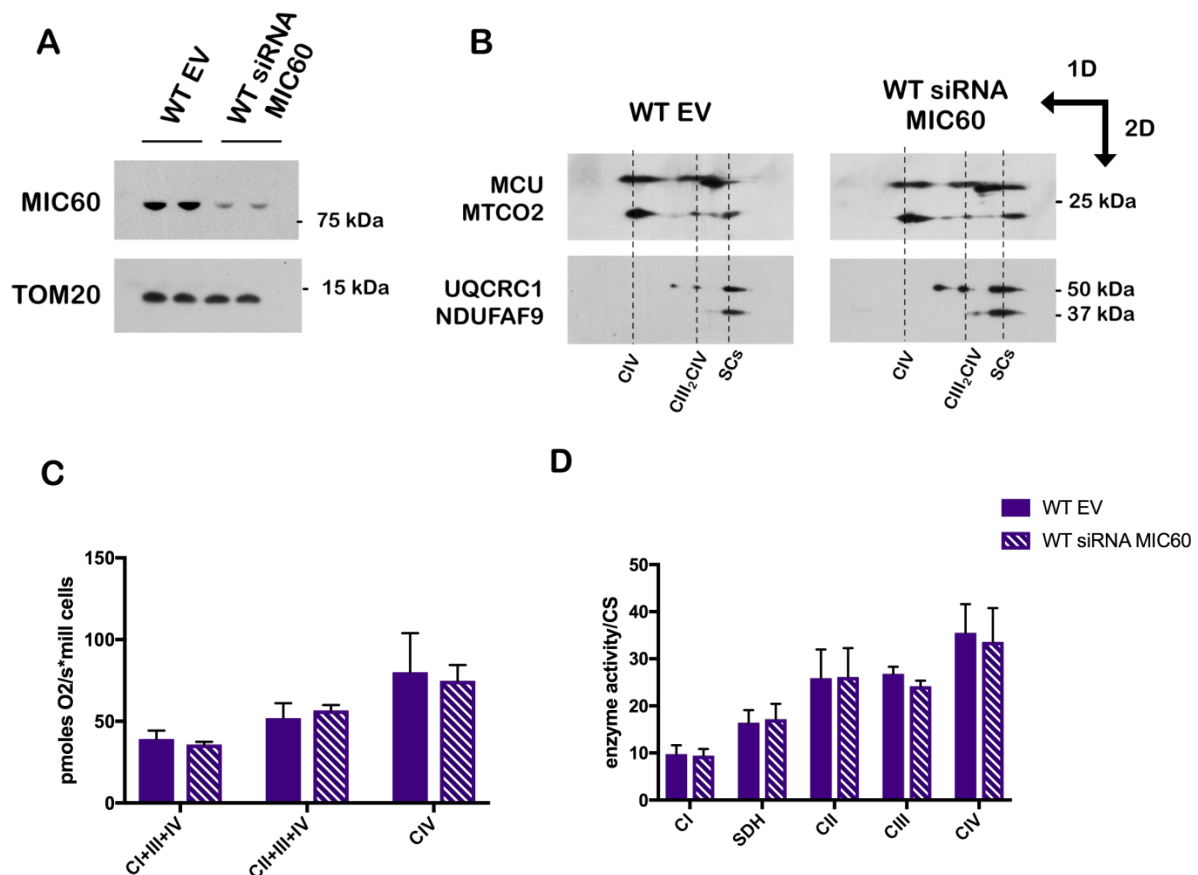


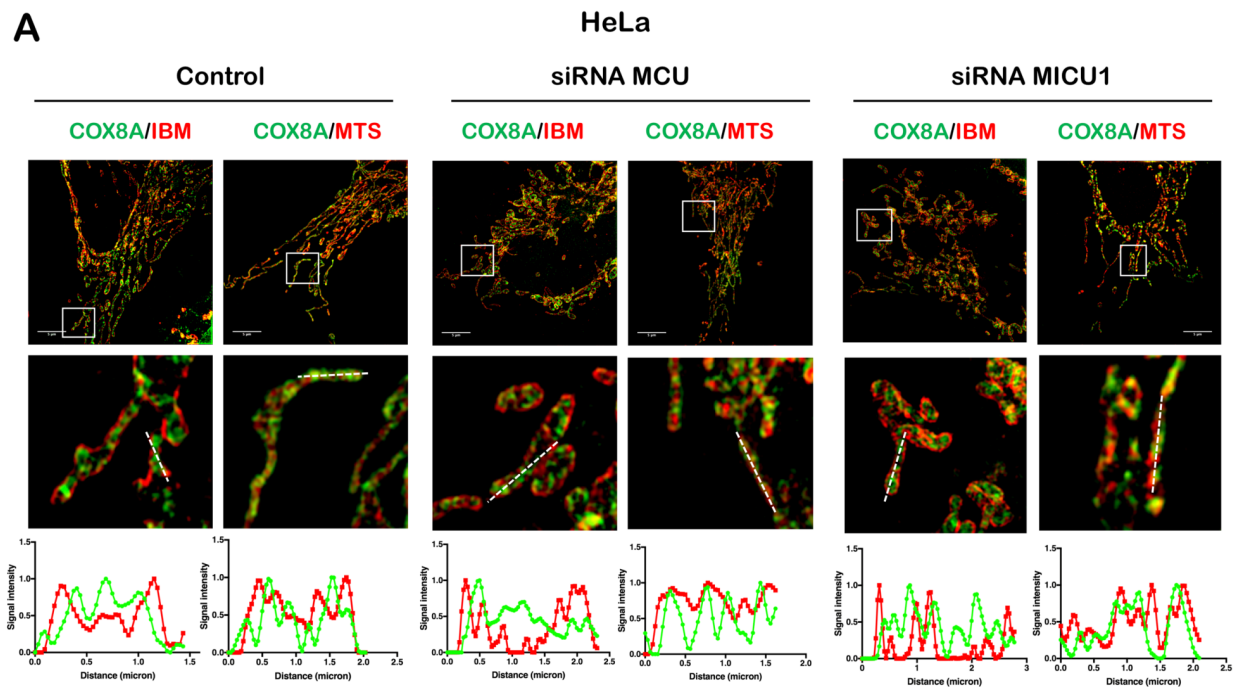
Figure 7.14: silencing of MIC60 does not lead to specific ETC enzymes deficiencies. A) SDS-PAGE, Western Blot, and immunodetection of total lysates from WT cells treated for 3 days with siRNA specific for MIC60 or the siRNA negative control (EV). TOM20 was used as loading control. B) 2D BN-PAGE, Western blot, and immunodetection of samples from the same cells as in (A) solubilised in 1% digitonin. C) Oxygen consumption rates measured in the same cells as in (A), permeabilised with 50 $\mu\text{g/ml}$ digitonin. CI+III+IV: difference between rate of oxygen consumption in the presence of glutamate and malate, and after inhibition of CI by rotenone. CII+III+IV: difference between rate of oxygen consumption in the presence of succinate and glycerol-3-phosphate, and after inhibition of CIII by antimycin A. CIV: difference between rate of oxygen consumption in the presence of TMPD and ascorbate, and after CIV inhibition by KCN. Results are expressed as mean \pm SD ($n=3$). D) Activities (mUnits/g of protein) of the respiratory chain enzymes measured on the same cells as in (A) by spectrophotometric kinetic measurements and normalised to citrate synthase (CS) activity. Results are expressed as mean \pm SD ($n=4$).

Then, we decided to test the second hypothesis and wondered if the interaction between CIV and the MCUC could have a role in the sub-mitochondrial localisation of these proteins in the IMM. To address this question, we decided to apply N-structured illuminated super-resolution microscopy (N-SIM) to identify the sub-mitochondrial distribution of COX8A (CIV) in the

absence of MCU or MICU1, and of MICU1 and MCU in CIV-deficient cells. MICU1, MCU, and COX8A were cloned with a green fluorescent protein (GFP) or a mCherry C-terminal tag and overexpressed in our cell models.

CIV localisation was studied in fixed HeLa cells (Figure 7.15A) and WT cybrids (Figure 7.15B) silenced for MCU and MICU1, or treated with control siRNA. For each condition, cells were co-transfected with COX8A-GFP, an inner boundary membrane (IBM) marker (IMM-mCherry-MITO7) or a matrix marker (pMTS-mScarlet-N1) to visualise the different sub-IMM compartments (Bindels et al., 2017; Olenych et al., 2007). Distributions were analysed measuring the cross-section intensity profiles of the two fluorophores in one representative mitochondrion and represented by plotting the peaks of both channels in one graph, as shown in Figure 7.15C.

In all the conditions tested, both in HeLa cells and in WT cybrids, COX8A-GFP co-localised with the matrix signal, while it appeared separated and externally surrounded by the IBM signal (Figure 7.15A, B). These experiments showed that fully assembled CIV exclusively localised in the cristae and that this distribution did not change when MCU and MICU1 expression was downregulated.



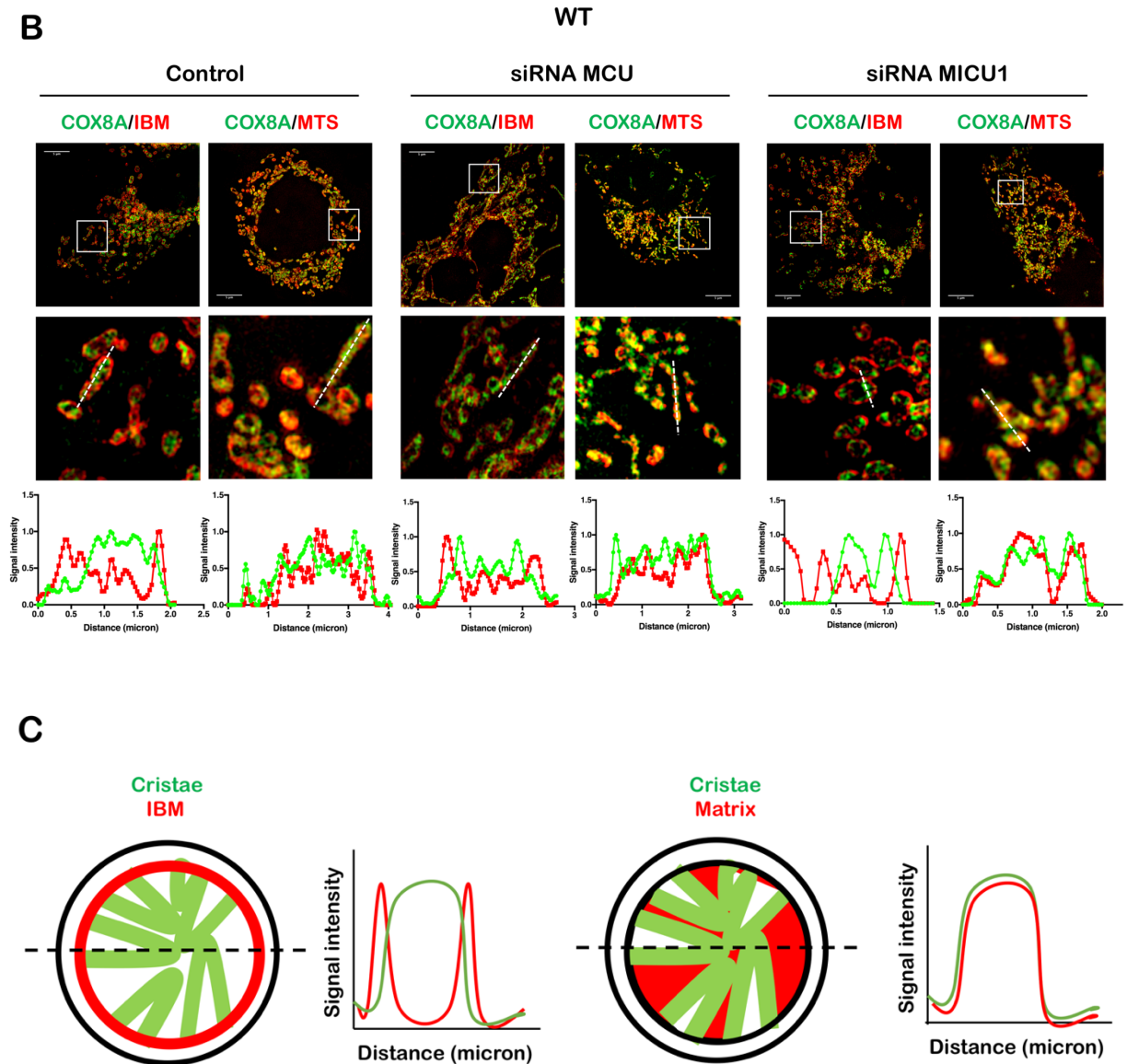
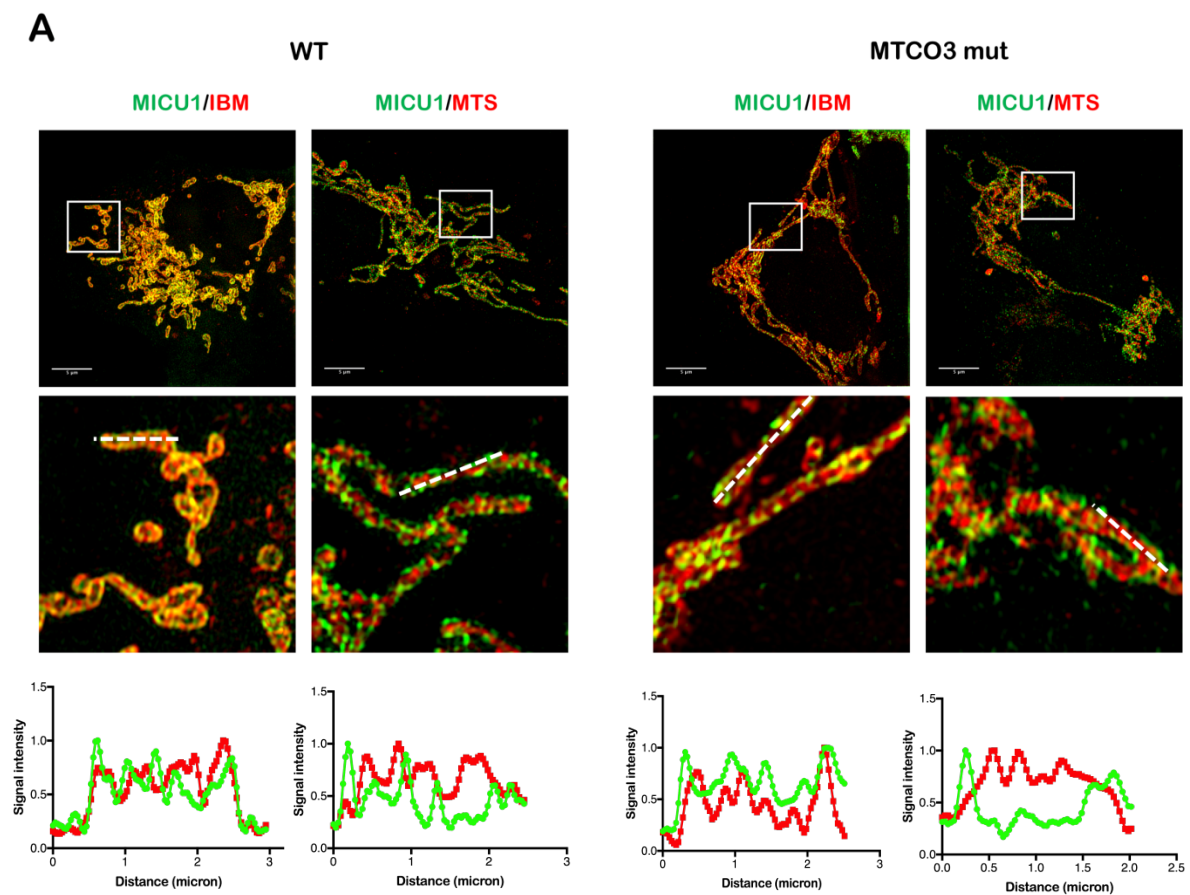


Figure 7.15: CIV localises in the cristae in control cells and in cells downregulating MCU and MICU1. Representative N-SIM images of HeLa cells (A) and WT cybrids (B) transfected with siRNAs targeting MCU or MICU1, or with siRNA Negative Control. Cells were transfected for 24 hours with plasmids transiently expressing COX8A-eGFP-N3 (CIV), pMTS-mScarlet-N1 (matrix marker), or IMM-mCherry-MITO7 (IBM marker). Panels at the bottom of each image show line plots of the two channels through mitochondria at locations indicated by the white dashed lines. At least 5 images were taken for each condition. Scale bars: 5 μ m. C) Graphic representation of expected line plots of CIV (green line) and the IBM or the matrix staining (red line) of regions marked with dashed lines.

As for CIV, we then studied MICU1 (Figure 7.16) and MCU (Figure 7.17) sub-mitochondrial localisation by co-transfecting cells with MICU1 or MCU-GFP, an IBM marker (IMM-mCherry-MITO7) or a matrix marker (pMTS-mScarlet-N1). To investigate the role of CIV in

MCUC components localisation, we compared our two CIV-deficient models (MTCO3 and MTCO1 mutants) to their respective WT cybrids. As reported in Gottschalk et al., 2019, in WT cells, MICU1 accumulated at the IBM (Figure 7.16), while MCU was distributed throughout the entire IMM (Figure 7.17). MICU1 localisation did not change in the MTCO3 and MTCO1 mutant cybrids, characterised by a still clear co-localisation pattern with the IBM marker and not with the matrix marker, representing the cristae, indicating that its distribution is independent of the physical presence or any direct interaction with CIV.



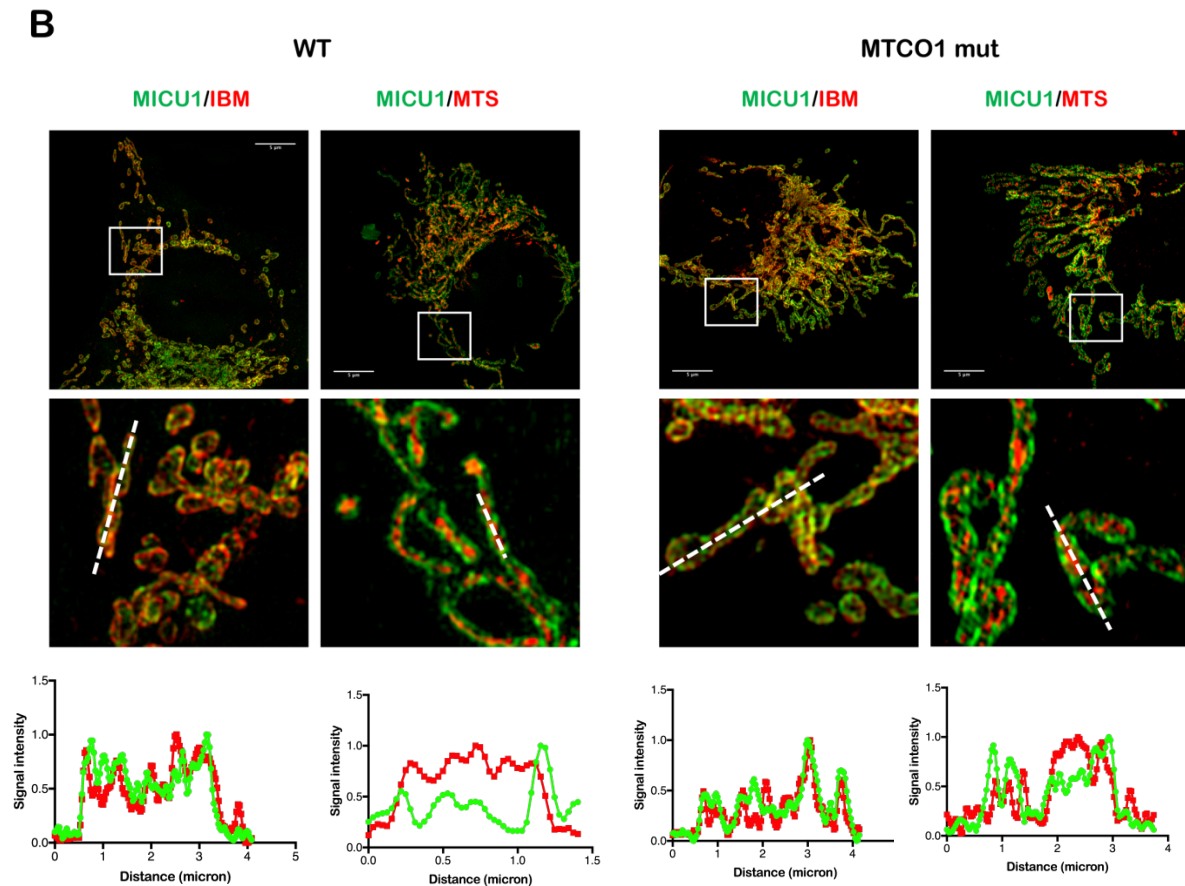
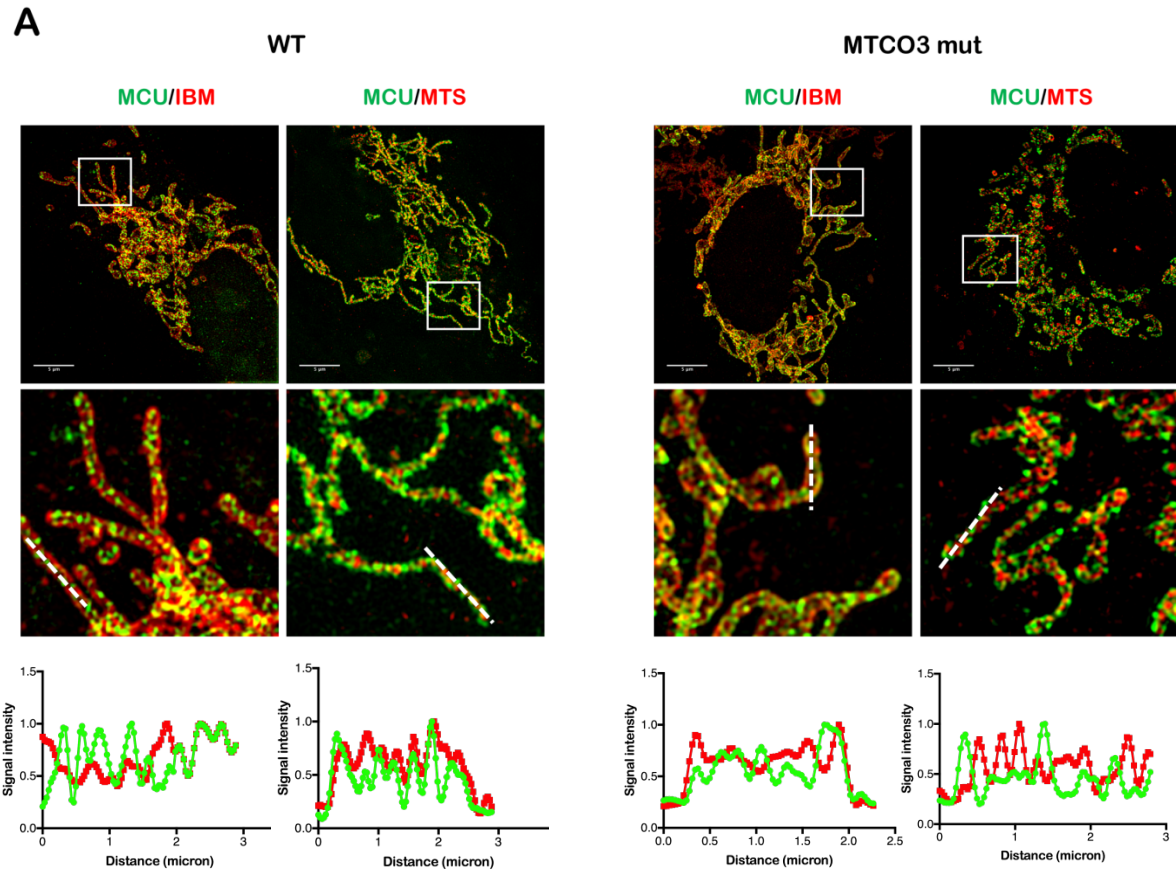


Figure 7.16: MICU1 localises at the IBM in both WT and CIV deficient cells. Representative N-SIM images of MTCO3 (A) and MTCO1 (B) mutant cybrids compared to the respective WT cybrids. Cells were transfected for 24 hours with plasmids transiently expressing MICU1-eGFP-N3, pMTS-mScarlet-N1 or IMM-mCherry-MITO7. Panels at the bottom of each image show line plots of the two channels through mitochondria at locations indicated by the white dashed lines. At least 5 images were taken for each condition. Scale bars: 5 μ m.

However, MCU sub-mitochondrial localisation was impacted in the cells lacking CIV. Indeed, N-SIM images analysis showed that MCU signals appeared distributed less in the cristae but instead accumulated more into the IBM, characterised by decreased co-localisation with the matrix marker and increased association with the IBM marker in MTCO3 and MTCO1 mutant cells (Figure 7.17). To further verify this observation, we co-expressed MICU1-GFP and MCU-mCherry in WT and MTCO1 mutant cells (Figure 7.18), where we observed a similar behaviour. Indeed, in accordance with the published data, MICU1 and MCU did not co-localise in WT cells, where MICU1 accumulated at the IBM whereas MCU was distributed along the cristae. However, in both mutant lines, we observed a decrease of MCU distribution at cristae

and an increased co-localisation with MICU1 at the IBM. These experiments suggest a rearrangement in MCU distribution, from CM to IBM, when CIV is absent.



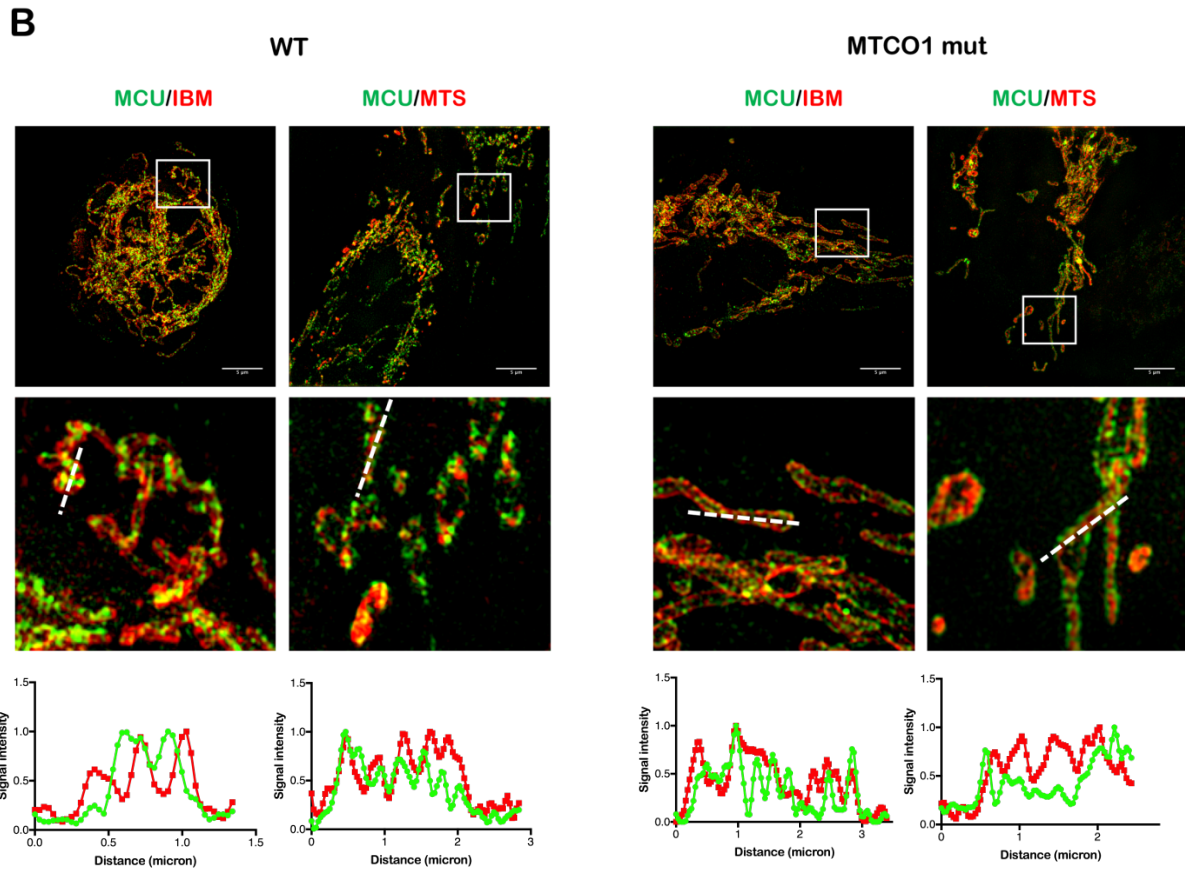


Figure 7.17: MCU localises in the cristae in WT cells, but accumulates more at the IBM in CIV deficient cells. Representative N-SIM images of MTCO3 (A) and MTCO1 (B) mutant cybrids compared to the respective WT cybrids. Cells were transfected for 24 hours with plasmids transiently expressing MCU-eGFP-N3, pMTS-mScarlet-N1 or IMM-mCherry-MITO7. Panels at the bottom of each image show line plots of the two channels through mitochondria at locations indicated by the white dashed lines. At least 5 images were taken for each condition. Scale bars: 5 μ m.

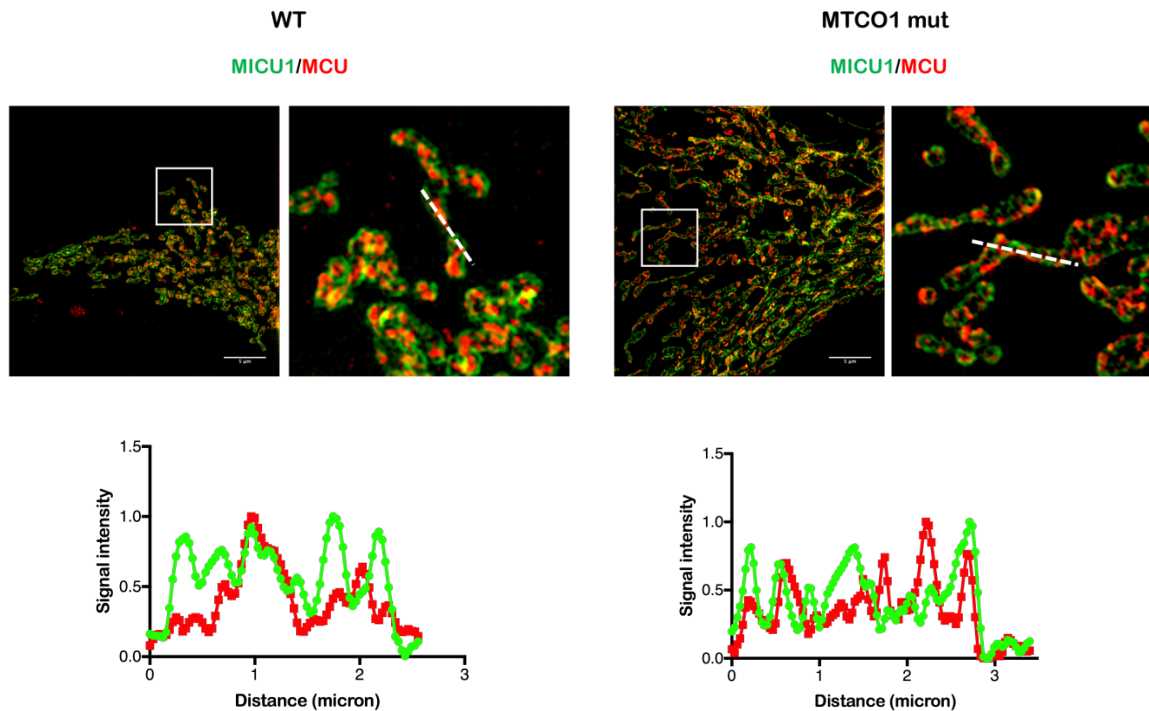


Figure 7.18: MCU localises with MICU1 at the IBM in CIV deficient cells. Representative N-SIM images of MTCO1 mutant cybrids compared to the respective WT cybrids. Cells were transfected for 24 hours with plasmids transiently expressing MICU1-eGFP-N3 and MCU-mCherry. Panels at the bottom of each image show line plots of the two channels through mitochondria at locations indicated by the white dashed lines. At least 5 images were taken for each condition. Scale bars: 5 μ m.

7.6 Conclusions

- Components of CIV and MCUC were found physically interacting or in close proximity by SILAC/Pulldown, BioID, and BN-PAGE experiments.
- CIV assembly or stability were not affected in the absence of all the tested MCUC subunits, but silencing of MICU1 or MICU2 induced the loss of an uncharacterised high-molecular-weight CIV-containing SC.
- In the absence of CIV, MCU-containing SC were re-arranged. Indeed, the \sim 230 kDa species observed in BN-PAGE in WT cells, decreased in CIV-deficient cells. This phenotype was specific for CIV defects and was not observed in CI and CIII-deficient cells.

- No CIV activity defect occurred in cells where MCU expression was silenced or treated with the MCU inhibitor, Ru360. On the other side, downregulation of MICU1 provoked a specific reduction in CIV activity and cellular respiration, while MICU2 silencing led to a general increase in ETC activity.
- MICU1 overexpression induced a small but significant reduction in CIV activity, an effect not observed in cells overexpressing MICU1^{EFmut}, unable to bind Ca²⁺.
- MICU1 role on CIV activity modulation is still unclear, but it did not seem to be linked to MICU1 function in cristae remodelling.
- CIV localised in the mitochondrial cristae membrane and its distribution was not affected by the expression of MCU or MICU1.
- MICU1 localised at the IBM both in WT cells and in cells lacking CIV, while MCU localised in the cristae in WT cells and was found redistributed at the IBM in the absence of CIV.

Section 8: Discussion and future directions

As discussed in the previous chapters, the formation of high-molecular-weight associations containing OXPHOS machinery complexes has been largely documented. BN-PAGE and proteomics analyses have been especially helpful in the identification of the main SC species (III_2IV_1 , I_1III_2 and the respirasomes $\text{I}_1\text{III}_2\text{IV}_1$ and $\text{I}_1\text{III}_2\text{IV}_2$), but they also have highlighted the presence of unknown species containing ETC enzymes, whose function still has to be investigated. For this reason, it is possible that certain SC types can originate from the interaction between the canonical ETC complexes and other IMM proteins or complexes.

This project started based on the finding of a physical interaction between CIV and MCU, when MCU peptides were identified by mass spectrometry within those detected by CIV-specific immunocapture. This observation was then extended from the pore-forming subunit of the uniporter, to the rest of the MCUC by BioID analysis, a technique that allows the identification of proteins in close spatial proximity (<10 nm) with a protein of interest, in living cells. In this context, a stable physical interaction is not strictly necessary and even transient or labile connections can be detected. In this experiment, we observed the MCUC-CIV relationship from the opposite perspective compared to the SILAC/Pulldown, fusing the biotin ligase to MCUC components. The results showed CIV subunits as some of the highest hits in MICU1, MICU2, EMRE, and MCUR1 BioID experiments, suggesting that not only MCU itself, but the whole complex is able to associate with the ETC complex. More interestingly, the candidate interactors presenting with the highest scores were almost consistently COX15, COX5A and COX4, which are respectively an early-stage CIV assembly factor involved in the synthesis of heme *a* for MTCO1 (Antonicka et al., 2003), and the first two nuclear-encoded subunits involved in the modular assembly of the enzyme (Vidoni et al., 2017). Of note, no CIV subunit or interactor were found in the BioID performed for MCU and MCUB, since the BirA enzyme was fused to the C-terminus of both proteins, which reside in the mitochondrial matrix. While negative, these data reinforce the specificity of the BioID method and the MCU/MCUB results have been recently published by our collaborators elsewhere (Antonicka et al., 2020). This finding initially implied the involvement of the MCUC in CIV assembly, or in the maturation of the mtDNA-encoded MTCO1 subunit. However, further experiments in

cells downregulating MCUC subunits did not show specific alterations in CIV biogenesis, nor the accumulation of intermediates or degradation products, ruling out this hypothesis. Nevertheless, the inability to find valid tools to modulate COX15 expression, such as siRNAs and functional overexpression of a tagged version of the protein, and the ability to visualise it in immunoblotting experiments, reduced the possibilities to explore this aspect in more depth.

To further characterise the nature of the MCUC-CIV interaction, we examined the formation of MCU-containing complexes and supercomplexes by BN-PAGE. Previous studies on the uniporter described the formation of a variety of higher-order MCU-containing species, between ~440 kDa (expected to include only MCU and EMRE) and ~1100 kDa (supposedly including also the dimer MICU1/MICU2) (Ghosh et al., 2020; König et al., 2016). However, these assemblies have not been confirmed in follow-up studies and the exact composition of each supercomplex could not be determined. In our experiments, this pattern appears different, presenting lower-molecular-weight MCU signals, both in WB and in complexome profiling, in addition to the already described higher-molecular-weight complexes. This discrepancy could be explained by the fact that, compared to OXPHOS enzymes, the BN-PAGE pattern of MCU complexes is strongly influenced by the amount of digitonin or DDM used in the solubilisation and the type of samples analysed. In König et al., for example, the study of the MCU complex was conducted on mice tissues, using 6 g digitonin/g protein, while our data were collected from digitonised cells or extracted mitochondria solubilised in 1% or 4 g digitonin/g protein, and 1% or 1.6 g DDM/g protein, respectively. As a result, in our 1D and 2D BN-PAGE experiments, in addition to higher-molecular-weight associations, we detected MCU in a ~230 kDa band, where it co-migrates with what is known to be non-associated or 'monomeric' form of CIV. This specific band disappears in cybrids with severe CIV assembly impairments, and this alteration in MCU pattern seems to be specific for the absence of CIV, since the same experiment conducted on cells lacking CI or CIII did not reproduce this result. We could therefore conclude that the loss of MCU-CIV interaction causes a re-arrangement in the formation of MCU supercomplexes, supporting the hypothesis of a stable association between CIV and MCU.

The analysis of the formation of SC containing the other MCUC subunit, instead, was more challenging. Indeed, no valid antibodies recognising EMRE on BN-PAGE are available and most of the MCUC components are often not detected in complexome analysis by mass spectrometry. MICU1 and MICU2 signal in 1D and 2D BN-PAGE showed a strong

accumulation of these subunits in low-molecular-weight species (<230 kDa), and only partially co-migrate with MCU (and supposedly EMRE). This observation was confirmed for MICU1 in complexome profiles (data not shown), while MICU2 has never been detected. The association within MCU and MICU1 appears to be lost in cells lacking CIV, but these data need to be further validated. However, the downregulation of both these subunits affects the formation of novel specific and high-molecular-weight CIV-containing SC, which supports the idea of a direct or indirect connection between MICU1/MICU2 and the ETC enzyme. These bands were clearly found missing in BN-PAGE experiments, but we were not able to confirm their composition through complexome profiling. Therefore, more investigations are needed to identify the molecular component of these SC species.

Once confirmed the existence of an interaction between CIV and MCUC using different approaches, we decided to investigate the physiological role of this association. Our initial analysis of CIV structure by BN-PAGE and complexome profiling ruled out the possibility that the MCUC has a function in the assembly or the stability of the enzyme. We then hypothesised that MCUC might be involved in the regulation of CIV and mitochondrial respiration, possibly through the modulation of Ca^{2+} entry. Indeed, it has been proposed that Ca^{2+} can regulate CIV activity directly or through the activation of other signalling pathways (Bender and Kadenbach, 2000; Vygodina et al., 2013). The association between the enzyme and MCUC could lead to the formation of a CIV subpopulation that localises specifically at the ER-mitochondria contact sites, where the activity modulation would take place, thanks to the high Ca^{2+} concentrations reached.

To address this question, we first performed enzyme activity and oxygen consumption measurements on cells downregulating each subunit of MCUC, to evaluate the impact of the different components separately. Cells lacking MCU or EMRE did not show ETC defects, while the modulation of MICU1 and MICU2 had the opposite effect: MICU2 silencing induced a general upregulation of ETC complexes activity and cellular respiration, while loss of MICU1 led to a specific 30% decrease in CIV activity and respiration capacity. Similar to its downregulation, the overexpression of MICU1 resulted in a small, but still significant reduction in CIV activity, not observed in cells overexpressing the inactive form MICU1^{EFmut}. These results suggested that the mechanism laying behind the modulation of ETC enzymes activity in the absence of one of the MICUs proteins is probably unrelated to MICU1 and MICU2 action on matrix Ca^{2+} regulation. Indeed, according to Patron et al., 2014, both MICU1 or

MICU2 silencing and MICU1 overexpression lead to mitochondrial calcium accumulation, phenomenon that would not explain the different phenotypes we observed between cells downregulating MICU1 and MICU2.

These observations were further confirmed by the study of matrix Ca^{2+} role on cellular respiration and CIV activity, via both acute and chronic treatments with Ru360, MCU inhibitor (Kirichok et al., 2004), and CGP37157, $\text{Na}^+/\text{Ca}^{2+}$ exchanger inhibitor (Baron and Thayer, 1997). The pharmacological inhibition of the uniporter is expected to reduce, even if not completely abolish, the import of Ca^{2+} in the matrix, despite leaving the MCU-CIV interaction still feasible. The block of Ca^{2+} export, on the other side, leads to matrix Ca^{2+} accumulation. However, no specific defect in CIV-linked respiration was detected in either these conditions, implying that the amount of Ca^{2+} in the matrix is not relevant for CIV activity modulation.

Nevertheless, Konstantinov's group's work (Vygodina et al., 2013; Vygodina et al., 2017) about Ca^{2+} -mediated CIV inhibition, proposed the existence of a cation binding site located on the IMS side of MTCO1, instead of the matrix, which would bind Ca^{2+} only at high concentrations. If this is true, MCU binding with CIV could be necessary to anchor the enzyme at the ER-mitochondria contact sites, where the necessary concentration of Ca^{2+} is reached independently from MCU transport activity. This hypothesis, however, was challenged by the fact that MCU silencing, which leads to both a reduction in matrix Ca^{2+} and loss of MCU-CIV interaction, did not seem to affect CIV and the ETC machinery activity. However, we cannot exclude that our knockdown model for MCU still expresses enough protein to maintain minimal interaction with the ETC enzyme and/or calcium import, enough to abolish any possible phenotype. A complete MCU knockout would need to be generated to confirm that the residual MCU is not enough to perform its CIV-related function.

Our results, therefore, suggest that the two MCUC roles, the established Ca^{2+} transporter function and the still unclear purpose linked to its association with CIV, do not overlap. However, this would not be the first time that MCUC components are found involved in parallel Ca^{2+} import-unrelated activities.

In 2019 two publications proposed a new role for MICU1: an involvement in the remodelling of cristae, resulting from direct interaction with components of the MICOS complex (Gottschalk et al., 2019; Tomar et al., 2019). Gottschalk and colleagues investigated the spatial

dynamics of the MCUC, finding that in resting conditions MICU1 localises to the IBM, while MCU and EMRE concentrate in the cristae. The uniporter is then transiently relocated in a MICU1-dependent manner to the non-cristae domain of the IMM during calcium spikes. Moreover, this study discovered that MICU1 contributes to cristae integrity and that its knockdown leads to mitochondrial fragmentation, and widening of the cristae junctions, with a phenotype that mimics OPA1 deficient cells. Similarly, Tomar's work indicated that while MICU1 can be found also co-localising with MCU, it distributes independently to sub-mitochondrial regions lacking MCU, and that it participates in cristae organisation, interacting with MIC60 and CHCHD2. The existence of a proportion of MICU1 not in a complex with MCU and EMRE, moreover, is supported by our 1D and 2D BN-PAGE data, which show both MICU1 and MICU2 accumulating in low-molecular-weight complexes that do not co-migrate with the MCU signal. It is therefore easy to speculate that most of MICU1 (and therefore MICU2) associates with the uniporter only in particular conditions, such as during calcium stimuli.

These new findings opened two important questions in the context of our research. Firstly, we wondered if the defect in CIV activity observed in MICU1 KD models was the result of a direct effect of the protein on CIV, or an indirect effect due to the cristae alteration. To rule out the second possibility, we repeated the structural and functional analysis of the OXPHOS machinery in WT hybrids transiently downregulating MIC60, since it is well established that loss of MIC60 results in drastically altered mitochondrial membrane ultrastructure (John et al., 2005) and has been shown to interact with MICU1 to control cristae organisation (Tomar et al., 2019). Previous analyses of ETC organisation and activity in yeast and human cell models silenced for MIC60 showed a moderate reduction in general respiratory capacity (Van Laar et al., 2016) or even no respiration defect (John et al., 2005), and never highlighted a specific defect in CIV. Our data showed no difference in oxygen consumption, enzyme activity, and CIV assembly or formation of supercomplexes in MIC60 KD cells compared to controls. Taken together with the data presented in Section 5, where no specific CIV defect was observed in cells stably downregulating MIC19, another component of the MICOS complex involved in cristae remodelling (Ott et al., 2015), we concluded that MICU1 effect on CIV is not related to alteration in the IMM organisation. However, the mechanism behind this phenotype is still unclear and we hypothesised that it might be linked to the spatial distribution of IMM complexes.

Indeed, we wondered if the interactions between CIV, MCU, and MICU1 might play a part in the sub-localisation of one or more of these proteins in the IMM. To evaluate this aspect, we generated MCU, MICU1 and CIV subunit COX8A fused with fluorescent proteins (GFP and mCherry), and analysed their spatial distribution in the membrane with a structured illumination super resolution microscopy (N-SIM). As expected, fully assembled CIV was confined to the mitochondrial cristae in control cells and its sub-localisation did not change when MCU or MICU1 expression levels were reduced by siRNAs. Similarly, we found MICU1 in the IBM of both WT and CIV deficient cells, confirming the data previously published and excluding a possible role for CIV in MICU1 spatial organisation.

MCU, however, was found in the cristae in control conditions and appeared to redistribute to the IBM in the absence of CIV. This behaviour suggested a possible CIV action in anchoring MCU to the cristae membrane in resting conditions, while this association would possibly be lost during calcium spikes, when MCU re-locates with MICU1. These results could explain the redistribution of MCU SC found in BN-PAGE analyses and open a new series of questions, which will be addressed in our future work. Beforehand, we want to validate these results analysing MCU localisation in CI- and CIII-deficient cells, in order to verify if this behaviour is specific for the absence of CIV or is due to OXPHOS impairments, possibly through secondary effects such as membrane potential decrease. The accumulation of protons in the cristae due to the activity of the respiration chain, indeed has been proven to be essential for MICU1 distribution (Gottschalk et al., 2019). Since MICU1 does not re-distribute in the cristae membrane in the CIV-deficient models analysed, we assume that these cells do not present a severe membrane potential loss, but it is possible that moderate changes are able to affect MCU IMM distribution without reaching the necessary threshold to re-locate MICU1.

We also plan to evaluate if MCU re-location in the absence of CIV is dependent on MICU1 and on its ability to bind Ca^{2+} . Firstly, we will repeat the sub-localisation experiment in WT and CIV-lacking cells after the siRNA-mediated silencing of MICU1. If MCU re-localisation in CIV-deficient cells appears influenced by MICU1 expression, we will investigate if the role of MICU1 is linked to its physical presence or to its calcium-binding function, re-expressing in siRNA-treated cells MICU1 or MICU1^{EFmut}. These results will hopefully give us a deeper understanding of how the axis CIV-MCU-MICU1 and Ca^{2+} affect the distribution of the calcium uniporter machinery in the IMM.

Future work will aim to integrate these observations with the study of another fundamental variable: Ca^{2+} . Indeed, Ca^{2+} was shown to be involved in the re-localisation of MCU, but it is not known yet if and how it affects CIV and its association with the MCUC. One possibility is that Ca^{2+} stimuli induce MCU detachment from CIV, in order to be recruited by MICU1 at the IBM, in a still unknown way. This mechanism could act as a modulator of Ca^{2+} entry in the matrix, keeping MCU and MICU1 separated in resting conditions. We are therefore planning to move our investigation in live cells and analyse by super resolution microscopy MCU localisation under resting conditions and in the presence of Ca^{2+} stimuli, in control cells and in cells not expressing CIV or MICU1. If this mechanism is real, the lack of CIV should translate in a less controlled MCU-MICU1 interaction and in a consequent rise in Ca^{2+} import. For this reason, mitochondrial Ca^{2+} content will be measured in cells carrying mutations in CIV, and compared with WT and CI- and CIII-deficient cells. On the other side, Ca^{2+} could affect CIV distribution as well, recruiting the complex CIV-MCU to the IBM. The live cell analysis of CIV distribution before and after Ca^{2+} stimuli will address this hypothesis.

The results collected so far in this project showed an unexpected interaction between the OXPHOS enzyme CIV and the mitochondrial Ca^{2+} import machinery MCUC. At the beginning of this study, we expected to find a correlation between Ca^{2+} regulation and CIV activity, but our results seem to rule out this hypothesis. Instead, our observations appear to point to a role of CIV in the localisation of MCU and possibly in the regulation of Ca^{2+} entry. Further analyses will be needed to verify this hypothesis.

Bibliography

Abrahams, J.P., Leslie, A.G., Lutter, R., and Walker, J.E. (1994). Structure at 2.8 Å resolution of F₁-ATPase from bovine heart mitochondria. *Nature* 370, 621-628.

Abu-Amero, K.K., Bosley, T.M. (2006). Mitochondrial abnormalities in patients with LHON-like optic neuropathies. *Invest. Ophthalmol. Vis. Sci.* 47, 4211-4220.

Abu-Libdeh, B., Douiev, L., Amro, S., Shahrour, M., Ta-Shma, A., Miller, C., Elpeleg, O., Saada, A. (2017). Mutation in the COX4I1 gene is associated with short stature, poor weight gain and increased chromosomal breaks, simulating Fanconi anemia. *Europ. J. Hum. Genet.* 25: 1142-1146.

Acin-Perez, R., and Enriquez, J.A. (2014). The function of the respiratory supercomplexes: the plasticity model. *Biochimica et biophysica acta* 1837, 444-450.

Acin-Perez, R., Bayona-Bafaluy, M.P., Fernandez-Silva, P., Moreno-Loshuertos, R., Perez-Martos, A., Bruno, C., Moraes, C.T., and Enriquez, J.A. (2004). Respiratory complex III is required to maintain complex I in mammalian mitochondria. *Molecular cell* 13, 805-815.

Acin-Perez, R., Fernandez-Silva, P., Peleato, M.L., Perez-Martos, A., and Enriquez, J.A. (2008). Respiratory active mitochondrial supercomplexes. *Molecular cell* 32, 529-539.

Ackerman, S.H., and Tzagoloff, A. (1990). Identification of two nuclear genes (ATP11, ATP12) required for assembly of the yeast F₁-ATPase. *Proceedings of the National Academy of Sciences of the United States of America* 87, 4986-4990.

Adeva-Andany, M.M., Carneiro-Freire, N., Seco-Filgueira, M., Fernández-Fernández, C., and Mouriño-Bayolo, D. (2019). Mitochondrial β -oxidation of saturated fatty acids in humans. *Mitochondrion* 46, 73-90.

Adjobo-Hermans, M.J.W., de Haas, R., Willems, P., Wojtala, A., van Emst-de Vries, S.E., Wagenaars, J.A., van den Brand, M., Rodenburg, R.J., Smeitink, J.A.M., Nijtmans, L.G., et al. (2020). NDUFS4 deletion triggers loss of NDUFA12 in *Ndufs4*(^{-/-}) mice and Leigh syndrome patients: A stabilizing role for NDUFAF2. *Biochimica et biophysica acta. Bioenergetics* 1861, 148213.

Agip, A.A., Blaza, J.N., Bridges, H.R., Viscomi, C., Rawson, S., Muench, S.P., and Hirst, J. (2018). Cryo-EM structures of complex I from mouse heart mitochondria in two biochemically defined states. *Nature structural & molecular biology* 25, 548-556.

Aich, A., Wang, C., Chowdhury, A., Ronsör, C., Pacheu-Grau, D., Richter-Dennerlein, R., Dennerlein, S., Rehling, P. (2018). COX16 promotes COX2 metallation and assembly during respiratory complex IV biogenesis. *Elife* 7.

Ajioka, R.S., Phillips, J.D., and Kushner, J.P. (2006). Biosynthesis of heme in mammals. *Biochimica et biophysica acta* 1763, 723-736.

Alberts, B., Johnson, A., Lewis, J., Raff, M., Roberts, K., and Walter, P. (2002). *Molecular Biology of the Cell*, 4th edition (New York: Garland Science).

Alston, C.L., Compton, A.G., Formosa, L.E., Strecker, V., Oláhová, M., Haack, T.B., Smet, J., Stouffs, K., Diakumis, P., Ciara, E., et al. (2016). Biallelic Mutations in TMEM126B Cause Severe Complex I Deficiency with a Variable Clinical Phenotype. *American journal of human genetics* 99, 217-227.

Alston, C.L., Davison, J. E., Meloni, F., van der Westhuizen, F. H., He, L., Hornig-Do, H.-T., Peet, A. C., Gissen, P., Goffrini, P., Ferrero, I., Wassmer, E., McFarland, R., Taylor, R. W. (2012). Recessive germline SDHA and SDHB mutations causing leukodystrophy and isolated mitochondrial complex II deficiency. *J. Med. Genet.* 49, 569-577.

Alston, C. L., Heidler, J., Dibley, M. G., Kremer, L. S., Taylor, L. S., Fratter, C., French, C. E., Glasgow, R. I. C., Feichtinger, R. G., Delon, I., Pagnamenta, A. T., Dolling, H., and 19 others. (2008) Bi-allelic mutations in NDUFA6 establish its role in early-onset isolated mitochondrial complex I deficiency. *Am. J. Hum. Genet.* 103: 592-601.

Alston, C. L., Veling, M. T., Heidler, J., Taylor, L. S., Alaimo, J. T., Sung, A. Y., He, L., Hopton, S., Broomfield, A., Pavaine, J., Diaz, J., Leon, E., Wolf, P., McFarland, R., Prokisch, H., Wortmann, S. B., Bonnen, P. E., Wittig, I., Pagliarini, D. J., Taylor, R. W. (2020). Pathogenic bi-allelic mutations in NDUFAF8 cause Leigh syndrome with an isolated complex I deficiency. *Am. J. Hum. Genet.* 106: 92-101.

An, J., Shi, J., He, Q., Lui, K., Liu, Y., Huang, Y., and Sheikh, M.S. (2012). CHCM1/CHCHD6, novel mitochondrial protein linked to regulation of mitofilin and mitochondrial cristae morphology. *The Journal of biological chemistry* 287, 7411-7426.

Andreu, A.L., Checcarelli, N., Iwata, S., Shanske, S., DiMauro, S. (2000). A missense mutation in the mitochondrial cytochrome b gene in a revisited case with histiocytoid cardiomyopathy. *Pediat. Res.* 48, 311-314.

Andreu, A.L., Hanna, M.G., Reichmann, H., Bruno, C., Penn, A.S., Tanji, K., Pallotti, F., Iwata, S., Bonilla, E., Lach, B., et al. (1999). Exercise intolerance due to mutations in the cytochrome b gene of mitochondrial DNA. *The New England journal of medicine* 341, 1037-1044.

Andrews, B., Carroll, J., Ding, S., Fearnley, I.M., and Walker, J.E. (2013). Assembly factors for the membrane arm of human complex I. *Proceedings of the National Academy of Sciences of the United States of America* 110, 18934-18939.

Angebault, C., Charif, M., Guegen, N., Piro-Megy, C., Mousson de Camaret, B., Procaccio, V., Guichet, P.-O., Hebrard, M., Manes, G., Leboucq, N., Rivier, F., Hamel, C. P., Lenaers, G., Roubertie, A. (2015) Mutation in NDUFA13/GRIM19 leads to early onset hypotonia, dyskinesia and sensorial deficiencies, and mitochondrial complex I instability. *Hum. Molec. Genet.* 24: 3948-3955.

Antonicka, H., Leary, S.C., Guercin, G.H., Agar, J.N., Horvath, R., Kennaway, N.G., Harding, C.O., Jaksch, M., Shoubridge, E.A. (2003a). Mutations in COX10 result in a defect in mitochondrial heme A biosynthesis and account for multiple, early-onset clinical phenotypes associated with isolated COX deficiency. *Human molecular genetics* 12, 2693-2702.

Antonicka, H., Lin, Z.Y., Janer, A., Aaltonen, M.J., Weraarpachai, W., Gingras, A.C., and Shoubridge, E.A. (2020). A High-Density Human Mitochondrial Proximity Interaction Network. *Cell metabolism* 32, 479-497.e479.

Antonicka, H., Mattman, A., Carlson, C.G., Glerum, D.M., Hoffbuhr, K.C., Leary, S.C., Kennaway, N.G., Shoubridge, E.A. (2003b). Mutations in COX15 produce a defect in the mitochondrial heme biosynthetic pathway, causing early-onset fatal hypertrophic cardiomyopathy. *Am J Hum Genet.* 72, 101-114.

Antony, A.N., Paillard, M., Moffat, C., Juskeviciute, E., Correnti, J., Bolon, B., Rubin, E., Csordas, G., Seifert, E.L., Hoek, J.B., et al. (2016). MICU1 regulation of mitochondrial Ca²⁺ uptake dictates survival and tissue regeneration. *Nature communications* 7, 10955.

Arnold, I., Folsch, H., Neupert, W., Stuart, R.A. (1998). Two distinct and independent mitochondrial targeting signals function in the sorting of an inner membrane protein, cytochrome c1. *J. Biol. Chem.*, 273, 1469-1476.

Astuti, D., Latif, F., Dallol, A., Dahia, P.L., Douglas, F., George, E., Sköldbberg, F., Husebye, E.S., Eng, C., Maher, E.R. (2001). Gene mutations in the succinate dehydrogenase subunit SDHB cause susceptibility to familial pheochromocytoma and to familial paraganglioma. *Am J Hum Genet* 69:49-54.

Atkinson, A., Khalimonchuk, O., Smith, P., Sabic, H., Eide, D., Winge, D.R. (2010). Mzm1 influences a labile pool of mitochondrial zinc important for respiratory function. *J Biol Chem.* 285, 19450-19459.

Atkinson, A., Smith, P., Fox, J.L., Cui, T.Z., Khalimonchuk, O., and Winge, D.R. (2011). The LYR protein Mzm1 functions in the insertion of the Rieske Fe/S protein in yeast mitochondria. *Mol Cell Biol* 31, 3988-3996.

Baertling, F., Al-Murshedi, F., Sanchez-Caballero, L., Al-Senaidi, K., Joshi, N. P., Venselaar, H., van den Brand, M. A. M., Nijtmans, L. G. J., Rodenburg, R. J. T. (2017). Mutation in mitochondrial complex IV subunit COX5A causes pulmonary arterial hypertension, lactic acidemia, and failure to thrive. *Hum. Mutat.* 38: 692-703.

Baertling, F., van den Brand, M., Hertecant, J.L., Al-Shamsi, A.P., van den Heuvel, L., Distelmaier, F., Mayatepek, E., Smeitink, J.A., Nijtmans, L.G., Rodenburg, R.J. (2015). Mutations in COA6 cause cytochrome c oxidase deficiency and neonatal hypertrophic cardiomyopathy. *Human mutation* 36, 34-38.

Bajzikova, M., Kovarova, J., Coelho, A.R., Boukalova, S., Oh, S., Rohlenova, K., Svec, D., Hubackova, S., Endaya, B., Judasova, K., et al. (2019). Reactivation of Dihydroorotate Dehydrogenase-Driven Pyrimidine Biosynthesis Restores Tumor Growth of Respiration-Deficient Cancer Cells. *Cell metabolism* 29, 399-416.e310.

Baker, R.A., Priestley, J.R.C., Wilstermann, A.M., Reese, K.J., and Mark, P.R. (2019). Clinical spectrum of BCS1L Mitopathies and their underlying structural relationships. *American journal of medical genetics. Part A* 179, 373-380.

Balcavage, W., Lloyd, J.L., Mattoon, J.R., Ohnishi, T., Scarpa, A. (1973). Cation movements and respiratory response in yeast mitochondria treated with high Ca^{2+} concentrations. *Biochimica et biophysica acta* 305, 41-51.

Balsa E, M.R., Perales-Clemente, E., Szklarczyk, R., Calvo, E., Landázuri, M.O., Enríquez, J.A. (2012). NDUFA4 is a subunit of complex IV of the mammalian electron transport chain. *Cell metabolism* 16, 378-386.

Baradaran, R., Wang, C., Siliciano, A.F., and Long, S.B. (2018). Cryo-EM structures of fungal and metazoan mitochondrial calcium uniporters. *Nature* 559, 580-584.

Barbot M, J.D., Schulz, C., Denkert, N., Kroppen, B., Hoppert, M., Jakobs, S., Meinecke, M. (2015). Mic10 Oligomerizes to Bend Mitochondrial Inner Membranes at Cristae Junctions. *Cell metabolism* 21, 756-763.

Barel, O., Shorer, Z., Flusser, H., Ofir, R., Narkis, G., Finer, G., Shalev, H., Nasasra, A., Saada, A., Birk, O. S. (2008). Mitochondrial complex III deficiency associated with a homozygous mutation in UQCRCQ. *Am. J. Hum. Genet.* 82, 1211-1216.

Baron, K.T., and Thayer, S.A. (1997). CGP37157 modulates mitochondrial Ca^{2+} homeostasis in cultured rat dorsal root ganglion neurons. *European journal of pharmacology* 340, 295-300.

Baughman, J.M., Perocchi, F., Girgis, H.S., Plovanich, M., Belcher-Timme, C.A., Sancak, Y., Bao, X.R., Strittmatter, L., Goldberger, O., Bogorad, R.L., et al. (2011). Integrative genomics identifies MCU as an essential component of the mitochondrial calcium uniporter. *Nature* 476, 341-345.

Baysal, B.E., Ferrell, R. E., Willett-Brozick, J. E., Lawrence, E. C., Myssiorek, D., Bosch, A., van der May, A., Taschner, P. E. M., Rubinstein, W. S., Myers, E. N., Richard, C. W., III, Cornelisse, C. J., Devilee, P., Devlin, B. (2000). Mutations in SDHD, a mitochondrial complex II gene, in hereditary paraganglioma. *Science (New York, N.Y.)* 287, 848-851.

Baysal, B.E., Willett-Brozick, J. E., Filho, P. A. A., Lawrence, E. C., Myers, E. N., Ferrell, R. E. (2004). An Alu-mediated partial SDHC deletion causes familial and sporadic paraganglioma. *J. Med. Genet.* 41, 703-709.

Beckmann, J.D., Ljungdahl, P.O., Lopez, J.L., and Trumpower, B.L. (1987). Isolation and characterization of the nuclear gene encoding the Rieske iron-sulfur protein (RIP1) from *Saccharomyces cerevisiae*. *The Journal of biological chemistry* 262, 8901-8909.

Beinert H, H.R., Münck E. (1997). Iron-sulfur clusters: nature's modular, multipurpose structures. *Science (New York, N.Y.)* 277, 653-659.

Bender, E., and Kadenbach, B. (2000). The allosteric ATP-inhibition of cytochrome c oxidase activity is reversibly switched on by cAMP-dependent phosphorylation. *FEBS Lett* 466, 130-134.

- Bénit, P., Beugnot, R., Chretien, D., Giurgea, I., De Lonlay-Debeney, P., Issartel, J.P., Corral-Debrinski, M., Kerscher, S., Rustin, P., Rötig, A., et al. (2003). Mutant NDUFV2 subunit of mitochondrial complex I causes early onset hypertrophic cardiomyopathy and encephalopathy. *Human mutation* 21, 582-586.
- Bénit, P., Chretien, D., Kadhom, N., de Lonlay-Debeney, P., Cormier-Daire, V., Cabral, A., Peudenier, S., Rustin, P., Munnich, A., and Rötig, A. (2001). Large-scale deletion and point mutations of the nuclear NDUFV1 and NDUFV3 genes in mitochondrial complex I deficiency. *American journal of human genetics* 68, 1344-1352.
- Bénit, P., Slama, A., Cartault, F., Giurgea, I., Chretien, D., Lebon, S., Marsac, C., Munnich, A., Rötig, A., and Rustin, P. (2004). Mutant NDUFV3 subunit of mitochondrial complex I causes Leigh syndrome. *Journal of medical genetics* 41, 14-17.
- Benjamini, Y., Hochberg, Y. (1995). Controlling the False Discovery Rate: A Practical and Powerful Approach to Multiple Testing. *Journal of the Royal Statistical Society: Series B (Methodological)* 57, 289-300.
- Berg, J.M., Tymoczko, J.L., and Stryer L. (2002). *Biochemistry*, 5th edition (New York: W H Freeman).
- Berger, I., Hershkovitz, E., Shaag, A., Edvardson, S., Saada, A., and Elpeleg, O. (2008). Mitochondrial complex I deficiency caused by a deleterious NDUFV1 mutation. *Annals of neurology* 63, 405-408.
- Berridge, M.J., Lipp, P., and Bootman, M.D. (2000). The versatility and universality of calcium signalling. *Nature reviews. Molecular cell biology* 1, 11-21.
- Berry EA, Z.Z., Bellamy, H.D., Huang, L. (2000). Crystallographic location of two Zn²⁺-binding sites in the avian cytochrome bc₁ complex. *Biochimica et Biophysica Acta (BBA) - Bioenergetics* 1459, 440-448.
- Berry, E., Huang, LS, Zhang, Z, Kim, SH. (1999). Structure of the avian mitochondrial cytochrome bc₁ complex. *J Bioenerg Biomembr.* 31, 177-190.
- Berry, E.A., De Bari, H., and Huang, L.S. (2013). Unanswered questions about the structure of cytochrome bc₁ complexes. *Biochimica et biophysica acta* 1827, 1258-1277.
- Bhosale, G., Sharpe, J.A., Koh, A., Kouli, A., Szabadkai, G., and Duchon, M.R. (2017). Pathological consequences of MICU1 mutations on mitochondrial calcium signalling and bioenergetics. *Biochimica et biophysica acta. Molecular cell research* 1864, 1009-1017.
- Bick, A.G., Calvo, S.E., and Mootha, V.K. (2012). Evolutionary diversity of the mitochondrial calcium uniporter. *Science (New York, N.Y.)* 336, 886.
- Bindels, D.S., Haarbosch, L., van Weeren, L., Postma, M., Wiese, K.E., Mastop, M., Aumonier, S., Gotthard, G., Royant, A., Hink, M.A., et al. (2017). mScarlet: a bright monomeric red fluorescent protein for cellular imaging. *Nature methods* 14, 53-56.

Blakely, E.L., Mitchell, A.L., Fisher, N., Meunier, B., Nijtmans, L.G., Schaefer, A.M., Jackson, M.J., Turnbull, D.M., and Taylor, R.W. (2005). A mitochondrial cytochrome b mutation causing severe respiratory chain enzyme deficiency in humans and yeast. *The FEBS journal* 272, 3583-3592.

Blaza, J.N., Serreli, R., Jones, A.J., Mohammed, K., and Hirst, J. (2014). Kinetic evidence against partitioning of the ubiquinone pool and the catalytic relevance of respiratory-chain supercomplexes. *Proceedings of the National Academy of Sciences of the United States of America* 111, 15735-15740.

Blázquez, A., Gil-Borlado, M.C., Morán, M., Verdú, A., Cazorla-Calleja, M.R., Martín, M.A., Arenas, J., and Ugalde, C. (2009). Infantile mitochondrial encephalomyopathy with unusual phenotype caused by a novel BCS1L mutation in an isolated complex III-deficient patient. *Neuromuscular disorders : NMD* 19, 143-146.

Bode, M., Woellhaf, M.W., Bohnert, M., van der Laan, M., Sommer, F., Jung, M., Zimmermann, R., Schroda, M., Herrmann, J.M. (2015). Redox-regulated dynamic interplay between Cox19 and the copper-binding protein Cox11 in the intermembrane space of mitochondria facilitates biogenesis of cytochrome c oxidase. *Molecular biology of the cell* 26, 2385-2401.

Bondarenko, A.I., Jean-Quartier, C., Parichatikanond, W., Alam, M.R., Waldeck-Weiermair, M., Malli, R., and Graier, W.F. (2014). Mitochondrial Ca(2+) uniporter (MCU)-dependent and MCU-independent Ca(2+) channels coexist in the inner mitochondrial membrane. *Pflugers Archiv : European journal of physiology* 466, 1411-1420.

Bonora, M., Wieckowski, M.R., Chinopoulos, C., Kepp, O., Kroemer, G., Galluzzi, L., and Pinton, P. (2015). Molecular mechanisms of cell death: central implication of ATP synthase in mitochondrial permeability transition. *Oncogene* 34, 1475-1486.

Bosley T.M., B.M.C., Glasier C.M., Abu-Amero K.K. (2008). Sporadic bilateral optic neuropathy in children: the role of mitochondrial abnormalities. *Invest. Ophthalmol. Vis. Sci.* 49, 5250–5256.

Bottani, E., Cerutti, R., Harbour, M.E., Ravaglia, S., Dogan, S.A., Giordano, C., Fearnley, I.M., D'Amati, G., Viscomi, C., Fernandez-Vizarra, E., et al. (2017). TTC19 Plays a Husbandry Role on UQCRFS1 Turnover in the Biogenesis of Mitochondrial Respiratory Complex III. *Molecular cell* 67, 96-105.e104.

Bourens, M., and Barrientos, A. (2017). Human mitochondrial cytochrome c oxidase assembly factor COX18 acts transiently as a membrane insertase within the subunit 2 maturation module. *The Journal of biological chemistry* 292, 7774-7783.

Bourens, M., Barrientos A. (2017). A CMC1-knockout reveals translation-independent control of human mitochondrial complex IV biogenesis. *EMBO Rep.* 18, 477-494.

Bourens, M., Boulet, A., Leary, S.C., Barrientos, A. (2014). Human COX20 cooperates with SCO1 and SCO2 to mature COX2 and promote the assembly of cytochrome c oxidase. *Hum Mol Genet.* 23, 2901-2913.

Bouzidi, M.F., Schagger, H., Collombet, J. M., Carrier, H., Flocard, F., Quard, S., Mousson, B., Godinot, C. (1993). Decreased expression of ubiquinol-cytochrome c reductase subunits in patients exhibiting mitochondrial myopathy with progressive exercise intolerance. *Neuromusc. Disord.* 3, 599-604.

Brandner, K., Mick, D.U., Frazier, A.E., Taylor, R.D., Meisinger, C., and Rehling, P. (2005). Taz1, an outer mitochondrial membrane protein, affects stability and assembly of inner membrane protein complexes: implications for Barth Syndrome. *Molecular biology of the cell* 16, 5202-5214.

Brandt, U. (2011). A two-state stabilization-change mechanism for proton-pumping complex I. *Biochimica et biophysica acta* 1807, 1364-1369.

Brandt, U., Uribe, S., Schagger, H., Trumpower, B.L. (1994). Isolation and characterization of QCR10, the nuclear gene encoding the 8.5-kDa subunit 10 of the *Saccharomyces cerevisiae* cytochrome bc1 complex. *J Biol Chem.* 269, 12947-12953.

Brandt, U., Yu, L., Yu, C.A., and Trumpower, B.L. (1993). The mitochondrial targeting presequence of the Rieske iron-sulfur protein is processed in a single step after insertion into the cytochrome bc1 complex in mammals and retained as a subunit in the complex. *The Journal of biological chemistry* 268, 8387-8390.

Brown, M.D., Starikovskaya, E., Derbeneva, O., Hosseini, S., Allen, J.C., Mikhailovskaya, I.E., Sukernik, R.I., and Wallace, D.C. (2002). The role of mtDNA background in disease expression: a new primary LHON mutation associated with Western Eurasian haplogroup J. *Human genetics* 110, 130-138.

Brown, M.D., Voljavec, A. S., Lott, M. T., Torroni, A., Yang, C.-C., Wallace, D. C. (1992). Mitochondrial DNA complex I and III mutations associated with Leber's hereditary optic neuropathy. *Genetics* 130, 163-173.

Brown, M.D., Voljavec, A.S., Lott, M.T., MacDonald, I., and Wallace, D.C. (1992). Leber's hereditary optic neuropathy: a model for mitochondrial neurodegenerative diseases. *FASEB journal: official publication of the Federation of American Societies for Experimental Biology* 6, 2791-2799.

Bruno, C., Martinuzzi, A., Tang, Y., Andreu, A.L., Pallotti, F., Bonilla, E., Shanske, S., Fu, J., Sue, C.M., Angelini, C., et al. (1999). A stop-codon mutation in the human mtDNA cytochrome c oxidase I gene disrupts the functional structure of complex IV. *American journal of human genetics* 65, 611-620.

Budde, S.M., van den Heuvel, L.P., Janssen, A.J., Smeets, R.J., Buskens, C.A., DeMeirleir, L., Van Coster, R., Baethmann, M., Voit, T., Trijbels, J.M., et al. (2000). Combined enzymatic complex I and III deficiency associated with mutations in the nuclear encoded NDUFS4 gene. *Biochemical and biophysical research communications* 275, 63-68.

Bugiani, M., Invernizzi, F., Alberio, S., Briem, E., Lamantea, E., Carrara, F., Moroni, I., Farina, L., Spada, M., Donati, M.A., et al. (2004). Clinical and molecular findings in children with complex I deficiency. *Biochimica et biophysica acta* 1659, 136-147.

Burgoyne, T., Patel, S., and Eden, E.R. (2015). Calcium signaling at ER membrane contact sites. *Biochimica et biophysica acta* 1853, 2012-2017.

Burnichon, N., Brière, J.J., Libé, R., Vescovo, L., Rivière, J., Tissier, F., Jouanno, E., Jeunemaitre, X., Bénit, P., Tzagoloff, A., Rustin, P., Bertherat, J., Favier, J., Gimenez-Roqueplo, A.P. (2010). SDHA is a tumor suppressor gene causing paraganglioma. *Hum Mol Genet* 19:3011-20.

Bych, K., Kerscher, S., Netz, D.J., Pierik, A.J., Zwicker, K., Huynen, M.A., Lill, R., Brandt, U., and Balk, J. (2008). The iron-sulphur protein Ind1 is required for effective complex I assembly. *The EMBO journal* 27, 1736-1746.

Cabrera-Orefice, A., Yoga, E.G., Wirth, C., Siegmund, K., Zwicker, K., Guerrero-Castillo, S. Zickermann, V., Hunte, C., Brandt, U. (2018). Locking loop movement in the ubiquinone pocket of complex I disengages the proton pumps. *Nat Commun* 9(1): 4500.

Calvo, S.E., Clauser, K.R. Mootha, V.K. (2016). MitoCarta2.0: an updated inventory of mammalian mitochondrial proteins. *Nucleic Acids Res* 44(D1): D1251-1257.

Calvo, S.E., Tucker, E.J., Compton, A.G., Kirby, D.M., Crawford, G., Burt, N.P., Rivas, M., Guiducci, C., Bruno, D.L., Goldberger, O.A., et al. (2010). High-throughput, pooled sequencing identifies mutations in NUBPL and FOXRED1 in human complex I deficiency. *Nature genetics* 42, 851-858.

Cao, C., Wang, S., Cui, T., Su, X.C., and Chou, J.J. (2017). Ion and inhibitor binding of the double-ring ion selectivity filter of the mitochondrial calcium uniporter. *Proceedings of the National Academy of Sciences of the United States of America* 114, E2846-e2851.

Capaldi, R.A. (1990). Structure and function of cytochrome c oxidase. *Annu Rev Biochem.* 59, 569-596.

Capaldi, R.A., and Aggeler, R. (2002). Mechanism of the F(1)F(0)-type ATP synthase, a biological rotary motor. *Trends in biochemical sciences* 27, 154-160.

Carafoli E, Lehninger, A.L. (1971). A survey of the interaction of calcium ions with mitochondria from different tissues and species. *Biochem J.* 122, 681-690.

Carafoli, E. (2002). Calcium signaling: A tale for all seasons. *PNAS* 99, 1115-1122.

Carilla-Latorre, S., Gallardo, M.E., Annesley, S.J., Calvo-Garrido, J., Grana, O., Accari, S.L., Smith, P.K., Valencia, A., Garesse, R., Fisher, P.R., et al. (2010). MidA is a putative methyltransferase that is required for mitochondrial complex I function. *J Cell Sci* 123, 1674-1683.

Carlson, C.G., Barrientos, A., Tzagoloff, A., Glerum, D.M. (2003). COX16 encodes a novel protein required for the assembly of cytochrome oxidase in *Saccharomyces cerevisiae*. *J Biol Chem.* 278, 3770-3775.

Carossa, V., Ghelli, A., Tropeano, C.V., Valentino, M.L., Iommarini, L., Maresca, A., Caporali, L., La Morgia, C., Liguori, R., Barboni, P., et al. (2014). A novel in-frame 18-bp

microdeletion in MT-CYB causes a multisystem disorder with prominent exercise intolerance. *Human mutation* 35, 954-958.

Carroll, J., Ding, S., Fearnley, I.M., and Walker, J.E. (2013). Post-translational modifications near the quinone binding site of mammalian complex I. *The Journal of biological chemistry* 288, 24799-24808.

Cavalier-Smith, T. (2006). Origin of mitochondria by intracellular enslavement of a photosynthetic purple bacterium. *Proceedings. Biological sciences* 273, 1943-1952.

Cecchini, G. (2003). Function and structure of complex II of the respiratory chain. *Annual review of biochemistry* 72, 77-109.

Cerqua, C., Morbidoni, V., Desbats, M.A., Doimo, M., Frasson, C., Sacconi, S., Baldoin, M.C., Sartori, G., Basso, G., Salviati, L., Trevisson, E. (2018). COX16 is required for assembly of cytochrome c oxidase in human cells and is involved in copper delivery to COX2. *Biochimica et biophysica acta* 1859, 244-252.

Chacinska, A., Pfannschmidt, S., Wiedemann, N., Kozjak, V., Sanjuan Szklarz, L.K., Schulze-Specking, A., Truscott, K.N., Guiard, B., Meisinger, C., and Pfanner, N. (2004). Essential role of Mia40 in import and assembly of mitochondrial intermembrane space proteins. *The EMBO journal* 23, 3735-3746.

Chance, B. (1955). On possible mechanisms for the control of electron transport in the respiratory chain. In *Proceedings of the Third International Congr. Biochem.*, Academic Press. (Brussels), pp. 300-304.

Chance, B., and Williams, G.R. (1955). A method for the localization of sites for oxidative phosphorylation. *Nature* 176, 250-254.

Chance, B., Mela, L. (1966). Calcium and manganese interactions in mitochondrial ion accumulation. *Biochemistry* 5, 3220-3223.

Chen, Y.C., Taylor, E.B., Dephoure, N., Heo, J.M., Tonhato, A., Papandreou, I., Nath, N., Denko, N.C., Gygi, S.P., and Rutter, J. (2012). Identification of a protein mediating respiratory supercomplex stability. *Cell metabolism* 15, 348-360.

Chiabrando, D., Vinchi, F., Fiorito, V., Mercurio, S., and Tolosano, E. (2014). Heme in pathophysiology: a matter of scavenging, metabolism and trafficking across cell membranes. *Frontiers in pharmacology* 5, 61.

Chinnaiyan, A.M. (1999). The apoptosome: heart and soul of the cell death machine. *Neoplasia* (New York, N.Y.) 1, 5-15.

Chinnery, P.F., and Hudson, G. (2013). Mitochondrial genetics. *British medical bulletin* 106, 135-159.

Chiurillo, M.A., Lander, N., Bertolini, M.S., Storey, M., Vercesi, A.E., and Docampo, R. (2017). Different Roles of Mitochondrial Calcium Uniporter Complex Subunits in Growth and Infectivity of *Trypanosoma cruzi*. *mBio* 8.

Choi, S., Quan, X., Bang, S., Yoo, H., Kim, J., Park, J., Park, K.S., and Chung, J. (2017). Mitochondrial calcium uniporter in *Drosophila* transfers calcium between the endoplasmic reticulum and mitochondria in oxidative stress-induced cell death. *The Journal of biological chemistry* 292, 14473-14485.

Christianson, T., Edwards, J.C., Mueller, D.M., Rabinowitz, M. (1983). Identification of a single transcriptional initiation site for the glutamic tRNA and COB genes in yeast mitochondria. *Proc. Natl. Acad. Sci. U. S. A.*, 80 5564-5568.

Church, C., Chapon, C., Poyton, R.O. (1996). Cloning and characterization of PET100, a gene required for the assembly of yeast cytochrome c oxidase. *The Journal of biological chemistry* 271, 18499-18507.

Church, C., Goehring, B., Forsha, D., Wazny, P., Poyton, R.O. (2005). A role for Pet100p in the assembly of yeast cytochrome c oxidase: interaction with a subassembly that accumulates in a pet100 mutant. *The Journal of biological chemistry* 280, 1854-1863.

Cipolat, S., Martins de Brito, O., Dal Zilio, B., and Scorrano, L. (2004). OPA1 requires mitofusin 1 to promote mitochondrial fusion. *Proceedings of the National Academy of Sciences of the United States of America* 101, 15927-15932.

Cizkova, A., Stranecky, V., Mayr, J.A., Tesarova, M., Havlickova, V., Paul, J., Ivanek, R., Kuss, A.W., Hansikova, H., Kaplanova, V., et al. (2008). TMEM70 mutations cause isolated ATP synthase deficiency and neonatal mitochondrial encephalomyopathy. *Nature genetics* 40, 1288-1290.

Clapham, D.E. (2007). Calcium signaling. *Cell* 131, 1047-1058.

Clark, K.M., Taylor R.W., Johnson M.A., Chinnery P.F., Chrzanowska-Lightowlers Z.M., Andrews R.M., Nelson I.P., Wood N.W., Lamont P.J., Hanna M.G. (1999). An mtDNA mutation in the initiation codon of the cytochrome C oxidase subunit II gene results in lower levels of the protein and a mitochondrial encephalomyopathy. *Am. J. Hum. Genet.* 64, 1330–1339.

Claros, M.G., and Vincens, P. (1996). Computational method to predict mitochondrially imported proteins and their targeting sequences. *European journal of biochemistry* 241, 779-786.

Clemente, P., Peralta, S., Cruz-Bermudez, A., Echevarría, L., Fontanesi, F., Barrientos, A., Fernandez-Moreno, M.A., Garesse, R. (2013). hCOA3 stabilizes cytochrome c oxidase 1 (COX1) and promotes cytochrome c oxidase assembly in human mitochondria. *J Biol Chem.* 288, 8321-8331.

Cogliati, S., Calvo, E., Loureiro, M., Guaras, A.M., Nieto-Arellano, R., Garcia-Poyatos, C., Ezkurdia, I., Mercader, N., Vazquez, J., and Enriquez, J.A. (2016a). Mechanism of super-assembly of respiratory complexes III and IV. *Nature* 539, 579-582.

Cogliati, S., Enriquez, J.A., and Scorrano, L. (2016b). Mitochondrial Cristae: Where Beauty Meets Functionality. *Trends in biochemical sciences* 41, 261-273.

Cogliati, S., Frezza, C., Soriano, M.E., Varanita, T., Quintana-Cabrera, R., Corrado, M., Cipolat, S., Costa, V., Casarin, A., Gomes, L.C., et al. (2013). Mitochondrial cristae shape determines respiratory chain supercomplexes assembly and respiratory efficiency. *Cell* 155, 160-171.

Colombini, M. (1989). Voltage gating in the mitochondrial channel, VDAC. *J. Membr. Biol.*, 111, 103-111.

Comi G.P., Bordoni, A., Salani, S., Franceschina, L., Sciacco, M., Prella, A., Fortunato, F., Zeviani, M., Napoli, L., Bresolin, N. (1998). Cytochrome c oxidase subunit I microdeletion in a patient with motor neuron disease. *Ann. Neurol.* 43, 110-116.

Cox, J., and Mann, M. (2008). MaxQuant enables high peptide identification rates, individualized p.p.b.-range mass accuracies and proteome-wide protein quantification. *Nature biotechnology* 26, 1367-1372.

Cox, J., and Mann, M. (2011). Quantitative, high-resolution proteomics for data-driven systems biology. *Annual review of biochemistry* 80, 273-299.

Crivellone, M. (1994). Characterization of CBP4, a new gene essential for the expression of ubiquinol-cytochrome c reductase in *Saccharomyces cerevisiae*. *J Biol Chem.* 269, 21284-21292.

Crompton, M. (1999). The mitochondrial permeability transition pore and its role in cell death. *The Biochemical journal* 341 (Pt 2), 233-249.

Cruciat, C.M., Hell, K., Fölsch, H., Neupert, W., Stuart, R.A. (1999). Bcs1p, an AAA-family member, is a chaperone for the assembly of the cytochrome bc₁ complex. *The EMBO journal* 18, 5226-5233.

Csordás, G., Golenár, T., Seifert, E.L., Kamer, K.J., Sancak, Y., Perocchi, F., Moffat, C., Weaver, D., de la Fuente Perez, S., Bogorad, R., Koteliensky, V., Adijanto, J., Mootha, V.K., Hajnóczky, G. (2013). MICU1 controls both the threshold and cooperative activation of the mitochondrial Ca²⁺ uniporter. *Cell metabolism* 17, 976-987.

Csordás, G., Renken, C., Várnai, P., Walter, L., Weaver, D., Buttle, K.F., Balla, T., Mannella, C.A., and Hajnóczky, G. (2006). Structural and functional features and significance of the physical linkage between ER and mitochondria. *The Journal of cell biology* 174, 915-921.

Cui, T.Z., Smith, P.M., Fox, J.L., Khalimonchuk, O., and Winge, D.R. (2012). Late-stage maturation of the Rieske Fe/S protein: Mzm1 stabilizes Rip1 but does not facilitate its translocation by the AAA ATPase Bcs1. *Mol Cell Biol* 32, 4400-4409.

D.C. Warthon, A.T. (1967). Cytochrome oxidase from beef heart mitochondria. *Methods Enzymol.*, 10, 245-250.

D'Aurelio, M., Pallotti, F., Barrientos, A., Gajewski, C.D., Kwong, J.Q., Bruno, C., Beal, M.F., Manfredi, G. (2001). In vivo regulation of oxidative phosphorylation in cells harboring a stop-

codon mutation in mitochondrial DNA-encoded cytochrome c oxidase subunit I. *J. Biol. Chem.*, 276, 46925–46932.

Dallabona, C., Abbink, T.E., Carrozzo, R., Torracco, A., Legati, A., van Berkel, C.G., Niceta, M., Langella, T., Verrigni, D., Rizza, T., et al. (2016). LYRM7 mutations cause a multifocal cavitating leukoencephalopathy with distinct MRI appearance. *Brain: a journal of neurology* 139, 782-794.

Danese, A., Patergnani, S., Bonora, M., Wieckowski, M.R., Previati, M., Giorgi, C., and Pinton, P. (2017). Calcium regulates cell death in cancer: Roles of the mitochondria and mitochondria-associated membranes (MAMs). *Biochimica et biophysica acta. Bioenergetics* 1858, 615-627.

Darshi, M., Mendiola, V.L., Mackey, M.R., Murphy, A.N., Koller, A., Perkins, G.A., Ellisman, M.H., and Taylor, S.S. (2011). ChChd3, an inner mitochondrial membrane protein, is essential for maintaining crista integrity and mitochondrial function. *The Journal of biological chemistry* 286, 2918-2932.

Davies, K.M., Blum, T.B., Kühlbrandt, W. (2018). Conserved in situ arrangement of complex I and III2 in mitochondrial respiratory chain supercomplexes of mammals, yeast, and plants. *Proc Natl Acad Sci U S A.* 115, 3024-3029.

Dawitz, H., Schäfer, J., Schaart, J.M., Magits, W., Brzezinski, P., and Ott, M. (2019). Rcf1 Modulates Cytochrome c Oxidase Activity Especially Under Energy-Demanding Conditions. *Frontiers in physiology* 10, 1555.

De Coo, I.F., Renier, W.O., Ruitenbeek, W., Ter Laak, H.J., Bakker, M., Schagger, H., Van Oost, B.A., and Smeets, H.J. (1999). A 4-base pair deletion in the mitochondrial cytochrome b gene associated with parkinsonism/MELAS overlap syndrome. *Annals of neurology* 45, 130-133.

De Haan, M., van Loon, A.P., Kreike, J., Vaessen, R.T., and Grivell, L.A. (1984). The biosynthesis of the ubiquinol-cytochrome c reductase complex in yeast. DNA sequence analysis of the nuclear gene coding for the 14-kDa subunit. *European journal of biochemistry* 138, 169-177.

de Lonlay, P., Valnot, I., Barrientos, A., Gorbatyuk, M., Tzagoloff, A., Taanman, J.W., Benayoun, E., Chretien, D., Kadhon, N., Lombes, A., et al. (2001). A mutant mitochondrial respiratory chain assembly protein causes complex III deficiency in patients with tubulopathy, encephalopathy and liver failure. *Nature genetics* 29, 57-60.

De Stefani, D., Bononi, A., Romagnoli, A., Messina, A., De Pinto, V., Pinton, P., and Rizzuto, R. (2012). VDAC1 selectively transfers apoptotic Ca²⁺ signals to mitochondria. *Cell death and differentiation* 19, 267-273.

De Stefani, D., Raffaello, A., Teardo, E., Szabo, I., and Rizzuto, R. (2011). A forty-kilodalton protein of the inner membrane is the mitochondrial calcium uniporter. *Nature* 476, 336-340.

Dean, D.R., and Dos Santos, P.C. (2015). Trading Places-Switching Frataxin Function by a Single Amino Acid Substitution within the [Fe-S] Cluster Assembly Scaffold. *PLoS genetics* 11, e1005192.

Deluca, H.F., and Engstrom, G.W. (1961). Calcium uptake by rat kidney mitochondria. *Proceedings of the National Academy of Sciences of the United States of America* 47, 1744-1750.

Demishtein-Zohary, K., Azem, A. (2017). The TIM23 mitochondrial protein import complex: function and dysfunction. *Cell and Tissue Research* 367, 33-41.

Dennerlein, S., Oeljeklaus, S., Jans, D., Hellwig, C., Bareth, B., Jakobs, S., Deckers, M., Warscheid, B., Rehling, P. (2015). MITRAC7 Acts as a COX1-Specific Chaperone and Reveals a Checkpoint during Cytochrome c Oxidase Assembly. *Cell reports* 12, 1644-1655.

Denton, R.M. (2009). Regulation of mitochondrial dehydrogenases by calcium ions. *Biochimica et biophysica acta* 1787, 1309-1316.

Diaz, F., Enríquez, J.A., and Moraes, C.T. (2012). Cells lacking Rieske iron-sulfur protein have a reactive oxygen species-associated decrease in respiratory complexes I and IV. *Mol Cell Biol* 32, 415-429.

Diaz, F., Fukui, H., Garcia, S., and Moraes, C.T. (2006). Cytochrome c oxidase is required for the assembly/stability of respiratory complex I in mouse fibroblasts. *Mol Cell Biol* 26, 4872-4881.

Diaz, F., Thomas, C.K., Garcia, S., Hernandez, D., Moraes, C.T. (2015). Mice lacking COX10 in skeletal muscle recapitulate the phenotype of progressive mitochondrial myopathies associated with cytochrome c oxidase deficiency. *Human molecular genetics* 14, 2737-2748.

Dieckmann, C., Pape, LK, Tzagoloff, A. (1982). Identification and cloning of a yeast nuclear gene (CBP1) involved in expression of mitochondrial cytochrome b. *Proc Natl Acad Sci U S A*. 79, 1805-1809.

Dieckmann, C., Tzagoloff, A. (1985). Assembly of the mitochondrial membrane system. CBP6, a yeast nuclear gene necessary for synthesis of cytochrome b. *J Biol Chem*. 260, 1513-1520.

Docampo, R., and Lukes, J. (2012). Trypanosomes and the solution to a 50-year mitochondrial calcium mystery. *Trends in parasitology* 28, 31-37.

Drago, I., and Davis, R.L. (2016). Inhibiting the Mitochondrial Calcium Uniporter during Development Impairs Memory in Adult *Drosophila*. *Cell reports* 16, 2763-2776.

Dudkina, N.V., Kudryashev, M., Stahlberg, H., Boekema, E.J. (2011). Interaction of complexes I, III, and IV within the bovine respirasome by single particle cryoelectron tomography. *Proc Natl Acad Sci U S A*. 108, 15196-15200.

Dudkina, N., Eubel, H., Keegstra, W., Boekema, E.J., Braun, H.P. (2005). Structure of a mitochondrial supercomplex formed by respiratory-chain complexes I and III. *PNAS* 102, 3225-3229.

Dumont, M.E., Ernst, J.F., Hampsey, D.M., and Sherman, F. (1987). Identification and sequence of the gene encoding cytochrome c heme lyase in the yeast *Saccharomyces cerevisiae*. *The EMBO journal* 6, 235-241.

Dumont, M.E., Schlichter, J.B., Cardillo, T.S., Hayes, M.K., Bethlenny, G., and Sherman, F. (1993). CYC2 encodes a factor involved in mitochondrial import of yeast cytochrome c. *Mol Cell Biol* 13, 6442-6451.

Dunning, C.J., McKenzie, M., Sugiana, C., Lazarou, M., Silke, J., Connelly, A., Fletcher, J.M., Kirby, D.M., Thorburn, D.R., and Ryan, M.T. (2007). Human CIA30 is involved in the early assembly of mitochondrial complex I and mutations in its gene cause disease. *The EMBO journal* 26, 3227-3237.

Dwight, T., Na, U., Kim, E., Zhu, Y., Richardson, A.L., Robinson, B.G., Tucker, K.M., Gill, A.J., Benn, D.E., Clifton-Bligh, R.J., Winge, D.R. (2017). Analysis of SDHAF3 in familial and sporadic pheochromocytoma and paraganglioma. *BMC Cancer*. 17, 497.

Eaton, S., Bursby, T., Middleton, B., Pourfarzam, M., Mills, K., Johnson, A.W., and Bartlett, K. (2000). The mitochondrial trifunctional protein: centre of a beta-oxidation metabolon? *Biochemical Society transactions* 28, 177-182.

Efremov, R.G., and Sazanov, L.A. (2011). Structure of the membrane domain of respiratory complex I. *Nature* 476, 414-420.

Elmore, S. (2007). Apoptosis: A Review of Programmed Cell Death. *Toxicol Pathol* 35, 495–516.

Ernster, L., Schatz, G. (1981). Mitochondria: a historical review. *Journal of Cell Biology* 91, 227-255.

Fan, C., Fan, M., Orlando, B.J., Fastman, N.M., Zhang, J., Xu, Y., Chambers, M.G., Xu, X., Perry, K., Liao, M., et al. (2018). X-ray and cryo-EM structures of the mitochondrial calcium uniporter. *Nature* 559, 575-579.

Fang, J.K., Prabu, S.K., Sepuri, N.B., Raza, H., Anandatheerthavarada, H.K., Galati, D., Spear, J., and Avadhani, N.G. (2007). Site specific phosphorylation of cytochrome c oxidase subunits I, IVi1 and Vb in rabbit hearts subjected to ischemia/reperfusion. *FEBS Lett* 581, 1302-1310.

Fato, R., Battino, M., Degli Esposti, M., Parenti Castelli, G., Lenaz, G. (1986). Determination of partition and lateral diffusion coefficients of ubiquinones by fluorescence quenching of n-(9-anthroyloxy)stearic acids in phospholipid vesicles and mitochondrial membranes. *Biochemistry* 25, 3378-3390.

Fedor, J.G., and Hirst, J. (2018). Mitochondrial Supercomplexes Do Not Enhance Catalysis by Quinone Channeling. *Cell metabolism* 28, 525-531.e524.

Feichtinger, R.G., Brunner-Krainz, M., Alhaddad, B., Wortmann, S.B., Kovacs-Nagy, R., Stojakovic, T., Erwa, W., Resch, B., Windischhofer, W., Verheyen, S., et al. (2017). Combined Respiratory Chain Deficiency and UQCC2 Mutations in Neonatal Encephalomyopathy: Defective Supercomplex Assembly in Complex III Deficiencies. *Oxidative medicine and cellular longevity* 2017, 7202589.

Fernandez-Moreira, D., Ugalde, C., Smeets, R., Rodenburg, R. J. T., Lopez-Laso, E., Ruiz-Falco, M. L., Briones, P., Martin, M. A., Smeitink, J. A. M., Arenas, J. (2007). X-linked NDUFA1 gene mutations associated with mitochondrial encephalomyopathy. *Ann. Neurol.* 61: 73-83.

Fernandez-Vizarra, E., and Zeviani, M. (2015). Nuclear gene mutations as the cause of mitochondrial complex III deficiency. *Frontiers in genetics* 6, 134.

Fernandez-Vizarra, E., and Zeviani, M. (2018). Mitochondrial complex III Rieske Fe-S protein processing and assembly. *Cell cycle (Georgetown, Tex.)* 17, 681-687.

Fernandez-Vizarra, E., Bugiani, M., Goffrini, P., Carrara, F., Farina, L., Procopio, E., Donati, A., Uziel, G., Ferrero, I., and Zeviani, M. (2007). Impaired complex III assembly associated with BCS1L gene mutations in isolated mitochondrial encephalopathy. *Human molecular genetics* 16, 1241-1252.

Fernandez-Vizarra, E., Ferrin, G., Perez-Martos, A., Fernandez-Silva, P., Zeviani, M., and Enriquez, J.A. (2010). Isolation of mitochondria for biogenetical studies: An update. *Mitochondrion* 10, 253-262.

Fieni, F., Lee, S.B., Jan, Y.N., and Kirichok, Y. (2012). Activity of the mitochondrial calcium uniporter varies greatly between tissues. *Nature communications* 3, 1317.

Fölsch, H., Guiard, B., Neupert, W., Stuart, R.A. (1996). Internal targeting signal of the BCS1 protein: a novel mechanism of import into mitochondria. *The EMBO journal* 15, 479-487.

Formosa, L.E., Mimaki, M., Frazier, A.E., McKenzie, M., Stait, T.L., Thorburn, D.R., Stroud, D.A., and Ryan, M.T. (2015). Characterization of mitochondrial FOXRED1 in the assembly of respiratory chain complex I. *Human molecular genetics* 24, 2952-2965.

Formosa, L.E., Muellner-Wong, L., Reljic, B., Sharpe, A.J., Jackson, T.D., Beilharz, T.H., Stojanovski, D., Lazarou, M., Stroud, D.A., and Ryan, M.T. (2020). Dissecting the Roles of Mitochondrial Complex I Intermediate Assembly Complex Factors in the Biogenesis of Complex I. *Cell reports* 31, 107541.

Fox, T. (2012). Mitochondrial Protein Synthesis, Import, and Assembly. *Genetics* 192, 1203-1234.

Frederick, R.L., and Shaw, J.M. (2007). Moving mitochondria: establishing distribution of an essential organelle. *Traffic (Copenhagen, Denmark)* 8, 1668-1675.

Frezza, C., Cipolat, S., Martins de Brito, O., Micaroni, M., Beznoussenko, G.V., Rudka, T., Bartoli, D., Polishuck, R.S., Danial, N.N., De Strooper, B., et al. (2006). OPA1 controls apoptotic cristae remodeling independently from mitochondrial fusion. *Cell* 126, 177-189.

Friederich, M.W., Erdogan, A.J., Coughlin, C.R., Elos, M.T., Jiang, H., O'Rourke, C.P., Lovell, M.A., Wartchow, E., Gowan, K., Chatfield, K.C., Chick, W.S., Spector, E.B, Van Hove, J.L. K., Riemer, J. (2017) Mutations in the accessory subunit NDUFB10 result in isolated complex I deficiency and illustrate the critical role of intermembrane space import for complex I holoenzyme assembly. *Hum. Molec. Genet.* 26: 702-716.

Friedman, J.R., Mourier, A., Yamada, J., McCaffery, J.M., and Nunnari, J. (2015). MICOS coordinates with respiratory complexes and lipids to establish mitochondrial inner membrane architecture. *Elife* 4.

Friedrich, T., Dekovic, D.K., and Burschel, S. (2016). Assembly of the Escherichia coli NADH:ubiquinone oxidoreductase (respiratory complex I). *Biochimica et biophysica acta* 1857, 214-223.

Fu, W., Japa, S., Beattie, D.S. (1990). Import of the iron-sulfur protein of the cytochrome b.c1 complex into yeast mitochondria. *J Biol Chem.* 265, 16541-16547.

Gaignard, P., Menezes, M., Schiff, M., Bayot, A., Rak, M., Ogier de Baulny, H., Su, C.H., Gilleron, M., Lombes, A., Abida, H., Tzagoloff, A., Riley, L., Cooper, S.T., Mina, K., Sivadorai, P., Davis, M.R., Allcock, R.J.N., Kresoje, N., Laing, N.G., Thorburn, D.R., Slama, A., Christodoulou, J., Rustin, P. (2013). Mutations in CYC1, encoding cytochrome c1 subunit of respiratory chain complex III, cause insulin-responsive hyperglycemia. *Am. J. Hum. Genet.* 93, 384-389.

Gellerich, F.N., Gizatullina, Z., Trumbeckaite, S., Nguyen, H.P., Pallas, T., Arandarcikaite, O., Vielhaber, S., Seppet, E., and Striggow, F. (2010). The regulation of OXPHOS by extramitochondrial calcium. *Biochimica et biophysica acta* 1797, 1018-1027.

Ghezzi, D., Arzuffi, P., Zordan, M., Da Re, C., Lamperti, C., Benna, C., D'Adamo, P., Diodato, D., Costa, R., Mariotti, C., Uziel, G., Smiderle, C., Zeviani, M. (2011). Mutations in TTC19 cause mitochondrial complex III deficiency and neurological impairment in humans and flies. *Nature Genet.* 43, 259-263.

Ghezzi, D., Goffrini, P., Uziel, G., Horvath, R., Klopstock, T., Lochmüller, H., D'Adamo, P., Gasparini, P., Strom, T.M., Prokisch, H., Invernizzi, F., Ferrero, I., Zeviani, M. (2009). SDHAF1, encoding a LYR complex-II specific assembly factor, is mutated in SDH-defective infantile leukoencephalopathy. *Nat Genet.* 41, 654-656.

Ghezzi, D., Zeviani, M. (2018). Human diseases associated with defects in assembly of OXPHOS complexes. *Essays Biochem.* 62, 271-286.

Ghosh, S., Basu Ball, W., Madaris, T.R., Srikantan, S., Madesh, M., Mootha, V.K., and Gohil, V.M. (2020). An essential role for cardiolipin in the stability and function of the mitochondrial calcium uniporter. *Proceedings of the National Academy of Sciences of the United States of America* 117, 16383-16390.

Giachin, G., Bouverot, R., Acajjaoui, S., Pantalone, S., Soler-López, M. (2016). Dynamics of Human Mitochondrial Complex I Assembly: Implications for Neurodegenerative Diseases.

- Gil-Borlado, M.C., Gonzalez-Hoyuela, M., Blazquez, A., Garcia-Silva, M.T., Gabaldon, T., Manzanares, J., Vara, J., Martin, M.A., Seneca, S., Arenas, J., et al. (2009). Pathogenic mutations in the 5' untranslated region of BCS1L mRNA in mitochondrial complex III deficiency. *Mitochondrion* 9, 299-305.
- Giles, R.E., Blanc, H., Cann, H.M., and Wallace, D.C. (1980). Maternal inheritance of human mitochondrial DNA. *Proceedings of the National Academy of Sciences of the United States of America* 77, 6715-6719.
- Gilkerson, R.W., Selker, J., Capaldi, R.A. (2003). The cristal membrane of mitochondria is the principal site of oxidative phosphorylation. *FEBS Lett.* 546, 355-358.
- Giorgi, C., Marchi, S., and Pinton, P. (2018). The machineries, regulation and cellular functions of mitochondrial calcium. *Nature reviews. Molecular cell biology* 19, 713-730.
- Giorgio, V., von Stockum, S., Antoniel, M., Fabbro, A., Fogolari, F., Forte, M., Glick, G.D., Petronilli, V., Zoratti, M., Szabó, I., et al. (2013). Dimers of mitochondrial ATP synthase form the permeability transition pore. *Proceedings of the National Academy of Sciences of the United States of America* 110, 5887-5892.
- Glancy, B., Willis, W., Chess, D.J., Balaban, R.S. (2013). Effect of calcium on the oxidative phosphorylation cascade in skeletal muscle mitochondria. *Biochemistry* 52, 2793-2809.
- Glerum, D., Shtanko A, Tzagoloff A. (1996). Characterization of COX17, a yeast gene involved in copper metabolism and assembly of cytochrome oxidase. *J Biol Chem.* 271, 14504-14509.
- Glerum, D.M., Muroff, I., Jin, C., and Tzagoloff, A. (1997). COX15 codes for a mitochondrial protein essential for the assembly of yeast cytochrome oxidase. *The Journal of biological chemistry* 272, 19088-19094.
- Glytsou, C., Calvo, E., Cogliati, S., Mehrotra, A., Anastasia, I., Rigoni, G., Raimondi, A., Shintani, N., Loureiro, M., Vazquez, J., et al. (2016). Optic Atrophy 1 Is Epistatic to the Core MICOS Component MIC60 in Mitochondrial Cristae Shape Control. *Cell reports* 17, 3024-3034.
- Gottschalk, B., Klec, C., Leitinger, G., Bernhart, E., Rost, R., Bischof, H., Madreiter-Sokolowski, C.T., Radulović, S., Eroglu, E., Sattler, W., et al. (2019). MICU1 controls cristae junction and spatially anchors mitochondrial Ca(2+) uniporter complex. *Nature communications* 10, 3732.
- Graham, L.A., Brandt, U., and Trumpower, B.L. (1994). Protease maturation of the Rieske iron-sulphur protein after its insertion into the mitochondrial cytochrome bc1 complex of *Saccharomyces cerevisiae*. *Biochemical Society transactions* 22, 188-191.
- Granatiero, V., Pacifici, M., Raffaello, A., De Stefani, D., and Rizzuto, R. (2019). Overexpression of Mitochondrial Calcium Uniporter Causes Neuronal Death. *Oxidative medicine and cellular longevity* 2019, 1681254.

Greggio, C., Jha, P., Kulkarni, S.S., Lagarrigue, S., Broskey, N.T., Boutant, M., Wang, X., Conde Alonso, S., Ofori, E., Auwerx, J., et al. (2017). Enhanced Respiratory Chain Supercomplex Formation in Response to Exercise in Human Skeletal Muscle. *Cell metabolism* 25, 301-311.

Große, L., Wurm, C.A., Brüser, C., Neumann, D., Jans, D.C., and Jakobs, S. (2016). Bax assembles into large ring-like structures remodeling the mitochondrial outer membrane in apoptosis. *The EMBO journal* 35, 402-413.

Gruschke, S., Kehrein, K., Römpler, K., Gröne, K., Israel, L., Imhof, A., Herrmann, J.M., Ott, M. (2011). Cbp3–Cbp6 interacts with the yeast mitochondrial ribosomal tunnel exit and promotes cytochrome b synthesis and assembly. *J Cell Biol.* 193, 101-114.

Gu, J., Wu, M., Guo, R., Yan, K., Lei, J., Gao, N., Yang, M. (2016). The architecture of the mammalian respirasome. *Nature* 537, 639-643.

Guarani, V., McNeill, E.M., Paulo, J.A., Huttlin, E.L., Frohlich, F., Gygi, S.P., Van Vactor, D., and Harper, J.W. (2015). QIL1 is a novel mitochondrial protein required for MICOS complex stability and cristae morphology. *Elife* 4.

Guarani, V., Paulo, J., Zhai, B., Huttlin, E.L., Gygi, S.P., and Harper, J.W. (2014). TIMMDC1/C3orf1 functions as a membrane-embedded mitochondrial complex I assembly factor through association with the MCIA complex. *Mol Cell Biol* 34, 847-861.

Guaras, A., Perales-Clemente, E., Calvo, E., Acin-Perez, R., Loureiro-Lopez, M., Pujol, C., Martinez-Carrascoso, I., Nunez, E., Garcia-Marques, F., Rodriguez-Hernandez, M.A., et al. (2016). The CoQH2/CoQ Ratio Serves as a Sensor of Respiratory Chain Efficiency. *Cell reports* 15, 197-209.

Guerrero-Castillo, S., Baertling, F., Kownatzki, D., Wessels, H.J., Arnold, S., Brandt, U., and Nijtmans, L. (2017). The Assembly Pathway of Mitochondrial Respiratory Chain Complex I. *Cell metabolism* 25, 128-139.

Gunter, T.E., and Pfeiffer, D.R. (1990). Mechanisms by which mitochondria transport calcium. *The American journal of physiology* 258, C755-786.

Guo, R., Zong, S., Wu, M., Gu, J., Yang, M. (2017). Architecture of Human Mitochondrial Respiratory Megacomplex I2III2IV2. *Cell.* 170, 1247-1257.

Gusic, M., Schottmann, G., Feichtinger, R.G., Du, C., Scholz, C., Wagner, M., Mayr, J.A., Lee, C.Y., Yépez, V.A., Lorenz, N., et al. (2020). Bi-Allelic UQCRFS1 Variants Are Associated with Mitochondrial Complex III Deficiency, Cardiomyopathy, and Alopecia Totalis. *American journal of human genetics* 106, 102-111.

Gustafsson, C.M., Falkenberg, M., and Larsson, N.G. (2016). Maintenance and Expression of Mammalian Mitochondrial DNA. *Annual review of biochemistry* 85, 133-160.

Haack, T.B., Danhauser, K., Haberberger, B., Hoser, J., Strecker, V., Boehm, D., Uziel, G., Lamantea, E., Invernizzi, F., Poulton, J., et al. (2010). Exome sequencing identifies ACAD9 mutations as a cause of complex I deficiency. *Nature genetics* 42, 1131-1134.

- Habersetzer, J., Ziani, W., Larrieu, I., Stines-Chaumeil, C., Giraud, M.F., Brèthes, D., Dautant, A., and Paumard, P. (2013). ATP synthase oligomerization: from the enzyme models to the mitochondrial morphology. *The international journal of biochemistry & cell biology* 45, 99-105.
- Habibzadeh, P., Inaloo, S., Silawi, M., Dastsooz, H., Farazi Fard, M.A., Sadeghipour, F., Faghihi, Z., Rezaeian, M., Yavarian, M., Böhm, J., et al. (2019). A Novel TTC19 Mutation in a Patient With Neurological, Psychological, and Gastrointestinal Impairment. *Frontiers in neurology* 10, 944.
- Hackenbrock, C., Chazotte, B., Gupte, S.S. (1986). The random collision model and a critical assessment of diffusion and collision in mitochondrial electron transport. *J Bioenerg Biomembr*.
- Hallberg, B., and Larsson, N.G. (2014). Making proteins in the powerhouse. *Cell Metab.* 20, 226–240.
- Hallmann, K., Kudin, A. P., Zsurka, G., Kornblum, C., Reimann, J., Stuve, B., Waltz, S., Hattingen, E., Thiele, H., Nurnberg, P., Rub, C., Voos, W., Kopatz, J., Neumann, H., Kunz, W. S. (2016). Loss of the smallest subunit of cytochrome c oxidase, COX8A, causes Leigh-like syndrome and epilepsy. *Brain* 139: 338-345.
- Hanna, M.G., Nelson I.P., Rahman S., Lane R.J., Land J., Heales S., Cooper M.J., Schapira A.H., Morgan-Hughes J.A., Wood N.W. (1998). Cytochrome c oxidase deficiency associated with the first stop-codon point mutation in human mtDNA. *Am J Hum Genet.* 63, 29-36.
- Hao, H.-X., Khalimonchuk, O., Schraders, M., Dephoure, N., Bayley, J.-P., Kunst, H., Devilee, P., Cremers, C. W. R. J., Schiffman, J. D., Bentz, B. G., Gygi, S. P., Winge, D. R., Kremer H., Rutter, J. (2009). SDH5, a gene required for flavination of succinate dehydrogenase, is mutated in paraganglioma. *Science (New York, N.Y.)* 325, 1139-1142.
- Hartley, A.M., Lukoyanova, N., Zhang, Y., Cabrera-Orefice, A., Arnold, S., Meunier, B., Pinotsis, N., and Maréchal, A. (2019). Structure of yeast cytochrome c oxidase in a supercomplex with cytochrome bc(1). *Nature structural & molecular biology* 26, 78-83.
- Hartley, A.M., Meunier, B., Pinotsis, N., and Maréchal, A. (2020). Rcf2 revealed in cryo-EM structures of hypoxic isoforms of mature mitochondrial III-IV supercomplexes. *Proceedings of the National Academy of Sciences of the United States of America* 117, 9329-9337.
- Hatefi, Y., Haavik, A.G., Fowler, L.R., and Griffiths, D.E. (1962). Studies on the electron transfer system. XLII. Reconstitution of the electron transfer system. *The Journal of biological chemistry* 237, 2661-2669.
- Haut, S., Brivet, M., Touati, G., Rustin, P., Lebon, S., Garcia-Cazorla, A., Saudubray, J. M., Boutron, A., Legrand, A., Slama, A. (2003). A deletion in the human QP-C gene causes a complex III deficiency resulting in hypoglycaemia and lactic acidosis. *Hum. Genet.* 113, 118-122.

Hayashi, T., Asano, Y., Shintani, Y., Aoyama, H., Kioka, H., Tsukamoto, O., Hikita, M., Shinzawa-Itoh, K., Takafuji, K., Higo, S., et al. (2015). Higd1a is a positive regulator of cytochrome c oxidase. *Proceedings of the National Academy of Sciences of the United States of America* 112, 1553-1558.

He, J., Ford, H.C., Carroll, J., Ding, S., Fearnley, I.M., and Walker, J.E. (2017). Persistence of the mitochondrial permeability transition in the absence of subunit c of human ATP synthase. *Proceedings of the National Academy of Sciences of the United States of America* 114, 3409-3414.

He, J., Ford, H.C., Carroll, J., Douglas, C., Gonzales, E., Ding, S., Fearnley, I.M., and Walker, J.E. (2018). Assembly of the membrane domain of ATP synthase in human mitochondria. *Proceedings of the National Academy of Sciences of the United States of America* 115, 2988-2993.

Heide, H., Bleier, L., Steger, M., Ackermann, J., Droese, S., Schwamb, B., Zornig, M., Reichert, A.S., Koch, I., Wittig, I., et al. (2012). Complexome profiling identifies TMEM126B as a component of the mitochondrial complex I assembly complex. *Cell metabolism* 16, 538-549.

Hejzlarová, K., Mráček, T., Vrbacký, M., Kaplanová, V., Karbanová, V., Nůsková, H., Pecina, P., and Houštěk, J. (2014). Nuclear genetic defects of mitochondrial ATP synthase. *Physiological research* 63 Suppl 1, S57-71.

Hell, K., Tzagoloff, A., Neupert, W., Stuart, R.A. (2000). Identification of Cox20p, a novel protein involved in the maturation and assembly of cytochrome oxidase subunit 2. *The Journal of biological chemistry* 275, 4571-4578.

Helling, S., Huttemann, M., Ramzan, R., Kim, S.H., Lee, I., Muller, T., Langenfeld, E., Meyer, H.E., Kadenbach, B., Vogt, S., et al. (2012). Multiple phosphorylations of cytochrome c oxidase and their functions. *Proteomics* 12, 950-959.

Hildenbeutel, M., Hegg, E.L., Stephan, K., Gruschke, S., Meunier, B., Ott, M. (2014). Assembly factors monitor sequential hemylation of cytochrome b to regulate mitochondrial translation. *J Cell Biol.* 205, 511-524.

Hill, B. (1993). The sequence of electron carriers in the reaction of cytochrome c oxidase with oxygen. *J. Bioenerg. Biomembr.* 25, 115-120.

Hill, M.M., Adrain, C., Duriez, P.J., Creagh, E.M., and Martin, S.J. (2004). Analysis of the composition, assembly kinetics and activity of native Apaf-1 apoptosomes. *The EMBO journal* 23, 2134-2145.

Hinson, J.T., Fantin, V.R., Schonberger, J., Breivik, N., Siem, G., McDonough, B., Sharma, P., Keogh, I., Godinho, R., Santos, F., et al. (2007). Missense mutations in the BCS1L gene as a cause of the Bjornstad syndrome. *The New England journal of medicine* 356, 809-819.

Hirst, J., and Roessler, M.M. (2016). Energy conversion, redox catalysis and generation of reactive oxygen species by respiratory complex I. *Biochimica et biophysica acta* 1857, 872-883.

Hiser, L., Di Valentin, M., Hamer, A.G., Hosler, J.P. (2000). Cox11p is required for stable formation of the Cu(B) and magnesium centers of cytochrome c oxidase. *The Journal of biological chemistry* 275, 619-623.

Höchli, M., and Hackenbrock, C. (1979). Lateral translational diffusion of cytochrome c oxidase in the mitochondrial energy-transducing membrane. *PNAS* 76, 1236-1240.

Hock, D.H., Reljic, B., Ang, C.S., Muellner-Wong, L., Mountford, H.S., Compton, A.G., Ryan, M.T., Thorburn, D.R., and Stroud, D.A. (2020). HIGD2A is required for assembly of the COX3 module of human mitochondrial complex IV. *Molecular & cellular proteomics : MCP*.

Hoefs, S.J.G., Dieteren, C.E.J., Distelmaier, F., Janssen, R.J., Eppelen, A., Swarts, H.G.P., Forkink, M., Rodenburg, R.J., Nijtmans, L.G., Willems, P.H., Smeitink, J.A. M., van den Heuvel, L.P. (2008). NDUFA2 complex I mutation leads to Leigh disease. *Am. J. Hum. Genet.* 82: 1306-1315.

Hoefs, S.J.G., van Spronsen, F.J., Lenssen, E.W.H., Nijtmans, L.G., Rodenburg, R.J., Smeitink, J.A.M., van den Heuvel, L.P. (2011). NDUFA10 mutations cause complex I deficiency in a patient with Leigh disease. *Europ. J. Hum. Genet.* 19: 270-274.

Hoffman, N.E., Chandramoorthy, H.C., Shamugapriya, S., Zhang, X., Rajan, S., Mallilankaraman, K., Gandhirajan, R.K., Vagnozzi, R.J., Ferrer, L.M., Sreerishnanilayam, K., et al. (2013). MICU1 motifs define mitochondrial calcium uniporter binding and activity. *Cell reports* 5, 1576-1588.

Hoffmann, A., and Spengler, D. (2018). The Mitochondrion as Potential Interface in Early-Life Stress Brain Programming. *Frontiers in behavioral neuroscience* 12, 306.

Hollenbeck, P.J., and Saxton, W.M. (2005). The axonal transport of mitochondria. *J Cell Sci* 118, 5411-5419.

Horvath, R., Scharfe, C., Hoeltzenbein, M., Do, B.H., Schroder, C., Warzok, R., Vogelgesang, S., Lochmuller, H., Muller-Hocker, J., Gerbitz, K.D. (2002). Childhood onset mitochondrial myopathy and lactic acidosis caused by a stop mutation in the mitochondrial cytochrome c oxidase III gene. *J Med Genet.* 39, 812–816.

Howell, N., Bindoff, L.A., McCullough, D.A., Kubacka, I., Poulton, J., Mackey, D., Taylor, L., and Turnbull, D.M. (1991). Leber hereditary optic neuropathy: identification of the same mitochondrial ND1 mutation in six pedigrees. *American journal of human genetics* 49, 939-950.

Huang, G., and Docampo, R. (2018). The Mitochondrial Ca(2+) Uniporter Complex (MCUC) of *Trypanosoma brucei* Is a Hetero-oligomer That Contains Novel Subunits Essential for Ca(2+) Uptake. *mBio* 9.

Huang, G., Vercesi, A.E., and Docampo, R. (2013). Essential regulation of cell bioenergetics in *Trypanosoma brucei* by the mitochondrial calcium uniporter. *Nature communications* 4, 2865.

- Hunte, C., Zickermann, V., and Brandt, U. (2010). Functional modules and structural basis of conformational coupling in mitochondrial complex I. *Science (New York, N.Y.)* 329, 448-451.
- Hunter, D.R., and Haworth, R.A. (1979). The Ca²⁺-induced membrane transition in mitochondria. I. The protective mechanisms. *Archives of biochemistry and biophysics* 195, 453-459.
- Huynen, M.A., Mühlmeister, M., Gotthardt, K., Guerrero-Castillo, S., and Brandt, U. (2016). Evolution and structural organization of the mitochondrial contact site (MICOS) complex and the mitochondrial intermembrane space bridging (MIB) complex. *Biochimica et biophysica acta* 1863, 91-101.
- Igney, F.H., and Krammer, P.H. (2002). Death and anti-death: tumour resistance to apoptosis. *Nature reviews. Cancer* 2, 277-288.
- Ikon, N., and Ryan, R.O. (2017). Cardiolipin and mitochondrial cristae organization. *Biochimica et biophysica acta. Biomembranes* 1859, 1156-1163.
- Imlay, J. (2006). Iron-sulphur clusters and the problem with oxygen. *Mol Microbiol.* 59, 1073-1082.
- Indrieri, A., van Rahden, V., Tiranti, V., Morleo, M., Iaconis, D., Tammaro, R., D'Amato, I., Conte, I., Maystadt, I., Demuth, S., Zvulunov, A., Kutsche, K., Zeviani, M., Franco, B. (2012). Mutations in COX7B cause microphthalmia with linear skin lesions, an unconventional mitochondrial disease. *Am J Hum Genet.* 91, 942-949.
- Inoue, M., Uchino, S., Iida, A., Noguchi, S., Hayashi, S., Takahashi, T., Fujii, K., Komaki, H., Takeshita, E., Nonaka, I., Okada, Y., Yoshizawa, T., Van Lommel, L., Schuit, F., Goto, Y., Mimaki, M., Nishino, I. (2019). COX6A2 variants cause a muscle-specific cytochrome c oxidase deficiency. *Ann. Neurol.* 86: 193-202.
- Invernizzi, F., Tigano, M., Dallabona, C., Donnini, C., Ferrero, I., Cremonte, M., Ghezzi, D., Lamperti, C., and Zeviani, M. (2013). A homozygous mutation in LYRM7/MZM1L associated with early onset encephalopathy, lactic acidosis, and severe reduction of mitochondrial complex III activity. *Human mutation* 34, 1619-1622.
- Ishigami, I., Zatspein, N.A., Hikita, M., Conrad, C.E., Nelson, G., Coe, J.D., Basu, S., Grant, T.D., Seaberg, M.H., Sierra, R.G., et al. (2017). Crystal structure of CO-bound cytochrome c oxidase determined by serial femtosecond X-ray crystallography at room temperature. *Proceedings of the National Academy of Sciences of the United States of America* 114, 8011-8016.
- Islas-Osuna, M.A., Ellis, T., Mittelmeier, T.M., Dieckmann, C.L. (2003). Suppressor mutations define two regions in the Cbp1 protein important for mitochondrial cytochrome b mRNA stability in *Saccharomyces cerevisiae*. *Current Genetics* 43, 327-336.
- Iverson, T.M. (2013). Catalytic mechanisms of complex II enzymes: a structural perspective. *Biochimica et biophysica acta* 1827, 648-657.
- Iwata, M., Bjorkman, J., and Iwata, S. (1999). Conformational change of the Rieske [2Fe-2S] protein in cytochrome bc1 complex. *J Bioenerg Biomembr* 31, 169-175.

Iwata, S., Lee, J.W., Okada, K., Lee, J.K., Iwata, M., Rasmussen, B., Link, T.A., Ramaswamy, S., and Jap, B.K. (1998). Complete structure of the 11-subunit bovine mitochondrial cytochrome bc₁ complex. *Science (New York, N.Y.)* 281, 64-71.

Janeway, K.A., Kim, S.Y., Lodish, M., Nosé, V., Rustin, P., Gaal, J., Dahia, P.L., Liegl, B., Ball, E.R., Raygada, M., Lai, A.H., Kelly, L., Hornick, J.L., O'Sullivan, M., de Krijger, R.R., Dinjens, W.N., Demetri, G.D., Antonescu, C.R., Fletcher, J.A., Helman, L., Stratakis, C.A. (2011). Defects in succinate dehydrogenase in gastrointestinal stromal tumors lacking KIT and PDGFRA mutations. *Proc Natl Acad Sci U S A* 108:314-8.

Janssen, R.J., Nijtmans, L.G., van den Heuvel, L.P., and Smeitink, J.A. (2006). Mitochondrial complex I: structure, function and pathology. *Journal of inherited metabolic disease* 29, 499-515.

John, G.B., Shang, Y., Li, L., Renken, C., Mannella, C.A., Selker, J.M., Rangell, L., Bennett, M.J., and Zha, J. (2005). The mitochondrial inner membrane protein mitofilin controls cristae morphology. *Molecular biology of the cell* 16, 1543-1554.

Johns, D.R., and Berman, J. (1991). Alternative, simultaneous complex I mitochondrial DNA mutations in Leber's hereditary optic neuropathy. *Biochemical and biophysical research communications* 174, 1324-1330.

Jonckheere, A.I., Hogeveen, M., Nijtmans, L.G., van den Brand, M.A., Janssen, A.J., Diepstra, J.H., van den Brandt, F.C., van den Heuvel, L.P., Hol, F.A., Hofste, T.G., Kapusta, L., Dillmann, U., Shamdeen, M.G., Smeitink, J.A., Rodenburg, R.J. (2008). A novel mitochondrial ATP8 gene mutation in a patient with apical hypertrophic cardiomyopathy and neuropathy. *J Med Genet.* 45, 129-133.

Jonckheere, A.I., Renkema, G.H., Bras, M., van den Heuvel, L.P., Hoischen, A., Gilissen, C., Nabuurs, S.B., Huynen, M.A., de Vries, M.C., Smeitink, J.A., et al. (2013). A complex V ATP5A1 defect causes fatal neonatal mitochondrial encephalopathy. *Brain: a journal of neurology* 136, 1544-1554.

Jonckheere, A.I., Smeitink, J.A., and Rodenburg, R.J. (2012). Mitochondrial ATP synthase: architecture, function and pathology. *Journal of inherited metabolic disease* 35, 211-225.

Jung, D.W., Bradshaw, P.C., and Pfeiffer, D.R. (1997). Properties of a cyclosporin-insensitive permeability transition pore in yeast mitochondria. *The Journal of biological chemistry* 272, 21104-21112.

Kadenbach, B., and Hüttemann, M. (2015). The subunit composition and function of mammalian cytochrome c oxidase. *Mitochondrion* 24, 64-76.

Kaila, V.R., Wikström, M., and Hummer, G. (2014). Electrostatics, hydration, and proton transfer dynamics in the membrane domain of respiratory complex I. *Proceedings of the National Academy of Sciences of the United States of America* 111, 6988-6993.

Kalani, K., Yan, S.F., and Yan, S.S. (2018). Mitochondrial permeability transition pore: a potential drug target for neurodegeneration. *Drug discovery today* 23, 1983-1989.

Kamer, K., Mootha, V.K. (2014). MICU1 and MICU2 play nonredundant roles in the regulation of the mitochondrial calcium uniporter. *EMBO Rep.*, 15, 299-307.

Kamer, K., Sancak, Y., Fomina, Y., Meisel, J.D., Chaudhuri, D., Grabarek, Z., Mootha, V.K. (2018). MICU1 imparts the mitochondrial uniporter with the ability to discriminate between Ca²⁺ and Mn²⁺. *Proceedings of the National Academy of Sciences of the United States of America* 115, E7960-E7969.

Kamer, K.J., and Mootha, V.K. (2015). The molecular era of the mitochondrial calcium uniporter. *Nature reviews. Molecular cell biology* 16, 545-553.

Kamer, K.J., Jiang, W., Kaushik, V.K., Mootha, V.K., and Grabarek, Z. (2019). Crystal structure of MICU2 and comparison with MICU1 reveal insights into the uniporter gating mechanism. *Proceedings of the National Academy of Sciences of the United States of America* 116, 3546-3555.

Kater, L., Wagener, N., Berninghausen, O., Becker, T., Neupert, W., and Beckmann, R. (2020). Structure of the Bcs1 AAA-ATPase suggests an airlock-like translocation mechanism for folded proteins. *Nature structural & molecular biology* 27, 142-149.

Kehrein, K., Schilling R, Möller-Hergt BV, Wurm CA, Jakobs S, Lamkemeyer T, Langer T, Ott M. (2015). Organization of mitochondrial gene expression in two distinct ribosome-containing assemblies. *Cell Rep.* 10, 843-853.

Keightley, J.A., Anitori, R., Burton, M. D., Quan, F., Buist, N. R. M., Kennaway, N. G. (2000). Mitochondrial encephalomyopathy and complex III deficiency associated with a stop-codon mutation in the cytochrome b gene. *Am. J. Hum. Genet.* 67, 1400-1410.

Keilin, D., and Hartree, E.F. (1947). Activity of the cytochrome system in heart muscle preparations. *The Biochemical journal* 41, 500-502.

Kim, H.J., Khalimonchuk, O., Smith, P.M., Winge, D.R. (2012). Structure, function, and assembly of heme centers in mitochondrial respiratory complexes. *Biochimica et Biophysica Acta (BBA) - Molecular Cell Research* 1823, 1604-1616.

Kirby, D.M., McFarland, R., Ohtake, A., Dunning, C., Ryan, M.T., Wilson, C., Ketteridge, D., Turnbull, D.M., Thorburn, D.R., and Taylor, R.W. (2004). Mutations of the mitochondrial ND1 gene as a cause of MELAS. *Journal of medical genetics* 41, 784-789.

Kirichenko, A.V., Pfitzner, U., Ludwig, B., Soares, C.M., Vygodina, T.V., and Konstantinov, A.A. (2005). Cytochrome c oxidase as a calcium binding protein. Studies on the role of a conserved aspartate in helices XI-XII cytoplasmic loop in cation binding. *Biochemistry* 44, 12391-12401.

Kirichok, Y., Krapivinsky, G., and Clapham, D.E. (2004). The mitochondrial calcium uniporter is a highly selective ion channel. *Nature* 427, 360-364.

Koch, J.R., and Schmid, F.X. (2014). Mia40 targets cysteines in a hydrophobic environment to direct oxidative protein folding in the mitochondria. *Nature communications* 5, 3041.

Konig, T., Troder, S.E., Bakka, K., Korwitz, A., Richter-Dennerlein, R., Lampe, P.A., Patron, M., Muhlmeister, M., Guerrero-Castillo, S., Brandt, U., et al. (2016). The m-AAA Protease Associated with Neurodegeneration Limits MCU Activity in Mitochondria. *Molecular cell* 64, 148-162.

Konji, V., Montag, A., Sandri, G., Nordenbrand, K., Ernster, L. (1985). Transport of Ca²⁺ and Mn²⁺ by mitochondria from rat liver, heart and brain. *Biochimie* 67, 1241–1250.

Kovacs-Bogdan, E., Sancak, Y., Kamer, K.J., Plovianich, M., Jambhekar, A., Huber, R.J., Myre, M.A., Blower, M.D., and Mootha, V.K. (2014). Reconstitution of the mitochondrial calcium uniporter in yeast. *Proceedings of the National Academy of Sciences of the United States of America* 111, 8985-8990.

Kraus, F., and Ryan, M.T. (2017). The constriction and scission machineries involved in mitochondrial fission. *J Cell Sci* 130, 2953-2960.

Krause-Buchholz, U., Schöbel, K., Lauffer, S., Rödel, G. (2005). *Saccharomyces cerevisiae* translational activator Cbs1p is associated with translationally active mitochondrial ribosomes. *Biol Chem.* 386, 407-415.

Kremer, L.S., Bader, D.M., Mertes, C., Kopajtich, R., Pichler, G., Iuso, A., Haack, T.B., Graf, E., Schwarzmayr, T., Terrile, C., et al. (2017). Genetic diagnosis of Mendelian disorders via RNA sequencing. *Nature communications* 8, 15824.

Krüger, V., Deckers, M., Hildenbeutel, M., van der Laan, M., Hellmers, M., Dreker, C., Preuss, M., Herrmann, J. M., Rehling, P., Wagner, R., Meinecke, M. (2012). The mitochondrial oxidase assembly protein1 (Oxa1) insertase forms a membrane pore in lipid bilayers. *J Biol Chem* 287(40): 33314-33326.

Kuhlbrandt, W. (2015). Structure and function of mitochondrial membrane protein complexes. *BMC biology* 13, 89.

Kuhlbrandt, W. (2019). Structure and Mechanisms of F-Type ATP Synthases. *Annual review of biochemistry* 88, 515-549.

Kwong, J.Q., Lu, X., Correll, R.N., Schwanekamp, J.A., Vagnozzi, R.J., Sargent, M.A., York, A.J., Zhang, J., Bers, D.M., and Molkentin, J.D. (2015). The Mitochondrial Calcium Uniporter Selectively Matches Metabolic Output to Acute Contractile Stress in the Heart. *Cell reports* 12, 15-22.

Lahiri, S., Toulmay, A., and Prinz, W.A. (2015). Membrane contact sites, gateways for lipid homeostasis. *Current opinion in cell biology* 33, 82-87.

Lam, A.K., and Galione, A. (2013). The endoplasmic reticulum and junctional membrane communication during calcium signaling. *Biochimica et biophysica acta* 1833, 2542-2559.

Lamantea, E., Carrara, F., Mariotti, C., Morandi, L., Tiranti, V., and Zeviani, M. (2002). A novel nonsense mutation (Q352X) in the mitochondrial cytochrome b gene associated with a combined deficiency of complexes I and III. *Neuromuscular disorders: NMD* 12, 49-52.

Lambert, J.P., Luongo, T.S., Tomar, D., Jadiya, P., Gao, E., Zhang, X., Lucchese, A.M., Kolmetzky, D.W., Shah, N.S., and Elrod, J.W. (2019). MCUB Regulates the Molecular Composition of the Mitochondrial Calcium Uniporter Channel to Limit Mitochondrial Calcium Overload During Stress. *Circulation* 140, 1720-1733.

Lambert, J.P., Murray, E.K., and Elrod, J.W. (2020). MCUB and mitochondrial calcium uptake - modeling, function, and therapeutic potential. *Expert opinion on therapeutic targets* 24, 163-169.

Lamperti, C., Diodato D., Lamantea E., Carrara F., Ghezzi D., Mereghetti P., Rizzi R., Zeviani M. (2012). MELAS-like encephalomyopathy caused by a new pathogenic mutation in the mitochondrial DNA encoded cytochrome c oxidase subunit I. *Neuromuscul. Disord.* 22, 990–994.

Lange, C., and Hunte, C. (2002). Crystal structure of the yeast cytochrome bc1 complex with its bound substrate cytochrome c. *Proc Natl Acad Sci U S A.* 99, 2800-2805.

Lapiente-Brun, E., Moreno-Loshuertos, R., Acin-Perez, R., Latorre-Pellicer, A., Colas, C., Balsa, E., Perales-Clemente, E., Quiros, P.M., Calvo, E., Rodriguez-Hernandez, M.A., et al. (2013). Supercomplex assembly determines electron flux in the mitochondrial electron transport chain. *Science (New York, N.Y.)* 340, 1567-1570.

Lasserre, J.P., Dautant, A., Aiyar, R.S., Kucharczyk, R., Glatigny, A., Tribouillard-Tanvier, D., Rytka, J., Blondel, M., Skoczen, N., Reynier, P., et al. (2015). Yeast as a system for modeling mitochondrial disease mechanisms and discovering therapies. *Disease models & mechanisms* 8, 509-526.

Lazarou, M., McKenzie, M., Ohtake, A., Thorburn, D.R., and Ryan, M.T. (2007). Analysis of the assembly profiles for mitochondrial- and nuclear-DNA-encoded subunits into complex I. *Mol Cell Biol* 27, 4228-4237.

Leary, S., Cobine P.A., Kaufman B.A., Guercin G.H., Mattman A., Palaty J., Lockitch G., Winge D.R., Rustin P., Horvath R., Shoubridge E.A. (2007). The human cytochrome c oxidase assembly factors SCO1 and SCO2 have regulatory roles in the maintenance of cellular copper homeostasis. *Cell metabolism* 5, 9-20.

Leary, S., Kaufman B.A., Pellicchia G., Guercin G.H., Mattman A., Jaksch M., Shoubridge EA. (2004). Human SCO1 and SCO2 have independent, cooperative functions in copper delivery to cytochrome c oxidase. *Human molecular genetics* 13, 1839-1848.

Leary, S.C., Sasarman F., Nishimura T., Shoubridge E.A. (2009). Human SCO2 is required for the synthesis of CO II and as a thiol-disulphide oxidoreductase for SCO1. *Hum. Mol. Genet.* 18, 2230–2240.

Lee, I., Bender, E., and Kadenbach, B. (2002). Control of mitochondrial membrane potential and ROS formation by reversible phosphorylation of cytochrome c oxidase. *Molecular and cellular biochemistry* 234-235, 63-70.

Lee, I., Salomon, A.R., Ficarro, S., Mathes, I., Lottspeich, F., Grossman, L.I., and Huttemann, M. (2005). cAMP-dependent tyrosine phosphorylation of subunit I inhibits cytochrome c oxidase activity. *The Journal of biological chemistry* 280, 6094-6100.

Lee, Y., Min, C.K., Kim, T.G., Song, H.K., Lim, Y., Kim, D., Shin, K., Kang, M., Kang, J.Y., Youn, H.S., et al. (2015). Structure and function of the N-terminal domain of the human mitochondrial calcium uniporter. *EMBO reports* 16, 1318-1333.

Lenaz, G., Fato, R., Di Bernardo, S., Jarreta, D., Costa, A., Genova, M.L., Parenti Castelli, G. (1999). Localization and mobility of coenzyme Q in lipid bilayers and membranes. *Biofactors*. 9, 87-93.

Lertrit, P., Noer, A.S., Jean-Francois, M.J., Kapsa, R., Dennett, X., Thyagarajan, D., Lethlean, K., Byrne, E., and Marzuki, S. (1992). A new disease-related mutation for mitochondrial encephalopathy lactic acidosis and strokelike episodes (MELAS) syndrome affects the ND4 subunit of the respiratory complex I. *American journal of human genetics* 51, 457-468.

Letts, J.A., Fiedorczuk, K., Sazanov, L.A. (2016). The architecture of respiratory supercomplexes. *Nature* 537, 644-648.

Letts, J.A., and Sazanov, L.A. (2017). Clarifying the supercomplex: the higher-order organization of the mitochondrial electron transport chain. *Nature structural & molecular biology* 24, 800-808.

Letts, J.A., Fiedorczuk, K., Degliesposti, G., Skehel, M., and Sazanov, L.A. (2019). Structures of Respiratory Supercomplex I+III(2) Reveal Functional and Conformational Crosstalk. *Molecular cell* 75, 1131-1146.e1136.

Levitas, A., Muhammad, E., Harel, G., Saada, A., Caspi, V.C., Manor, E., Beck, J.C., Sheffield, V., and Parvari, R. (2010). Familial neonatal isolated cardiomyopathy caused by a mutation in the flavoprotein subunit of succinate dehydrogenase. *Eur J Hum Genet* 18:1160-5.

Lewis-Smith, D., Kamer, K.J., Griffin, H., Childs, A.M., Pysden, K., Titov, D., Duff, J., Pyle, A., Taylor, R.W., Yu-Wai-Man, P., et al. (2016). Homozygous deletion in MICU1 presenting with fatigue and lethargy in childhood. *Neurology. Genetics* 2, e59.

Lim, S.K., Stroud, D.A., Compton, A.G., Tucker, E.J., Dasvarma, A., Gandolfo, L.C., Marum, J.E., McKenzie, M., Peters, H.L., Mowat, D., Procopis, P.G., Wilcken, B., Christodoulou, J., Brown, G.K., Ryan, M.T., Bahlo, M., Thorburn, D.R. (2014). A founder mutation in PET100 causes isolated complex IV deficiency in Lebanese individuals with Leigh syndrome. *Am J Hum Genet.* 94, 209-222.

Liolitsa, D., Rahman, S., Benton, S., Carr, L.J., and Hanna, M.G. (2003). Is the mitochondrial complex I ND5 gene a hot-spot for MELAS causing mutations? *Annals of neurology* 53, 128-132.

Liu, J.C., Liu, J., Holmstrom, K.M., Menazza, S., Parks, R.J., Fergusson, M.M., Yu, Z.X., Springer, D.A., Halsey, C., Liu, C., et al. (2016). MICU1 Serves as a Molecular Gatekeeper to Prevent In Vivo Mitochondrial Calcium Overload. *Cell reports* 16, 1561-1573.

Liu, J.C., Parks, R.J., Liu, J., Stares, J., Rovira, II, Murphy, E., and Finkel, T. (2017). The In Vivo Biology of the Mitochondrial Calcium Uniporter. *Advances in experimental medicine and biology* 982, 49-63.

Liu, J.C., Syder, N.C., Ghorashi, N.S., Willingham, T.B., Parks, R.J., Sun, J., Fergusson, M.M., Liu, J., Holmstrom, K.M., Menazza, S., et al. (2020a). EMRE is essential for mitochondrial calcium uniporter activity in a mouse model. *JCI insight* 5.

Liu, Y., Jin, M., Wang, Y., Zhu, J., Tan, R., Zhao, J., Ji, X., Jin, C., Jia, Y., Ren, T., et al. (2020b). MCU-induced mitochondrial calcium uptake promotes mitochondrial biogenesis and colorectal cancer growth. *Signal transduction and targeted therapy* 5, 59.

Llorente-Garcia, I., Lenn, T., Erhardt, H., Harriman, O.L., Liu, L.N., Robson, A., Chiu, S.W., Matthews, S., Willis, N.J., Bray, C.D., et al. (2014). Single-molecule in vivo imaging of bacterial respiratory complexes indicates delocalized oxidative phosphorylation. *Biochimica et biophysica acta* 1837, 811-824.

Lobo-Jarne, T., and Ugalde, C. (2018). Respiratory chain supercomplexes: Structures, function and biogenesis. *Seminars in cell & developmental biology* 76, 179-190.

Lobo-Jarne, T., Nyvltova, E., Perez-Perez, R., Timon-Gomez, A., Molinie, T., Choi, A., Mourier, A., Fontanesi, F., Ugalde, C., and Barrientos, A. (2018). Human COX7A2L Regulates Complex III Biogenesis and Promotes Supercomplex Organization Remodeling without Affecting Mitochondrial Bioenergetics. *Cell reports* 25, 1786-1799.e1784.

Lobo-Jarne, T., Pérez-Pérez, R., Fontanesi, F., Timón-Gómez, A., Wittig, I., Peñas, A., Serrano-Lorenzo, P., García-Consuegra, I., Arenas, J., Martín, M.A., et al. (2020). Multiple pathways coordinate assembly of human mitochondrial complex IV and stabilization of respiratory supercomplexes. *The EMBO journal* 39, e103912.

Lodish, H., Berk, A., Zipursky, S.L., Matsudaira, P., Baltimore, D., and Darnell, J. (2000). *Molecular Cell Biology*, 4th edition (New York: W. H. Freeman).

Loeffen, J., Elpeleg, O., Smeitink, J., Smeets, R., Stöckler-Ipsiroglu, S., Mandel, H., Sengers, R., Trijbels, F., and van den Heuvel, L. (2001). Mutations in the complex I NDUFS2 gene of patients with cardiomyopathy and encephalomyopathy. *Annals of neurology* 49, 195-201.

Loeffen, J., Smeitink, J., Triepels, R., Smeets, R., Schuelke, M., Sengers, R., Trijbels, F., Hamel, B., Mullaart, R., and van den Heuvel, L. (1998). The first nuclear-encoded complex I mutation in a patient with Leigh syndrome. *American journal of human genetics* 63, 1598-1608.

Logan, C.V., Szabadkai, G., Sharpe, J.A., Parry, D.A., Torelli, S., Childs, A.M., Kriek, M., Phadke, R., Johnson, C.A., Roberts, N.Y., et al. (2014). Loss-of-function mutations in MICU1 cause a brain and muscle disorder linked to primary alterations in mitochondrial calcium signaling. *Nature genetics* 46, 188-193.

Lopez-Fabuel, I., Le Douce, J., Logan, A., James, A.M., Bonvento, G., Murphy, M.P., Almeida, A., and Bolanos, J.P. (2016). Complex I assembly into supercomplexes determines

differential mitochondrial ROS production in neurons and astrocytes. *Proceedings of the National Academy of Sciences of the United States of America* 113, 13063-13068.

López-Gallardo, E., Solano, A., Herrero-Martín, M.D., Martínez-Romero, I., Castaño-Pérez, M.D., Andreu, A.L., Herrera, A., López-Pérez, M.J., Ruiz-Pesini, E., and Montoya, J. (2009). NARP syndrome in a patient harbouring an insertion in the MT-ATP6 gene that results in a truncated protein. *Journal of medical genetics* 46, 64-67.

Lorenzi, I., Oeljeklaus S., Aich A., Ronsör C., Callegari S., Dudek J., Warscheid B., Dennerlein S., Rehling P. (2018). The mitochondrial TMEM177 associates with COX20 during COX2 biogenesis. *Biochim Biophys Acta Mol Cell Res.* 1865, 323-333.

Luongo, T.S., Lambert, J.P., Yuan, A., Zhang, X., Gross, P., Song, J., Shanmughapriya, S., Gao, E., Jain, M., Houser, S.R., et al. (2015). The Mitochondrial Calcium Uniporter Matches Energetic Supply with Cardiac Workload during Stress and Modulates Permeability Transition. *Cell reports* 12, 23-34.

Lytovchenko, O., Naumenko, N., Oeljeklaus, S., Schmidt, B., von der Malsburg, K., Deckers, M., Warscheid, B., van der Laan, M., Rehling, P. (2014) The INA complex facilitates assembly of the peripheral stalk of the mitochondrial F₁F_o-ATP synthase. *EMBO J* 33:1624–1638.

Maarse, A.C., and Grivell, L.A. (1987). Nucleotide sequence of the gene encoding the 11-kDa subunit of the ubiquinol-cytochrome-c oxidoreductase in *Saccharomyces cerevisiae*. *European journal of biochemistry* 165, 419-425.

Maas, M.F., Krause, F., Dencher, N.A., and Sainsard-Chanet, A. (2009). Respiratory complexes III and IV are not essential for the assembly/stability of complex I in fungi. *Journal of molecular biology* 387, 259-269.

Maio, N., Ghezzi D., Verrigni D., Rizza T., Bertini E., Martinelli D., Zeviani M., Singh A., Carozzo R., Rouault T.A. (2016). Disease- Causing SDHAF1 Mutations Impair Transfer of Fe-S Clusters to SDHB. *Cell Metab.* 23, 292-302.

Maio, N., Rouault T.A. (2015). Iron –sulfur cluster biogenesis in mammalian cells: New insights into the molecular mechanisms of cluster delivery. *Biochimica et Biophysica Acta (BBA) - Bioenergetics* 6, 1493-1512.

Mallilankaraman, K., Doonan, P., Cárdenas, C., Chandramoorthy, H.C., Müller, M., Miller, R., Hoffman, N.E., Gandhirajan, R.K., Molgó, J., Birnbaum, M.J., Rothberg, B.S., Mak, D.O., Foskett, J.K., Madesh, M. (2012). MICU1 is an essential gatekeeper for MCU-mediated mitochondrial Ca(2+) uptake that regulates cell survival. *Cell* 151, 630-644.

Mallilankaraman, K., Cardenas, C., Doonan, P.J., Chandramoorthy, H.C., Irrinki, K.M., Golenar, T., Csordas, G., Madireddi, P., Yang, J., Muller, M., et al. (2012). MCUR1 is an essential component of mitochondrial Ca²⁺ uptake that regulates cellular metabolism. *Nat Cell Biol* 14, 1336-1343.

Mansilla, N., Racca S., Gras D.E., Gonzalez D.H., Welchen E. (2018). The Complexity of Mitochondrial Complex IV: An Update of Cytochrome c Oxidase Biogenesis in Plants. *Int J Mol Sci.* 19.

Maranzana, E., Barbero, G., Falasca, A.I., Lenaz, G., and Genova, M.L. (2013). Mitochondrial respiratory supercomplex association limits production of reactive oxygen species from complex I. *Antioxidants & redox signaling* 19, 1469-1480.

Marcet-Houben M, M.G., Gabaldón T. (2009). Phylogenomics of the oxidative phosphorylation in fungi reveals extensive gene duplication followed by functional divergence. *BMC Evol Biol.* 9.

Marechal, A., Iwaki, M., and Rich, P.R. (2013). Structural changes in cytochrome c oxidase induced by binding of sodium and calcium ions: an ATR-FTIR study. *Journal of the American Chemical Society* 135, 5802-5807.

Margulis, L. (1970). *Origin of eukaryotic cells: evidence and research implications for a theory of the origin and evolution of microbial, plant, and animal cells on the Precambrian earth.* (New Haven: Yale University Press).

Marotta, R., Chin, J., Kirby, D.M., Chiotis, M., Cook, M., Collins, S.J. (2011). Novel single base pair COX III subunit deletion of mitochondrial DNA associated with rhabdomyolysis. *J. Clin. Neurosci.* 18, 290–292.

Martinez Lyons, A., Ardisson, A., Reyes, A., Robinson, A.J., Moroni, I., Ghezzi, D., Fernandez-Vizarrá, E., Zeviani, M. (2016). COA7 (C1orf163/RESA1) mutations associated with mitochondrial leukoencephalopathy and cytochrome c oxidase deficiency. *J Med Genet.* 53, 846-849.

Massa, V., Fernandez-Vizarrá, E., Alshahwan, S., Bakhsh, E., Goffrini, P., Ferrero, I., Mereghetti, P., D'Adamo, P., Gasparini, P., Zeviani, M. (2008). Severe infantile encephalomyopathy caused by a mutation in COX6B1, a nucleus-encoded subunit of cytochrome c oxidase. *Am J Hum Genet.* 82, 1281-1289.

Matesanz-Isabel, J., Arias-del-Val, J., Alvarez-Illera, P., Fonteriz, R.I., Montero, M., Alvarez, J. (2016). Functional roles of MICU1 and MICU2 in mitochondrial Ca(2+) uptake. *Biochim Biophys Acta.* 1858, 1110-1117.

Mathieu, L., Marsy, S., Saint-Georges, Y., Jacq, C., Dujardin, G. (2011). A transcriptome screen in yeast identifies a novel assembly factor for the mitochondrial complex III. *Mitochondrion* 11, 391-396.

Mayr, J.A., Havlíčková, V., Zimmermann, F., Magler, I., Kaplanová, V., Jesina, P., Pecinová, A., Nusková, H., Koch, J., Sperl, W., Houstek, J. (2010). Mitochondrial ATP synthase deficiency due to a mutation in the ATP5E gene for the F1 epsilon subunit. *Human molecular genetics* 19, 3430-3439.

McEwen, J., Hong, K.H., Park, S., Preciado, G.T. (1993). Sequence and chromosomal localization of two PET genes required for cytochrome c oxidase assembly in *Saccharomyces cerevisiae*. *Curr Genet.* 23, 9-14.

McFarland, R., Kirby, D.M., Fowler, K.J., Ohtake, A., Ryan, M.T., Amor, D.J., Fletcher, J.M., Dixon, J.W., Collins, F.A., Turnbull, D.M., et al. (2004). De novo mutations in the

mitochondrial ND3 gene as a cause of infantile mitochondrial encephalopathy and complex I deficiency. *Annals of neurology* 55, 58-64.

McKenzie, M., Lazarou, M., Thorburn, D.R., and Ryan, M.T. (2006). Mitochondrial respiratory chain supercomplexes are destabilized in Barth Syndrome patients. *Journal of molecular biology* 361, 462-469.

McKenzie, M., Tucker, E.J., Compton, A.G., Lazarou, M., George, C., Thorburn, D.R., and Ryan, M.T. (2011). Mutations in the gene encoding C8orf38 block complex I assembly by inhibiting production of the mitochondria-encoded subunit ND1. *Journal of molecular biology* 414, 413-426.

McWhinney, S.R., Pasini, B., Stratakis, C.A. (2007). Familial gastrointestinal stromal tumors and germ-line mutations. *N Engl J Med* 357:1054-6.

Melchionda, L., Haack, T.B., Hardy, S., Abbink, T.E., Fernandez-Vizarra, E., Lamantea, E. (2014). Mutations in APOPT1, encoding a mitochondrial protein, cause cavitating leukoencephalopathy with cytochrome c oxidase deficiency. *Am J Hum Genet.* 95, 315–325.

Meng, H., Yamashita, C., Shiba-Fukushima, K., Inoshita, T., Funayama, M., Sato, S., Hatta, T., Natsume, T., Umitsu, M., Takagi, J., et al. (2017). Loss of Parkinson's disease-associated protein CHCHD2 affects mitochondrial crista structure and destabilizes cytochrome c. *Nature communications* 8, 15500.

Michel, H. (1999). Proton pumping by cytochrome c oxidase. *Nature* 402, 602-603.

Mick, D., Dennerlein S, Wiese H, Reinhold R, Pacheu-Grau D, Lorenzi I, Sasarman F, Weraarpachai W, Shoubridge EA, Warscheid B, Rehling P. (2012). MITRAC links mitochondrial protein translocation to respiratory-chain assembly and translational regulation. *Cell* 15, 1528-1541.

Mick, D., Vukotic M, Piechura H, Meyer HE, Warscheid B, Deckers M, Rehling P. (2010). Coa3 and Cox14 are essential for negative feedback regulation of COX1 translation in mitochondria. *J Cell Biol.* 191, 141-154.

Milenkovic, D., Blaza, J.N., Larsson, N.G., and Hirst, J. (2017). The Enigma of the Respiratory Chain Supercomplex. *Cell metabolism* 25, 765-776.

Milenkovic, D., Ramming, T., Muller, J.M., Wenz, L.S., Gebert, N., Schulze-Specking, A., Stojanovski, D., Rospert, S., and Chacinska, A. (2009). Identification of the signal directing Tim9 and Tim10 into the intermembrane space of mitochondria. *Molecular biology of the cell* 20, 2530-2539.

Mileykovskaya, E., Penczek, P.A., Fang, J., Mallampalli, V.K., Sparagna, G.C., and Dowhan, W. (2012). Arrangement of the respiratory chain complexes in *Saccharomyces cerevisiae* supercomplex III₂IV₂ revealed by single particle cryo-electron microscopy. *The Journal of biological chemistry* 287, 23095-23103.

Mitchell, P. (1976). Possible molecular mechanisms of the protonmotive function of cytochrome systems. *Journal of theoretical biology* 62, 327-367.

- Miyake, N., Yano, S., Sakai, C., Hatakeyama, H., Matsushima, Y., Shiina, M., Watanabe, Y., Bartley, J., Abdenur, J. E., Wang, R. Y., Chang, R., Tsurusaki, Y., Doi, H., Nakashima, M., Saito, H., Ogata, K., Goto, Y., Matsumoto, N. (2013). Mitochondrial Complex III Deficiency Caused by a Homozygous UQCRC2 Mutation Presenting with Neonatal-Onset Recurrent Metabolic Decompensation Hum. Mutat. 34, 446-452.
- Mkaouar-Rebai E., E.E., Chamkha I., Kammoun F., Triki C., Fakhfakh F. (2011). Molecular-clinical correlation in a family with a novel heteroplasmic Leigh syndrome missense mutation in the mitochondrial cytochrome c oxidase III gene. J. Child Neurol. 26, 12-20.
- Montero, M., Alonso, M.T., Carnicero, E., Cuchillo-Ibanez, I., Albillos, A., Garcia, A.G., Garcia-Sancho, J., and Alvarez, J. (2000). Chromaffin-cell stimulation triggers fast millimolar mitochondrial Ca²⁺ transients that modulate secretion. Nat Cell Biol 2, 57-61.
- Moran, M., Marin-Buera, L., Gil-Borlado, M.C., Rivera, H., Blazquez, A., Seneca, S., Vazquez-Lopez, M., Arenas, J., Martin, M.A., and Ugalde, C. (2010). Cellular pathophysiological consequences of BCS1L mutations in mitochondrial complex III enzyme deficiency. Human mutation 31, 930-941.
- Mordas, A., and Tokatlidis, K. (2015). The MIA pathway: a key regulator of mitochondrial oxidative protein folding and biogenesis. Accounts of chemical research 48, 2191-2199.
- Mordaunt, D.A., Jolley, A., Balasubramaniam, S., Thorburn, D.R., Mountford, H.S., Compton, A.G., Nicholl, J., Manton, N., Clark, D., Bratkovic, D., et al. (2015). Phenotypic variation of TTC19-deficient mitochondrial complex III deficiency: a case report and literature review. American journal of medical genetics. Part A 167, 1330-1336.
- Moreno-Lastres, D., Fontanesi, F., Garcia-Consuegra, I., Martin, M.A., Arenas, J., Barrientos, A., and Ugalde, C. (2012). Mitochondrial complex I plays an essential role in human respirasome assembly. Cell metabolism 15, 324-335.
- Mori, M., Terada, K. (1998). Mitochondrial protein import in animals. Biochimica et biophysica acta 1403, 12-27.
- Morino, H., Miyamoto, R., Ohnishi, S., Maruyama, H., Kawakami, H. (2014). Exome sequencing reveals a novel TTC19 mutation in an autosomal recessive spinocerebellar ataxia patient. BMC Neurol. 14.
- Mourier, A., Matic, S., Ruzzenente, B., Larsson, N.G., and Milenkovic, D. (2014). The respiratory chain supercomplex organization is independent of COX7a2l isoforms. Cell metabolism 20, 1069-1075.
- Munnich, A., Rustin, P. (2001). Clinical spectrum and diagnosis of mitochondrial disorders. Am J Med Genet. 106, 4-17.
- Munujos, P., Coll-Canti, J., Gonzalez-Sastre, F., and Gella, F.J. (1993). Assay of succinate dehydrogenase activity by a colorimetric-continuous method using iodinitrotetrazolium chloride as electron acceptor. Anal Biochem 212, 506-509.

- Murphy, A.N., Kelleher, J.K., and Fiskum, G. (1990). Submicromolar Ca^{2+} regulates phosphorylating respiration by normal rat liver and AS-30D hepatoma mitochondria by different mechanisms. *The Journal of biological chemistry* 265, 10527-10534.
- Murphy, E., Pan, X., Nguyen, T., Liu, J., Holmstrom, K.M., and Finkel, T. (2014). Unresolved questions from the analysis of mice lacking MCU expression. *Biochemical and biophysical research communications* 449, 384-385.
- Musa, S., Eyaid, W., Kamer, K., Ali, R., Al-Mureikhi, M., Shahbeck, N., Al Mesaifri, F., Makhseed, N., Mohamed, Z., AlShehhi, W.A., et al. (2019). A Middle Eastern Founder Mutation Expands the Genotypic and Phenotypic Spectrum of Mitochondrial MICU1 Deficiency: A Report of 13 Patients. *JIMD reports* 43, 79-83.
- Naithani, S., Saracco, S.A., Butler, C.A., and Fox, T.D. (2003). Interactions among COX1, COX2, and COX3 mRNA-specific translational activator proteins on the inner surface of the mitochondrial inner membrane of *Saccharomyces cerevisiae*. *Mol. Biol. Cell* 14, 324-333.
- Ndi, M., Marin-Buera, L., Salvatori, R., Singh, A.P., and Ott, M. (2018). Biogenesis of the bcl Complex of the Mitochondrial Respiratory Chain. *Journal of molecular biology* 430, 3892-3905.
- Neupert, W. (1997). Protein import into mitochondria. *Annu Rev Biochem.* 66, 863-917.
- Nicholls, D.G. (1974). The influence of respiration and ATP hydrolysis on the proton-electrochemical gradient across the inner membrane of rat-liver mitochondria as determined by ion distribution. *European journal of biochemistry* 50, 305-315.
- Nichols, B.J., and Denton, R.M. (1995). Towards the molecular basis for the regulation of mitochondrial dehydrogenases by calcium ions. *Molecular and cellular biochemistry* 149-150, 203-212.
- Nijtmans, L.G., Taanman, J., Muijsers, A.O., Speijer, D., Van den Bogert, C. (1998). Assembly of cytochrome-c oxidase in cultured human cells. *Eur J Biochem.* 254, 389-394.
- Nishigaki, Y., Ueno, H., Coku, J., Koga, Y., Fujii, T., Sahashi, K., Nakano, K., Yoneda, M., Nonaka, M., Tang, L. (2010). Extensive screening system using suspension array technology to detect mitochondrial DNA point mutations. *Mitochondrion* 10, 300-308.
- Nobrega, F., Nobrega, M.P., Tzagoloff, A. (1992). BCS1, a novel gene required for the expression of functional Rieske iron-sulfur protein in *Saccharomyces cerevisiae*. *EMBO J.* 11, 3821-3829.
- Nobrega, F.G., and Tzagoloff, A. (1980). Assembly of the mitochondrial membrane system. DNA sequence and organization of the cytochrome b gene in *Saccharomyces cerevisiae* D273-10B. *The Journal of biological chemistry* 255, 9828-9837.
- Nobrega, M., Bandeira, S.C., Beers, J., Tzagoloff, A. (2002). Characterization of COX19, a widely distributed gene required for expression of mitochondrial cytochrome oxidase. *The Journal of biological chemistry* 277, 40206-40211.

Nobrega, M., Nobrega, F.G., Tzagoloff, A. (1990). COX10 codes for a protein homologous to the ORF1 product of *Paracoccus denitrificans* and is required for the synthesis of yeast cytochrome oxidase. *The Journal of biological chemistry* 265, 14220-14226.

Nogueira, C., Barros, J., Sa, M. J., Azevedo, L., Taipa, R., Torraco, A., Meschini, M. C., Verrigni, D., Nesti, C., Rizza, T., Teixeira, J., Carozzo, R., Pires, M. M., Vilarinho, L., Santorelli, F. M. (2013). Novel TTC19 mutation in a family with severe psychiatric manifestations and complex III deficiency. *Neurogenetics* 14, 153-160.

Nouet, C., Truan, G., Mathieu, L., Dujardin, G. (2009). Functional analysis of yeast *bcs1* mutants highlights the role of Bcs1p-specific amino acids in the AAA domain. *Journal of molecular biology* 388, 252-261.

Nouws, J., Nijtmans, L., Houten, S.M., van den Brand, M., Huynen, M., Venselaar, H., Hoefs, S., Gloerich, J., Kronick, J., Hutchin, T., et al. (2010). Acyl-CoA dehydrogenase 9 is required for the biogenesis of oxidative phosphorylation complex I. *Cell metabolism* 12, 283-294.

Ogilvie, I., Kennaway, N.G., and Shoubridge, E.A. (2005). A molecular chaperone for mitochondrial complex I assembly is mutated in a progressive encephalopathy. *The Journal of clinical investigation* 115, 2784-2792.

Ogun, A.S., Valentine, M. (2019). *Biochemistry, Heme Synthesis*. StatPearls Publishing.

Oka, T., Sayano, T., Tamai, S., Yokota, S., Kato, H., Fujii, G., and Mihara, K. (2008). Identification of a novel protein MICS1 that is involved in maintenance of mitochondrial morphology and apoptotic release of cytochrome c. *Molecular biology of the cell* 19, 2597-2608.

Oláhová, M., Ceccatelli Berti, C., Collier, J.J., Alston, C.L., Jameson, E., Jones, S.A., Edwards, N., He, L., Chinnery, P.F., Horvath, R., et al. (2019). Molecular genetic investigations identify new clinical phenotypes associated with BCS1L-related mitochondrial disease. *Human molecular genetics* 28, 3766-3776.

Oláhová, M., Haack, T.B., Alston, C.L., Houghton, J.A., He, L., Morris, A.A., Brown, G.K., McFarland, R., Chrzanowska-Lightowlers, Z.M., Lightowlers, R.N., et al. (2015). A truncating PET100 variant causing fatal infantile lactic acidosis and isolated cytochrome c oxidase deficiency. *European journal of human genetics: EJHG* 23, 935-939.

Olenych, S.G., Claxton, N.S., Ottenberg, G.K., and Davidson, M.W. (2007). The fluorescent protein color palette. *Current protocols in cell biology* Chapter 21, Unit 21.25.

Olsen, J.V., Vermeulen, M., Santamaria, A., Kumar, C., Miller, M.L., Jensen, L.J., Gnad, F., Cox, J., Jensen, T.S., Nigg, E.A., et al. (2010). Quantitative phosphoproteomics reveals widespread full phosphorylation site occupancy during mitosis. *Science signaling* 3, ra3.

Ostergaard, E., Rodenburg, R. J., van den Brand, M., Thomsen, L. L., Duno, M., Batbayli, M., Wibrand, F., Nijtmans, L. (2011) Respiratory chain complex I deficiency due to NDUFA12 mutations as a new cause of Leigh syndrome. *J. Med. Genet.* 48: 737-740.

Ott, C., Dorsch, E., Fraunholz, M., Straub, S., and Kozjak-Pavlovic, V. (2015). Detailed analysis of the human mitochondrial contact site complex indicate a hierarchy of subunits. *PLoS One* 10, e0120213.

Oudshoorn, P., Van Steeg, H., Swinkels, B.W., Schoppink, P., and Grivell, L.A. (1987). Subunit II of yeast QH2:cytochrome-c oxidoreductase. Nucleotide sequence of the gene and features of the protein. *European journal of biochemistry* 163, 97-103.

Oxenoid, K., Dong, Y., Cao, C., Cui, T., Sancak, Y., Markhard, A.L., Grabarek, Z., Kong, L., Liu, Z., Ouyang, B., et al. (2016). Architecture of the mitochondrial calcium uniporter. *Nature* 533, 269-273.

Pacheu-Grau, D., Bareth, B., Dudek, J., Juris, L., Vögtle, F.N., Wissel, M., Leary, S.C., Dennerlein, S., Rehling, P., Deckers, M. (2015). Cooperation between COA6 and SCO2 in COX2 maturation during cytochrome c oxidase assembly links two mitochondrial cardiomyopathies. *Cell metabolism* 21, 823-833.

Pagliarini, D.J., Calvo, S.E., Chang, B., Sheth, S.A., Vafai, S.B., Ong, S.E., Walford, G.A., Sugiana, C., Boneh, A., Chen, W.K., et al. (2008). A mitochondrial protein compendium elucidates complex I disease biology. *Cell* 134, 112-123.

Paillard, M., Csordas, G., Huang, K.T., Varnai, P., Joseph, S.K., and Hajnoczky, G. (2018). MICU1 Interacts with the D-Ring of the MCU Pore to Control Its Ca(2+) Flux and Sensitivity to Ru360. *Molecular cell* 72, 778-785.e773.

Paillusson, S., Stoica, R., Gomez-Suaga, P., Lau, D.H.W., Mueller, S., Miller, T., and Miller, C.C.J. (2016). There's Something Wrong with my MAM; the ER-Mitochondria Axis and Neurodegenerative Diseases. *Trends in neurosciences* 39, 146-157.

Palade, G.E. (1953). An electron microscope study of the mitochondrial structure. *The journal of histochemistry and cytochemistry: official journal of the Histochemistry Society* 1, 188-211.
Palmieri F, P.C. (2010). Mitochondrial metabolite transport. *Essays Biochem.* 47, 37-52.

Palmieri, L., Pardo, B., Lasorsa, F.M., del Arco, A., Kobayashi, K., Iijima, M., Runswick, M.J., Walker, J.E., Saheki, T., Satrustegui, J., et al. (2001). Citrin and aralar1 are Ca(2+)-stimulated aspartate/glutamate transporters in mitochondria. *The EMBO journal* 20, 5060-5069.

Palty, R., Silverman, W.F., Hershinkel, M., Caporale, T., Sensi, S.L., Parnis, J., Nolte, C., Fishman, D., Shoshan-Barmatz, V., Herrmann, S., et al. (2010). NCLX is an essential component of mitochondrial Na⁺/Ca²⁺ exchange. *Proceedings of the National Academy of Sciences of the United States of America* 107, 436-441.

Pan, X., Liu, J., Nguyen, T., Liu, C., Sun, J., Teng, Y., Fergusson, M.M., Rovira, II, Allen, M., Springer, D.A., et al. (2013). The physiological role of mitochondrial calcium revealed by mice lacking the mitochondrial calcium uniporter. *Nat Cell Biol* 15, 1464-1472.

Papadopoulou, L.S., CM.; Davidson, MM.; Tanji, K.; Nishino, I.; Sadlock, J.E.; Krishna, S.; Walker, W.; Selby, J.; Glerum, D.M.; Coster, R.V.; Lyon, G.; Scalais, E.; Lebel, R.; Kaplan, P.; Shanske, S.; De Vivo, D.C.; Bonilla, E.; Hirano, M.; DiMauro, S.; Schon, E.A. (1999). Fatal

infantile cardioencephalomyopathy with COX deficiency and mutations in SCO2, a COX assembly gene. *Nature genetics* 23, 333-337.

Parfait, B., Chretien, D., Rötig, A., Marsac, C., Munnich, A., and Rustin P (2000). Compound heterozygous mutations in the flavoprotein gene of the respiratory chain complex II in a patient with Leigh syndrome. *Hum Genet* 106:236-43.

Park, J., Lee, Y., Park, T., Kang, J.Y., Mun, S.A., Jin, M., Yang, J., and Eom, S.H. (2020). Structure of the MICU1-MICU2 heterodimer provides insights into the gatekeeping threshold shift. *IUCrJ* 7, 355-365.

Patron, M., Granatiero, V., Espino, J., Rizzuto, R., and De Stefani, D. (2019). MICU3 is a tissue-specific enhancer of mitochondrial calcium uptake. *Cell death and differentiation* 26, 179-195.

Patron, M., Checchetto, V.; Raffaello, A.; Teardo, E.; Vecellio Reane, D.; Mantoan, M.; Granatiero, V.; Szabò, I.; De Stefani, D.; Rizzuto, R. (2014). MICU1 and MICU2 finely tune the mitochondrial Ca²⁺ uniporter by exerting opposite effects on MCU activity. *Mol. Cell*, 53, 726-737.

Paumard, P., Vaillier, J., Couлары, B., Schaeffer, J., Soubannier, V., Mueller, D.M., Brethes, D., di Rago, J.P., and Velours, J. (2002). The ATP synthase is involved in generating mitochondrial cristae morphology. *The EMBO journal* 21, 221-230.

Paupе, V., and Prudent, J. (2018). New insights into the role of mitochondrial calcium homeostasis in cell migration. *Biochemical and biophysical research communications* 500, 75-86.

Paupе, V., Prudent, J., Dassa, E.P., Rendon, O.Z., and Shoubridge, E.A. (2015). CCDC90A (MCUR1) is a cytochrome c oxidase assembly factor and not a regulator of the mitochondrial calcium uniporter. *Cell metabolism* 21, 109-116.

Perales-Clemente, E., Bayona-Bafaluy, M.P., Perez-Martos, A., Barrientos, A., Fernandez-Silva, P., and Enriquez, J.A. (2008). Restoration of electron transport without proton pumping in mammalian mitochondria. *Proceedings of the National Academy of Sciences of the United States of America* 105, 18735-18739.

Pérez-Pérez, R., Lobo-Jarne, T., Milenkovic, D., Mourier, A., Bratic, A., García-Bartolomé, A., Fernández-Vizarra, E., Cadenas, S., Delmiro, A., García-Consuegra, I., Arenas, J., Martín, M.A., Larsson, N.G., Ugalde, C. (2016). COX7A2L Is a Mitochondrial Complex III Binding Protein that Stabilizes the III₂+IV Supercomplex without Affecting Respirasome Formation. *Cell reports* 16, 2387-2398.

Perocchi, F., Gohil, V.M., Girgis, H.S., Bao, X.R., McCombs, J.E., Palmer, A.E., and Mootha, V.K. (2010). MICU1 encodes a mitochondrial EF hand protein required for Ca²⁺ uptake. *Nature* 467, 291-296.

Peters, J.W., Beratan, D.N., Bothner, B., Dyer, R.B., Harwood, C.S., Heiden, Z.M., Hille, R., Jones, A.K., King, P.W., Lu, Y., et al. (2018). A new era for electron bifurcation. *Current opinion in chemical biology* 47, 32-38.

Petrungaro, C., Zimmermann, K.M., Kuttner, V., Fischer, M., Dengjel, J., Bogeski, I., and Riemer, J. (2015). The Ca²⁺-Dependent Release of the Mia40-Induced MICU1-MICU2 Dimer from MCU Regulates Mitochondrial Ca²⁺ Uptake. *Cell metabolism* 22, 721-733.

Pfanner, N., van der Laan, M., Amati, P., Capaldi, R.A., Caudy, A.A., Chacinska, A., Darshi, M., Deckers, M., Hoppins, S., Icho, T., et al. (2014). Uniform nomenclature for the mitochondrial contact site and cristae organizing system. *The Journal of cell biology* 204, 1083-1086.

Phillips, J., Graham, L.A., Trumpower, B.L. (1993). Subunit 9 of the *Saccharomyces cerevisiae* cytochrome bc₁ complex is required for insertion of EPR-detectable iron-sulfur cluster into the Rieske iron-sulfur protein. *J Biol Chem.* 268, 11727-11736.

Phillips, J., Schmitt, M.E., Brown, T.A., Beckmann, J.D., Trumpower, B.L. (1990). Isolation and characterization of QCR9, a nuclear gene encoding the 7.3-kDa subunit 9 of the *Saccharomyces cerevisiae* ubiquinol-cytochrome c oxidoreductase complex. An intron-containing gene with a conserved sequence occurring in the intron of COX4. *J Biol Chem.* 265, 20813-20821.

Pickles, S., Vigie, P., and Youle, R.J. (2018). Mitophagy and Quality Control Mechanisms in Mitochondrial Maintenance. *Current biology: CB* 28, R170-r185.

Pilet, E., Jasaitis, A., Liebl, U., and Vos, M.H. (2004). Electron transfer between hemes in mammalian cytochrome c oxidase. *Proceedings of the National Academy of Sciences of the United States of America* 101, 16198-16203.

Pitceathly, R., Rahman, S., Wedatilake, Y., Polke, J.M., Cirak, S., Foley, A.R., Sailer, A., Hurler, M.E., Stalker, J., Hargreaves, I., Woodward, C.E., Sweeney, M.G., Muntoni, F., Houlden, H., Taanman, J.W., Hanna, M.G; UK10K Consortium. (2013). NDUFA4 mutations underlie dysfunction of a cytochrome c oxidase subunit linked to human neurological disease. *Cell reports* 3, 1795-1805.

Plovanich, M., Bogorad, R.L., Sancak, Y., Kamer, K.J., Strittmatter, L., Li, A.A., Girgis, H.S., Kuchimanchi, S., De Groot, J., Speciner, L., Taneja, N., Oshea, J., Kotliansky, V., Mootha, V.K. (2013). MICU2, a paralog of MICU1, resides within the mitochondrial uniporter complex to regulate calcium handling. *PLoS One* 8.

Pozzan, T., Rizzuto, R., Volpe, P., and Meldolesi, J. (1994). Molecular and cellular physiology of intracellular calcium stores. *Physiological reviews* 74, 595-636.

Pronicki, M., Kowalski P, Piekutowska-Abramczuk D, Taybert J, Karkucinska-Wieckowska A, Szymanska-Debinska T, Karczmarewicz E, Pajdowska M, Migdal M, Milewska-Bobula B, Sykut-Cegielska J, Popowska E. (2010). A homozygous mutation in the SCO2 gene causes a spinal muscular atrophy like presentation with stridor and respiratory insufficiency. *Eur J Paediatr Neurol.* 14, 253-260.

Protasoni, M., Bruno, C., Donati, M.A., Mohamoud, K., Severino, M., Allegri, A., Robinson, A.J., Reyes, A., Zeviani, M., and Garone, C. (2020). Novel compound heterozygous pathogenic

variants in nucleotide-binding protein like protein (NUBPL) cause leukoencephalopathy with multi-systemic involvement. *Molecular genetics and metabolism* 129, 26-34.

Prudent, J., Popgeorgiev, N., Bonneau, B., Thibaut, J., Gadet, R., Lopez, J., Gonzalo, P., Rimokh, R., Manon, S., Houart, C., et al. (2013). Bcl-wav and the mitochondrial calcium uniporter drive gastrula morphogenesis in zebrafish. *Nature communications* 4, 2330.

Raffaello, A., De Stefani, D., Sabbadin, D., Teardo, E., Merli, G., Picard, A., Checchetto, V., Moro, S., Szabo, I., and Rizzuto, R. (2013). The mitochondrial calcium uniporter is a multimer that can include a dominant-negative pore-forming subunit. *The EMBO journal* 32, 2362-2376.

Raffaello, A., Mammucari, C., Gherardi, G., and Rizzuto, R. (2016). Calcium at the Center of Cell Signaling: Interplay between Endoplasmic Reticulum, Mitochondria, and Lysosomes. *Trends in biochemical sciences* 41, 1035-1049.

Ragan, C.I., Wilson, M.T., Darley-USmar, V.M., Lowe P.M. (1987). Sub-fractionation of mitochondria and isolation of the proteins of oxidative phosphorylation (M. Darley-USmar, D. Rickwood, M.T. Wilson (Eds.), *Mitochondria: A Practical Approach*, IRL Press, Oxford).

Rahman, S., Taanman J.W., Cooper J.M., Nelson I., Hargreaves I., Meunier B., Hanna M.G., Garcia J.J., Capaldi R.A., Lake B.D. (1999). A missense mutation of cytochrome oxidase subunit II causes defective assembly and myopathy. *Am J Hum Genet.* 65, 1030-1039.

Rak, M., Gokova, S., Tzagoloff, A. (2011) Modular assembly of yeast mitochondrial ATP synthase. *EMBO J* 30:920–930.

Rampelt, H., Zerbes, R.M., van der Laan, M., Pfanner, N. (2017). Role of the mitochondrial contact site and cristae organizing system in membrane architecture and dynamics. *Biochim Biophys Acta Mol Cell Res.* 1864, 737-746.

Rana, M., de Coo, I., Diaz, F., Smeets, H., and Moraes, C.T. (2000). An out-of-frame cytochrome b gene deletion from a patient with parkinsonism is associated with impaired complex III assembly and an increase in free radical production. *Annals of neurology* 48, 774-781.

Rathore, S., Berndtsson, J., Marin-Buera, L., Conrad, J., Carroni, M., Brzezinski, P., and Ott, M. (2019). Cryo-EM structure of the yeast respiratory supercomplex. *Nature structural & molecular biology* 26, 50-57.

Ravn, K., Wibrand, F., Hansen, F.J., Horn, N., Rosenberg, T., and Schwartz, M. (2001). An mtDNA mutation, 14453G-->A, in the NADH dehydrogenase subunit 6 associated with severe MELAS syndrome. *European journal of human genetics: EJHG* 9, 805-809.

Rebelo, A., Saade, D., Pereira, C.V., Farooq, A., Huff, T.C., Abreu, L., Moraes, C.T., Mnatsakanova, D., Mathews, K., Yang, H., Schon, E.A., Zuchner, S., Shy, M.E.. (2018). SCO2 mutations cause early-onset axonal Charcot-Marie-Tooth disease associated with cellular copper deficiency. *Brain: a journal of neurology* 141, 662-672.

Rehling, P., Model, K., Brandner, K., Kovermann, P., Sickmann, A., Meyer, H.E., Kühlbrandt, W., Wagner, R., Truscott, K.N., Pfanner, N. (2003). Protein insertion into the mitochondrial inner membrane by a twin-pore translocase. *Science (New York, N.Y.)* 299, 1747-1751.

Reid, R.A., Moyle, J., and Mitchell, P. (1966). Synthesis of adenosine triphosphate by a protonmotive force in rat liver mitochondria. *Nature* 212, 257-258.

Reinders, J., Wagner, K., Zahedi, R.P., Stojanovski, D., Eyrich, B., van der Laan, M., Rehling, P., Sickmann, A., Pfanner, N., and Meisinger, C. (2007). Profiling phosphoproteins of yeast mitochondria reveals a role of phosphorylation in assembly of the ATP synthase. *Molecular & cellular proteomics : MCP* 6, 1896-1906.

Ren, T., Zhang, H., Wang, J., Zhu, J., Jin, M., Wu, Y., Guo, X., Ji, L., Huang, Q., Zhang, H., et al. (2017). MCU-dependent mitochondrial Ca²⁺ inhibits NAD⁺/SIRT3/SOD2 pathway to promote ROS production and metastasis of HCC cells. *Oncogene* 36, 5897-5909.

Rendón, O., Antonicka, H., Horvath, R., and Shoubridge, E.A. (2016). A mutation in the FAD-dependent oxidoreductase FOXRED1 results in cell-type specific assembly defects in oxidative phosphorylation complexes I and II *Molecular and cellular biology* 36, 2132-2140.

Renkema, G.H., Visser, G., Baertling, F., Wintjes, L.T., Wolters, V.M., van Montfrans, J., de Kort, G.A.P., Nikkels, P.G.J., van Hasselt, P.M., van der Crabben, S.N., Rodenburg, R.J.T. (2017). Mutated PET117 causes complex IV deficiency and is associated with neurodevelopmental regression and medulla oblongata lesions. *Hum. Genet.* 136, 759-769.

Rhein, V.F., Carroll, J., Ding, S., Fearnley, I.M., and Walker, J.E. (2013). NDUFAF7 methylates arginine 85 in the NDUFS2 subunit of human complex I. *The Journal of biological chemistry* 288, 33016-33026.

Rhein, V.F., Carroll, J., Ding, S., Fearnley, I.M., and Walker, J.E. (2016). NDUFAF5 Hydroxylates NDUFS7 at an Early Stage in the Assembly of Human Complex I. *The Journal of biological chemistry* 291, 14851-14860.

Rieger, B., Shalaeva, D.N., Sohnel, A.C., Kohl, W., Duwe, P., Mulkidjanian, A.Y., and Busch, K.B. (2017). Lifetime imaging of GFP at CoxVIIIa reports respiratory supercomplex assembly in live cells. *Scientific reports* 7, 46055.

Rizzuto, R., Bernardi, P., and Pozzan, T. (2000). Mitochondria as all-round players of the calcium game. *The Journal of physiology* 529 Pt 1, 37-47.

Rizzuto, R., Brini, M., Murgia, M., and Pozzan, T. (1993). Microdomains with high Ca²⁺ close to IP₃-sensitive channels that are sensed by neighboring mitochondria. *Science (New York, N.Y.)* 262, 744-747.

Rizzuto, R., De Stefani, D., Raffaello, A., and Mammucari, C. (2012). Mitochondria as sensors and regulators of calcium signalling. *Nature reviews. Molecular cell biology* 13, 566-578.

Rizzuto, R., Pinton, P., Carrington, W., Fay, F.S., Fogarty, K.E., Lifshitz, L.M., Tuft, R.A., and Pozzan, T. (1998). Close contacts with the endoplasmic reticulum as determinants of mitochondrial Ca²⁺ responses. *Science (New York, N.Y.)* 280, 1763-1766.

- Roche, B., Aussel, L., Ezraty, B., Mandin, P., Py, B., and Barras, F. (2013). Iron/sulfur proteins biogenesis in prokaryotes: formation, regulation and diversity. *Biochimica et biophysica acta* 1827, 455-469.
- Rödel, G., Michaelis, U., Forsbach, V., Kreike, J., Kaudewitz, F. (1986). Molecular cloning of the yeast nuclear genes CBS1 and CBS2. *Curr Genet.* 11, 47-53.
- Roux, K.J., Kim, D.I., Raida, M., and Burke, B. (2012). A promiscuous biotin ligase fusion protein identifies proximal and interacting proteins in mammalian cells. *The Journal of cell biology* 196, 801-810.
- Rutter, J., Winge, D., Schiffman, J.D. (2010). Succinate dehydrogenase—assembly, regulation and role in human disease. *Mitochondrion* 10, 393-401.
- Rutter, G.A., and Denton, R.M. (1989). Rapid purification of pig heart NAD⁺-isocitrate dehydrogenase. Studies on the regulation of activity by Ca²⁺, adenine nucleotides, Mg²⁺ and other metal ions. *The Biochemical journal* 263, 445-452.
- Rutter, G.A., and Rizzuto, R. (2000). Regulation of mitochondrial metabolism by ER Ca²⁺ release: an intimate connection. *Trends in biochemical sciences* 25, 215-221.
- Saada, A., Edvardson, S., Rapoport, M., Shaag, A., Amry, K., Miller, C., Lorberboum-Galski, H., and Elpeleg, O. (2008). C6ORF66 is an assembly factor of mitochondrial complex I. *American journal of human genetics* 82, 32-38.
- Saada, A., Vogel, R.O., Hoefs, S.J., van den Brand, M.A., Wessels, H.J., Willems, P.H., Venselaar, H., Shaag, A., Barghuti, F., Reish, O., et al. (2009). Mutations in NDUFAF3 (C3ORF60), encoding an NDUFAF4 (C6ORF66)-interacting complex I assembly protein, cause fatal neonatal mitochondrial disease. *American journal of human genetics* 84, 718-727.
- Sadler, I., Suda, K., Schatz, G., Kaudewitz, F., and Haid, A. (1984). Sequencing of the nuclear gene for the yeast cytochrome c1 precursor reveals an unusually complex amino-terminal presequence. *The EMBO journal* 3, 2137-2143.
- Salvador-Gallego, R., Mund, M., Cosentino, K., Schneider, J., Unsay, J., Schraermeyer, U., Engelhardt, J., Ries, J., and García-Sáez, A.J. (2016). Bax assembly into rings and arcs in apoptotic mitochondria is linked to membrane pores. *The EMBO journal* 35, 389-401.
- Salvatori, R., Kehrein, K., Singh, A.P., Aftab, W., Möller-Hergt, B.V., Forne, I., Imhof, A., and Ott, M. (2020). Molecular Wiring of a Mitochondrial Translational Feedback Loop. *Molecular cell* 77, 887-900.e885.
- Samanta, K., Mirams, G.R., and Parekh, A.B. (2018). Sequential forward and reverse transport of the Na⁽⁺⁾ Ca⁽²⁺⁾ exchanger generates Ca⁽²⁺⁾ oscillations within mitochondria. *Nature communications* 9, 156.
- Sancak, Y., Markhard, A.L., Kitami, T., Kovacs-Bogdan, E., Kamer, K.J., Udeshi, N.D., Carr, S.A., Chaudhuri, D., Clapham, D.E., Li, A.A., et al. (2013). EMRE is an essential component of the mitochondrial calcium uniporter complex. *Science (New York, N.Y.)* 342, 1379-1382.

- Sánchez-Caballero, L., Elurbe, D.M., Baertling, F., Guerrero-Castillo, S., van den Brand, M., van Strien, J., van Dam, T.J.P., Rodenburg, R., Brandt, U., Huynen, M.A., et al. (2020). TMEM70 functions in the assembly of complexes I and V. *Biochimica et biophysica acta. Bioenergetics* 1861, 148202.
- Sanchez-Caballero, L., Guerrero-Castillo, S., and Nijtmans, L. (2016). Unraveling the complexity of mitochondrial complex I assembly: A dynamic process. *Biochimica et biophysica acta* 1857, 980-990.
- Sánchez-Caballero, L., Ruzzenente, B., Bianchi, L., Assouline, Z., Barcia, G., Metodiev, M.D., Rio, M., Funalot, B., van den Brand, M.A., Guerrero-Castillo, S., et al. (2016). Mutations in Complex I Assembly Factor TMEM126B Result in Muscle Weakness and Isolated Complex I Deficiency. *American journal of human genetics* 99, 208-216.
- Sanchez, E., Lobo, T., Fox, J.L., Zeviani, M., Winge, D.R., and Fernandez-Vizarra, E. (2013). LYRM7/MZM1L is a UQCRC1 chaperone involved in the last steps of mitochondrial Complex III assembly in human cells. *Biochimica et biophysica acta* 1827, 285-293.
- Saraste, M. (1999). Oxidative phosphorylation at the fin de siècle. *Science (New York, N.Y.)* 283, 1488-1493.
- Saris, N.E. (1963). The calcium pump in mitochondria. *Societas Scientiarum Fennica Commentationes Physico-Mathematicae.* 28, 3-59.
- Sastri, M., Darshi, M., Mackey, M., Ramachandra, R., Ju, S., Phan, S., Adams, S., Stein, K., Douglas, C.R., Kim, J.J., et al. (2017). Sub-mitochondrial localization of the genetic-tagged mitochondrial intermembrane space-bridging components Mic19, Mic60 and Sam50. *J Cell Sci* 130, 3248-3260.
- Schaefer, A.M., Taylor, R.W., Turnbull, D.M., and Chinnery, P.F. (2004). The epidemiology of mitochondrial disorders--past, present and future. *Biochimica et biophysica acta* 1659, 115-120.
- Schäfer, E., Seelert, H., Reifschneider, N.H., Krause, F., Dencher, N.A., Vonck, J. (2006). Architecture of active mammalian respiratory chain supercomplexes.
- Schägger, H., Pfeiffer, K. (2000). Supercomplexes in the respiratory chains of yeast and mammalian mitochondria. *The EMBO journal* 19, 1777-1783.
- Schägger, H., Pfeiffer, K. (2001). The ratio of oxidative phosphorylation complexes I-V in bovine heart mitochondria and the composition of respiratory chain supercomplexes. *J Biol Chem.* 276, 37861-37867.
- Schagger, H. (2002). Respiratory chain supercomplexes of mitochondria and bacteria. *Biochimica et biophysica acta* 1555, 154-159.
- Schagger, H., Link, T.A., Engel, W.D., and von Jagow, G. (1986). Isolation of the eleven protein subunits of the bc₁ complex from beef heart. *Methods in enzymology* 126, 224-237.

- Schägger, H., von Jagow, G. (1991). Blue native electrophoresis for isolation of membrane protein complexes in enzymatically active form. *Analytical Biochemistry* 199, 223-231.
- Scharwey, M., Tatsuta, T., and Langer, T. (2013). Mitochondrial lipid transport at a glance. *J Cell Sci* 126, 5317-5323.
- Scheffler, I.E. (1999). *Mitochondria* (Wiley-Liss).
- Scheffler, I.E. (2015). Mitochondrial disease associated with complex I (NADH-CoQ oxidoreductase) deficiency. *Journal of inherited metabolic disease* 38, 405-415.
- Schlehe, J.S., Journal, M.S., Taylor, K.P., Amodeo, K.D., and LaVoie, M.J. (2013). The mitochondrial disease associated protein Ndufa2 is dispensable for Complex-I assembly but critical for the regulation of oxidative stress. *Neurobiology of disease* 58, 57-67.
- Schuelke, M., Smeitink, J., Mariman, E., Loeffen, J., Plecko, B., Trijbels, F., Stöckler-Ipsiroglu, S., and van den Heuvel, L. (1999). Mutant NDUFV1 subunit of mitochondrial complex I causes leukodystrophy and myoclonic epilepsy. *Nature genetics* 21, 260-261.
- Schulze, M., Rodel, G. (1988). SCO1, a yeast nuclear gene essential for accumulation of mitochondrial cytochrome c oxidase subunit II. *Mol Gen Genet.* 211, 492-498.
- Scorrano, L., De Matteis, M.A., Emr, S., Giordano, F., Hajnóczky, G., Kornmann, B., Lackner, L.L., Levine, T.P., Pellegrini, L., Reinisch, K., et al. (2019). Coming together to define membrane contact sites. *Nature communications* 10, 1287.
- Shamseldin, H.E., Alasmari, A., Salih, M.A., Samman, M.M., Mian, S.A., Alshidi, T., Ibrahim, N., Hashem, M., Faqeih, E., Al-Mohanna, F., et al. (2017). A null mutation in MICU2 causes abnormal mitochondrial calcium homeostasis and a severe neurodevelopmental disorder. *Brain : a journal of neurology* 140, 2806-2813.
- Sheftel, A.D., Stehling, O., Pierik, A.J., Netz, D.J., Kerscher, S., Elsasser, H.P., Wittig, I., Balk, J., Brandt, U., and Lill, R. (2009). Human ind1, an iron-sulfur cluster assembly factor for respiratory complex I. *Mol Cell Biol* 29, 6059-6073.
- Sickmann, A., Reinders, J., Wagner, Y., Joppich, C., Zahedi, R., Meyer, H.E., Schonfisch, B., Perschil, I., Chacinska, A., Guiard, B., et al. (2003). The proteome of *Saccharomyces cerevisiae* mitochondria. *Proceedings of the National Academy of Sciences of the United States of America* 100, 13207-13212.
- Siddiqi, S., Siddiq, S., Mansoor, A., Oostrik, J., Ahmad, N., Kazmi, S. A. R., Kremer, H., Qamar, R., Schraders, M. (2013). Novel mutation in AAA domain of BCS1L causing Bjornstad syndrome. *J. Hum. Genet.* 58, 819-821.
- Sideris, D.P., Petrakis, N., Katrakili, N., Mikropoulou, D., Gallo, A., Ciofi-Baffoni, S., Banci, L., Bertini, I., and Tokatlidis, K. (2009). A novel intermembrane space-targeting signal docks cysteines onto Mia40 during mitochondrial oxidative folding. *The Journal of cell biology* 187, 1007-1022.

Signes, A, Cerutti, R., Dickson, A.S., Benincá, C., Hinchy, E.C., Ghezzi, D., Carozzo, R., Bertini, E., Murphy, M.P., Nathan, J.A., Viscomi, C., Fernandez-Vizarra, E., Zeviani, M. (2019). APOPT1/COA8 assists COX assembly and is oppositely regulated by UPS and ROS. *EMBO Molecular Medicine* 11.

Signes, A., and Fernandez-Vizarra, E. (2018). Assembly of mammalian oxidative phosphorylation complexes I-V and supercomplexes. *Essays in biochemistry* 62, 255-270.

Simon, D.K., Friedman, J., Breakefield, X.O., Jankovic, J., Brin, M.F., Provias, J., Bressman, S.B., Charness, M.E., Tarsy, D., Johns, D.R., et al. (2003). A heteroplasmic mitochondrial complex I gene mutation in adult-onset dystonia. *Neurogenetics* 4, 199-205.

Sinkler, C.A., Kalpage, H., Shay, J., Lee, I., Malek, M.H., Grossman, L.I., and Hüttemann, M. (2017). Tissue- and Condition-Specific Isoforms of Mammalian Cytochrome c Oxidase Subunits: From Function to Human Disease. *Oxidative medicine and cellular longevity* 2017, 1534056.

Sirrenberg, C., Bauer, M.F., Guiard, B., Neupert, W., Brunner, M. (1996). Import of carrier proteins into the mitochondrial inner membrane mediated by Tim22. *Nature* 384, 582-585.

Skoldberg, F., Grimelius, L., Woodward, E. R., Rorsman, F., Van Schothorst, E. W., Winqvist, O., Karlsson, F. A., Akerstrom, G., Kampe, O., Husebye, E. S. (1998). A family with hereditary extra-adrenal paragangliomas without evidence for mutations in the von Hippel-Lindau disease or ret genes. *Clin. Endocr.* 48.

Slater, E.C., and Cleland, K.W. (1953). The effect of calcium on the respiratory and phosphorylative activities of heart-muscle sarcosomes. *The Biochemical journal* 55, 566-590.

Smeitink, J., and van den Heuvel, L. (1999). Human mitochondrial complex I in health and disease. *American journal of human genetics* 64, 1505-1510.

Smeitink, J.A., Zeviani, M., Turnbull, D.M., and Jacobs, H.T. (2006). Mitochondrial medicine: a metabolic perspective on the pathology of oxidative phosphorylation disorders. *Cell metabolism* 3, 9-13.

Smith, D., Gray, J., Mitchell, L., Antholine, W.E., and Hosler, J.P. (2005). Assembly of Cytochrome-c Oxidase in the Absence of Assembly Protein Surf1p Leads to Loss of the Active Site Heme. *Journal of Biological Chemistry* 280, 17652-17656.

Smith, P.M., Fox, J.L., and Winge, D.R. (2012). Biogenesis of the cytochrome bc(1) complex and role of assembly factors. *Biochimica et biophysica acta* 1817, 276-286.

Sousa, J.S., D'Imprima, E., Vonck, J. (2018). *Mitochondrial Respiratory Chain Complexes.*, Vol 87 (Singapore: Springer).

Souza, R.L., Green-Willms, N., Fox, T.D., Tzagoloff, A., Nobrega, F.G. (2000). Cloning and characterization of COX18, a *Saccharomyces cerevisiae* PET gene required for the assembly of cytochrome oxidase. *J Biol Chem.* 275, 14898-14902.

- Sowers, A.E., Hackenbrock, C. (1981). Rate of lateral diffusion of intramembrane particles: measurement by electrophoretic displacement and rerandomization. *PNAS* 78, 6246-6250.
- Spiegel, R., Shaag, A., Mandel, H., Reich, D., Penyakov, M., Hujeriat, Y., Saada, A., Elpeleg, O., and Shalev, S.A. (2009). Mutated NDUFS6 is the cause of fatal neonatal lactic acidemia in Caucasus Jews. *European journal of human genetics: EJHG* 17, 1200-1203.
- Spinazzi, M., Radaelli, E., Horre, K., Arranz, A.M., Gounko, N.V., Agostinis, P., Maia, T.M., Impens, F., Morais, V.A., Lopez-Lluch, G., et al. (2019). PARL deficiency in mouse causes Complex III defects, coenzyme Q depletion, and Leigh-like syndrome. *Proceedings of the National Academy of Sciences of the United States of America* 116, 277-286.
- Steenart, N.A., and Shore, G.C. (1997). Mitochondrial cytochrome c oxidase subunit IV is phosphorylated by an endogenous kinase. *FEBS Lett* 415, 294-298.
- Stephan, K., and Ott, M. (2020). Timing of dimerization of the bc(1) complex during mitochondrial respiratory chain assembly. *Biochimica et biophysica acta. Bioenergetics* 1861, 148177.
- Sterea, A.M., and El Hiani, Y. (2020). The Role of Mitochondrial Calcium Signaling in the Pathophysiology of Cancer Cells. *Advances in experimental medicine and biology* 1131, 747-770.
- Stoldt, S., Wenzel, D., Kehrein, K., Riedel, D., Ott, M., Jakobs, S. (2018). Spatial orchestration of mitochondrial translation and OXPHOS complex assembly. *Nat Cell Biol* 20, 528-534.
- Strauss, M., Hofhaus, G., Schroder, R.R., and Kuhlbrandt, W. (2008). Dimer ribbons of ATP synthase shape the inner mitochondrial membrane. *The EMBO journal* 27, 1154-1160.
- Strogolova, V., Hoang, N.H., Hosler, J., and Stuart, R.A. (2019). The yeast mitochondrial proteins Rcf1 and Rcf2 support the enzymology of the cytochrome c oxidase complex and generation of the proton motive force. *The Journal of biological chemistry* 294, 4867-4877.
- Stroh, A., Anderka, O., Pfeiffer, K., Yagi, T., Finel, M., Ludwig, B., Schägger, H. (2004). Assembly of respiratory complexes I, III, and IV into NADH oxidase supercomplex stabilizes complex I in *Paracoccus denitrificans*. *J Biol Chem.* 279, 5000-5007.
- Stroud, D., Becker, T., Qiu, J., Stojanovski, D., Pfannschmidt, S., Wirth, C., Hunte, C., Guiard, B., Meisinger, C., Pfanner, N., Wiedemann, N. (2011). Biogenesis of mitochondrial β -barrel proteins: the POTRA domain is involved in precursor release from the SAM complex. *Mol Biol Cell.* 22, 2823-2833.
- Stroud, D., Maher, M.J., Lindau, C., Vögtle, F.N., Frazier, A.E., Surgenor, E., Mountford, H., Singh, A.P., Bonas, M., Oeljeklaus, S., Warscheid, B., Meisinger, C., Thorburn, D.R., Ryan, M.T. (2015). COA6 is a mitochondrial complex IV assembly factor critical for biogenesis of mtDNA-encoded COX2. *Hum Mol Genet.* 24, 5404-5415.
- Stroud, D.A., Surgenor, E.E., Formosa, L.E., Reljic, B., Frazier, A.E., Dibley, M.G., Osellame, L.D., Stait, T., Beilharz, T.H., Thorburn, D.R., et al. (2016). Accessory subunits are integral for assembly and function of human mitochondrial complex I. *Nature* 538, 123-126.

Sugiana, C., Pagliarini, D.J., McKenzie, M., Kirby, D.M., Salemi, R., Abu-Amero, K.K., Dahl, H.H., Hutchison, W.M., Vascotto, K.A., Smith, S.M., et al. (2008). Mutation of C20orf7 disrupts complex I assembly and causes lethal neonatal mitochondrial disease. *American journal of human genetics* 83, 468-478.

Sun, F., Huo, X., Zhai, Y., Wang, A., Xu, J., Su, D., Bartlam, M., Rao, Z. (2005). Crystal structure of mitochondrial respiratory membrane protein complex II. *Cell* 121, 1043-1057.

Suzuki, J., Kanemaru, K., and Iino, M. (2016). Genetically Encoded Fluorescent Indicators for Organellar Calcium Imaging. *Biophysical journal* 111, 1119-1131.

Szklarczyk, R., Wanschers, B., Cuypers, T.D., Esseling, J.J., Riemersma, M., van den Brand, M.A., Gloerich, J., Lasonder, E., van den Heuvel, L.P., Nijtmans, L.G., Huynen, M.A. (2012). Iterative orthology prediction uncovers new mitochondrial proteins and identifies C12orf62 as the human ortholog of COX14, a protein involved in the assembly of cytochrome c oxidase. *Genome Biol.* 13, R12.

Szklarczyk, R., Wanschers, B., Nijtmans, L.G., Rodenburg, R.J., Zschocke, J., Dikow, N., van den Brand, M.A., Hendriks-Franssen, M.G., Gilissen, C., Veltman, J.A., Nootboom, M., Koopman, W.J., Willems, P.H., Smeitink, J.A., Huynen, M.A., van den Heuvel, L.P. (2013). A mutation in the FAM36A gene, the human ortholog of COX20, impairs cytochrome c oxidase assembly and is associated with ataxia and muscle hypotonia. *Human molecular genetics* 22, 656-667.

Tabebi, M., Mkaouar-Rebai, E., Mnif, M., Kallabi, F., Ben Mahmoud, A., Ben Saad, W., Charfi, N., Keskes-Ammar, L., Kamoun, H., Abid, M. (2015). A novel mutation MT-COIII m.9267G>C and MT-COI m.5913G>A mutation in mitochondrial genes in a Tunisian family with maternally inherited diabetes and deafness (MIDD) associated with severe nephropathy. *Biochem. Biophys. Res. Commun.* 459, 353–360.

Tait, S.W., and Green, D.R. (2013). Mitochondrial regulation of cell death. *Cold Spring Harbor perspectives in biology* 5.

Tamargo, J., and Lopez-Sendon, J. (2011). Novel therapeutic targets for the treatment of heart failure. *Nature reviews. Drug discovery* 10, 536-555.

Tamiya, G, Makino, S., Hayashi, M., Abe, A., Numakura, C., Ueki, M., Tanaka, A., Ito, C., Toshimori, K., Ogawa, N., Terashima, T., Maegawa, H., Yanagisawa, D., Tooyama, I., Tada, M., Onodera, O., Hayasaka, K. (2014). A mutation of COX6A1 causes a recessive axonal or mixed form of Charcot-Marie-Tooth disease. *Am J Hum Genet.* 95, 294-300.

Tang, W.K., Borgnia, M.J., Hsu, A.L., Esser, L., Fox, T., de Val, N., and Xia, D. (2020). Structures of AAA protein translocase Bcs1 suggest translocation mechanism of a folded protein. *Nature structural & molecular biology* 27, 202-209.

Tatuch, Y., and Robinson, B.H. (1993). The mitochondrial DNA mutation at 8993 associated with NARP slows the rate of ATP synthesis in isolated lymphoblast mitochondria. *Biochemical and biophysical research communications* 192, 124-128.

Taylor, S.S., Harris, N.J., Germany, E.M., Fox, J.L., Khalimonchuk, O. (2017). The Assembly Factor Pet117 Couples Heme a Synthase Activity to Cytochrome Oxidase Assembly. *The Journal of biological chemistry* 292, 1815-1825.

Territo, P.R., Mootha, V.K., French, S.A., and Balaban, R.S. (2000). Ca²⁺ activation of heart mitochondrial oxidative phosphorylation: role of the F(0)/F(1)-ATPase. *American journal of physiology. Cell physiology* 278, C423-435.

Tilokani, L., Nagashima, S., Paupe, V., and Prudent, J. (2018). Mitochondrial dynamics: overview of molecular mechanisms. *Essays in biochemistry* 62, 341-360.

Timón-Gómez, A., Nývltová, E., Abriata, L.A., Vila, A.J., Hosler, J., Barrientos, A. (2018). Mitochondrial cytochrome c oxidase biogenesis: Recent developments. *Semin Cell Dev Biol.* 76, 163-178.

Timón-Gómez, A., Garlich, J., Stuart, R.A., Ugalde, C., and Barrientos, A. (2020). Distinct Roles of Mitochondrial HIGD1A and HIGD2A in Respiratory Complex and Supercomplex Biogenesis. *Cell reports* 31, 107607.

Tiranti, V., Hoertnagel, K., Carrozzo, R., Galimberti, C., Munaro, M., Granatiero, M., Zelante, L., Gasparini, P., Marzella, R., Rocchi, M., Bayona-Bafaluy, M.P., Enriquez, J.A., Uziel, G., Bertini, E., Dionisi-Vici, C., Franco, B., Meitinger, T., Zeviani, M. (1998). Mutations of SURF-1 in Leigh disease associated with cytochrome c oxidase deficiency. *Am. J. Hum. Genet.* 63, 1609-1621.

Tiranti, V., Corona, P., Greco, M., Taanman, J.W., Carrara, F., Lamantea, E., Nijtmans, L., Uziel, G., and Zeviani, M. (2000). A novel frameshift mutation of the mtDNA COIII gene leads to impaired assembly of cytochrome c oxidase in a patient affected by Leigh-like syndrome. *Human molecular genetics* 9, 2733-2742.

Tiranti, V., Corona, P., Greco, M., Taanman, J.W., Carrara, F., Lamantea, E., Nijtmans, L., Uziel, G., and Zeviani, M. (2000). A novel frameshift mutation of the mtDNA COIII gene leads to impaired assembly of cytochrome c oxidase in a patient affected by Leigh-like syndrome. *Human molecular genetics* 9, 2733-2742.

Tomar, D., Dong, Z., Shanmughapriya, S., Koch, D.A., Thomas, T., Hoffman, N.E., Timbalia, S.A., Goldman, S.J., Breves, S.L., Corbally, D.P., et al. (2016). MCUR1 Is a Scaffold Factor for the MCU Complex Function and Promotes Mitochondrial Bioenergetics. *Cell reports* 15, 1673-1685.

Tomar, D.T., M.; Garbincius, J.F.; Kolmetzky, D.W.; Salik, O.; Jadiya, P.; Carpenter, A.C.; Elrod, J.W. (2019). MICU1 regulates mitochondrial cristae structure and function independent of the mitochondrial calcium uniporter channel. *BioRxiv*.

Tondera, D., Grandemange, S., Jourdain, A., Karbowski, M., Mattenberger, Y., Herzig, S., Da Cruz, S., Clerc, P., Raschke, I., Merkwirth, C., et al. (2009). SLP-2 is required for stress-induced mitochondrial hyperfusion. *The EMBO journal* 28, 1589-1600.

Torrioni, A., Petrozzi, M., D'Urbano, L., Sellitto, D., Zeviani, M., Carrara, F., Carducci, C., Leuzzi, V., Carelli, V., Barboni, P., et al. (1997). Haplotype and phylogenetic analyses suggest

that one European-specific mtDNA background plays a role in the expression of Leber hereditary optic neuropathy by increasing the penetrance of the primary mutations 11778 and 14484. *American journal of human genetics* 60, 1107-1121.

Traba, J., Del Arco, A., Duchen, M.R., Szabadkai, G., and Satrustegui, J. (2012). SCaMC-1 promotes cancer cell survival by desensitizing mitochondrial permeability transition via ATP/ADP-mediated matrix Ca(2+) buffering. *Cell death and differentiation* 19, 650-660.

Trouillard, M., Meunier, B., and Rappaport, F. (2011). Questioning the functional relevance of mitochondrial supercomplexes by time-resolved analysis of the respiratory chain. *Proceedings of the National Academy of Sciences of the United States of America* 108, E1027-1034.

Trumpower, B.L. (1990). The protonmotive Q cycle. Energy transduction by coupling of proton translocation to electron transfer by the cytochrome bc1 complex. *The Journal of biological chemistry* 265, 11409-11412.

Tsai, M.F., Phillips, C.B., Ranaghan, M., Tsai, C.W., Wu, Y., Williams, C., and Miller, C. (2016). Dual functions of a small regulatory subunit in the mitochondrial calcium uniporter complex. *Elife* 5.

Tucker, E.J., Wanschers, B.F., Szklarczyk, R., Mountford, H.S., Wijeyeratne, X.W., van den Brand, M.A., Leenders, A.M., Rodenburg, R.J., Reljic, B., Compton, A.G., et al. (2013). Mutations in the UQCC1-interacting protein, UQCC2, cause human complex III deficiency associated with perturbed cytochrome b protein expression. *PLoS genetics* 9, e1004034.

Tufi, R., Gleeson, T.P., von Stockum, S., Hewitt, V.L., Lee, J.J., Terriente-Felix, A., Sanchez-Martinez, A., Ziviani, E., and Whitworth, A.J. (2019). Comprehensive Genetic Characterization of Mitochondrial Ca(2+) Uniporter Components Reveals Their Different Physiological Requirements In Vivo. *Cell reports* 27, 1541-1550.e1545.

Turrens, J.F. (2003). Mitochondrial formation of reactive oxygen species. *The Journal of physiology* 552, 335-344.

Tyanova, S., Temu, T., Sinitcyn, P., Carlson, A., Hein, M.Y., Geiger, T., Mann, M., and Cox, J. (2016). The Perseus computational platform for comprehensive analysis of (prote)omics data. *Nature methods* 13, 731-740.

Tzagoloff, A., Capitanio, N., Nobrega, M.P., Gatti, D. (1990). Cytochrome oxidase assembly in yeast requires the product of COX11, a homolog of the *P. denitrificans* protein encoded by ORF3. *The EMBO journal* 9, 2759-2764.

Tzagoloff, A., Wu, M.A., and Crivellone, M. (1986). Assembly of the mitochondrial membrane system. Characterization of COR1, the structural gene for the 44-kilodalton core protein of yeast coenzyme QH₂-cytochrome c reductase. *The Journal of biological chemistry* 261, 17163-17169.

Urban, P.F., and Klingenberg, M. (1969). On the redox potentials of ubiquinone and cytochrome b in the respiratory chain. *European journal of biochemistry* 9, 519-525.

Vais, H., Mallilankaraman, K., Mak, D.D., Hoff, H., Payne, R., Tanis, J.E., and Foskett, J.K. (2016). EMRE Is a Matrix Ca(2+) Sensor that Governs Gatekeeping of the Mitochondrial Ca(2+) Uniporter. *Cell reports* 14, 403-410.

Valente, L., Piga, D., Lamantea, E., Carrara, F., Uziel, G., Cudia, P., Zani, A., Farina, L., Morandi, L., Mora, M. (2009). Identification of novel mutations in five patients with mitochondrial encephalomyopathy. *Biochim. Biophys. Acta* 1787, 491-501.

van den Bosch, B. J. C., Gerards, M., Sluiter, W., Stegmann, A. P. A., Jongen, E. L. C., Hellebrekers, D. M. E. I., Oegema, R., Lambrichs, E. H., Prokisch, H., Danhauser, K., Schoonderwoerd, K., de Coo, I. F. M., Smeets, H. J. M. (2012). Defective NDUFA9 as a novel cause of neonatally fatal complex I disease. *J. Med. Genet.* 49: 10-15.

Van Laar, V.S., Berman, S.B., and Hastings, T.G. (2016). Mic60/mitofilin overexpression alters mitochondrial dynamics and attenuates vulnerability of dopaminergic cells to dopamine and rotenone. *Neurobiology of disease* 91, 247-261.

van Loon, A., Brandli, A.W., Pesold-Hurt, B., Blank, D., Schatz, G. (1987). Transport of proteins to the mitochondrial intermembrane space: the 'matrix-targeting' and the 'sorting' domains in the cytochrome c1 presequence. *The EMBO journal* 6, 2433-2439.

Van Loon, A.P., De Groot, R.J., De Haan, M., Dekker, A., and Grivell, L.A. (1984). The DNA sequence of the nuclear gene coding for the 17-kd subunit VI of the yeast ubiquinol-cytochrome c reductase: a protein with an extremely high content of acidic amino acids. *The EMBO journal* 3, 1039-1043.

van Rahden, V. A., Fernandez-Vizarra, E., Alawi, M., Brand, K., Fellmann, F., Horn, D., Zeviani, M., Kutsche, K. (2011). Mutations in NDUFB11, encoding a complex I component of the mitochondrial respiratory chain, cause microphthalmia with linear skin defects syndrome. *Am. J. Hum. Genet.* 96: 640-650.

Van Vranken, J., Na U, Winge DR, Rutter J. (2015). Protein-mediated assembly of succinate dehydrogenase and its cofactors. *Crit Rev Biochem Mol Biol.* 50, 168-180.

Vartak, R.S., Semwal, M.K., and Bai, Y. (2014). An update on complex I assembly: the assembly of players. *J Bioenerg Biomembr* 46, 323-328.

Vasington, F.D., and Murphy, J.V. (1962). Ca ion uptake by rat kidney mitochondria and its dependence on respiration and phosphorylation. *The Journal of biological chemistry* 237, 2670-2677.

Vecellio Reane, D., Vallesio, F., Checchetto, V., Acquasaliente, L., Butera, G., De Filippis, V., Szabò, I., Zanotti, G., Rizzuto, R., Raffaello, A. (2016). A MICU1 Splice Variant Confers High Sensitivity to the Mitochondrial Ca²⁺ Uptake Machinery of Skeletal Muscle. *Mol. Cell.* 64, 760-773.

Verkhovsky, M., Bloch, D.A., and Verkhovskaya, M. (2012). Tightly-bound ubiquinone in the *Escherichia coli* respiratory complex I. *Biochimica et biophysica acta* 1817, 1550-1556.

Vidoni, S.H., Harbour, M.E., Guerrero-Castillo, S., Signes, A., Ding, S., Fearnley, I.M., Taylor, R.W. Tiranti, V. Arnold, S. Fernandez-Vizarra, E., Zeviani, M. (2017). MR-1S Interacts with

PET100 and PET117 in Module-Based Assembly of Human Cytochrome c Oxidase. *Cell reports* 18, 1727-1738.

Vinothkumar, K.R., Zhu, J., and Hirst, J. (2014). Architecture of mammalian respiratory complex I. *Nature* 515, 80-84.

Visapaa, I., Fellman, V., Varilo, T., Palotie, A., Raivio, K. O., Peltonen, L. (1998). Assignment of the locus for a new lethal neonatal metabolic syndrome to 2q33-37. *Am. J. Hum. Genet.* 63, 1396-1403.

Viscomi, C., Bottani, E., Civiletto, G., Cerutti, R., Moggio, M., Fagiolari, G., Schon, E.A., Lamperti, C., and Zeviani, M. (2011). In vivo correction of COX deficiency by activation of the AMPK/PGC-1 α axis. *Cell metabolism* 14, 80-90.

Vogel, F., Bornhövd, C., Neupert, W., Reichert, A.S. (2006). Dynamic subcompartmentalization of the mitochondrial inner membrane. *J Cell Biol.* 175, 237-247.

Vogel, R.O., Janssen, R.J., Ugalde, C., Grovenstein, M., Huijbens, R.J., Visch, H.J., van den Heuvel, L.P., Willems, P.H., Zeviani, M., Smeitink, J.A., et al. (2005). Human mitochondrial complex I assembly is mediated by NDUFAF1. *The FEBS journal* 272, 5317-5326.

Vogel, R.O., Janssen, R.J., van den Brand, M.A., Dieteren, C.E., Verkaart, S., Koopman, W.J., Willems, P.H., Pluk, W., van den Heuvel, L.P., Smeitink, J.A., et al. (2007). Cytosolic signaling protein Ecsit also localizes to mitochondria where it interacts with chaperone NDUFAF1 and functions in complex I assembly. *Genes & development* 21, 615-624.

Vögtle, F.N., Burkhart, J., Rao, S., Gerbeth, C., Hinrichs, J., Martinou, J.C., Chacinska, A., Sickmann, A., Zahedi, R.P., Meisinger, C. (2012). Intermembrane space proteome of yeast mitochondria. *Mol Cell Proteomics.* 11, 1840-1852.

Vukotic, M., Oeljeklaus, S., Wiese, S., Vogtle, F.N., Meisinger, C., Meyer, H.E., Zieseniss, A., Katschinski, D.M., Jans, D.C., Jakobs, S., et al. (2012). Rcf1 mediates cytochrome oxidase assembly and respirasome formation, revealing heterogeneity of the enzyme complex. *Cell metabolism* 15, 336-347.

Vultur, A., Gibhardt, C.S., Stanisiz, H., and Bogeski, I. (2018). The role of the mitochondrial calcium uniporter (MCU) complex in cancer. *Pflugers Archiv : European journal of physiology* 470, 1149-1163.

Vygodina, T., Kirichenko, A., and Konstantinov, A.A. (2013). Direct regulation of cytochrome c oxidase by calcium ions. *PLoS One* 8, e74436.

Vygodina, T.V., Mukhaleva, E., Azarkina, N.V., and Konstantinov, A.A. (2017). Cytochrome c oxidase inhibition by calcium at physiological ionic composition of the medium: Implications for physiological significance of the effect. *Biochimica et biophysica acta. Bioenergetics* 1858, 982-990.

Wagener, N., Ackermann, M., Funes, S., Neupert, W. (2011). A pathway of protein translocation in mitochondria mediated by the AAA-ATPase Bcs1. *Mol Cell.* 44, 191-202.

Walker, J.E. (2013). The ATP synthase: the understood, the uncertain and the unknown. *Biochemical Society transactions* 41, 1-16.

Walkinshaw, E., Gai, Y., Farkas, C., Richter, D., Nicholas, E., Keleman, K., and Davis, R.L. (2015). Identification of genes that promote or inhibit olfactory memory formation in *Drosophila*. *Genetics* 199, 1173-1182.

Wang, L., Yang, X., Li, S., Wang, Z., Liu, Y., Feng, J., Zhu, Y., and Shen, Y. (2014). Structural and mechanistic insights into MICU1 regulation of mitochondrial calcium uptake. *The EMBO journal* 33, 594-604.

Wang, Y., Nguyen, N.X., She, J., Zeng, W., Yang, Y., Bai, X.C., Jiang, Y. (2019). Structural Mechanism of EMRE-Dependent Gating of the Human Mitochondrial Calcium Uniporter. *Cell*. 177, 1252-1261.

Wanschers, B.F.J., Szklarczyk, R., van den Brand, M. A. M., Jonckheere, A., Suijskens, J., Smeets, R., Rodenburg, R. J., Stephan, K., Helland, I. B., Elkamil, A., Rootwelt, T., Ott, M., van den Heuvel, L., Nijtmans, L. G., Huynen, M. A. (2014). A mutation in the human CBP4 ortholog UQCC3 impairs complex III assembly, activity and cytochrome b stability. *Hum. Molec. Genet.* 23, 6356-6365.

Watt, I.N., Montgomery, M.G., Runswick, M.J., Leslie, A.G., and Walker, J.E. (2010). Bioenergetic cost of making an adenosine triphosphate molecule in animal mitochondria. *Proceedings of the National Academy of Sciences of the United States of America* 107, 16823-16827.

Weber, T.A., Koob, S., Heide, H., Wittig, I., Head, B., van der Blik, A., Brandt, U., Mittelbronn, M., and Reichert, A.S. (2013). APOOL is a cardiolipin-binding constituent of the Mitofilin/MINOS protein complex determining cristae morphology in mammalian mitochondria. *PLoS One* 8, e63683.

Wei, Y.L., Yu, C.A., Yang, P., Li, A.L., Wen, J.Y., Zhao, S.M., Liu, H.X., Ke, Y.N., Campbell, W., Zhang, Y.G. (2006). Novel mitochondrial DNA mutations associated with Chinese familial hypertrophic cardiomyopathy. *Clin. Exp. Pharmacol. Physiol.* 36, 933-939.

Weraarpachai, W., Antonicka, H., Sasarman, F., Seeger, J., Schrank, B., Kolesar, J.E., Lochmüller, H., Chevrette, M., Kaufman, B.A., Horvath, R., Shoubridge, E.A. (2009). Mutation in TACO1, encoding a translational activator of COX I, results in cytochrome c oxidase deficiency and late-onset Leigh syndrome. *Nature genetics* 41, 833-837.

Weraarpachai, W., Sasarman, F., Nishimura, T., Antonicka, H., Aure, K., Rotig, A., Lombes, A., Shoubridge, E. A. (2012). Mutations in C12orf62, a factor that couples COX I synthesis with cytochrome c oxidase assembly, cause fatal neonatal lactic acidosis. *Am. J. Hum. Genet.* 90, 142-151.

Wibrand, F., Ravn, K., Schwartz, M., Rosenberg, T., Horn, N., Vissing, J. (2001). Multisystem disorder associated with a missense mutation in the mitochondrial cytochrome b gene. *Ann. Neurol.* 50.

Wiedemann, N., Kozjak, V., Chacinska, A., Schönfisch, B., Rospert, S., Ryan, M.T., Pfanner, N., Meisinger, C. (2003). Machinery for protein sorting and assembly in the mitochondrial outer membrane. *Nature* 424, 565-571.

Wiel, C., Lallet-Daher, H., Gitenay, D., Gras, B., Le Calvé, B., Augert, A., Ferrand, M., Prevarskaya, N., Simonnet, H., Vindrieux, D., et al. (2014). Endoplasmic reticulum calcium release through ITPR2 channels leads to mitochondrial calcium accumulation and senescence. *Nature communications* 5, 3792.

Wikstrom, M. (2004). Cytochrome c oxidase: 25 years of the elusive proton pump. *Biochimica et biophysica acta* 1655, 241-247.

Williams, E.G., Wu, Y., Jha, P., Dubuis, S., Blattmann, P., Argmann, C.A., Houten, S.M., Amariuta, T., Wolski, W., Zamboni, N., et al. (2016). Systems proteomics of liver mitochondria function. *Science (New York, N.Y.)* 352, aad0189.

Wittig, I., and Schagger, H. (2008). Structural organization of mitochondrial ATP synthase. *Biochimica et biophysica acta* 1777, 592-598.

Wu, M., Tzagoloff, A. (1989). Identification and characterization of a new gene (CBP3) required for the expression of yeast coenzyme QH₂-cytochrome c reductase. *J Biol Chem.* 264, 11122-11130.

Wu, W., Shen Q., Lei, Z., Qiu, Z., Li, D., Pei, H., Zheng, J., Jia, Z. (2019). The crystal structure of MICU2 provides insight into Ca²⁺ binding and MICU1-MICU2 heterodimer formation. *EMBO Rep.*

Xia, D., Yu, C.A., Kim, H., Xia, J.Z., Kachurin, A.M., Zhang, L., Yu, L., Deisenhofer, J. (1997). Crystal structure of the cytochrome bc₁ complex from bovine heart mitochondria. *Science (New York, N.Y.)* 277, 60-66.

Xu, F., Ackerley, C., Maj, M.C., Addis, J.B., Levandovskiy, V., Lee, J., Mackay, N., Cameron, J.M., Robinson, B.H. (2008). Disruption of a mitochondrial RNA-binding protein gene results in decreased cytochrome b expression and a marked reduction in ubiquinol-cytochrome c reductase activity in mouse heart mitochondria. *Biochem J.* 416, 15-26.

Xu, F., Morin, C., Mitchell, G., Ackerley, C., Robinson, B.H. (2004). The role of the LRPPRC (leucine-rich pentatricopeptide repeat cassette) gene in cytochrome oxidase assembly: mutation causes lowered levels of COX (cytochrome c oxidase) I and COX III mRNA. *Biochem J.* 382, 331-336.

Xu, S., and Chisholm, A.D. (2014). *C. elegans* epidermal wounding induces a mitochondrial ROS burst that promotes wound repair. *Developmental cell* 31, 48-60.

Yamamoto, T., Yamagoshi, R., Harada, K., Kawano, M., Minami, N., Ido, Y., Kuwahara, K., Fujita, A., Ozono, M., Watanabe, A., et al. (2016). Analysis of the structure and function of EMRE in a yeast expression system. *Biochimica et biophysica acta* 1857, 831-839.

Ye, H., and Rouault, T. (2010). Erythropoiesis and iron sulfur cluster biogenesis. *Adv Hematol.*

Yoo, J., Wu, M., Yin, Y., Herzik, M.A., Jr., Lander, G.C., and Lee, S.Y. (2018). Cryo-EM structure of a mitochondrial calcium uniporter. *Science (New York, N.Y.)* 361, 506-511.

Yoshikawa, S., and Shimada, A. (2015). Reaction mechanism of cytochrome c oxidase. *Chemical reviews* 115, 1936-1989.

Yu, C., Wang, Y., Peng, J., Shen, Q., Chen, M., Tang, W., Li, X., Cai, C., Wang, B., Cai, S., et al. (2017). Mitochondrial calcium uniporter as a target of microRNA-340 and promoter of metastasis via enhancing the Warburg effect. *Oncotarget* 8, 83831-83844.

Yu, C., Xia JZ, Kachurin, A.M., Yu, L., Xia, D., Kim, H., Deisenhofer, J. (1996). Crystallization and preliminary structure of beef heart mitochondrial cytochrome-bc1 complex. *Biochim Biophys Acta.* 1275, 47-53.

Yun, C.H., Gennis, R.B. (1991). Assignment of the histidine axial ligands to the cytochrome bH and cytochrome bL components of the bc1 complex from *Rhodobacter sphaeroides* by site-directed mutagenesis. *Biochemistry* 30, 6747-6754.

Zara V., Conte, L., Trumpower, B.L. (2004). Further insights into the assembly of the yeast cytochrome bc1 complex based on analysis of single and double deletion mutants lacking supernumerary subunits and cytochrome b. *Eur J Biochem.* 271, 1209-1218.

Zara, V., Conte, L., and Trumpower, B.L. (2007). Identification and characterization of cytochrome bc(1) subcomplexes in mitochondria from yeast with single and double deletions of genes encoding cytochrome bc(1) subunits. *The FEBS journal* 274, 4526-4539.

Zara, V., Conte, L., and Trumpower, B.L. (2009). Evidence that the assembly of the yeast cytochrome bc1 complex involves the formation of a large core structure in the inner mitochondrial membrane. *The FEBS journal* 276, 1900-1914.

Zara, V., Conte, L., and Trumpower, B.L. (2009a). Biogenesis of the yeast cytochrome bc1 complex. *Biochimica et biophysica acta* 1793, 89-96.

Zara, V., Conte, L., and Trumpower, B.L. (2009b). Evidence that the assembly of the yeast cytochrome bc1 complex involves the formation of a large core structure in the inner mitochondrial membrane. *The FEBS journal* 276, 1900-1914.

Zeng, X., Barros, M.H., Shulman, T., Tzagoloff, A. (2008) ATP25, a new nuclear gene of *Saccharomyces cerevisiae* required for expression and assembly of the Atp9p subunit of mitochondrial ATPase. *Mol Biol Cell* 19:1366–1377.

Zhang, Z, Huang, L., Shulmeister, V.M., Chi, Y., Kim, K.K., Hung, L., Crofts, A.R., Berry, E.A., Kim, S. (1998). Electron transfer by domain movement in cytochrome bc1. *Nature* 392, 677-684.

Zhao, R.Z., Jiang, S., Zhang, L., and Yu, Z.B. (2019). Mitochondrial electron transport chain, ROS generation and uncoupling (Review). *International journal of molecular medicine* 44, 3-15.

Zheng, X.X., Shoffner, J.M., Voljavec, A.S., and Wallace, D.C. (1990). Evaluation of procedures for assaying oxidative phosphorylation enzyme activities in mitochondrial myopathy muscle biopsies. *Biochimica et biophysica acta* 1019, 1-10.

Zheng, Y.R., Zhang, X.N., and Chen, Z. (2019). Mitochondrial transport serves as a mitochondrial quality control strategy in axons: Implications for central nervous system disorders. *CNS neuroscience & therapeutics* 25, 876-886.

Zollner, A., Rodel, G., Haid, A. (1992). Molecular cloning and characterization of the *Saccharomyces cerevisiae* CYT2 gene encoding cytochrome-c1-heme lyase *The FEBS journal* 207, 1093-1100.

Zong, S., Wu, M., Gu, J., Liu, T., Guo, R., and Yang, M. (2018). Structure of the intact 14-subunit human cytochrome c oxidase. *Cell research* 28, 1026-1034.

9.1 Appendix A

Respiratory supercomplexes act as a platform for complex III-mediated maturation of human mitochondrial complexes I and IV.

Protasoni M, Pérez-Pérez R, Lobo-Jarne T, Harbour ME, Ding S, Peñas A, Diaz F, Moraes CT, Fearnley IM, Zeviani M, Ugalde C, Fernández-Vizarra E.

EMBO J. 2020 Feb 3;39(3)

Respiratory supercomplexes act as a platform for complex III-mediated maturation of human mitochondrial complexes I and IV

Margherita Protasoni¹ , Rafael Pérez-Pérez² , Teresa Lobo-Jarne² , Michael E Harbour¹, Shujing Ding¹, Ana Peñas², Francisca Diaz³, Carlos T Moraes³ , Ian M Fearnley¹, Massimo Zeviani^{1,4} , Cristina Ugalde^{2,5,*}  & Erika Fernández-Vizarra^{1,**} 

Abstract

Mitochondrial respiratory chain (MRC) enzymes associate in supercomplexes (SCs) that are structurally interdependent. This may explain why defects in a single component often produce combined enzyme deficiencies in patients. A case in point is the alleged destabilization of complex I in the absence of complex III. To clarify the structural and functional relationships between complexes, we have used comprehensive proteomic, functional, and biogenetical approaches to analyze a MT-CYB-deficient human cell line. We show that the absence of complex III blocks complex I biogenesis by preventing the incorporation of the NADH module rather than decreasing its stability. In addition, complex IV subunits appeared sequestered within complex III subassemblies, leading to defective complex IV assembly as well. Therefore, we propose that complex III is central for MRC maturation and SC formation. Our results challenge the notion that SC biogenesis requires the pre-formation of fully assembled individual complexes. In contrast, they support a cooperative-assembly model in which the main role of complex III in SCs is to provide a structural and functional platform for the completion of overall MRC biogenesis.

Keywords complex I; complex III; cytochrome b mutation; mitochondrial respiratory chain assembly; supercomplexes

Subject Category Membranes & Trafficking

DOI 10.15252/embj.2019102817 | Received 29 June 2019 | Revised 2 November 2019 | Accepted 26 November 2019

The EMBO Journal (2020) e102817

Introduction

The mitochondrial respiratory chain (MRC) complex III (cIII) or *bc₁* complex is a trans-inner-membrane enzyme that couples the transfer of electrons from ubiquinol (reduced coenzyme Q or CoQ) to cytochrome *c* with the translocation of protons from the mitochondrial matrix to the intermembrane space, by means of the Q-cycle catalytic mechanism (Trumpower, 1990). Biochemically, cIII occupies a central position in the MRC, since it receives electrons from complex I (cI) and complex II (cII) through CoQ and donates them to complex IV (cIV) via cytochrome *c*. cIII is also at the crossroads of alternative electron transfer pathways, such as those from the glycerol-3-phosphate dehydrogenase, electron transfer flavoprotein (ETF), sulfide-quinone reductase (SQR), and dihydroorotate dehydrogenase (DHODH), all converging onto CoQ (Lenaz *et al.*, 2007). The quaternary structure of the complex is always dimeric (cIII₂), with each monomer being composed of ten different subunits (Iwata *et al.*, 1998; Berry *et al.*, 1999, 2000), only one of which (MT-CYB) is encoded by the mitochondrial genome (mtDNA). Structurally, cIII₂ is part of all known respiratory supercomplexes (SCs), where it physically interacts with both cI and cIV in the SCs cI+cIII₂+cIV_n (Schagger & Pfeiffer, 2000), structures known as “respirasomes” because they are in principle able to transfer electrons from NADH to O₂ (Acin-Perez *et al.*, 2008; Gu *et al.*, 2016; Letts *et al.*, 2016; Wu *et al.*, 2016; Guo *et al.*, 2017). It is well known that severe cIII₂ deficiency in patients carrying null mutations in genes encoding some cIII₂ structural components and assembly factors are associated with a concomitant decrease in cI activity (Lamantea *et al.*, 2002; Bruno *et al.*, 2003; Acin-Perez *et al.*, 2004; Barel *et al.*, 2008; Tucker *et al.*, 2013; Carossa *et al.*, 2014; Feichtinger *et al.*, 2017) and, in some cases, in cIV activity as well (Carossa *et al.*, 2014). These pleiotropic effects have been traditionally interpreted as a loss of cI and cIV stability in the absence of their SC partner (Acin-Perez *et al.*, 2004),

1 Medical Research Council-Mitochondrial Biology Unit, University of Cambridge, Cambridge, UK

2 Instituto de Investigación Hospital 12 de Octubre (i+12), Madrid, Spain

3 Department of Neurology, Miller School of Medicine, University of Miami, Miami, FL, USA

4 Department of Neurosciences, University of Padova, Padova, Italy

5 Centro de Investigación Biomédica en Red de Enfermedades Raras (CIBERER), U723, Madrid, Spain

*Corresponding author. Tel: +34 91 7792784; E-mail: cugalde@h12o.es

**Corresponding author. Tel: +44 1223 252700; E-mail: emfvb2@mrc-mbu.cam.ac.uk

which is based on the premise that the biogenesis of MRC SCs proceeds by the incorporation of pre-made fully assembled individual complexes (Acin-Perez *et al*, 2008).

Here, we have used proteomics and biogenetic approaches to comprehensively characterize the biogenesis and organization of the MRC components in a homoplasmic MT-CYB null mutant human cell line, devoid of fully assembled cIII₂ (de Coo *et al*, 1999; Rana *et al*, 2000; Perez-Perez *et al*, 2016). Contrary to the current model (Acin-Perez *et al*, 2004), our data demonstrate that the severe cI deficiency associated with the absence of cIII₂ does not originate from destabilization of the fully assembled cI holoenzyme but rather from assembly stalling of nascent cI. MT-CYB mutant cybrid mitochondria accumulate a cI assembly intermediate lacking the catalytic N-module (Mimaki *et al*, 2012; Moreno-Lastres *et al*, 2012; Sanchez-Caballero *et al*, 2016), which is stabilized by the cI assembly factor NDUFAF2 (Ogilvie *et al*, 2005). In addition, we found that specific cIII₂ subunits were recruited into stalled protein structures that sequestered cIV subunits, affecting the maturation of the cIV holo-enzyme. These data explain the molecular mechanisms leading to combined respiratory chain deficiency associated with the absence of cIII₂, challenge the concept of SC assembly by incorporation of fully assembled individual complexes, and demonstrate the essential role of SCs as cIII₂-driven factories carrying out efficient assembly and maturation of the overall mitochondrial respiratory chain.

Results

Combined mitochondrial respiratory chain deficiency in Δ 4-CYB cybrids

Enzymatic activities of respiratory chain complexes I, II, III, and IV were measured in the #17.3E Δ 4-CYB clone, homoplasmic for the 4-bp deletion in MT-CYB (heretofore referred to as Δ 4-CYB), in comparison with clone #4.1, containing 100% wild-type (heretofore referred to as WT) mitochondrial DNA (mtDNA). Both cybrid clones, obtained from 143B TK⁻ ρ^0 cells (King & Attadi, 1996a; King & Attardi, 1996b), were populated with mitochondria from the same heteroplasmic patient (Rana *et al*, 2000). In the Δ 4-CYB cells, cIII₂ activity was virtually absent and the activities of cI and cIV were significantly lower than the WT values, to $25 \pm 13\%$ and $64 \pm 11\%$, respectively (Fig 1A). The profound reduction in cI amounts and activity of Δ 4-CYB was confirmed by in-gel activity assays (IGA) and by immunodetection, with a specific antibody against the cI subunit NDUFS1, following blue-native gel electrophoresis (BNGE) separation of the native MRC complexes in mitochondrial extracts from the Δ 4-CYB and WT cell lines (Fig 1B and C). The amounts of assembled complexes V and II were not drastically affected by the MT-CYB mutation in two different Δ 4-CYB clones: #17.3E (E) and #17.3B (B) (Fig 1C).

To investigate the origin of the combined respiratory chain deficiency, we performed stable isotope labeling by amino acids in cell culture (SILAC)-based quantitative proteomics, to compare the relative abundance of proteins from mitochondrial extracts of the two cell lines. Both the Δ 4-CYB and the WT cybrids were cultured in "Heavy (H)" and "Light (L)" media and then mixed before mitochondrial isolation by cell disruption, differential centrifugation

(Fernández-Vizcarra *et al*, 2010), and solubilization with 1.6 mg n-dodecyl β -D-maltoside (DDM)/mg protein. This experiment was performed in duplicate using reciprocal labeling of the mutant and control cells (Vidoni *et al*, 2017). The resulting fractions were resolved by blue-native gel electrophoresis (BNGE); each lane was then excised in 64 1-mm-thick slices and analyzed by mass spectrometry (MS). This analysis included the relative quantification of 1,263 proteins, the most downregulated of which were structural subunits of cIII and cI (Figs 2A and EV1). The amounts of nine known cI assembly factors (ACAD9, ECSIT, FOXRED1, NDUFAF1, NDUFAF2, NDUFAF3, NDUFAF4, NDUFAF6, and TMEM126B) did not differ significantly between the Δ 4-CYB and WT cells (Fig 2A). Conversely, the tenth cI assembly factor detected in this analysis, NDUFAF2 (Ogilvie *et al*, 2005), and the cII assembly factor SDHAF2 (Hao *et al*, 2009) were significantly more abundant in Δ 4-CYB mitochondria. Other proteins were also upregulated in the mutant cells. These included CHCHD2, whose knock-down causes cIV deficiency (Baughman *et al*, 2009; Imai *et al*, 2019), HIGD2A, one of the human orthologs of yeast Rcf1, which stabilizes the interaction between cIII₂ and cIV (Chen *et al*, 2012; Strogolova *et al*, 2012; Vukotic *et al*, 2012; Rieger *et al*, 2017), and GHITM or growth hormone-inducible transmembrane protein, a member of the BAX inhibitor motif-containing (TMBIM) family. GHITM localizes to the inner mitochondrial membrane, interacts with CHCHD2, and is deemed to participate in the maintenance of mitochondrial morphology and integrity (Oka *et al*, 2008; Meng *et al*, 2017).

To further examine the expression of the structural components of the MRC complexes and the ATP synthase (cV) in the Δ 4-CYB cells, we performed metabolic labeling of the thirteen mtDNA-encoded subunits. This analysis indicated that only MT-CYB was not translated in the Δ 4-CYB cybrids and that there was no clear reduction in the synthesis of any of the seven ND (cI) subunits (Fig 2B). Next, we tested the steady-state levels of several cI, cII, cIII₂, cIV, and cV subunits from whole-cell lysates, separated by SDS-PAGE, and immunovisualized by Western blot (WB) with specific antibodies. cIII₂ subunits were in general the most reduced in the Δ 4-CYB cybrids, with significantly lower levels of UQCRC1, UQCRC2, UQCRB, UQCRFS1, and UQCRQ (Fig 2C). Conversely, cytochrome cI (CYC1) showed comparable steady-state levels in both cybrid lines. Likewise, immunodetection using an anti-UQCRQ monoclonal antibody (Abcam ab110255) visualized a band of molecular mass smaller than 10 kDa and revealed equal levels in both cell lines (Fig 2C). Subsequent experiments suggested that this antibody fails to reliably detect UQCRQ, whereas it seems to cross react with UQCR10 (Fig 4C). Several cI subunits also showed variable reduction in their steady-state levels, depending on the structural module with which they associate (Stroud *et al*, 2016; Zhu *et al*, 2016). The lowest levels were detected for NDUFS1, a component of the catalytic N-module, followed by NDUFB8, belonging to the ND5-module, and NDUFS3, belonging to the Q-module. The amounts of NDUFA9 and NDUFB11, assigned to the ND2 and ND4 modules, respectively, were not significantly affected in the mutant cells (Fig 2D). The steady-state levels of mitochondrial and nuclear-encoded cIV subunits were similar to WT cells, except for significantly lower amounts of COX6B1 (Fig 2E), one of the subunits incorporated in the late stages of cIV assembly (Vidoni *et al*, 2017). SDHB of cII was also markedly reduced, to about half in Δ 4-CYB cybrids compared with WT

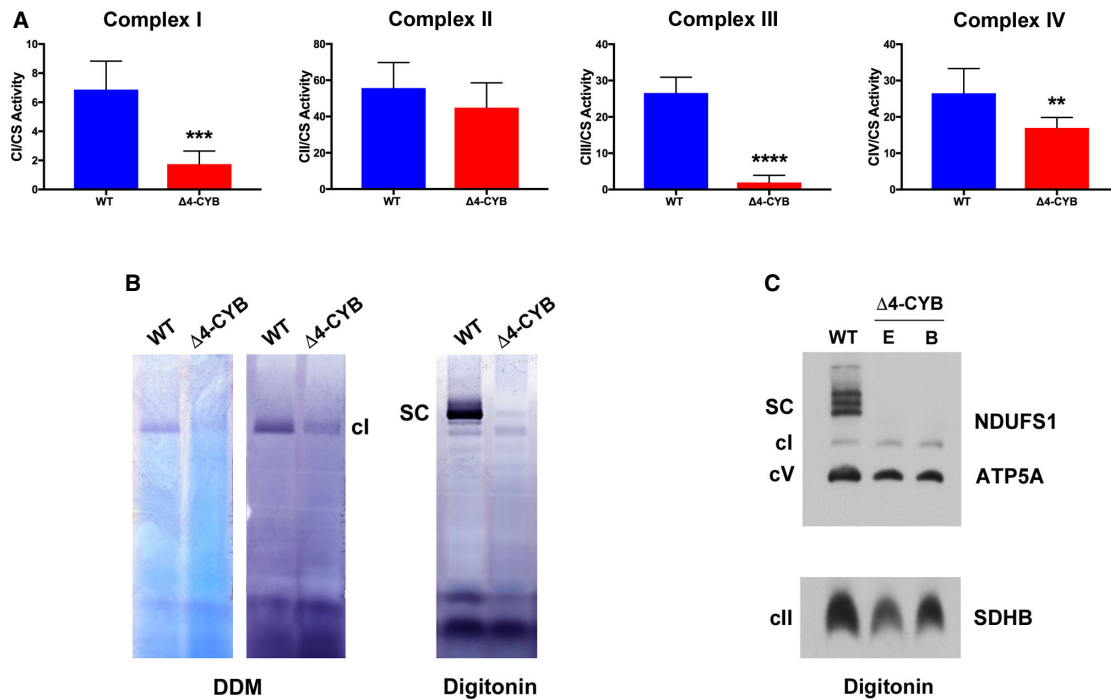


Figure 1. Complex I and IV enzymatic deficiencies in $\Delta 4$ -CYB cells.

A The activities (mUnits/g of protein) of the MRC enzymes were determined by spectrophotometric kinetic measurements in WT and $\Delta 4$ -CYB cells and normalized by the percentage of citrate synthase (CS) activity. Results are expressed as mean \pm SD ($n = 4-6$ biological replicates). Unpaired Student's t -test ** $P = 0.0100$; *** $P = 0.0002$; **** $P < 0.0001$.

B Complex I in-gel activity assays (IGA) after blue-native gel electrophoresis (BNGE) of WT and $\Delta 4$ -CYB samples solubilized with either 1.6 mg DDM/mg protein or 4 mg digitonin/mg protein. The gels were incubated in the reaction mixture for 1.5 h (lighter signals in DDM gels) or were left to continue the reaction for 24 h to obtain darker signals (DDM and Digitonin gels).

C BNGE, Western blot, and immunodetection, with anti-NDUF51 (cl), anti-ATP5A (cV), and anti-SDHB (cll) antibodies, of samples from the WT cybrids and from $\Delta 4$ -CYB clones E (#17.3E) and B (#17.3B). Clone E was the cell line of choice for the analysis shown in panels (A and B), and all the figures hereafter.

Source data are available online for this figure.

(Fig 2F), whereas cV subunits showed no differences between the two cell lines (Fig 2G).

The absence of MT-CYB causes accumulation of specific CIII assembly intermediates

Differentially labeled mitochondria solubilized with either 4 mg digitonin (Figs 3 and EV1A and B) or 1.6 mg DDM/mg protein were resolved by BNGE (Fig EV1C and D). Each lane was excised in 64, 1-mm-thick slices, and "complexome profiles" of protein distribution through the gel were obtained by LC/MS analysis (Heide *et al*, 2012; Vidoni *et al*, 2017). By this approach, we compared the relative migration and abundance of the cIII₂ components in $\Delta 4$ -CYB versus WT clones, in conditions that allow the analysis of individual MRC complexes (DDM) and supercomplexes (SCs, visualized in digitonin-solubilized samples). As expected, fully assembled cIII₂ and cIII₂-containing SCs were missing in the $\Delta 4$ -CYB cells (Fig EV1). Peptides corresponding to six structural cIII₂ subunits, UQCRC1, MT-CYB, UQCRH, UQCRB, UQCRC2, and UQCR11 and to one

assembly factor, UQCC2, were found only in the datasets corresponding to WT mitochondria (Fig EV1), reflecting again their virtual absence in $\Delta 4$ -CYB cells. UQCC2 binds to nascent MT-CYB in the very early stages of cIII₂ assembly (Gruschke *et al*, 2012; Tucker *et al*, 2013), and its presence seems to depend on the existence of a functional MT-CYB. In contrast, peptides corresponding to the remaining four subunits, UQCRC2, CYC1, UQCRFS1, and UQCR10; and two assembly factors, BCS1L and MZM1L (LYRM7), were detected in both control and mutated mitochondria (Figs 3A and D, and EV1). To validate the findings obtained from the complexome profiling, we performed BNGE followed by WB and immunodetection analyses of digitonin-solubilized mitochondria. 2D BNGE of $\Delta 4$ -CYB samples (Fig 3B) confirmed the presence of CYC1 in several protein structures ranging from low to high molecular mass, and the absence of UQCRC2, UQCRFS1, and UQCRC2 from cIII₂ structures and from higher molecular size bands visible in $\Delta 4$ -CYB. Conversely, these subunits were always found in the cIII₂ holocomplex and canonical SCs of WT cells (Fig 3B). Indeed, in the $\Delta 4$ -CYB cells, residual amounts of UQCRC2, CYC1, and UQCRQ subunits were

immunodetected in a high-molecular size area of 2D-BNGE WB, which does not correspond to that of WT SCs and does not contain UQCRFS1. This protein aggregate was also detected in the top gel slices by MS complexome analyses (Fig EV2).

The relative abundance of each subunit in the assembled species was estimated by calculating the area under the peaks defined by the relative peptide intensity in the complexome profiles obtained from the digitonin-solubilized samples. As “internal standard” experimental controls, we used the amount and distribution within the gel lanes of MRC-unrelated mitochondrial proteins, such as

TOM20, TOM22, and citrate synthase (CS), which were not significantly different between the two cell lines (Fig EV2). These measurements (Fig 3C) confirmed that CYC1 and UQCR10 were more abundant in $\Delta 4$ -CYB cybrids than UQCR2 or UQCRFS1, present at extremely low levels and mainly found at the gel migration front (Fig 3A). Conversely, CYC1 and UQCR10 were distributed in several peaks with molecular sizes ranging from 25 to 2,952 kDa, indicating their stabilization inside different assembly intermediates or structural aggregates that accumulate when MT-CYB is lacking and $cIII_2$ biogenesis is impaired. Notably, the amounts and

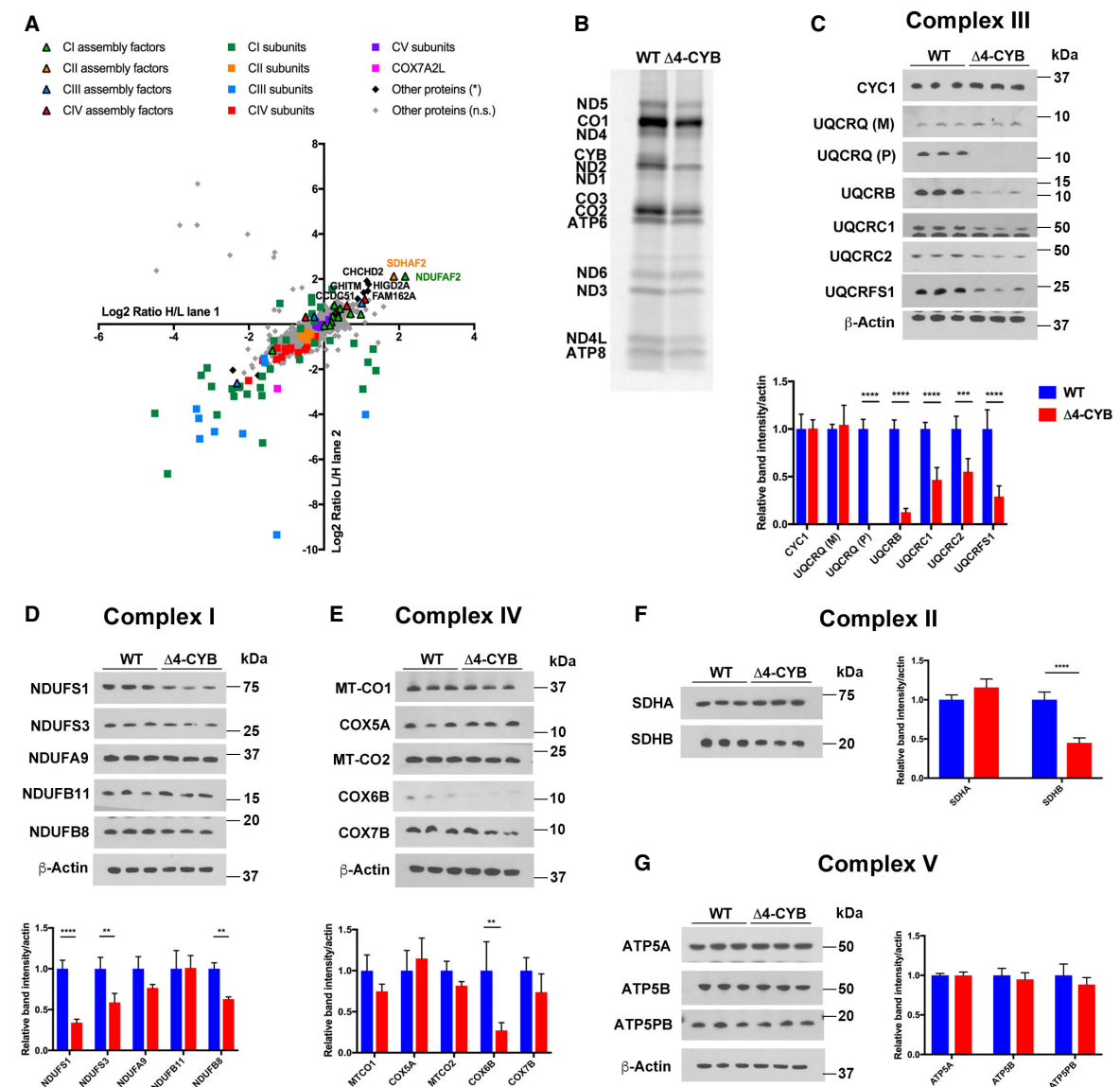


Figure 2.

Figure 2. Reduced steady-state levels of structural MRC subunits in $\Delta 4$ -CYB cells.

- A Scatter plot generated from the peptide content analyzed by mass spectrometry in each of the 64 slices excised from BNGE and after quantifying the heavy-to-light (H/L) and light-to-heavy (L/H) ratios in both reciprocal labeling experiments performed with mitochondria isolated from WT and $\Delta 4$ -CYB cells (see also Fig EV1). The logarithmic ratios were calculated using MaxQuant (Cox & Mann, 2008), and the statistical significance of the differences for the enrichment or depletion of the proteins was determined with Perseus (Cox & Mann, 2011; Tyanova et al, 2016).
- B Labeling of the thirteen mtDNA-encoded MRC structural subunits. Cells were incubated with [³⁵S]-L-Met for 1 h in the presence of emetine 100 μ g/ml to inhibit cytoplasmic translation.
- C Immunodetection of complex III structural subunits on Western blots of total cell lysates separated by SDS-PAGE, from three independent replicates of WT and $\Delta 4$ -CYB cells. The graph shows the densitometric quantification of the signals corresponding to each subunit normalized to that of the β -Actin. The mean of the three control (WT) samples was set to 1.0, and all the measurements were referenced to that value. The values plotted in the graphs are the mean \pm SD ($n = 3$). Two-way ANOVA with Sidak's multiple comparisons test **** $P < 0.0001$; *** $P = 0.0007$.
- D Immunodetection of complex I structural subunits on Western blots of total cell lysates separated by SDS-PAGE, from three independent replicates of WT and $\Delta 4$ -CYB cells. The graph shows the densitometric quantification of the signals corresponding to each subunit normalized to that of the β -actin. The mean of the three control (WT) samples was set to 1.0, and all the measurements were referenced to that value. The values plotted in the graphs are the mean \pm SD ($n = 3$). Two-way ANOVA with Sidak's multiple comparisons test **** $P < 0.0001$; ** $P = 0.0024$ (NDUFS3); ** $P = 0.0061$ (NDUFB8).
- E Immunodetection of complex IV structural subunits on Western blots of total cell lysates separated by SDS-PAGE, from three independent replicates of WT and $\Delta 4$ -CYB cells. The graph shows the densitometric quantification of the signals corresponding to each subunit normalized to that of the β -Actin. The mean of the three control (WT) samples was set to 1.0, and all the measurements were referenced to that value. The values plotted in the graphs are the mean \pm SD ($n = 3$). Two-way ANOVA with Sidak's multiple comparisons test ** $P = 0.0011$.
- F Immunodetection of complex II structural subunits on Western blots of total cell lysates separated by SDS-PAGE, from three independent replicates of WT and $\Delta 4$ -CYB cells. The graph shows the densitometric quantification of the signals corresponding to each subunit normalized to that of the β -actin. The mean of the three control (WT) samples was set to 1.0, and all the measurements were referenced to that value. The values plotted in the graphs are the mean \pm SD ($n = 3$). Two-way ANOVA with Sidak's multiple comparisons test **** $P < 0.0001$.
- G Immunodetection of complex V structural subunits on Western blots of total cell lysates separated by SDS-PAGE, from three independent replicates of WT and $\Delta 4$ -CYB cells. The graph shows the densitometric quantification of the signals corresponding to each subunit normalized to that of the β -actin. The mean of the three control (WT) samples was set to 1.0, and all the measurements were referenced to that value. The values plotted in the graphs are the mean \pm SD ($n = 3$). There were no differences in the steady-state levels of the tested subunits (2-way ANOVA with Sidak's multiple comparisons test).

Source data are available online for this figure.

distribution of the UQCRFS1-related assembly factors BCS1L (Fernandez-Vizarrá et al, 2007) and MZM1L (Sanchez et al, 2013) were comparable in both cell lines (Fig 3D).

To determine the composition of the UQCR10-containing assembly intermediates by immunopurification, an HA-tagged version of UQCR10 (UQCR10^{HA}) was constitutively transduced in WT and $\Delta 4$ -CYB cells (Fig 4A and B). Its expression was detectable in both cell lines, contrary to UQCRQ^{HA} that was absent in the mutant $\Delta 4$ -CYB but present in WT. Notably, the anti-UQCRQ antibody cross reacted with UQCR10 (Fig 4C). Both UQCR10^{HA}-expressing cybrid lines were grown in "H" and "L" SILAC medium according to a duplicate experimental protocol using reciprocal labeling (Andrews et al, 2013) and used for immunopurification of the tagged protein with an anti-HA antibody conjugated to Sepharose beads. MS analysis of immunopurified fractions showed more similar abundance for CYC1 and UQCRH (≈ -1 log₂ ratio) than for other cIII₂ subunits, indicating that the interaction with UQCR10^{HA} was not significantly different in the mutant relative to WT cell lines (Fig 4D). Contrariwise, < -5 log₂ ratios (32-fold lower) were detected in $\Delta 4$ -CYB versus WT cells for a number of cIII₂ components including UQCRC1, UQCRC2, UQCRFS1, UQCRQ, and UQCRB, in agreement with their very low levels in $\Delta 4$ -CYB cells. Immunopurified COX7A2L levels, also known as SCAFI (Lapiente-Brun et al, 2013), were also much lower in mutant cells, reflecting its preferential binding to cIII₂ (Perez-Perez et al, 2016). In addition, several cIV structural subunits belonging to the MT-CO2 module (MT-CO2, COX5B, COX6C) or to the MT-CO3 module (COX6B1) were found in the immunopurified fractions, suggesting their physical interaction with UQCR10 in both cell lines, although in lower amount in $\Delta 4$ -CYB cells (between -2 and -4 in log₂ ratio). Three proteins appeared with positive log₂ ratios, indicating higher levels of interaction with UQCR10^{HA} in the $\Delta 4$ -CYB mutants, and therefore are candidates to bind the

UQCR10-containing assembly intermediates found in the mutant cell line. These proteins were as follows: GHITM (Fig 2A); CHCHD3 (MIC19), a member of the mitochondrial contact site (MICOS) complex (Kozjak-Pavlovic, 2017); and HADHB, subunit beta of the fatty acid beta-oxidation trifunctional enzyme (Eaton et al, 2000). Upon SILAC-based relative quantification of the total mitochondrial extracts, the only protein showing a change in abundance and distribution associated with the absence of MT-CYB was GHITM (Figs 4E and 2A). However, shRNA-based stable knock-down of either CHCHD3 or GHITM expression did not produce a clear cIII₂ assembly or enzymatic defect, ruling out these proteins as *bona fide* cIII₂ assembly factors (Fig EV3).

Likewise, CYC1^{HA} expressed in both cell lines (Fig 4F) was perfectly incorporated into cIII₂ and SCs in WT cybrids, whereas it presented an atypical CYC1 accumulation pattern in $\Delta 4$ -CYB cells (Fig 4G), similar to that already seen in the complexome profiles (Fig 3A). These CYC1^{HA} overexpressing cells were then used to perform another duplicate experiment of anti-HA immunopurification combined with SILAC, to compare the interactions of CYC1^{HA} in the two cell lines (Fig 4H). The results further confirmed the low abundance of UQCRC1, UQCRC2, and UQCRFS1 subunits in the mutant cells and again showed a direct interaction of CYC1-containing structures with CIV subunit MT-CO2.

Incomplete complex I maturation in the absence of MT-CYB

Consistent observations have established that drastic MT-CYB mutations are associated with concomitant cIII₂ and cI deficiencies (Lamantea et al, 2002; Bruno et al, 2003; Acin-Perez et al, 2004; Carossa et al, 2014). This phenomenon was deemed to reflect destabilization of cI after its complete assembly, as reported in a mouse fibroblast cell line carrying a missense mutation in *Mt-Cyb* that

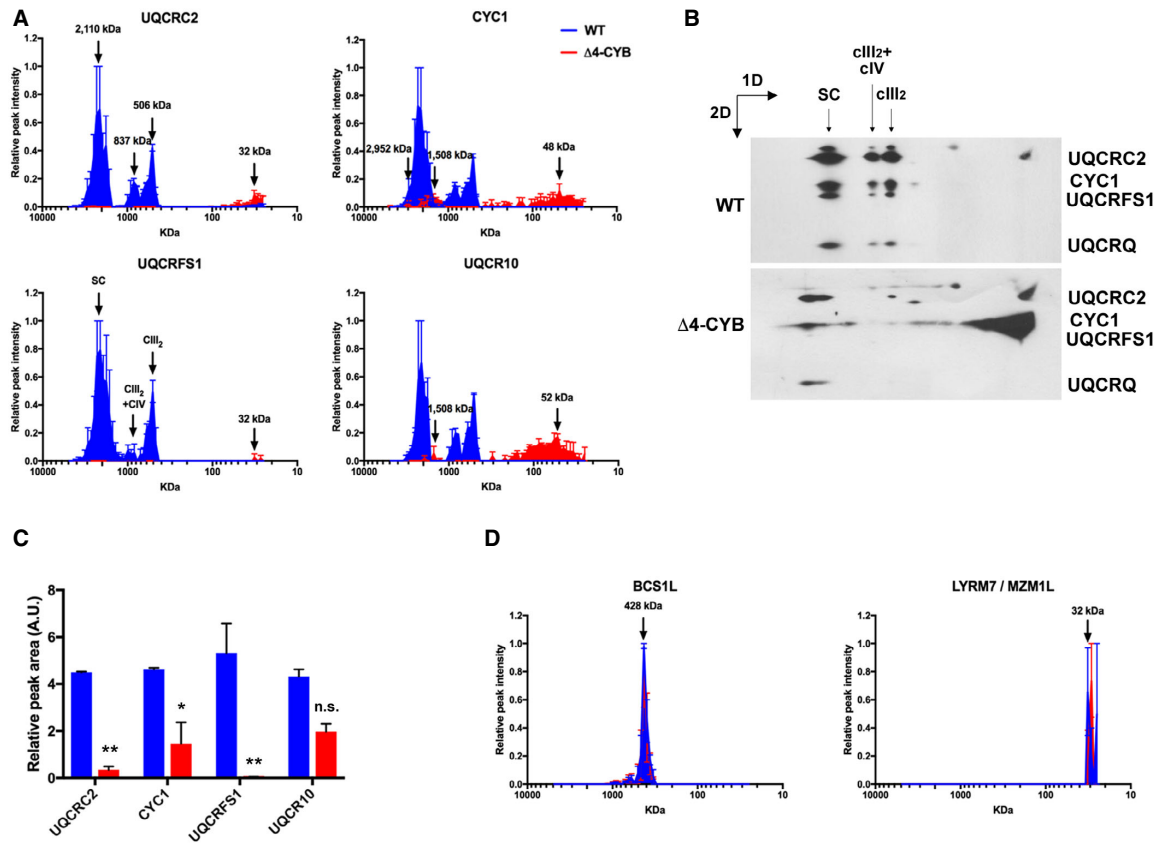


Figure 3. Blue-native gel electrophoresis (BNGE) mass spectrometry and immunodetection analysis of *cIII*₂-related proteins.

A Complexome profiles of *cIII*₂ structural subunits generated by analyzing the peptide content in each of the 64 slices in which the gel lanes were excised (see also Figs EV1 and EV2). The graphs plot the relative peptide peak intensities along the lane, setting the maximum to 1.0, versus the molecular mass calculated using the individual complexes and supercomplexes as the standards to generate a calibration curve. The relative amounts of the proteins between the two cell lines were determined by calculating the H/L ratios of peptides that were present in both WT (blue traces) and Δ4-CYB samples (red traces). The represented values are the mean ± SEM of the two reciprocal labeling experiments.

B Second-dimension BNGE of digitonin-solubilized samples from WT and Δ4-CYB cells, Western blot and immunodetection of the indicated *cIII*₂ structural subunits with specific antibodies. The immunodetection patterns were equivalent to the complexome profiles.

C Quantification of the total peak area under the curves (AUC) defined by the peptide intensity peaks for the indicated *cIII*₂ subunits. The x-axis values were the slice number (1–64), and the y-axis values were the relative peptide intensity. The graph shows the mean ± SD (*n* = 2). Two-way ANOVA with Sidak's multiple comparisons test ***P* = 0.0083 (UQCRC2); ***P* = 0.0033 (UQCRFS1); **P* = 0.0224; n.s. = non-significant.

D Complexome profiles of two *cIII*₂ assembly factors (BCS1L and LYRM7 or MZM1L) generated in the same way as in (A). The represented values are the mean ± SEM of the two reciprocal labeling experiments.

Source data are available online for this figure.

resulted in the total loss of the protein (Acin-Perez *et al*, 2004). However, our comparative complexome profiling data between human Δ4-CYB homoplasmic cybrids and their isogenic WT controls clearly demonstrate stalling of nascent ci rather than destabilization of the ci holocomplex (Figs 5 and EV4). Peptides corresponding to 31 of the 44 ci structural subunits were detected in both control and mutant samples. To simplify the analysis and data interpretation, the subunits were grouped according to the structural modules in which they are incorporated (Stroud *et al*, 2016; Guerrero-Castillo *et al*, 2017). Quantitative proteomics showed

profoundly decreased amounts of all ci structural subunits in the Δ4-CYB mitochondria (Fig 5A and C). In addition, in the mutant cell line, most of the ci subunits, except those of the N-module, were preferentially accumulating in a peak at an apparent molecular mass of 991 kDa in mitochondria solubilized with digitonin (Fig 5A), or 812 kDa upon solubilization with DDM (Fig EV5A). By contrast, only small amounts ($6.1 \pm 0.4\%$ of the control) of N-module subunits were found in a peak approximating 1,172 kDa in digitonin-solubilized or 1,002 kDa in DDM-solubilized samples, corresponding to the fully assembled “free” complex I (Figs 5A and D, and

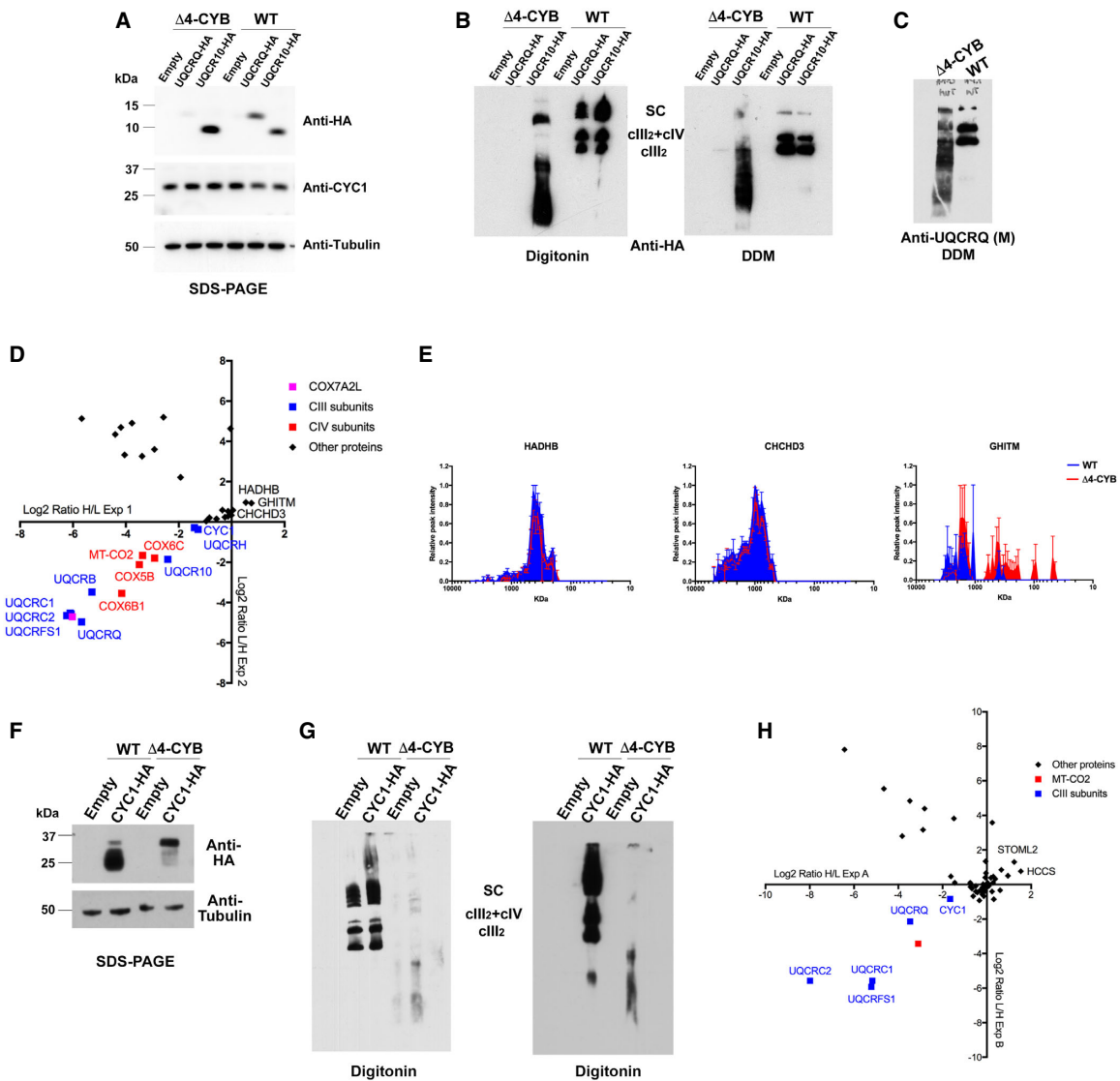


Figure 4. Proteomic analyses of UQCRI0 and CYC1-containing protein associations in $\Delta 4$ -CYB cells. See also Fig EV3.

A SDS-PAGE, Western blot, and immunodetection, with the indicated specific antibodies, of $\Delta 4$ -CYB and WT cells expressing HA-tagged versions of UQCRI0 and UQCRI0 and of cells transduced with the lentiviral expression vector without any cDNA insert (Empty).

B BNGE, Western blot, and immunodetection, with an anti-HA tag antibody, of samples from the same cell lines as in (A) solubilized either with digitonin or DDM.

C BNGE, Western blot, and immunodetection, with the monoclonal (M) anti-UQCRI0 antibody (Abcam ab110255), of non-transduced $\Delta 4$ -CYB and WT cells. The mitoplast samples were solubilized with DDM (See also Fig EV1).

D Scatter plot generated from the analysis of the logarithmic heavy (H)-to-light (L) ratios in the x-axis and the reverse in the y-axis, in the two reciprocal labeling SILAC experiments (1 and 2) and anti-HA immunopurification of $\Delta 4$ -CYB and WT cells expressing UQCRI0^{HA}.

E Complexome profiles, generated as in Fig 3, for the proteins found specifically enriched in $\Delta 4$ -CYB UQCRI0^{HA}, according to the SILAC immunopurification experiments shown in (D). The represented values are the mean \pm SEM of the two reciprocal labeling experiments.

F SDS-PAGE, Western blot, and immunodetection, with the indicated specific antibodies, of $\Delta 4$ -CYB and WT cells expressing an HA-tagged version of CYC1 and of cells transduced with the lentiviral expression vector without any cDNA insert (Empty).

G BNGE, Western blot, and immunodetection, with an anti-HA tag antibody, of samples from the same cell lines as in (F) solubilized either with digitonin.

H Scatter plot generated from the analysis of the logarithmic heavy (H)-to-light (L) ratios in the x-axis and the reverse in the y-axis, in the two reciprocal labeling SILAC experiments (A and B) of anti-HA immunopurification of $\Delta 4$ -CYB and WT cells expressing CYC1^{HA}.

Source data are available online for this figure.

EV5A). This pattern was different from that found in the WT samples solubilized with digitonin, in which all the N-module subunits were exclusively located in the SCs, including the “respirasomes” (I+III₂+IV_n), peaking at 2,110 kDa (Figs 5A and EV4). Also, in $\Delta 4$ -CYB cells, increased amounts of NDUFV1 and NDUFV2 were accumulated at sizes ranging from 25 to 49 kDa, further demonstrating impaired incorporation of the N-module. These profiles indicated that the prominent peak at 991 kDa (digitonin) or 812 kDa (DDM) corresponds to the “pre-complex I” (pre-cI) intermediate that accumulates immediately before the incorporation of the N-module. This is supported by the detection of large amounts of NDUFAF2 in the 991 kDa peak in $\Delta 4$ -CYB, while it was absent in WT cells (Figs 5B and EV4). NDUFAF2 is a cI assembly factor that stabilizes pre-cI, when the incorporation of the N-module is impaired. The accumulation of this pre-cI species, also known as “~830 kDa intermediate” (Ogilvie *et al.*, 2005), was clearly distinct from the 1,002 kDa signal corresponding to the whole cI in both WT and $\Delta 4$ -CYB mitochondria solubilized in DDM (Fig EV5A). Given their sequence homology, NDUFAF2 probably occupies the binding site of the N-module subunit NDUFA12 in the cI structure, and its upregulation in $\Delta 4$ -CYB mitochondria could induce cI assembly stalling at the pre-cI stage by preventing the incorporation of the N-module. However, NDUFAF2 overexpression did not prompt the accumulation of pre-cI in the WT cells, and the amount of mature active cI was the same as in the cells transfected with an empty vector (Fig EV5B–D). In addition, downregulation of NDUFAF2 expression had no drastic effects on cI assembly or activity in the WT cells, as previously described (Schlehe *et al.*, 2013), and did not promote cI maturation in the $\Delta 4$ -CYB cells (Fig EV5E–G). These results clearly indicate the occurrence of stalled assembly of cI in the absence of MT-CYB.

To unequivocally determine whether the residual holo-cI observed in the $\Delta 4$ -CYB cells was due to either degradation of fully assembled holo-enzyme, or assembly stalling of the nascent enzyme, we studied cI assembly dynamics. Pulse-chase [³⁵S]-L-Met metabolic labeling was first used to follow the stability and incorporation of the mtDNA-encoded subunits. SDS-PAGE analysis of the individual mitochondrial peptides after a 2-h radioactive pulse and chase times of 2, 5, and 24 h indicated comparable turnover rates of the MT-ND subunits in the presence or absence of MT-CYB (Fig 6A). In addition, 1D-BNGE of these samples ruled out the detection of fully assembled cI and its subsequent degradation over time (Fig 6B). 2D-BNGE analysis of the same samples from WT and $\Delta 4$ -CYB cells (Fig 6C) showed comparable assembly incorporation of all the mtDNA-encoded subunits in both cell lines at the initial stages (pulse), except for the absence of MT-CYB in the mutant. At this point, the MT-ND subunits accumulated in their respective assembly modules and, to a lesser extent, in the pre-cI. However, after a 2-h chase, while in the WT the MT-ND subunits started to be detected into the SCs, in the $\Delta 4$ -CYB mutant cells they were exclusively present in the pre-cI spot. At 5- and 24-h chase times, cI assembly progressed directly from pre-cI to SCs in WT, whereas it remained mainly stuck in pre-cI in $\Delta 4$ -CYB, with very scarce formation of free cI and no trace of SCs.

Then, the incorporation of the cI nuclear-encoded subunits was analyzed at different time points after the recovery of mitochondrial protein synthesis and cI assembly in cells that were pre-treated with the inhibitor doxycycline for 6 days, in order to deplete cells from

MRC mature complexes. 1D-BNGE followed by cI-IGA analysis of samples collected between 0 and 72 h after removal of doxycycline showed the progressive appearance of strong NADH-dehydrogenase activity within the SCs in the WT, whereas in $\Delta 4$ -CYB cells very faint NADH-dehydrogenase reactive signals were present at a molecular size around 1,000 kDa, corresponding to free cI holocomplex (Fig 6D). IGA analysis also detected faint reactivity in a band of $\Delta 4$ -CYB with slower electrophoretic mobility, most likely corresponding to a second peak containing the N-module, found in the complexome profile analysis with an apparent molecular size of 1,386 kDa (Fig 5A). Furthermore, 2D-BNGE analysis followed by WB with four different antibodies recognizing specific subunits from distinct cI structural modules (NDUFA9, NDUFB8, NDUFS1, and NDUFV1) was used to determine the cI assembly dynamics on samples collected at the same time points from both cell lines (Fig 6E). In WT cells, the tested cI nuclear subunits were robustly expressed in a position corresponding to SCs with no obvious accumulation of assembly intermediates. By contrast, in $\Delta 4$ -CYB cells much lower amounts of cI subunits NDUFA9 and NDUFB8 were mostly detected in assembly intermediates as well as in the pre-cI structure. In accordance with the poor cI-IGA signals (Fig 6D), the NDUFS1 and NDUFV1 subunits, belonging to the N-module, were either undetected or detected in two very faint spots corresponding to the cI holocomplex and the higher molecular size structure (asterisk), the complete composition of which must be elucidated. The blots of mutant samples had to be exposed 10 times longer than those of the controls, in order to obtain detectable signals (Fig 6E). These observations further confirmed cI assembly stalling, with very residual incorporation of the N-module and accumulation of pre-cI in the absence of MT-CYB.

Complex I assembly stalling is due to both structural and functional loss of complex III

To distinguish whether the cI assembly blockage in $\Delta 4$ -CYB cells is merely due to the structural absence of cIII₂ or to the lack of ubiquinol oxidase activity, leading to a CoQ pool redox imbalance, we stably expressed an HA-tagged version of the *Emericella nidulans* alternative oxidase (AOX) (Perales-Clemente *et al.*, 2008; Guaras *et al.*, 2016) in WT and $\Delta 4$ -CYB cybrids. AOX is naturally expressed in plants as well as in some fungi and parasites, and its catalytic activity is able to bypass mitochondrial respiratory chain cIII₂ and cIV by directly oxidizing CoQ and reducing oxygen (Young *et al.*, 2013). AOX overexpression was previously shown to restore CoQ redox balance and to promote cI assembly in *Podospira anserina* fungal strains as well as in mouse cultured cells lacking complex III or IV (Maas *et al.*, 2009; Guaras *et al.*, 2016). Upon stable transduction of a lentiviral vector containing the AOX^{HA} coding sequence, the protein was readily expressed in both WT and $\Delta 4$ -CYB cybrids (Fig 7A). AOX^{HA} was shown to be functional in the human cells because its expression reversed the pyrimidine auxotrophy of the $\Delta 4$ -CYB cybrids, enabling them to grow in culture medium without uridine (Fig 7B), and indirectly indicating the restoration of the CoQ pool redox balance (King & Attardi, 1989). AOX^{HA} expression was associated with a partial recovery of the levels and assembly of cI subunits into the mature enzyme in the $\Delta 4$ -CYB cells (Fig 7C–E). In agreement, there was a significant change in cI enzymatic activity, increasing from 25 to 55% of the

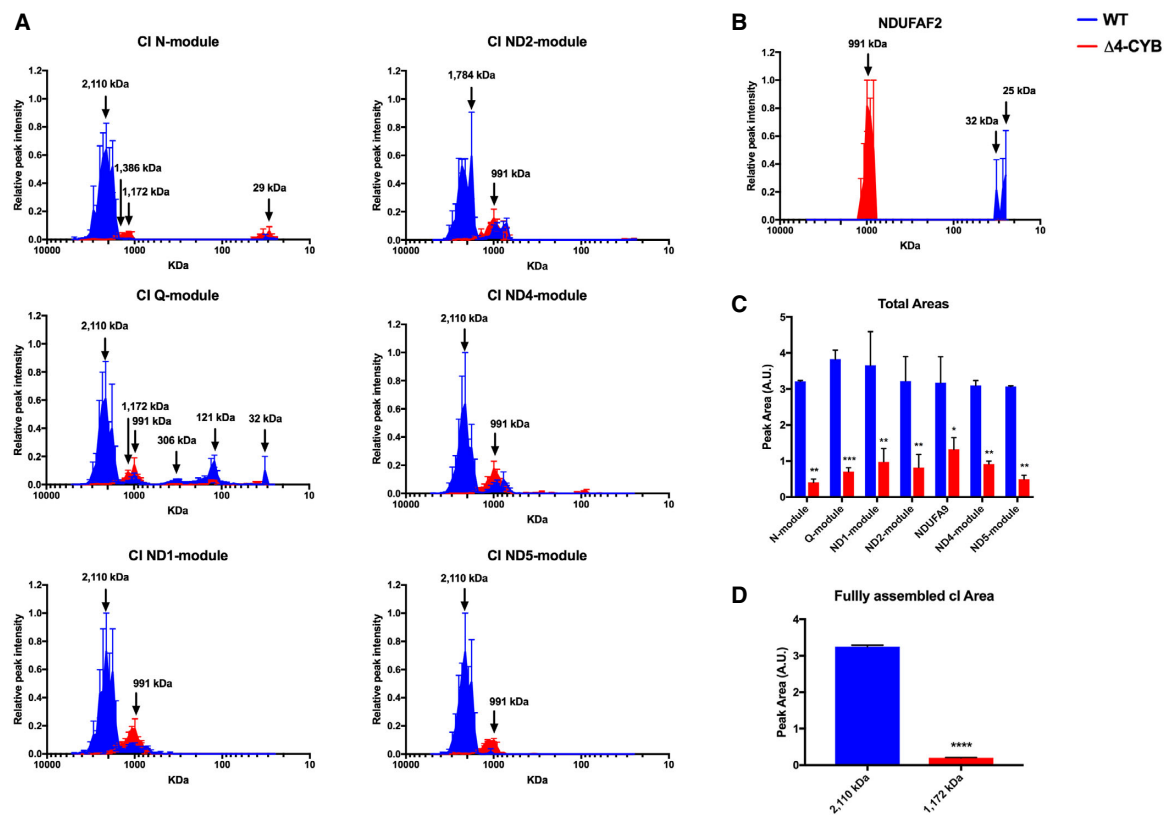


Figure 5. Complex I alterations in $\Delta 4$ -CYB cells.

- A** Complexome profiles of the different cI structural modules. The graphs were generated as in Fig 3, but in this case, the peptide intensity values for the individual subunits belonging to each module (Stroud *et al*, 2016) were averaged to simplify the analysis (see also Figs EV4 and EV5). The represented values are the mean \pm SEM of the two reciprocal labeling experiments.
- B** Complexome profiles of the cI assembly factor NDUFAF2 (see main text for details) in WT (blue) and $\Delta 4$ -CYB (red) mitochondria (see also Figs EV4 and EV5). The represented values are the mean \pm SEM of the two reciprocal labeling experiments.
- C** Quantification of the total area under the curve (calculated as in Fig 3C) in the profiles corresponding to each cI module (top graph). The area of the NDUFA9 subunit was calculated separately as its profile did not correspond to any of the other structural subunit modules. The plotted values are the mean \pm SD ($n = 2$). Two-way ANOVA with Sidak's multiple comparisons test *** $P = 0.0006$; ** $P = 0.0012$ (N-module); ** $P = 0.0016$ (ND1-module); ** $P = 0.0032$ (ND2-module); ** $P = 0.0057$ (ND4-module); *** $P = 0.0020$ (ND5-module); * $P = 0.0140$.
- D** Quantification of the area of the N-module peak corresponding to the molecular mass of the fully assembled cI: 1,172 kDa in $\Delta 4$ -CYB samples and the respirasome (cI+cIII₂+cIV) SCs in #4:1 WT samples (2,110 kDa). The plotted values are the mean \pm SD ($n = 2$). Unpaired Student's t -test **** $P < 0.0001$.

WT values (Fig 7F), which was reflected on a maximal respiratory capacity in the $\Delta 4$ -CYB AOX^{HA} cells of 50% of the WT (Fig 7G). In addition, readily detectable amounts of NDUFAF2 were still bound to pre-cI in the $\Delta 4$ -CYB AOX^{HA} cells (Fig 7D). Therefore, these results indicate that stable overexpression of functional AOX can only achieve a partial rescue of cI assembly in the absence of cIII₂.

To determine whether the impairment of the CoQ redox balance by abolishment of cIII₂ activity was sufficient to induce a similar cI assembly defect, WT cells stably expressing AOX^{HA} and their corresponding mock-transduced (EV) controls were cultured for 7 days in the presence of the specific inhibitor antimycin A (AA), which effectively inhibited mitochondrial respiration in the control cells (Fig 7H). Long-term inhibition of cIII₂ activity in these cells did not

induce any significant destabilization of cIII₂, cI, or SCs (Fig 7I). As expected, WT cells expressing functional AOX^{HA} treated with AA showed normal respiration (Fig 7H), again without affecting the relative distribution and levels of cI and SCs (Fig 7I). These results indicate that adjustment of the CoQ redox state by itself barely influences cI assembly or stability.

The absence of MT-CYB alters biogenesis of complexes II and IV, but not of complex V

SILAC-complexome experiments allowed us to systematically analyze the assembly state of the remaining OXPHOS enzymes in $\Delta 4$ -CYB versus WT cells systematically. Mass spectrometry analysis

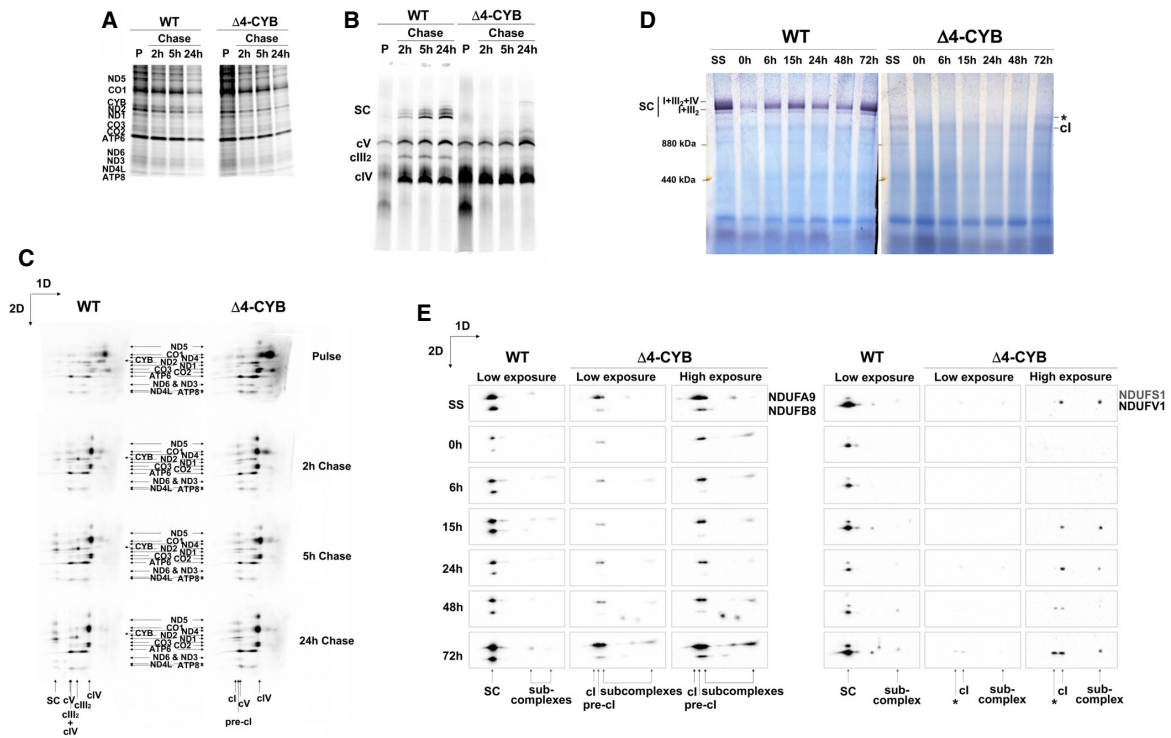


Figure 6. Complex I assembly kinetics in $\Delta 4$ -CYB cells.

A SDS-PAGE resolving the radioactively labeled mitochondrial translation products after a 2-h pulse (P). The ^{35}S -Met and the cycloheximide were removed from the medium, and cells were collected at the indicated chase times (2, 5, and 24 h).
B First-dimension (1D) BNGE analysis of the same cells as in (A), prepared with digitonin.
C Denaturing second-dimension (2D) BNGE analysis of the same samples allowed following the incorporation of the individual labeled subunits inside their corresponding complex and supercomplex species.
D Complex I-IGA (cI-IGA) analysis of digitonin-solubilized samples after inhibiting mitochondrial translation with doxycycline for 6 days (0 h). After removing the drug and restoring synthesis of the mtDNA-encoded subunits, the cells were collected at the indicated times to follow the appearance of cI reactivity with time. The gels were incubated in the reaction mixture for 24 h. SS = steady state. The asterisk indicates the presence of a high-molecular-weight cI-containing band of unknown nature (see main text).
E 2D BNGE, Western blot, and immunodetection analysis of WT and $\Delta 4$ -CYB mitochondria from cells collected at the same times after doxycycline treatment to follow the incorporation kinetics of the indicated cI nuclear-encoded subunits, belonging to different structural modules. The blots shown were either exposed for 16 s. (low exposures) or 160 s. (high exposures) in order to visualize the qualitative signals in the $\Delta 4$ -CYB samples.

Source data are available online for this figure.

detected subunits of cV belonging to its two distinct assembly modules (He *et al*, 2018). The F1 particle included α (ATP5A1), β (ATP5B), γ (ATP5C1), and ϵ (ATP5E) subunits, whereas the peripheral stalk included subunits b (ATP5F1), d (ATP5H), F6 (ATP5J), OSCP (ATP5O), e (ATP5I), f (ATP5J2), g (ATP5L), MT-ATP6, MT-ATP8, 6.8PL (MP68), and DAPIT. These results indicate that ATP synthase biogenesis was essentially unaffected in $\Delta 4$ -CYB (Fig 8A). As for cII subunits, SDHA showed decreased incorporation into the fully assembled enzyme (calculated MW 156 kDa) in the $\Delta 4$ -CYB cell line, as well as accumulation of sub-assembled species of lower molecular mass. These results could be related to the upregulation of cII assembly factor SDHAF2 (Fig 2A). Accordingly, the amounts of SDHB and SDHC incorporated into cII were about half of the control, and SDHC was also accumulated in subcomplexes (Fig 8B).

However, these alterations in cII biogenesis were not sufficient to determine an overt enzymatic deficiency (Fig 1A) and did not become evident by semi-quantitative Western blot analysis of BNGE samples (Fig 1C).

On the other hand, analysis of the relative amount and distribution of cIV subunits that define each of the assembly modules (Vidoni *et al*, 2017) revealed structural alterations and impaired assembly of cIV in $\Delta 4$ -CYB cells, compatible with the observed cytochrome c oxidase (COX) deficiency (Fig 1A). Subunits from the early, intermediate (MT-CO2), and late (MT-CO3) assembly modules were clearly reduced in free cIV and absent in the positions corresponding to cIII₂+cIV and “respirasome” (cI+cIII₂+cIV_n) SCs. The most affected subunit was NDUFA4 (COXFA4) (Pitceathly & Taanman, 2018), which was shown to have a weaker interaction

with the complex, being incorporated after the assembly of the “canonical” thirteen COX subunits (Balsa *et al*, 2012; Pitceathly *et al*, 2013; Vidoni *et al*, 2017). In addition, the “early” module

composed of COX4I1, COX5A, and HIGD1A appeared to accumulate in subcomplexes in $\Delta 4$ -CYB mitochondria (Fig 8C). MT-CO1 and COX7B were not detected in this complex analysis, but BNGE

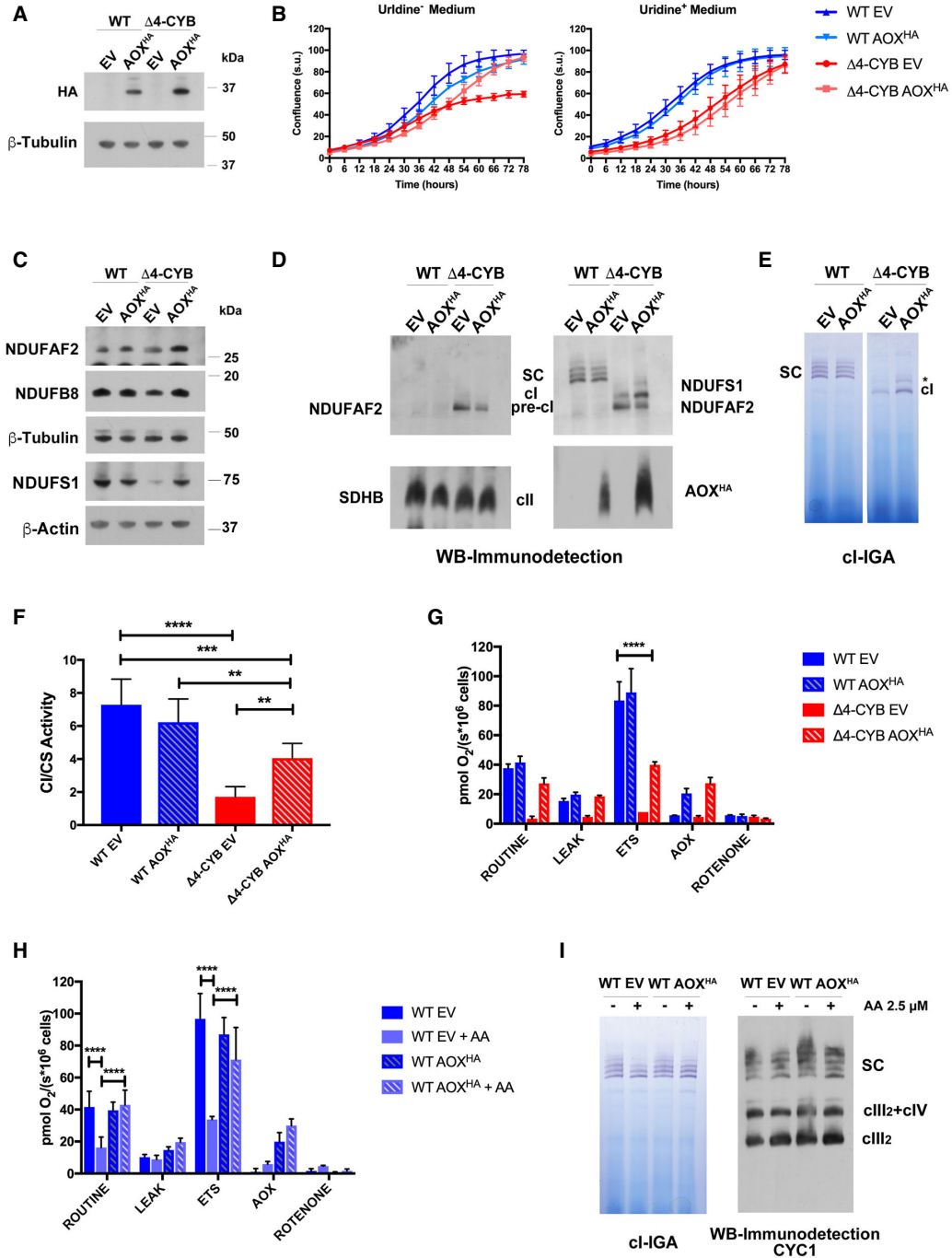


Figure 7.

Figure 7. Alternative oxidase (AOX) expression and function in WT and Δ 4-CYB cells.

- A SDS-PAGE, Western blot, and immunodetection of AOX^{H/A} expression in whole-cell lysates from WT and Δ 4-CYB cells transduced with the AOX^{H/A}/pWPXLd-ires-Hygro^R lentiviral vector. The transduction and selection controls were the same cell lines transfected with an empty pWPXLd-ires-Hygro^R vector (EV).
- B Growth curves of the AOX^{H/A} expressing cell lines and their corresponding EV controls. Cell growth was monitored every 6 h after substituting the medium in two replicate 24-well plates, one plate with medium without uridine (Uridine⁻), and the second plate with medium supplemented with 50 μ g/ml uridine (Uridine⁺). The graphs show the average confluence \pm SD at each time point ($n = 6$ wells per cell line).
- C Immunodetection of cI structural subunits and NDUFAF2 in the same samples as in panel (A).
- D 1D BNGE, Western blot, and immunodetection analyses of digitonin-solubilized mitochondria from WT and Δ 4-CYB cybrids expressing AOX^{H/A} and their corresponding EV controls.
- E Complex I in-gel activity assays (IGA) after BNGE as in panel (D). The gels were incubated in the IGA reaction mixture for 5 h. The asterisk indicates the presence of a high-molecular-weight cI-containing band of unknown nature (see main text).
- F Spectrophotometric kinetic measurements of cI activity in WT and Δ 4-CYB AOX^{H/A} and EV samples normalized by the percentage of citrate synthase (CS) activity. Results are expressed as mean \pm SD ($n = 5$ biological replicates). Two-way ANOVA with Tukey's multiple comparisons test $^{**}P = 0.0077$ (WT AOX^{H/A} versus Δ 4-CYB AOX^{H/A}); $^{**}P = 0.0044$ (Δ 4-CYB EV versus Δ 4-CYB AOX^{H/A}); $^{***}P = 0.0003$; $^{****}P < 0.0001$.
- G High-resolution respirometry analyses performed in intact cells in an Oroboros instrument. ROUTINE: cellular basal oxygen consumption rate (in pmol O₂/sec per million cells in DMEM medium. LEAK is the non-phosphorylating respiration in the presence of the ATP synthase inhibitor oligomycin. ETS: maximal respiration rate in the presence of the uncoupler CCCP. AOX: oxygen consumption in the presence of antimycin A, inhibiting cIII₂ activity but not that of AOX. ROTENONE: oxygen consumption in the presence of the cI inhibitor rotenone. In all cases, this was equal to the background. Results are expressed as mean \pm SD ($n = 2$ biological replicates). Two-way ANOVA with Tukey's multiple comparisons test $^{****}P < 0.0001$.
- H Respirometry analyses, performed as in panel (G), in WT EV controls and AOX^{H/A}-expressing cells untreated or treated with 2.5 μ M antimycin A for 7 days (+AA). Results are expressed as mean \pm SD ($n = 4$ biological replicates). Two-way ANOVA with Tukey's multiple comparisons test $^{****}P < 0.0001$.
- I 1D BNGE followed by cI-IGA (right) or Western blot and immunodetection of cIII₂ subunit CYC1 (left) in digitonin-solubilized samples from WT EV controls and AOX^{H/A}-expressing cells untreated (-) or treated (+) with 2.5 μ M antimycin A for 7 days.

Source data are available online for this figure.

combined with WB and immunodetection with specific antibodies also showed the increased accumulation of these subunits in cIV subassemblies of Δ 4-CYB versus WT cell lines (Fig 8D). Moreover, the assembly factor MR-1S was accumulated in the cIV intermediates of mutant samples migrating around the size of mature cIV molecular mass (Vidoni *et al*, 2017) (Fig 8C). The increased binding of the intermediate assembly factor MR-1S, despite the reduced amount of cIV in the Δ 4-CYB cells, indicated that the absence of MT-CYB also hampers the maturation and induces stalling of cIV assembly in a series of intermediates.

Discussion

In order to elucidate the mechanisms controlling the biogenesis of the human respiratory chain in health and disease, we have taken advantage of modern high-throughput proteomics techniques to evaluate the structural re-organization of the MRC complexes in human cybrids characterized by the complete loss of holo-cIII₂ (de Coo *et al*, 1999; Rana *et al*, 2000). In addition to the absence of cIII₂ enzymatic activity, these cells showed a marked defect in

cI activity. This confirmed the well-established connection between severe cIII₂ deficiency and cI impairment. Interestingly, the activity of cIV was also significantly reduced in our system, as previously reported in a subset of patients with severe cIII deficiency (Carossa *et al*, 2014; Feichtinger *et al*, 2017). Accordingly, the absence of fully assembled cIII₂ led to the complete loss of SCs containing cIII₂ and cI, and to the accumulation of an inactive pre-cI lacking the catalytic N-module; fully assembled cIV levels were also decreased and, to a lesser extent, those of cII as well. Our work gives a straightforward explanation of the combined respiratory chain enzyme deficiency associated with cIII₂ depletion, by providing evidence that cIII₂-containing SCs are essential to efficiently promote the assembly of the other MRC complexes, particularly of cI.

Previous experimental work in a mouse cell line led to propose a mechanism by which a severe *Mt-Cyb* mutation determined cI instability and degradation once the cI holo-enzyme was fully formed (Acin-Perez *et al*, 2004). The origin of this instability was deemed to be the oxidative damage to cI protein components due to reverse electron transfer (RET) originated by high reduced CoQ to total CoQ (CoQH₂/CoQ) ratios, triggering a response to degrade damaged cI

Figure 8. Assembly state of cV, cII, and cIV in Δ 4-CYB cells.

- A Complexome profiles of the two cV structural and assembly modules. The graphs were generated as in Fig 3, but in this case, the peptide intensity values for the individual subunits belonging to each module (He *et al*, 2018) were averaged to simplify the analysis. The represented values are the mean \pm SEM of the two reciprocal labeling experiments.
- B Complexome profiles of the three detected cII subunits. The graphs were generated as in Fig 3. The represented values are the mean \pm SEM of the two reciprocal labeling experiments.
- C Complexome profiles of the different cIV assembly modules and of the last subunit to be incorporated (NDUFA4). The graphs were generated as in Fig 3, but in this case, the peptide intensity values for the individual subunits belonging to each assembly module (Vidoni *et al*, 2017) were averaged to simplify the analysis. The represented values are the mean \pm SEM of the two reciprocal labeling experiments. The bar graph represents the quantification of the total area under the curve (calculated as in Fig 3C) in the profiles corresponding to each cIV module. The plotted values are mean \pm SD ($n = 2$). Two-way ANOVA with Sidak's multiple comparisons test $^{**}P = 0.0088$ (Early); $^{**}P = 0.0063$ (MT-CO2); $^{**}P = 0.0040$ (NDUFA4); $^{*}P = 0.0264$.
- D 1D BNGE, Western blot, and immunodetection of two cIV subunits (MT-CO1 and COX7B) in samples from WT and Δ 4-CYB cells solubilized with DDM and digitonin (Dig).

Source data are available online for this figure.

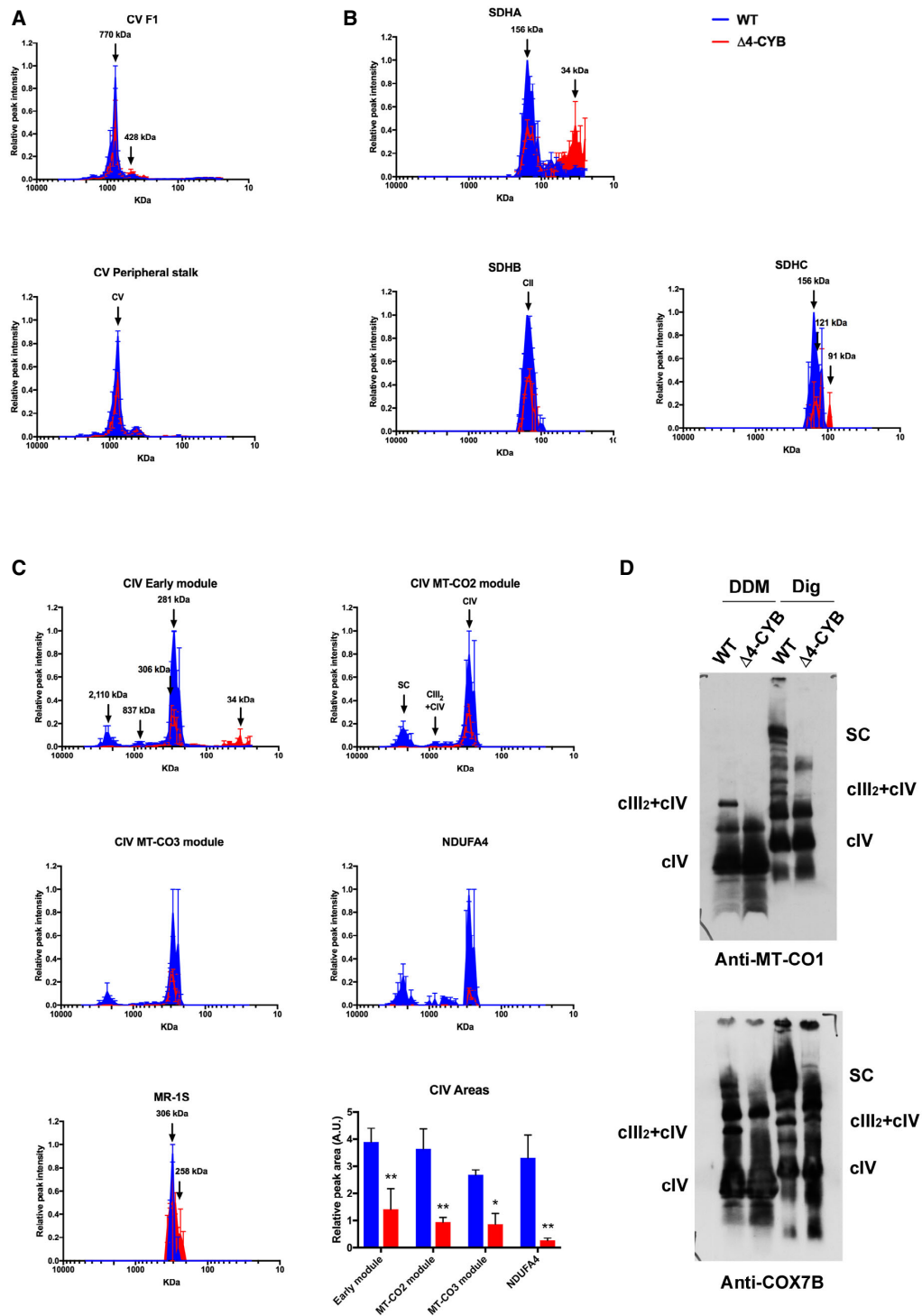


Figure 8.

by undefined mechanisms and proteases (Guaras *et al*, 2016). However, this explanation is incompatible with the fact that long-term exposure to cIII₂ inhibitors, which would also increase the CoQH₂/CoQ ratio, does not result in cI destabilization (Acin-Perez *et al*, 2004; Guaras *et al*, 2016; this work).

The results shown in this report clearly prove that the absence of cIII₂ originates a block in the assembly process of nascent cI, demonstrating that the efficient maturation of human cI strictly depends on its association to cIII₂ within SCs in physiological conditions. Our conclusion is based on the following evidence. First, NDUFAF2, the factor that holds pre-cI (or ~830 kDa intermediate) in a competent state to complete the assembly process by adding the N-module (Ogilvie *et al*, 2005; Sanchez-Caballero *et al*, 2016), is overexpressed in Δ4-CYB mitochondria as a consequence of cI assembly stalling and was detected bound to immature pre-cI. Second, pulse-chase labeling of the mtDNA-encoded subunits showed comparable turnover of the MT-ND subunits between the mutated and control cells, contrary to the model based on instability and degradation of fully assembled cI. Third, the kinetics of incorporation of both mitochondrial and nuclear cI subunits into the nascent complex over time indicated the accumulation of most cI subunits in the pre-cI at all times in the mutant, rather than the prior formation of a complete “free” cI able to be incorporated into SCs and then degraded in the absence of cIII₂. Several arguments may explain the different experimental interpretation in mouse cells carrying a *Mt-Cyb* mutation (Acin-Perez *et al*, 2004). In addition to using cells from different species, in which the turnover rates of the MRC complexes may differ, the times used in the pulse-chase experiments of Acin-Perez *et al* missed intermediate points (e.g., 2 and 5 h), and samples were solubilized using DDM instead of digitonin, which prevents the visualization of respirasomes. Indeed, Acin-Perez *et al* describe the appearance of a second faster-migrating cI band of “unknown nature” accumulating in the *Mt-Cyb*-mutated cells, that could very well be pre-cI, which was still unknown at the time (Ogilvie *et al*, 2005). Importantly, our detailed analysis of respiratory chain complex subunit incorporation dynamics supports the view that full and proper maturation of human cI preferentially occurs within the SC structures (Moreno-Lastres *et al*, 2012). By increasing the intermediate time points of our experiments, we demonstrated that the temporal gap between the complete assembly of cI and its incorporation into SCs, as previously proposed (Acin-Perez *et al*, 2008; Guerrero-Castillo *et al*, 2017), did not occur. Notably, the existence of such a kinetic “gap” had previously set the basis to propose the “plasticity model” for the structural and functional organization of the respiratory chain, which, in view of our data, deserves further confirmation.

The replacement of cIII₂ function by xeno-expression of AOX in Δ4-CYB cells partially increased the levels of functional cI, as reported in mutant mouse cells (Guaras *et al*, 2016). However, pre-cI accumulation was still evident, and cI-linked activities remained at approximately half of the control values. These observations are consistent with the idea that promotion of efficient cI maturation has two components: a functional component sensing the redox state of the CoQ pool and a structural component induced by the physical binding of cIII₂ to pre-cI. Concerning the CoQ redox balance, one could speculate that a highly reduced CoQ pool can change the redox state of pre-cI within which the Fe-S clusters would be reduced, thus possibly changing the milieu polarity and

impeding the incorporation of the N-module through electrostatic forces. From the structural point of view, there is no direct contact between cIII₂ and the N-module of cI in the respirasome (Gu *et al*, 2016; Letts *et al*, 2016; Wu *et al*, 2016; Guo *et al*, 2017), but it has now been demonstrated that there is a structural cross-talk between cI and cIII₂ (Letts *et al*, 2019). Therefore, it is conceivable that the binding of cIII₂ to pre-cI could induce a conformational change facilitating the exchange of NDUFAF2 for the N-module.

Our analyses also showed stabilization of novel cIII₂ intermediates containing catalytic CYC1 and accessory UQCR10 subunits. This finding was surprising since MT-CYB, the only mtDNA-encoded subunit of cIII₂, has consistently been considered as the “seed” around which the rest of cIII₂ builds up, assuming that no intermediates could be assembled independently from MT-CYB (Ndi *et al*, 2018). Moreover, the current cIII₂ assembly model establishes an early interaction of CYC1 with UQCR1 and UQCR2 (Zara *et al*, 2009; Signes & Fernandez-Vizcarra, 2018). Our data are not compatible with this hypothesis since CYC1 accumulated in different protein structures, whereas UQCR1 and UQCR2, whose stability critically depends on the presence of MT-CYB, were virtually undetected. Although we found UQCR10- and CYC1-containing protein structures within a wide range of molecular sizes, mass spectrometry analysis on immunopurified fractions overexpressing UQCR10^{HA} and CYC1^{HA} failed to detect convincing novel partners potentially acting as cIII₂ chaperones or assembly factors. By contrast, these analyses provided evidence for the co-existence of cIV structural subunits, mainly belonging to the MT-CO2 assembly module (Vidoni *et al*, 2017), within the cIII₂ stalled intermediates present in the *MT-CYB* mutant cells, where SCs are totally absent. Overall, these findings suggest that cIV subunits are sequestered within aberrant cIII₂ subcomplexes, possibly as a signal to avoid the full assembly and maturation of cIV in a cellular environment lacking SCs. Accordingly, the overall biogenesis of cIV was affected by the loss of cIII₂ without enhanced turnover of cIV subunits and holo-cIV. This suggests stalling of cIV maturation, further supported by the increased amounts of MR-1S, a mammalian COX assembly factor found within the advanced cIV intermediates (Vidoni *et al*, 2017). Likewise, our analyses showed general assembly adaptations of cII in the mutant cells, supported by overexpression of SDHAF2, a cII assembly factor binding SDHA and mediating its flavinylation (Hao *et al*, 2009; Kim *et al*, 2012). However, these alterations were not drastic enough to induce a significant functional impairment of cII.

In conclusion, our data have uncovered a fundamental function for MRC SCs, as the platform for regulated assembly of complexes I and IV, and possibly cII as well, in which cIII₂ is central. Thus, SC could act as “mitochondrial factories” to control the stoichiometry of the MRC complexes in different metabolic settings or even assist in the overall repair of respiratory chain modules damaged during respiratory work. Both possibilities will be addressed in future investigations.

Materials and Methods

Cell culture

143B-TK⁻ osteosarcoma-derived cybrid cells were grown in High-Glucose (4.5 g/l) DMEM containing Sodium Pyruvate and

GlutaMAX™ (Gibco-Thermo Fisher Scientific) supplemented with 10% fetal bovine serum (Gibco-Thermo Fisher Scientific) and 50 µg/ml uridine (Sigma-Aldrich). Cells transduced with expression vectors containing a puromycin resistance cassette were grown in the presence of 1 µg/ml Puromycin (InvivoGen). If it was hygromycin, the final concentration of the Hygromycin B was 100 µg/ml (InvivoGen), and for neomycin-resistant cells, the final concentration of geneticin was 500 µg/ml (Gibco-Thermo Fisher Scientific).

The cells used in the SILAC experiments were grown in DMEM for SILAC (Gibco-Thermo Fisher Scientific) plus 10% dialyzed serum (Gibco-Thermo Fisher Scientific) and 50 µg/ml uridine, supplemented either with unlabeled L-lysine monohydrochloride (K₀), L-arginine (R₀), and L-proline ("Light" conditions) or with L-lysine-¹³C₆, ¹⁵N₂ hydrochloride (K₈), L-arginine-¹³C₆, ¹⁵N₄ hydrochloride (R₁₀), and L-proline ("Heavy" conditions), all from Sigma-Aldrich.

Denaturing and native electrophoresis, western blot, and immunodetection

Total protein extracts from cultured cells or fractions were resolved by SDS-PAGE using Novex NuPAGE 4–12% Bis-Tris Precast Gels (Thermo Fisher Scientific).

Samples for blue-native gel electrophoresis (BNGE) were prepared either from digitonized cellular extracts (Nijtmans *et al*, 2002) or from isolated mitochondria (Fernández-Vizarrá *et al*, 2010). For the solubilizations, either 1.6 mg DDM/mg protein or 4 mg digitonin/mg protein was used (Wittig *et al*, 2006; Acin-Perez *et al*, 2008). Approximately 50 µg of protein was loaded into Native PAGE Novex 3–12% Bis-Tris Protein Gels (Thermo Fisher Scientific) and electrophoresed in the conditions indicated by the manufacturer.

Proteins were electroblotted to PVDF membranes and immunodetected using commercial antibodies (Table 1). Immunoreactive bands were visualized using ECL Western Blotting Detection Reagents (GE Healthcare) and X-Ray films (Fuji) or using a digital Amersham Imager 680 (GE Healthcare). Signal intensities were quantified by densitometry using ImageJ.

Enzymatic activity assays

For the biochemical kinetic reaction assays, digitonin-solubilized cell samples were used (Tiranti *et al*, 1995). Individual cI (NADH: decylubiquinone oxidoreductase, rotenone sensitive), cII (succinate: CoQ₁ oxidoreductase), cIII (decylubiquinol:cytochrome c oxidoreductase), cIV (cytochrome c oxidase), and citrate synthase (CS) activities were measured as described (Kirby *et al*, 2007), with slight modifications. The reactions were performed for 2 min in 96-well plates in a final volume of 200 µl.

Complex I in-gel activity (IGA) assays were performed on the samples electrophoresed in native conditions as described (Calvaruso *et al*, 2008). To allow for cI activity to appear, gels were incubated between 1.5 and 24 h in cI-IGA reaction buffer.

Complexome profiling

Mitochondria isolated from 1:1 mixtures of differentially SILAC labeled #4.1 WT and #17.1 Δ4-CYB cybrids were used to analyze

Table 1. Antibodies used in this study.

Antibody	Source	Catalogue number
Rabbit monoclonal anti-NDUFS1	Abcam	ab169540
Mouse monoclonal anti-NDUFS3	Abcam	ab110246
Mouse monoclonal anti-NDUFA9	Life Technologies	LS459100
Mouse monoclonal anti-NDUFB11	Proteintech	16720-1-AP
Mouse monoclonal anti-NDUFB8	Abcam	ab110242
Rabbit polyclonal anti-NDUFAF2	Proteintech	13891-1-AP
Mouse monoclonal anti-SDHA	Abcam	ab14715
Mouse monoclonal anti-SDHB	Abcam	ab14714
Mouse monoclonal anti-UQCRC1	Abcam	ab110252
Mouse monoclonal anti-UQCRC2	Abcam	ab14745
Mouse monoclonal anti-UQCRCF1	Abcam	ab14746
Rabbit polyclonal anti-CYC1	Proteintech	10242-1-AP
Mouse monoclonal anti-UQCRQ	Abcam	ab110255
Rabbit polyclonal anti-UQCRQ	Abcam	ab136679
Rabbit monoclonal anti-UQCRB	Abcam	ab190360
Mouse monoclonal anti-COX5A	Abcam	ab110262
Mouse monoclonal anti-COX6B1	Abcam	ab110266
Mouse monoclonal anti-COX7B	Abcam	ab197379
Mouse monoclonal anti-MTCO1	Abcam	ab14705
Mouse monoclonal anti-MTCO2	Abcam	ab110258
Mouse monoclonal anti-ATP5A	Abcam	ab14748
Rabbit polyclonal anti-ATPbeta	Santa Cruz Biotechnology	SC-33618
Mouse monoclonal anti-ATPb	Santa Cruz Biotechnology	SC-514419
Mouse monoclonal anti-β-actin	Sigma-Aldrich	A1978
Mouse monoclonal anti-β-tubulin	Sigma-Aldrich	T5201
Rat monoclonal anti-HA	Roche	11867423001
Mouse monoclonal Anti-FLAG M2	Sigma-Aldrich	F3165
Goat anti-Mouse IgG	PROMEGA	W402B
Goat anti-Rabbit IgG	PROMEGA	W401B
Goat anti-Rat IgG	Cell Signaling Technology	70775
Rabbit monoclonal anti-HA (Sepharose® Bead Conjugate)	Cell Signaling Technology	3956S

the samples and generate the complexome profiles as described (Vidoni *et al*, 2017).

Overexpression of tagged proteins

For the amplification of UQCRQ and UQCR10 cDNAs, total RNA was extracted from control human fibroblasts (TRIZol Plus RNA Purification System, Invitrogen) and retrotranscribed (Omniscript RT Kit, Qiagen). Approximately 200 ng of cDNA were used as templates for the amplification of UQCRQ and UQCR10 using specific primers (sequences available upon request). The PCR products were cloned

directly into the pCR2.1 TA-cloning vector. After sequence verification, selected clones were used to add the C-terminal HA tags by PCR amplification. The CYC1^{HA} PCR product was generated using DNA from synthetic clone containing the CYC1 sequence as the template. The HA-tagged *Emericella nidulans* AOX cDNA insert cloned into the pTNT vector was a kind gift from M^a Pilar Bayona-Bafaluy (University of Zaragoza, Spain). The insert was amplified by PCR with specific oligos using this vector as a template. The PCR-generated HA-tagged fragments were again cloned in the pCR2.1 TA-cloning vector (Invitrogen). These inserts were then introduced into the pWPXLd-ires-Puro^R or pWPXLd-ires-Hygro^R lentiviral expression vectors, modified versions of pWPXLd (Addgene #12258), by restriction enzyme digestion with EcoRV/PmeI and BamHI and ligation with T4 DNA ligase (New England Biolabs).

Lentiviral particles were generated in HEK293T packaging cells by co-transfection, with FuGENE 6 (Promega), of the target vector with the packaging psPAX2 (Addgene plasmid #12260) and envelope pMD2.G (Addgene #12259) vectors. The lentiviral vectors were a gift from Didier Trono. Target cells were transduced as described (Perales-Clemente *et al.*, 2008). Twenty-four hours after transduction, cells were selected for puromycin or hygromycin resistance.

The Myc-DDK (FLAG)-tagged NDUFAF2 cDNA clone (Cat# RC207387) and the “empty” pCMV6-Entry mammalian expression vector (Cat# PS100001) were purchased from OriGene Technologies. WT and Δ 4-CYB cybrids were transfected with these vectors using FuGENE HD (Promega). Forty-eight hours after transfection, cells were selected for neomycin resistance.

Immunopurification and quantitative proteomics

The immunopurification of the HA-tagged cIII₂ subunits UQCR10 and CYC1 expressed in the SILAC labeled WT and Δ 4-CYB cybrids was performed and analyzed as described (Andrews *et al.*, 2013; Vidoni *et al.*, 2017).

Assembly kinetics assays

[³⁵S]-L-Methionine pulse and pulse-chase labeling of the mitochondrial peptides were performed as described (Chomyn, 1996; Fernandez-Silva *et al.*, 2007). Labeled samples from cells in one 10-cm petri dish were prepared for BNGE using the digitonization method (Nijtmans *et al.*, 2002).

Mitochondrial translation was blocked by adding 15 μ g/ml doxycycline to the cell culture medium for 6 days, and the cells were collected at different time points after removal of the drug and prepared for BNGE as described (Ugalde *et al.*, 2004).

Cell growth

Growth curves were assessed using an IncuCyte HD instrument (Essen Bioscience) using an algorithm to calculate cell confluency based on inverted microscope imaging. Images of each of the 24 wells in the plates were taken every 6 h for a total period of 78 h.

Respirometry

Oxygen consumption measurements were performed in intact cells using an Oroboros Instruments High-Resolution

Respirometer (Pesta & Gnaiger, 2012). Measurements were performed using approximately 5×10^6 cells in the same supplemented culture medium used to grow them. Basal (ROUTINE) respiration was recorded until the steady state was reached and was continued for an additional 5 min. To inhibit the ATP synthase (cV) and measure the non-phosphorylating respiration (LEAK), 2.5 μ M oligomycin was added to the chambers and the respiration rates left to reach the steady state. The uncoupled state (ETS) was achieved by titrating CCCP in 0.5 μ M steps until the respiratory rates did not increase any further. Next, 2.5 μ M antimycin A was added to the chambers to inhibit cIII and to evaluate AOX-driven respiration. Finally, 1 μ M rotenone was added to inhibit cI.

Statistical analysis

Numerical data in graphs are shown as mean \pm SD. Student's *t*-test was used for pair-wise comparison, while 2-way ANOVA with Sidak's or Tukey's (depending on the software recommendation) *post hoc* test was used for multiple comparisons. GraphPad Prism v.7.0e for Mac OS was the software used for the statistical analyses and for calculation of the area under the curves (AUC) defined by the peptide intensity in each gel slice in the MS complexome profiling analyses.

Data availability

The mass spectrometry proteomics data have been deposited to the ProteomeXchange Consortium (<https://www.ebi.ac.uk/pride/>) via the PRIDE partner repository with the dataset identifier PXD016521.

Expanded View for this article is available online.

Acknowledgements

We are grateful to Antonio Barrientos (University of Miami, USA) for critically revising the manuscript and to Justin G. Fedor (Mitochondrial Biology Unit, Cambridge, UK), Leonid A. Sazanov (IST Austria, Klosterneuburg, Austria), and James A. Letts (University of California, Davis, USA) for scientific discussions. We also thank Irenaeus F. de Coo (Erasmus University, The Netherlands) for the original patient fibroblasts used to produce cybrids and Ester Perales-Clemente and M. Pilar Bayona-Bafaluy (University of Zaragoza, Spain) for providing the Puro^R and Hygro^R lentiviral expression vectors. Our research was supported by the Core Grant from the Medical Research Council (Grant MC_UU_00015/5), ERC Advanced Grant FP7-3222424 and NRJ-Institut de France Grant (to M.Z.), Association Française contre les Myopathies (AFM) grant 16086 (to E.F.-V.), Instituto de Salud Carlos III-MINECO/European ERDF-ESF grant PI17-00048, Comunidad Autónoma de Madrid/ERDF-ESF grant P2018/BAA-4403, and NIH-RO1 grant GM105781 (to C.U.).

Author contributions

Conceptualization, EF-V and CU; Methodology, MEH, IMF, CU, and EF-V; Software, MEH; Investigation, MP, RP-P, TL, MEH, SD, AP, and EF-V; Formal Analysis, MP, RP-P, MEH, SD, CU, and EF-V; Resources, FD, CTM, MZ, CU, and EF-V; Writing—Original Draft, EF-V; Writing—Reviewing and Editing, MEH, FD, CTM, IMF, MZ, CU, and EF-V; Visualization, MP, RP-P, CU, and EF-V; Supervision, CU and EF-V; Funding Acquisition, CU, EF-V, and MZ.

Conflict of interest

The authors declare that they have no conflict of interest.

References

- Acin-Perez R, Bayona-Bafaluy MP, Fernandez-Silva P, Moreno-Loshuertos R, Perez-Martos A, Bruno C, Moraes CT, Enriquez JA (2004) Respiratory complex III is required to maintain complex I in mammalian mitochondria. *Mol Cell* 13: 805–815
- Acin-Perez R, Fernandez-Silva P, Peleato ML, Perez-Martos A, Enriquez JA (2008) Respiratory active mitochondrial supercomplexes. *Mol Cell* 32: 529–539
- Andrews B, Carroll J, Ding S, Fearnley IM, Walker JE (2013) Assembly factors for the membrane arm of human complex I. *Proc Natl Acad Sci USA* 110: 18934–18939
- Balsa E, Marco R, Perales-Clemente E, Szklarczyk R, Calvo E, Landazuri MO, Enriquez JA (2012) NDUFA4 is a subunit of complex IV of the mammalian electron transport chain. *Cell Metab* 16: 378–386
- Barel O, Shorer Z, Flusser H, Ofir R, Narkis G, Finer G, Shalev H, Nasasra A, Saada A, Birk OS (2008) Mitochondrial complex III deficiency associated with a homozygous mutation in UQCRCQ. *Am J Hum Genet* 82: 1211–1216
- Baughman JM, Nilsson R, Gohil VM, Arlow DH, Gauhar Z, Mootha VK (2009) A computational screen for regulators of oxidative phosphorylation implicates SLIRP in mitochondrial RNA homeostasis. *PLoS Genet* 5: e1000590
- Berry EA, Huang LS, Zhang Z, Kim SH (1999) Structure of the avian mitochondrial cytochrome bc1 complex. *J Bioenerg Biomembr* 31: 177–190
- Berry EA, Guergova-Kuras M, Huang LS, Crofts AR (2000) Structure and function of cytochrome bc complexes. *Annu Rev Biochem* 69: 1005–1075
- Bruno C, Santorelli FM, Assereto S, Tonoli E, Tessa A, Traverso M, Scapolan S, Bado M, Tedeschi S, Minetti C (2003) Progressive exercise intolerance associated with a new muscle-restricted nonsense mutation (G142X) in the mitochondrial cytochrome b gene. *Muscle Nerve* 28: 508–511
- Calvaruso MA, Smeitink J, Nijtmans L (2008) Electrophoresis techniques to investigate defects in oxidative phosphorylation. *Methods* 46: 281–287
- Carossa V, Ghelli A, Tropeano CV, Valentino ML, Iommarini L, Maresca A, Caporali L, La Morgia C, Liguori R, Barboni P et al (2014) A novel in-frame 18-bp microdeletion in MT-CYB causes a multisystem disorder with prominent exercise intolerance. *Hum Mutat* 35: 954–958
- Chen YC, Taylor EB, Dephoure N, Heo JM, Tonhato A, Papandreou I, Nath N, Denko NC, Gygi SP, Rutter J (2012) Identification of a protein mediating respiratory supercomplex stability. *Cell Metab* 15: 348–360
- Chomyn A (1996) *In vivo* labeling and analysis of human mitochondrial translation products. *Methods Enzymol* 264: 197–211
- de Coo IF, Renier WO, Ruitenbeek W, Ter Laak HJ, Bakker M, Schagger H, Van Oost BA, Smeets HJ (1999) A 4-base pair deletion in the mitochondrial cytochrome b gene associated with parkinsonism/MELAS overlap syndrome. *Ann Neurol* 45: 130–133
- Cox J, Mann M (2008) MaxQuant enables high peptide identification rates, individualized p.p.b.-range mass accuracies and proteome-wide protein quantification. *Nat Biotechnol* 26: 1367–1372
- Cox J, Mann M (2011) Quantitative, high-resolution proteomics for data-driven systems biology. *Annu Rev Biochem* 80: 273–299
- Eaton S, Bursby T, Middleton B, Pourfarzang M, Mills K, Johnson AW, Bartlett K (2000) The mitochondrial trifunctional protein: centre of a beta-oxidation metabolon? *Biochem Soc Trans* 28: 177–182
- Feichtinger RG, Brunner-Krainz M, Alhaddad B, Wortmann SB, Kovacs-Nagy R, Stojakovic T, Erwa W, Resch B, Windischhofer W, Verheyen S et al (2017) Combined respiratory chain deficiency and UQC22 mutations in neonatal encephalomyopathy: defective supercomplex assembly in complex III deficiencies. *Oxid Med Cell Longev* 2017: 7202589
- Fernandez-Silva P, Acin-Perez R, Fernandez-Vizarrá E, Perez-Martos A, Enriquez JA (2007) *In vivo* and in organello analyses of mitochondrial translation. *Methods Cell Biol* 80: 571–588
- Fernandez-Vizarrá E, Bugiani M, Goffrini P, Carrara F, Farina L, Procopio E, Donati A, Uziel G, Ferrero I, Zeviani M (2007) Impaired complex III assembly associated with BCS1L gene mutations in isolated mitochondrial encephalopathy. *Hum Mol Genet* 16: 1241–1252
- Fernández-Vizarrá E, Ferrín G, Pérez-Martos A, Fernández-Silva P, Zeviani M, Enriquez JA (2010) Isolation of mitochondria for biogenetical studies: an update. *Mitochondrion* 10: 253–262
- Gruschke S, Rompler K, Hildenbeutel M, Kehrein K, Kuhl I, Bonnefoy N, Ott M (2012) The Cbp3-Cbp6 complex coordinates cytochrome b synthesis with bc1 complex assembly in yeast mitochondria. *J Cell Biol* 199: 137–150
- Gu J, Wu M, Guo R, Yan K, Lei J, Gao N, Yang M (2016) The architecture of the mammalian respirasome. *Nature* 537: 639–643
- Guaras A, Perales-Clemente E, Calvo E, Acin-Perez R, Loureiro-Lopez M, Pujol C, Martinez-Carrascoso I, Nunez E, Garcia-Marques F, Rodriguez-Hernandez MA et al (2016) The CoQH2/CoQ ratio serves as a sensor of respiratory chain efficiency. *Cell Rep* 15: 197–209
- Guerrero-Castillo S, Baertling F, Kownatzki D, Wessels HJ, Arnold S, Brandt U, Nijtmans L (2017) The assembly pathway of mitochondrial respiratory chain complex I. *Cell Metab* 25: 128–139
- Guo R, Zong S, Wu M, Gu J, Yang M (2017) Architecture of human mitochondrial respiratory megacomplex I2III2IV2. *Cell* 170: 1247–1257 e12
- Hao HX, Khalimonchuk O, Schraders M, Dephoure N, Bayley JP, Kunst H, Devilee P, Cremers CW, Schiffman JD, Bentz BG et al (2009) SDHS, a gene required for flavination of succinate dehydrogenase, is mutated in paraganglioma. *Science* 325: 1139–1142
- He J, Ford HC, Carroll J, Douglas C, Gonzales E, Ding S, Fearnley IM, Walker JE (2018) Assembly of the membrane domain of ATP synthase in human mitochondria. *Proc Natl Acad Sci USA* 115: 2988–2993
- Heide H, Bleier L, Steger M, Ackermann J, Drose S, Schwamb B, Zornig M, Reichert AS, Koch I, Wittig I et al (2012) Complexome profiling identifies TMEM126B as a component of the mitochondrial complex I assembly complex. *Cell Metab* 16: 538–549
- Imai Y, Meng H, Shiba-Fukushima K, Hattori N (2019) Twin CHCH proteins, CHCHD2, and CHCHD10: key molecules of Parkinson's disease, amyotrophic lateral sclerosis, and frontotemporal dementia. *Int J Mol Sci* 20: E908
- Iwata S, Lee JW, Okada K, Lee JK, Iwata M, Rasmussen B, Link TA, Ramaswamy S, Jap BK (1998) Complete structure of the 11-subunit bovine mitochondrial cytochrome bc1 complex. *Science* 281: 64–71
- Kim HJ, Jeong MY, Na U, Winge DR (2012) Flavinylation and assembly of succinate dehydrogenase are dependent on the C-terminal tail of the flavoprotein subunit. *J Biol Chem* 287: 40670–40679
- King MP, Attardi G (1989) Human cells lacking mtDNA: repopulation with exogenous mitochondria by complementation. *Science* 246: 500–503
- King MP, Attadi G (1996a) Mitochondria-mediated transformation of human rho(0) cells. *Methods Enzymol* 264: 313–334
- King MP, Attardi G (1996b) Isolation of human cell lines lacking mitochondrial DNA. *Methods Enzymol* 264: 304–313
- Kirby DM, Thorburn DR, Turnbull DM, Taylor RW (2007) Biochemical assays of respiratory chain complex activity. *Methods Cell Biol* 80: 93–119
- Kozjak-Pavlovic V (2017) The MICOS complex of human mitochondria. *Cell Tissue Res* 367: 83–93

- Lamantea E, Carrara F, Mariotti C, Morandi L, Tiranti V, Zeviani M (2002) A novel nonsense mutation (Q352X) in the mitochondrial cytochrome b gene associated with a combined deficiency of complexes I and III. *Neuromuscul Disord* 12: 49–52
- Lapiente-Brun E, Moreno-Loshuertos R, Acin-Perez R, Latorre-Pellicer A, Colas C, Balsa E, Perales-Clemente E, Quiros PM, Calvo E, Rodriguez-Hernandez MA et al (2013) Supercomplex assembly determines electron flux in the mitochondrial electron transport chain. *Science* 340: 1567–1570
- Lenaz G, Fato R, Formiggini G, Genova ML (2007) The role of Coenzyme Q in mitochondrial electron transport. *Mitochondrion* 7(Suppl): S8–S33
- Letts JA, Fiedorczuk K, Sazanov LA (2016) The architecture of respiratory supercomplexes. *Nature* 537: 644–648
- Letts JA, Fiedorczuk K, Degliesposti G, Skehel M, Sazanov LA (2019) Structures of respiratory supercomplex I+III2 reveal functional and conformational crosstalk. *Mol Cell* 75: 1131–1146 e6
- Maas MF, Krause F, Dencher NA, Sainsard-Chanet A (2009) Respiratory complexes III and IV are not essential for the assembly/stability of complex I in fungi. *J Mol Biol* 387: 259–269
- Meng H, Yamashita C, Shiba-Fukushima K, Inoshita T, Funayama M, Sato S, Hatta T, Natsume T, Umitsu M, Takagi J et al (2017) Loss of Parkinson's disease-associated protein CHCHD2 affects mitochondrial crista structure and destabilizes cytochrome c. *Nat Commun* 8: 15500
- Mimaki M, Wang X, McKenzie M, Thorburn DR, Ryan MT (2012) Understanding mitochondrial complex I assembly in health and disease. *Biochim Biophys Acta* 1817: 851–862
- Moreno-Lastres D, Fontanesi F, Garcia-Consuegra I, Martin MA, Arenas J, Barrientos A, Ugalde C (2012) Mitochondrial complex I plays an essential role in human respirasome assembly. *Cell Metab* 15: 324–335
- Ndi M, Marin-Buera L, Salvatori R, Singh AP, Ott M (2018) Biogenesis of the bc1 complex of the mitochondrial respiratory chain. *J Mol Biol* 430: 3892–3905
- Nijtmans LG, Henderson NS, Holt IJ (2002) Blue Native electrophoresis to study mitochondrial and other protein complexes. *Methods* 26: 327–334
- Ogilvie I, Kennaway NG, Shoubridge EA (2005) A molecular chaperone for mitochondrial complex I assembly is mutated in a progressive encephalopathy. *J Clin Invest* 115: 2784–2792
- Oka T, Sayano T, Tamai S, Yokota S, Kato H, Fujii G, Mihara K (2008) Identification of a novel protein MIC51 that is involved in maintenance of mitochondrial morphology and apoptotic release of cytochrome c. *Mol Biol Cell* 19: 2597–2608
- Perales-Clemente E, Bayona-Bafaluy MP, Perez-Martos A, Barrientos A, Fernandez-Silva P, Enriquez JA (2008) Restoration of electron transport without proton pumping in mammalian mitochondria. *Proc Natl Acad Sci USA* 105: 18735–18739
- Perez-Perez R, Lobo-Jarne T, Milenkovic D, Mourier A, Bratic A, Garcia-Bartolome A, Fernandez-Vizarras E, Cadenas S, Delmiro A, Garcia-Consuegra I et al (2016) COX7A2L is a mitochondrial complex III binding protein that stabilizes the III2+IV supercomplex without affecting respirasome formation. *Cell Rep* 16: 2387–2398
- Pesta D, Gnaiger E (2012) High-resolution respirometry: OXPHOS protocols for human cells and permeabilized fibers from small biopsies of human muscle. *Methods Mol Biol* 810: 25–58
- Pitceathly RD, Rahman S, Wedatilake Y, Polke JM, Cirak S, Foley AR, Sailer A, Hurler ME, Stalker J, Hargreaves I et al (2013) NDUFA4 mutations underlie dysfunction of a cytochrome c oxidase subunit linked to human neurological disease. *Cell Rep* 3: 1795–1805
- Pitceathly RDS, Taanman JW (2018) NDUFA4 (Renamed COXFA4) is a cytochrome-c oxidase subunit. *Trends Endocrinol Metab* 29: 452–454
- Rana M, de Coo I, Diaz F, Smeets H, Moraes CT (2000) An out-of-frame cytochrome b gene deletion from a patient with parkinsonism is associated with impaired complex III assembly and an increase in free radical production. *Ann Neurol* 48: 774–781
- Rieger B, Shalaeva DN, Sohnel AC, Kohl W, Duwe P, Mulikidjanian AY, Busch KB (2017) Lifetime imaging of GFP at CoxVIIIa reports respiratory supercomplex assembly in live cells. *Sci Rep* 7: 46055
- Sanchez E, Lobo T, Fox JL, Zeviani M, Winge DR, Fernandez-Vizarras E (2013) LYRM7/MZM1L is a UQCRCF1 chaperone involved in the last steps of mitochondrial complex III assembly in human cells. *Biochim Biophys Acta* 1827: 285–293
- Sanchez-Caballero L, Guerrero-Castillo S, Nijtmans L (2016) Unraveling the complexity of mitochondrial complex I assembly: a dynamic process. *Biochim Biophys Acta* 1857: 980–990
- Schagger H, Pfeiffer K (2000) Supercomplexes in the respiratory chains of yeast and mammalian mitochondria. *EMBO J* 19: 1777–1783
- Schlehe JS, Journel MS, Taylor KP, Amodeo KD, LaVoie MJ (2013) The mitochondrial disease associated protein Ndufa2 is dispensable for complex-I assembly but critical for the regulation of oxidative stress. *Neurobiol Dis* 58: 57–67
- Signes A, Fernandez-Vizarras E (2018) Assembly of mammalian oxidative phosphorylation complexes I-V and supercomplexes. *Essays Biochem* 62: 255–270
- Strogolova V, Furness A, Robb-McGrath M, Garlich J, Stuart RA (2012) Rcf1 and Rcf2, members of the hypoxia-induced gene 1 protein family, are critical components of the mitochondrial cytochrome bc1-cytochrome c oxidase supercomplex. *Mol Cell Biol* 32: 1363–1373
- Stroud DA, Surgenor EE, Formosa LE, Reljic B, Frazier AE, Dibley MG, Osellame LD, Stait T, Beilharz TH, Thorburn DR et al (2016) Accessory subunits are integral for assembly and function of human mitochondrial complex I. *Nature* 538: 123–126
- Tiranti V, Munaro M, Sandona D, Lamantea E, Rimoldi M, DiDonato S, Bisson R, Zeviani M (1995) Nuclear DNA origin of cytochrome c oxidase deficiency in Leigh's syndrome: genetic evidence based on patient's-derived rho degrees transformants. *Hum Mol Genet* 4: 2017–2023
- Trumpower BL (1990) The protonmotive Q cycle. Energy transduction by coupling of proton translocation to electron transfer by the cytochrome bc1 complex. *J Biol Chem* 265: 11409–11412
- Tucker EJ, Wanschers BF, Szklarczyk R, Mountford HS, Wijeyeratne XW, van den Brand MA, Leenders AM, Rodenburg RJ, Reljic B, Compton AG et al (2013) Mutations in the UQCC1-interacting protein, UQCC2, cause human complex III deficiency associated with perturbed cytochrome b protein expression. *PLoS Genet* 9: e1004034
- Tyanova S, Temu T, Sinitcyn P, Carlson A, Hein MY, Geiger T, Mann M, Cox J (2016) The Perseus computational platform for comprehensive analysis of (prote)omics data. *Nat Methods* 13: 731–740
- Ugalde C, Vogel R, Huijbers R, van den Heuvel B, Smeitink J, Nijtmans L (2004) Human mitochondrial complex I assembles through the combination of evolutionary conserved modules: a framework to interpret complex I deficiencies. *Hum Mol Genet* 13: 2461–2472
- Vidoni S, Harbour ME, Guerrero-Castillo S, Signes A, Ding S, Fearnley IM, Taylor RW, Tiranti V, Arnold S, Fernandez-Vizarras E et al (2017) MR-15 interacts with PET100 and PET117 in module-based assembly of human cytochrome c oxidase. *Cell Rep* 18: 1727–1738
- Vukotic M, Oeljeklaus S, Wiese S, Vogtle FN, Meisinger C, Meyer HE, Ziesenis A, Katschinski DM, Jans DC, Jakobs S et al (2012) Rcf1 mediates cytochrome oxidase assembly and respirasome formation, revealing heterogeneity of the enzyme complex. *Cell Metab* 15: 336–347

- Wittig I, Braun HP, Schagger H (2006) Blue native PAGE. *Nat Protoc* 1: 418–428
- Wu M, Gu J, Guo R, Huang Y, Yang M (2016) Structure of mammalian respiratory supercomplex I1III2IV1. *Cell* 167: 1598–1609 e10
- Young L, Shiba T, Harada S, Kita K, Albury MS, Moore AL (2013) The alternative oxidases: simple oxidoreductase proteins with complex functions. *Biochem Soc Trans* 41: 1305–1311
- Zara V, Conte L, Trumpower BL (2009) Biogenesis of the yeast cytochrome bc1 complex. *Biochim Biophys Acta* 1793: 89–96

- Zhu J, Vinothkumar KR, Hirst J (2016) Structure of mammalian respiratory complex I. *Nature* 536: 354–358



License: This is an open access article under the terms of the Creative Commons Attribution 4.0 License, which permits use, distribution and reproduction in any medium, provided the original work is properly cited.

9.2 Appendix B

Novel compound heterozygous pathogenic variants in nucleotide-binding protein like protein (NUBPL) cause leukoencephalopathy with multi-systemic involvement.

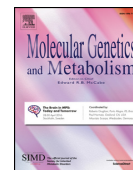
Protasoni M, Bruno C, Donati MA, Mohamoud K, Severino M, Allegri A, Robinson AJ, Reyes A, Zeviani M, Garone C.

Mol Genet Metab. 2020 Jan;129(1):26-34.



Contents lists available at ScienceDirect

Molecular Genetics and Metabolism

journal homepage: www.elsevier.com/locate/ymgme

Novel compound heterozygous pathogenic variants in nucleotide-binding protein like protein (*NUBPL*) cause leukoencephalopathy with multi-systemic involvement

Margherita Protasoni^a, Claudio Bruno^b, Maria Alice Donati^c, Khadra Mohamoud^a, Mariasavina Severino^d, Anna Allegri^e, Alan J. Robinson^a, Aurelio Reyes^a, Massimo Zeviani^{a,*}, Caterina Garone^{a,f,*}

^a Medical Research Council Mitochondrial Biology Unit, University of Cambridge, Hills Road, CB20XY Cambridge, UK

^b Center of Translational and Experimental Myology, IRCCS Giannina Gaslini Institute, via Gerolamo Gaslini 5, 16147 Genoa, Italy

^c Metabolic Unit, A. Meyer Children's Hospital, viale Pieraccini 24, 50139 Florence, Italy

^d Neuroradiology Unit, IRCCS Istituto Giannina Gaslini, via Gerolamo Gaslini 5, 16147 Genoa, Italy

^e Pediatric Clinic Unit, IRCCS Istituto Giannina Gaslini, via Gerolamo Gaslini 5, 16147, Genoa, Italy

^f Dipartimento di Scienze Mediche e Chirurgiche, Centro di Ricerca Biomedica Applicata, Università di Bologna, via Massarenti, 11, 40100 Bologna, Italy



ARTICLE INFO

Keywords:

Mitochondrial disorders
NUBPL
Human complex I
Complex I assembly
Complex I assembly factors
Brain MRI

ABSTRACT

NUBPL (Nucleotide-binding protein like) protein encodes a member of the Mrp/NBP35 ATP-binding proteins family, deemed to be involved in mammalian complex I (CI) assembly process. Exome sequencing of a patient presenting with infantile-onset hepatopathy, renal tubular acidosis, developmental delay, short stature, leukoencephalopathy with minimal cerebellar involvement and multiple OXPHOS deficiencies revealed the presence of two novel pathogenic compound heterozygous variants in *NUBPL* (p.Phe242Leu/p.Leu104Pro). We investigated patient's and control immortalised fibroblasts and demonstrated that both the peripheral and the membrane arms of complex I are undetectable in mutant *NUBPL* cells, resulting in virtually absent CI holocomplex and loss of enzyme activity. In addition, complex III stability was moderately affected as well. Lentiviral-mediated expression of the wild-type *NUBPL* cDNA rescued both CI and CIII assembly defects, confirming the pathogenicity of the variants. In conclusion, this is the first report describing a complex multi-systemic disorder due to *NUBPL* defect. In addition, we confirmed the role of *NUBPL* in Complex I assembly associated with secondary effect on Complex III stability and we demonstrated a defect of mtDNA-related translation which suggests a potential additional role of *NUBPL* in mtDNA expression.

1. Introduction

The primary function of mitochondria is to provide energy to the cells. This role is carried out by the oxidative phosphorylation (OXPHOS) pathway, composed of five multi-subunit complexes and two mobile electron carriers (ubiquinone and cytochrome *c*), embedded in the inner mitochondrial membrane (IMM). Complexes I to IV carry out respiration, i.e. the transport of electrons extracted from nutrients to molecular oxygen, that sustains the generation of a proton gradient across the membrane, exploited by complex V to phosphorylate ADP, converting it into ATP. Human complex I (CI) is an initial step of the electron transport chain. It is composed of 45 different subunits [22] organized in three structural domains: a membrane arm, or P module,

and two peripheral domains, the N and the Q modules, protruding in the mitochondrial matrix. In the N module, Nicotinamide Dehydrogenase (NADH) is oxidised by flavin mononucleotide (FMN) and electrons are passed through a chain of 8 iron-sulfur (Fe–S) clusters, and eventually transferred to ubiquinone, bound to the Q module. For every oxidised NADH molecule, the P-module pumps four protons across the inner membrane from the matrix to the intermembrane space of mitochondria, contributing to the formation of the protonmotive force [2,11]. Isolated mitochondrial CI deficiency (MIM# 252010), due to pathogenic variants in CI subunits or assembly factors, causes severe decrease of energy production and is the most common cause of OXPHOS disorders [15]. Nucleotide-binding protein like (*NUBPL*) (MIM# 613621) encodes a member of the Mrp/NBP35 ATP-binding proteins

* Corresponding authors at: Medical Research Council Mitochondrial Biology Unit, University of Cambridge, Wellcome Trust/MRC Building, Cambridge Biomedical Campus, Hills Road, Cambridge CB2 0XY, UK.

E-mail addresses: mdz21@mrc-mbu.cam.ac.uk (M. Zeviani), caterina.garone@unibo.it (C. Garone).

<https://doi.org/10.1016/j.ymgme.2019.11.003>

Received 19 August 2019; Received in revised form 14 November 2019; Accepted 16 November 2019

Available online 21 November 2019

1096-7192/ © 2019 Published by Elsevier Inc.

Table 1
– Clinical, molecular genetics and biochemical features of NUBPL patients.

Patient	NUBPL Pathogenic variants	F/M	Onset (m)	Age at last follow-up (yy)	Neurological	Brain MRI Abnormalities	Other systemic manifestation	Disease course	OXPHOS defect		REF.
									Muscle	Fibroblasts	
P1	c.166G > A; p.Gly56Arg (Ex2) 240-kb deletion (exons 1–4); 137-kb duplication (exon 7) c.815-27 T > C; p.Asp273Glnfs*32 (intron 9)	M	24	11.5	Developmental delay Ataxia Speech difficulties Spasticity Myopathy Vertical and horizontal nystagmus	Extensive cerebellar and cerebellar WM abnormalities	-	Step-wise with episodes of regression	I	I	[5] Tucker et al., 2011 [8]
P2	c.205_206delGT; p.Val69Tyrfs*80 (Ex2) c.815-217 T > C; p.Asp273Glnfs*32(intron 9)	M	NA	23	Ataxia Spasticity Dysarthria Nystagmus	T2 abnormalities in cerebellum, anterior brainstem, pyramidal tract	NA	Progressive	I	-	[20]
P3	c.166G > A; p.Gly56Arg (Ex2) c.815-27 T > C; p.Asp273Glnfs*32(intron 9)	M	8	+/9	Motor regression Ataxia Spasticity Rotatory nystagmus	Severe cerebellum, corpus callosum and brain stem atrophy WM abnormalities in cerebral (fronto-parietal), cerebellum, basal ganglia and brainstem area	-	Progressive	-	-	[8]
P4	c.166G > A; p.Gly56Arg (Ex2) c.667_668insCCTTGCTGCTG; p.Glu223Alafs*4(Ex8) c.815-27 T > C; p.Asp273Glnfs*32(intron 9)	M	8	11.6	Motor regression Ataxia Spasticity Dysarthria Nystagmus Motor regression Ataxia Dysarthria Nystagmus	Severe cerebellum and brain stem atrophy WM abnormalities in cerebral (fronto-parietal), cerebellum, basal ganglia and brainstem area	-	Continuing development	-	I	[8]
P5*	c.166G > A; p.Gly56Arg (Ex2) c.313G > T; p.Asp105Tyr (Ex4) c.815-7 T > C; p.Asp273Glnfs*32(intron 9)	F	13	8.6	Motor regression Ataxia Dysarthria Nystagmus	Severe cerebellum and brainstem atrophy WM abnormalities in cerebellum, basal ganglia and brainstem area	-	Continuing development	-	I	[8]
P6*	c.166G > A; p.Gly56Arg (Ex2) c.313G > T; p.Asp105Tyr (Ex4) c.815-27 T > C; p.Asp273Glnfs*32(intron 9)	F	13	7.1	Motor regression Ataxia Spasticity Dysarthria Nystagmus	Severe cerebellum and brainstem atrophy WM abnormalities in cerebral (frontal), cerebellum, basal ganglia and brainstem area	-	Step-wise with episodes of regression	I	I	[8]
P7	c.166G > A; p.Gly56Arg (Ex2) 693 + 1G > A; p.? (intron 8) 815-27 T > C; p.Asp273Glnfs*32(intron 9)	F	21	7.25	Motor regression Ataxia Spasticity Rotatory nystagmus	Extensive cerebellar and cerebellar WM abnormalities	-	Continuing development	-	-	[8]
P8	c.166G > A; p.Gly56Arg (Ex2) c.579A > C; p.Leu193Phe (Ex7) c.815-27 T > C; p.Asp273Glnfs*32(intron 9)	F	10	4.2	Motor regression Ataxia Spasticity Myopathy	Extensive cerebellar and cerebellar WM abnormalities	-	Step-wise with episodes of regression	I	I	[8]
P9*	c.311 T > C; p.Leu104Pro (Ex4) c.287A > T; p.Asp96Val(Ex3)	F	At Birth	25yy	Developmental delay Hypotonia Dysarthria Severe generalized dystonia	bilateral putaminal atrophy with T2 hyperintensities cerebellar atrophy	-	Step-wise with episodes of regression	NA	NA	[1]
P10*	c.311 T > C; p.Leu104Pro (Ex4) c.287A > T; p.Asp96Val (Ex3)	F	At birth	17yy	Bilateral nystagmus Developmental delay Ataxia Mild generalized dystonia Intention tremor	bilateral putaminal atrophy with T2 hyperintensities cerebellar atrophy	-	NA	NA	NA	[1]
P11		F	18 m	13yy			7	Slowly progressive		I	(continued on next page)

Table 1 (continued)

Patient	NUBPL Pathogenic variants	F/M	Onset (m)	Age at last follow-up (yy)	Neurological	Brain MRI	Age	Other systemic manifestation	Disease course	OXPHOS defect	REF.
	c.311 T > C; p.Leu104Pro (Ex4); c.726C > G; p.Phe242Leu (Ex9)				Developmental delay Generalized Hypotonia Myopathy	Abnormalities Cerebral and cerebellar white matter abnormalities with cerebellar lesion		Type III renal tubular acidosis Hepatomegaly Severe osteoporosis Growth hormone deficiency interstitial lung disease		Muscle Fibroblasts	Current report

M = month; Y = year; WM = White matter; I = Complex I, NADH-Cytochrome C reductase; III = Complex III, Succinate-Cytochrome C reductase.

family [4,18]. Similar to cytosolic members of this protein family, e.g. Cfd1 and Nbp35, NUBPL is able to bind Fe–S clusters thanks to the presence of two highly conserved cysteine residues in a CxxC motif in the C-terminal domain of the protein, but the precise molecular mechanism remains unclear [18]. NUBPL defect causes a leukoencephalopathy with a distinct brain MRI pattern predominantly involving cerebellar cortex, deep white matter and corpus callosum at early stage and progressing to severe cerebellar atrophy and brainstem involvement at the late stage [8]. Currently, 10 patients with NUBPL pathogenic variants are reported in the literature [1,5,8,20,21] presenting a neurodevelopmental disorder with mild to severe ataxia, dystonia, spasticity and dysarthria (Table 1 and Fig. 1). Here, we report for the first time a complex multisystemic syndrome due to novel compound heterozygous pathogenic variants in NUBPL in a 13-year-old girl. Functional analyses were previously limited to the determination of CI enzymatic activity and steady-state levels in human defective NUBPL samples. In this study, we have performed an extensive biochemical, genetic and protein analysis of our patient-derived fibroblast cell line harbouring compound heterozygous NUBPL pathogenic single nucleotide variants bringing new insights into the disease mechanism of NUBPL.

2. Case Report

A 13-year-old girl, the first child of healthy unrelated parents, was born at term after uneventful pregnancy and normal delivery. Birth weight was 3330 g. Perinatal period was normal (APGAR score 8/10). At age 18 months, she presented with failure to thrive (HP:0001508) and developmental delay (HP:0001263). At age 30 months, a type III renal tubular acidosis (HP:0001947) was identified. Laboratory investigations showed increased levels of lactate in plasma and in urine.

At this age neurological assessment documented generalized hypotonia (HP:0001290), wasting and weakness with positive Gowers sign (HP:0003198). Brain MRI revealed an asymmetric leukoencephalopathy (HP:0002352) with predominant fronto-parietal involvement, swelling of the corpus callosum and restricted diffusion at the edges of the affected white matter, associated with a small cortical cerebellar lesion (Fig. 2A–E). Brain MR spectroscopy revealed lactate peaks at the level of both affected and normal-appearing cerebral white matter (Fig. 2K, L).

At 6 years, mild hepatomegaly (HP:0002240), short stature (HP:0004322) and severe osteoporosis (HP:0000939) were noted. Endocrinological evaluation detected a complete growth hormone deficiency (HP:0000824) and replacement treatment was started. At 7 years of age, pulmonary CT scan revealed interstitial lung disease (HP:0006530). Sweat test was negative. At this time, the child showed generalized muscle hypotrophy, hyposthenia and signs of peripheral reduced oxygenation with nail clubbing. Follow-up brain MRI showed improvement of the cerebral white matter abnormalities, with decrease in both white matter swelling and extent of the signal abnormalities, whereas the cerebellar abnormalities had slightly worsened (Fig. 2F–J). Brain MR spectroscopy demonstrated absence of lactate peaks in the affected white matter (Fig. 2M). Cardiac (including ECG and echocardiography), funduscopy, and hearing assessments were normal. Over the following years the clinical course remained stable with satisfactory electrolyte balance and metabolic compensation and stability of motor functions. At 12 years of age she presented a critical episode characterized by hypertonia to the limbs with loss of contact and tachypnea. EEG showed significant slowing in right frontal seat.

Laboratory results indicated the presence of increased plasma levels of alanine, lactic and butyric acid. A muscle biopsy performed at 36 months revealed an irregular pattern of Cytochrome C Oxidase (COX) activity. In addition, mitochondrial respiratory chain activities measured in muscle homogenate showed a significant reduction in CI + III (NADH-Cytochrome C reductase) and a marginal reduction in CII + III (Succinate cytochrome c reductase) (Table 2). At her last

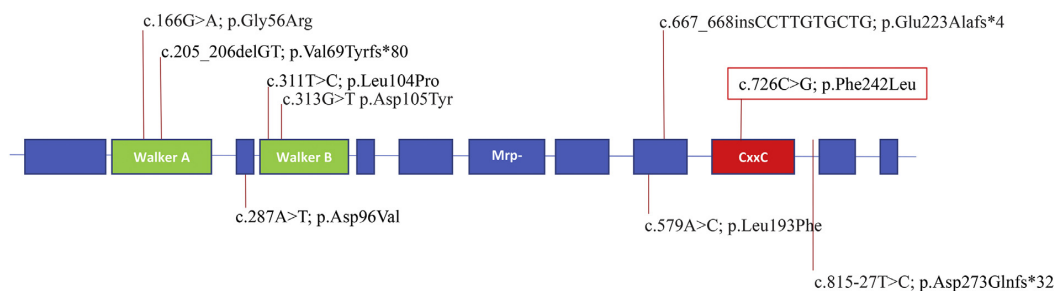


Fig. 1. – Schematic representation of *NUBPL* exons and reported pathogenic variants. The red box highlights the novel pathogenic variant described in the current report. (For interpretation of the references to colour in this figure legend, the reader is referred to the web version of this article.)

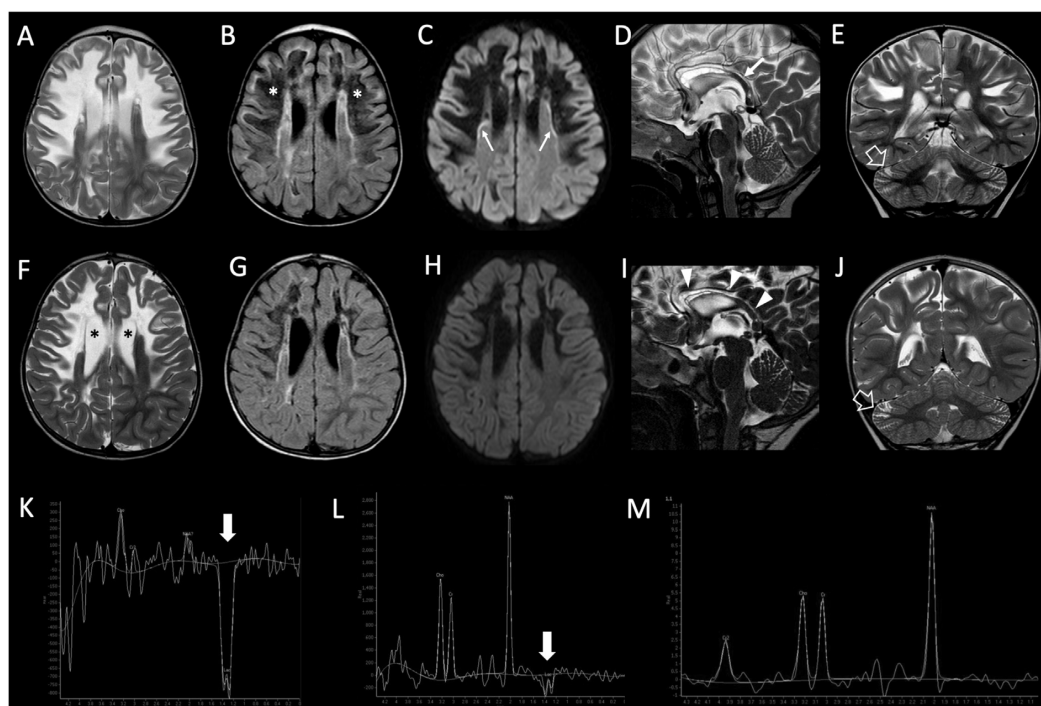


Fig. 2. Brain MRI and MR Spectroscopy findings of the patient obtained at 2.5 years (A-E, K, L) and 7 years of age (F-J, M). Axial T2-weighted (A, F), fluid-attenuated inversion recovery (FLAIR) (B, G), diffusion-weighted images (DWI) (C, H), sagittal T2-weighted (D, I) and coronal T2-weighted (E, J) images are shown. The initial MRI shows diffuse cerebral white matter abnormalities, mainly in the frontal and right parietal lobes (A, B), involving both the periventricular and subcortical regions, with central rarefaction (asterisks, B). The abnormal cerebral white matter is surrounded by a rim of abnormal solid tissue, with linear areas of restricted diffusion (arrows, C). There is swelling and T2-hyperintensities at the level of the anterior portions of the corpus callosum and splenium, with preservation of the fibres connecting the pericentral cortex (arrow, D). There is a very small area of signal abnormality of the cerebellar cortex in the right hemisphere (empty arrow, E). The late MRI reveals improvement of the deep white matter changes with absence of restricted diffusion (G, H), and thinning of the affected white matter with mild enlargement of the lateral ventricles (asterisks, F). There is atrophy of the corpus callosum (arrowheads, I). The cerebellar abnormalities slightly worsen (empty arrow, J). MR spectroscopy at 2.5 years of age demonstrate very high lactate peaks in the affected white matter (arrow, K) and smaller lactate peaks in the spared, normal-appearing white matter (arrow, L). Follow-up MR spectroscopy performed at 7 years of age reveals no significant lactate peaks in the affected cerebral white matter (M).

examination, at 13 years of age, she complained of easy fatigability and she started enteral nutrition.

3. Results

3.1. Genetics

Exome sequencing of patient's blood DNA identified two pathogenic variants in *NUBPL* (NM_025152.3; NP_079428.2; #MIM 613621):

c.726C > G, p.Phe242Leu, in exon 9, not previously reported; c.311 T > C, p.Leu104Pro, in exon 4, previously reported in compound heterozygosity with another pathogenic variant. Sanger's sequencing in the parents, proved that the pathogenic variants were allelic, the c.726C > G being transmitted by the heterozygous father and the c.311 T > C by the heterozygous mother. Both parents are healthy carrier. The two pathogenic variants are localized in two different functional domains of the protein, and are both highly conserved in different species. ClustalW alignment of *NUBPL* and the human

Table 2
mitochondrial respiratory chain activities ($\mu\text{mole}/\text{min}/\text{g}$) in muscle homogenate.

	Patient	Controls
NADH dehydrogenase	20.1	28.67–39.53
Succinate dehydrogenase	0.96	0.49–0.73
NADH-cytochrome C reductase (complexes I + III)	0.10	0.66–1.52
Succinate-cytochrome C reductase (complexes II + III)	0.46	0.46–0.88
Cytochrome C oxidase	3.92	1.78–2.46
Citrate synthase	21.3	7.82–10.90

orthologues of cytosolic Fe/S proteins Cfd1/Nbp35 (NUBP1/NUBP2) (Fig. S1) shows that the first pathogenic variant (p.Leu104Pro) localizes in the Walker B motif, essential for nucleotide binding and hydrolysis [10]. The second pathogenic variant (p.Phe242Leu) is in close proximity to the CxxC binding residues and may affect the ability of the protein to bind the Fe–S clusters or to form homodimers [13]. MutationTaster and SIFT softwares predicted both pathogenic variants to be deleterious for protein function.

3.2. Biochemistry

We first analyzed the steady-state levels of respiratory chain subunits, particularly those forming the different CI submodules in immortalised patient-derived skin fibroblasts [19]. SDS-PAGE based Western blot (WB) immunodetection showed strong reduction of the steady-state level of CI subunits localized in both the peripheral and membrane arms, suggesting a deleterious effect of the *NUBPL* pathogenic variants on the whole enzyme (Fig. 3A–S2). Steady-state levels of subunits of other respiratory chain complexes (Fig. 3A) and of Aconitase 2 (ACO2) (Fig. 4A), a mitochondrial matrix protein containing a 4Fe–4S cluster involved in the conversion of Citrate to Isocitrate, did not show abnormalities. Likewise, the amount of the Fe–S containing structural components of CIII (UQCRC1) was not affected. 1st and 2nd dimension (1D and 2D) BN-PAGE analysis of DDM-treated samples demonstrated a dramatic reduction of the fully assembled CI in patient's fibroblasts, whereas both CIII and CII, as well as CIV, holocomplexes were normal (Fig. 3B and C). These results confirm the high specificity of *NUBPL* for the assembly/stability of CI subunits.

In order to study the effect of the two pathogenic variants in the formation of supercomplexes (SC), we analyzed mitochondria extracted from fibroblasts treated with 1% digitonin by 1D and 2D BN-PAGE WB (Fig. 3D and E). This analysis showed a marked reorganization of the SC in the patient, including the loss of the respirasome (CI + CIII₂ + CIV), with the maintenance of the CIII₂ + CIV species. However, WB analysis of 2D BN using UQCRC1, the only CIII subunit containing an iron-sulfur cluster, and UQCRC1, a CIII core subunit, showed accumulation of CIII sub-assemblies in the patient's cells (Fig. 3E). Interestingly, similar results, although less drastic, were obtained from the analysis of another human cell line defective for the complex I assembly factor ACAD9, including the decrease in the amount of SC (Fig. S3). [6]

Besides Complex I assembly, *NUBPL* has been deemed to play a role in mitochondrial translation in *Arabidopsis thaliana* [24]. We analyzed mitochondrial translation by [³⁵S]-L-methionine metabolic labelling, and found that the amount of mtDNA-related subunits was moderately decreased in mutant fibroblasts compared to controls (Fig. 3F–S4), and also to the ACAD9 defective fibroblasts (Fig. S5).

Spectrophotometric analysis of the respiratory chain complexes confirmed severe CI deficiency with 22% residual activity of patient's vs controls' fibroblasts (Fig. 3G), whereas the activities of the other complexes, including those containing mtDNA encoded subunits, were normal. These results indicate again the specificity of the *NUBPL* defect on CI function, and suggest that the mild reduction in mtDNA translation is unlikely to affect the function of the remaining complexes.

3.3. Functional complementation assay

To further confirm the pathogenicity of the pathogenic variants, we performed complementation experiments by overexpressing *NUBPL* wild-type cDNA in patient's and control fibroblasts by stable lentivirus transduction. The overexpression of the native protein fully restored the steady-state whole CI amount, assembly and enzyme activity and the correction of the mtDNA translation defect in the patient's cells (Fig. 4A–F; Fig. S6–7).

4. Discussion

NUBPL defect cause leukoencephalopathy with early onset (0–24 m) of developmental delay or motor regression and mild to severe ataxia, spasticity, dystonia, dysarthria and myopathy. Currently, 10 patients have been reported with variable disease course: four patients presented episodes of regression, two patients a progressive disease course; three had a stable disease course with acquisition of some milestones. Here, we describe for the first time a progressive multisystem clinical phenotype with type III renal tubular acidosis, osteoporosis, hepatomegaly, growth hormone deficiency, interstitial lung disease. Brain MRI confirmed the association of leukoencephalopathy with cerebellar, corpus callosum and deep cortical involvement. However, neurological features were not the most predominantly debilitating symptoms and they were including myopathy, hypotonia and neurocognitive deficit. *NUBPL* defect in our patient was due to compound heterozygous pathogenic variants: one very recently described variant in a different compound heterozygosity (c.311 T > C, p.Leu104Pro) [1] and a novel unreported variant (c.726 C > G, p.Phe242Leu). While the first pathogenic variant is localized in a Walker B motif essential for nucleotide bind, the second pathogenic variant is localized in proximity to the CxxC binding residues to the Fe–S clusters. Therefore, we can hypothesize a genotype-phenotype correlation with the c.726 C > G, p.Phe242Leu pathogenic variant responsible of the most severe and complex phenotype of our patient. Further studies with additional identified patients are needed to confirmed our hypothesize. *NUBPL* has been identified as a CI assembly factor, involved in the insertion of 4Fe–4S clusters in the CI N module [18], and in two 4Fe–S metallated subunits of the Q module, NDUFS2 and NDUFS3 [17,18]. We have performed an extensive functional analysis of our patient fibroblast cell line and we have demonstrated that *NUBPL* defect compromises the assembly of the whole CI. The assembly pathway of CI has recently been described as a modular process, which requires the synthesis of six independent multiprotein sub-modules (Q, P_{P-a}, P_{P-b}, P_{D-a}, P_{D-b}, N), subsequently integrated to form the holoenzyme via a stepwise process involving at least 13 assembly factors and chaperons [7]. Both the N and the Q modules are pre-assembled before their incorporation in the holoenzyme. However, whilst the Q module is added to the membrane arm at an early stage, the insertion of the N module is one of the final steps of the complete assembly of CI [7,17]. Previous structural analysis of CI by blue native gel electrophoresis in patients' cells with pathogenic variants in N and Q module subunits has shown the accumulation of stable CI intermediates corresponding to the unconnected N module and to the incomplete membrane arm, which can contain also Q module subunits, such as NDUFA9 and NDUFS2 [9]. Therefore, pathogenic variants causing the destabilization of either the N or the Q modules are not sufficient to determine the complete loss of the enzyme. Contrariwise, our results demonstrate a drastic effect on CI impaired *NUBPL* activity, leading to a decrease of CI subunits belonging to all three modules and a general loss of the fully assembled complex. This observation suggests that *NUBPL* is involved in the formation of both the peripheral and membrane arms of the enzyme. The analysis of mitochondrial complexes extracted with digitonin in 1D and 2D blue native gels allowed us to investigate the formation and the stability of supercomplexes in our patient cell line. As expected, in the absence of CI there is a redistribution of the remaining complexes, which leads to

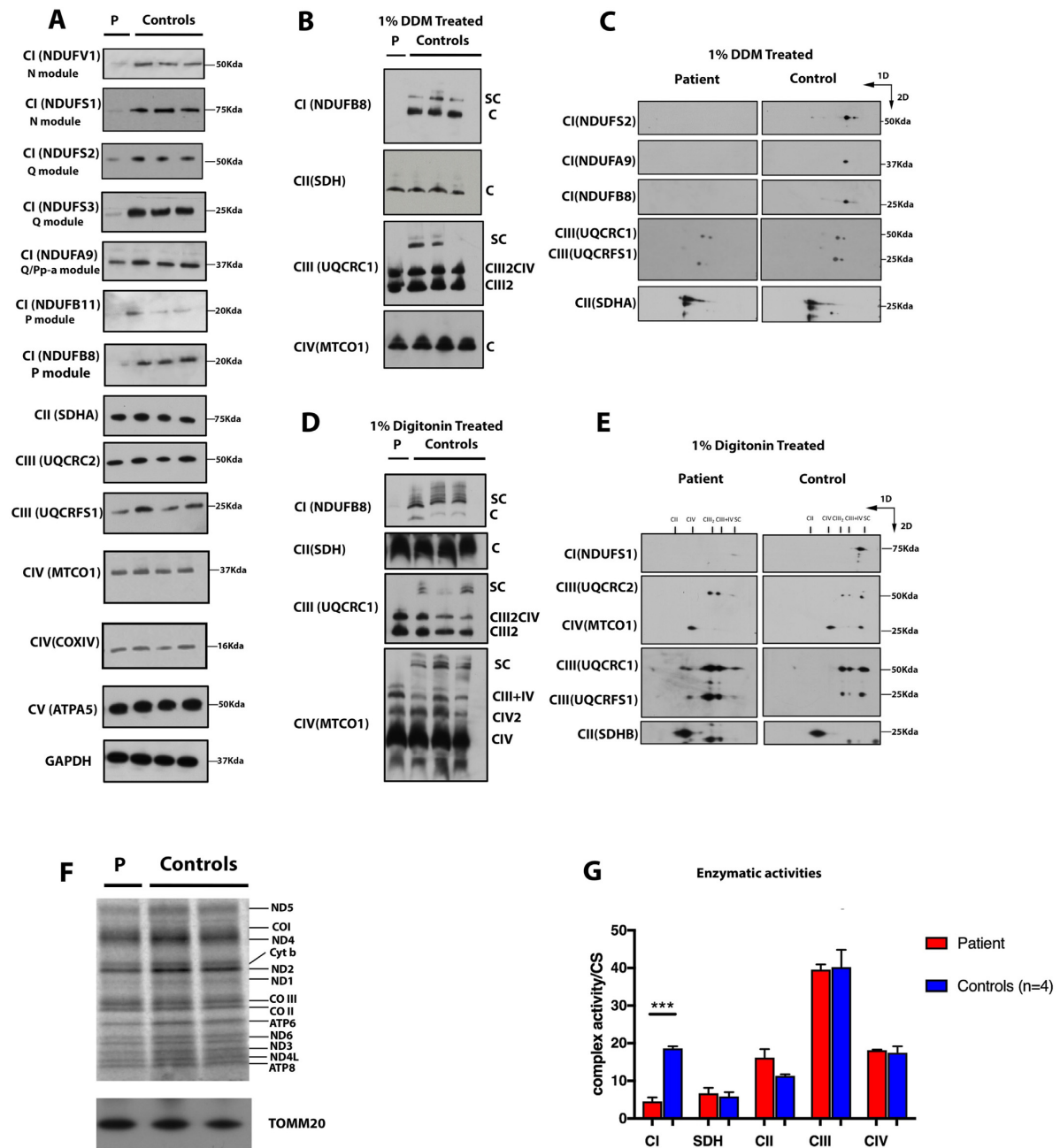


Fig. 3. - Functional characterisation of NUBPL defective immortalised fibroblasts vs three independent controls: the analyses of A) steady-state level of CI (NDUFV1, NDUFS1, NDUFS2, NDUFS3, NDUFA9, NDUFB11, NDUFB8), CII (SDHA), CIII (UQCRC2, UQCRFS1), CIV (MTCO1, COXIV), CV (ATPA5) and loading control (GAPDH) by WB analysis of SDS page from fibroblast lysates; B) 1D BN-PAGE and C) 2D BN-PAGE WB study with 1%DDM treated proteins; D) 1D BN-PAGE and E) 2D BN-PAGE study with 1% Digitonin treated proteins; F) ³⁵S-methionine labelling for mitochondrial protein translation were performed in patient's and controls immortalised fibroblasts; and, G) Spectrophotometer analysis of mitochondrial respiratory chain complex activities in fibroblast lysates. Data in figures are given as mean +/- SEM based on at least 3 biological replicates.

CI = NADH:ubiquinone oxidoreductase; CII = succinate:ubiquinone oxidoreductase; SDH=Succinate dehydrogenase; CIII = quinol-cytochrome c reductase; CIV = cytochrome c oxidase; CV=F₀F₁-ATPase.

an increase in CIII₂ and CIII₂ + CIV species, while monomer CIV does not seem to be affected. Interestingly, NUBPL defective cell line showed also reduced stability or impaired assembly of CIII. The formation of SC

seems to be important for the structural stabilization of the individual enzymes [12]. A current standard model suggests that partially assembled CIII₂ is incorporated in CI + CIII₂ + CIV SC, before the

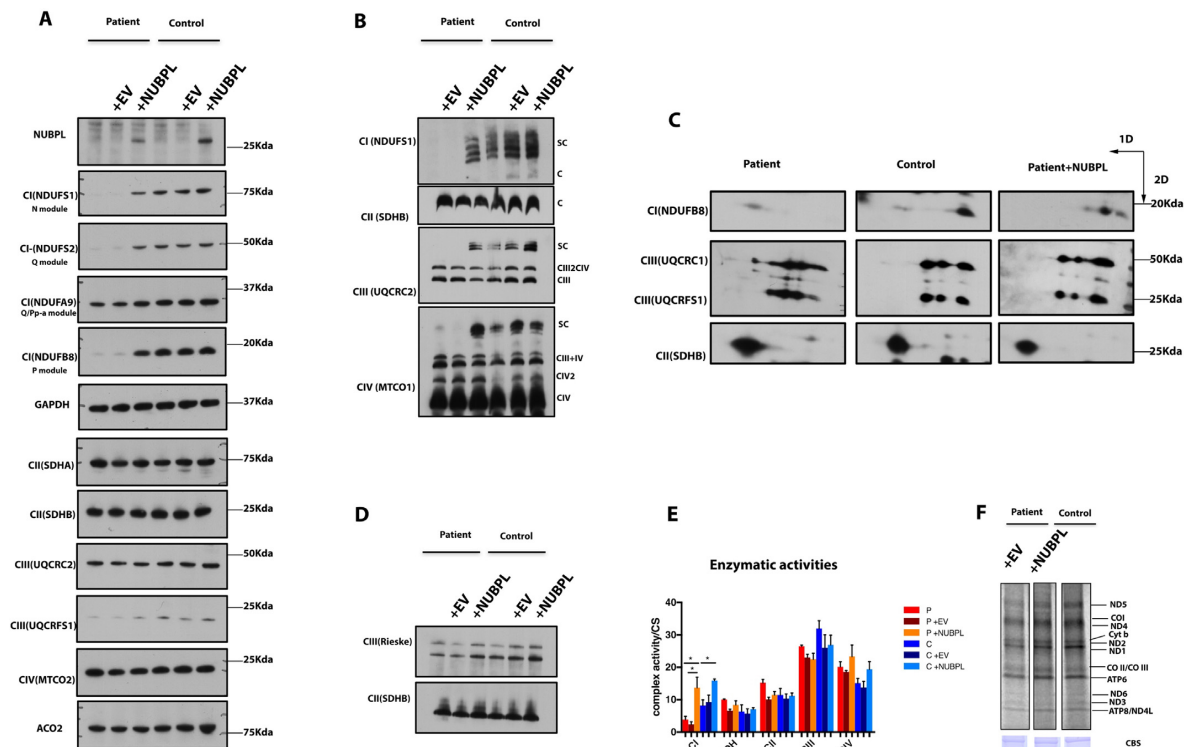


Fig. 4. – Stable lentiviral transfection of wild-type NUBPL restored the defective Complex I as demonstrated by analysing the A) Steady state levels of NUBPL and CI subunits (NDUFS1, NDUFS2, NDUFA9, NDUFB8) by SDS page analysis; B) 1D and C) 2D BN PAGE WB of samples treated with 1% DDM and D) 1D BN PAGE of Rieske protein in 1%DDM treated samples; E) spectrophotometer analysis of mitochondrial respiratory chain activities; F) 35 S-methionine labelling for mitochondrial proteins translation. Data in figures are given as mean \pm SEM based on at least 3 biological replicates. CI = NADH:ubiquinone oxidoreductase; CII = succinate:ubiquinone oxidoreductase; SDH = Succinate dehydrogenase; CIII = ubiquinol-cytochrome c reductase; CIV = cytochrome c oxidase.

insertion of the Rieske protein (UQCRC1), which is preferentially localized in SC rather than in free CIII₂ [30]. This hypothesis is supported by the partial de-stabilization and degradation of CIII₂ in our mutant cells, shown by 2D BN WB.

We also observed a moderate defect in mitochondrial protein synthesis rate in the patient cells analyzed by [35 S]-methionine labelling. This mildly affects all the mitochondrial encoded proteins, partially supporting a previous hypothesis on a role of NUBPL in mitochondrial translation [24]. The defect in the mitochondrial translation can be also responsible of instability of Complex III.

In conclusion, our results confirm the role of NUBPL in the assembly of CI and suggest an involvement of the protein in the stability of the whole enzyme. Further investigation is warranted to establish as whether this effect is due to a direct function of NUBPL on assembly of holo-CI, or to a severely disruptive structural consequence of impaired CI Fe–S metallation.

5. Methods

5.1. Editorial policies and ethical considerations

This study was approved by the ethics committee of the Children's Hospital Giannina Gaslini Institute, Genova (Italy) and it has been carried out in accordance with the Code of Ethics of the World Medical Association (Declaration of Helsinki). The patient's parents signed an informed consent approved by the Ethics Committee of the Gaslini Institute (available upon request), on the treatment of the biological

material obtained from the patient.

None of the Authors has conflicts of interest concerning the present work.

5.2. Cell biology

Human fibroblasts were grown in Dulbecco's Modified Eagle Medium (DMEM, Gibco #10569010), supplemented with 10% foetal bovine serum (Gibco #10270–106), 1% penicillin and streptomycin (Gibco #15070–063) and 50 μ g/ml uridine. Fibroblasts were immortalised by lentiviral transduction using the pLOX-Ttag-iresTK vector (Tronolab, Addgene #12246).

Cells were lysed in TG lysis buffer (20 mM Tris-HCl pH 7.5, 500 mM NaCl, 1 mM EDTA, 1% Triton-X-100, 10% Glycerol, 1.5 mM MgCl₂) and 1 \times protease inhibitor cocktail (Roche #05056489001). The protein amount was detected with DC protein assay kit (BioRad #5000111) and 20 μ g of protein were loaded in SDS-PAGE Nu-PAGE 4–12% Bis-Tris gel (Invitrogen #NP0321). Proteins were transferred to a PVDF membrane (Immobilon-P #IPVH00010) at 100 V for 1 h at 4 $^{\circ}$ C in Tris-Glycine transfer buffer, 20% methanol, 0.25% SDS.

5.3. Biochemistry

Samples for Blue Native Gel Electrophoresis (BNGE) were prepared as described previously [14,23] with DDM or Digitonin in order to analyse the supercomplexes. Native samples were run through pre-cast NativePAGE 3%–12% Bis-Tris gels, while Novex NuPAGE 4%–12% Bis-

Tris Gels (Life Technologies) were used for denaturing conditions. Proteins were blotted to a PVDF membrane (Immobilon-P #IPVH00010) at 300 mA for 1.5 h in bicarbonate transfer buffer (0.318 mg/ml Na₂CO₃, 0.84 mg/ml NaHCO₃).

Samples were immunodetected using commercial specific antibodies. A detailed list can be found in Supp. Table 1.

In order to analyse the mitochondrial respiratory chain activities, cells samples were snap-frozen in liquid nitrogen and homogenized in 10 mM phosphate buffer (pH 7.4). The spectrophotometric activity of CI, CII, CIII, CIV, and CS, was measured as described in Bugiani et al. [3].

CI activity was measured by following the decrease of NADH absorbance at 340 nm. Proteins were incubated during 2 min at 30 °C in a reaction mix containing 20 mM KP buffer pH 8, 0.2 mM NADH, 1 mM sodium azide, 0.1% BSA in 1 mM EDTA pH = 7.4. The reaction was initiated adding 50 μM CoQ, followed for 2 min, and then inhibited with 5 μM rotenone. CII activity was performed at 30 °C pre incubating proteins with 50 mM KP Buffer pH = 7.0, 1.5 mM KCN and 0.1 mM DCPIP. This reaction was followed after the injection of 16 mM succinate (SDH activity) and 50 mM CoQ (CII activity) at 600 nm for two minutes. Complex III was assessed measuring the reduction of cytochrome c at 550 nm for 2 min at 30 °C. Proteins were incubated with 50 mM KP buffer pH = 7.4, 2 mM NaN₃, 1 mg/ml BSA (in EDTA 10 mM pH = 7.4), 50 mM Cytochrome c (SIGMA #C7752), and 50 mM reduced decylubiquinone (DBH2, Sigma #D7911). CIV activity was measured at 550 nm following cytochrome c oxidation for two minutes at 37 °C. Assay was performed in 90–95% reduced cytochrome c (1.3 mg/ml, SIGMA #C7752) in 50 mM KP buffer pH = 7.0. All enzymatic activities were normalized for protein quantification (DC assay kit, Bio-Rad) and for citrate synthase (CS) activity. For CS activity measurements, proteins were incubated at 30 °C with 75 mM Tris-HCl Buffer pH = 8.0, 0.1 mM 5,5'-Dithiobis-(2-nitrobenzoic acid) (DTNB) and 0.4 mM Acetyl-CoA. The reaction was initiated adding 0.5 mM Oxalacetate and followed at 412 nm for two minutes.

To analyse translation of mitochondrially encoded proteins metabolic labelling was performed as previously described [16]. Cells were grown as described and, then the standard medium was replaced with methionine/cysteine free DMEM (Sigma-Aldrich) supplemented with 2 mM L-glutamine, 48 μg/ml cysteine, and 50 μg/ml uridine. The cells were incubated for 2 × 10 min in this medium and then transferred to methionine/cysteine-free DMEM containing 10% (vol/vol) dialyzed FCS and emetine dihydrochloride (100 μg/ml) to inhibit cytosolic translation. Cells were incubated for 10 min before addition of 120 μCi/ml of [³⁵S]methionine. Labeling was performed for 60 min, and then the cells were washed twice with standard growth medium. Protein samples (30 μg) were separated on 10–20% SDS-PAGE gels, and products were visualized and quantified using a PhosphorImager system with ImageQuant software (Molecular Dynamics, GE Healthcare).

5.4. Statistics

Statistical analyses were performed using GraphPad Prism software version XXX. *P* values less than 0.05 according to a two-tailed Student's *t*-test were considered significant.

Acknowledgments

We thank Dr. Erika Fernandez-Vizarrá for her help and advice. Our work was supported by the Core Grant from the MRC (Grant MC_UU_00015/5); ERC Advanced under Grant FP7-322424 and NRJ-Institut de France Grant (to M.Z.); European Commission under 'Marie Skłodowska-Curie Actions', Individual Fellowship – Reintegration Panel (Mitobiopath-705560)(CG).

Grant numbers

Core Grant from the MRC (Grant MC_UU_00015/5);
ERC Advanced under Grant FP7322424 and NRJ-Institut de France Grant.
European Commission under 'Marie Skłodowska-Curie Actions', Individual Fellowship-Reintegration Panel (Mitobiopath-705,560)(CG).

Appendix A. Supplementary data

Supplementary data to this article can be found online at <https://doi.org/10.1016/j.ymgme.2019.11.003>.

References

- [1] B. Balint, G. Charlesworth, M. Stamelou, L. Carr, N.E. Mencacci, N.W. Wood, K.P. Bhatia, Mitochondrial complex I NUBPL mutations cause combined dystonia with bilateral striatal necrosis and cerebellar atrophy, *Eur. J. Neurol.* 26 (9) (2019) 1240–1243, <https://doi.org/10.1111/ene.13956>.
- [2] J.A. Birrell, K. Morina, H.R. Bridges, T. Friedrich, J. Hirst, Investigating the function of [2Fe-2S] cluster N1a, the off-pathway cluster in complex I, by manipulating its reduction potential, *Biochem. J.* 456 (1) (2013) 139–146, <https://doi.org/10.1042/BJ20130606>.
- [3] M. Bugiani, F. Invernizzi, S. Alberio, E. Briem, E. Lamantea, F. Carrara, ... M. Zeviani, Clinical and molecular findings in children with complex I deficiency, *Biochim Biophys Acta* 1659 (2–3) (2004) 136–147, <https://doi.org/10.1016/j.bbabi.2004.09.006>.
- [4] K. Bych, S. Kerscher, D.J. Netz, A.J. Pierik, K. Zwicker, M.A. Huynen, ... J. Balk, The iron-sulphur protein Ind1 is required for effective complex I assembly, *EMBO J* 27 (12) (2008) 1736–1746, <https://doi.org/10.1038/emboj.2008.98>.
- [5] S.E. Calvo, E.J. Tucker, A.G. Compton, D.M. Kirby, G. Crawford, N.P. Burt, ... V.K. Mootha, High-throughput, pooled sequencing identifies mutations in NUBPL and FOXRED1 in human complex I deficiency, *Nat Genet* 42 (10) (2010) 851–858, <https://doi.org/10.1038/ng.659>.
- [6] C. Garone, M.A. Donati, M. Sacchini, B. Garcia-Diaz, C. Bruno, S. Calvo, ... S. Dimauro, Mitochondrial encephalomyopathy due to a novel mutation in ACAD9, *JAMA Neurol* 70 (9) (2013) 1177–1179, <https://doi.org/10.1001/jamaneuro.2013.3197>.
- [7] S. Guerrero-Castillo, F. Baertling, D. Kownatzki, H.J. Wessels, S. Arnold, U. Brandt, L. Nijtmans, The assembly pathway of mitochondrial respiratory chain complex I, *Cell Metab.* 25 (1) (2017) 128–139, <https://doi.org/10.1016/j.cmet.2016.09.002>.
- [8] S.H. Kevelam, R.J. Rodenburg, N.I. Wolf, P. Ferreira, R.J. Lunsing, L.G. Nijtmans, ... M.S. van der Knaap, NUBPL mutations in patients with complex I deficiency and a distinct MRI pattern, *Neurology* 80 (17) (2013) 1577–1583, <https://doi.org/10.1212/WNL.0b013e31828f1914>.
- [9] M. Lazarou, M. McKenzie, A. Ohtake, D.R. Thorburn, M.T. Ryan, Analysis of the assembly profiles for mitochondrial- and nuclear-DNA-encoded subunits into complex I, *Mol. Cell. Biol.* 27 (12) (2007) 4228–4237, <https://doi.org/10.1128/MCB.00074-07>.
- [10] D.D. Leipe, E.V. Koonin, L. Aravind, Evolution and classification of P-loop kinases and related proteins, *J. Mol. Biol.* 333 (4) (2003) 781–815 Retrieved from <https://www.ncbi.nlm.nih.gov/pubmed/14568537>.
- [11] M. Mimaki, X. Wang, M. McKenzie, D.R. Thorburn, M.T. Ryan, Understanding mitochondrial complex I assembly in health and disease, *Biochim. Biophys. Acta* 1817 (6) (2012) 851–862, <https://doi.org/10.1016/j.bbabi.2011.08.010>.
- [12] D. Moreno-Lastres, F. Fontanesi, I. Garcia-Consuegra, M.A. Martin, J. Arenas, A. Barrientos, C. Ugalde, Mitochondrial complex I plays an essential role in human respirasome assembly, *Cell Metab.* 15 (3) (2012) 324–335, <https://doi.org/10.1016/j.cmet.2012.01.015>.
- [13] D.J. Netz, A.J. Pierik, M. Stumpf, E. Bill, A.K. Sharma, L.J. Pallesen, ... R. Lill, A bridging [4Fe-4S] cluster and nucleotide binding are essential for function of the Cfd1-Nbp35 complex as a scaffold in iron-sulfur protein maturation, *J Biol Chem* 287 (15) (2012) 12365–12378, <https://doi.org/10.1074/jbc.M111.328914>.
- [14] L.G. Nijtmans, N.S. Henderson, L.J. Holt, Blue native electrophoresis to study mitochondrial and other protein complexes, *Methods* 26 (4) (2002) 327–334, [https://doi.org/10.1016/S1046-2023\(02\)00038-5](https://doi.org/10.1016/S1046-2023(02)00038-5).
- [15] J. Nouws, L.G. Nijtmans, J.A. Smeitink, R.O. Vogel, Assembly factors as a new class of disease genes for mitochondrial complex I deficiency: cause, pathology and treatment options, *Brain* 135 (Pt 1) (2012) 12–22, <https://doi.org/10.1093/brain/awr261>.
- [16] J. Rorbach, P. Boesch, P.A. Gammage, T.J. Nicholls, S.F. Pearce, D. Patel, ... M. Minczuk, MRM2 and MRM3 are involved in biogenesis of the large subunit of the mitochondrial ribosome, *Mol Biol Cell* 25 (17) (2014) 2542–2555, <https://doi.org/10.1091/mbc.E14-01-0014>.
- [17] L. Sanchez-Caballero, S. Guerrero-Castillo, L. Nijtmans, Unraveling the complexity of mitochondrial complex I assembly: a dynamic process, *Biochim. Biophys. Acta* 1857 (7) (2016) 980–990, <https://doi.org/10.1016/j.bbabi.2016.03.031>.
- [18] A.D. Sheftel, O. Stehling, A.J. Pierik, D.J. Netz, S. Kerscher, H.P. Elsasser, ... R. Lill, Human ind1, an iron-sulfur cluster assembly factor for respiratory complex I, *Mol Cell Biol* 29 (22) (2009) 6059–6073, <https://doi.org/10.1128/MCB.00817-09>.
- [19] A. Signes, E. Fernandez-Vizarrá, Assembly of mammalian oxidative

- phosphorylation complexes I-V and supercomplexes, *Essays Biochem.* 62 (3) (2018) 255–270, <https://doi.org/10.1042/EBC20170098>.
- [20] E.V. Tenisch, A.S. Lebre, D. Grevent, P. de Lonlay, M. Rio, M. Zilbovicius, ... N. Boddaert, Massive and exclusive pontocerebellar damage in mitochondrial disease and NUBPL mutations, *Neurology* 79 (4) (2012) 391, <https://doi.org/10.1212/WNL.0b013e3182611232>.
- [21] E.J. Tucker, M. Mimaki, A.G. Compton, M. McKenzie, M.T. Ryan, D.R. Thorburn, Next-generation sequencing in molecular diagnosis: NUBPL mutations highlight the challenges of variant detection and interpretation, *Hum. Mutat.* 33 (2) (2012) 411–418, <https://doi.org/10.1002/humu.21654>.
- [22] K.R. Vinothkumar, J. Zhu, J. Hirst, Architecture of mammalian respiratory complex I, *Nature* 515 (7525) (2014) 80–84, <https://doi.org/10.1038/nature13686>.
- [23] I. Wittig, H.P. Braun, H. Schagger, Blue native PAGE, *Nat. Protoc.* 1 (1) (2006) 418–428, <https://doi.org/10.1038/nprot.2006.62>.
- [24] M.M. Wydro, P. Sharma, J.M. Foster, K. Bych, E.H. Meyer, J. Balk, The evolutionarily conserved iron-sulfur protein INDH is required for complex I assembly and mitochondrial translation in Arabidopsis [corrected], *Plant Cell* 25 (10) (2013) 4014–4027, <https://doi.org/10.1105/tpc.113.117283>.